RQT

NASA CR-134848

(NASA-CR-134848) QUIET CLEAN SHORT-HAUL EXPERIMENTAL ENGINE (QCSEE) OVER THE WING (OTW) DESIGN REPORT Final Report (General Electric Co.) 530 p HC A23/MF A01 CSCL 21E

N80-15086

Unclas
G3/07 33463

QUIET CLEAN SHORT-HAUL EXPERIMENTAL ENGINE (QCSEE) Over-the-Wing (OTW) Final Design Report

June, 1977

by

Advanced Engineering & Technology Programs Department
Group Engineering Division

Prepared For

National Aeronautics and Space Administration

NASA Lewis Research Center
Contract NAS3-18021

TABLE OF CONTENTS

TABLE OF CONTENTS (Continued)

TABLE OF CONTENTS (Continued)

TABLE OF CONTENTS (Continued)

TABLE OF CONTENTS (Continued)

TABLE OF CONTENTS (Concluded)

LIST OF ILLUSTRATIONS

LIST OF ILLUSTRATIONS (Continued)

LIST OF ILLUSTRATIONS (Continued)

LIST OF ILLUSTRATIONS (Continued)

LIST OF ILLUSTRATIONS (Continued)

LIST OF ILLUSTRATIONS (Continued)

LIST OF ILLUSTRATIONS (Continued)

LIST OF ILLUSTRATIONS (Continued)

LIST OF ILLUSTRATIONS (Continued)

LIST OF ILLUSTRATIONS (Continued)

LIST OF ILLUSTRATIONS (Continued)

LIST OF ILLUSTRATIONS (Continued)

LIST OF ILLUSTRATIONS (Continued)

LIST OF ILLUSTRATIONS (Concluded)

LIST OF TABLES

LIST OF TABLES (Continued)

LIST OF TABLES (Continued)

LIST OF TABLES (Continued)

LIST OF TABLES (Concluded)

SECTION 1.0

INTRODUCTION

The Quiet Clean Short-Haul Experimental Engine (QCSEE) Program provides for the design, fabrication, and testing of experimental, high-bypass, geared turbofan engines and propulsion systems for short-haul passenger aircraft. The overall objective of the program is to develop the propulsion technology required for future externally blown flap types of aircraft with engines located both under the wing and over the wing. This technology encompasses the following elements:

- Variable-pitch and fixed-pitch fans
- Geared fans
- Low noise
- Low exhaust emissions
- High thrust-to-weight ratio
- Composite fan blades
- Composite fan frames
- Lightweight low-drag nacelles
- Digital electronic controls
- Thrust reverse means
- Rapid response to thrust demand
- Low fan pressure ratio, low fuel consumption cycles

Two experimental propulsion systems are being developed and will be tested as a part of the QCSEE Program (Contract NAS3-18021). The under-the-wing (UTW) engine features a low-tip-speed, low-pressure-ratio, variable-pitch fan, while the over-the-wing (OTW) engine features a fixed-pitch fan having a higher design pressure ratio accomplished with a higher tip speed.

The overall engine design process included the preliminary design of optimized UTW and OTW flight engine configurations during the initial phase of the program, which involved the participation of representatives of NASA-Lewis, the Douglas Aircraft Company, The Boeing Company, and American Airlines.

The preliminary design of the two experimental engines was conducted in parallel with the design of the flight engines. Design of the experimental engines duplicated the flight engines in all areas except those where considerable cost savings could be accomplished through simplification or utilization of existing component hardware without compromising the basic program objectives.

Following approval of the preliminary engine designs by NASA, detail design of the experimental engines was initiated. This report summarizes the final detail design of the OTW experimental engine. Any discussions relating to the OTW flight engine are included only for the purpose of defining specific differences which exist between the experimental and flight engine configurations. Reference to the UTW engine in certain sections is made only where it was felt necessary to provide a better understanding of the overall engine design process.

SECTION 2.0

SUMMARY

This report summarizes the detail design of the over-the-wing (OTW) experimental engine. The results of the detail design provide a high degree of confidence that the experimental engine will meet all of the stated program objectives. Design simplification in certain areas and application of available component hardware to the experimental engine design to minimize program expenditures have not resulted in any compromise of the program technical objectives.

2.1 PROGRAM OBJECTIVES

The major purpose of the QCSEE Program is to develop and demonstrate the technology required for propulsion systems for quiet, clean, and economically viable commercial short-haul aircraft. This comprehensive program includes the following objectives:

- To develop the propulsion system technology which will permit a short-haul aircraft to achieve the system noise goal of 95 EPNdB along a 152 m (500 ft) sideline when the engines are scaled to a total installed thrust of 400,300 N (90,000 lb). The design shall also minimize the ground area (footprint) exposed to objectionable noise levels.

- To demonstrate a propulsion system which will meet advanced pollution goals under all operating conditions.

- To develop the technology for very-high-bypass-ratio engines with quiet low-pressure-ratio geared variable-pitch fans.

- To develop the technology required to meet propulsion system performance, control, weight, and operational characteristics.

- To develop the material, design, and fabrication technology for quiet propulsion systems which will yield engine designs which have an uninstalled thrust-to-weight ratio greater than 6 to 1 and installed thrust-to-weight ratios greater than 3.5 to 1.

- To develop the technology which will yield engine thrust response characteristics required for powered lift operations.

- To provide the technology which will permit the design of quiet, efficient, lightweight thrust reversing systems for powered lift aircraft.

- To provide the technology to permit the design of integrated engine and nacelle installations which will be tolerant to aerodynamic distortions expected with operating flight conditions (such as high crosswinds, large angles of attack, and side slip) and still provide good cruise performance.

- To provide the digital electronic engine control technology required to improve engine and fan pitch control, thrust response, operational monitoring, and relief of some of the pilot's workload especially during powered lift flight operations in the terminal area.

2.2 SPECIFIC TECHNICAL OBJECTIVES

The following specific design objectives have been established for the flight and experimental QTW propulsion systems.

2.2.1 Noise

The QTW experimental engine shall be designed to meet the following noise objectives when scaled to fit a four-engined, 400,300 N (90,000 lb) thrust aircraft:

Takeoff and approach - 95 EPNdB @ 152 m (500 ft) SL

Max. Reverse Thrust* - 100 PNdB @ 152 m (500 ft) SL

The conceptual flight design engine will meet these same noise objectives when installed on a typical short-haul commercial aircraft. The design shall also minimize the aircraft acoustic footprint.

2.2.2 Pollution

The engines shall be designed to minimize exhaust emissions of carbon monoxide (CO), unburned hydrocarbons (HC), oxides of nitrogen (NO_x), and visible smoke.

2.2.3 Thrust to Weight

The full-scale QTW experimental engine shall be designed to meet the following thrust and thrust-to-weight objectives:

	Uninstalled	Installed
Thrust	93,408 N (21,000 lb)	90,294 N (20,300 lb)
Thrust/wt	7.4	4.7

*35° Max. Forward Thrust

Uninstalled thrust includes all engine internal pressure losses up to the nozzle throat; installed thrust includes additional losses due to inlet ram recovery.

Uninstalled weight includes the dry weight of all engine components and engine accessories. Installed weight includes the following additions:

- Inlet and inlet anti-icing system
- Exhaust ducts and nozzles
- Fan duct and splitter
- Engine mounts to interface with aircraft structure
- Nozzle controls and hydraulic system
- Fire detection and extinguishing systems
- Drains, vents, and oil cooler
- Instrumentation

Thrust/weight shall be representative of a flight engine design. This shall include analytically predicted flight weight of all boiler plate and non-flight design components.

2.2.4 Thrust Reversal

The OTW propulsion system shall provide the following thrust reversal capability:

- Operation down to 5.1 m/sec (10 knots)
- Max. forward to max. reverse thrust transient in less than 1.5 seconds
- At least 35% static takeoff thrust in reverse
- Noise levels as specified in Section 2.2.1

2.2.5 Engine Bleed

The engines shall be capable of safely providing up to 13% engine core bleed (not to be demonstrated).

2.2.6 Power Extraction

The engines shall be capable of supplying a minimum of 1640 W/4448 N (2.2 horsepower per 1000 lb) of installed thrust for customer takeoff power (not to be demonstrated).

2.2.7 Dynamic Thrust Response

The engine thrust response shall be designed to meet an acceleration from 62% to 95% thrust in one second [sea level to 1830 m (6000 ft) altitude].

2.2.8 Distortion Tolerance

The engine shall be capable of satisfactory operation at inlet upwash angles of 0 to 50°, with 18 m/sec (35 knot) 90° crosswinds.

2.2.9 Oil Consumption

Engine oil consumption shall not exceed 0.906 kg/hr (2 lb/hr).

2.2.10 Dumping

No fuels or lubricants shall be dumped.

2.2.11 General Design Criteria

In addition to the specific objectives listed above, the experimental engine shall meet the following general criteria:

1. The propulsion system shall be designed for ground static and altitude chamber operation.

2. The propulsion system shall be designed for flight operation except in specific areas where nonflight hardware can be used to save costs.

3. Propulsion system characteristics, such as temperatures, specific fuel consumption, and overall pressure ratio shall be selected to be appropriate for short-haul commercial aircraft.

4. All propulsion system components shall be designed for life which is compatible with expected commercial short-haul operation.

5. The propulsion system control system shall be designed with digital logic and signal paths capable of interfacing with an aircraft onboard flight digital computer. The control system shall be designed to provide selectable programmed power management and failure indication and/or corrective action over the entire propulsion system operating envelope.

6. The propulsion system shall be designed with the objective of achieving high performance, but it is not essential that hardware development be carried to the point where ultimate performance is achieved for the experimental propulsion system. The Contractor shall show that his analytical extrapolation of performance data to a fully developed propulsion system is reasonably accurate, and that deviations in performance do not significantly affect acoustic or pollution characteristics of the experimental propulsion systems.

The experimental engine nacelle shall be designed with the following features:

1. Internal aerodynamic contours representative of the flight nacelle (except as modified for commonality with UTW hardware).

2. Acoustic treatment that is representative of the flight-type design.

3. All electrical, fuel, oil, cooling, fire detection and prevention, control, and instrumentation systems required to test the propulsion systems.

4. Convenient access for maintenance.

The propulsion system shall be designed for the following maintenance features:

1. The engine shall be easily removable from the nacelle without requiring removal of the fan exhaust duct.

2. The engine shall be capable of being trimmed on a test stand with no additional trimming required if installed on an aircraft.

3. Accessories shall be located for easy inspection.

4. Access to borescope ports shall be provided without requiring removal of any engine component.

5. Any propulsion system accessory shall be replaceable in 45 minutes*.

6. Fans shall have an even number of blades to permit replacement in pairs without rebalancing. Blades shall be capable of rapid inspection and replacement.

7. Modular construction is used to facilitate maintenance.

---

* Exception to this objective has been taken in the design of the experimental engine in those areas where significant cost savings could be effected through utilization of existing accessory component hardware.

The propulsion system shall be designed to perform within the flight maneuver forces envelope per MIL-E-5007C data December 30, 1965, paragraph 3.14, with the exception of conditions of catapult flight maneuver and precession rates.

2.3 OPERATING REQUIREMENTS

The foregoing specific objectives and general criteria are further amplified by the following propulsion system operating requirements.

2.3.1 Life and Duty Cycle

The engines shall be designed for a useful life of 36,000 hours over a 15 year period, based on the typical 403 km (250 mile) mission cycle shown in Table 2-I.

Table 2-I. Flight Duty Cycle.

Segment	Altitude		Mach No.	% Power	Time	
	km	ft			Min	% Time
Start	0	0	0	-	0.5	1.11
Idle-Taxi	0	0	0	4-20	3.1	6.89
Takeoff	0	0	0.12	100	1.22	2.71
Climb (1st seg)	0-3.05	0-10K	128.6 m/sec (250 kts) IAS	Max.Cont.	5.0	11.11
(2nd seg)	3.05-7.63	10-25K	154.3 m/s (350 kts) IAS	Max.Cont.	5.0	11.11
Cruise	6.41-7.63	21K-25K	.70	Max.Cruise	14.0	31.11
Descent	6.1-0.06	20K-200ft	.60	F.I.	10.0	22.22
Approach	0.06	200 ft	0.12	65	3.0	6.67
Reverse Thrust	0	0	0.12-0	Max.Rev.	0.08	0.18
Idle-Taxi	0	0	0	4-20	3.1	6.89
					45.00	100.00

Cyclic life shall be based on 48,000 mission cycles plus 1000 ground checkout cycles to full power.

The engine shall be capable of operation throughout the flight envelope shown in Figure 2.1. The combustor shall meet commercial relight requirements as shown on the flight envelope.

ORIGINAL PAGE IS
OF POOR QUALITY

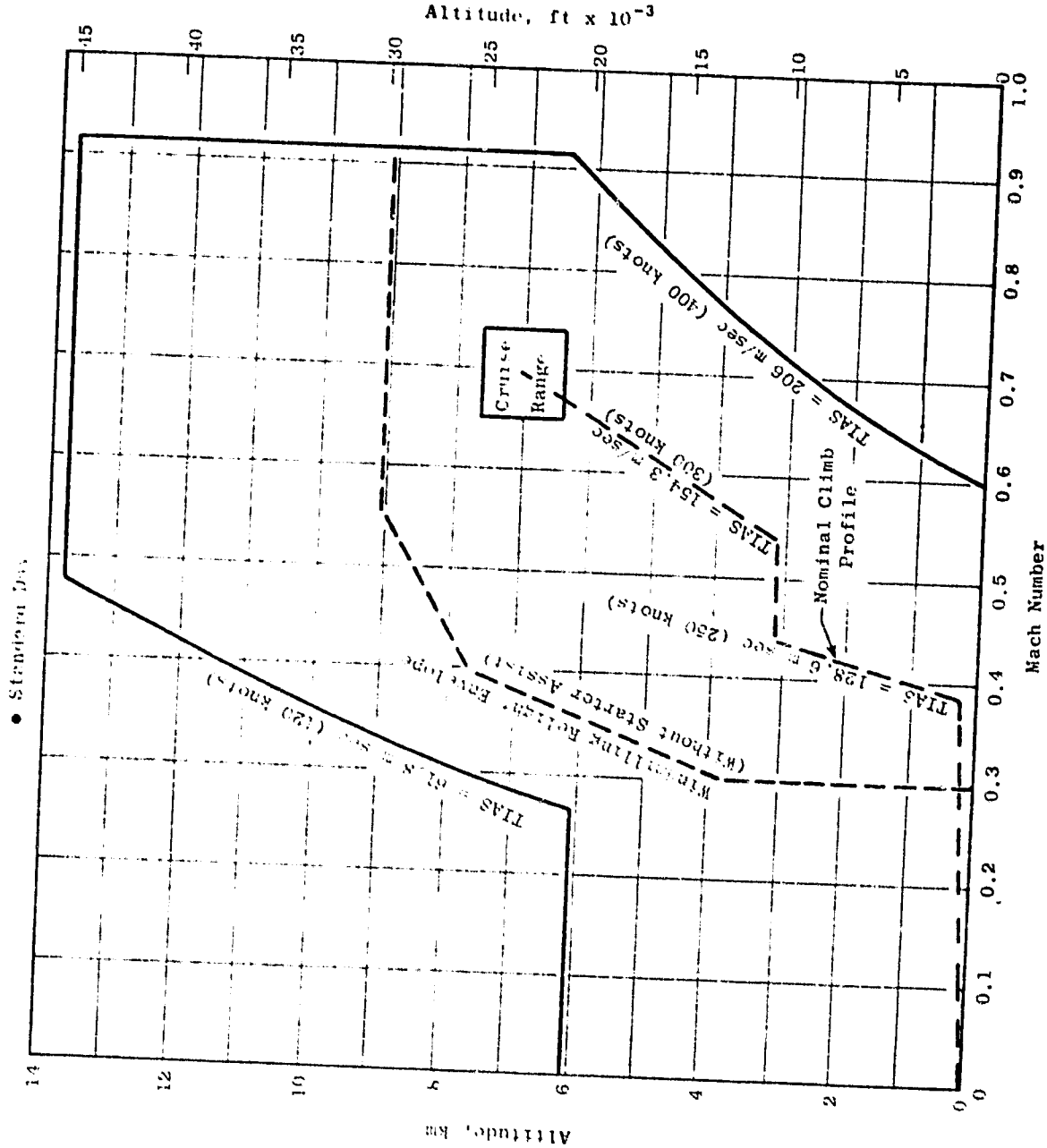

Figure 2.1. QCSEE Operating Envelope.

The engine shall be capable of withstanding loads caused by seizure of either rotor with deceleration from maximum rpm to zero rpm in one second. (Figure 2.2).

Composite parts shall be capable of withstanding unbalanced loads caused by loss of five adjacent composite fan blades at maximum rpm. Metal parts shall be capable of withstanding loss of one equivalent metal blade.

2.3.2 Flight Attitudes

The engine shall be capable of operating within the range of flight attitudes shown in Figure 2.3.

2.4 OTW EXPERIMENTAL PROPULSION SYSTEM

The OTW experimental propulsion system, shown in Figure 2.4, features: a high Mach (accelerating) inlet, a gear driven fan, a composite fan vane-frame, a treated fan duct with an acoustic splitter ring, a variable geometry confluent flow exhaust nozzle, an advanced (F101) core and low pressure turbine, a treated core exhaust, top-mounted engine accessories, and a digital electronic control system.

The fundamental design criterion which established the engine design approach was the fan engine cycle required to meet the noise objective. The fan and core exhaust pressure ratios were dictated by jet-flap noise constraints and by the powered lift requirements of an over-the-wing installation.

The fan is a low-pressure-ratio (1.35)*, low-tip-speed [350.5 m/sec (1150 ft/sec]* configuration sized to provide 405.5 kg/sec (894 lb/sec)* of corrected airflow.

The fan contains 28 titanium blades having an aerodynamic contour capable of conversion to composite material in a flight system. The fan is driven by the F101 low pressure turbine through a main reduction gear. The reduction gear is an eight-star epicyclic configuration with a gear ratio of 2.0617 and a takeoff power rating of 12,813 kw (17,183 HP).

The fan frame is a flight-weight composite structure containing integral acoustic treatment, outer casing, containment, and fan tip treatment. Thirty-three integral outlet guide vanes also act as structural struts. The outer casing of the frame provides both inner and outer nacelle flowpaths and containment for failed composite**. Core inlet flowpath and mounts for the forward bearings, gears, radial drive, etc., are integrally provided.

The nacelle components include a hybrid inlet providing acoustic suppression by means of a high throat Mach number (0.79) and integral acoustic treatment. The boilerplate fan duct which includes an acoustic splitter and the

*Takeoff power setting.
**Flight engine design.

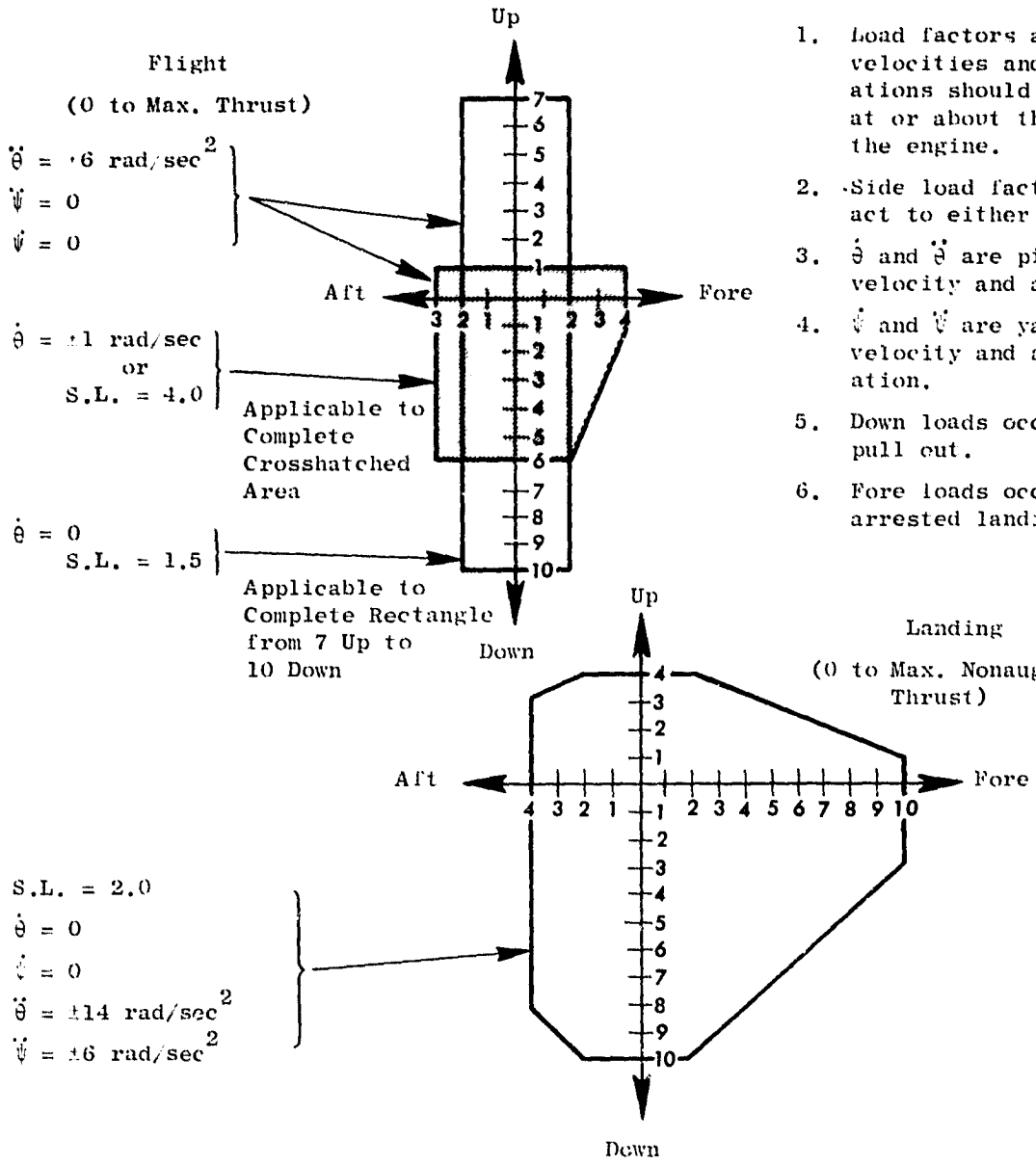

Figure 2-2. QCSEE Design Loads.

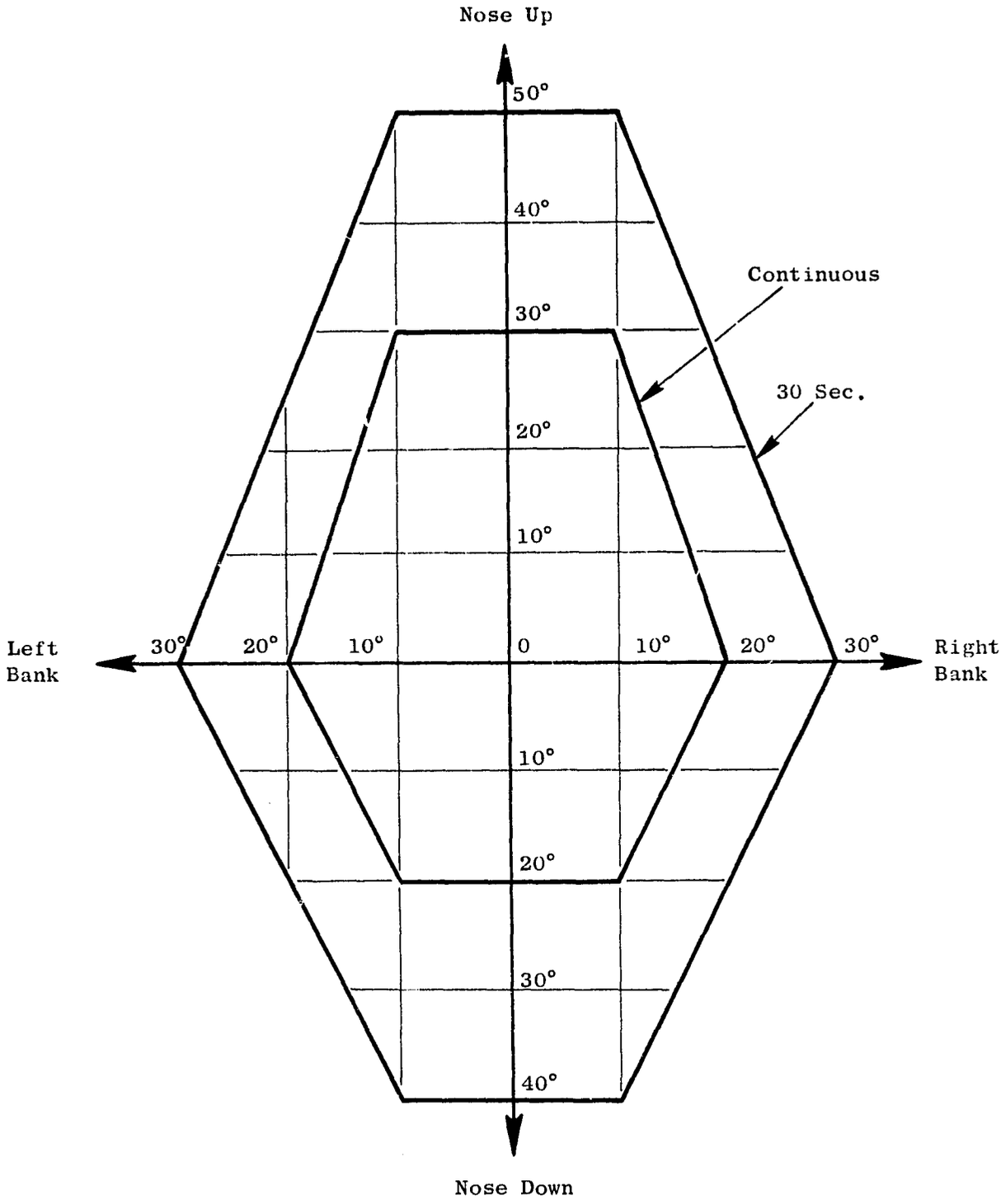

Figure 2.3. QCSEE Flight Attitudes.

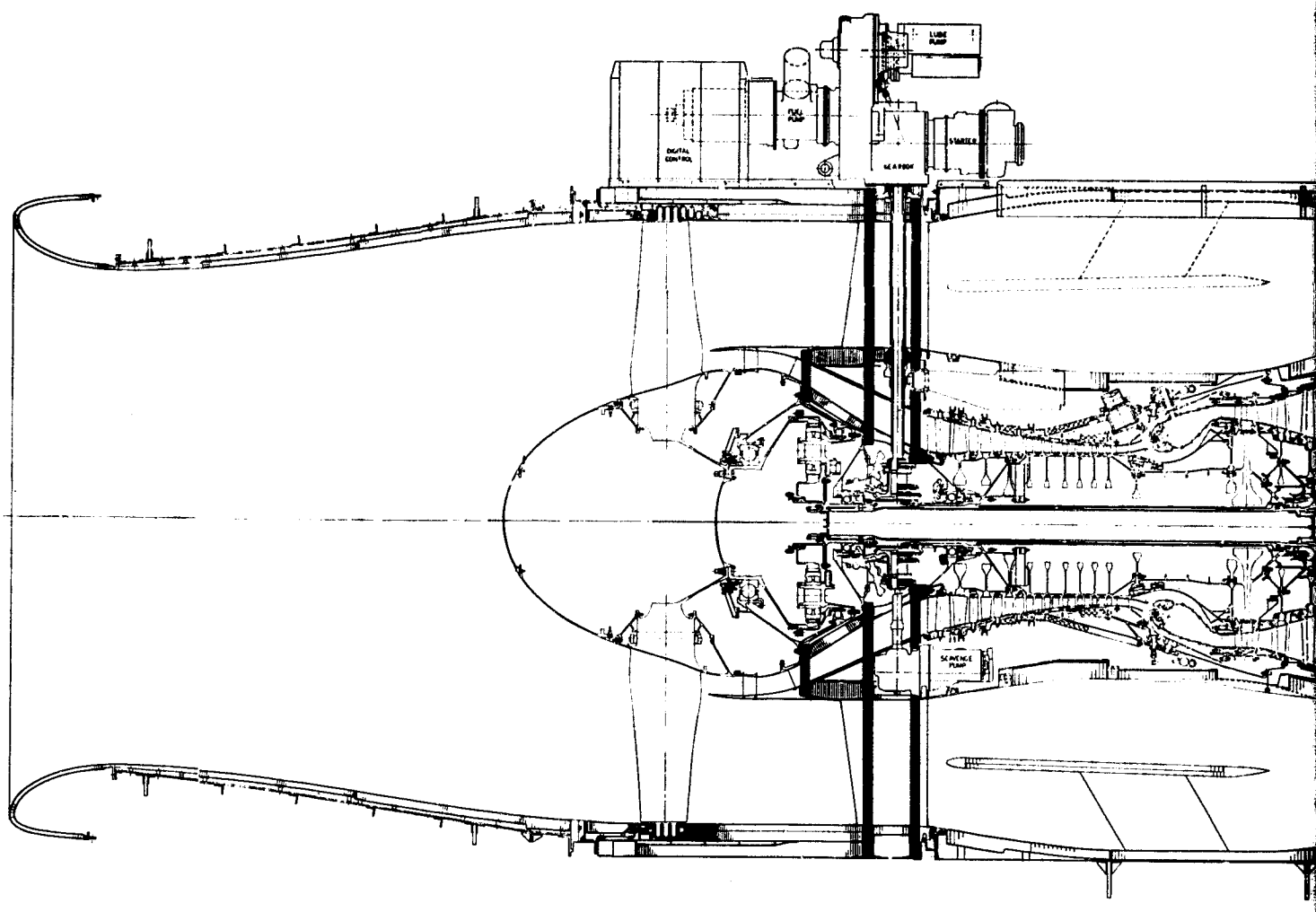

Figure 2.4. OTW Experimental

FOLDOUT FRAME 1

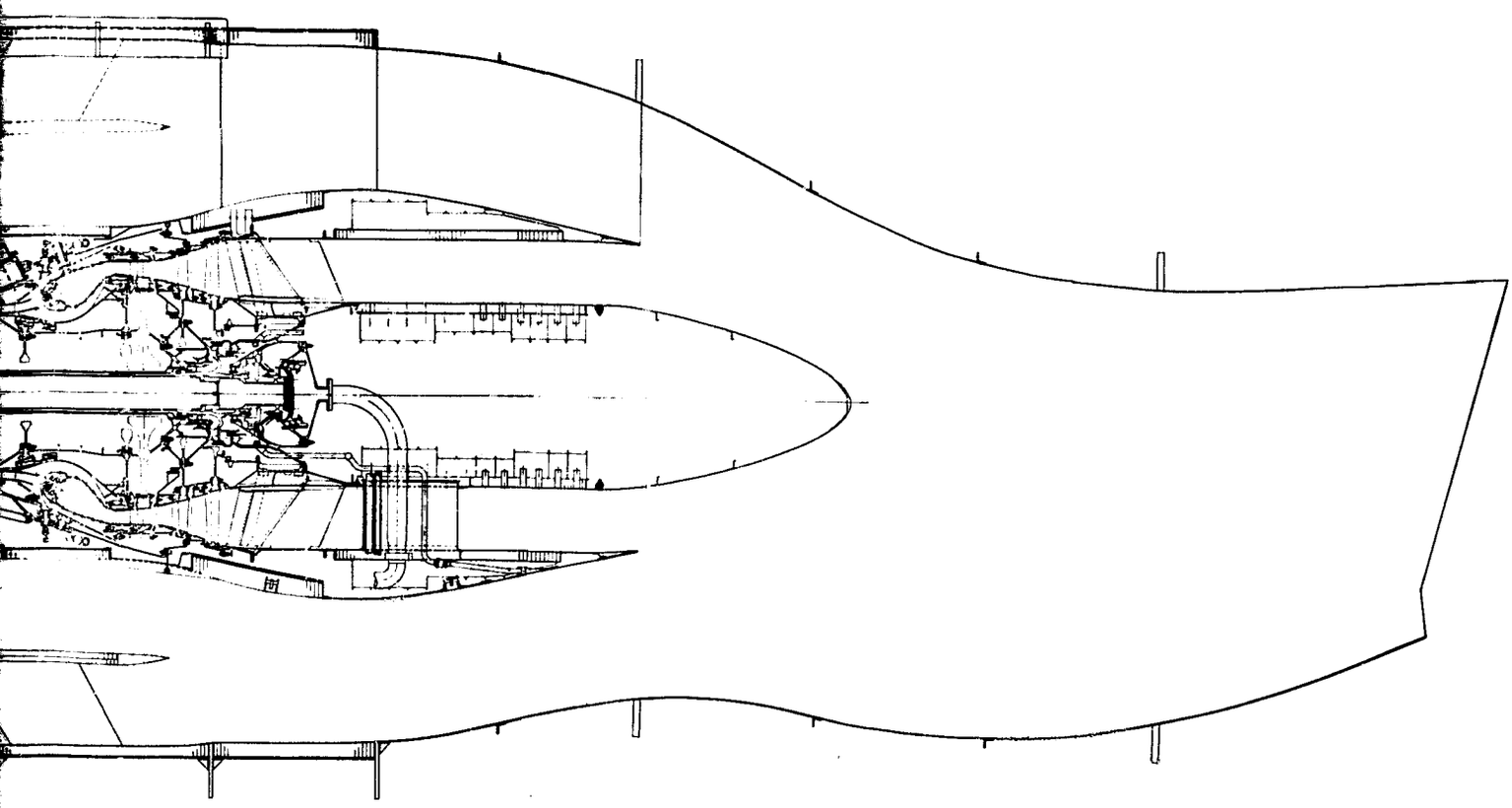

TW Experimental Propulsion System.

FOLDOUT FRAME 2

core cowl are hinged from the pylon to provide access for engine maintenance. The core exhaust and plug are acoustically treated to reduce aft-radiated noise. The "D" shaped confluent flow exhaust nozzle incorporates side doors to vary the area from takeoff to cruise. No actuation system is provided for the experimental engine, so that exhaust areas must be preset before starting the engine. A blocker-type thrust reverser is integral with the nozzle and can be manually preset to the reverse thrust position for testing.

Engine fuel flow is controlled by a full-authority digital electronic control which schedules core stators and provides starting, acceleration, and deceleration schedules. Major engine accessories are mounted on a boilerplate gearbox on top of the fan frame. This accessory package is common with that of the UTW engine, requiring that the OTW engine be tested in an inverted position relative to an aircraft installation.

All experimental engine components have been designed to meet the engine life and operating requirements defined in Section 2.3.

The OTW experimental propulsion system is designed to provide 93,408 N (21,000 lb) of uninstalled thrust and 90,294 N (20,300 lb) of installed thrust at takeoff on a 305.6° K (90° F) day. Analysis indicates that, when scaled in accordance with the specified ground rules, the engine will meet all of the program noise objectives.

2.5 OTW FLIGHT PROPULSION SYSTEM

The OTW flight propulsion system cross section is shown in Figure 2.5. Comparing Figure 2.5 with Figure 2.4, it will be noted that the major configurational difference between the flight and experimental propulsion systems is the "D" nozzle and accessory orientation. Also the fan duct is modified and an acoustic splitter is added to satisfy the experimental engine noise goal and to utilize common UTW hardware. The noise goal for the experimental engine is based on a 609.6 m (2000 ft) takeoff, while the acoustic design of the flight propulsion system is based on a noise goal set for a 914.4 m (3000 ft) takeoff.

Structural component differences are also in the areas of the turbine rear frame and core nozzle. The experimental engine utilizes a modified F101 rear frame, while the flight engine configuration is based on an optimized flightweight design. The core nozzle of the experimental engine is a non-coated boilerplate design to minimize cost.

Other differences between the two configurations are primarily in the areas of material substitutions and utilization of existing accessory components in the experimental engine to minimize program cost. For example, the experimental engine uses steel rather than titanium for fan shafting, reduction gear carrier, and bearing support cones. Cost savings in the accessory area are based on utilization of an available oil tank, heat exchanger, pumps, filters, etc., which would be optimized in the flight engine. Several changes in the core also have been considered, consistent with the lower cycle compressor discharge pressure.

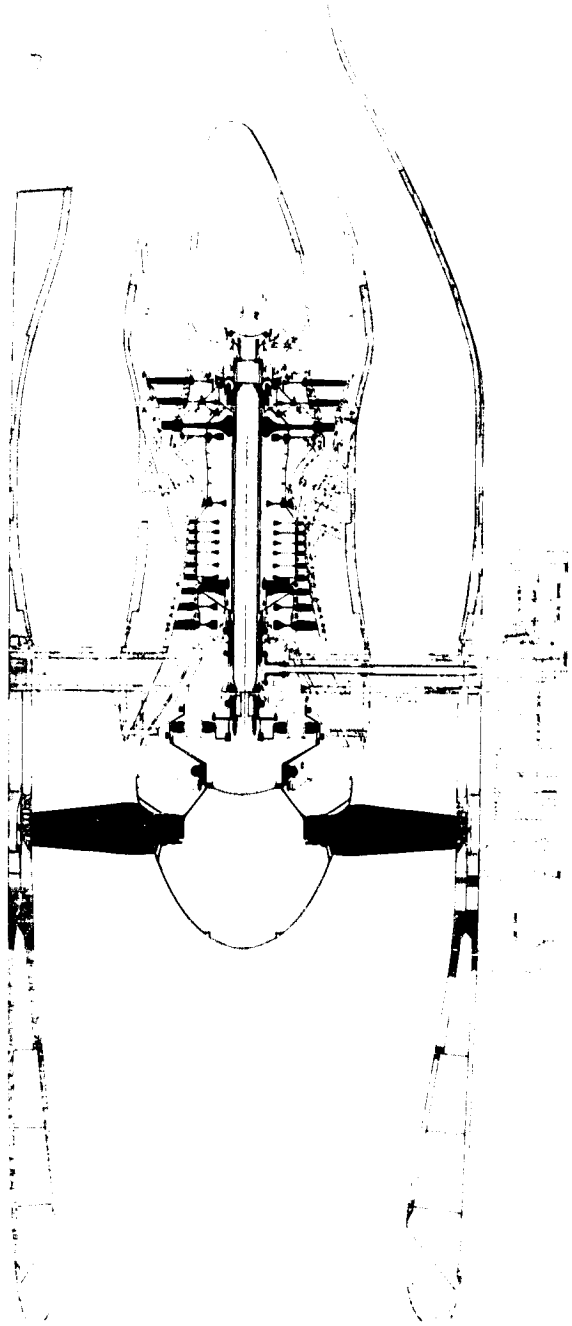

Figure 2.5. OTW Flight Propulsion System.

The flight propulsion system also includes: an inlet anti-icing provision which is not included in the experimental system inlet, a flight-type fire detection and extinguishing system in place of a facility system, and a double-wall fuel system. The flight system also would include the necessary bleed manifolding for cabin air conditioning and for high lift systems requiring engine bleed air.

The experimental QTW engine is top mounted from a pylon similar to the UTW engine. The flight engine would be trunnion mounted from a structural arch extending forward from the wing box section. By opening the bypass duct and core cowl, the engine and inlet can be removed from the pylon in the downward direction.

Analyses conducted to date indicate that the uninstalled thrust/weight of the flight engine will be within 3% of meeting the program goal of 7.4, and that the installed (total propulsion system) thrust/weight will meet the program goal of 4.7.

SECTION 3.0

ACOUSTIC DESIGN

3.1 SUMMARY

The preliminary acoustic design (Reference 1 and 2) of the OTW engine defined a configuration which meets the takeoff, approach, and reverse thrust noise goals. Table 3-I summarizes the current system noise levels at the three design points.

Table 3-I. Summary of OTW Noise Levels at 152 m (500 ft) Sideline.

- 90,000-lb thrust
- 4 engines

	EPNdB	
	Requirement	Current Estimates
Takeoff	95	95
Approach	95	90.6
Reverse Thrust	100	100

The noise levels have been obtained by estimating unsuppressed noise from existing test data of similar fan and core configurations, analytically suppressing the dominant engine noise sources with the advanced technology concepts to be developed under the QCSEE program, and extrapolating these levels to inflight conditions. Jet/flap noise was added to the engine noise levels to obtain total system or aircraft noise levels.

The preliminary acoustic design effort has attempted to establish OTW engine configurations which have balanced suppression in the fan inlet, fan exhaust, and core. To establish the balanced system suppression, detailed predictions have been made for these 10 different noise sources:

1. Fan inlet
2. Fan exhaust
3. Turbine
4. Combustor
5. Compressor
6. Gears
7. Flow
8. Struts
9. Splitter
10. Jet/Flap

By predicting the noise levels of the various sources which could represent noise floors, the required treatment can be determined and applied to the engine only to the extent which is beneficial to the total system.

Figure 3.1 summarizes the main acoustic features of the OTW engine. A high throat Mach number inlet (0.79) is used to suppress inlet noise at takeoff and reverse thrust. Inlet wall treatment having a length equal to 0.74 fan diameters is added to provide suppression at approach. The rotor-stator combination has a 1.93 rotor tip chord spacing and a vane/blade ratio of 1.18. The vane/blade ratio is lower than would normally be selected for minimum noise generation; however, the vane row is the same as that used on the UTW engine (V/B = 1.83). The effect of low V/B ratio on the OTW engine is somewhat offset by the large spacing. Fan exhaust suppression utilizes inner and outer wall treatment with varying thickness to obtain increased suppression bandwidth. A 76.2 cm (30 inch) splitter is employed to obtain the required suppression level. A major concern in the aft duct is noise generated by flow over the treated surfaces, struts, and splitter. To keep these sources below the suppressed fan noise, the average duct Mach number is limited to 0.47 over the splitter. Core suppression utilizes a low frequency design for combustor noise reduction with thinner treated panels on the inner and outer walls to reduce the high frequency turbine noise. Treatment also is applied in the core inlet to reduce forward-radiated compressor noise.

3.2 DESIGN REQUIREMENTS

The noise requirements for the OTW engine are specified as a total system or aircraft noise level at the operating conditions associated with takeoff and approach operation. Reverse thrust requirements also are specified for static aircraft conditions. These are shown graphically on Figure 3.2.

The takeoff noise requirement is 95 EPNdB on a 152 m (500 ft) sideline with the aircraft at a 61.0 m (200 ft) altitude and the engines at 100% thrust. Takeoff flap angle and aircraft speed are given in Table 3-II. Also shown in Table 3-II are inlet angle of attack and upwash angles which must be accounted for with regard to fan inlet noise generation and high Mach inlet suppression.

At approach the noise requirement is the same as at takeoff, but the engine is operated at 65% thrust. Flap angles, defined in Table 3-II, however, are increased for the powered lift approach.

Reverse thrust noise is limited to 100 PNdB at a reverse thrust equivalent to 35% of takeoff thrust with the aircraft static. For the OTW engine, this thrust level is accomplished by operating the engine at 100% speed, thus providing engine noise and suppression equivalent to takeoff. Due to the reverser, however, the aft noise is redirected into the forward quadrant.

Since the engine noise levels will be measured only during static testing, a procedure for determining in-flight EPNdB levels from static data has been established as part of the contract. This procedure, Appendix A of Reference 2, establishes the following:

• P/P = 1.34 • Tip Speed = 370.5 m/sec (1150 ft/sec) • Blade No. = 28

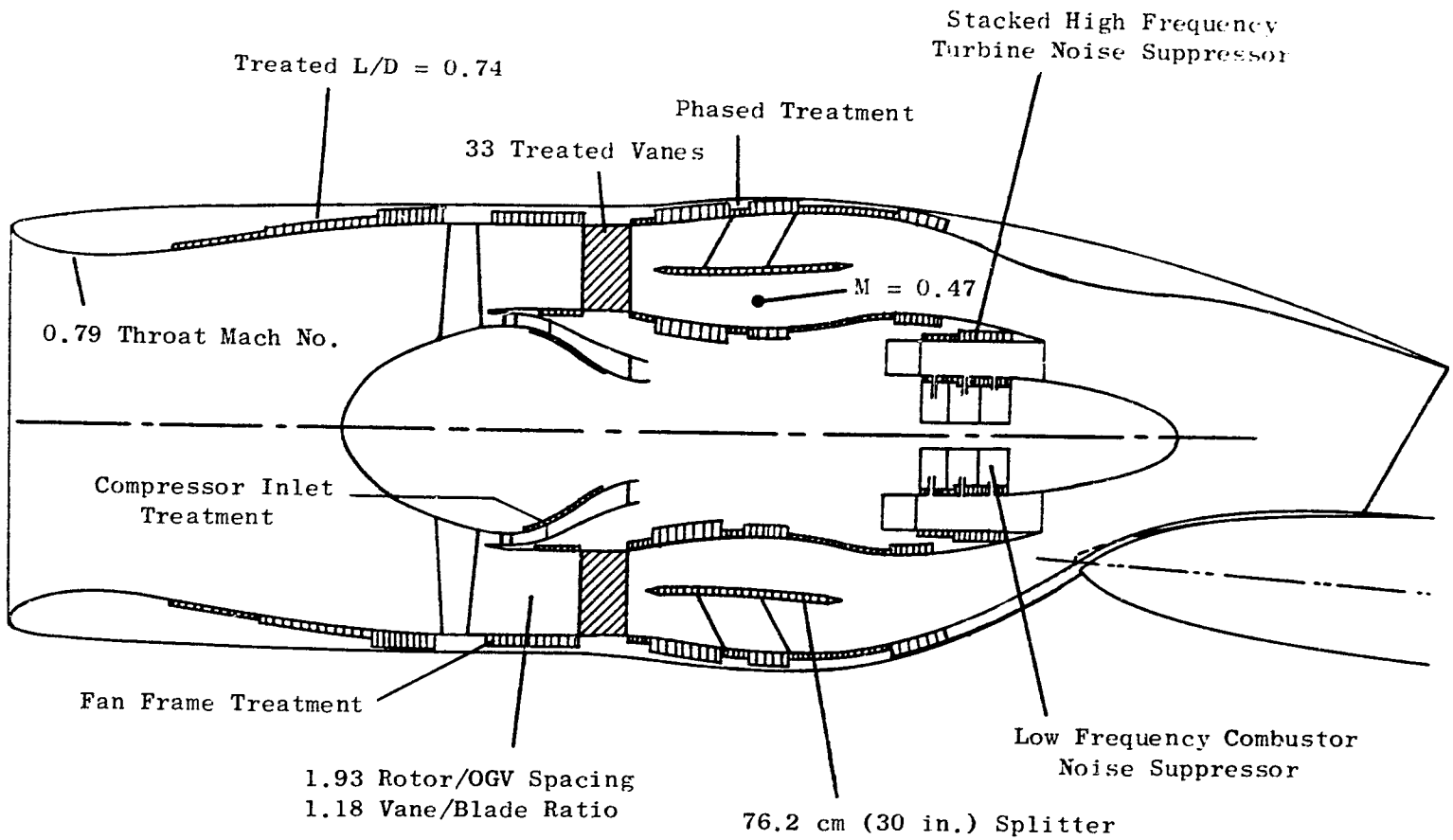

Figure 3.1. QCSEE OTW Engine - Acoustic Treatment Schematic.

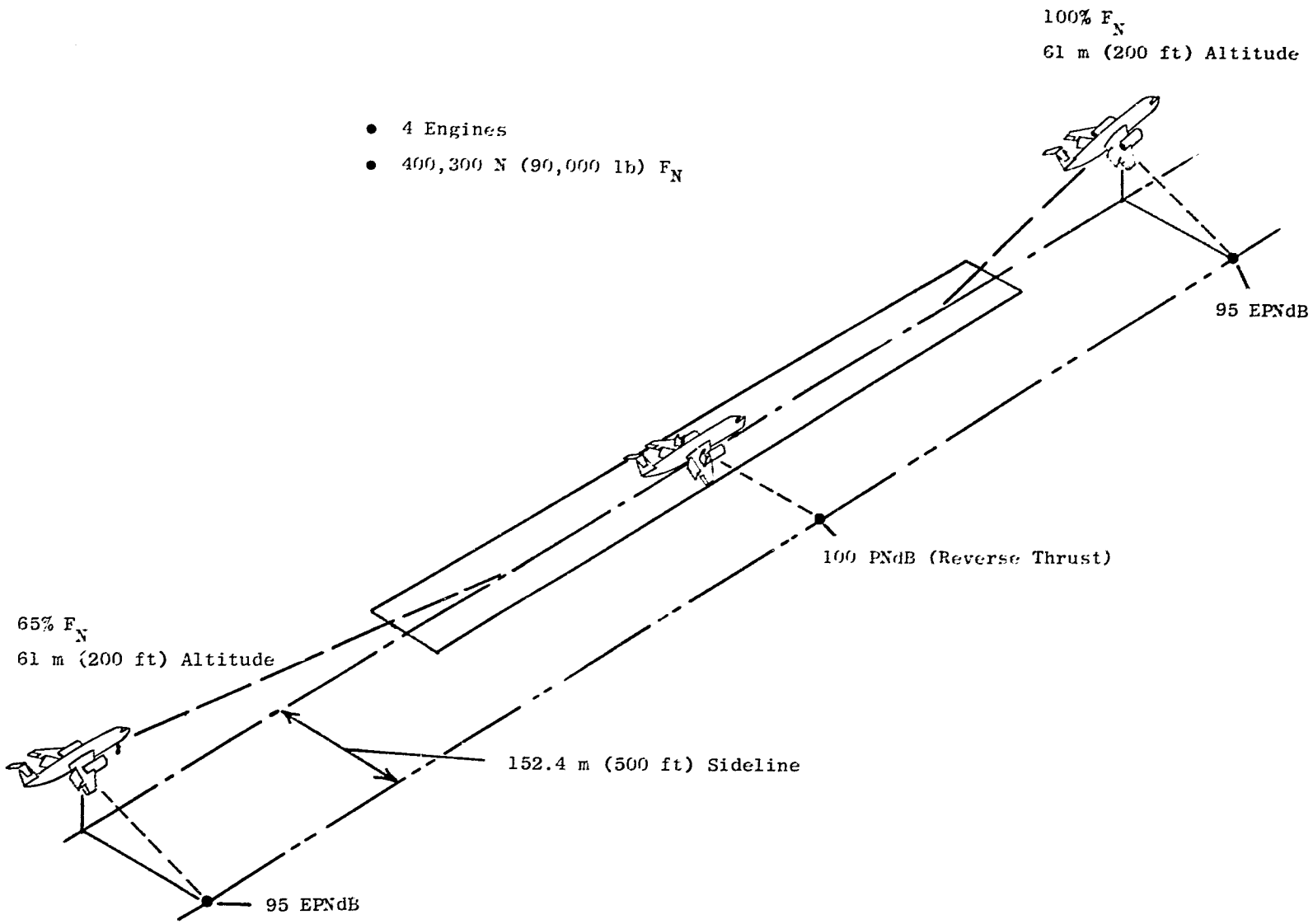

Figure 3.2. QCSEE Acoustic Requirements.

Table 3-II. OTW Aircraft Flight Characteristics for Acoustic Calculations.

Flight Conditions	Takeoff	Approach
Aircraft Speed, m/sec (knots)	41.15 (80)	41.15 (80)
Flap Chord Line Angle, radians (degrees)	.524 (30)	1.047 (60)
Climb or Glide Angle, radians (degrees)	.218 (12.5)	.105 (6)
Angle of Attack, radians (degrees)	.105 (6)	.035 (2)
Upwash Angle, radians (degrees)	.262 (15)	.192 (11)
Installed Net Thrust, percent	100	65

1. Jet/flap noise calculation procedure
2. Extrapolation procedures
3. Doppler shift correction
4. Dynamic effect correction
5. In-flight clean-up and upwash angle correction
6. Relative velocity correction for jet/flap noise
7. Fuselage shielding and wing shielding
8. PNdB to EPNdB calculation

This procedure has been used in all noise estimates for the OTW engine.

3.3 SYSTEM ACOUSTIC DESIGN CONSIDERATIONS

Many features of the OTW engine designs have been selected based on the low system noise requirements for a 100,080 N (22,500 lb) thrust engine installed in an over-the-wing configuration. The two major noise sources considered were the fan noise and the jet/flap noise. Forward-radiated fan noise is primarily a function of fan tip speed. Fan noise in the inlet quadrant can be reduced with lower tip speed, and tip speeds lower than 366 m/sec (1200 ft/sec) avoid the increased noise levels due to the multiple pure tones associated with supersonic-tip-speed fans. The lowest tip speed, 350 m/sec (1150 ft/sec), consistent with the fan pressure ratio and engine cycle requirements was therefore selected for the OTW fan.

Aft-radiated fan noise levels have been correlated primarily with fan pressure ratio. In addition to controlling aft fan noise, the fan pressure ratio also determines the fan jet velocity. Since the jet/flap noise is proportional to the velocity to the sixth power, low fan pressure ratios result in rapidly reduced aft system noise levels. Since aft-generated fan noise can be suppressed with acoustic treatment, the fan-pressure ratio was selected primarily based on the need to achieve low levels of jet/flap noise. Since the OTW design provides some wing shielding of jet/flap noise, the selected pressure ratio was slightly higher than that acceptable for the UTW designs.

The UTW engine rotor-OGV spacing of 1.5 rotor chords was selected in order to reduce fan source noise levels and minimize the need for splitters in the fan inlet and exhaust. Wider rotor-OGV spacing would produce additional reduction which also can be achieved with a lengthened exhaust splitter; the latter produces a smaller weight increase than the frame length required for additional spacing. Since the OTW engine uses the same frame as the UTW, the axial spacing was fixed. With the shorter chord blades, the spacing ratio increased to 1.93. This increased spacing ratio and, hence, lower source noise was offset by a nonoptimum vane/blade ratio for the OTW which resulted from using the common vane frame. For the UTW engine, a vane/blade ratio of 1.83 was selected to minimize the fan tone second harmonic level which makes a large contribution to the perceived noise levels. This ratio for the OTW becomes 1.18 due to the larger number of fan blades.

Table 3-III shows the major design features in the OTW design which impact the projected noise levels. The engine system trades discussed above have produced an engine preliminary design which meets the noise goals of the program as well as the performance and thrust-to-weight requirements.

Table 3-III. QCSEE OTW Design Parameters (Takeoff).

Number of fan blades	28
Fan diameter, cm (inches)	180.4 (71)
Fan pressure ratio	1.34
Fan rpm	3778
Fan tip speed, m/sec (ft/sec)	350.5 (1150)
Number of OGV's	33
Fan weight flow (corrected), kg/sec (lb/sec)	405.5 (894)
Inlet Mach number (throat)	0.79
Rotor/OGV spacing	1.93
Inlet treatment length/fan diameter	0.74
Effective exhaust area, m^2 ($in.^2$)	1.747 (2708)
Gross thrust (uninstalled), KN (lb)	93.4 (21,000)
Blade passing frequency, Hz	1760
Vane/blade ratio	1.179
Exhaust weight flow, kg/sec (lb/sec)	402.3 (886.8)
Exhaust velocity, m/sec (ft/sec)	230.7 (757.0)

3.4 NOISE COMPONENTS

Details of the critical noise sources were presented in the Preliminary Design Report (PDR). The following gives updated levels which are based on the data and prediction procedures previously discussed.

3.4.1 Takeoff Noise

Noise levels for the OTW engine at takeoff are shown on Figure 3.3 in bar chart form. Unsuppressed noise is dominated by the fan in the forward and aft quadrants. Suppressed noise levels are balanced between the fan and jet/flap noise in the forward and aft quadrants. Forward quadrant noise is higher than the aft for the suppressed configuration.

The constituent levels shown are at the angle of maximum noise for the suppressed engine; thus, in the forward quadrant, 1.57 radians (90°) is selected, since the total of the dominant sources (jet/flap and fan inlet noise) are a maximum at that angle. This comparison shows that the takeoff noise is more sensitive to fan inlet noise than aft noise.

Gear noise and compressor noise are not shown as they were not contributing noise sources.

3.4.2 Approach Noise

To obtain 65% thrust at approach, the OTW engine is operated at 82% fan speed.

The approach noise constituents are shown on Figure 3.4. Jet/flap and fan inlet noise in the forward quadrant are the dominant sources for the suppressed levels with fan exhaust and aft jet/flap noise approximately 5 PNdB lower. Unsuppressed, the fan forward and aft noise are dominant. Additional approach noise reductions would require nozzle area variation to reduce the jet/flap noise by reducing the exhaust velocity.

3.4.3 Reverse Thrust Noise

The predicted noise constituents for the OTW engine operating in the reverse thrust mode are given in Figure 3.5. The constituents are at a 152.4 m (500 ft) sideline at takeoff fan speed with a corresponding thrust level at 35 percent of the engine rated thrust in the forward mode at takeoff power. The major noise source in reverse thrust is the reverser jet noise and the fan inlet noise in the forward quadrant. Due to a redirection of the exhaust flow, the fan exhaust noise also is shown in the forward quadrant. As with takeoff, the fan inlet suppression is critical to meeting the noise goal.

3.5 COMPONENT DESIGN

This section provides the acoustic design approach selected for each engine noise source and the design status. These suppression techniques were selected for detailed study as part of the acoustic design development programs and were based on studies conducted after the PDR. In several cases the design approach is the same as that presented in the PDR, but additional substantiating data were obtained to confirm the earlier selections.

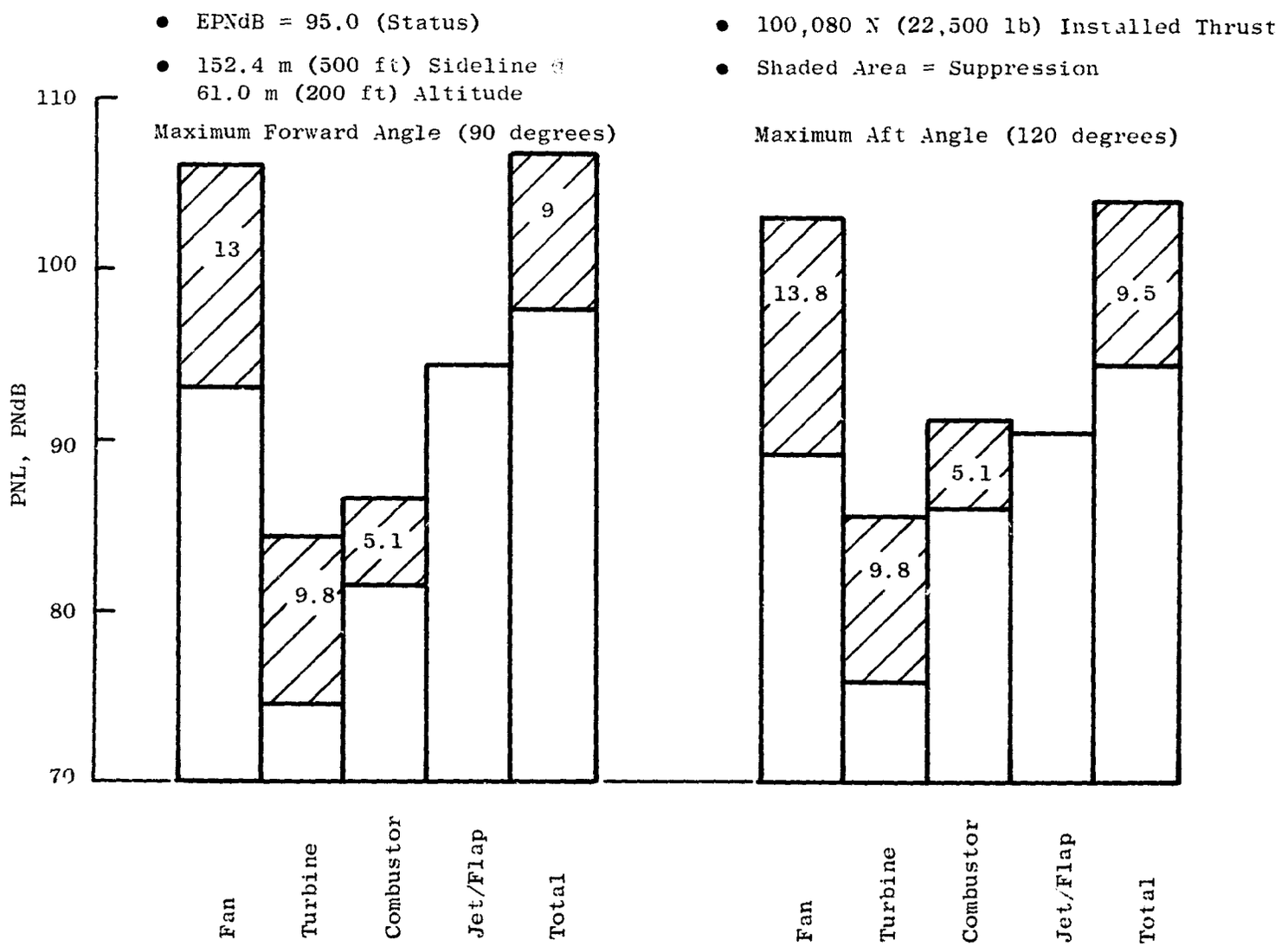

Figure 3.3. OTW Takeoff Noise Constituents.

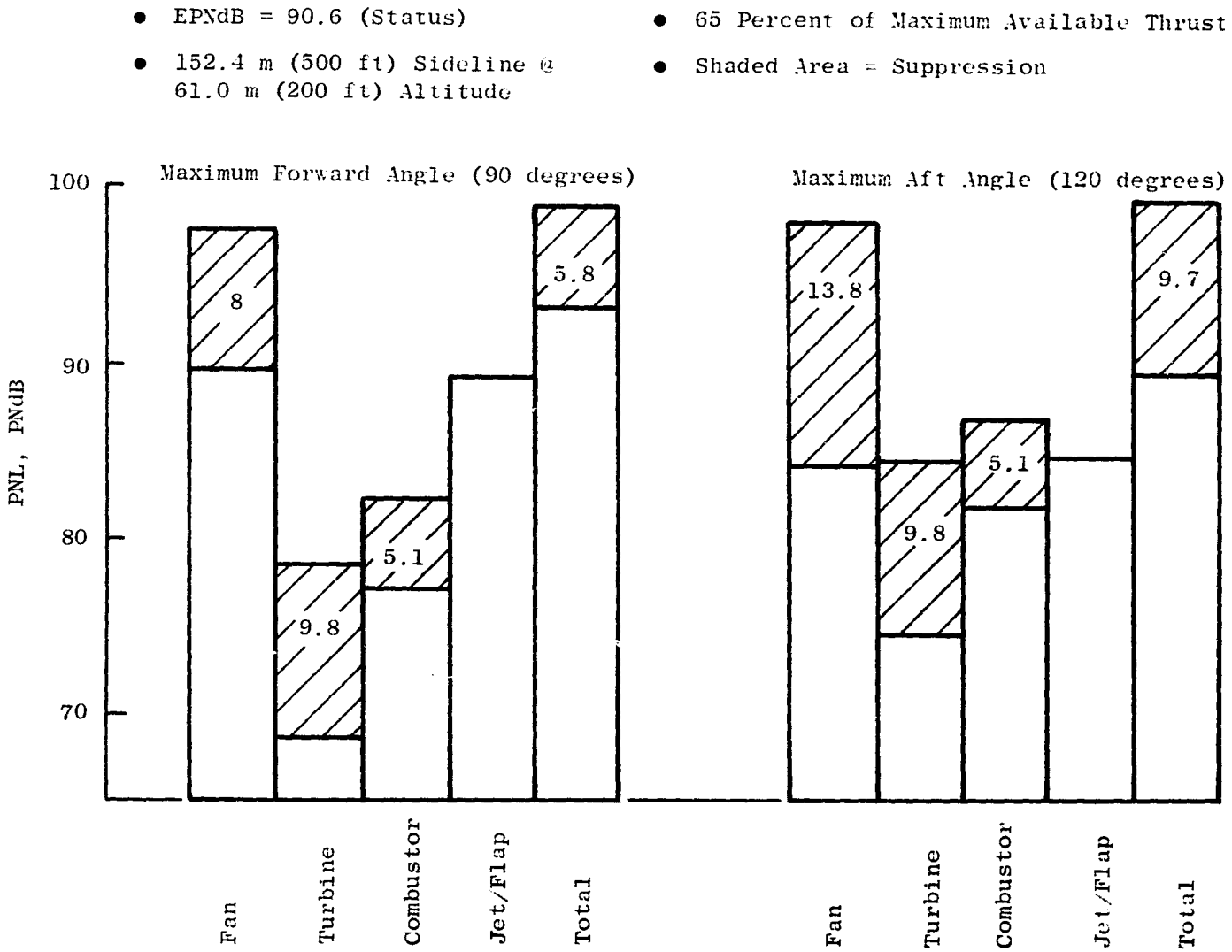

Figure 3.4. OTW Approach Noise Constituents.

- Maximum PNdB = 100.0
- 152.4 m (500 ft) Sideline
- 35 Percent of Takeoff Thrust
- Shaded Area = Suppression

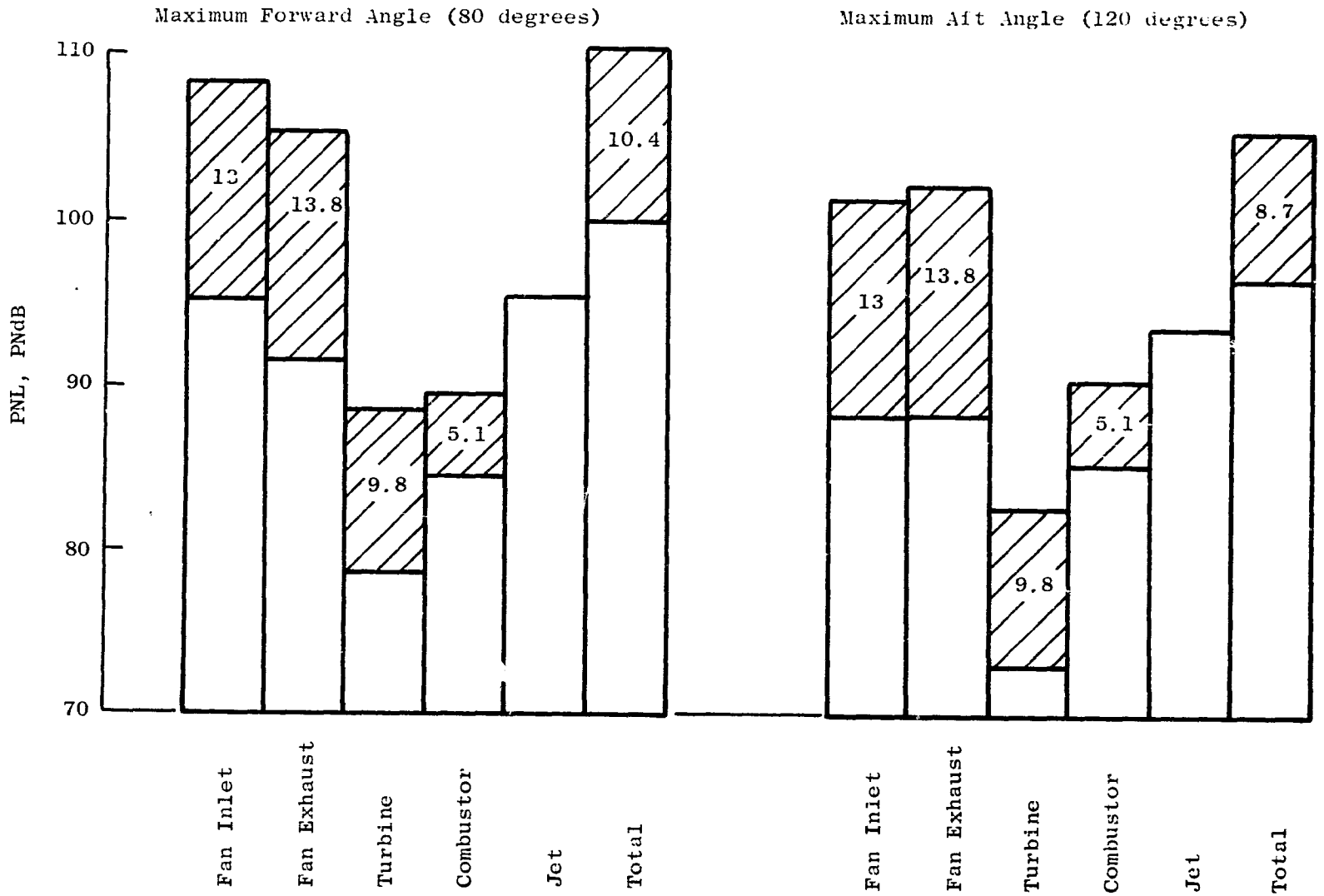

Figure 3.5. OTW Reverse Thrust Noise Constituents.

Since the PDR, the following have been completed:

1. Vane/blade ratio selected
2. Rotor/stator spacing selected
3. Treated vane-frame defined
4. Fan inlet throat Mach number selected
5. Fan inlet length defined
6. Exhaust splitter length selected
7. Aft duct Mach number distribution defined
8. Core nozzle treatment defined
9. Core compressor inlet treatment defined

A detailed discussion of the data and analyses used to establish the above follows.

3.5.1 Fan Inlet Design

The accelerating inlet, Figure 3.6, has been selected as the primary design. This inlet provides suppression at takeoff and reverse thrust with a 0.79 throat Mach number plus wall treatment. At approach, suppression is obtained by the use of wall treatment.

Tests have been completed on a scale model, 20 inch-diameter UTW fan with an accelerating inlet. Results of these tests are shown in Figure 3.7. With wall treatment, the inlet provided 13 PNdB reduction and met the suppression goal. These data, applied to the OTW engine, also showed 13 PNdB reduction. The resulting spectra are shown on Figure 3.8.

The aerodynamic lines for the accelerating inlet have been selected as a result of 30.40 cm (12 in.) inlet tests at the NASA-Lewis 9 × 15 Wind Tunnel. During these tests, noise data were obtained with the accelerating inlet operating at 0.79 throat Mach number and various angles of attack. These data, Figure 3.9, show the inlet to be acoustically insensitive to angle of attack.

3.5.2 Fan Exhaust Design

Several design techniques have been used to establish 13.8 PNdB aft fan noise reduction. These are:

1. Phased wall treatment
2. Acoustic splitter
3. Rotor - OGV treatment
4. Flow noise floor definition
5. Treated vane row

The aft duct design is shown in Figure 3.10

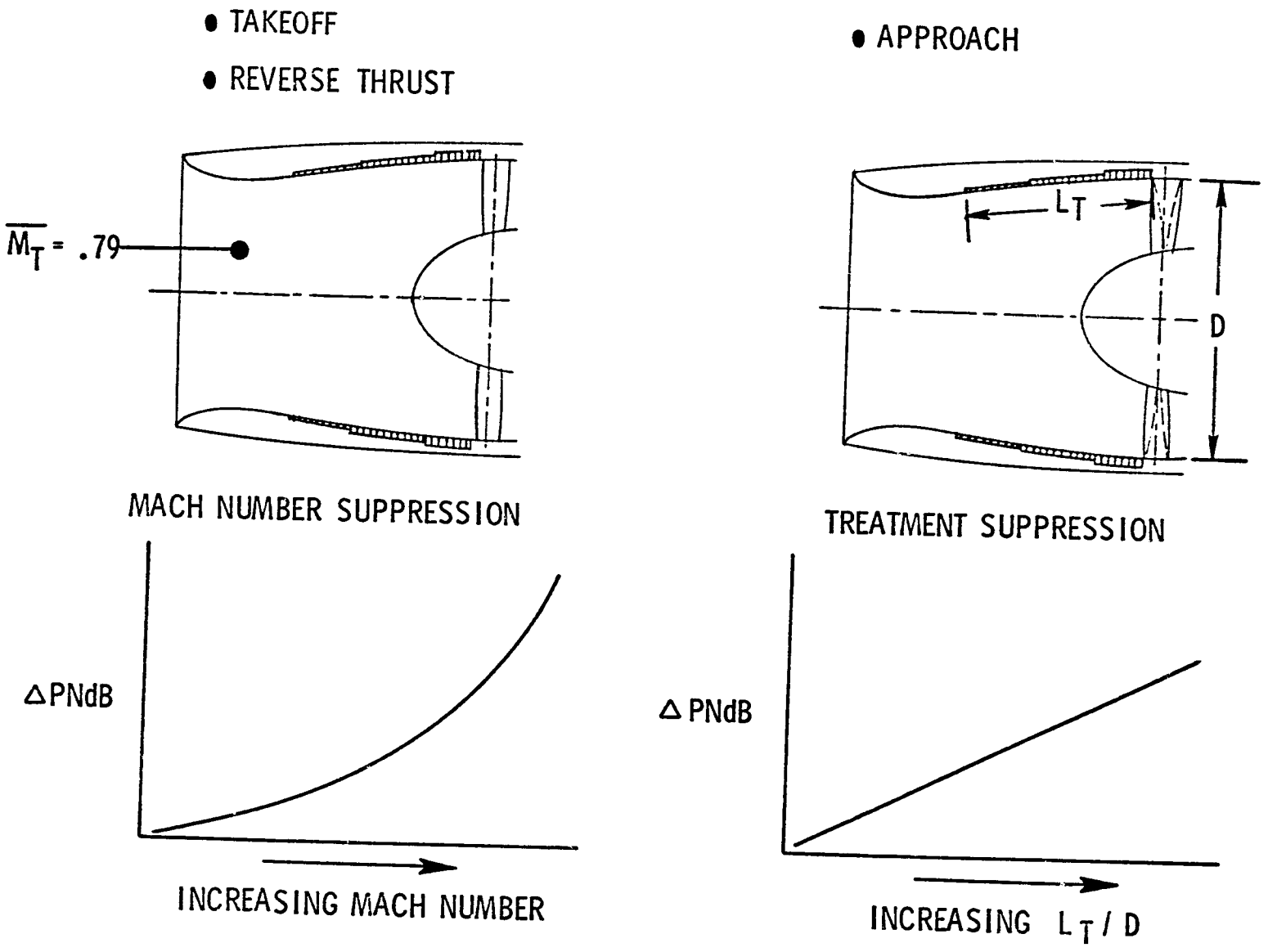

Figure 3.6. OTW Inlet Noise Reduction Concepts.

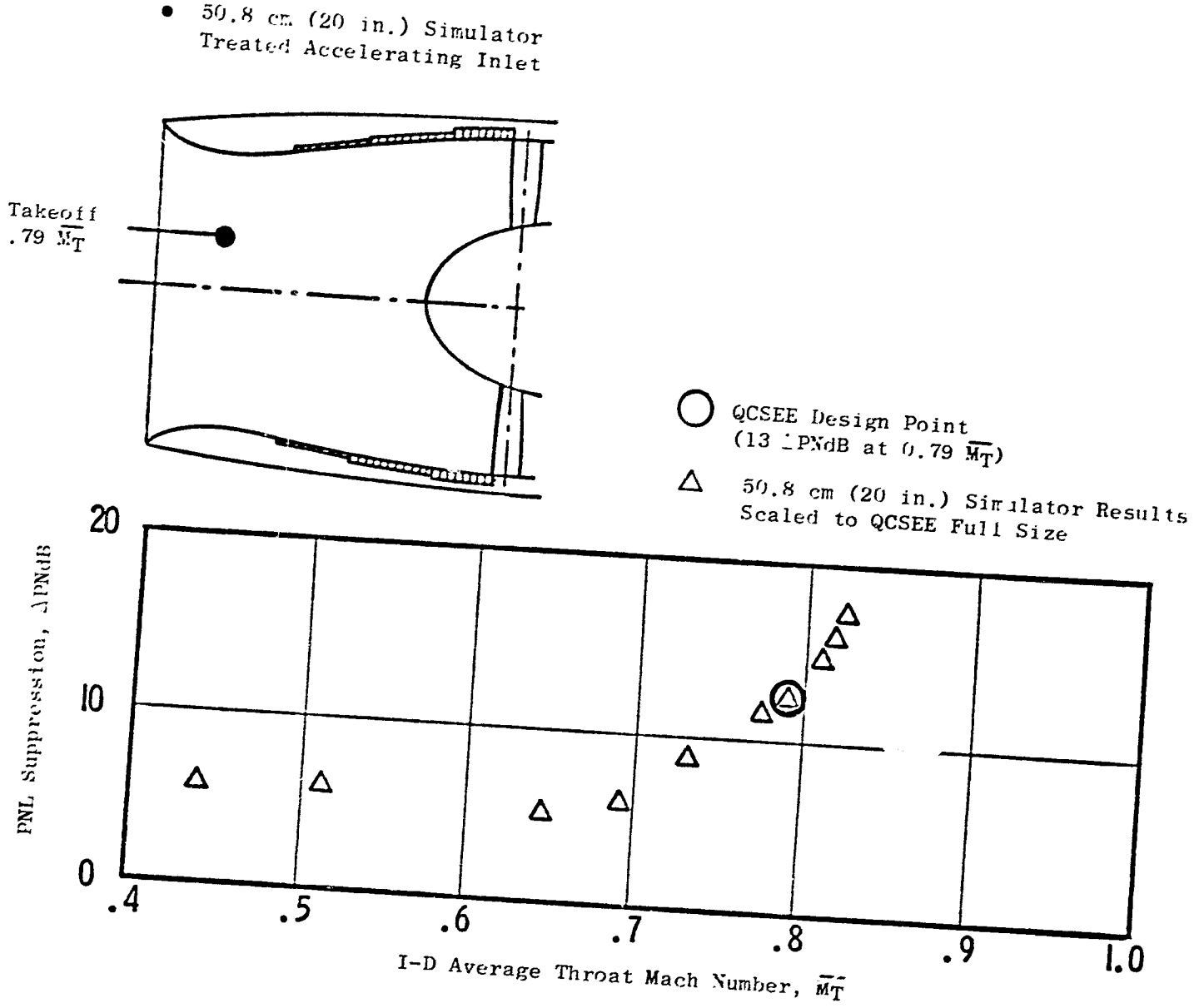

Figure 3.7. QCSEE Accelerating Inlet Suppression.

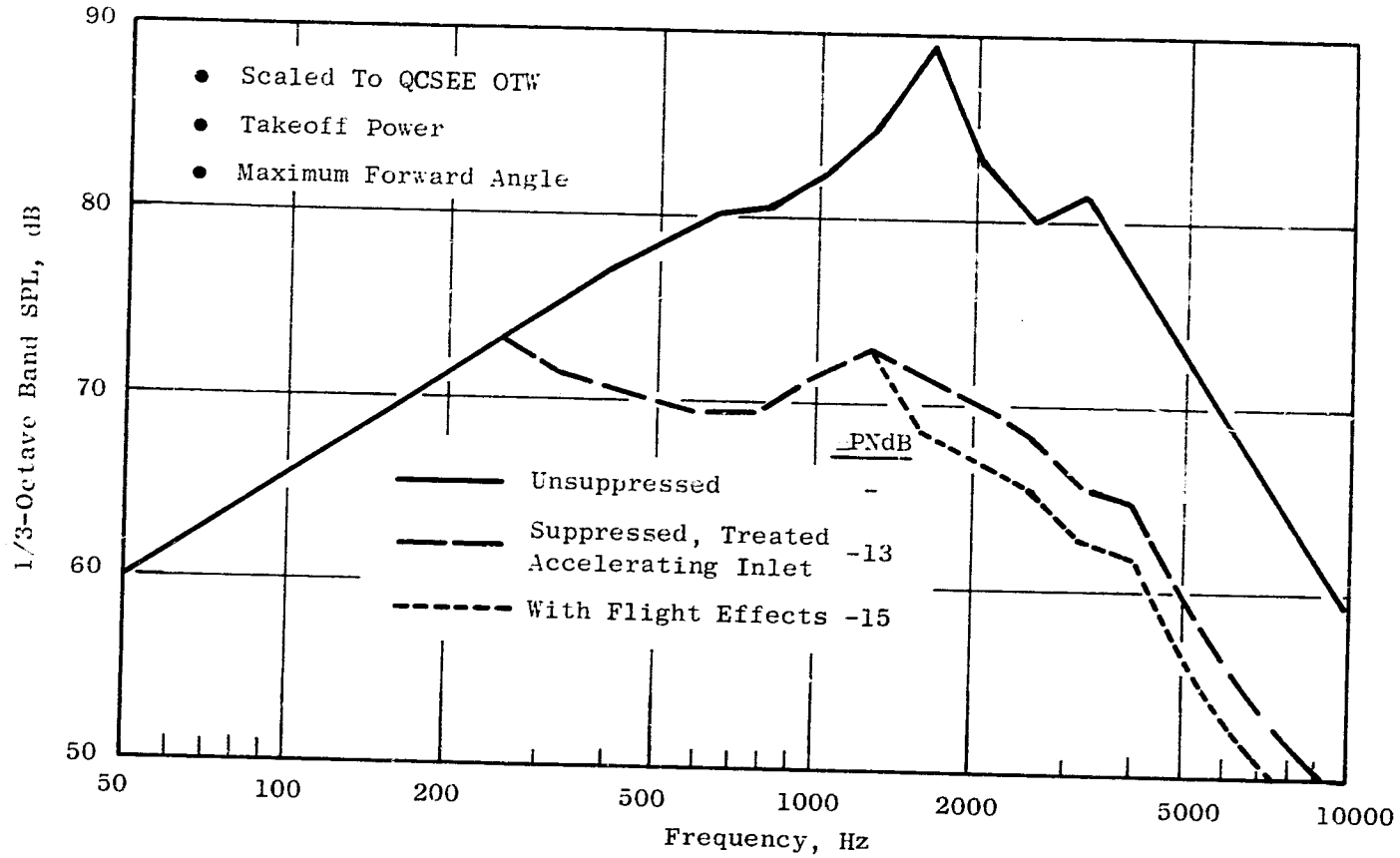

Figure 3.8. 50.8 cm (20 inch) Simulator Treated Accelerating Inlet Suppression.

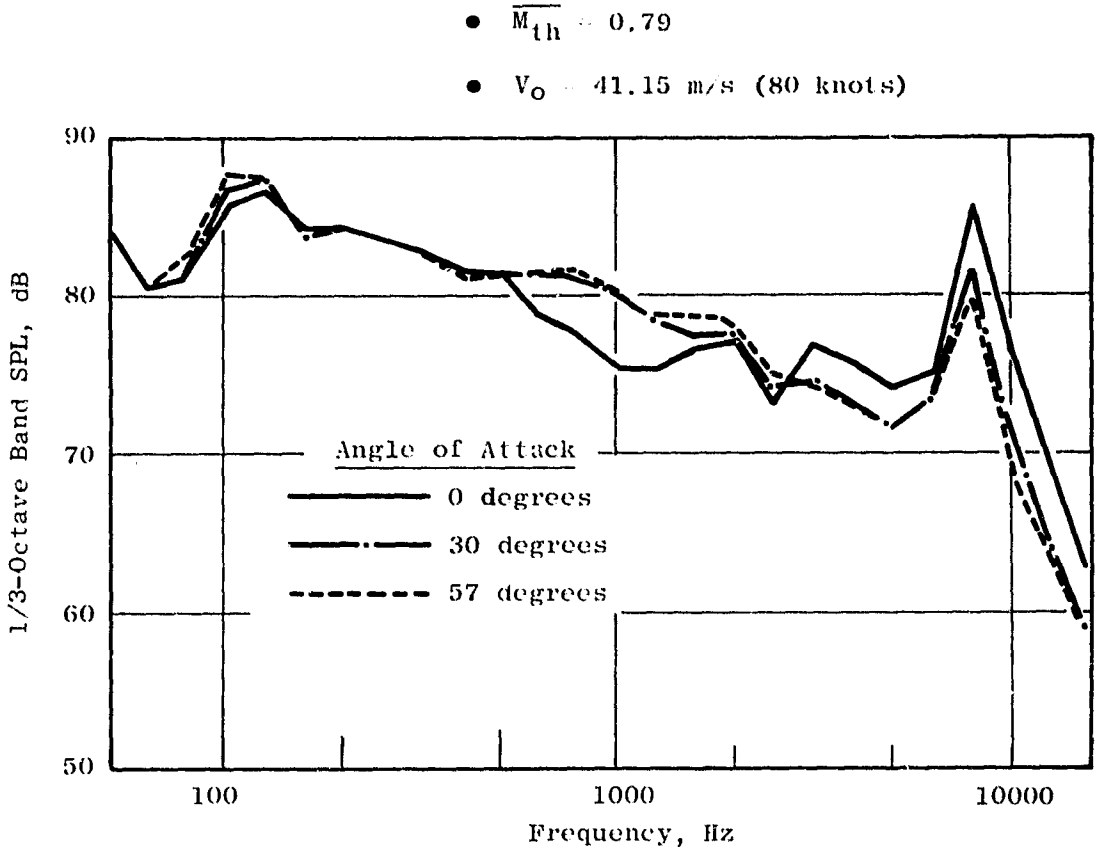

Figure 3.9. Effect of Angle of Attack on Acceleration Suppression.

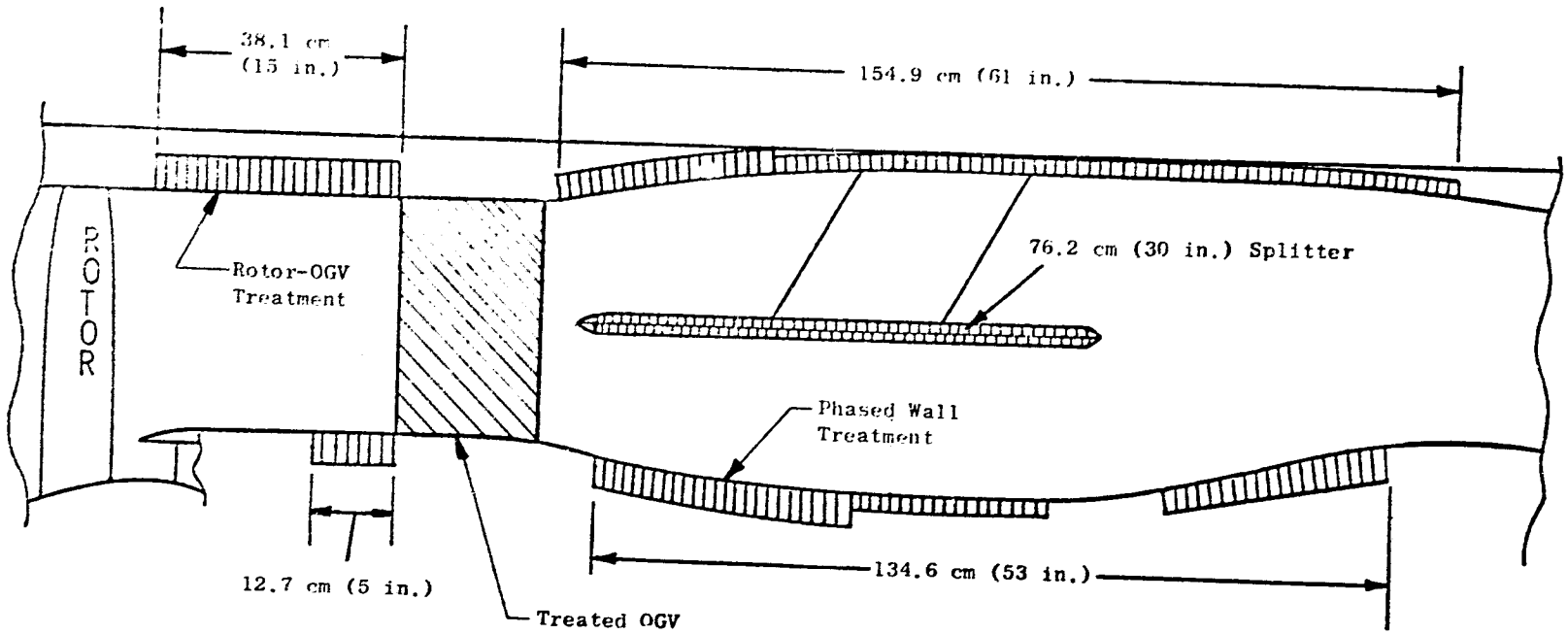

Figure 3.10. OTW Fan Exhaust Duct.

Figure 3.11 shows the unsuppressed and suppressed aft fan noise spectrum. As seen by the spectra, the suppression occurs over a very wide frequency range and results in a noy-weighted spectra (also shown) which is very flat from 500 to 6300 Hz. This is the basic problem in designing for large suppression levels and the reason for varying treatment depths to obtain increased suppression bandwidth.

Cold flow duct test results had shown an interaction or phasing effect which increased suppression bandwidth when treatment panels were arranged with varying thickness. The suppression obtained was greater than that expected from the summation of the individual panel suppressions. The concept was investigated using a 50.8 cm (20 in.) diameter low-tip-speed fan (NASA Rotor 55) in the General Electric Anechoic Chamber beginning October 1974. These data (Figure 3.12 show a slightly increased high frequency suppression relative to normal prediction values. These results are being incorporated into the OTW design.

Rotor OGV treatment was applied to the OTW engine to reduce the BPF tone since the aft duct treatment was designed to reduce the higher frequencies. This type of treatment also was tested on the 50.8 cm (20 in.) diameter fan and showed broadband suppression as well as tone reduction (Figure 3.13).

Flow noise generated by air passing over the treated surfaces (the splitter and the support struts) represents a floor which limits the amount of suppression attainable in the aft duct. The 50.8 cm (20 in.) Rotor 55 was tested with nominal and open nozzles to vary duct Mach number for a configuration having an acoustic splitter. These results are shown on Figure 3.14. For a change in Mach number from 0.465 to 0.515, the aft suppression did not vary, indicating that a noise floor had not been reached at 0.515 Mach number. The engine aft duct flow lines have been selected to provide an average Mach number of only 0.45, thus no flow noise limitation is expected on the engine.

A treated OGV is shown on Figure 3.10, however, no credit has been taken for suppression due to this treatment. During the engine testing the suppression benefit of the treated OGV will be evaluated.

3.5.3 Core Exhaust Design

Prediction of low frequency combustor noise had been based on data correlations from various engine tests. In order to check these predictions, core noise measurements were obtained on an F101 engine which uses the QCSEE core. Figure 3.15 shows the test configuration and the location of the acoustic probe in the core nozzle. Far-field measurements also were obtained during the test. Figure 3.16 is a comparison of far-field levels as a function of jet velocity or engine power setting. At higher power settings, jet noise is the dominant source at 400 Hz; but, as power is reduced, the jet noise decays at a V^9 rate and the combustor noise becomes dominant. This is indicated by the break or flattening of the predicted total noise. Other sources may be influencing the 400 Hz level in the far field; thus, the

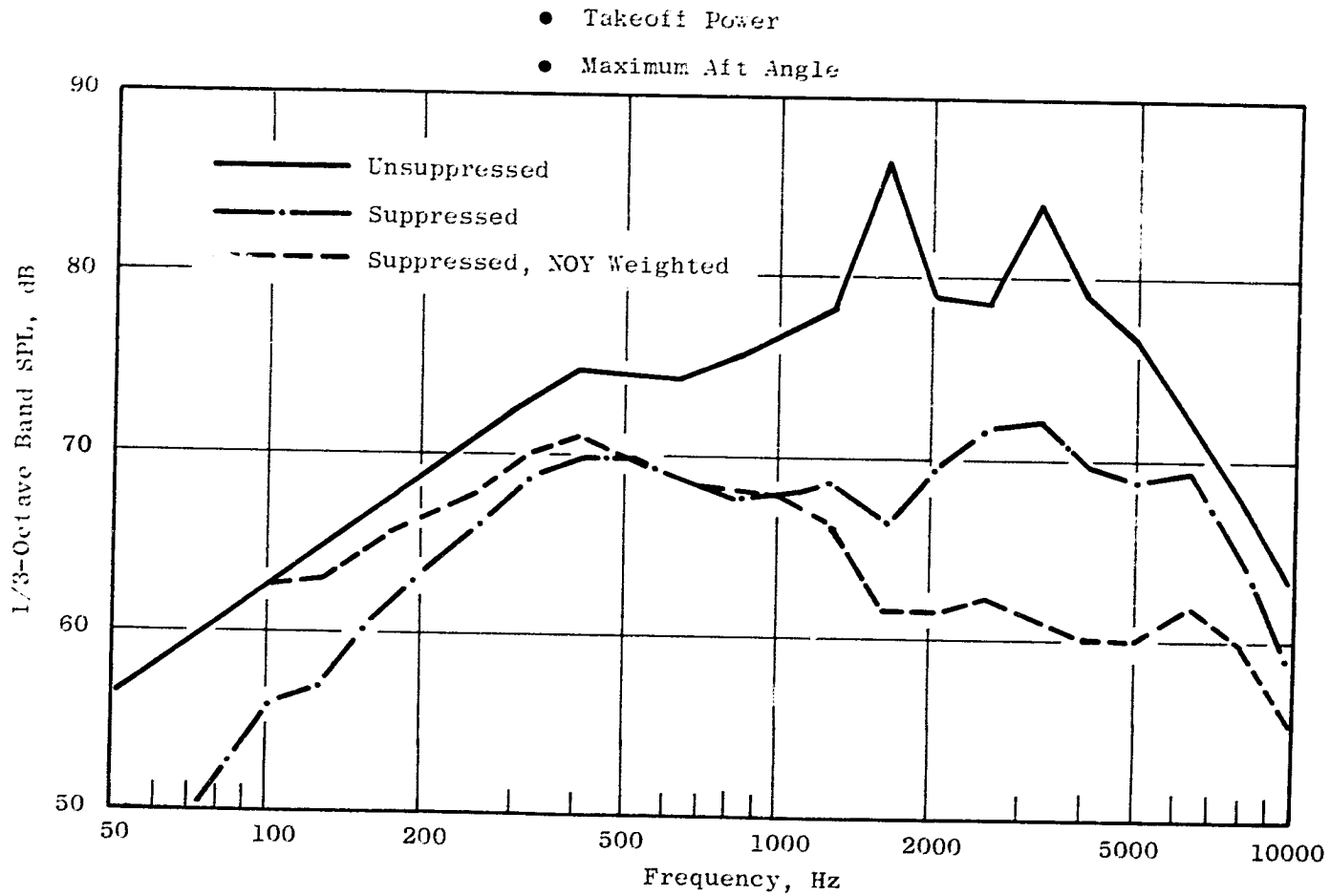

Figure 3.11. OTW Unsuppressed and Suppressed Fan Spectra.

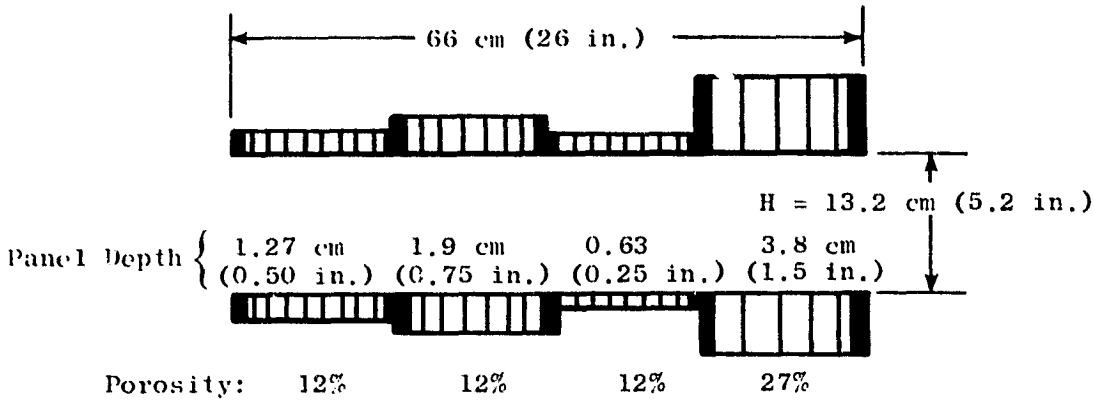

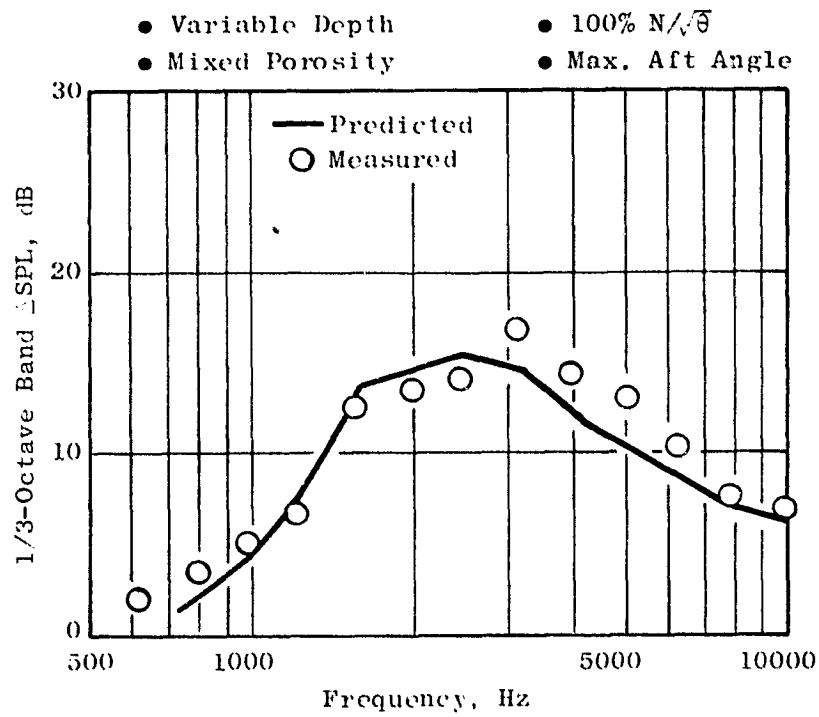

Figure 3.12. Predicted Vs. Measured Suppression Spectra - Variable Depth, Mixed Porosity Panels.

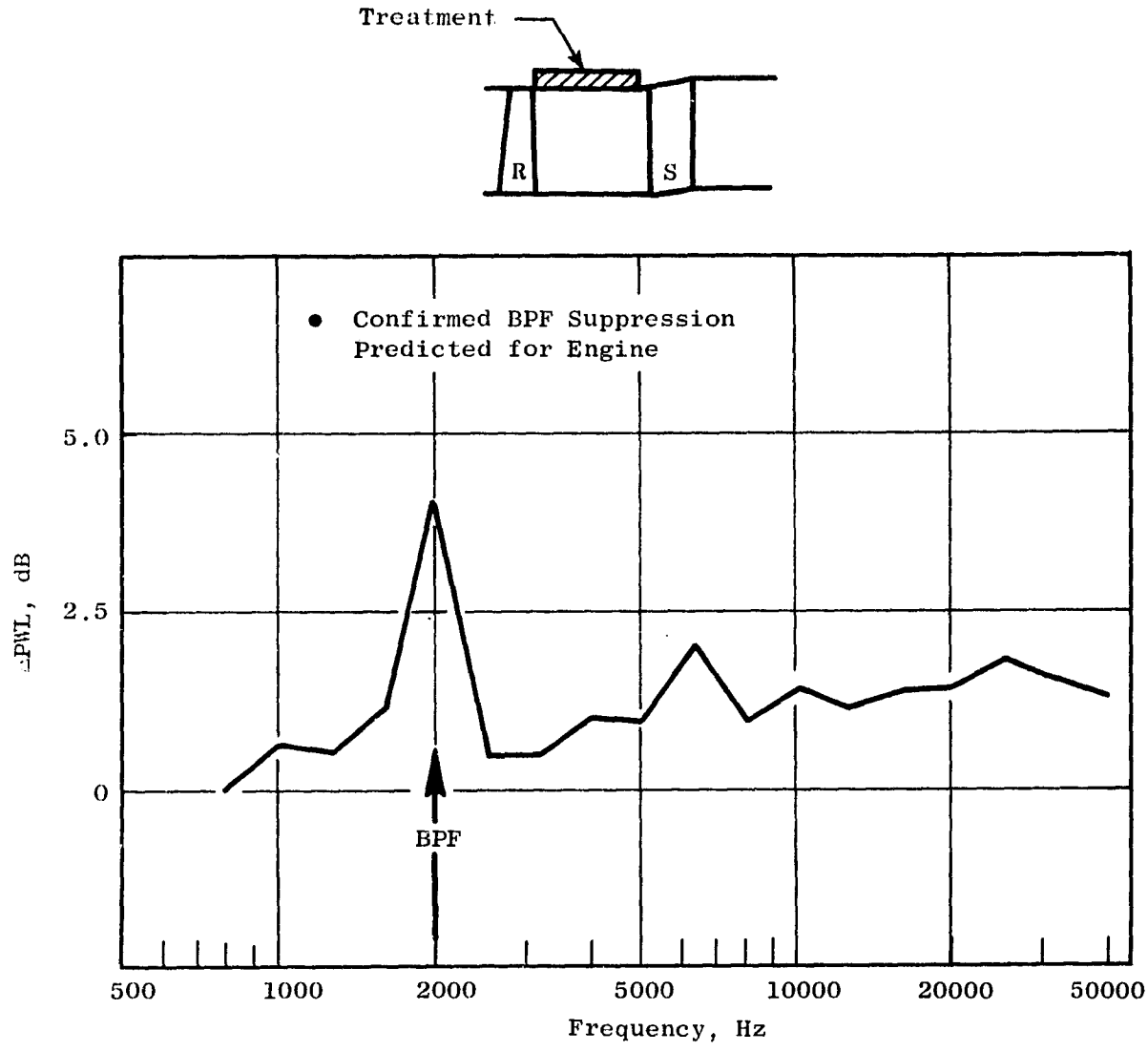

Figure 3.13. Rotor, OGV Treatment Suppression.

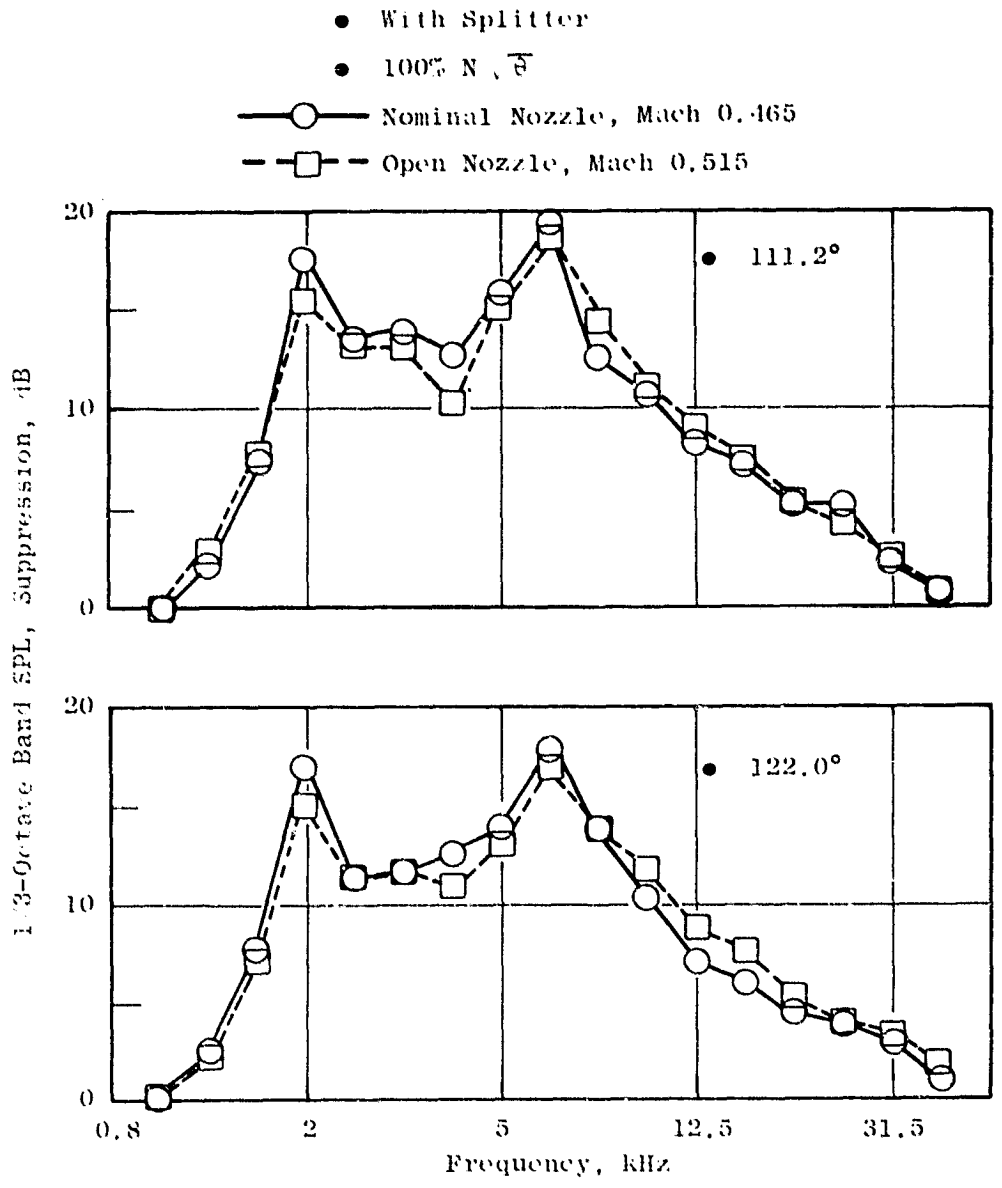

Figure 3.14. Flow Noise Effects.

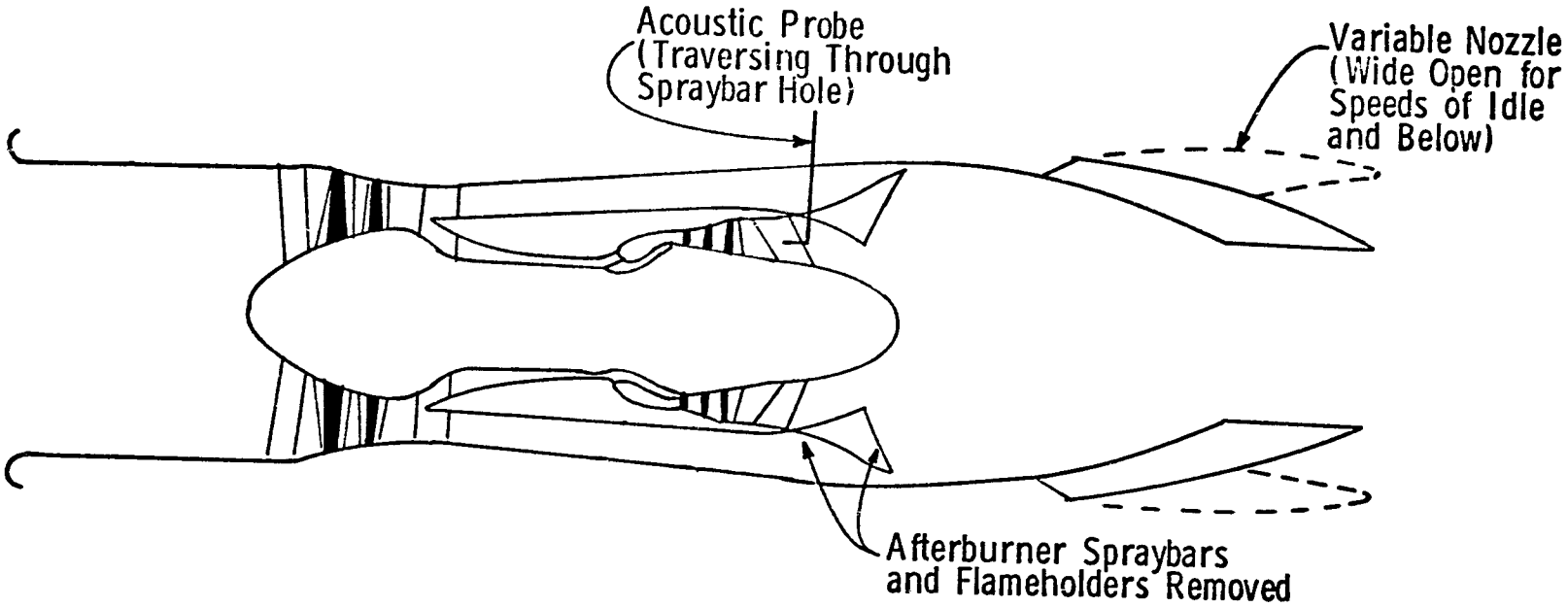

Figure 3.15. F101 Core Noise Measurement.

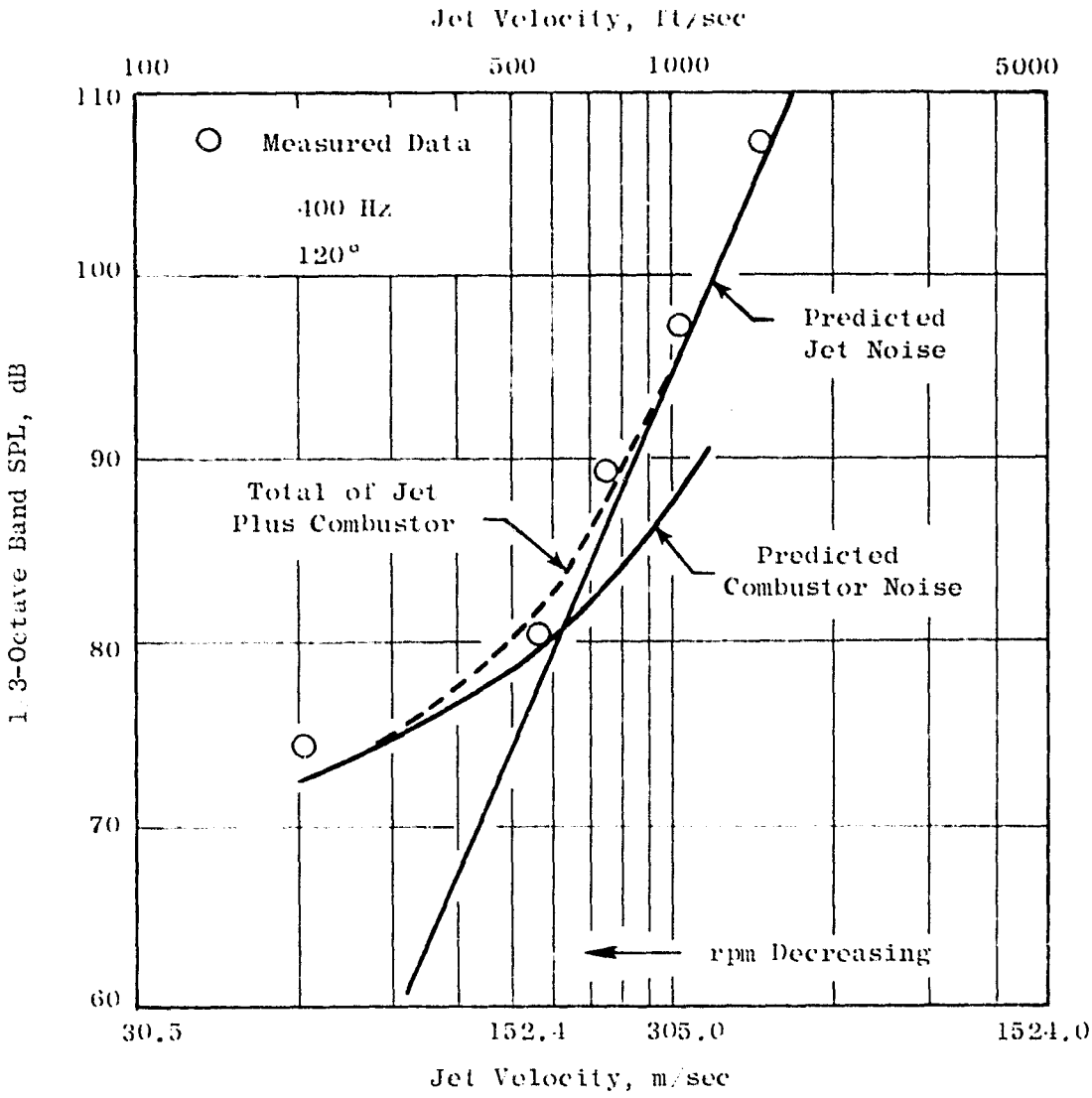

Figure 3.16. Farfield Core Noise Measurements Vs. Predictions

absolute level is not significant; it is significant, however, that the prediction procedure is not underpredicting the absolute level.

Probe data, which are not influenced by other sources, also agreed well with the predicted levels (Figure 3.17) on an absolute level basis.

Figure 3.18 shows the core suppressor design selected for the OTW engine. This design incorporates stacked treatment which has high frequency turbine suppression panels placed over deeper, low frequency combustor noise suppression panels. Hot duct tests were conducted to evaluate the design, and the results are shown on Figure 3.18 relative to predicted levels. Table 3-IV compares the resulting PNdB reductions. Both the turbine and combustor suppression objectives are exceeded by the design.

Table 3-IV. QCSEE OTW Core Suppression ΔPNdB.

	Design Requirement	Component Test Data
Combustor	4.6	5.1
Turbine	5.0	9.8

Based on these data, it was concluded that the predicted levels were attainable and, with development of the suppressor concept, the core noise level would be accounted for.

3.6 SYSTEM NOISE LEVELS

The primary constituents in the acoustic design are:

- Fan inlet noise
- Fan exhaust noise
- Core noise

Each has a significant development program defined to arrive at the design objectives. The levels for these three noise sources involve both unsuppressed noise estimates and suppression estimates. If either or both are different than the current evaluation, there will be an impact on the system EPNdB.

Figure 3.19 is a carpet plot showing variations in the suppression level for fan inlet and fan exhaust noise. The variation in suppression shown on the figures also can be interpreted as a variation in the unsuppressed levels with constant suppression. The OTW design is more sensitive to inlet noise variation than aft noise. A change of 3 PNdB in inlet noise would increase the system levels from 95 to 96.3 EPNdB, while a 3 PNdB change in aft noise would result in only 95.2 EPNdB.

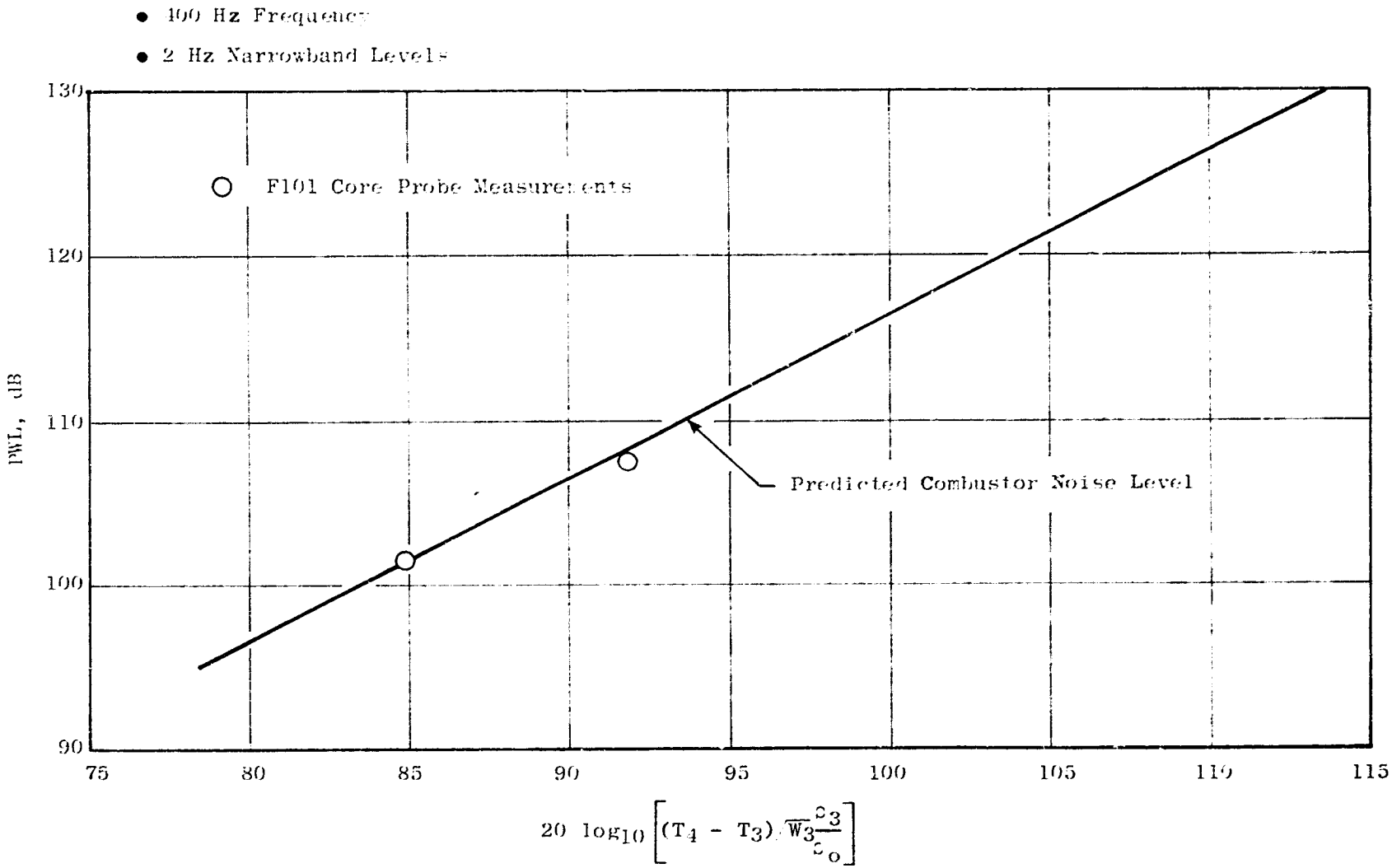

Figure 3.17. Probe Measured Vs. Predicted Combustor Noise.

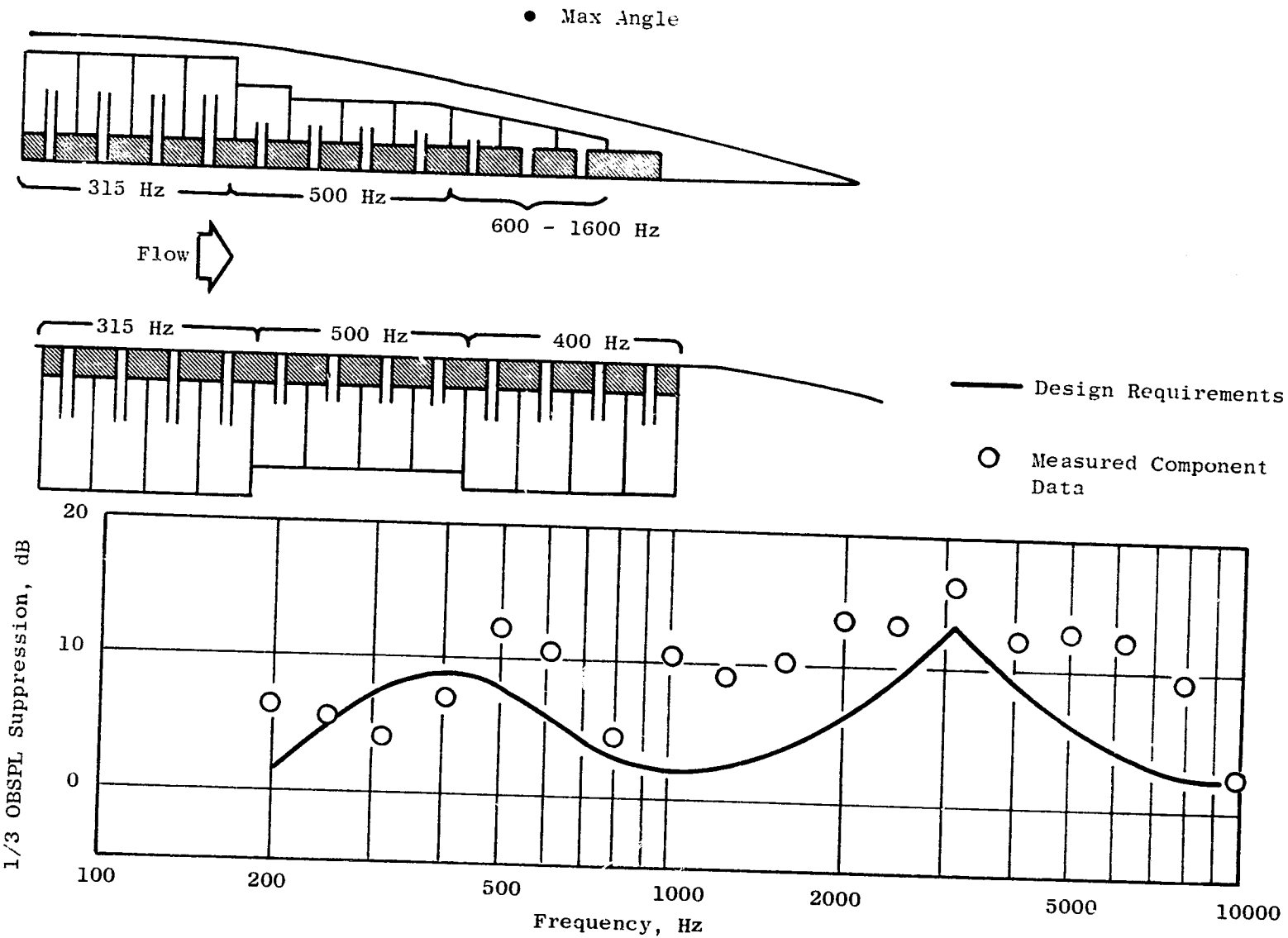

Figure 3.18. OTW Stacked Treatment Configuration.

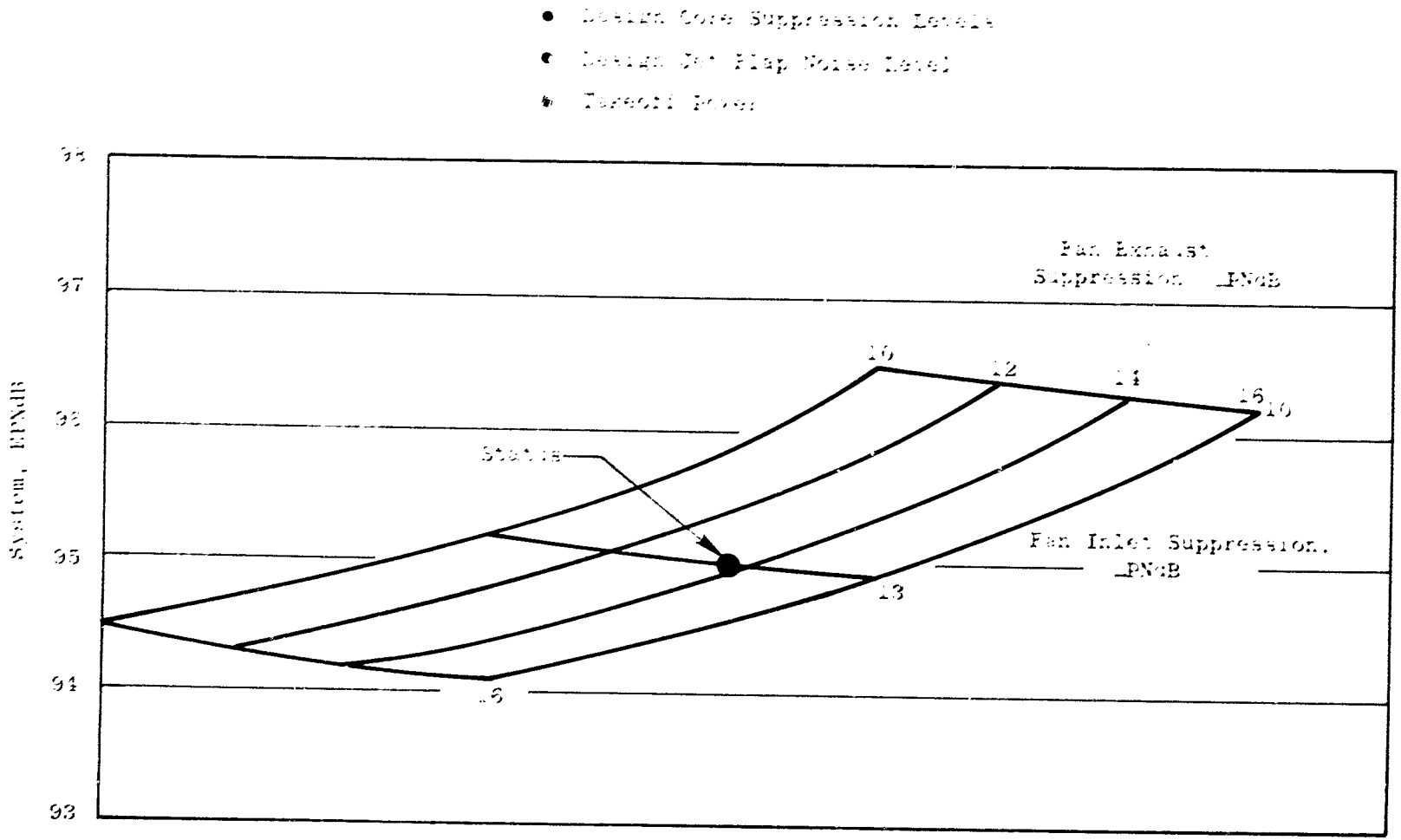

Figure 3.19. Effect of Constituent Noise Suppression on OTW System Noise.

Figure 3.20 gives the footprint or contour plot for the OTW system. The takeoff footprint is slightly larger than at approach, due to the increased jet/flap noise. The total 90 EPNdB footprint area is only 17.9 km^2 (444 acres).

References

1. Quiet Clean Short-Haul Experimental Engine (QCSEE) - Preliminary Analyses and Design Report Volume I, NASA CR-134838, 1974.

2. Quiet Clean Short-Haul Experimental Engine (QCSEE) - Preliminary Analyses and Design Report Volume II, NASA CR-134839, 1974.

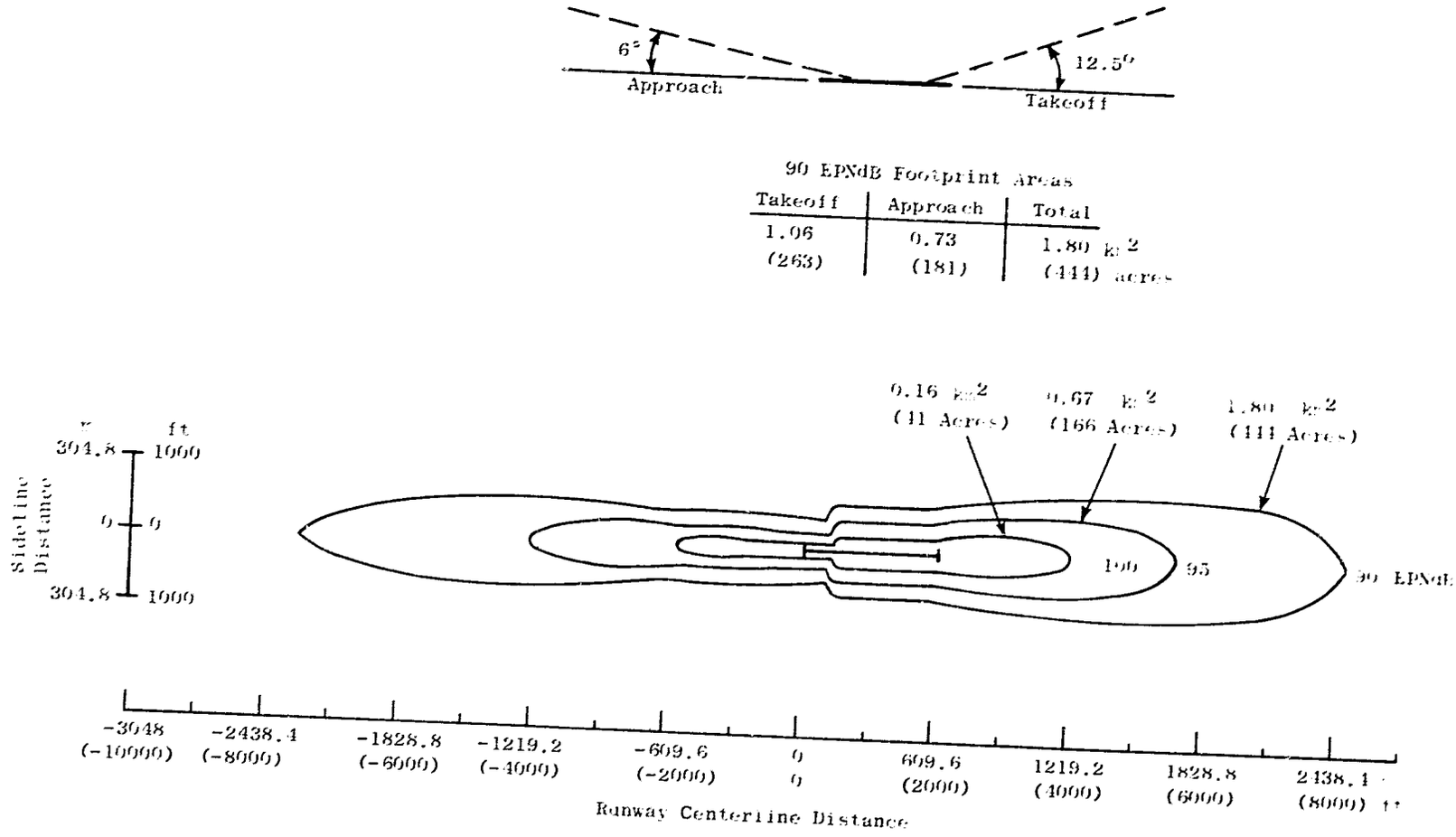

Figure 3.20. OTW Approach and Takeoff Contours.

SECTION 4.0

OTW EMISSIONS CONTROL

4.1 SUMMARY

The objective of the OTW combustor design program was to select a clean combustion system for the OTW engine based on available components and combustion technology being developed under other concurrent component development and technology programs.

The F101 PFRT combustor, selected for the OTW engine, is an advanced combustor design that has demonstrated excellent performance characteristics and favorable pollutant emissions characteristics in development tests of the F101 and CFM56 engines. A consideration in the selection of the PFRT configuration was the readily available hardware and vast amount of development experience associated with this design.

C_xH_y, CO, and NO_x, and smoke emission level predictions have been prepared for the OTW engine based on recent data from a QCSEE OTW component test with a F101 PFRT combustor. These estimates indicate that the OTW engine will meet the contract goals for smoke and NO_x emissions with the use of an unmodified F101 PFRT combustor. However, because of the relatively low cycle pressure ratio of the OTW engine, its predicted C_xH_y and CO emissions levels will exceed the goals. Methods of reducing the levels of these two emissions categories are being investigated. Several approaches for obtaining these reductions in the OTW engine have been identified based on the results of emissions control technology development programs currently underway at General Electric, including the NASA Experimental Clean Combustor Program. These approaches involve modifications of the operating conditions within the combustor at engine idle power, since virtually all of the C_xH_y and CO emissions are produced in this engine operating mode. These approaches are:

- Increased compressor discharge pressure (CDP) bleed air extraction at idle
- Circumferential sector fuel staging at idle

Both of these operational approaches were simulated in development tests of the QCSEE OTW combustor to evaluate their application to the QCSEE OTW engine program. The results of these tests indicated that sector fuel staging and compressor discharge bleed both provide significant reductions in CO and C_xH_y emissions levels. Since the QCSEE OTW engine is not currently configured for compressor discharge bleed, it is planned to utilize only sector fuel staging at idle.

Based on these development test data, which are in fair agreement with previously obtained engine data, either of these operational approaches

appears to be suitable for use in an OTW flight engine without compromising any other combustor performance requirements. Application of sector fuel staging in the OTW experimental engine is expected to provide reductions in CO and C_xH_y emission levels. However, the resulting CO and C_xH_y emission levels will exceed the program goal for these emission categories.

Although the PFRT combustor will be used in the OTW engine tests, additional work is under consideration which would involve applying advanced emission reduction technology from the NASA-GE Clean Combustor program to develop a new Double Annular Dome Combustor for QCSEE. This combustor development will be conducted in a sector test rig and will concentrate on reducing idle emissions to meet the program goals. This technology can then be applied to a new annular combustor design for the QCSEE OTW engine which would be expected to meet all the program goals.

4.2 EXHAUST EMISSIONS DESIGN GOALS

The goal maximum emissions levels to be demonstrated with the OTW engine are consistent with the Environmental-Protection-Agency-defined (EPA) emissions standards, which become effective January 1, 1979, for Class T2 aircraft turbine engines. Engines in this EPA-defined category are all engines with a rated thrust of 35,580 N (8,000 lb) or greater. These standards set maximum limits on the quantities of C_xH_y, CO, NO_x, and smoke emissions that can be discharged by engines.

The Class T2 engine standards in the three categories of gaseous emissions are shown in Table 4-I. The standards are defined in terms of pounds of emission per 1000-pound thrust-hours for a prescribed takeoff/landing mission cycle. This prescribed cycle is shown in Table 4-II. The intent of these standards is to limit the quantities of these exhaust constituents that can be discharged within and around airports.

The smoke standards are expressed in terms of the SAE ARP 1179 Smoke Number. The maximum allowable smoke number is dependent on rated engine thrust, as shown in Figure 4.1. For the OTW engine, the smoke number standard is 22. Also shown in Figure 4.1 are the standards for several other General Electric commercial engines.

4.3 SELECTED COMBUSTOR DESIGN

The F101 PFRT engine combustor will be used in the OTW engine. A cross section of this combustor design is presented in Figure 4.2.

The F101 PFRT combustor is an advanced, short-length configuration which features the use of a unique airblast-type fuel introduction and atomization design approach. In this combustor design, the dome comprises 20 carbureting swirl cups. Fuel is supplied to each of these swirl cups at low pressure by means of a simple, open-end fuel delivery tube. The carbureting swirl cups have three stages through which air is introduced and mixed with the fuel, as

Table 4-I. EPA Gaseous Emissions Standards for Class T2 Engines.

GASEOUS EMISSIONS (C_xH_y, CO, and NO_x)

- Earliest effective date - January 1, 1979
- Firm standards for engines newly manufactured on or after 1/1/79:
- Emissions index expressed as: pounds emissions per 1000-pound thrust-hours for a prescribed cycle

C_xH_y	0.8
CO	4.3
NO_x	3.0

Table 4-II. EPA Gaseous Emissions Standards, Turbojets and Turbofans.

- EPA index expressed as: pounds emissions per 1000-pound thrust-hours for a prescribed cycle
- Prescribed cycle for Class T2 engines:

Mode	% Power	Time, Minutes
Taxi-idle	Ground idle	19.0
Takeoff	100	0.7
Climbout	85	2.2
Approach	30	4.0
Taxi-idle	Ground idle	7.0

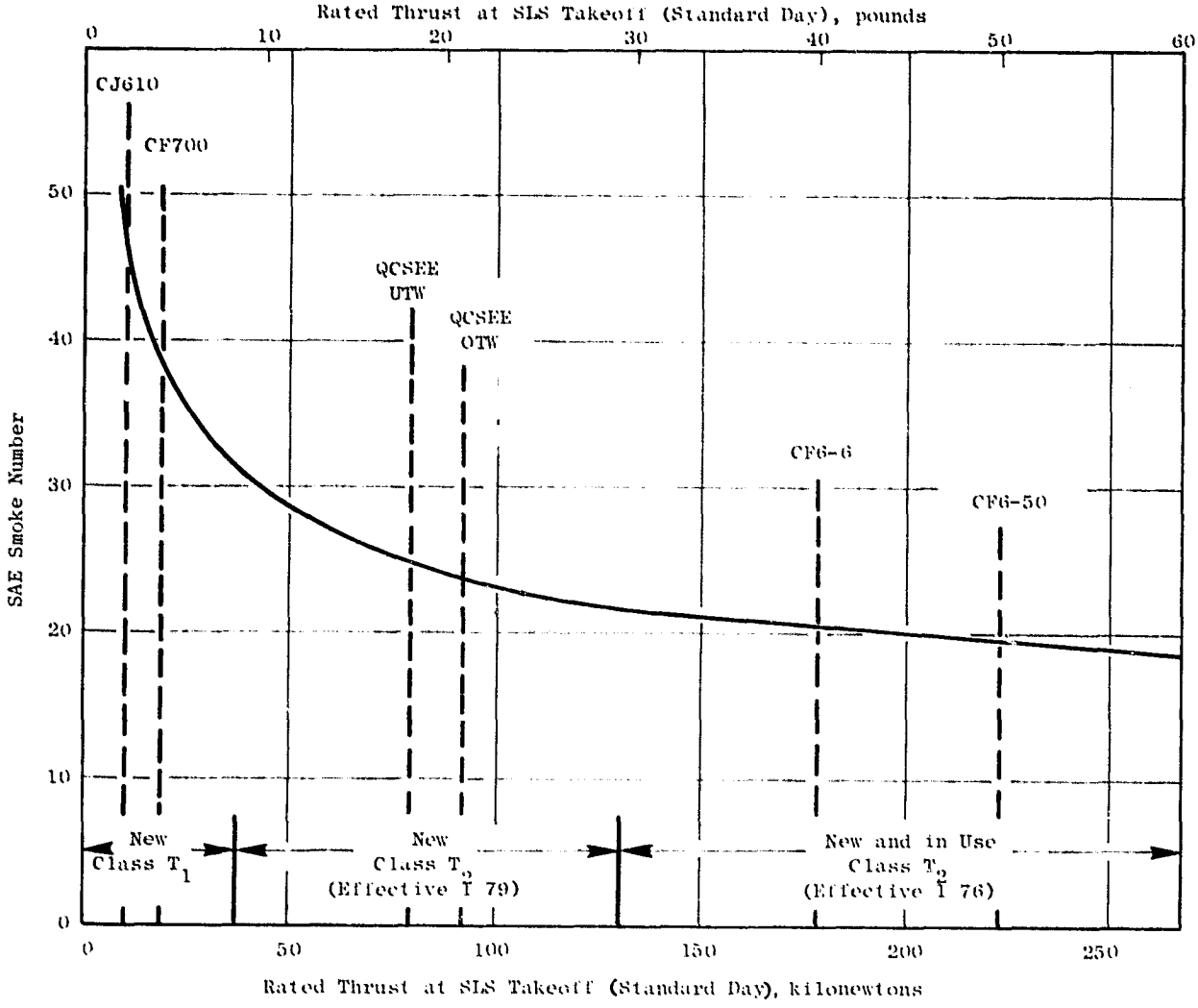

Figure 4.1. EPA Smoke Emission Standards.

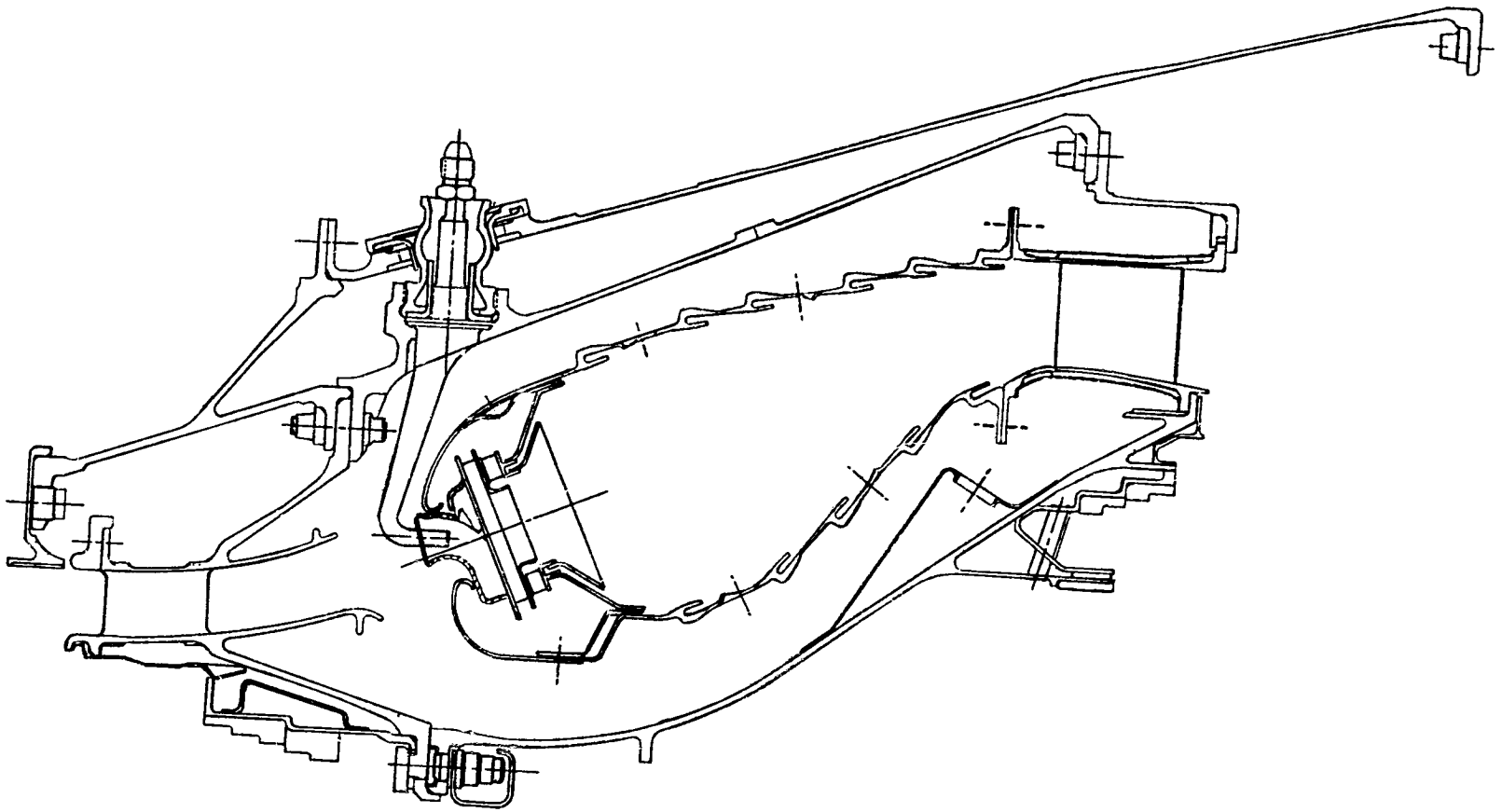

Figure 4.2. F101 PFRT Combustor Cross Section.

is shown in Figure 4.3. In the first stage, the fuel is premixed in a scroll device with a small amount of the combustor airflow, upstream of the flow areas that meter the airflow into the primary combustion zone (dome) of the combustor. Additional airflow is introduced through the primary air swirler which further energizes the fuel-air mixture and carries it to the primary cup exit. At this point, the secondary air swirler introduces air which rotates in a direction opposite to that of air from the primary swirler. Fuel leaving the downstream edge of the primary cup venturi enters the shear region created by the mixing boundaries of the counterrotating flows, and the high aerodynamic shear stress imposed on the fuel produces very fine atomization and highly effective fuel-air mixing over wide ranges of combustor operating conditions.

With these excellent atomization and mixing capabilities, very-short-length combustor designs are possible. Accordingly, the F101 PFRT combustor is a compact design with very short length compared to other current technology turbofan engine combustors. Its very short overall axial length is illustrated in Figure 4.4.

Extensive development testing of the F101 PFRT combustor design has been conducted to perfect its operating characteristics. Excellent performance, including low exit temperature pattern and profile factors (Figure 4.5) and acceptable altitude relight capabilities have been demonstrated in these tests.

One of the key accomplishments of these development efforts was the attainment of the altitude relight performance shown in Figure 4.6. This flight map, of course, is representative of a military engine application. The OTW engine, on the other hand, will operate over a commercial engine flight map, similar to that of the CF6-50 engine. The windmilling of the CF6-50 engine is shown in Figure 4.7, where it is compared with the F101 engine flight map. A commonly employed parameter for evaluating ignition severity is PT/V_{ref}, where P and T represent the combustor inlet pressure and temperature and V_{ref} the combustor reference velocity. Regions of low PT/V_{ref} on the windmilling map represent the most difficult areas in which to achieve ignition. The F101 combustor has demonstrated relight capability with PT/V_{ref} values down to 7.4 atmospheres ° K seconds/meter (60 psi ° R/fps), which is also the minimum PT/V_{ref} encountered in the CF6-50 envelope, as is shown in Figure 4.7. Therefore, it is expected that the OTW engine combustor will meet the anticipated altitude relight requirements. Further assessments of the OTW engine combustor relight capabilities will be made as the windmilling characteristics of this engine are better defined.

To date, the PFRT combustor has been used in the F101 and other engines. The engine tests have included both ground and flight test evaluations. These engine tests along with extensive component development testing of this combustor design have been conducted to optimize its operating characteristics.

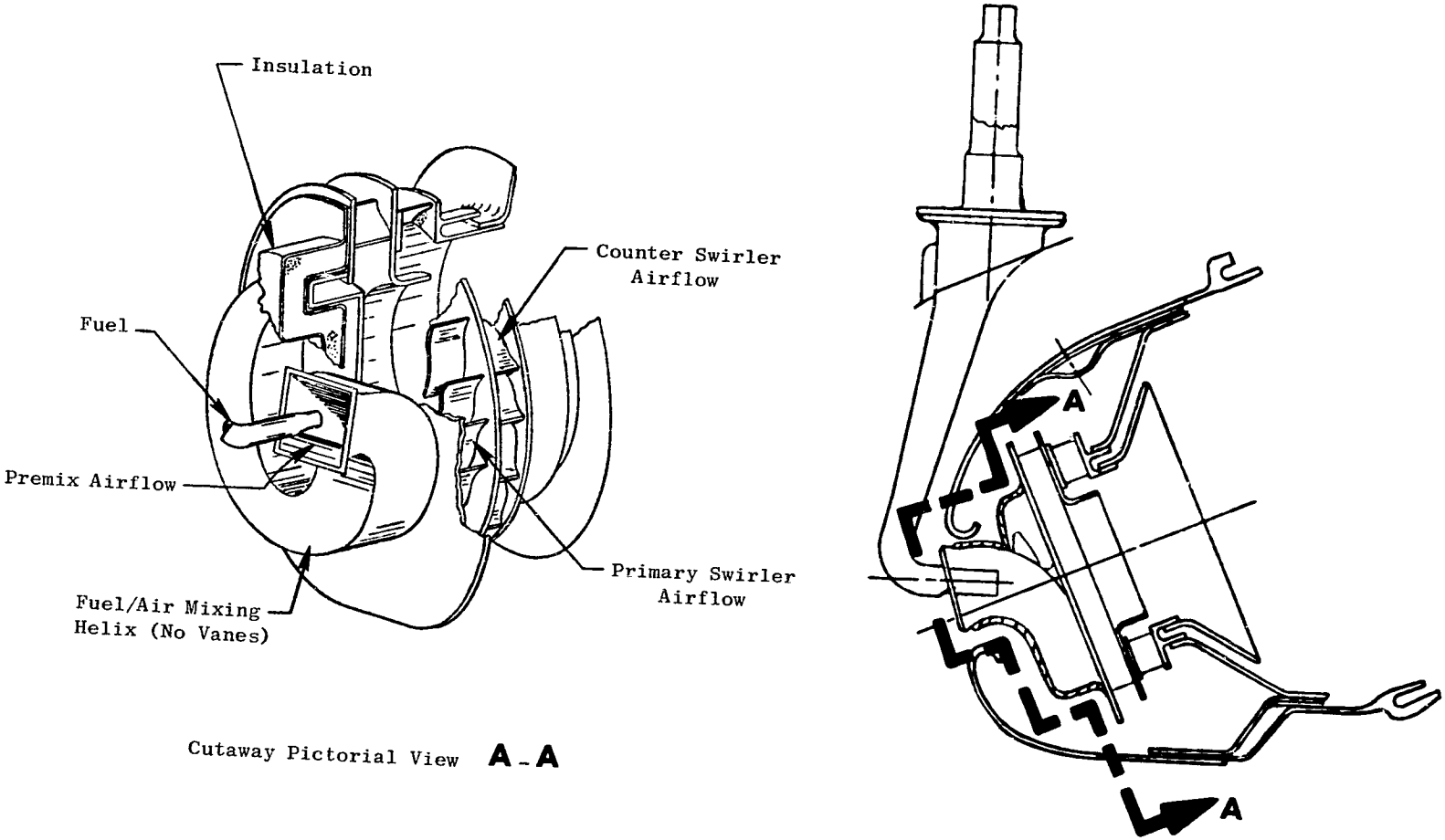

Cutaway Pictorial View **A-A**

Figure 4.3. F101 PFRT Three-Stage Carburetor.

Figure 4.4. F101 PFRT Engine Combustor.

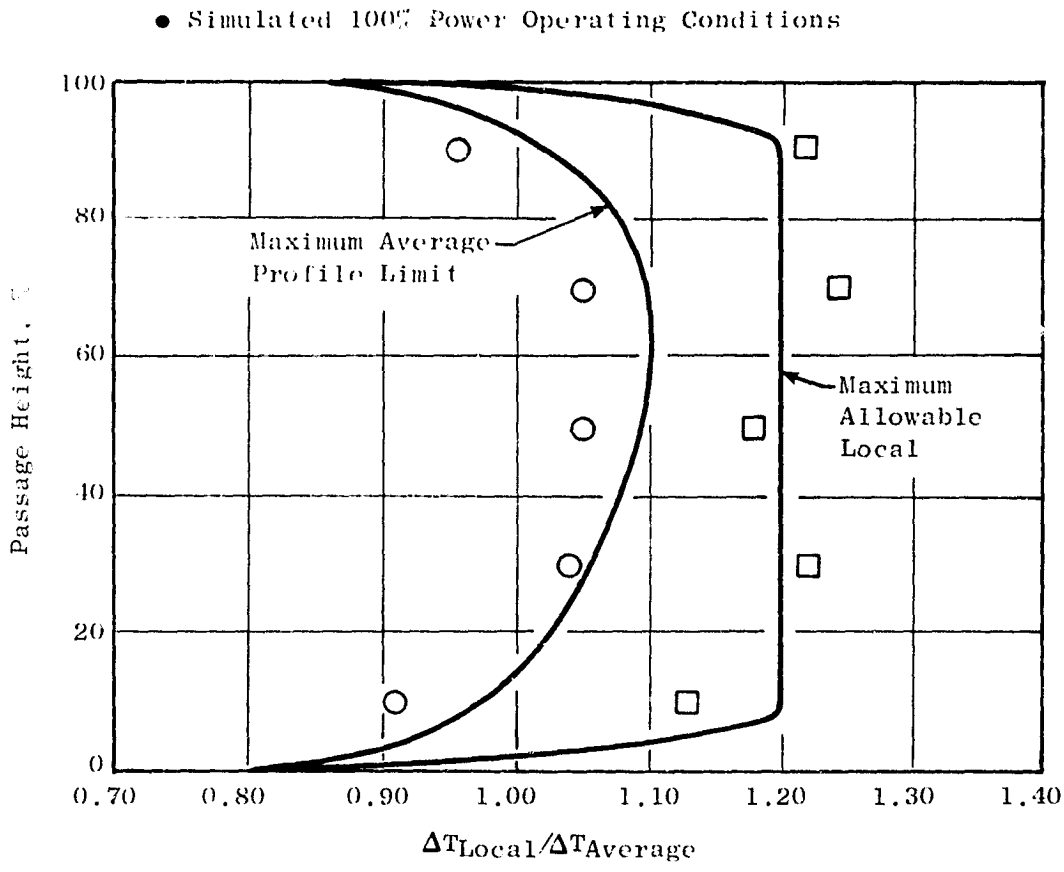

Figure 1.5. F101 PFRT Combustor Exit Temperature Characteristics.

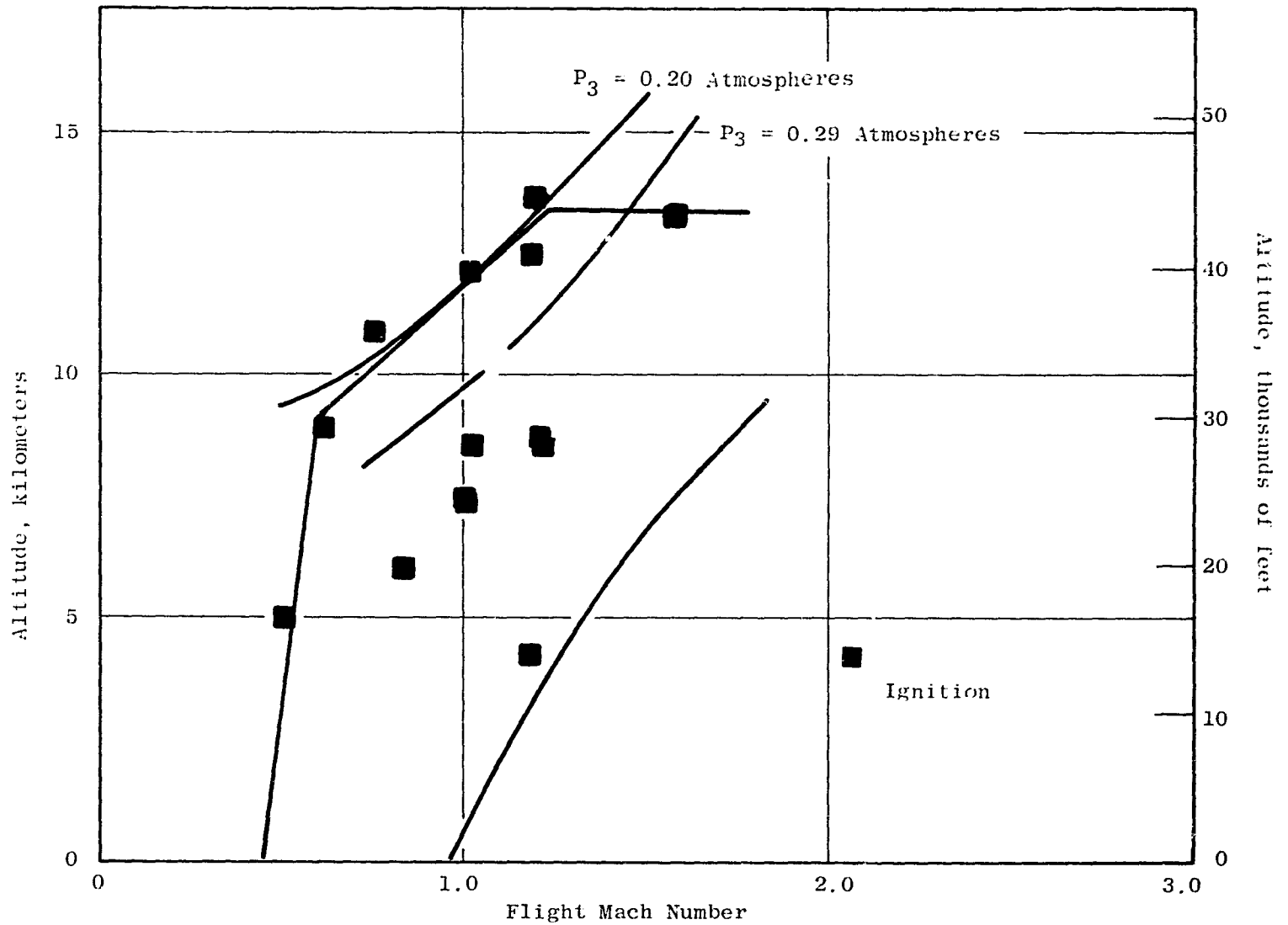

Figure 4.6. F101 PFRT Combustor Altitude Relight Performance.

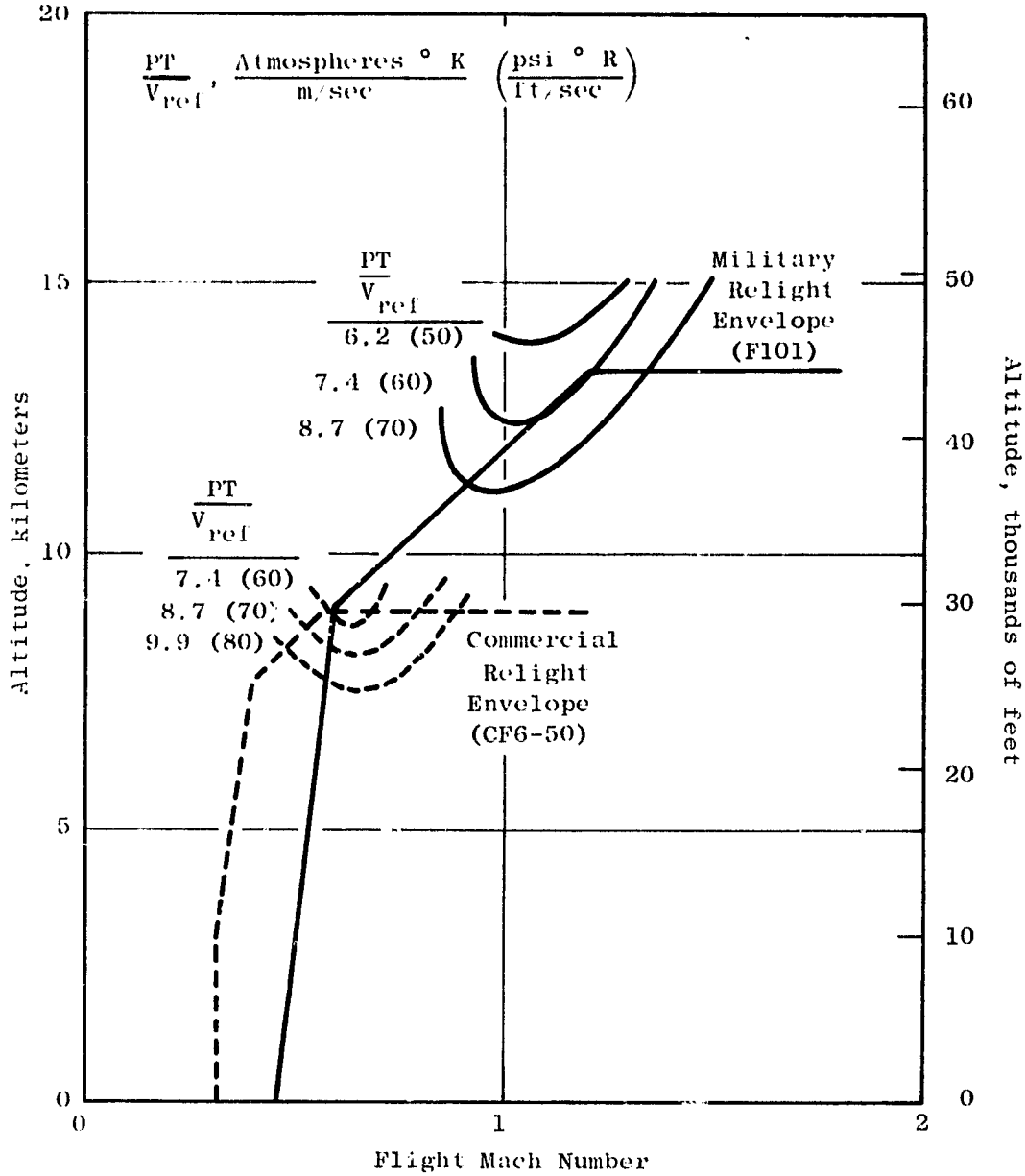

Figure 4.7. Comparison of Typical Commercial and Military Relight Envelopes.

4.4 PREDICTED ENGINE EMISSIONS CHARACTERISTICS

4.4.1 Smoke Emissions

The predicted peak smoke emission level of the OTW engine is shown in Figure 4.8. This peak level occurs at takeoff operating conditions. This predicted value is based on data obtained in the F101 PFRT combustor component tests conducted as a part of the QCSEE Program. In the component test, a smoke number of 42 was measured at the combustor exit. These component data are generally in good agreement with engine data obtained at combustor operating conditions close to those of the QCSEE OTW engine. Because it is a mixed-flow engine, it is predicted to have a peak smoke emission level of about 7 which satisfies the contract goals with significant margin as is shown in Figure 4.8. The smoke emission levels of other General Electric commercial aircraft engines are also presented in Figure 4.8 for comparison.

4.4.2 Gaseous Emissions

The predicted gaseous pollutant emissions characteristics of the OTW engine are shown in Figure 4.9. The predicted CO, C_xH_y, and NO_x levels are based on data obtained in the recently conducted OTW combustor component test. Although the component test data is in generally good agreement with data from other engine tests with this same combustor design, some adjustments to the CO and C_xH_y emissions levels could result due to the uncertainty of the true combustor fuel-air ratios in the engine at idle operating conditions. The NO_x data is in very good agreement with engine data obtained at the same combustor operating conditions.

Using these estimated emissions indices, the emissions levels in terms of the EPA-defined parameter can be calculated. A copy of the computer summary sheet showing these calculations for the OTW engine are presented as Figure 4.10. Comparisons of these calculated emissions levels with the EPA standards are presented in Table 4-III for C_xH_y, CO, and NO_x emissions, respectively. As shown the OTW engine is expected to meet the NO_x emission standard. However, significant reductions in the C_xH_y and CO emissions levels of the OTW engine will be required to meet the contract goals.

Relative to those of other turbofan engine combustors, the emissions characteristics of the F101 PFRT combustor generally are favorable because of its advanced design features including its short length as is indicated by the comparative emissions level data presented in Figures 4.11, 4.12, and 4.13. At the same combustor inlet air operating conditions, its C_xH_y and NO_x emissions levels are significantly lower than those of other modern combustors. However, in the OTW engine application, its CO and C_xH_y emissions levels in terms of the EPA takeoff-landing mission parameter cycle are well in excess of the prescribed standards because of the adverse combustor operating conditions

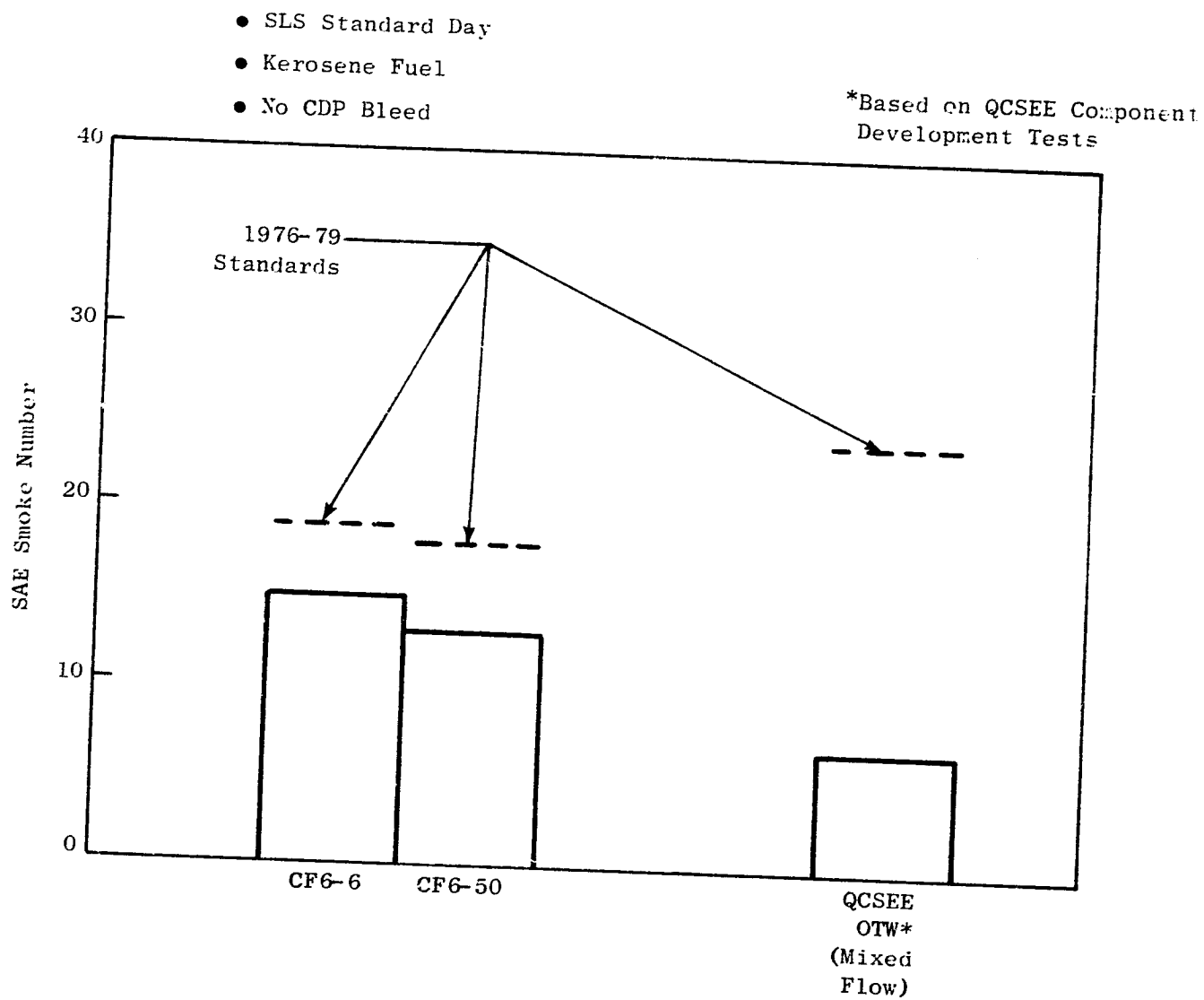

Figure 4.8. Peak Emission Characteristics of GE-AEG Class T2 Engines.

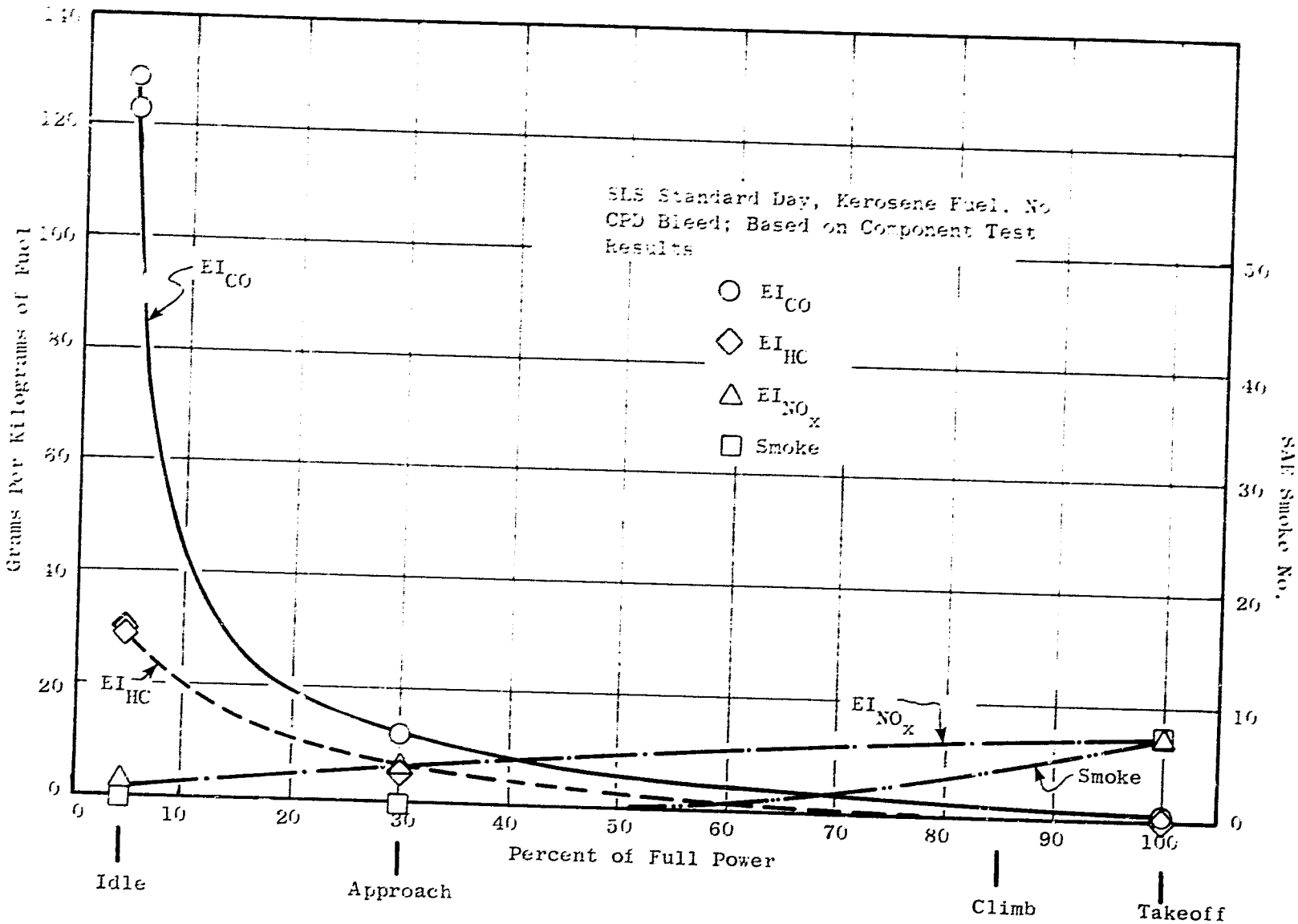

Figure 4.9. Estimated Gaseous Exhaust Emission Characteristics of OTW Engine.

Date: 6/75
Engine Performance Source: QCSEE OTW SLS/Std. Day Operation Line
Emissions Data Source: QCSEE OTW Combustor Component Test
Fuel Type: JP5
Engine Class: T2

Based on Component Test Emissions Data

	EPA Cycle Condition			
	Idle	Takeoff	Climb	Approach
Engine Parameters				
Time (minutes)	26.00	0.70	2.20	4.00
Percent Power	4.50	100.00	85.00	30.00
Thrust (pounds)	913.0	30300.0	17255.0	6090.0
Fuel Flow (pph)	665.0	6881.0	5501.0	1884.0
SFC (pph/lb Thrust)	0.7284	0.3390	0.3188	0.3094
Thrust-Hours	395.63	236.83	632.68	406.00
Emissions Parameters				
Carbon Monoxide				
lb/1000 lb Fuel	123.000	0.900	2.000	12.500
lb/Hour	81.795	6.193	11.002	22.550
pounds	35.444	0.072	0.403	1.570
% of Total lbs	94.543	0.193	1.076	4.188
Hydrocarbons				
lb/1000 lb Fuel	30.500	0.000	0.400	1.200
lb/Hour	20.282	0.000	2.200	2.261
pounds	8.789	0.000	0.081	0.151
% of Total lbs	97.435	0.000	0.894	1.671
Oxides of Nitrogen				
lb/1000 lb Fuel	1.600	13.900	11.800	6.200
lb/Hour	1.064	95.646	64.912	11.681
pounds	0.461	1.116	2.380	0.779
% of Total lbs	9.736	23.563	50.258	16.443

Summary

	EPA Parameter (lb Emission/1000 lb Thrust-Hr-Cycle)		
	Calculated Level	1979 Standard	Percent Red. Required
Carbon Monoxide	22.43	4.30	80.83
Hydrocarbons	5.40	0.80	85.18
Oxides of Nitrogen	2.83	3.00	0.00

Figure 4.10. Emissions Calculations Using Prescribed EPA Landing - Takeoff Cycle.

Table 4-III. Predicted QCSEE OTW Engine Emissions Characteristics.

- Based on QCSEE component test data
- 4.5% power at idle
- No CDP bleed

Emission	1979 Standard*	With F101 Combustor As Is
C_xH_y	0.8	5.3
CO	4.3	23.0
NO_x	3.0	2.8
Smoke, SAE SN	22	<10

*Pounds emissions per 1000-pound thrust-hours for a prescribed cycle as numerically and dimensionally expressed by the EPA.

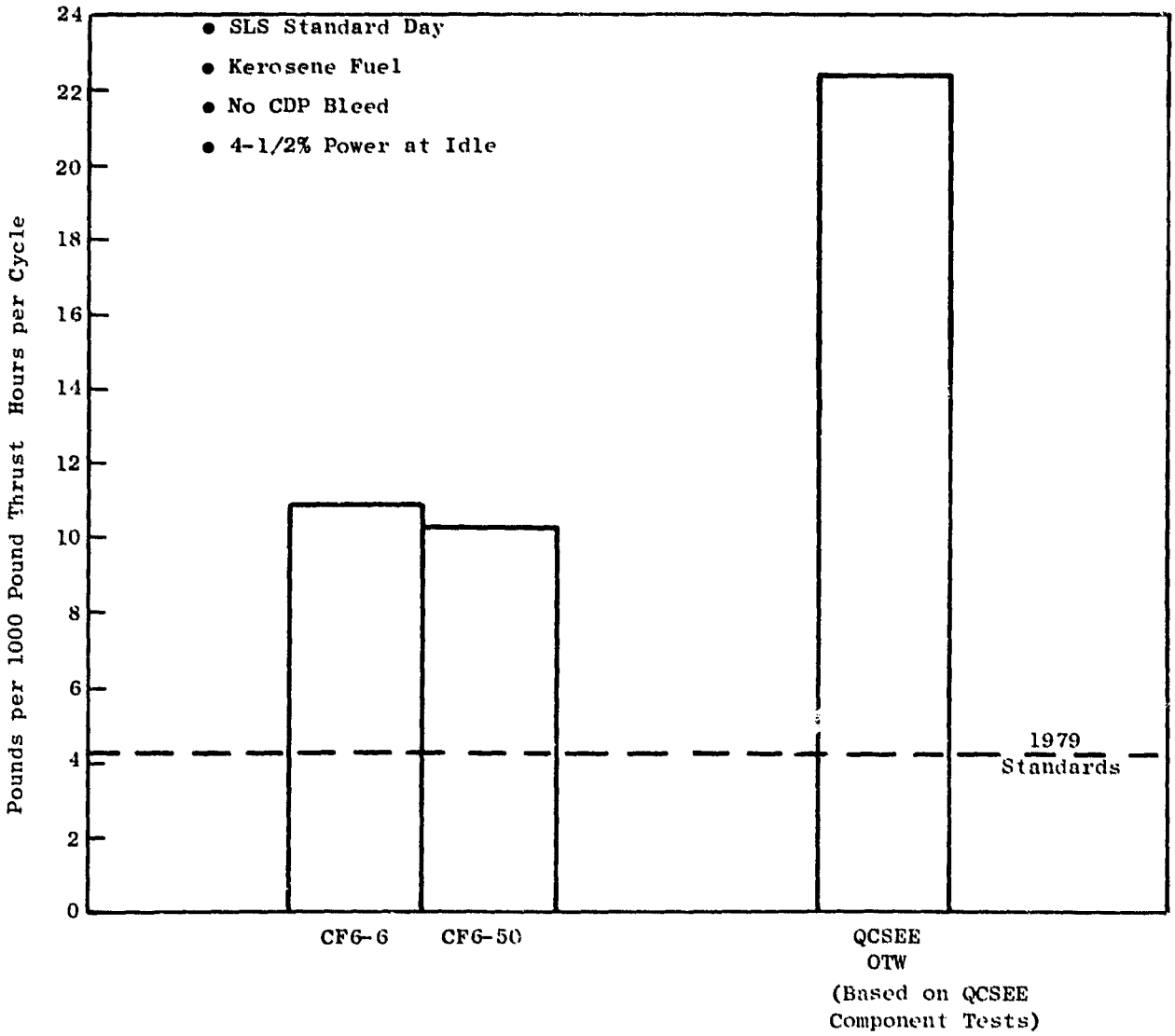

Figure 4.11. CO Emissions Characteristics of AEG Commercial Engines (Class T2).

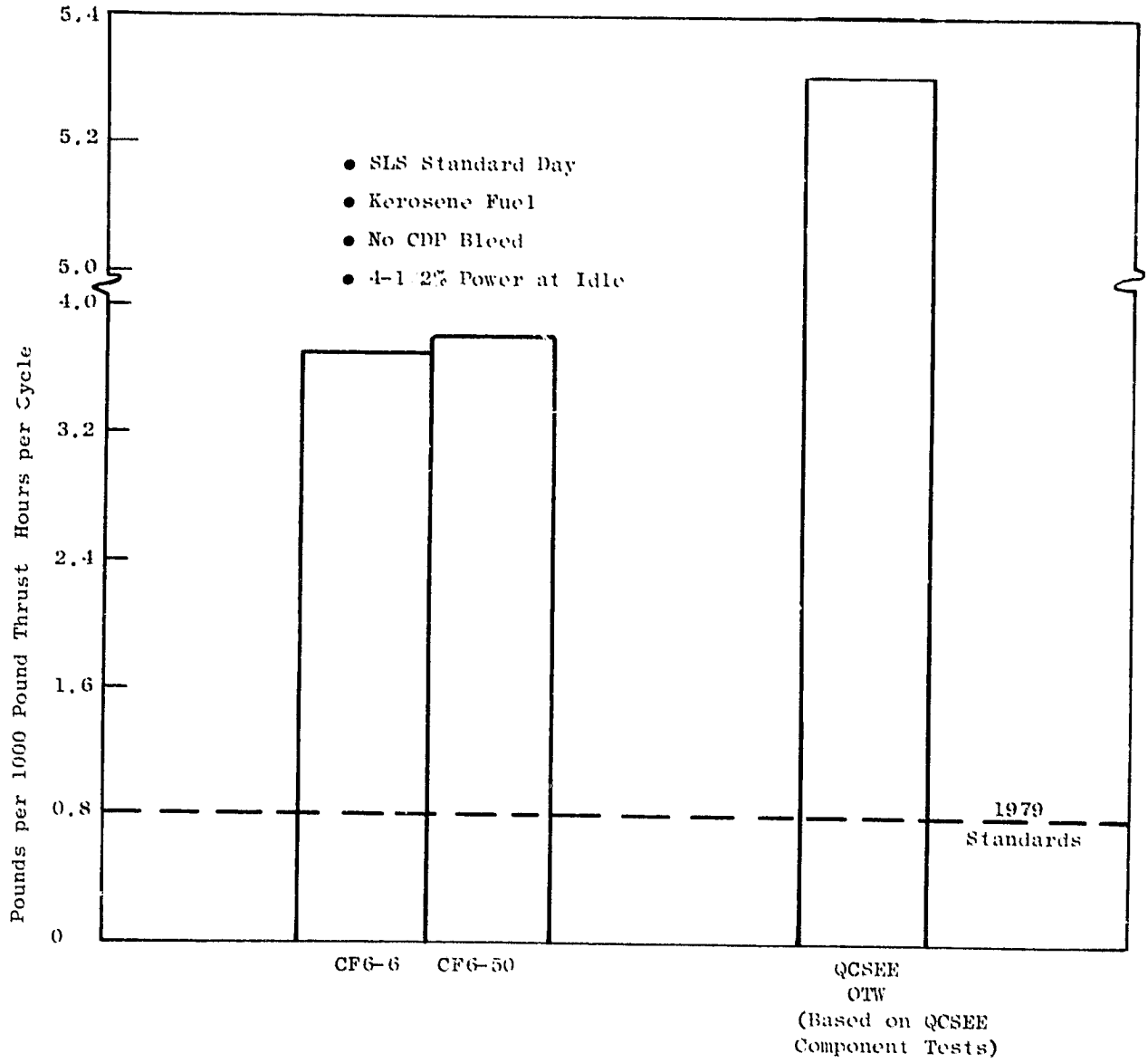

Figure 4.12. C_xH_y Emissions Characteristics of AEG Commercial Engines (Class T2).

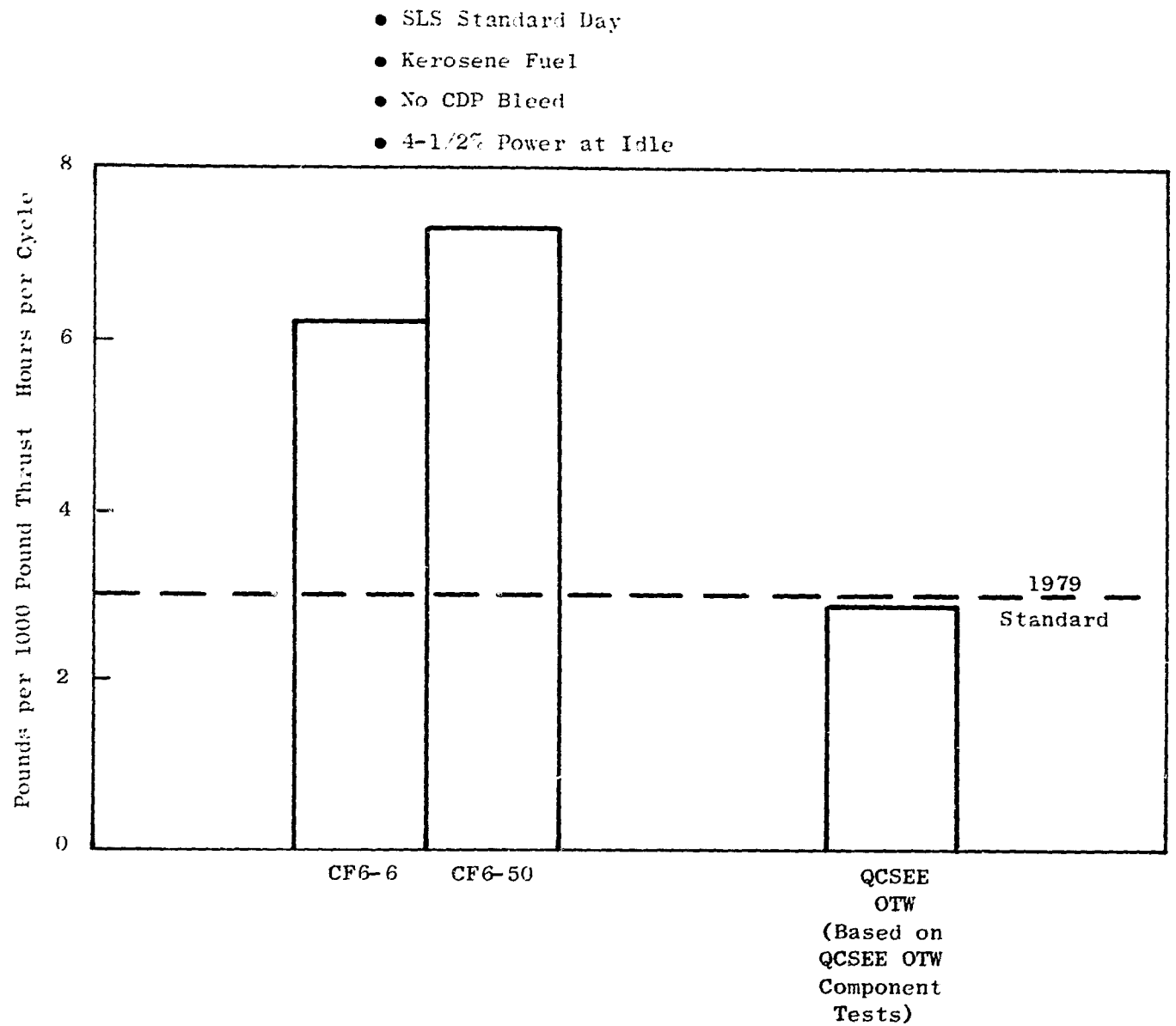

Figure 4-13. NO_x Emissions Characteristics of AEG Commercial Engines (Class T2).

that prevail at ground idle. These adverse operating conditions are associated with the comparatively low cycle pressure ratio of the OTW engine. This low cycle pressure, however, does result in somewhat lower NO_x emissions levels, as is shown in Figure 4-13.

The key combustor operating conditions, which are the primary cause of the differences between the emissions levels of the OTW and higher pressure ratio engines are presented in Table 4-IV. The Specific effects of combustor operating conditions, primarily inlet temperature and pressure, on the CO and C_xH_y emissions indices of the F101 PFRT combustor are shown in Figure 4.14. The higher C_xH_y and CO emissions indices associated with the OTW engine result in proportionately higher calculated mission cycle EPA parameters for this engine. To meet the applicable CO and C_xH_y emissions standards, as defined by the EPA, emissions indices at idle of about 20 and 4 grams per kilogram of fuel, respectively, are required. These target emissions indices and the estimated OTW engine emissions indices are presented in the form of combustion efficiency values in Figure 4.15. As is shown in Figure 4.15, an improvement of over 5.0 percent in combustion efficiency at idle is required to obtain the emissions indices required at idle to meet the EPA goals.

4.5 PERTINENT EMISSIONS REDUCTION TECHNOLOGY

As is discussed in the preceding section, features to reduce the C_xH_y and CO emissions levels of the OTW engine are needed to meet EPA requirements.

The CO and C_xH_y emissions, of course, are products of inefficient combustion. As illustrated in Figure 4.9, these emissions are primarily produced at idle and other low power operating conditions. These emissions mainly occur at these operating conditions because the combustion efficiencies (degree to which the available chemical energy of the fuel is converted to heat energy) of most present-day engines at these low engine power operating conditions are not optimum, typically falling in the 90 to 96 percent range. At higher engine power settings, the combustion efficiency levels of most engines are generally well in excess of 99 percent and, therefore, virtually all of the fuel is converted to the ideal combustion products, carbon dioxide and water, at these operating conditions. The somewhat reduced combustion efficiency performance of most existing aircraft turbine engines at idle and other low engine power operating conditions is due to the adverse combustor operating conditions that normally prevail at these engine operating conditions. At the low engine power operating conditions, the combustor inlet air temperature and pressure levels are relatively low; the overall combustor fuel-air ratios are generally low; and, the quality of the fuel atomization and its distribution within the primary combustion zone is usually poor because of the low fuel and airflows. In any given engine, all of these adverse combustor operating conditions are rapidly eliminated as the engine power setting is increased above idle power levels and, accordingly, its combustion efficiency performance is quickly increased to near-optimum levels.

To meet the CO and C_xH_y emissions standards defined by the EPA for Class T2 aircraft engines, combustion efficiency values at the ground idle operating

Table 4-IV. Comparison of Operating Conditions of OTW and Higher Pressure Ratio Engines at Ground Idle and Takeoff.

	OTW Engine	Higher Pressure Ratio Engine
Standard Day Ground Idle		
Combustor air flow kg/s (pps)	5.5 (12.3)	7.39 (16.3)
Combustor inlet air temperature ° C (° F)	145.5 (287)	163.9 (327)
Combustor inlet air pressure kN/m^2 (psia)	248.2 (36)	324.1 (47)
Combustor fuel-air ratio	0.0159	0.0160
Standard Day Takeoff		
Combustor air flow kg/s (pps)	28.5 (62.7)	40.6 (89.4)
Combustor inlet air temperature ° C (° F)	453 (847)	509.4 (949)
Combustor inlet air pressure kN/m^2 (psia)	1724 (250)	2455 (356)
Combustor fuel-air ratio	0.0309	0.0234

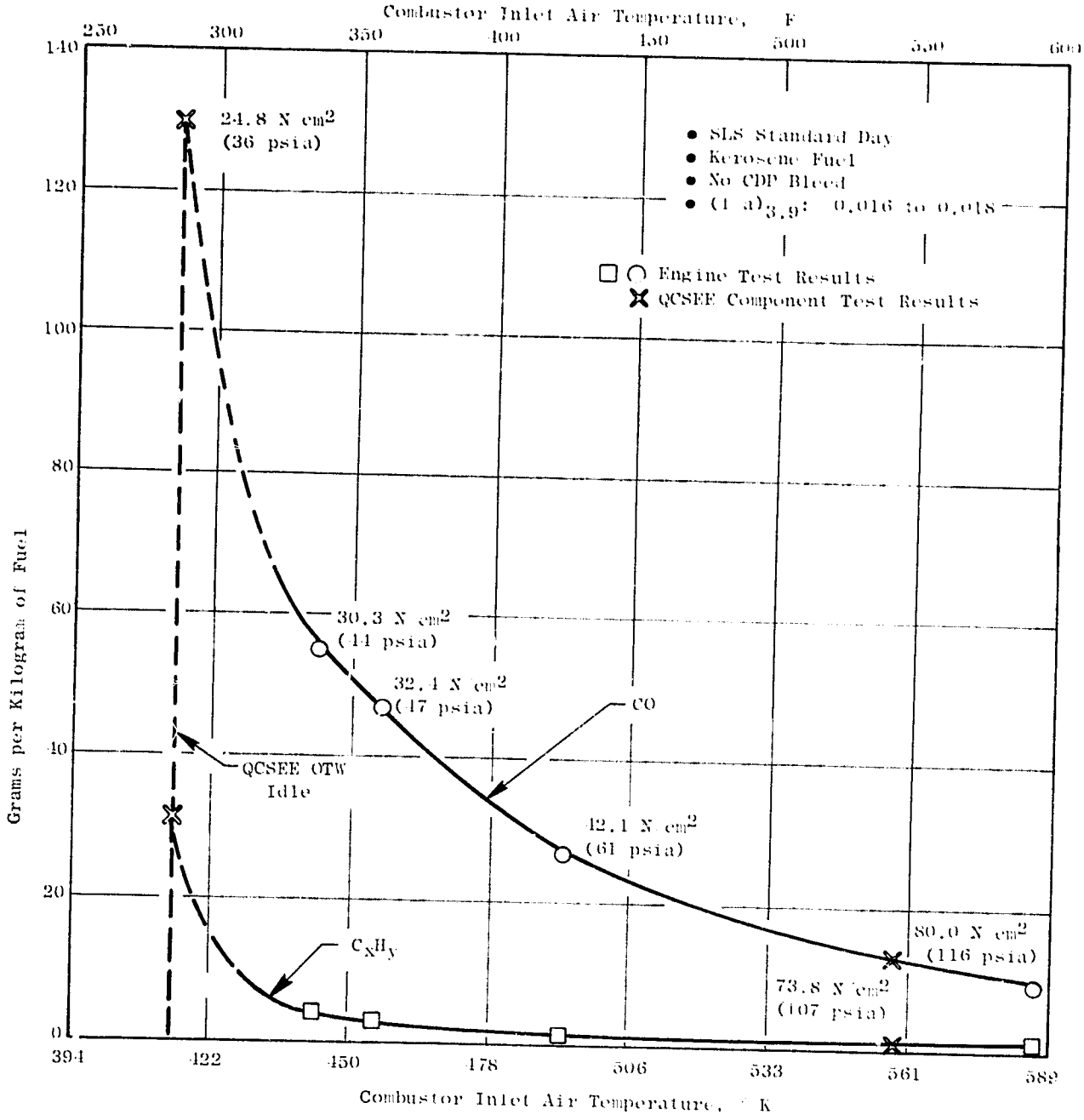

Figure 4.14. CO and C_xH_y Emissions Characteristics of F101 PFRT Engine Combustor.

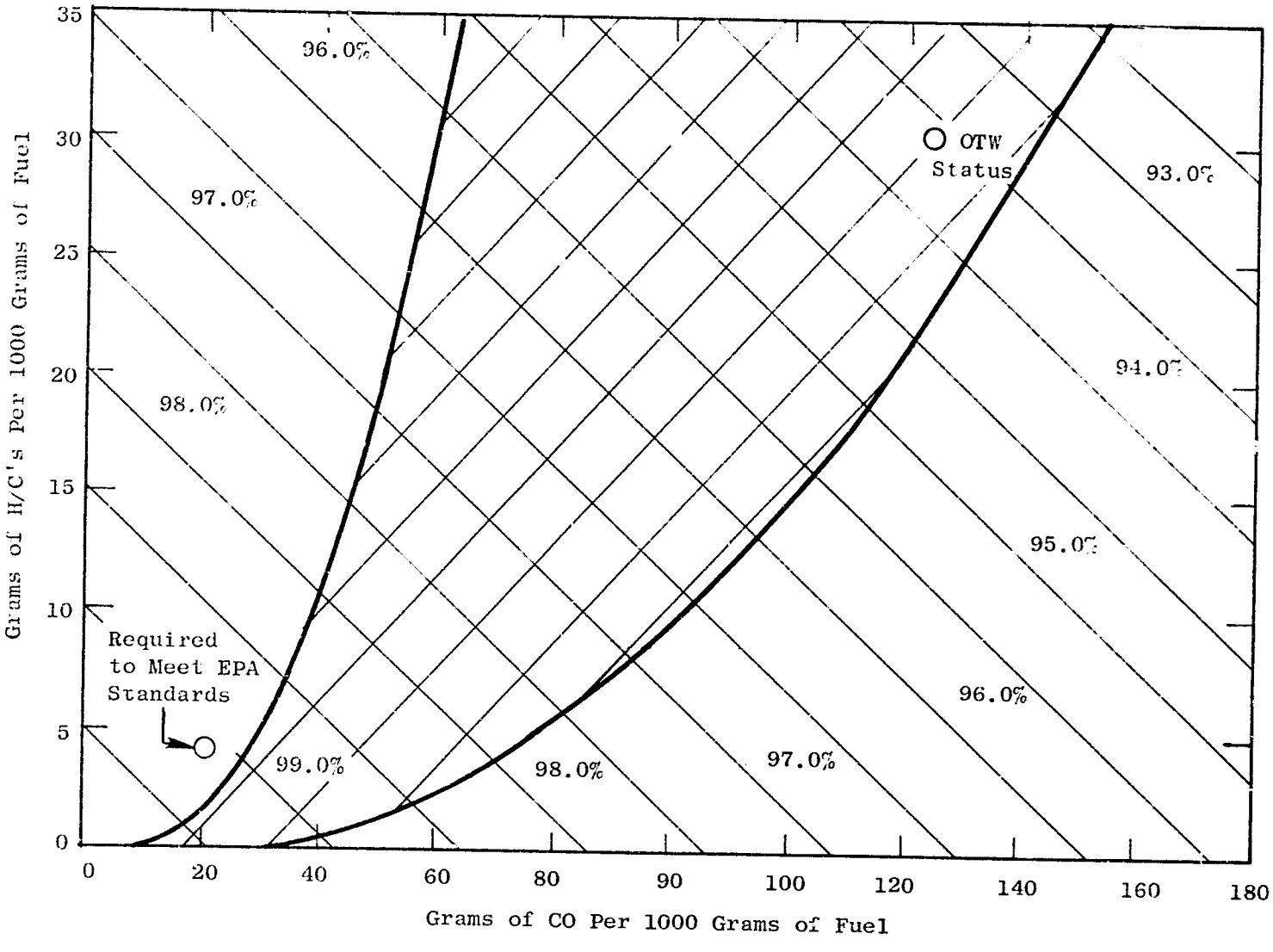

Figure 4.15. Relationship Between CO and H/C's Emissions and Combustion Efficiency.

conditions of 99 percent or higher are required. For example, in the case of the OTW engine, CO and C_xH_y emissions levels of about 20 and 4 grams per kilogram of fuel, respectively, are required at idle to meet the EPA standards. This combination of emissions levels is equivalent to a combustion efficiency value of 99 percent. Thus, significant improvements in the combustion efficiency performance levels, which are typical of present-day engines at the ground idle operating conditions, are required to meet these EPA standards.

Based on combustion chemical kinetics considerations, these required significant improvements in combustion efficiency performance at idle appear to be obtainable in engine combustors, providing that improved control of the various processes which occur in the primary combustion zones of the combustors can be attained at idle operating conditions. CO is formed in combustors as a result of the combustion of near-stoichiometric or over-stoichiometric fuel-air mixtures in the primary zone, because it is a thermochemical equilibrium product resulting from the combustion of such mixtures. Even in combustors designed to have relatively lean primary zone fuel-air mixtures at all operating conditions, relatively rich mixtures generally exist locally within the primary zone since the fuel-air mixing process is not instantaneous. Considerable amounts of CO can be generated as a result of the combustion of these localized rich primary zone mixtures. At idle, any CO that is so generated is not rapidly consumed and, therefore, can escape from the combustion zones of the combustor. Therefore, to obtain low CO emissions levels at idle operating conditions in any given combustor, very precise control of the equivalent ratios in the primary combustion zone and in the dilution zone immediately downstream and of the associated residence times in these zones is essential.

Unlike CO, the C_xH_y emissions are not thermochemical equilibrium combustion products. Moreover, combustion chemical kinetics data show that vaporized hydrocarbons, and any partially oxidized hydrocarbons, are consumed much more rapidly than CO. Thus, as long as these constituents reside in a flame zone for even a very brief time period, they are largely consumed. One of the products of this consumption process may be CO, depending on the flame zone stoichiometry and other factors. Thus, at idle operating conditions, relatively low C_xH_y emissions levels should be obtainable, based on these combustion chemical kinetics considerations, provided that the fuel is properly vaporized and mixed to some degree with air within the primary combustion zone. In any given combustor, the primary causes of this category of idle power emissions appear to be associated with its fuel injection characteristics. In particular, coarse fuel atomization may result in large numbers of large fuel droplets which can escape from the primary zone before they are fully vaporized. In many present-day combustors, the fuel atomization quality tends to be relatively coarse at the low engine power operating conditions because of the low fuel flows associated with these engine operating conditions. Also, the fuel spray pattern of a given combustor may be such that some of the fuel is directed into the relatively cold air streams used to cool the combustor liners and other parts. At idle, any fuel that is so entrained by these cooling air streams tends to be carried out of the primary combustion zones as unreacted fuel. Accordingly, to obtain reduced C_xH_y emissions levels as well as low CO emission levels, very effective fuel atomization at idle is an important need.

The effective atomization is needed both to facilitate rapid and satisfactorily controlled fuel-air mixing in the primary combustion zone and to prevent fuel droplets from escaping from the primary zone.

At General Electric, investigations to identify and develop means of reducing CO and C_xH_y emissions levels at idle by providing improved fuel atomization and improved control of the primary combustion zone fuel-air ratios at idle have been underway for the past several years. For the most part, these investigations have been primarily conducted with CF6 engine combustors, which have already developed low smoke emission characteristics. A major objective of these annular combustor development investigations therefore, has been to retain these already developed low smoke emission characteristics. One of the major development programs of this kind, which is currently underway, is the NASA Experimental Clean Combustor Program. To date, some promising methods of obtaining significant reductions in the CO and C_xH_y emissions levels of these combustors have been identified in these programs.

One relatively simple means of obtaining more optimum primary zone fuel-air ratios at idle, without adversely affecting combustion performance characteristics at high power operating conditions, is to extract and dump overboard increased amounts of compressor discharge airflow when operating at idle. This approach results in increased fuel-air ratios throughout the combustor. Tests of CF6-6 and other engines, in which various amounts of compressor discharge airflow were extracted, were conducted. The results (Figures 4.16 and 4.17) illustrate the beneficial effects of increasing the primary combustion zone fuel-air ratio, at a constant fuel flow rate. The use of increased bleed air extraction also results in small, but beneficial, increases in primary zone gas residence time, which are the result of the lower air mass flows through the combustor. Significant CO and C_xH_y emissions levels reductions were obtained in these investigations. Since many advanced engines have provisions for extracting large amounts of compressor discharge airflow, this concept appears to be an attractive one.

Still another means of obtaining the higher primary zone fuel-air ratios is to use the fuel injection staging techniques at idle operating conditions. In this approach, fuel is valved to only selected fuel nozzles, or fuel injectors, instead of to the full complement of nozzles. This approach results in higher primary zone fuel-air ratios in the portions of the combustor annulus where the fuel is concentrated. Various forms of such fuel injection staging can be considered, depending on the nature of the combustor design. Some fuel injection staging techniques that can be conveniently used in conventional annular combustors are illustrated in Figure 4.18. Tests of these fuel staging approaches have been conducted with both a CF6-50 combustor and an F101 PFRT combustor.

As shown in Figures 4.19 and 4.20, the use of circumferential sector staging, in which the fuel was supplied to groups of adjacent nozzles, was found to be highly effective. With this type of staging the enrichened fuel-air mixtures in the fueled zones are obtained and, at the same time, the number of boundaries between fueled and nonfueled regions are minimized. Circumferential fuel staging of this kind appears to be an attractive approach for

C-2

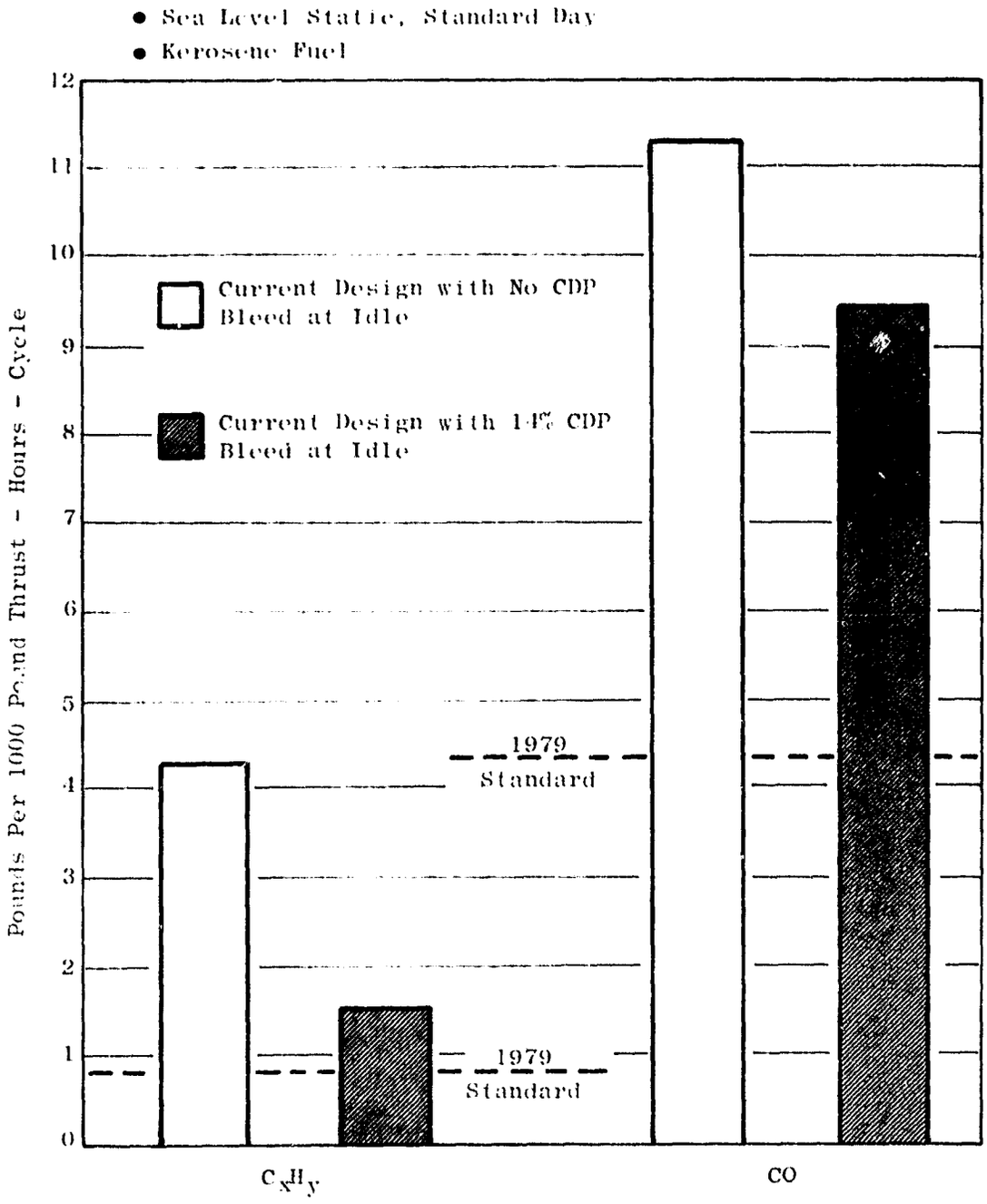

Figure 4.16. C_xH_y and CO Reductions in CF6-6 Engine with Increased CDP Bleed Air Extraction.

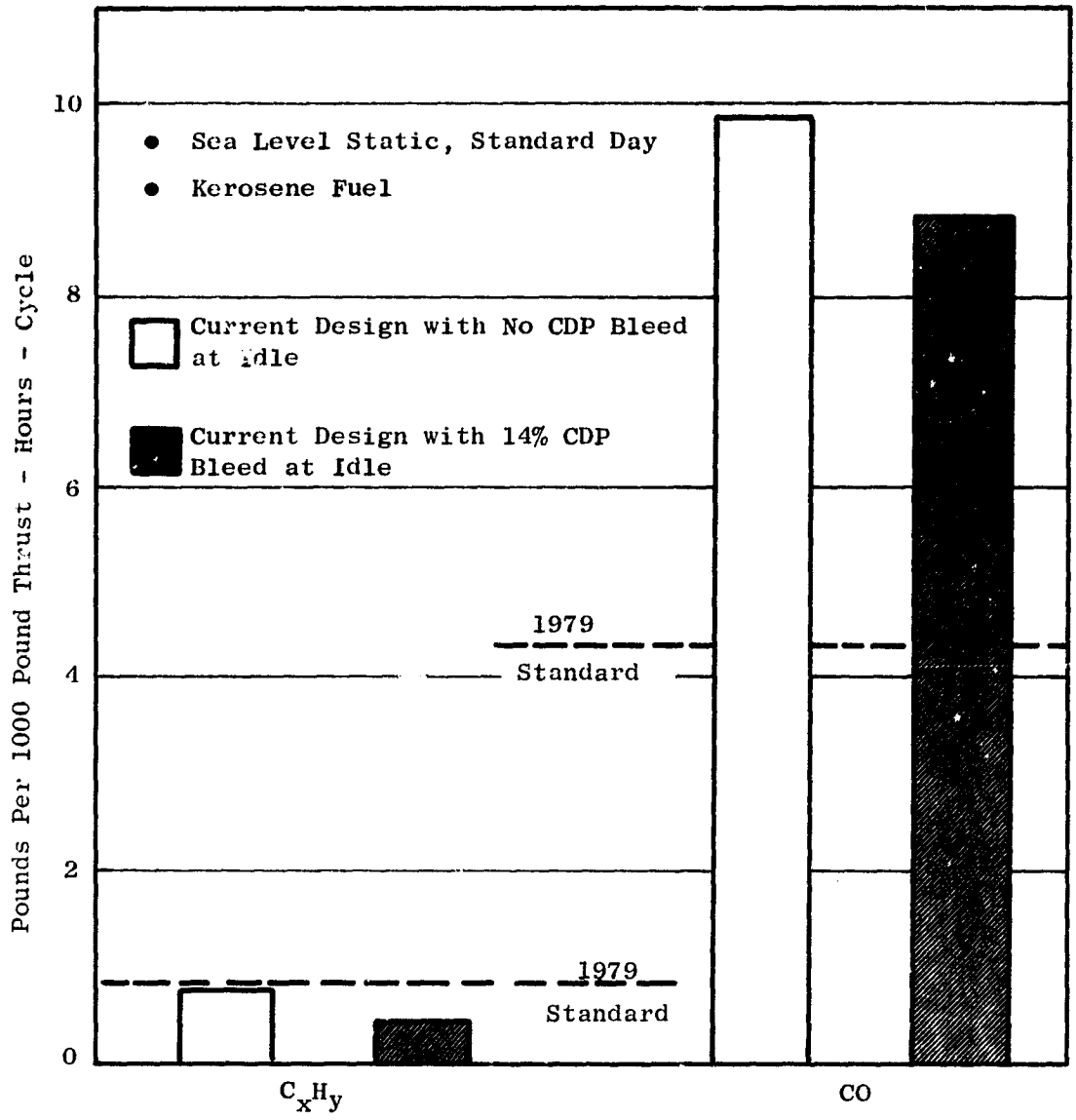

Figure 4.17. C_xH_y and CO Reductions in Higher Pressure Ratio Engine with Increased CDP Bleed Air Extraction.

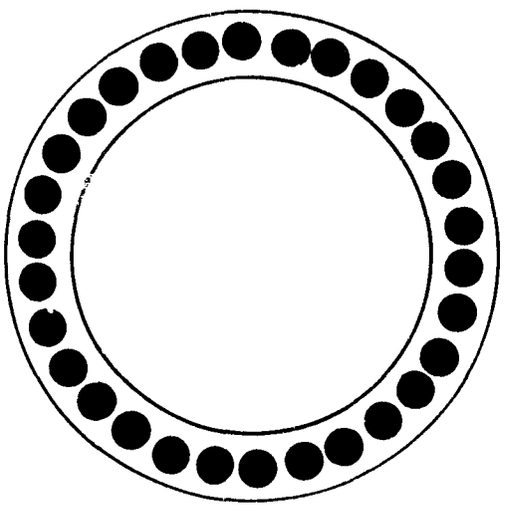

All Nozzles Fueled

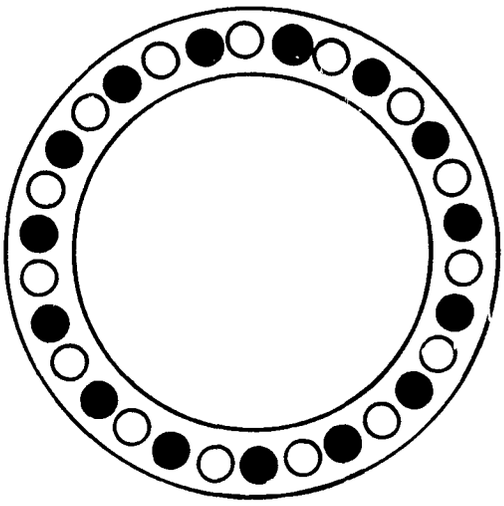

Alternate Nozzles Fueled

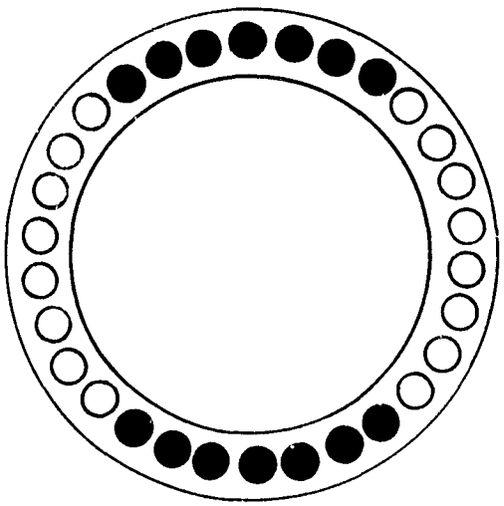

Opposing Sectors Fueled

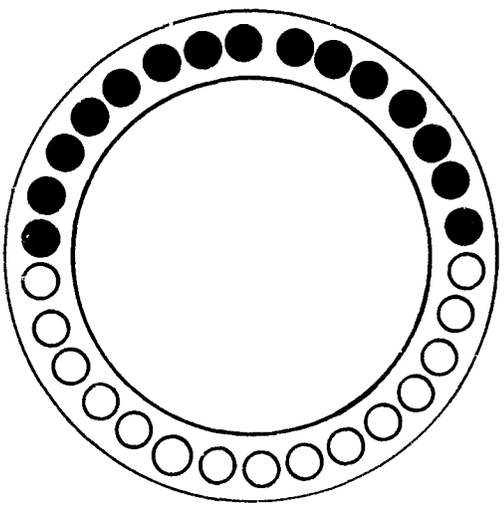

Single Sector Fueled

Figure 4.18. Fuel Staging Methods at Idle in the CF6 Engine.

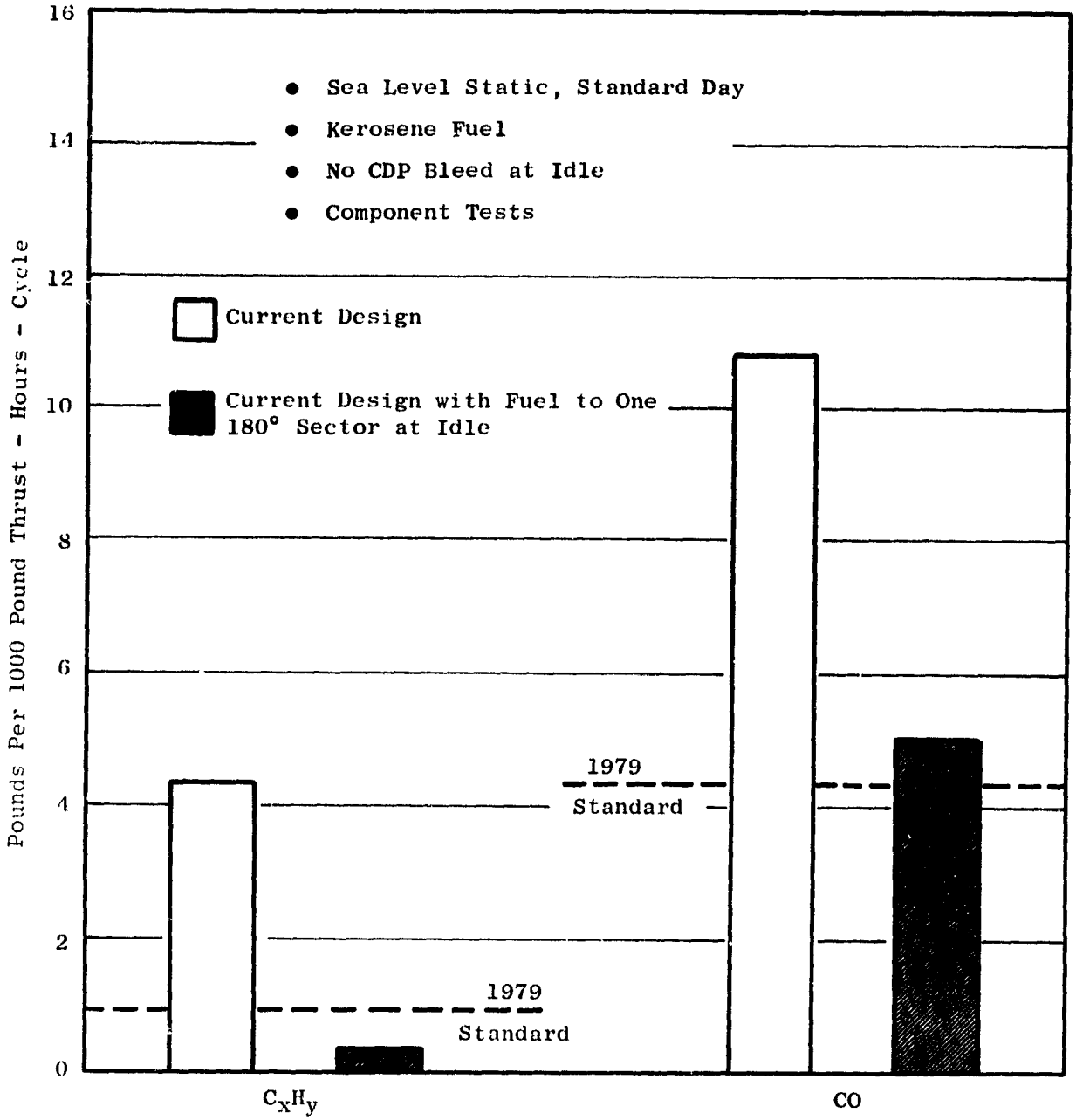

Figure 4.19. C_xH_y and CO Reductions in a CF6-50 Engine Combustor.

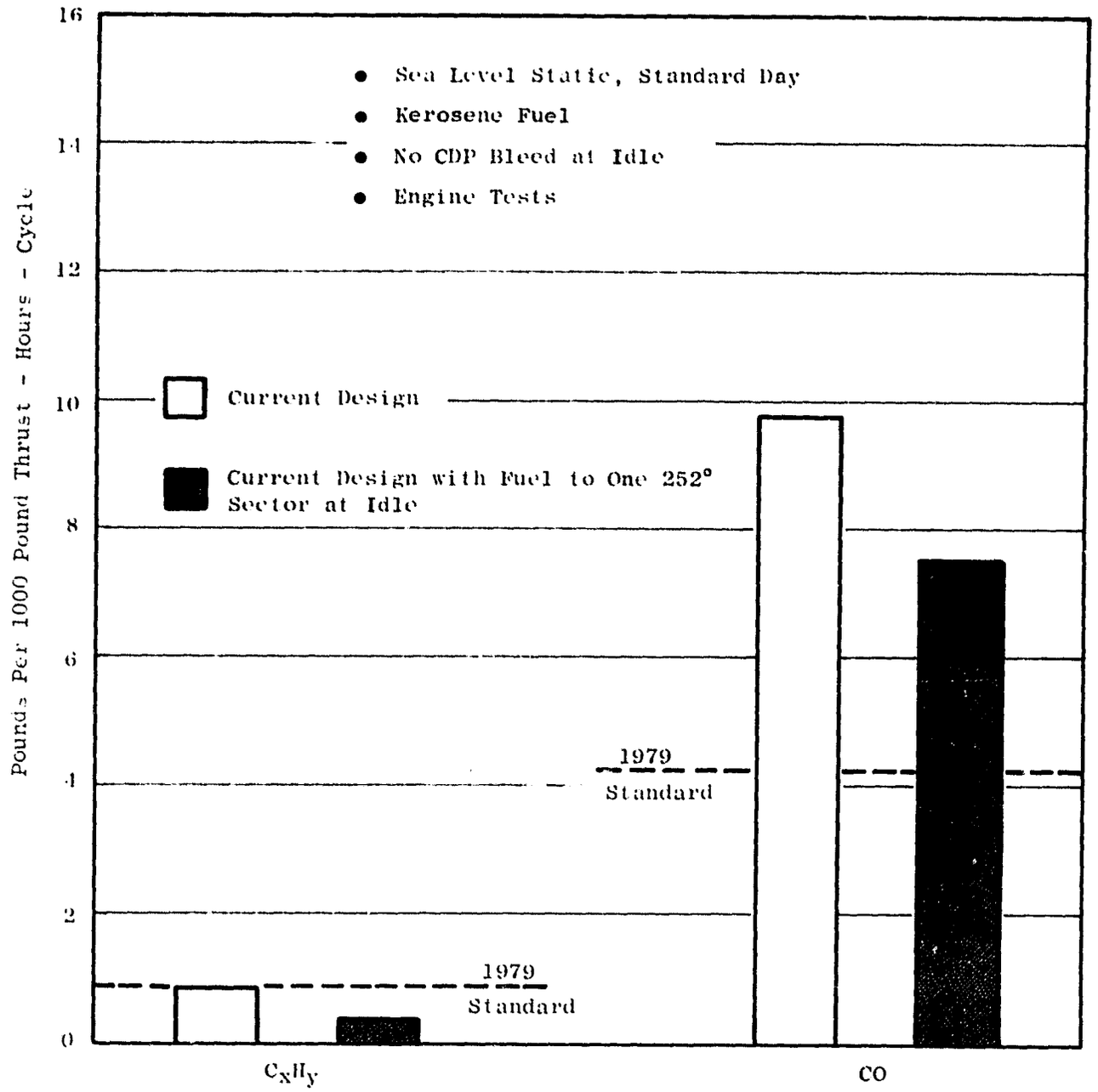

Figure 4.20. C_xH_y and CO Reductions in a High Pressure Ratio Combustor.

use at idle to obtain much reduced CO and C_xH_y emissions levels. As part of the QCSEE Program, development tests of the QCSEE OTW combustor were conducted to evaluate these different approaches. The results of this test indicate that both sector fuel staging and compressor discharge bleed provide substantial reductions in CO and C_xH_y emissions levels at the QCSEE OTW engine idle conditions. Idle emissions reductions of CO and C_xH_y similar to those obtained in the other engine tests were obtained in the QCSEE OTW development tests of the F101 PFRT combustor as shown in Figures 4.21 and 4.22. Further studies are underway to assess the practicality and suitability of applying this approach in advanced engines such as the QCSEE OTW.

Based on the results obtained to date in the General Electric and other investigations, it appears that reductions in the CO and C_xH_y emissions levels of advanced combustors can be obtained by approaches involving primary zone stoichiometry control at idle. In general, these approaches can be used without adversely affecting either the combustion performance or the smoke and NO_x emission characteristics of these combustors at the high engine power operating conditions. In some instances, the use of these approaches can be accompanied by small increases in NO_x emissions at the low engine power operating conditions, but the NO_x emissions levels at these engine operating conditions are still quite low.

4.6 PREDICTED EMISSIONS CHARACTERISTICS WITH ADDED CONTROL FEATURES

Based on the above described results, sector fuel staging at idle has been selected for possible use in reducing CO and C_xH_y emissions in the OTW engine at idle.

Increased CDP bleed air extraction, although an effective means of reducing CO and C_xH_y emissions at idle, could not be employed in the current QCSEE OTW engine program as it is not configured for CDP bleed capability.

Estimates have been made of the emissions characteristics of the OTW engine with the use of sector fuel staging at idle. The estimates are based on the results of the investigations described above which used CF6 and QCSEE OTW engine combustors. As shown in Table 4-V, the predicted CO and C_xH_y emission levels for the OTW engine are still above the prescribed standard. These predictions were based on the OTW combustor component test results. Further evaluation of this emissions reduction technique will be made during the OTW engine tests.

Additional effort is under consideration which would involve applying the advanced emission reduction technology developed in the NASA-GE Clean Combustor program to a double annular combustor design for QCSEE. This new design would be developed in a sector test program concentrating on reducing idle emissions to meet the program goals.

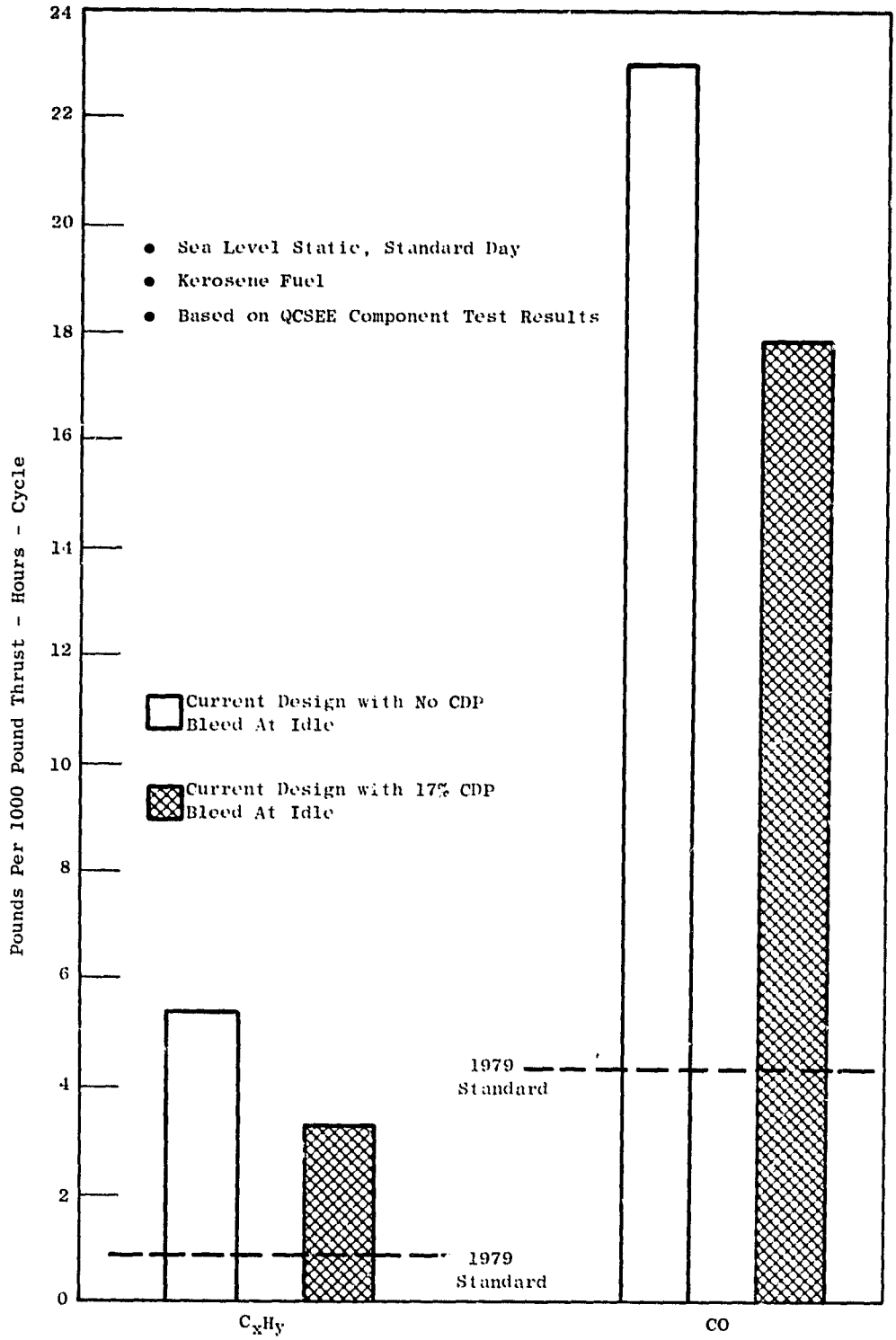

Figure 4.21. C_xH_y and CO Reductions in QCSEE OTW (F101 PFRT) Combustor.

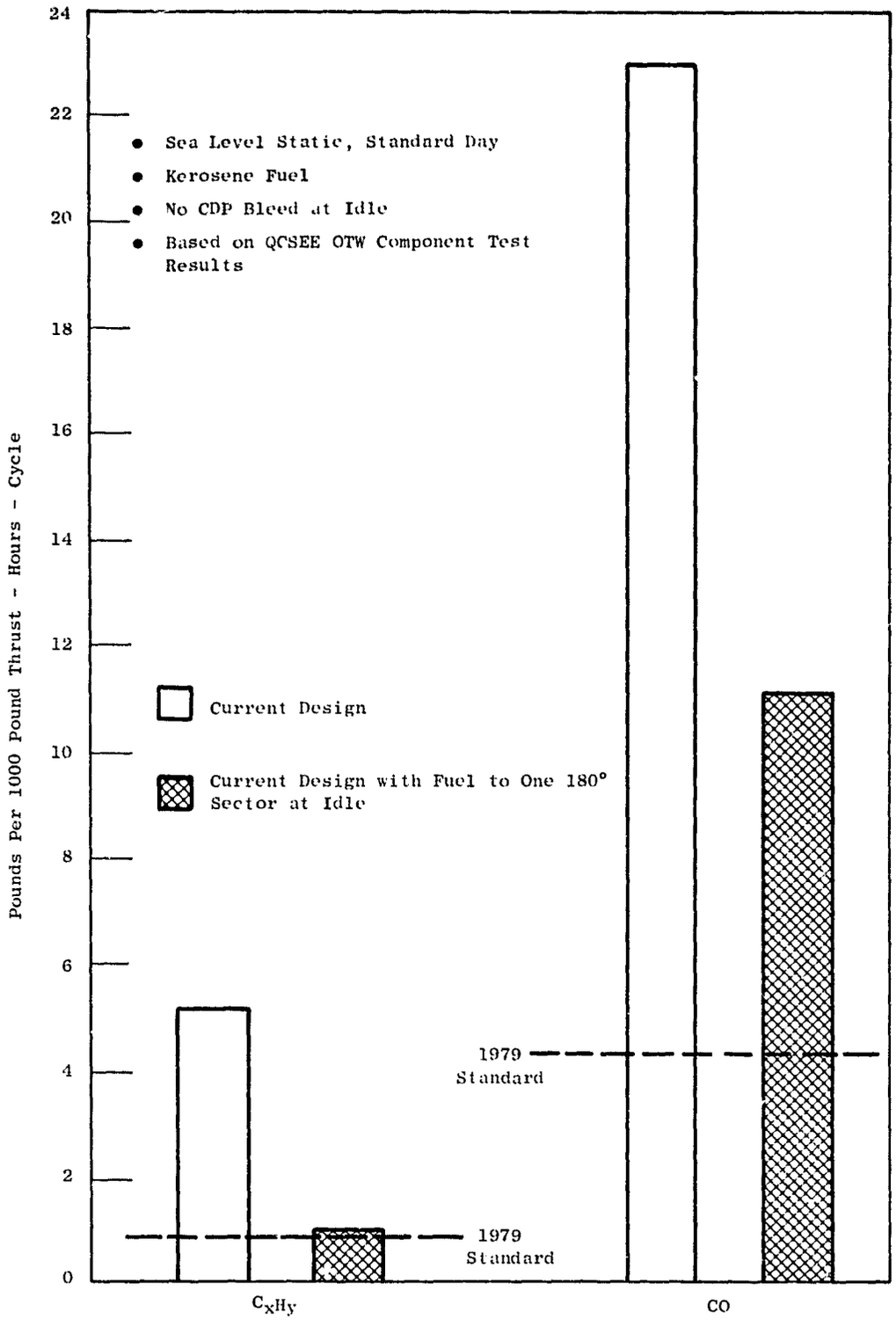

Figure 4.22. C_xH_y and CO Reductions in QCSEE OTW (F101 PFRT) Combustor.

Table 4-V. Predicted OTW Engine Emissions Characteristics.

- Based on QCSEE OTW Component Test Data
- 4.5% Power at Idle
- No CDP Bleed
- Kerosene Fuel

	Pounds Per 1000 Pound Thrust - Hours Per Cycle		
Emission	1979 Standard	Combustor As Is	With Sector Burning At Idle
CO	4.3	23.0	11.2
C_xH_y	0.8	5.3	0.94
NO_x	3.0	2.8	2.8
Smoke (SAE SN)	22	<10	<10

SECTION 5.0

ENGINE CYCLE AND PERFORMANCE

5.1 SUMMARY

The QCSEE OTW engine has a mixed-flow cycle, utilizing a single-stage, gear-driven fan. A physical mixer is not utilized; the fan and core exhaust streams exit confluently through a common exhaust nozzle. Objective thrust levels are 93,413 N (21,000 lb) thrust uninstalled at sea level static, and 21,129 N (4,750 lb) thrust uninstalled at cruise, Mach 0.8, 9144 m (30,000 ft). Design cycle and performance data are presented for these flight conditions as well as for the noise rating conditions, 41.2 m/sec, 61.0 m (80 knot, 200 ft) sideline. The predicted fan performance map also is shown.

5.2 CYCLE SELECTION CRITERIA

Primary constraints on the QCSEE engine cycle include low-noise and low exhaust emissions. The particular cycle defined under this program also was selected to allow usage of several major propulsion system components in common with the QCSEE under-the-wing engine. These components include:

- Inlet
- Fan frame
- Fan bypass duct
- Core engine
- Low pressure turbine
- Turbine frame

An inlet throat Mach number of 0.79 is required at maximum power at the noise rating condition [41.2 m/sec, 61.0 m (80 knot, 200 ft) sideline], thus establishing the airflow at that flight condition. Ram recovery characteristics of the selected inlet are shown in Figure 5.1. In Figure 5.2, the corrected airflow characteristics are shown as a function of flight Mach number. Also shown is the inlet throat Mach number for 406 kg/sec (894 lb/sec) corrected airflow, selected as the design value at all flight conditions for control mode purposes.

Performance objectives are summarized in Table 5-I. As shown in Table 5-1, the engine has an uninstalled thrust at takeoff of 93,413 N (21,000 lb). At cruise the thrust is 21,129 N (4,750 lb).

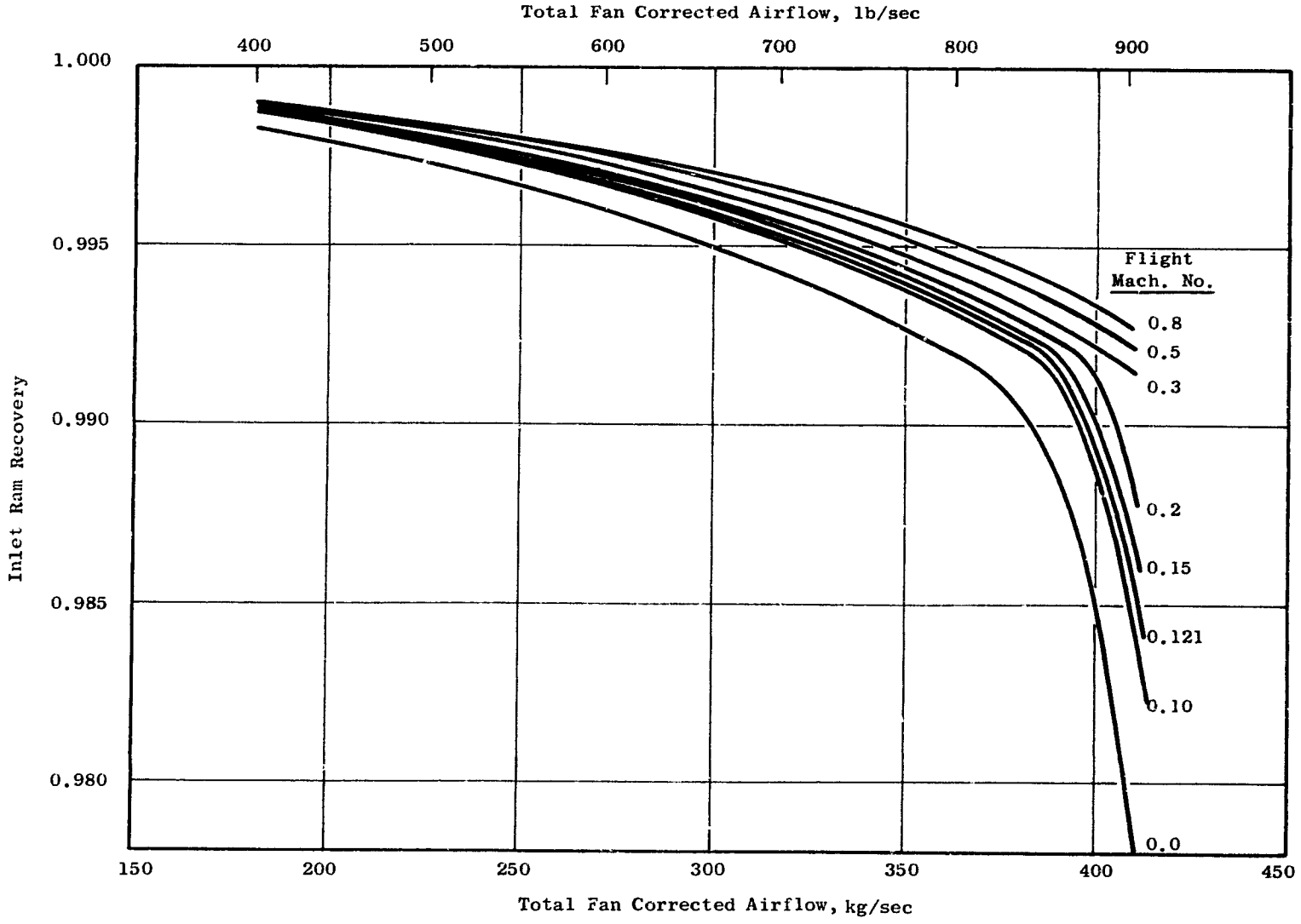

Figure 5.1. QCSEE Inlet Ram Recovery Characteristics.

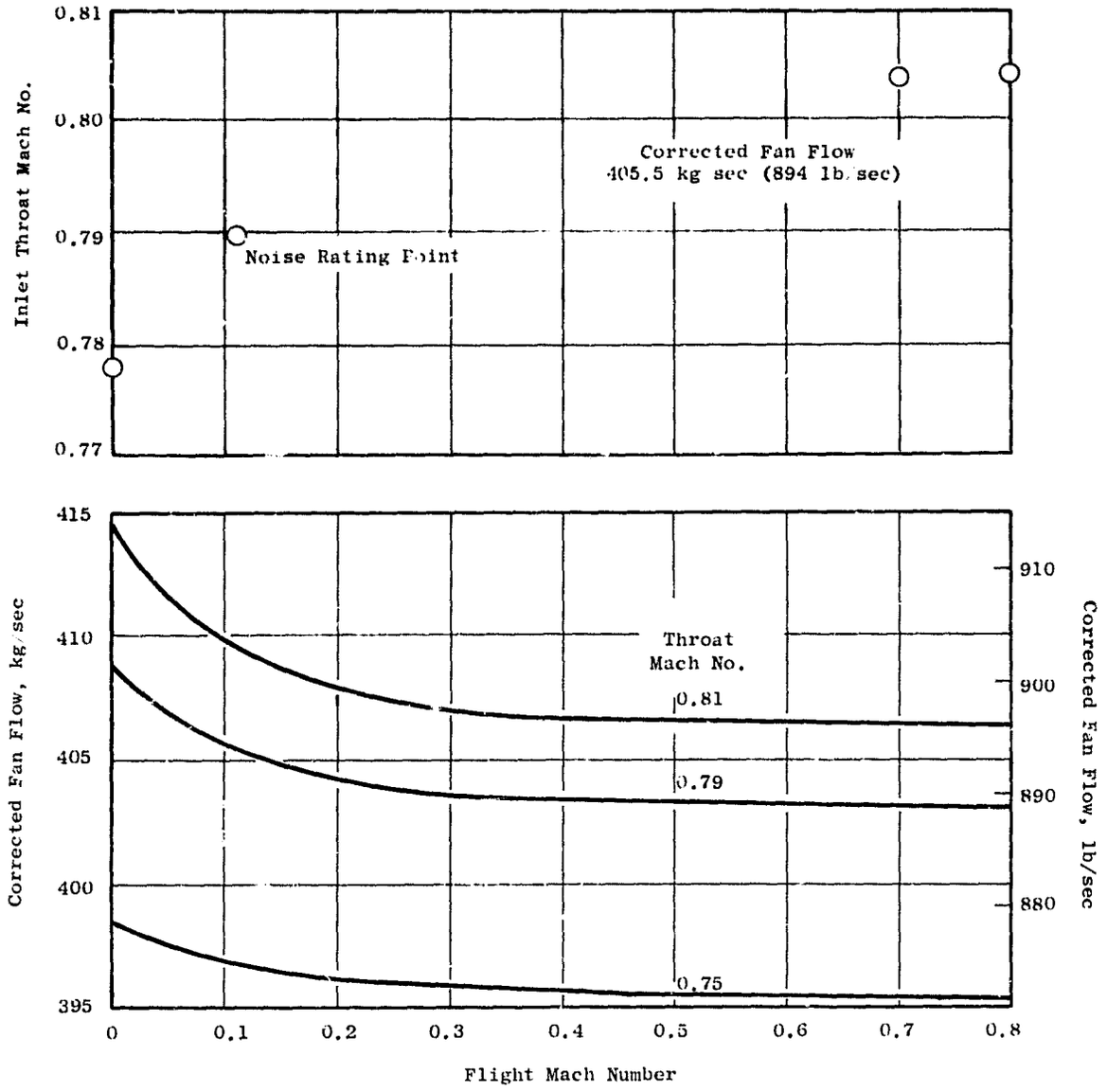

Figure 5.2. QCSEE Inlet Characteristics.

Table 5-I QCSEE OTW Engine Performance Objectives.

Takeoff, SLS, 305° K (90° F) Day		
Uninstalled net thrust, (1) N (lb)	93,413	(21,000)
Uninstalled sfc, kg/Ns (lb/hr/lb)	1.0×10^{-5}	(0.36)
Turbine rotor inlet temperature, ° K (° F) (maximum)	1678	(2560)
Bypass ratio (approximate)	10.2	
Cycle pressure ratio (approximate)	15.5	
Installed net thrust, (1) N (lb)	90,299	(20,300)
Takeoff, SLS, Standard Day		
Uninstalled net thrust, (1) N (lb)	93,413	(21,000)
Uninstalled sfc, kg/Ns (lb/hr/lb)	9.9×10^{-6}	(0.35)
Turbine rotor inlet temperature, ° K (° F) (maximum)	1650	(2510)
Cruise, Mach 0.8, 9144 m (30,000 feet), Standard Day		
Uninstalled net thrust, (1) N (lb)	21,129	(4,750)
Reverse Thrust		
35% of static takeoff thrust N (lb) (minimum)	32,694	(7,350)

(1) No bleed or power extraction

The experimental engine is based on utilization of PFRT F101 core engine and low pressure turbine components. The fan is gear driven with the gear ratio selected to match the available LP turbine; the gear ratio is 2.0617.

5.3 ENGINE AND SYSTEM PERFORMANCE

The OTW propulsion system incorporates a single-stage, gear-driven fan. The fan and core streams mix (without a physical mixer) and exhaust confluently through the two-position exhaust nozzle. PFRT level F101 core engine components are utilized. The cycle provides 93,413 N (21,000 lb) thrust uninstalled, at sea level static conditions, flat rated to a 305° K (90° F) day. Installed, with the effect on inlet ram recovery allowed for, the thrust level is 90,299 N (20,300 lb) at sea level static. At the Mach 0.8, 9144 m (30,000 ft) flight condition, the maximum thrust level uninstalled is 21,129 N (4,750 lbs).

The performance of the OTW experimental engine has been revised from that shown in the preliminary design report. The major factors contributing to the revision are the updating of core performance to represent demonstrated PFRT levels and the revision of duct pressure losses to reflect single splitters.

The predicted OTW experimental engine fan map is shown in Figure 5.3. Design pressure ratio is 1.36 at 406 kg/sec (900 lb/sec) corrected flow; the hub pressure ratio is 1.43. Also shown on the map are the SLS operating line and the takeoff and climb operating conditions.

During the takeoff runway roll, corrected airflow is held at 406 kg/sec (894 lb/sec), which results in 0.79 inlet throat Mach number at the critical sideline noise condition. The exhaust nozzle remains open at the takeoff area [1.802 m^2 (2793 $in.^2$)], while the throttle is in the takeoff position. Fan pressure decreases during the roll as shown on the fan map.

When the throttle is cut back above 0.3 flight Mach number, the exhaust nozzle closes to the cruise area 1.488 m^2 (2307 $in.^2$). This transition shifts the operating point on the map to a lower-flow/higher-pressure-ratio condition at the start of the climb leg. Climb is assumed to be at 129 m/sec (250 knots) indicated air speed to 3048 m (10,000 ft) where acceleration is then made to 154.0 m/sec (300 knots) indicated air speed for climb to the 0.7 Mach number 7520 m (25,000 ft) cruise condition shown on the map.

Two predicted stall lines are included on the map in Figure 5.3. At the time the OTW map was defined, it was not planned to include tip treatment; so, the stall line without treatment was incorporated in the cycle deck. Later the decision was made to use tip treatment in the experimental engine. The expected effect on the stall line is shown in Figure 5.3.

Parasitic and cooling flows for the OTW engine cycle are shown in Figure 5.4.

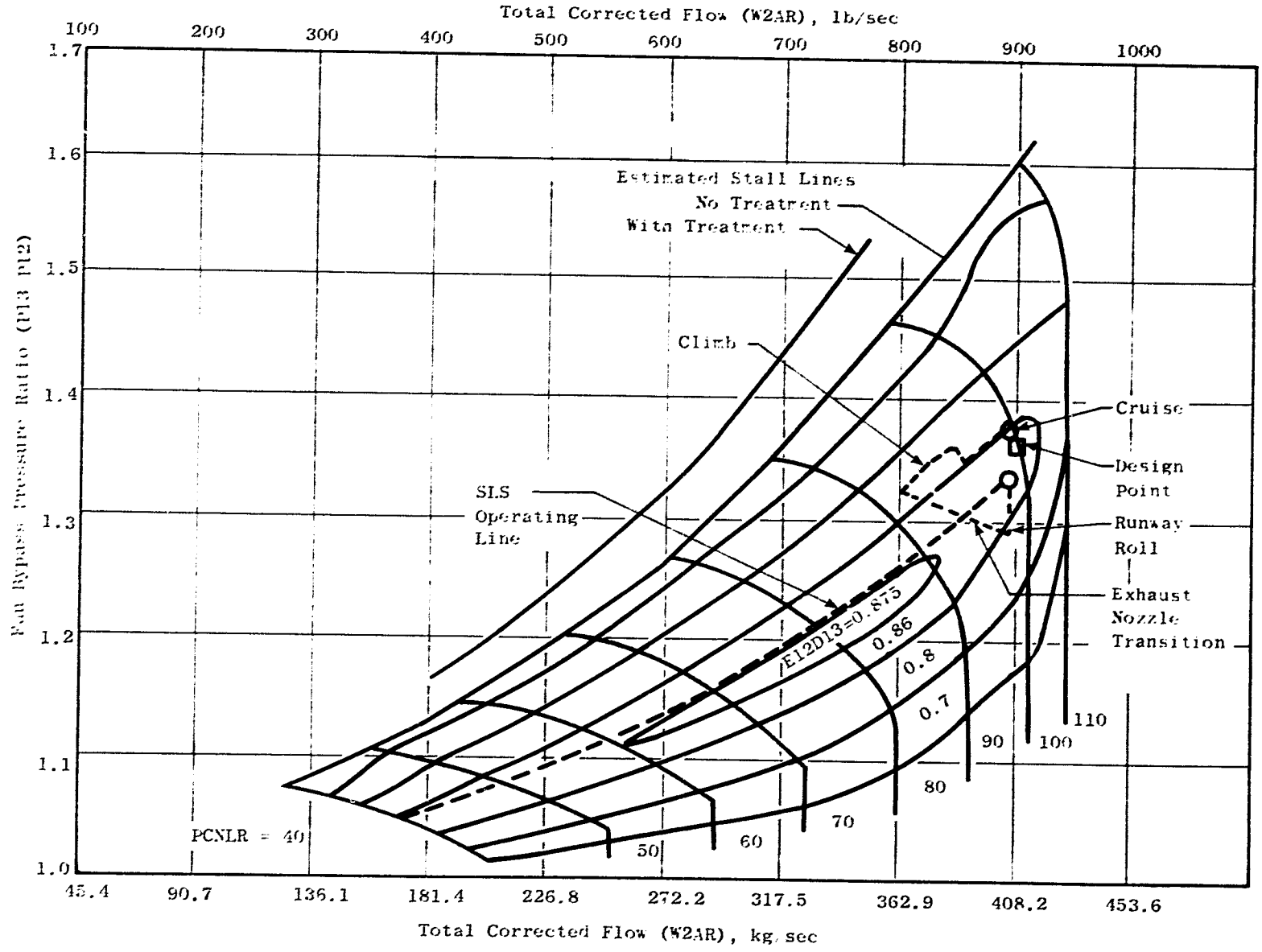

Figure 5.3. Predicted OTW Fan Performance.

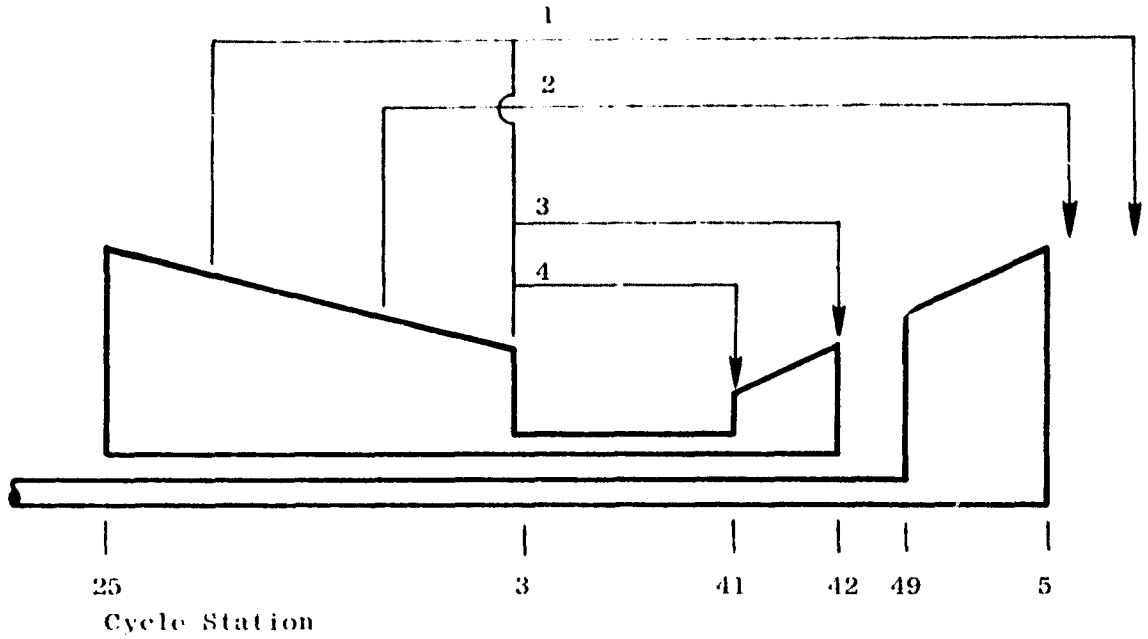

		Source	Sink	Quantity (% of W_{25})
1	Balance Piston, LP Shaft and Rear Bearing Cooling	Stage 3 & CDP	LP Discharge	2.01
2	LP Turbine Rotor Discharge and Dovetail Cooling, LP Turbine Nozzle Vane and Band Cooling	Stage 5	LP Discharge	1.84
3	CDP Seal Leakage, HP Turbine Rotor Cooling	CDP	HP Discharge	5.46
4	HP Nozzle Vane & Band Cooling (Nonchargeable)	CDP	HP Rotor Inlet	11.0

Figure 5.4. Cooling Flow Schematic.

Cycle parameters and performance for the experimental engine are shown in Table 5-II [see cycle nomenclature (Table 5-III) and station designations (Figure 5.5)].

The first three columns in Table 5-II show sea level static takeoff conditions corresponding to the objective levels presented in Table 5-I. The installed data (Column 3) include the effect of inlet ram recovery.

Cruise performance at 0.8 Mach, 9144 m (30,000 ft) is shown in Table 5-II, Column 4 (uninstalled) and Column 5 (installed). An uninstalled thrust of 21,129 N (4750 lb) is the objective level as identified in Table 5-I.

In Columns 6 and 7 of Table 5-II are shown performance parameters at 0.7 Mach number, 7620 m (25,000 ft), which has developed as the cruise condition of principal interest in aircraft studies.

At the approach flight condition [41.2 m/sec, 61.0 m (80 knots, 200 ft)], maximum power is established at 406 kg/sec (894 lb/sec) corrected fan flow, resulting in an inlet throat Mach number of 0.79. Performance at this condition is shown in Column 8 of Table 5-II. Approach thrust is assumed to be 65 percent of the maximum (takeoff) thrust at this flight condition, as shown in Column 9.

The thrust levels shown in Table 5-II are based on an axial discharge exhaust nozzle rather than the "D" nozzle planned for testing. Thus, the performance shown does not reflect the loss in forward thrust associated with the off-axial orientation of the "D" nozzle, or the offsetting gain in lift due to deflection of the exhaust gases over the aircraft flap system. The relationship between an axial discharge nozzle and the selected kickdown "D" nozzle performance will be established from model testing and applied to test results when the engine demonstrator test program is underway.

Fan rotor speed over a range of representative flight conditions is shown in Figure 5.6. During the takeoff roll, the fan speed is essentially constant. It drops off as the throttle is cut back to climb or cruise conditions and the two-position exhaust nozzle closes.

Flight idle is assumed to be 15 percent of maximum cruise power. In Figure 5.6, the resulting fan speed is shown for both open and closed nozzle areas at the flight idle power level. The higher speeds associated with the open nozzle would offer an acceleration time advantage. However, a specific nozzle area switchover point has not been identified and possibly significant thrust jumps could occur dependent on its selection.

Table 5-II. OTW Experimental Engine Performance.

Parameter	Case Number								
	1	2	3	4	5	6	7	8	9
RATING	T/O	T/O	T/O	MXCR	MXCR	MXCR	MXCR	T/O	APP
ALT	0	0	0	30000	30000	25000	25000	200	200
XM	0	0	0	0.8	0.8	0.7	0.7	0.121	0.121
DTAMB	+31	0	+31	+18	+18	+18	+18	0	0
FN	21000†	21000†	20300‡	4750†	4647‡	5544†	5422‡	16877‡	10970‡
SFC	0.339	0.329	0.355	0.711	0.722	0.680	0.691	0.402	0.384
BPR	10.20	10.28	10.09	10.00	10.00	9.99	9.99	10.31	10.93
PAMB	14.696	14.696	14.696	4.361	4.361	5.454	5.454	14.590	14.590
XM11	---	---	0.778	---	0.803	---	0.785	0.790	0.564
T1A	519.67	518.67	549.67	484.92	484.92	491.56	491.56	519.48	519.48
P1A	14.696	14.696	14.432	6.657	6.610	7.568	7.515	14.557	14.658
P12Q11	1.0	1.0	0.982	1.0	0.993	1.0	0.993	0.988	0.994
XNL	3818	3739	3860	3661	3664	3657	3657	3738	3104
PCNLR	98.56	98.59	98.87	99.91	99.91	99.05	99.04	98.48	81.78
W2AR	894.0	891.2	894.0	894.0	891.0	887.4	887.2	894.0	749.5
W2A	868.4	894.2	852.8	418.8	415.8	469.4	466.1	884.8	747.0
P13Q12	1.336	1.336	1.346	1.375	1.375	1.368	1.368	1.333	1.215
E12D13	0.868	0.868	0.867	0.861	0.861	0.862	0.862	0.868	0.877
P21Q2	1.426	1.426	1.428	1.436	1.436	1.429	1.429	1.425	1.289
E2D21	0.792	0.791	0.792	0.786	0.786	0.789	0.789	0.791	0.801
W15	790.9	814.9	775.9	380.7	378.0	426.7	423.7	806.6	684.4
T15	604	570	606	539	539	545	545	571	553
P15	19.63	19.63	19.42	9.16	9.09	10.35	10.28	19.40	17.81
P16Q15	0.991	0.991	0.991	0.992	0.992	0.992	0.992	0.991	0.993
P16	19.46	19.46	19.25	9.08	9.01	10.27	10.19	19.22	17.68
T25	624	589	624	552	552	559	559	590	568
P25	20.60	20.60	20.25	9.39	9.32	10.63	10.55	20.40	18.67
P25Q21	0.983	0.983	0.983	0.983	0.983	0.983	0.983	0.983	0.988
T19	2321	2215	2348	2213	2213	2212	2212	2210	1871
P48	64.39	64.23	64.27	31.02	30.80	34.74	34.50	63.27	46.36
E15D5	0.902	0.901	0.901	0.898	0.898	0.898	0.898	0.902	0.895
P48Q5	3.473	3.469	3.489	3.539	3.539	3.508	3.507	3.463	2.775
XNL48	7934	7709	7959	7555	7554	7511	7539	7707	6400
P55Q5	0.992	0.992	0.992	0.991	0.991	0.992	0.992	0.992	0.990
P56Q55	0.991	0.991	0.991	0.991	0.991	0.991	0.991	0.991	0.991
T56	1761	1680	1784	1672	1672	1674	1671	1675	1477
P56	18.22	18.20	18.10	8.61	8.55	9.73	9.67	17.97	16.51
T58	720	679	725	653	653	659	659	679	637
P58	19.10	19.10	18.91	8.93	8.86	10.10	10.03	18.87	17.43
W8	870.4	896.1	854.8	419.3	416.8	470.5	467.1	886.8	748.2
T8	720	679	725	653	653	659	659	679	637
P8	19.05	19.05	18.86	8.90	8.81	10.07	10.00	18.82	17.39
A8	2771	2771	2793	2307	2307	2307	2307	2793	2793
AE8	2688	2688	2707	2267	2267	2257	2258	2707	2710
V9	787	761	771	1141	1141	1128	1123	757	612
FG9	21000	21000	20300	15339	15160	16142	25944	20590	14105
FRAM	0	0	0	10589	10513	10598	10522	3713	3135

† Uninstalled
‡ Installed

Table 5-III. Mixed-Flow Turbofan Nomenclature.

ALT	Altitude, feet
XM	Flight Mach number
DTAMB	Temperature increment from standard day ambient temperature, ° R
FN	Net thrust, lb
stc	Specific fuel consumption, lb/hr/lb
BPR	Bypass ratio
PAMB	Ambient pressure, psia
XM11	Engine inlet throat Mach number
T1A	Fan inlet total temperature, ° R
P1A	Fan inlet total pressure, psia
P12Q11	Inlet duct pressure ratio
XNL	Fan physical speed, rpm
PCNLR	Fan corrected speed, percent
W2AR	Engine inlet total corrected flow, lb/sec
W2A	Engine inlet total flow, lb/sec
P13Q12	Fan bypass pressure ratio
E12D13	Fan bypass adiabatic efficiency
P21Q2	Fan hub pressure ratio
E2D21	Fan hub adiabatic efficiency
W15	Bypass duct total flow, lb/sec
T15	Bypass duct total temperature, ° R
P15	Bypass duct inlet total pressure, psia
P16Q15	Bypass duct pressure ratio
P16	Bypass duct discharge total pressure, psia
T25	Fan hub discharge total temperature, ° R
P25	Fan hub discharge total pressure, psia
P25Q21	Intercompressor transition duct pressure ratio
XNH	HP compressor physical speed, rpm
PCNHR	HP compressor corrected speed, percent
W25R	HP compressor corrected inlet airflow, lb/sec
W25	HP compressor inlet airflow, lb/sec

Table 5-III. Mixed-Flow Turbofan Nomenclature (concluded).

P3Q25	HP compressor pressure ratio
E25D3	HP compressor adiabatic efficiency
P3Q2	Overall cycle pressure ratio
T3	HP compressor discharge total temperature, ° R
P3	HP compressor discharge total pressure, psia
P4Q3	Combustor pressure ratio
E36D4	Main combustion efficiency
T4	HP turbine 1st stage nozzle inlet total temperature, ° R
W41	HP turbine rotor inlet gas flow, lb/sec
T41	HP turbine rotor inlet total temperature, ° R
E4D42	HP turbine adiabatic efficiency
P4Q42	HP turbine pressure ratio
T42	HP turbine discharge total temperature, ° R
W49	LP turbine rotor inlet total gas flow, lb/sec
T49	LP turbine rotor inlet total temperature, ° R
P48	LP turbine rotor inlet total pressure, psia
E48D5	LP turbine rotor adiabatic efficiency
P48Q5	LP turbine pressure ratio
XNL48	LP turbine physical speed, rpm
P55Q5	LP turbine frame pressure ratio
P56Q55	Core duct pressure ratio
T56	Core duct discharge temperature, ° R
P56	Core duct discharge pressure, psia
T58	Exhaust duct inlet temperature, ° R
P58	Exhaust duct inlet total pressure, psia
W8	Jet nozzle throat total gas flow, lb/sec
T8	Jet nozzle throat total temperature, ° R
P8	Jet nozzle throat total pressure, psia
A8	Jet nozzle throat actual area, sq in.
AE8	Jet nozzle throat effective area, sq in.
V9	Jet nozzle exit velocity, ft/sec
FG9	Gross thrust, lb
FRAM	Ram drag, lb

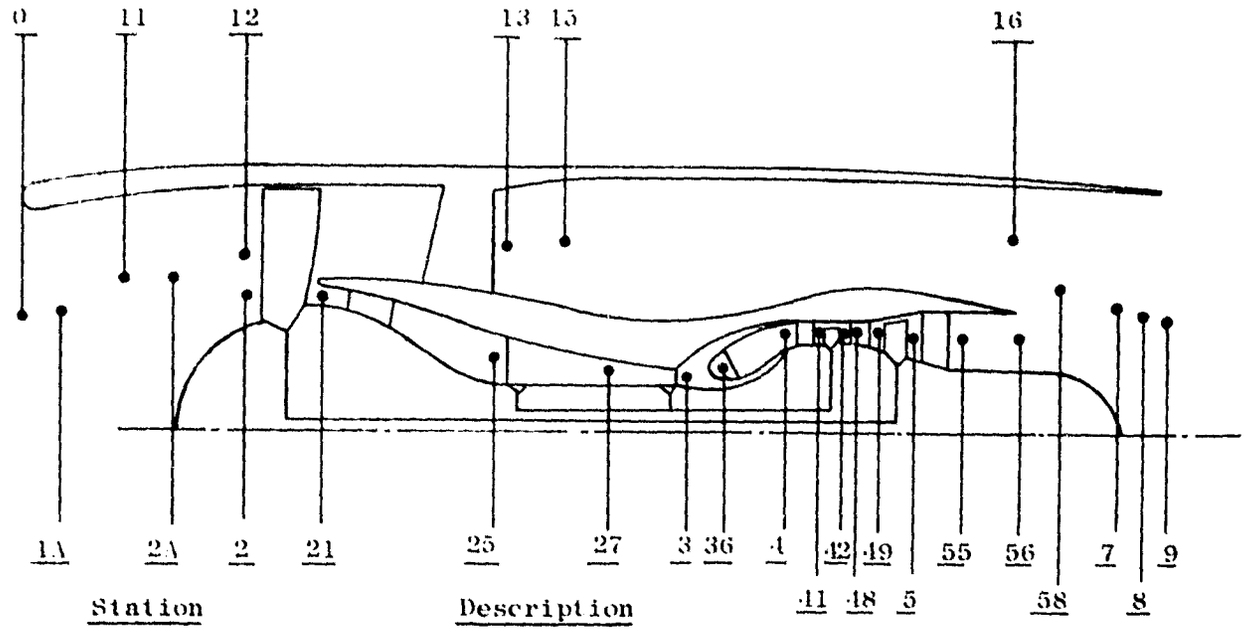

Station	Description
0	Free Stream Air Conditions
1A	Total Nacelle Inlet
11	Inlet Throat
2A	Total Fan Front Face
2	Fan Hub Inlet
21	Fan Hub Discharge
25	HP Compressor Inlet
27	HP Compressor 5th Stage (Stator Exit)
3	HP Compressor Discharge (Stator Exit)
36	Combustor Inlet
4	Combustor Discharge (HP Turbine Vane Inlet)
41	HP Turbine Rotor Inlet
42	HP Turbine Discharge
48	LP Turbine Vane Inlet
49	LP Turbine Rotor Inlet
5	LP Turbine Discharge
55	LP Turbine Frame Discharge
56	Core Duct Discharge
58	Mixing Plane
7	Exhaust Nozzle Inlet
8	Exhaust Nozzle Throat
9	Exhaust Nozzle Discharge
12	Fan Tip Inlet
13	Fan Tip Discharge
15	Bypass Duct Inlet
16	Bypass Duct Discharge

Figure 5.5. Station Designations.

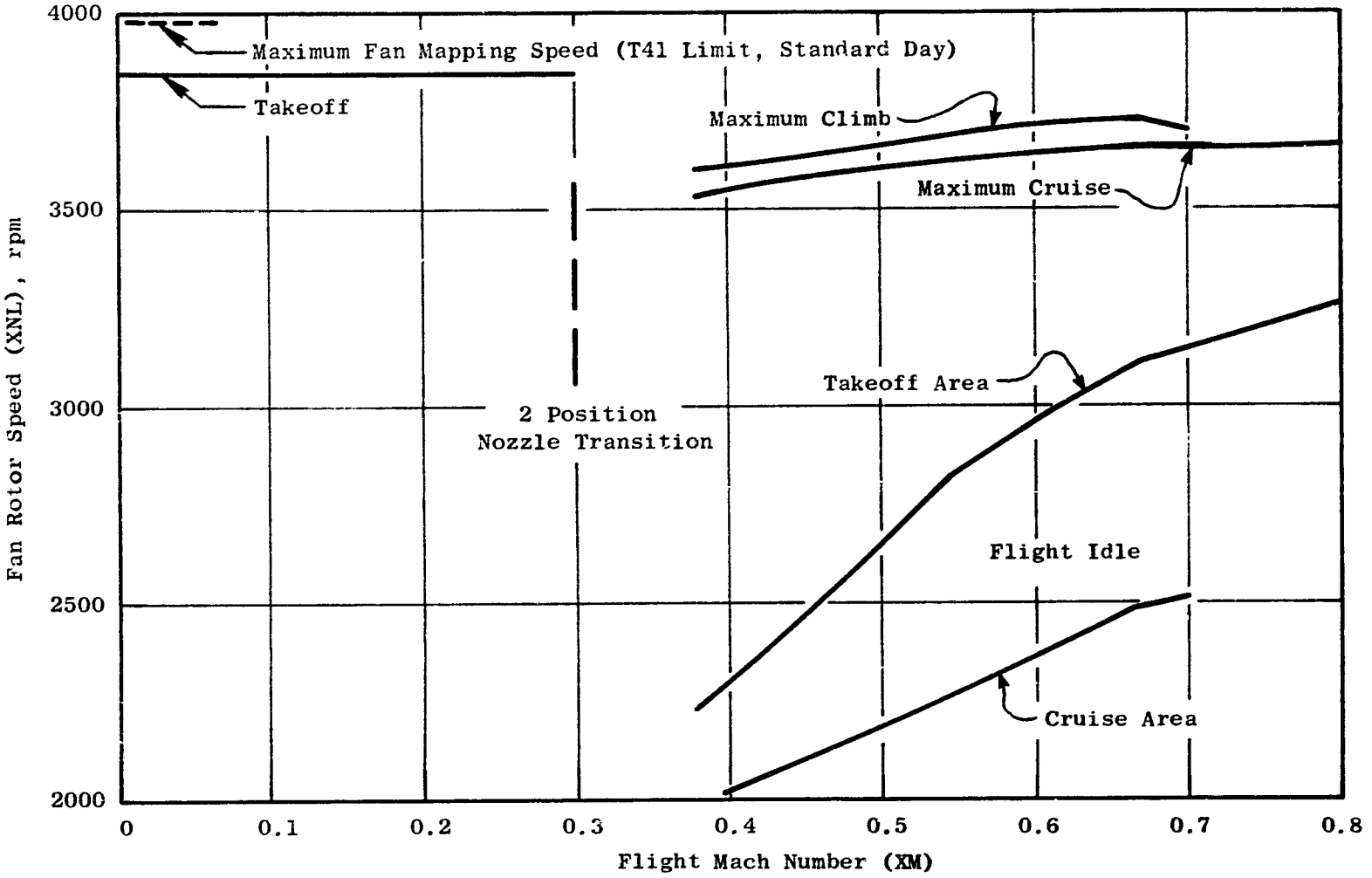

Figure 5.6. OTW Engine Fan Speed Versus Mach Number (Hot Day).

SECTION 6.0

FAN AERODYNAMIC DESIGN

6.1 SUMMARY

The aerodynamic design of both the variable-pitch UTW and fixed-pitch OTW geared fans was completed during the Preliminary Design Phase.

At the major operating conditions of takeoff and maximum cruise, a corrected flow of 405.5 kg/sec (894 lbm/sec) was selected for both fans, which enables common inlet hardware to yield the desired 0.79 average throat Mach number at the critical takeoff noise measurement condition. The aerodynamic design bypass pressure ratio is 1.36 for the OTW fan, which is intermediate between the takeoff and maximum cruise power settings. The takeoff pressure ratio is 1.34. The takeoff corrected tip speed is 354 m/sec (1162 ft/sec). The pressure ratio and speed were selected on the basis of minimum noise within the constraints of adequate stall margin and core engine supercharging.

THE OTW fan employs 28 fixed-pitch fan blades. A flight version of the design would use composite fan blades, but titanium fan blades will be used in the experimental fan as a cost saving measure. The conceptual design with composite blades was used to establish the number of fan blades and, in conjunction with the aerodynamic design, the blade airfoil shape. The metal blades require a larger fan disk rim than would be required for composite blades. The fan disk support cone and the remaining fan components on the experimental engine will be of flight design.

6.2 DESIGN REQUIREMENTS

Major operating requirements for the over-the-wing (OTW) fan, Figure 6.1, are takeoff, where noise and thrust are of primary importance, and maximum cruise, where economy and thrust are of primary importance. A secondary requirement was to utilize hardware common to the UTW fan when no significant performance penalty was involved. At takeoff, a low fan pressure ratio of 1.34 was selected to minimize the velocity of the bypass stream at the nozzle exit. A corrected flow of 405.5 kg/sec (894 lb/sec), the same as for the UTW, at this pressure ratio yields the required engine thrust. The inlet throat is sized at this condition for an average Mach number of 0.79 to minimize forward propagation of any noise. This sizing of the inlet throat prohibits higher corrected flow at altitude cruise. Required maximum cruise thrust is obtained by raising the fan pressure ratio to 1.38. The aerodynamic design point was selected at an intermediate condition, which is a pressure ratio of 1.36 and a corrected flow of 408 kg/sec (900 lb/sec). Table 6-1 summarizes the key parameters for these three conditions:

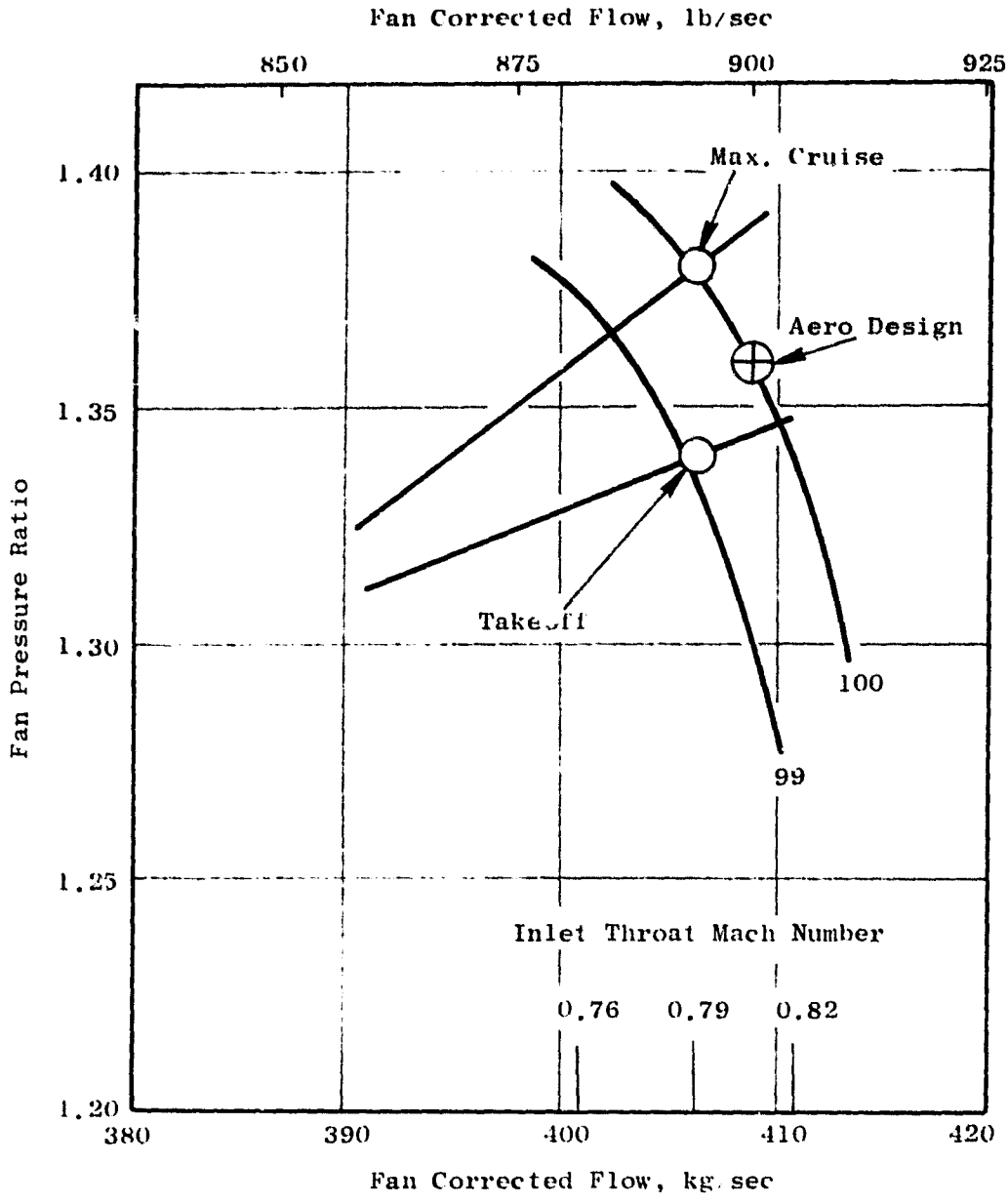

Figure 6.1. Major Operating Requirements for OTW Fan.

Table 6-I. QCSEE OTW Fan.

Parameter	Design Point	Takeoff	Maximum Cruise
Total fan flow	408 kg/sec (900 lb/sec)	405.5 kg/sec (894 lb/sec)	405.5 kg/sec (894 lb/sec)
Pressure ratio - bypass flow	1.36	1.34	1.38
Pressure ratio core flow	1.43	1.43	1.44
Bypass ratio	9.9	10.1	9.8
Corrected tip speed	358 m/sec (1175 ft/sec	354 m/sec (1162 ft/sec)	359 m/sec (1178 ft/sec)

BASIC DESIGN FEATURES

A cross section of the selected OTW fan configuration is shown in Figure 6.2. The fan outer flowpath, vane-frame (including outer and inner flowpath), and transition duct (including the six frame struts) are all common to the UTW fan configuration. Thus the integrated nacelle vane-frame assembly is common to both propulsion systems. There are 28 fixed-pitch rotor blades. The overall proportions for the rotor blades, blade number, and radial distributions of thickness and chord were selected to provide a satisfactory aeromechanical flight-type composite configuration. However, to minimize overall program costs, titanium was substituted for the actual blade construction. The stall margin for the OTW fan is projected to be adequate. The circumferential grooved casing treatment is retained from the UTW fan to provide added protection against stall. The rotor was positioned axially such that the trailing edge hub intersects the hub flowpath at the same axial station as the UTW which puts the aft face of the fan disk at approximately the same engine station. A tip axial spacing between rotor trailing edge and vane/frame leading edge equal to 1.9 true rotor tip chords results. The vane/blade ratio is 1.18. Immediately following the rotor, in the hub region, is a splitter which divides the flow into the bypass portion and core portion. The proximity of the splitter leading edge to the rotor blade is to enable additional design control on the streamlines in the hub region to provide improved surface velocity and loading distributions. The 156 OGV's for the fan hub flow, or core portion, are in the annular space under the splitter. There are six struts in the gooseneck which guides the fan hub flow into the core compressor.

Figure 6.2. Cross Section of OTW Fan.

In the vane/frame, which is common with the UTW Fan, the vanes are nonaxisymmetric in that five vane geometries, each with a different camber and stagger, are employed around the annulus. This nonaxisymmetric geometry is required to conform the vane-frame downstream flow field to the geometry of the pylon, which protrudes forward into the vane-frame, and simultaneously maintains a condition of minimum circumferential static pressure distortion upstream of the vane/frame. There are 33 vanes in the vane/frame which yield a vane/blade ratio of 1.18.

6.4 DETAILED CONFIGURATION DESIGN

The corrected tip speed at the aerodynamic design point was selected at 358 m/sec (1175 ft/sec). This was selected for design purposes, as a compromise between the takeoff and cruise tip speed requirements. The objective design point adiabatic efficiency is 88% for the bypass portion and 78% for the core portion. Requirements include 16% stall margin at takeoff and a high fan hub pressure ratio to provide good core engine supercharging. An inlet radius ratio of 0.42 was selected, compared to 0.44 for the UTW fan, to provide additional annulus area covergence at the rotor hub which reduces the hub aerodynamic loading. Discharge radius ratios are approximately the same for the two fans. For the 1.803 m (71 in.) tip diameter, a flow per annulus area of 194 kg/sec-m^2 (39.8 lb/sec-ft^2) results.

The standard General Electric axisymmetric flow computation procedure was employed in calculating the velocity diagrams. Several calculation stations were included internal to the rotor blade to improve the overall accuracy of the solution in this region. The physical splitter geometry is represented in the calculations. Forward of the splitter, calculation stations span the radial distance from OD to ID. Aft of the splitter, calculation stations span the radial distance between the OD and the topside of the splitter and between the underside of the splitter and the hub contour. At each calculation station effective area coefficients, consistent with established design practice, were assumed.

The design radial distribution of rotor total-pressure ratio is shown in Figure 6.3. This distribution is consistent with a stage average pressure ratio of 1.36 in the bypass region. The higher-than-average pressure ratio in the hub region provides maximum core engine supercharging subject to a balance between the constraints of acceptable rotor diffusion factors, stator inlet absolute Mach numbers, and stator diffusion factors. A stage average pressure ratio of 1.43 results at the core OGV exit. The assumed radial distribution of rotor efficiency for the design is shown in Figure 6.4, which was based on measured results from similar configurations (Quiet Engine, Fan B). The assumption of efficiency rather than total-pressure-loss coefficient is a General Electric design practice for rotors of this type. The radial distribution of rotor diffusion factor which results from these assumptions is shown in Figure 6.5. Figures 6.6 and 6.7 show the radial distributions of rotor relative Mach number and air angle, respectively. At the rotor hub the flow turns 16° past axial which corresponds to a work coefficient of 2.6.

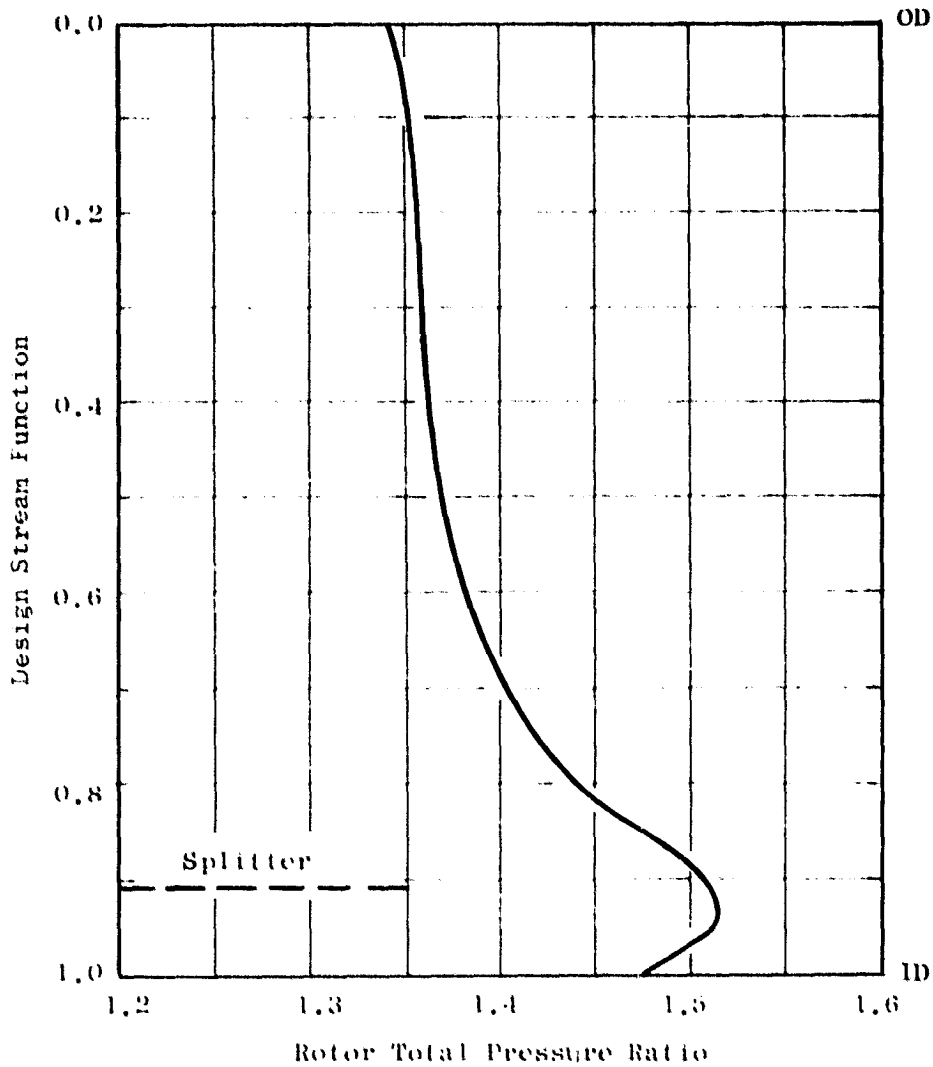

Figure 6.3. OTW Radial Distribution of Rotor Total Pressure Ratio.

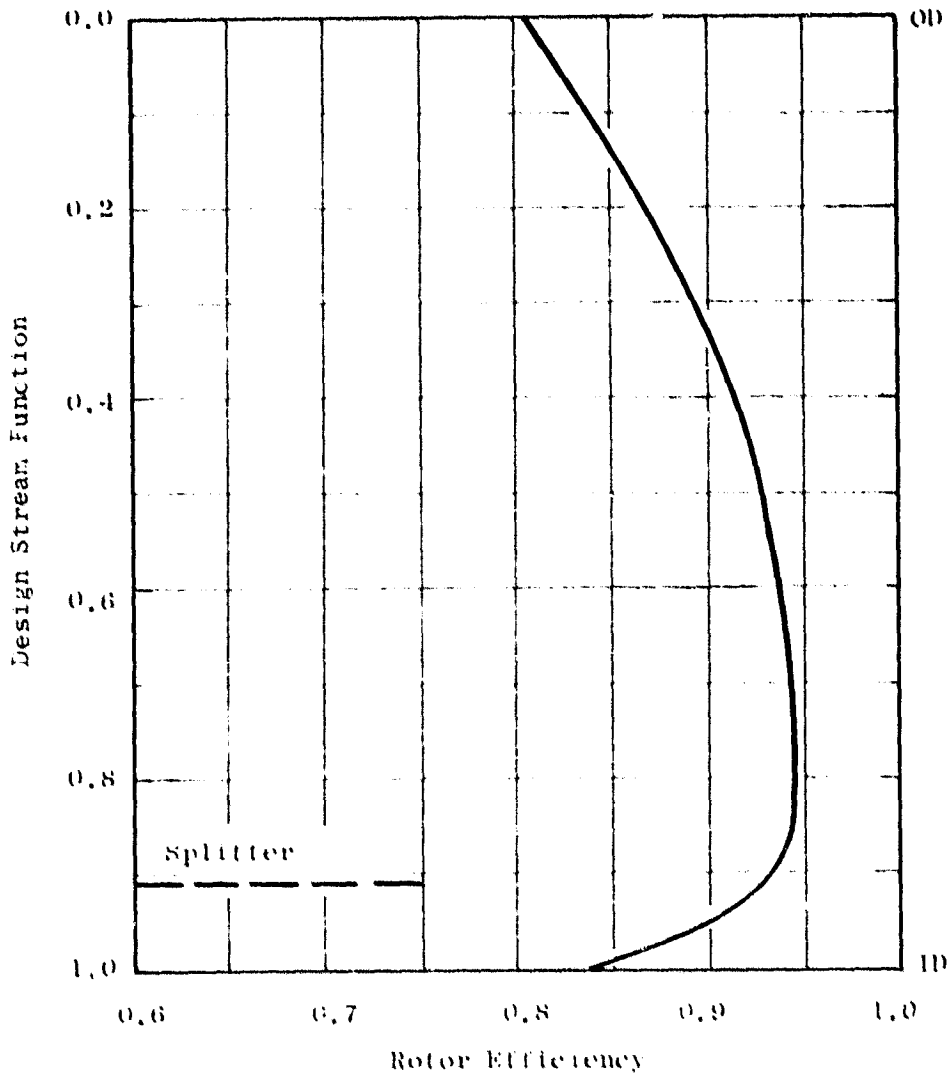

Figure 6.4. OTW Radial Distribution of Rotor Efficiency.

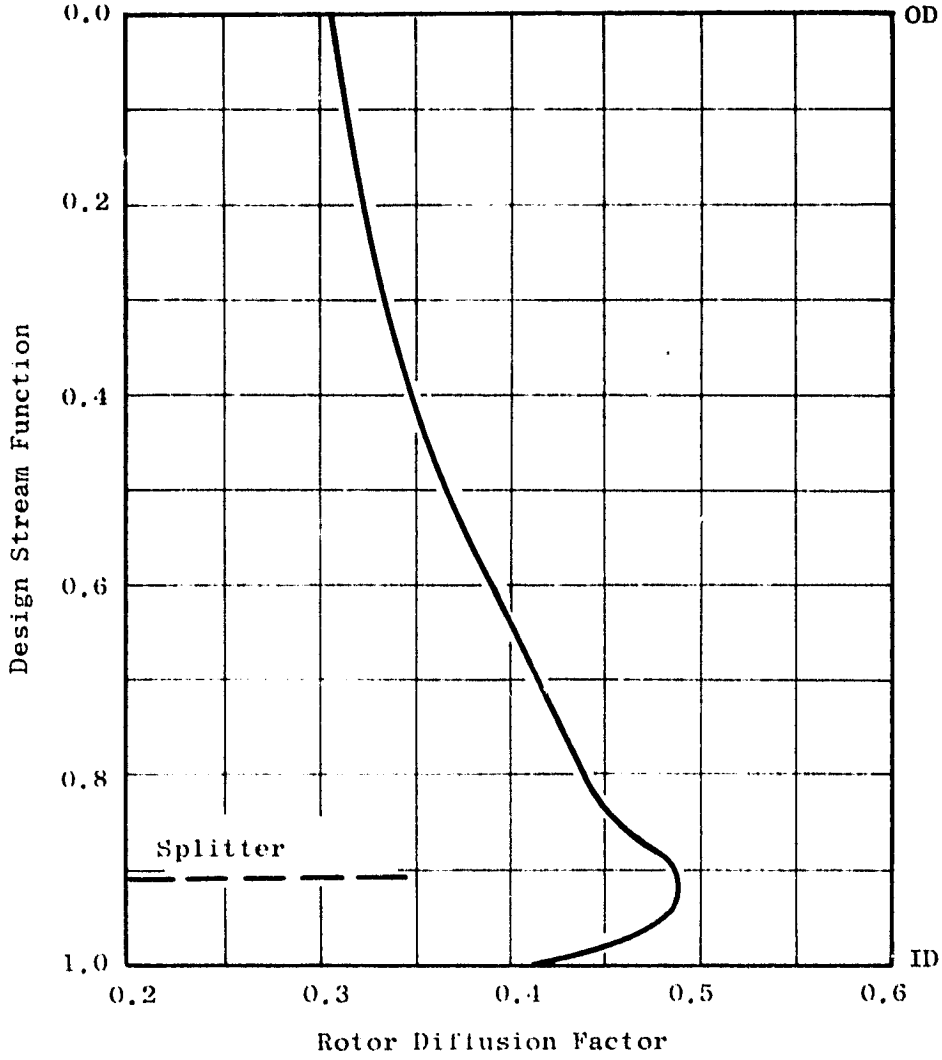

Figure 6.5. OTW Radial Distribution of Rotor Diffusion Factor.

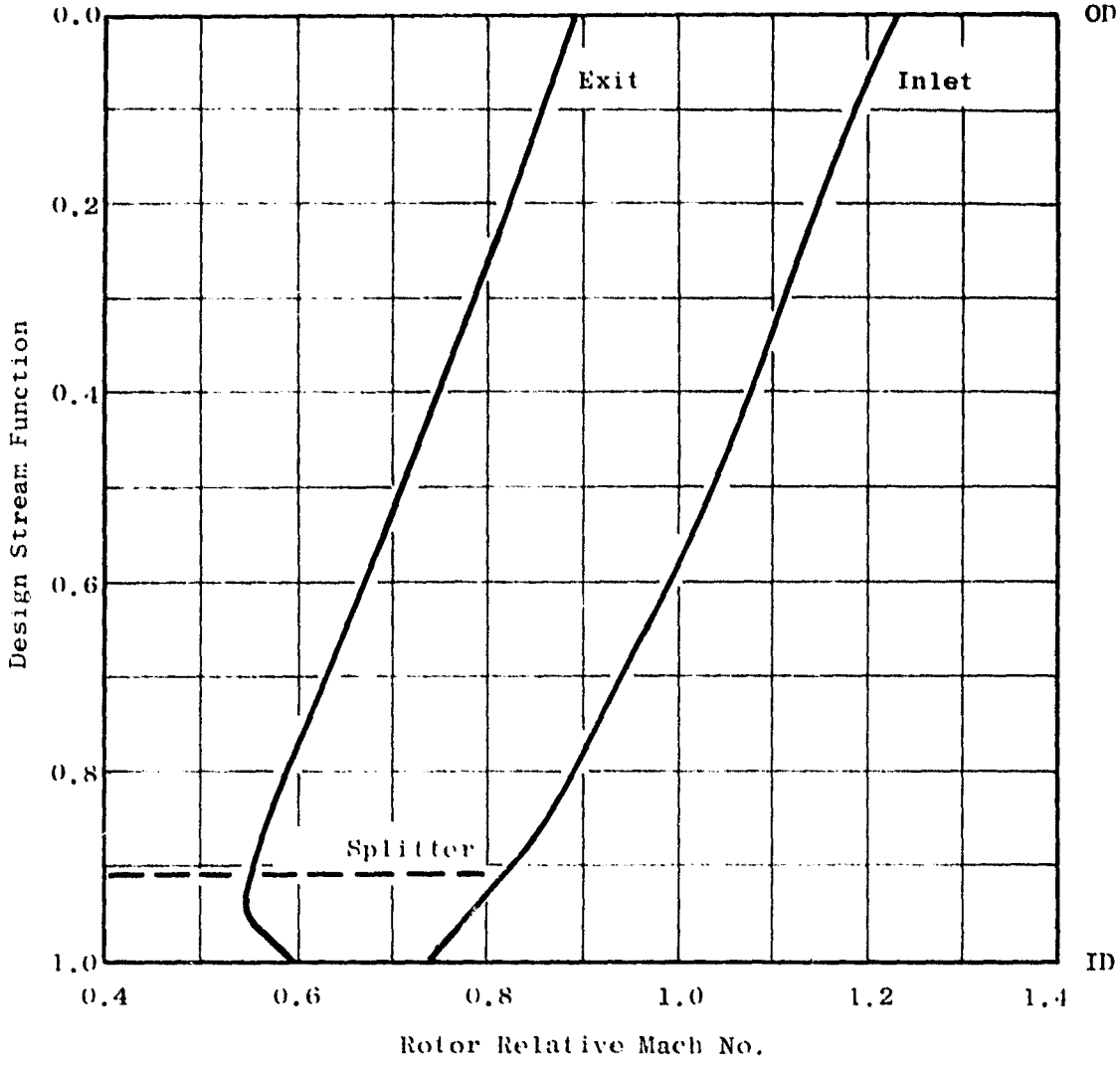

Figure 6.6. OTW Radial Distribution of Rotor Relative Mach Number.

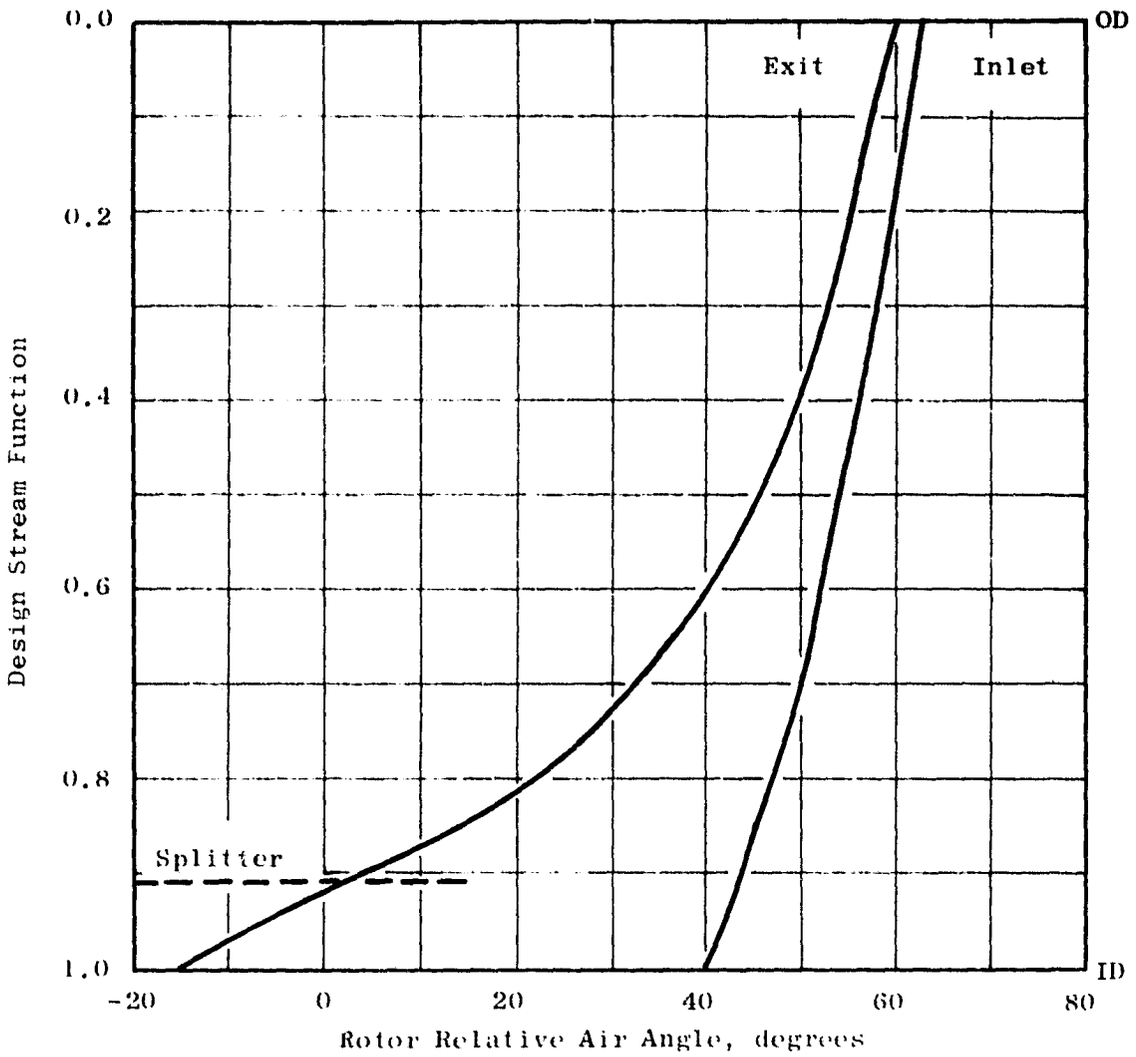

Figure 6.7. OTW Radial Distribution of Rotor Relative Air Angle.

The assumed radial distribution of total-pressure-loss coefficient for the core portion OGV is shown in Figure 6.8. The relatively high level, particularly in the ID region, is in recognition of the very high bypass ratio of the OTW engine and, accordingly, the small relative size of the core OGV compared to the rotor. The annulus height of the core stator is approximately 70% of the rotor staggered spacing, a significant dimension when analyzing secondary flow phenomena. It is anticipated that a significant portion of the core OGV will be influenced by the rotor secondary flows. The moderately high core OGV diffusion factors, turning angles, and inlet Mach numbers, as shown in Figure 6.8, were contributing factors in the total-pressure-loss coefficient assumptions. An average swirl of 6° is retained in the fluid upon exit from the core OGV, like the UTW configuration. This was done to lower its aerodynamic loading. The transition duct struts designed for the UTW configuration were cambered to accept this swirl.

6.5 ROTOR BLADE DESIGN

The rotor blade tip solidity was selected as 1.3. With a rotor tip inlet relative Mach number of 1.22, a reduction in tip solidity would lower the overall performance potential of the configuration. The rotor hub solidity was selected as 2.2. The primary factors in this selection were the rotor hub loading and sufficient passage length to do the required 56° turning. The radial chord distribution is linear with radius. Mechanical input was provided to ensure that this chord distribution and the selected thickness distribution, as shown in Figures 6.9 and 6.10, produced a satisfactory aeromechanical configuration.

The detailed layout procedure employed in the design of the fan blade geometry generally parallels established design procedures. In the tip region of the blade where the inlet relative flow is supersonic, the uncovered portion of the suction surface was set to ensure that the maximum flow passing capacity is consistent with the design flow requirement. The incidence angles in the tip region were selected according to transonic blade design practice which has yielded good overall performance for previous designs. In the hub region, where the inlet flow is subsonic, incidence angles were selected from NASA cascade data correlations with adjustments from past design experience. The blade trailing edge angle was established by the deviation angle which was obtained from Carter's Rule applied to the camber of an equivalent two-dimensional cascade with an additive empirical adjustment, X. This adjustment is derived from aerodynamic design and performance synthesis for this general type of rotor. However, in the rotor hub, the significant turning past axial results in profile shapes that resemble impulse turbine blades. Design practice in turbine blade layout suggested that blade sections using the full empirical adjustment would result in an overturning of the flow. This overturning by the rotor would aggravate a relatively high-Mach-number/high-loading condition on the core OGV. Consequently the empirical adjustment was reduced 2° in this region. The incidence and deviation angles and the empirical adjustment angle employed in the design are shown in Figure 6.11.

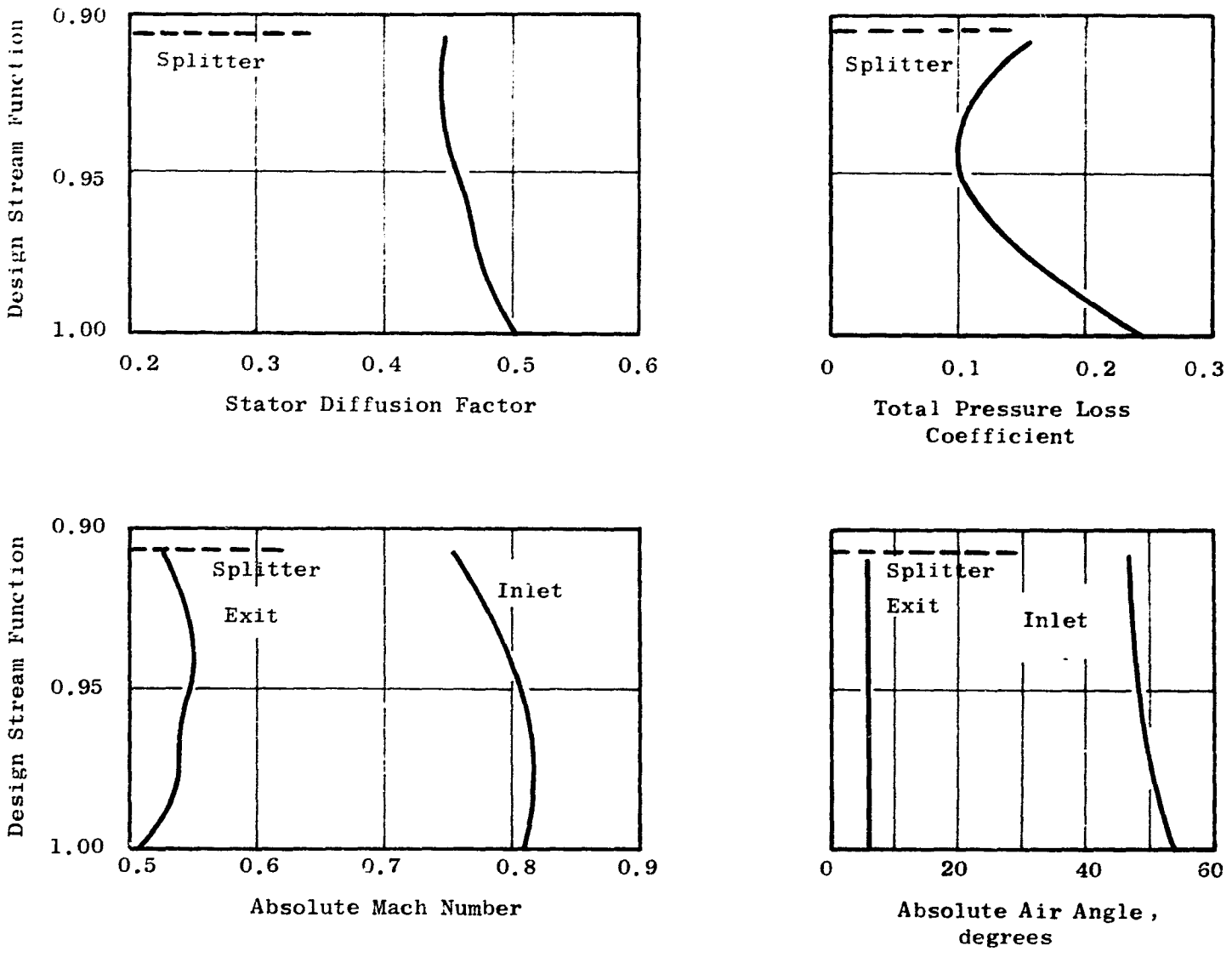

Figure 6.8. OTW Radial Distribution for Core OGV.

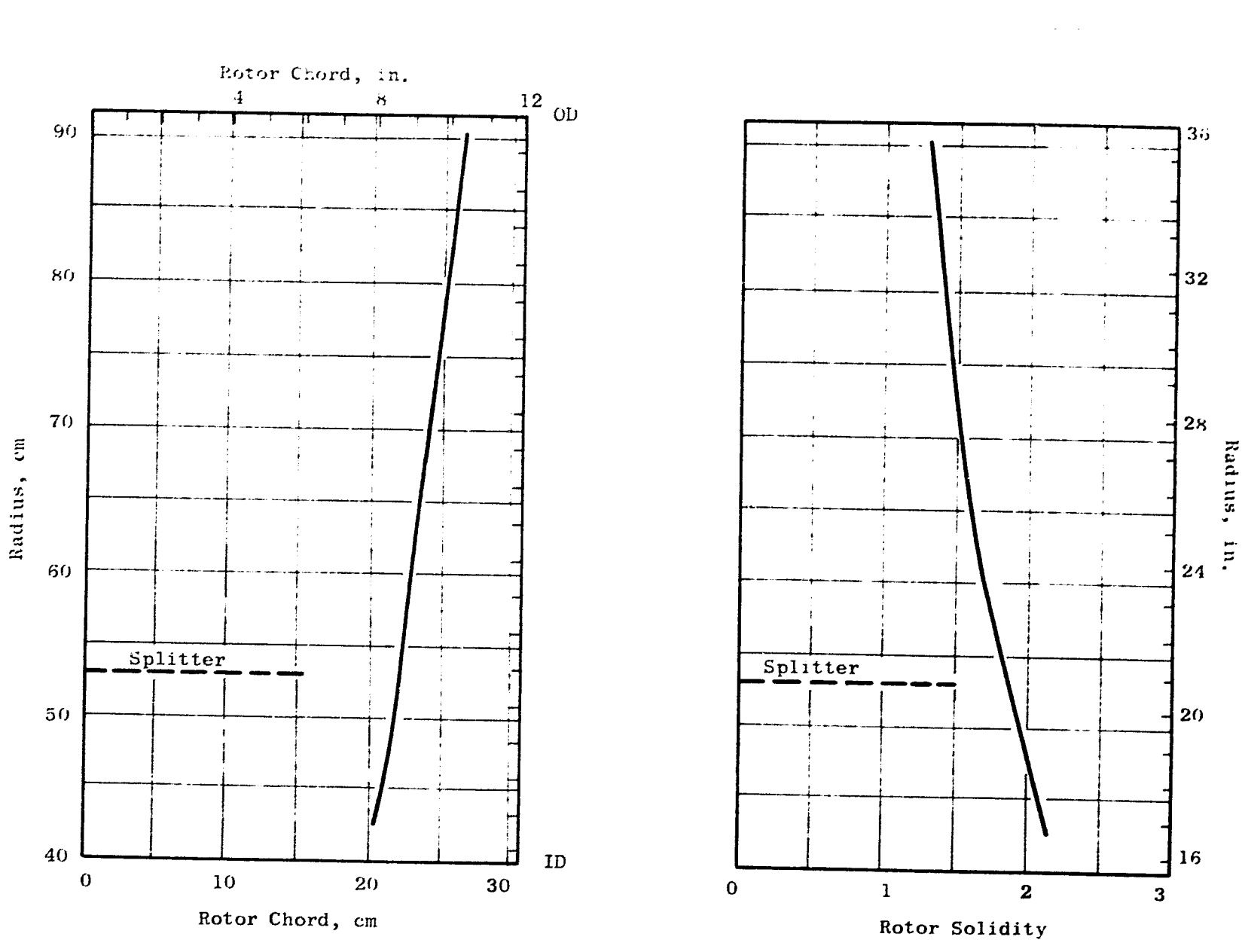

Figure 6.9. OTW Rotor Chord Distribution.

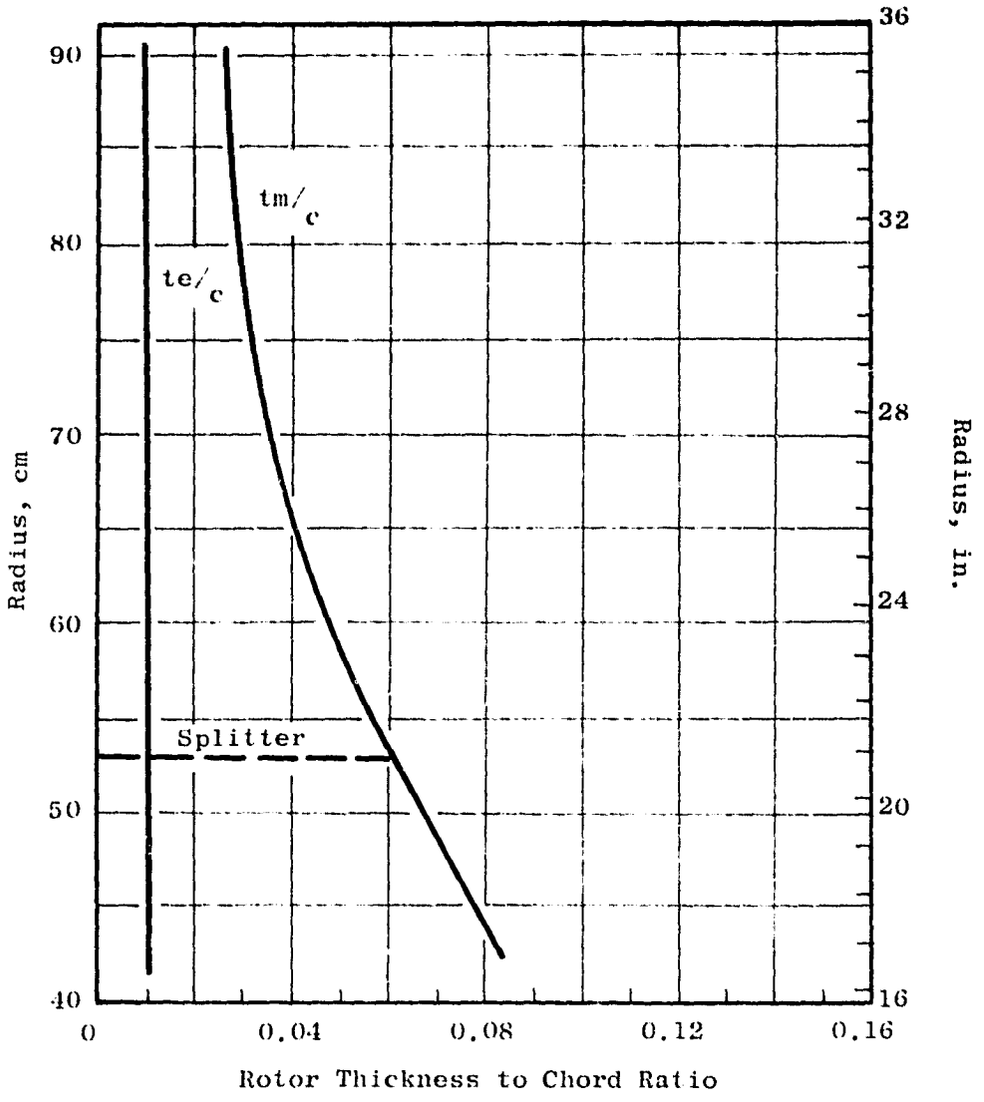

Figure 6.10. OTW Rotor Thickness Distribution.

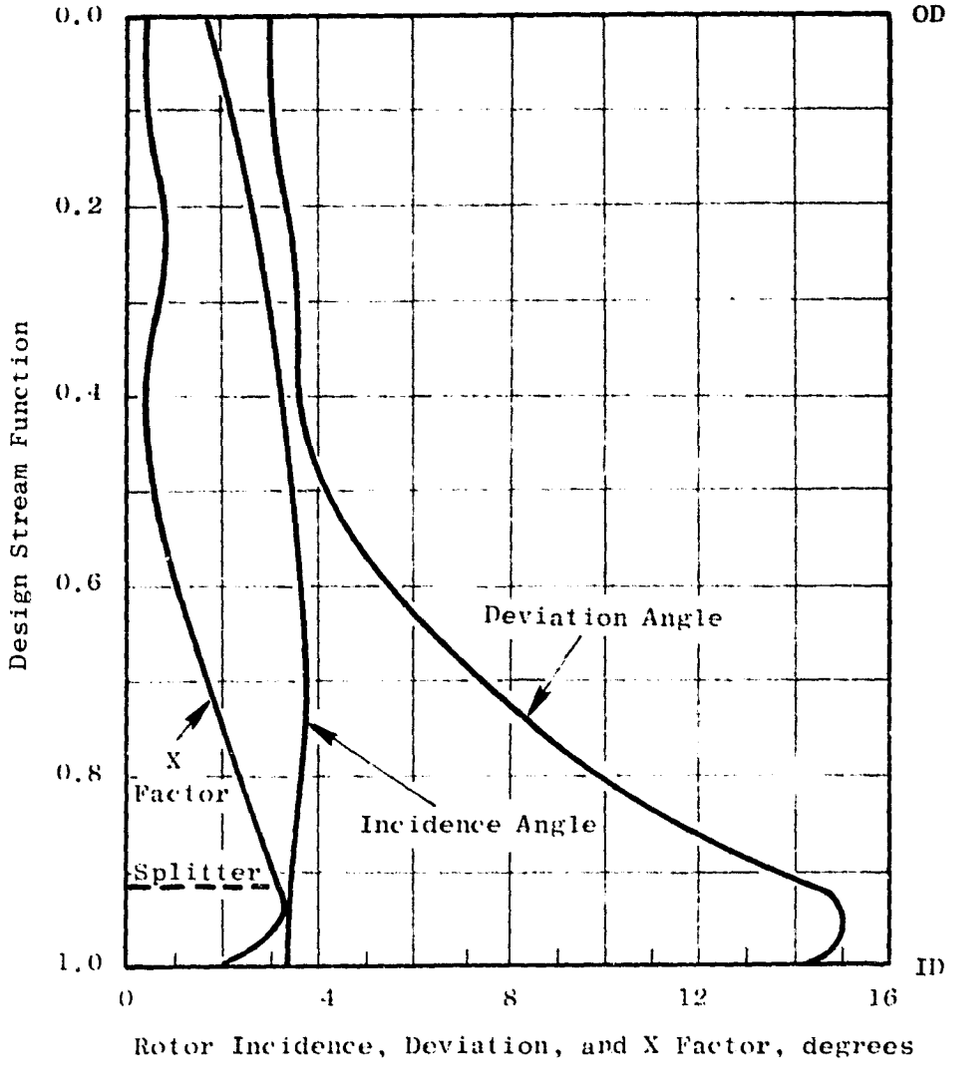

Figure 6.11. OTW Rotor Incidence, Deviation, and Empirical Adjustment Angles.

Over the entire blade span, the minimum passage area, or throat, must be sufficient to pass the design flow including allowances for boundary layer losses and flow nonuniformities. In the transonic and supersonic region, the smallest throat area, consistent with permitting the design flow to pass, is desirable since this minimizes overexpansions on the suction surface. A further consideration was to minimize disturbances to the flow along the forward portion of the suction surface to minimize forward-propagating waves that might provide an additional noise source. Design experience guided the degree to which each of these desires was applied to individual section layouts. The percent throat margin, the percentage by which the ratio of the effective throat area to the capture area exceeds the critical area ratio, is shown in Figure 6.12. The values employed are generally consistent with past experience.

The resulting blade shapes have very little camber in the tip region. In the mid-span region, the shapes generally resemble multiple circular arc sections with the majority of the camber occurring in the aft portion. In the inner region, the shapes are similar to a double circular arc. Figure 6.13 shows plane sections through the blade at several radial locations. The resulting camber and stagger radial distributions are shown in Figure 6.14.

6.6 CORE OGV DESIGN

A moderately low aspect ratio of 1.3 was selected for the core portion OGV to provide a rugged mechanical system. This selection was in recognition of the potentially severe aeromechanical environment of the core OGV, i.e., large rotor blade wakes, because of its small size in relationship to that of the rotor blade. A solidity at the ID of 2.24 was selected to yield reasonable levels of diffusion factor, Figure 6.8. The number of OGV's which results is 156.

Profiles for the core OGV are multiple circular arcs. The incidence angle over the outer portion of the span was selected from a correlation of the NASA low-speed cascade data. Locally, in the ID region, the incidence angle was reduced 4°. This local reduction in incidence was in recognition of traverse data results on other high bypass fan configurations which show core stator inlet air angles several degrees higher than the axisymmetric calculated values. The deviation angle was obtained from Carter's Rule as was described for the rotor blade, but no empirical adjustment was made. The resulting incidence and deviation angles are shown in Figure 6.15. An average throat area 5% greater than the critical contraction ratio was employed in the design. The throat area margin is shown in Figure 6.15. Locally, in the ID region, the margin is zero for the axisymmetric vector diagrams. However, as noted above, the anticipated inlet air angle in this region will be several degrees higher; and, therefore, the capture area will be several percent lower than the axisymmetric calculation. The effective throat-to-capture area ratio, therefore, will increase to provide adequate margin.

The multiple circular arc mean line consisted of a maximum radius arc forward of the throat, which occurs at the passage leading edge. This arc

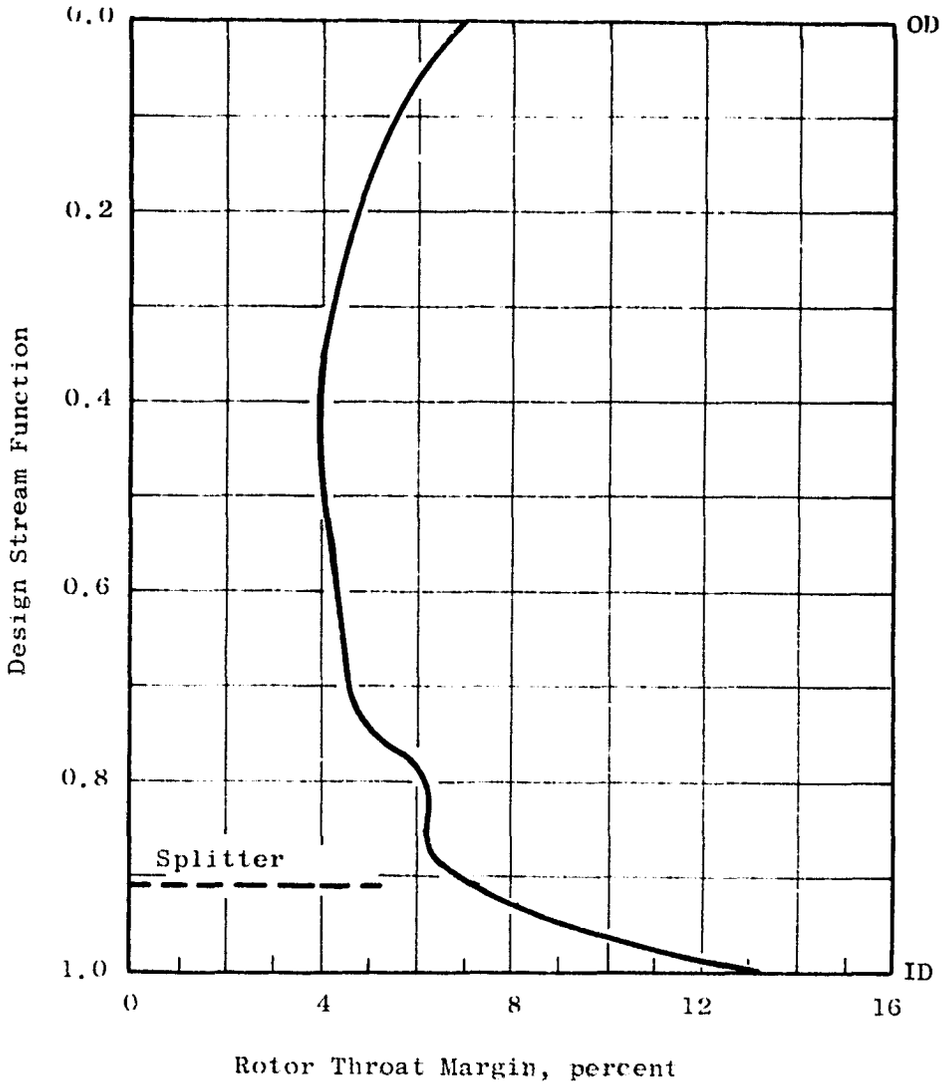

Figure 6.12. OTW Rotor, Percent Throat Margin.

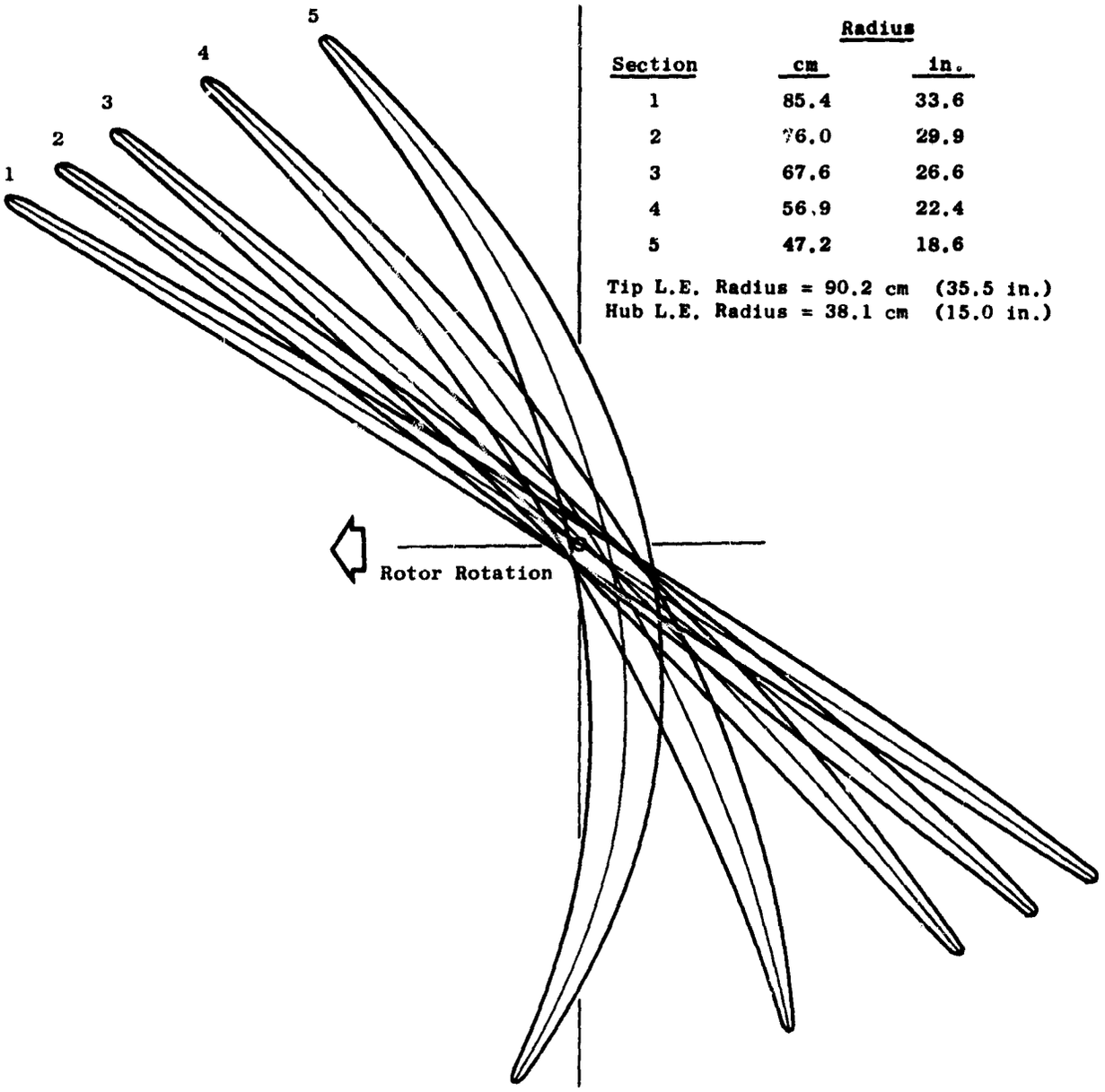

Section	Radius cm	Radius in.
1	85.4	33.6
2	76.0	29.9
3	67.6	26.6
4	56.9	22.4
5	47.2	18.6

Tip L.E. Radius = 90.2 cm (35.5 in.)
Hub L.E. Radius = 38.1 cm (15.0 in.)

Figure 6.13. OTW Fan Blade Plane Sections.

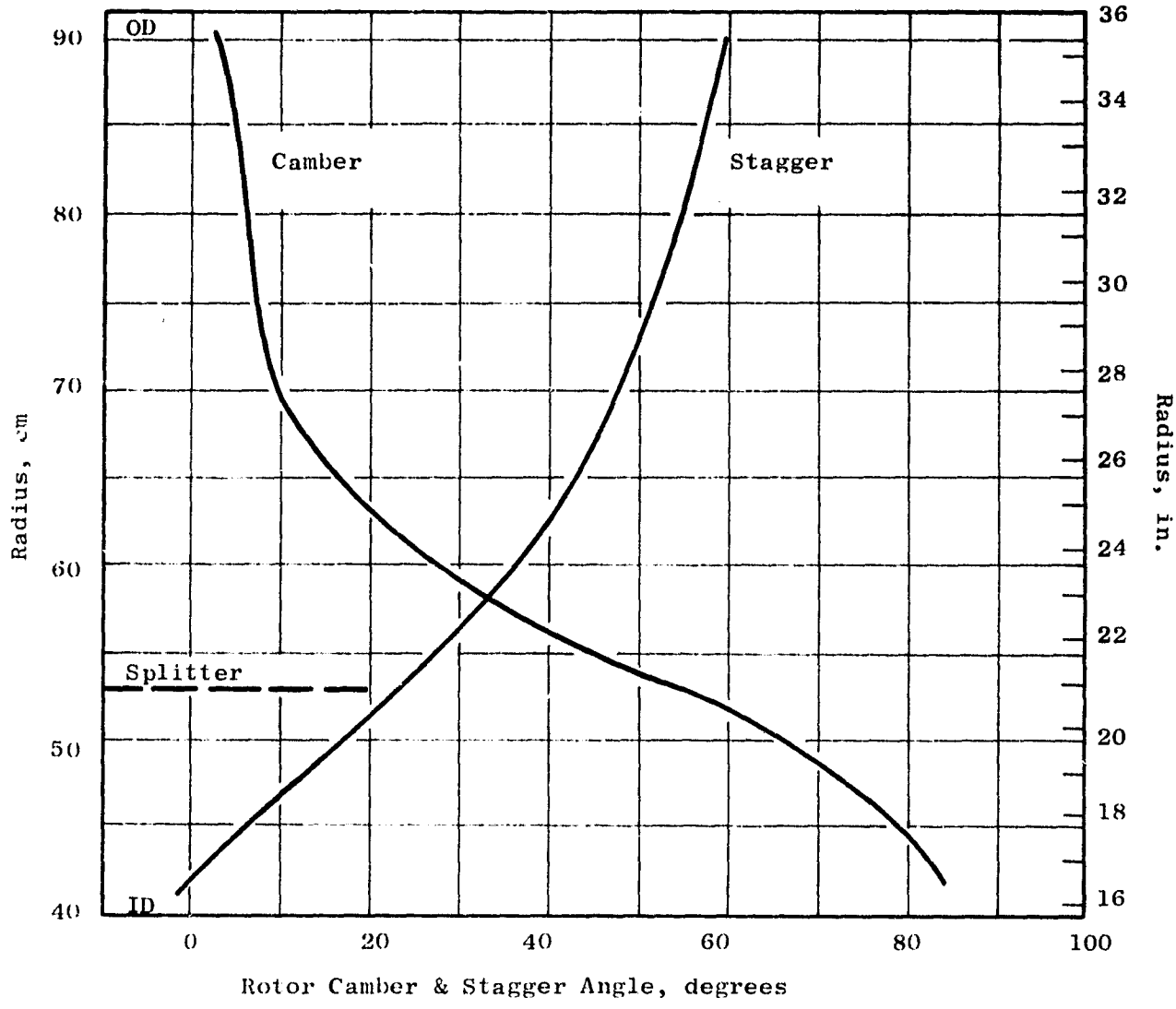

Figure 6.14. OTW Camber and Stagger Radial Distribution.

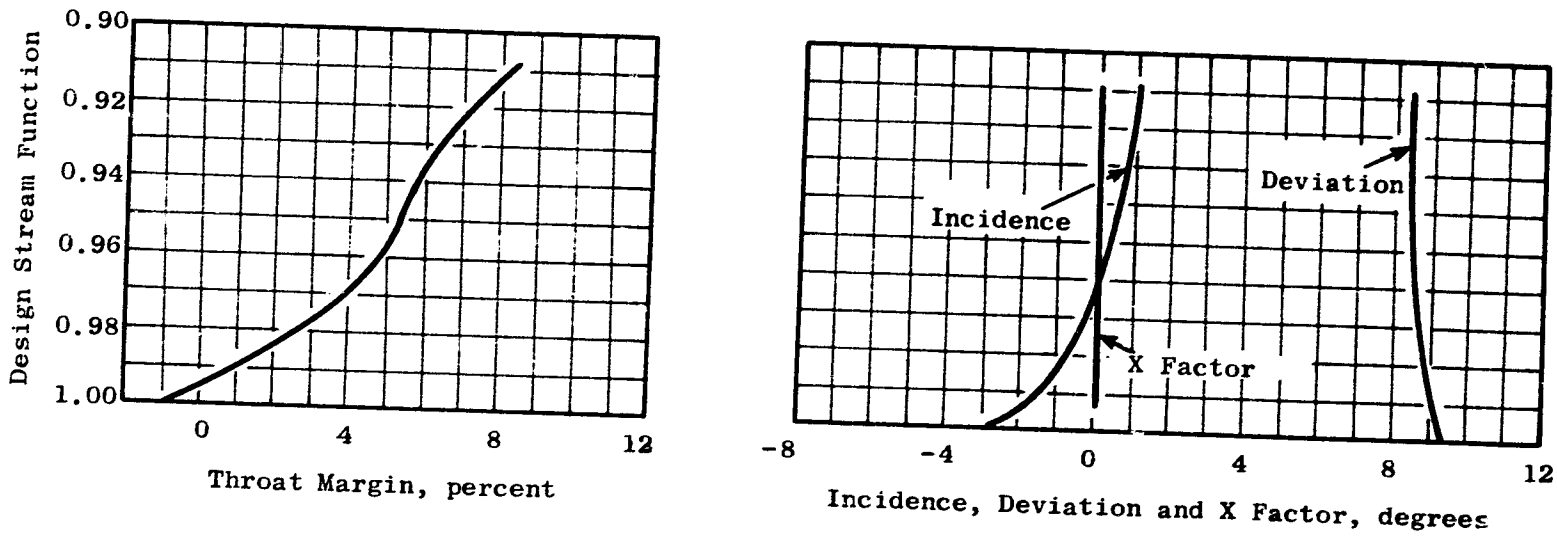

Figure 6.15. OTW Core OGV Aero Design Characteristics.

was determined by the incidence and throat area selection. A small blend region transitioned into a second arc prescribed by the overall camber requirement. The resulting radial distributions of camber, stagger, solidity, chord, and thickness-to-chord ratio are given in Figure 6.16. Figure 6.17 is a cylindrical section of the OGV at the pitch-line radius.

6.7 TRANSITION DUCT STRUT DESIGN

The transition duct flowpath is shown in Figure 6.18. It is common to both the UTW and OTW engines. The ratio of duct exit to duct inlet flow area is 1.02. There are six struts in the transition duct which are aerodynamically configured to remove the 0.105 radian (6°) of swirl left in the air by the core OGV's and to house the structural spokes of the composite wheels (see Figure 6.2). In addition, at engine station 196.5 (Figure 6.2), the 6 and 12 o'clock strut positions must house radial accessory drive shafts. The number of struts and axial position of the strut trailing edge were selected identical with the F101 engine to minimize unknowns in the operation of the core engine system. The axial positions and thickness requirements of the composite wheel spokes were dictated by mechanical considerations. The axial location of the strut leading edge at the OD was determined by its proximity to the splitter leading edge in the UTW engine configuration. At the OD flowpath, the strut leading edge is 17.8 mm (0.7 in.) forward of the wheel spoke. A relatively blunt strut leading edge results from the 26.7 mm (1.05 in.) wheel spoke thickness requirement. The wheel spoke is radial. The axial lean of the strut leading edge provides relief from the LE bluntness at lower radii and makes the LE approximately normal to the incoming flow. A NASA 65-series thickness distribution was selected for the basic profile thickness which was modified for the special considerations required in this design. The strut thickness is the same for all radii aft of the forward shell spoke LE (Figure 6.18) to facilitate fabrication. A cylindrically cut cross section showing the strut geometry at three radii is shown in Figure 6.19. The thickness distribution for the 6 and 12 o'clock struts was modified for the envelope of the radial drive shaft. The leading edge 40% chord of these further modified sections is identical to that of the nominal strut geometry; and, aft of the forward shell spoke LE, the strut thickness is the same for all radii. The core engine has demonstrated operation in the presence of a similar thick strut in the F101 application without duress.

6.8 VANE/FRAME DESIGN

The vane/frame performs the dual function of an outlet guide vane for the bypass flow and a frame support for the engine components and nacelle. It is a common piece of hardware for both the UTW and OTW engine fans. It is integrated with the pylon which houses the radial drive shaft at engine station 196.50 (see Figure 6.2), houses the engine mount at approximate engine station 210, provides an interface between the propulsion system with the aircraft system, and houses the forward thrust links. The vane/frame, furthermore, acts as an inlet guide vane for the UTW fan when in the reverse mode of operation.

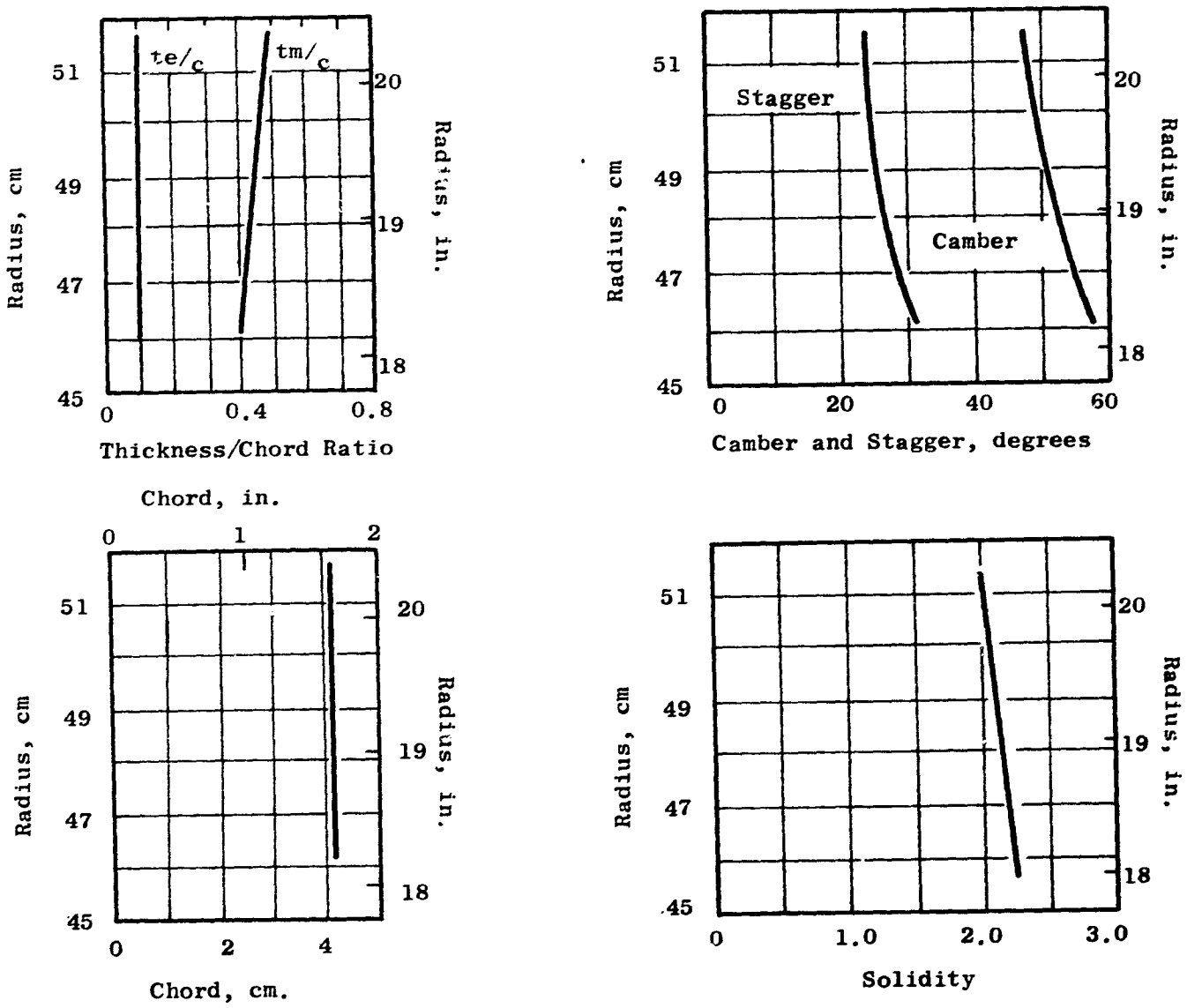

Figure 6.16. OTW Core OGV Aero Design Characteristics.

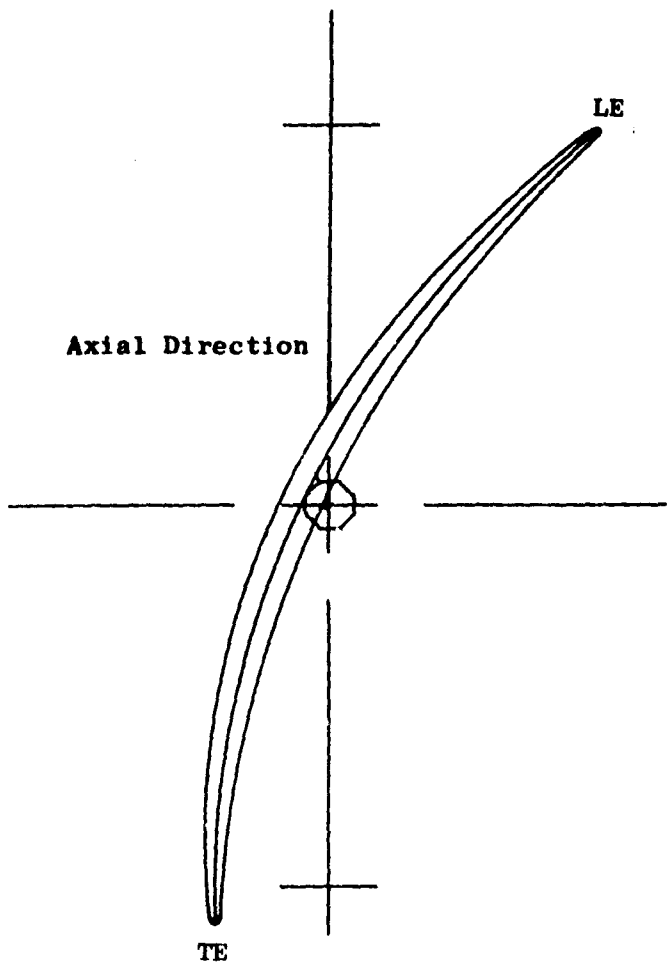

Figure 6.17. Cyclindrical Section of OTW Core OGV at the Pitch Line Radius.

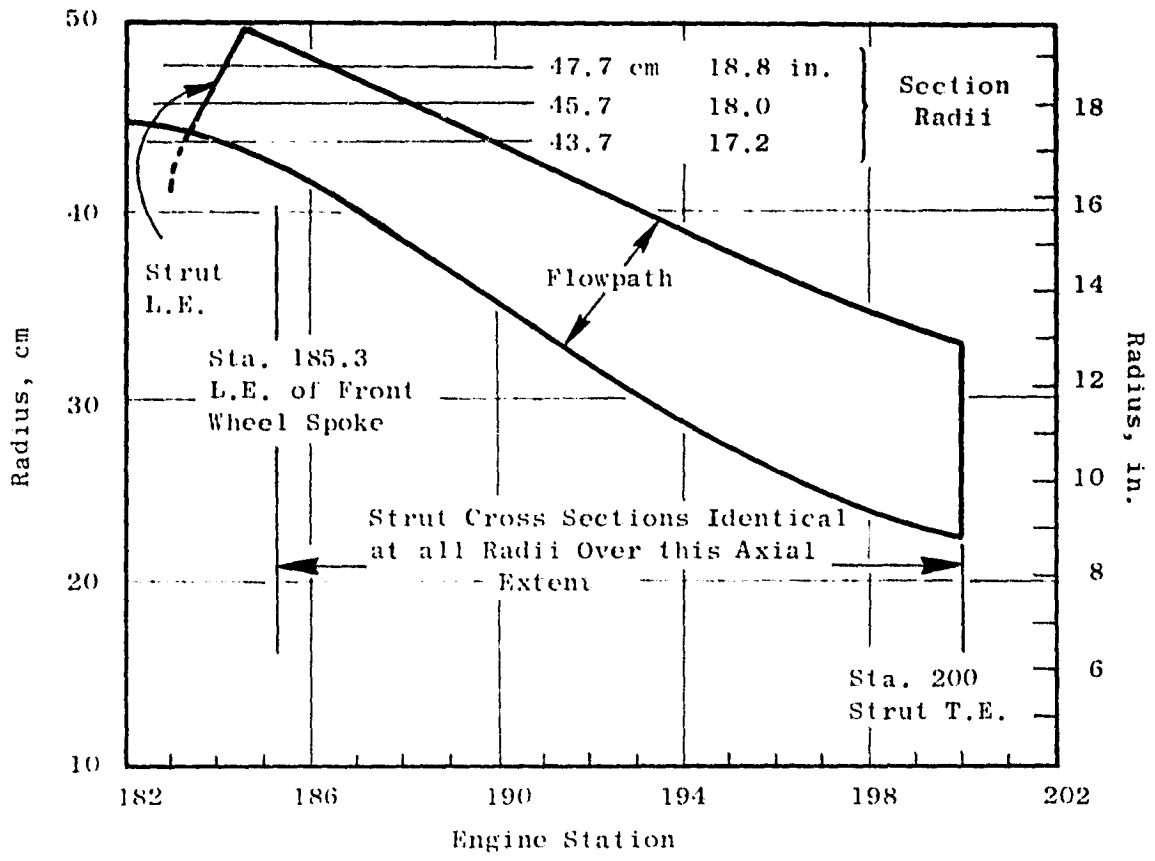

Figure 6.18. Transition Duct Flowpath.

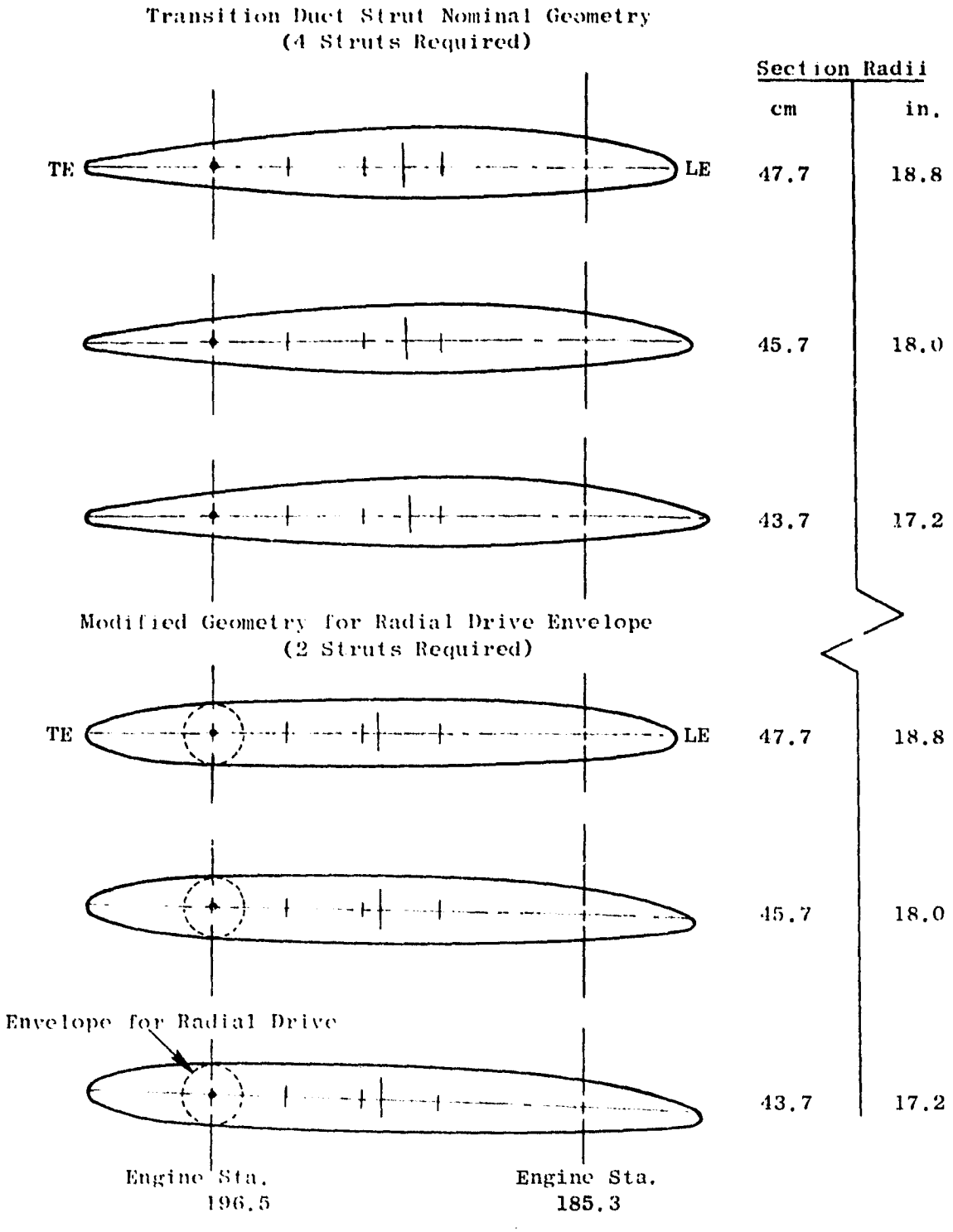

Figure 6.19. Nominal and Modified Transition Duct Strut.

A conventional OGV system turns the incoming flow to axial. Housing requirements of the pylon dictate a geometry which requires the OGV's to underturn approximately 0.174 radian (10°) on one side and to overturn approximately 0.174 radian (10°) on the other side. The vanes must be tailored to downstream vector diagrams which conform to the natural flow field around the pylon to avoid creating velocity distortions in the upstream flow. Ideally, each vane would be individually tailored. However, to avoid excessive costs, five vane geometry groups were selected as adequate.

The Mach number and air angle at inlet to the vane/frame are shown in Figure 6.20 for both the UTW and OTW fans. In the outer portion of the bypass duct annulus, the larger air angle in the UTW environment results in a less negative incidence angle than for the OTW environment. Mach number in the outer portion of the annulus is also higher in the UTW environment. When selecting incidence angles, a higher Mach number environment naturally leads to the desire to select a less negative incidence angle. The amount by which the incidence angle would naturally be increased, due to the higher Mach number UTW environment, is approximately equal to the increase in the inlet air angle of the UTW environment. In the inner portion of the annulus, the inlet Mach number and air angle are higher for the OTW environment. The natural increase in incidence angle desired because of the higher Mach number is approximately the same as the increase in the inlet air angle. As a result of these considerations, no significant aerodynamic performance penalty is assessed to using common hardware for both the UTW and OTW fans.

Locally, near the bypass duct ID, there is a discontinuity of the aerodynamic environment of the UTW configuration. This discontinuity represents that portion of the flow which passes under the island but bypasses the splitter. The calculation ignored mixing across the vortex sheet. In the design of the vane geometry no special considerations were incorporated because of this discontinuity, since it is believed that in a real fluid the mixing process will greatly diminish the vortex strength.

The vane chord at the OD was selected largely by the mechanical requirement of axial spacing between the composite frame spokes. At the ID the vane leading edge was lengthened primarily to obtain an aerodynamically reasonable leading edge fairing on the pylon compatible with the envelope requirements of the radial drive shaft. The ID region is significantly more restrictive in this regard because of choking considerations, particularly for the OTW environment, with the reduced circumferential spacing between vanes. The solidity resulting from 33 vanes, an acoustic requirement, was acceptable from an aerodynamic loading viewpoint as shown in Figure 6.21. The two diffusion factor curves are a result of the two aerodynamic environments, UTW and OTW, to which the common vane/frame geometry is exposed. The thickness is a modified NASA 65-series distribution. Maximum-thickness- and trailing-edge-thickness-to-chord ratios of 0.08 and 0.02, respectively, were selected at the OD. The same maximum thickness and trailing edge thickness were used at all other radii which results in a maximum-thickness- and trailing-edge-thickness-to-chord ratios of 0.064 and 0.016, respectively, at the ID.

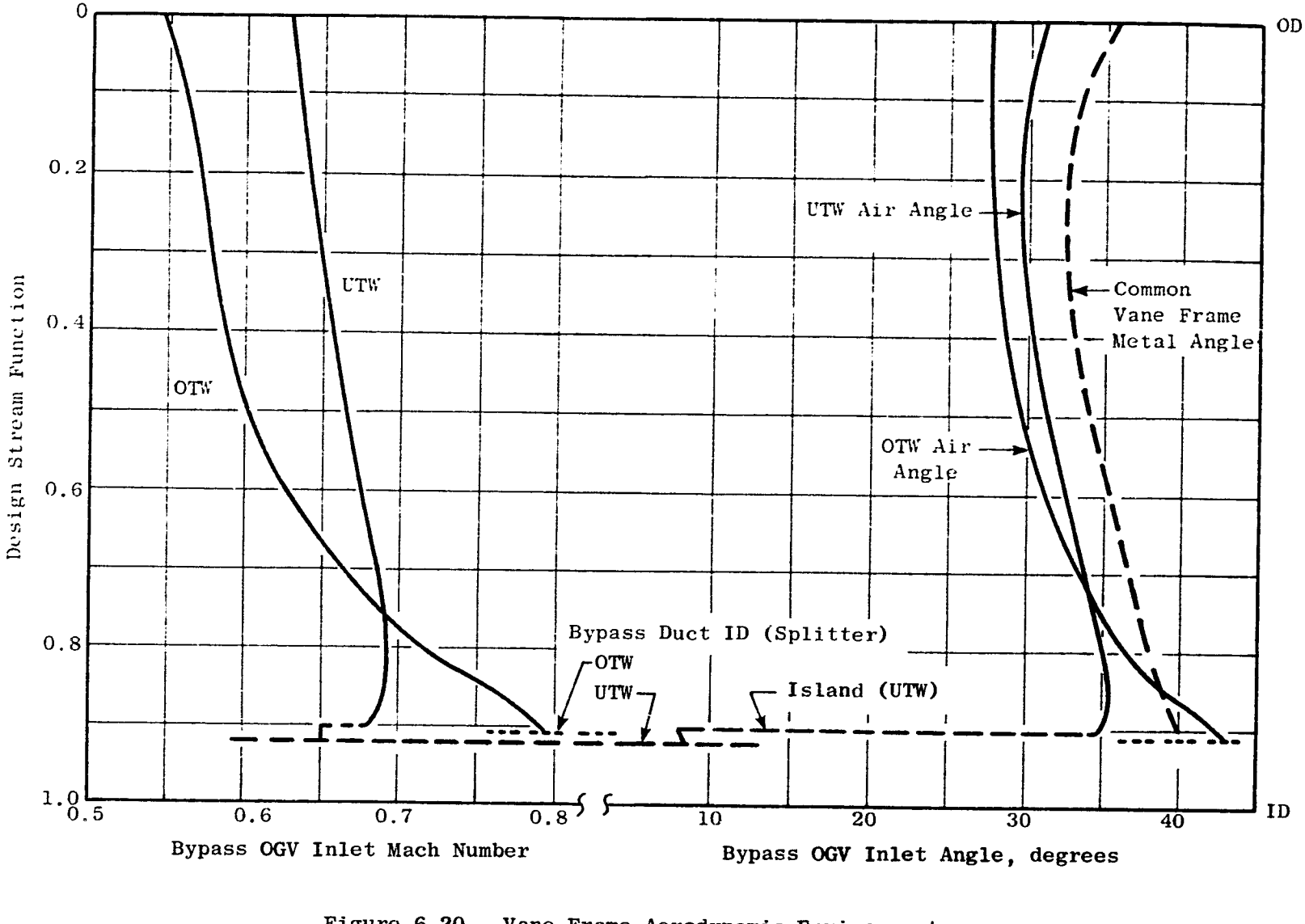

Figure 6.20. Vane Frame Aerodynamic Environment.

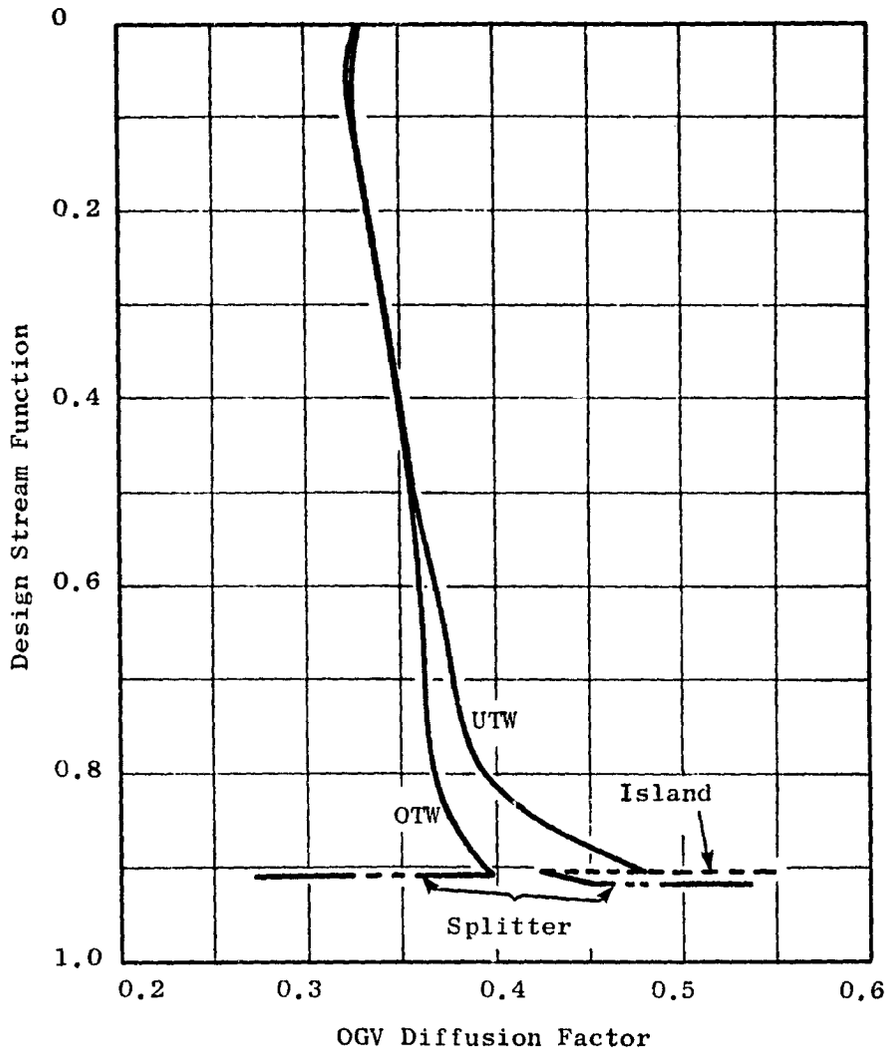

Figure 6.21. Diffusion Factors for Vane-Frame Nominal Vane Configuration.

As a guide in the selection of the overall vector diagram requirements of the vane/frame, a circumferential analysis of an approximate vane geometry, including the pylon, was performed. This analysis indicated that, for uniform flow at vane inlet, the vane discharge Mach number was approximately constant circumferentially and that the discharge air angle was nearly linear circumferentially between the pylon wall angles. Figure 6.22, an unwrapped cross section at the ID, shows the flow-field calculated by this analysis. The specific design criteria selected for the layout of the five-vane geometry groups was to change the average discharge vector diagram with zero swirl to vector diagrams with $\pm$ 5° of swirl and $\pm$ 10° of swirl.

The meanline shapes for each of the five-vane groups vary. For the vane group which overturns the flow by +10°, the meanline is approximately a circular arc. As a result of passage area distribution and choking considerations, the meanline shape employed in the forward 25% chord region of this vane group was retained for the other four groups.

The incidence angle for all vane groups was the same and was selected for the group with the highest camber. A correlation of NASA low-speed cascade data was the starting point for the incidence selection. Over the outer portion of the vane, where the inlet Mach number is lower, the incidence angles were slanted to the low side of the correlation. This was done in consideration of the reverse thrust mode of operation for the UTW fan. In this mode, the OGV's impart a swirl counter to the direction of rotor rotation. Additional vane leading edge camber tends to increase the counter-swirl and, therefore, the pumping capacity of the fan. In the inner portion of the vane the incidence angles are higher than suggested by the correlation because of the higher inlet Mach number. Also, in the reverse mode of operation, this reduction in vane leading edge camber in the ID region reduces the swirl for that portion of the fluid which enters the core engine and tends to reduce its pressure drop.

The deviation angle for each of the five vane groups was calculated from Carter's Rule as described for the rotor. The portion of the meanline aft of the 25% chord point approximates a circular arc blending between the front circular arc and the required trailing edge angle. For the vane group which underturns the flow by 10°, the aft portion of the blade has little camber. Figure 6.23 shows an unwrapped cross section at the ID of two of the 10° overcambered vanes and two of the 10° undercambered vanes adjacent to the pylon. Note that the spacing between the pylon and the first undercambered vane is 50% larger than average. This increased spacing was required to open the passage internal area, relative to the capture area, to retrieve the area blocked by the radial drive shaft envelope requirements.

The radial distributions of camber and stagger for the nominal and two extreme vane geometries are shown in Figure 6.24. The radial distributions of chord and solidity for the nominal vane are shown in Figure 6.25. The design held the leading and trailing edge axial projection common for all five groups which results in slightly different chord lengths for the other four vane types.

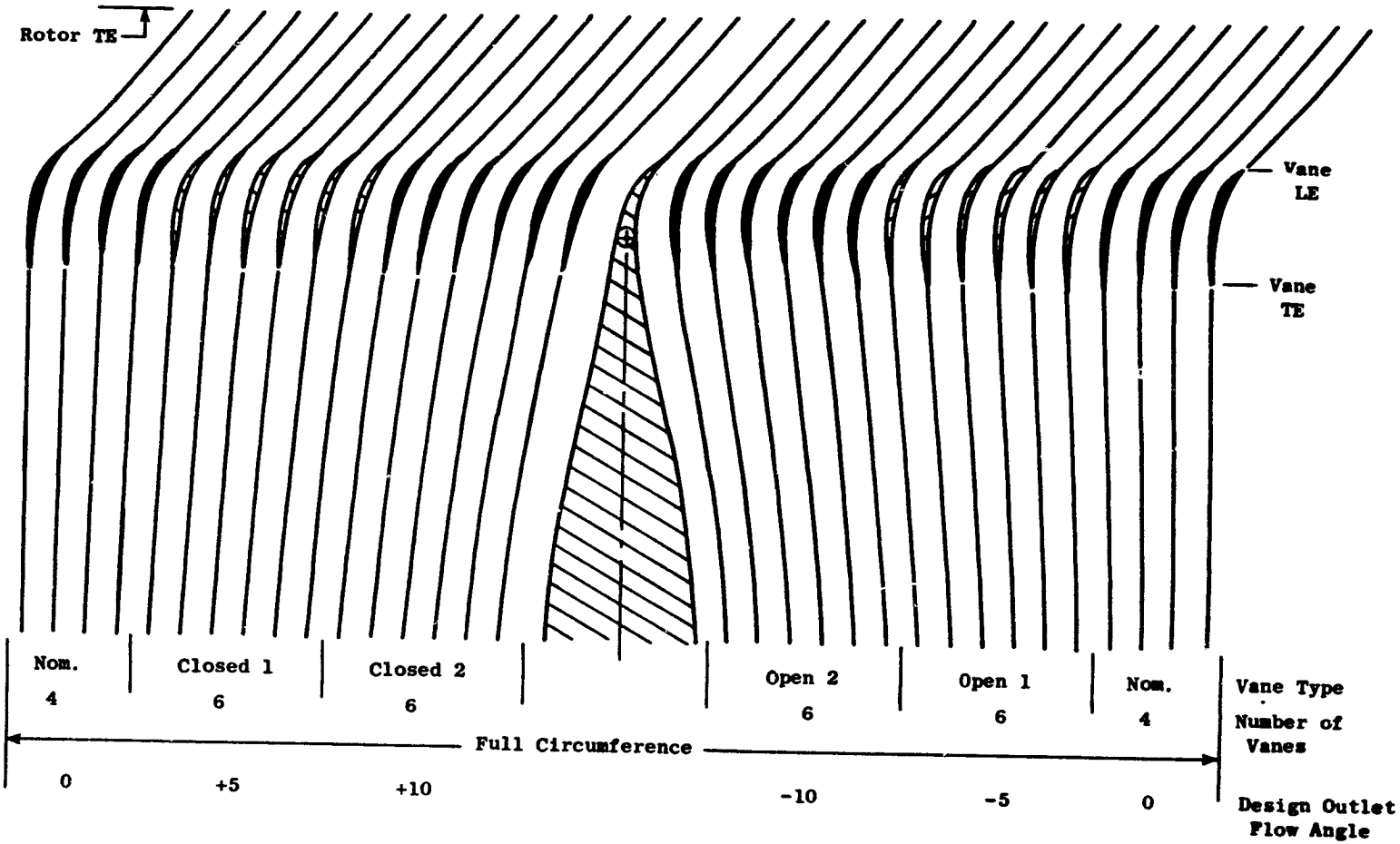

Figure 6.22. Vane Frame Unwrapped Section at I.D.

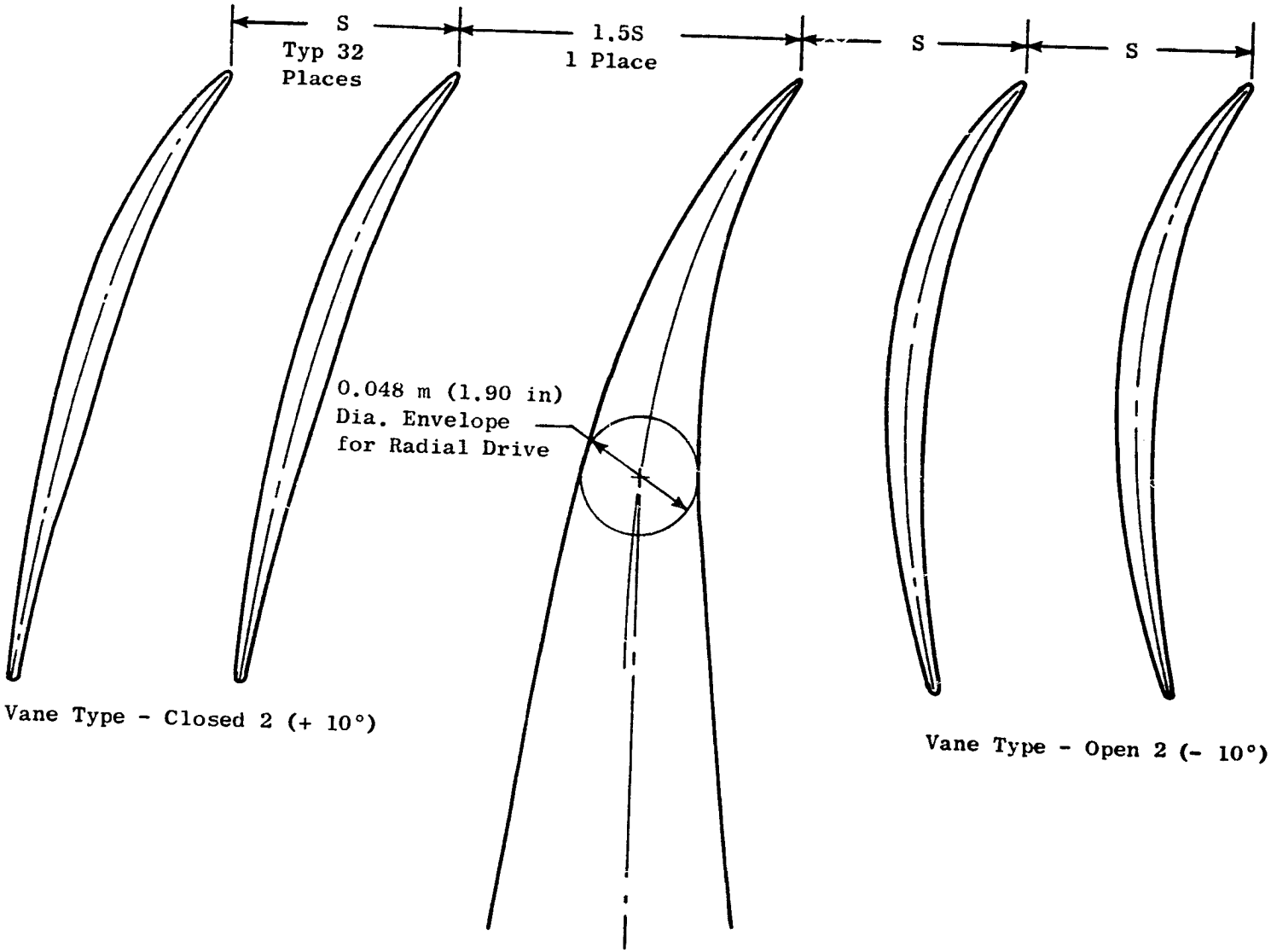

Figure 6.23. Vane-Frame Unwrapped Section at ID, 32 Vanes Plus Pylon LE Fairing.

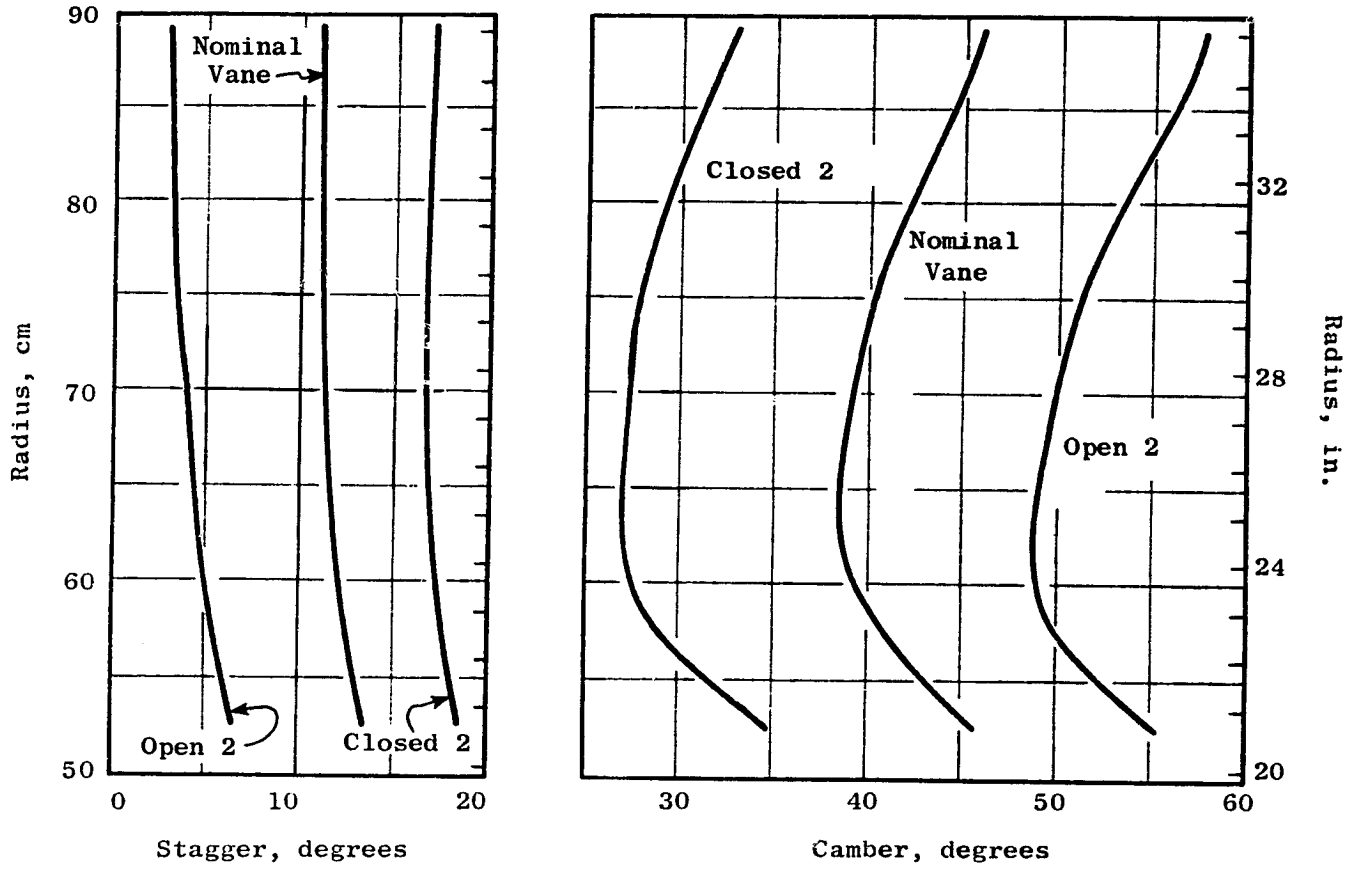

Figure 6.24. QCSEE Vane Frame.

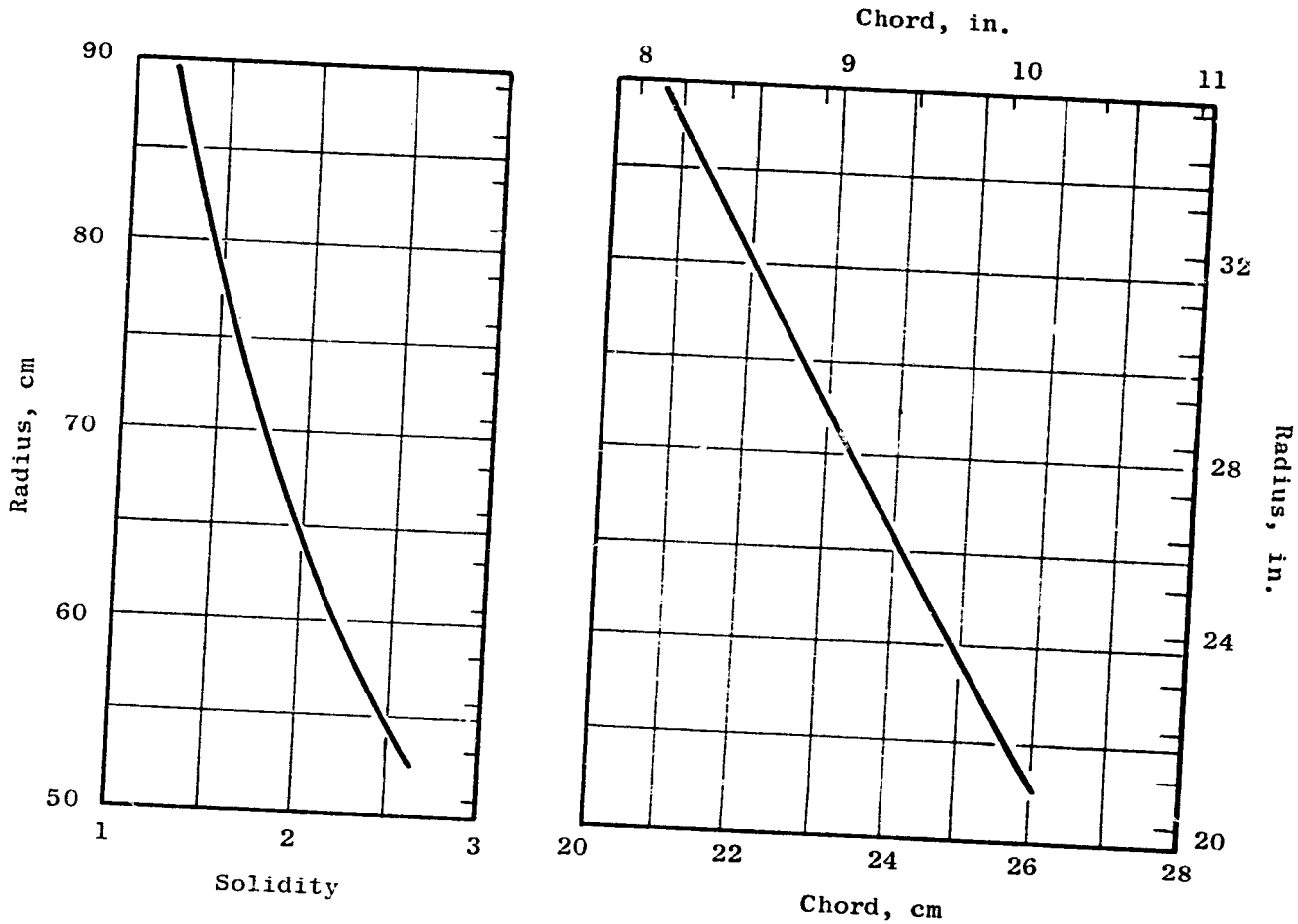

Figure 6.25. QCSEE Vane Frame.

SECTION 7.0

FAN MECHANICAL DESIGN

7.1 SUMMARY

The OTW experimental fan has 28 fixed-pitch metal blades with a 180-cm (71-in.) fan tip diameter similar to that of UTW fan. This rotor is shown in Figure 7.1. The conceptual design of this is based on using composite fan blades, but metal blades will be used for reasons of economy and low risk. The conceptual composite blade design dictates the absence of blade shrouds, determines the number of fan blades, and affects the sizing of such parameters as the blade solidity, reduced velocity, and leading edge thickness. In the flight engine, composite blades would be substituted for the metal blades without aerodynamic change or compromise in the composite blade mechanical design. While the demonstrator fan disk is heavier than the composite bladed flight weight disk, it reflects a flight configuration in both design criteria and material selection. A comparison between the experimental and flight OTW fan design criteria is given in Table 7-I.

The OTW fan has both a forward rotating spinner and aft flowpath adapter. The inner flowpath formed by these two parts and the blade platform is identical to the inner flowpath of the UTW fan from a point near the blade trailing edge aft. The tip speed of the OTW fan is about 17% higher than that of the UTW fan.

The fan blades and disk are fabricated of 6-4 titanium. 6-4 titanium couplings on the fore and aft sides of the disk isolate the relatively high stresses in the disk from the 6061 aluminum forward and aft spinners. Increased blade retention capability is provided to prevent axial movement of the blades (benefiting from General Electric experience in large fan design). Fan rotor materials and allowable stresses are shown in Figure 7.2.

Two-plane balance of the fan rotor will be provided at the forward and aft disk flanges. In addition, the forward spinner will be permanently balanced in two planes. Blade retainers will be pan weighted and blades will be moment weighed, all to be preprogrammed into the rotor. Final trim balancing or field balancing is accomplished through balance bolts mounted in the spinner.

7.2 DESIGN REQUIREMENTS

Design life of the fan rotor is 36,000 hours, including 48,000 flight cycles and 1000 full-power ground cycles. To match the rotor low cycle fatigue life to these design requirements, stress levels were kept to appropriate levels, and contouring and flange scalloping were used to minimize stress concentrations.

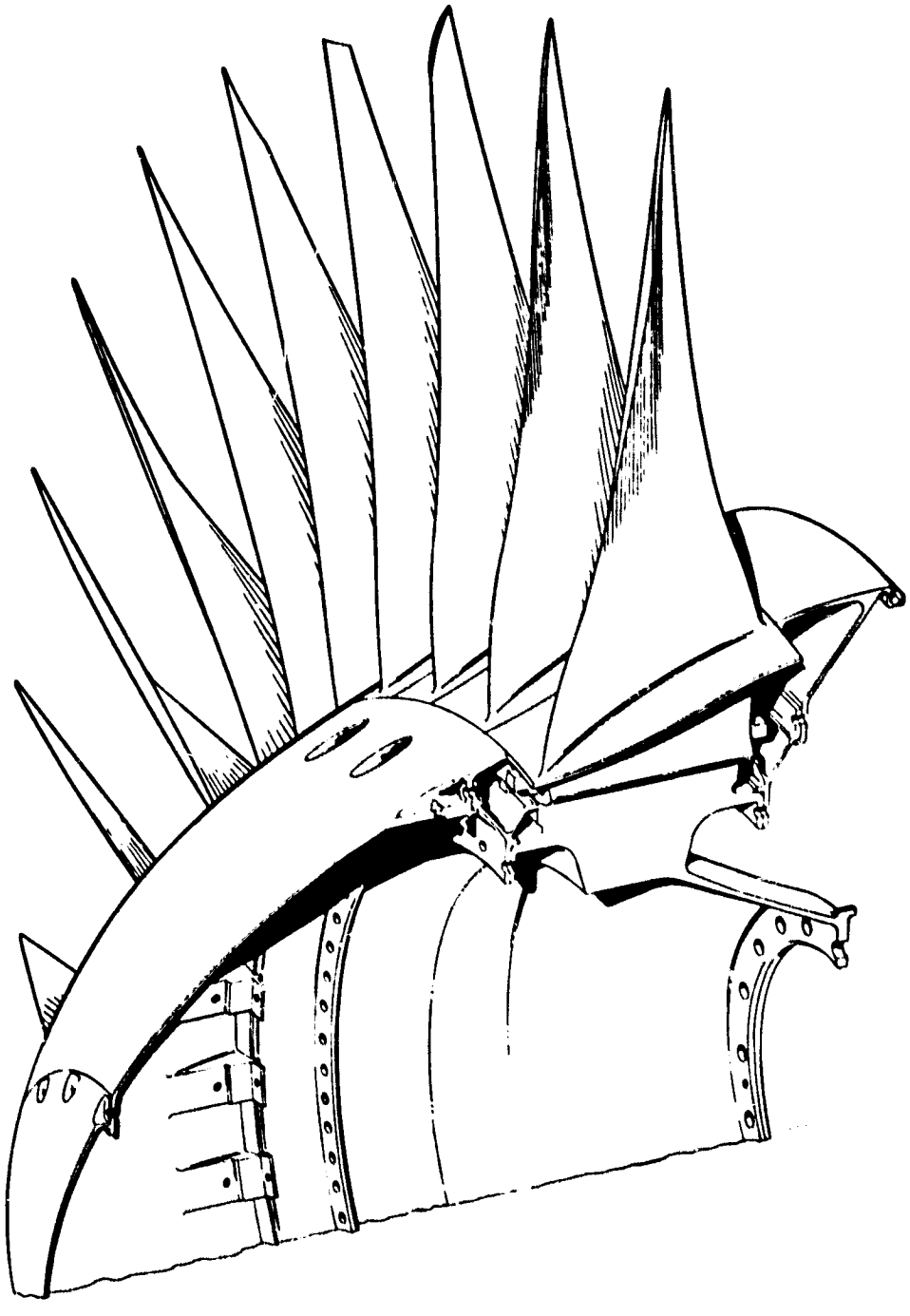

Figure 7.1. OTW Fan Rotor.

Table 7-I. QCSEE OTW Fan Design Criteria.

Component	Materials	
	Demonstrator	Flight
Disk	Titanium	Titanium
Blades	Titanium	Composite
Number of Blades	28	28
Per Blade Centrifugal Load, N (lb)	558,696 (125,600)	184,156 (41,400)
Design Point Speed, rpm	3792	3792
Design Burst Speed, rpm	5615	5615
Disk Low-Cycle Fatigue Life (Minimum)	>48,000 Flight Cycles	>48,000 Flight Cycles
Disk Low-Cycle Fatigue Life with Initial 0.025 × 0.076 cm (0.01 × 0.03 in.) Defect	>16,000 Flight Cycles	>16,000 Flight Cycles

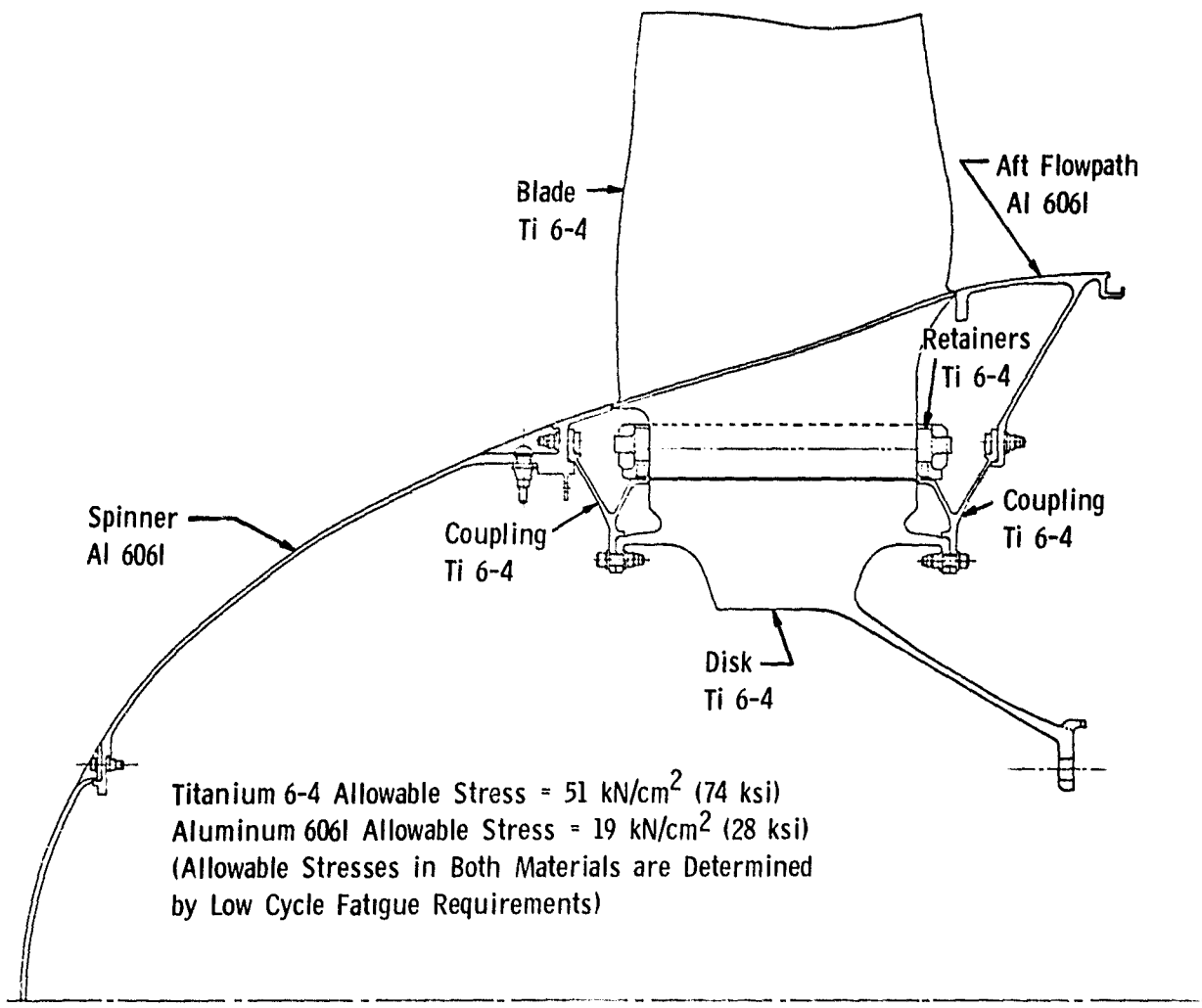

Figure 7.2. OTW Rotor Layout.

Fan blades can be individually replaced without removal of the fan rotor. Openings in the aft flowpath support permit access for the removal of the entire fan rotor package and gearbox.

7.3 FAN BLADE DESIGN

The OTW fan blades (Figure 7.3) are machined from 6-Al-4V titanium forgings, a finished blade weighing 5.94 kg (13.1 lb). Blade geometry is summarized in Table 7-II and Figures 7.4 and 7.5. Operating steady-state stresses are summarized in Figure 7.6 and Table 7-III. Blade airfoil stresses and vibratory frequencies were calculated by the use of standard General Electric mechanical design programs in the computer library. These include a twisted blade program for calculating airfoil stresses and frequencies and a shell program to determine blade root boundary conditions due to the flexibility of the disk and adjacent shells. Blade dovetail and disk poststresses were calculated by a computer time-sharing program based on the dovetail analysis of Dr. H.J. Macke (Report Nos. R59FPD611 and R63FPD21).

The steady-state effective stress shown in Figure 7.6 is composed of the resultant of bending, induced tensile, and centralized stresses. This permits a level of vibratory stress consistent with GE practice (minimum of 6.9 kN/cm^2 or 10 ksi, as shown in Figure 7.11). Since the blade leading and trailing edges are in compression except at the root, where the tensile stresses are very low, the blade is rather insensitive to foreign object damage on the edges. At the root, assuming damage that will produce a stress concentration of 3, the blade is capable of tolerating a vibratory stress of 31 kN/cm^2 (45 ksi) single amplitude. The uncorrected gas bending stress is an indicator of stall stress levels; in the case of the OTW fan blade, the stall stress is projected to be less than the allowable vibratory stress.

The fan blades are a "low-flexed" design, i.e., the first flexural frequency of the blades crosses the two per rev line in the fan operating speed range. Without a thicker blade root, which would have been aerodynamically unsatisfactory, low-flexing was necessary because of the lack of blade shrouds. This approach, though not common, is used successfully on General Electric's TF34 fan and J79 stage 1 compressor blade and was successful on NASA's Quiet Engine C fan. The blade Campbell diagram is shown in Figure 7.7. The frequency of the disk-blade assembly (dashed lines) is somewhat lower than the fixed blade frequency (solid lines) due to the flexibility of the supporting fan disk. The frequency margin between the N=2 disk-blade mode and the two per rev resonance line is 19 percent at 100% fan speed. The two per rev resonance crossover occurs at about 66% speed which is in the flight idle range. However, in the experimental engine which is not a flight engine, there will be no reason to operate other than transiently in this speed range, so no problem is anticipated. In a flight engine utilizing composite blades, the resonant frequency of the blade is subject to some adjustment by a rearrangement and recomposition of the fabric plies; also, the flight idle speed of the engine can be varied somewhat. Experience with the 20 inch UTW simulator which had a similar low flex blade design showed that the vibratory stresses at crossover were only 30% of scope limits.

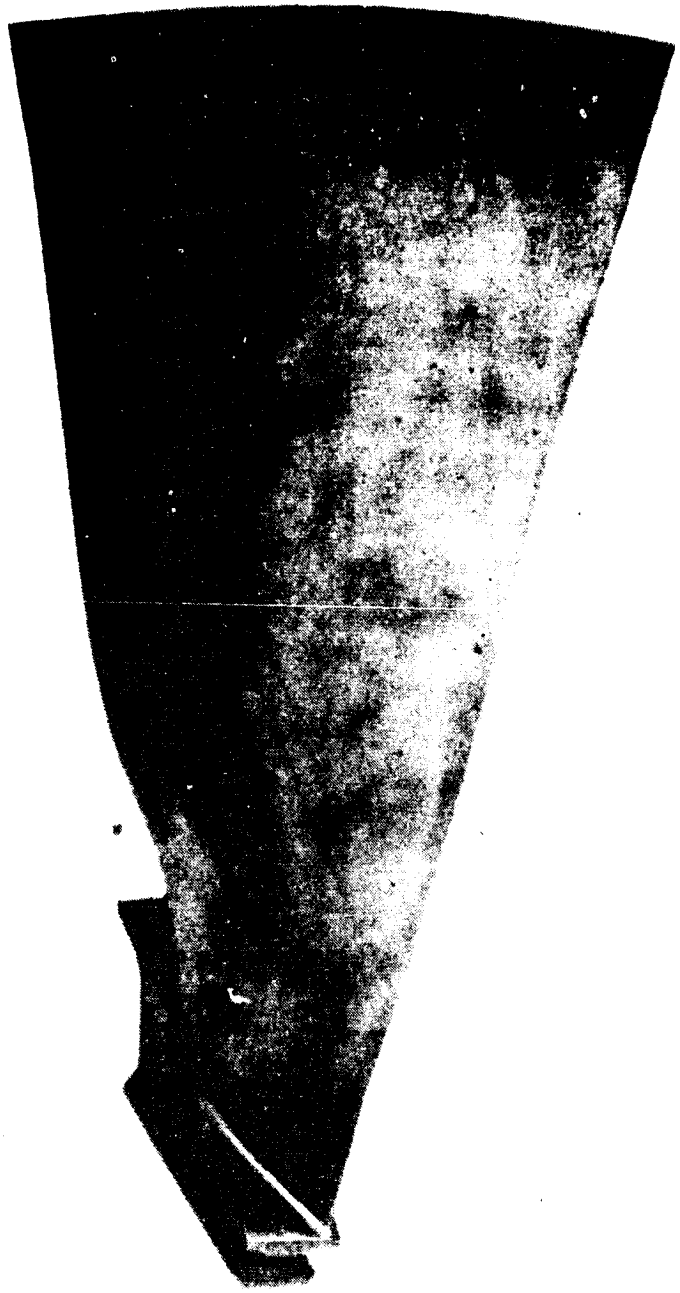

Figure 7.3. OTW Fan Blade.

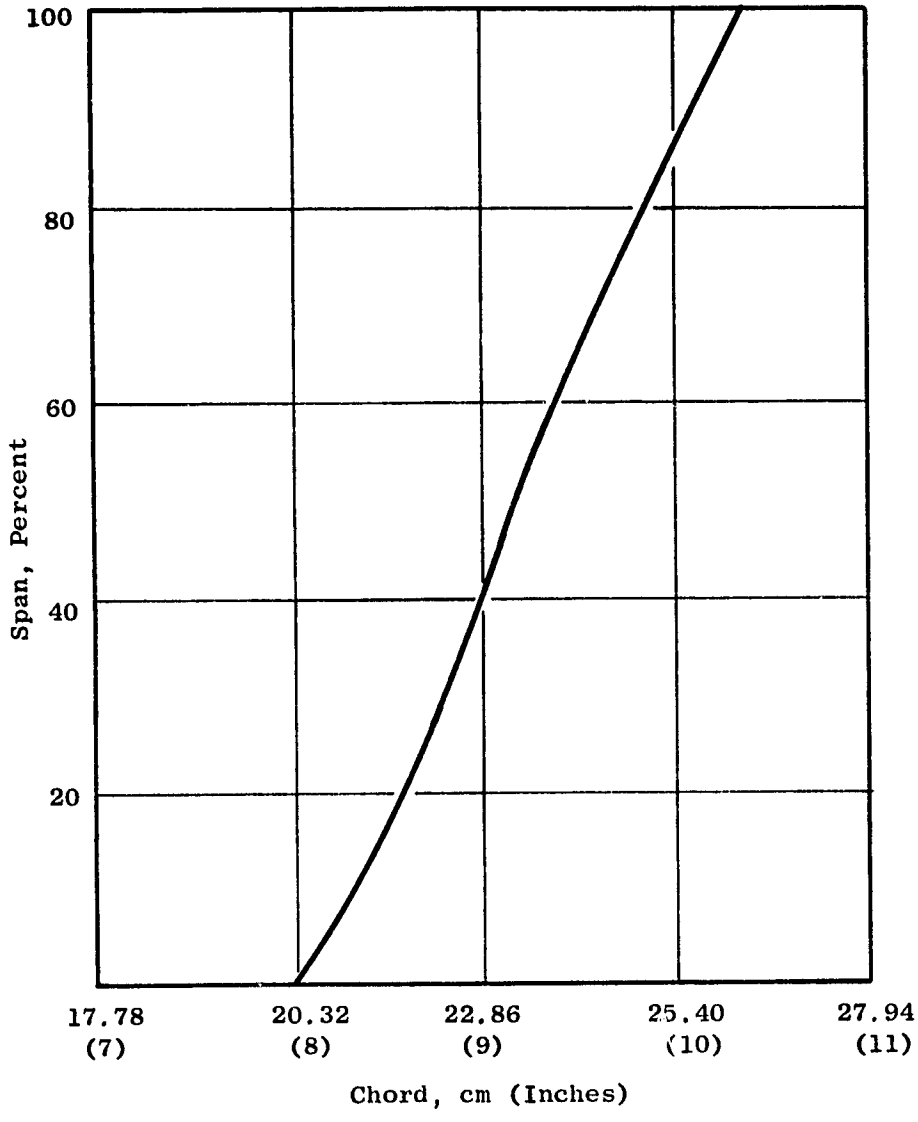

Figure 7.4. OTW Fan Blade Chord Vs. Span.

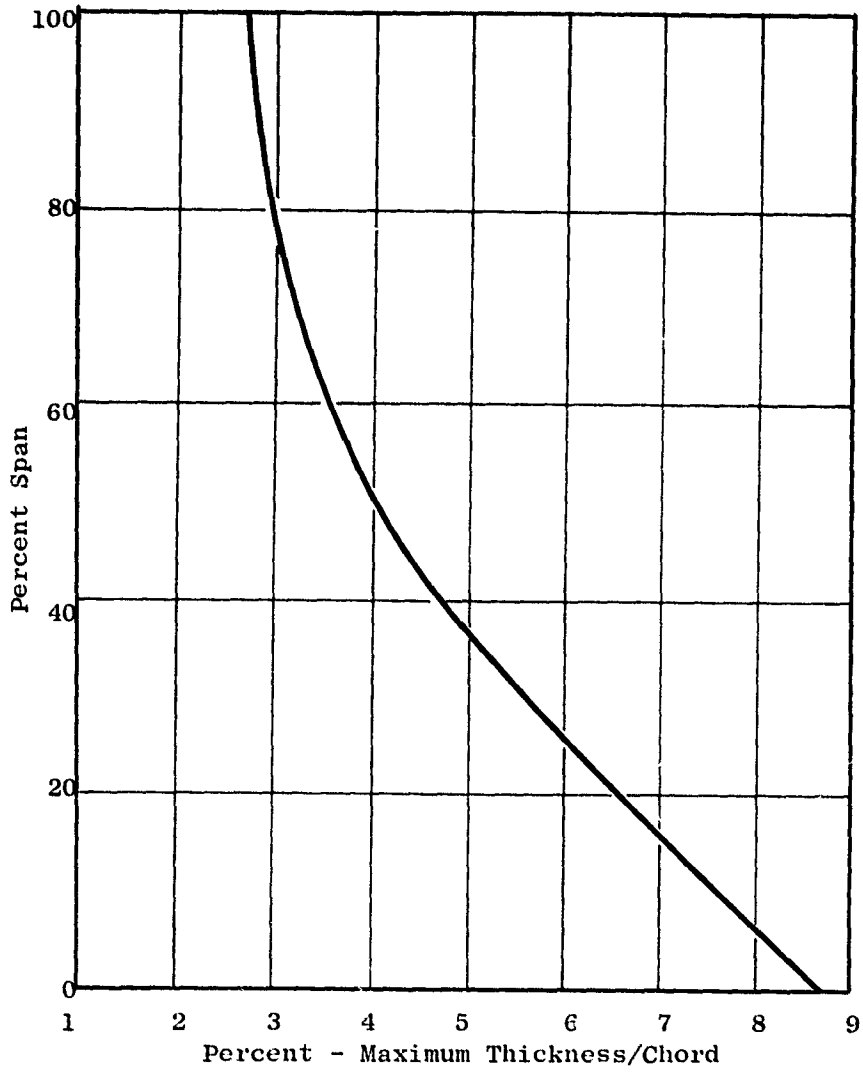

Figure 7.5. OTW Fan Blade Maximum Thickness Chord Vs. Span.

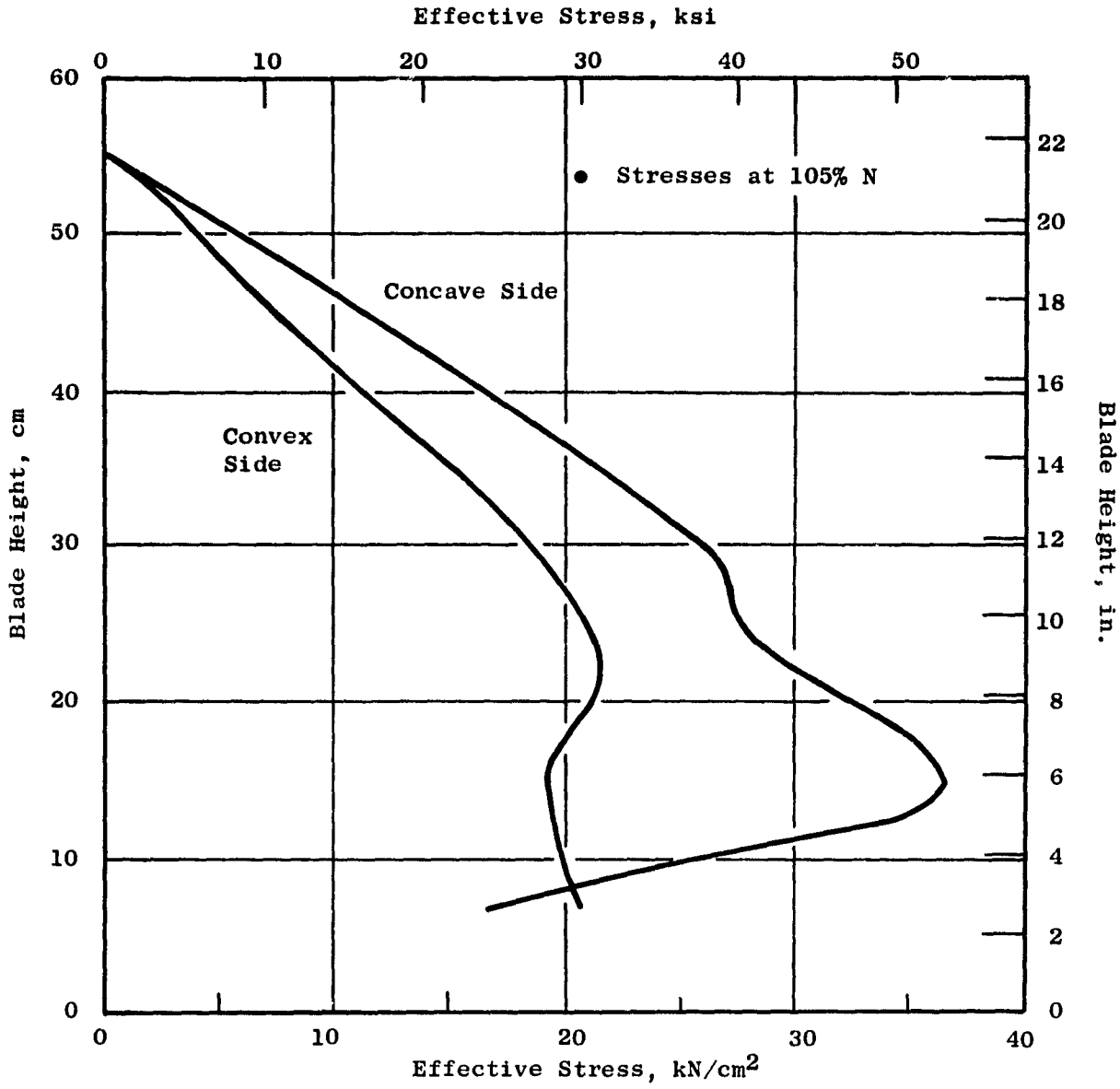

Figure 7.6. Blade Steady-State Effective Stress.

Table 7-II. QCSEE OTW Fan Blade.

Number of Blades	28	
Fan Tip Diameter	180.3 cm (71 inches)	
Airfoil Length	52.1 cm (20.5 inches)	
Aspect Ratio	2.1	
	Blade Tip	Blade Root
Chord	26.31 cm (10.36 inches)	20.68 cm (8.14 inches)
Max. Thickness/ Chord	2.65 percent	8.6 percent
Solidity	1.3	2.34

Table 7-III. Blade Stresses.

- Max. Centrifugal — 16.6 kN/cm^2 (24 ksi) @ 105% N, 7.62 cm (3 in.) from root
- Max. Effective — 36.5 kN/cm^2 (53 ksi) @ 105% N, 15.2 cm (6 in.) from root
- Leading and trailing edges in compression except at root - low tensile stresses permit an allowable vibratory stress of 31 kN/cm^2 (45 ksi SA) with a stress concentration of 3 (FOD)
- Anticipated vibratory stress at first flex - 2/rev crossing is approximately 30% of scope limits.
- Uncorrected gas bending stress = 12.4 kN/cm^2 (18 ksi).

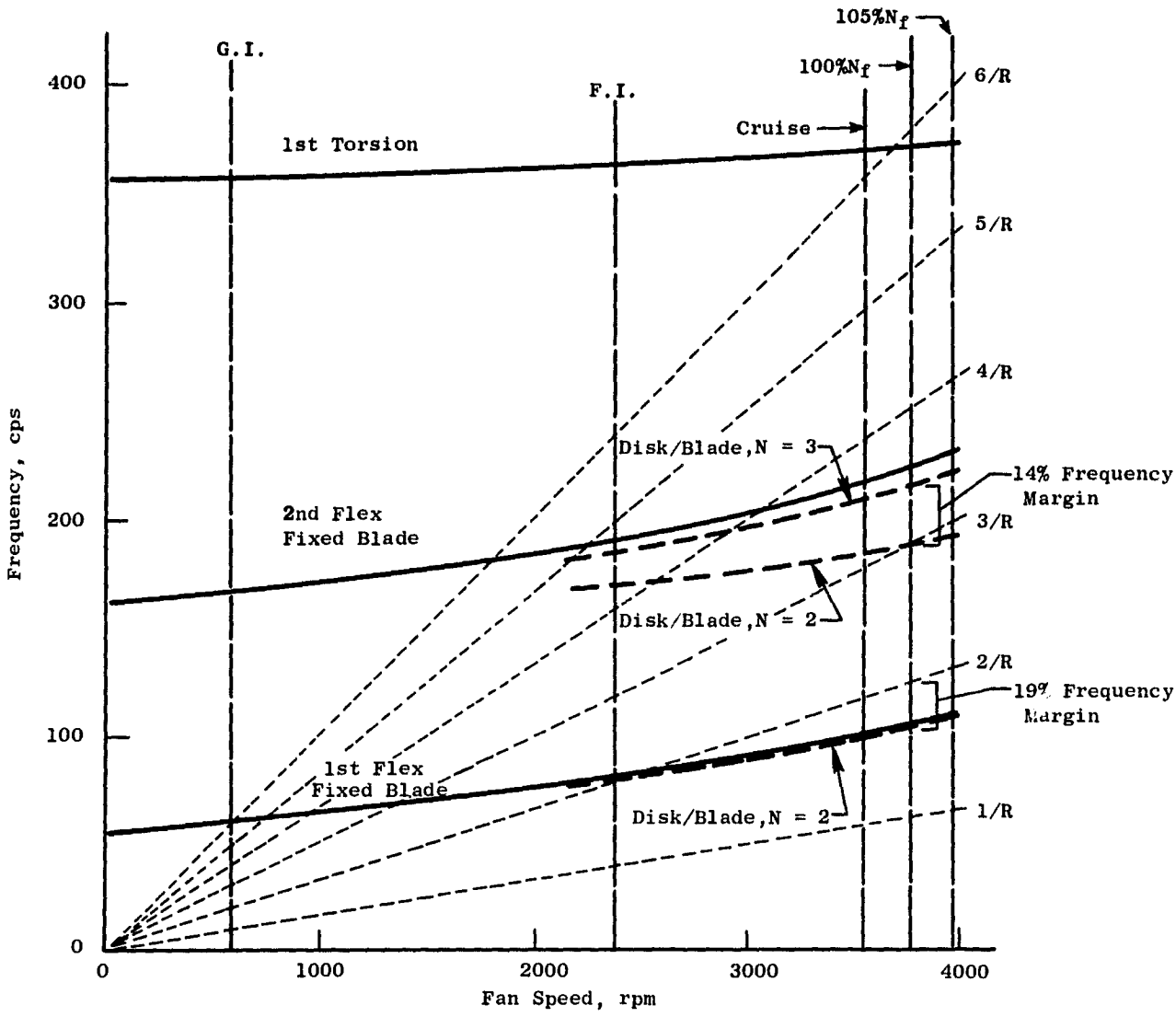

Figure 7.7. OTW Fan Blade Campbell Diagram.

The combined blade (second flex) disk (N=3) mode has a frequency margin of 14 percent from the 3 per rev line at 100% speed. In the absence of frame struts or inlet guide vanes ahead of the fan, higher order resonances have not been a problem on similar configuration engines such as the TF34 and CF6.

It is desirable to have a minimum of 12% frequency margin from the combined blade-disk mode to a per rev stimulus at 100% speed. The present blade design, with a margin of 19% between the first flex N=2 blade-disk mode and the two per rev line, and a margin of 14% between the second flex N=3 blade-disk mode and the three per rev line (Reference Figure 7.7), is considered to have adequate margin in these two modes of greatest concern.

Blade "instability" or "limit cycle vibration" can be a problem on fans. It is characterized by a high amplitude vibration in a single mode (normally the first flexural or torsional mode) at a nonintegral per rev frequency. It is not one of the classical airfoil flutter cases and is apparently confined to cascades. Because of the nonlinearity in the aerodynamics involved, it has resisted practical solutions by solely theoretical means. Accordingly, General Electric has adopted a semiempirical "reduced velocity" approach for limit cycle avoidance. Reduced velocity gives a measure of a blade's stability against self-excited vibration. This parameter is defined as $V_R = W/bf_t$,

where: b = 1/2 chord at 5/6 span - (meters)

W = average air velocity relative to the blade over the outer third of the span - (meters/sec)

f_t = first torsional frequency at design rpm - (Hertz)

The basic criterion used for setting the design of the OTW metal blade was the requirement of having a reduced velocity parameter no higher than 1.5. This allowable range is based on previous testing of a variety of fan configurations in combination with the specific aerodynamic design of the OTW blade.

Blade instability does not occur once the blades are stalled. The current design practice is to design blades such that when the fan is throttled, stall occurs before the empirically predicted blade instability is encountered. The blade stability is affected by varying the blade chord and thickness distribution which changes the reduced velocity parameter. The operating and stall characteristics of this blade are presented in Figure 7.8 in terms of reduced velocity versus incidence angle. This shows an acceptable blade design with the design point reduced velocity parameter at 1.3, and in which the throttled fan should stall before encountering the expected blade stability limit. The predicted blade stall line includes the effects of special casing treatment.

OTW composite flight blade would have additional stability margin due to the higher stiffness-to-weight ratio possible in composite designs.

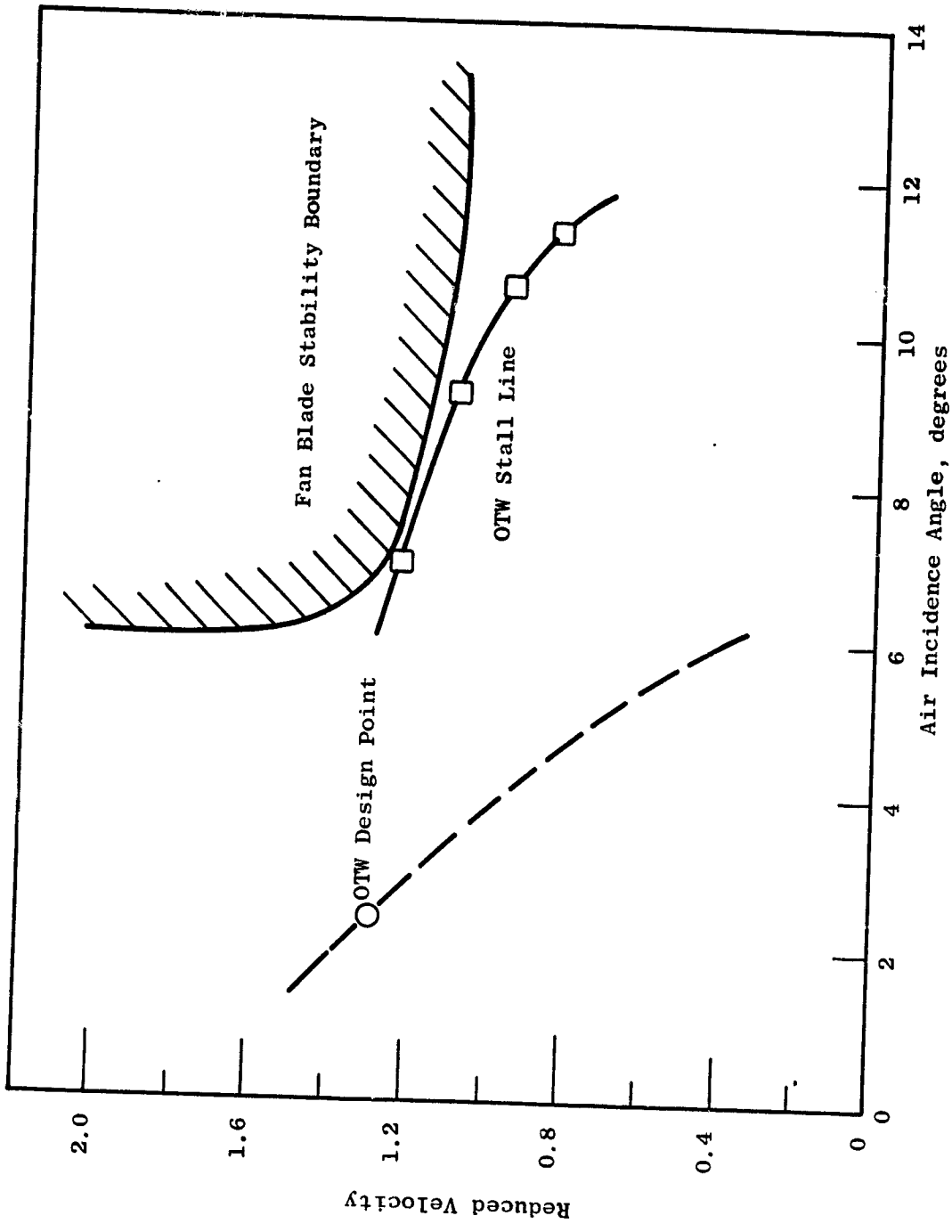

Figure 7.8. OTW Fan Limit Cycle Boundary.

The blade is attached to the disk by an axially oriented 55° flank angle dovetail (Figure 7.9). Maximum blade dovetail steady-state stress is 29.7 kN/cm^2 (43 ksi) in combined bending and tensile stress. Dovetail crush stress is 51 kN/cm^2 (74 ksi) and is life limiting by the mechanism of wear or fretting, not by low cycle fatigue, since neither a tensile stress nor a stress concentration is involved. Dovetail flanks are plasma sprayed with copper-nickel-indium and coated with Molydag to protect against fretting. In the event of loss of a blade airfoil, the resulting combination of tensile and bending stress on the disk post is 44 kN/cm^2 (64 ksi) within an allowable stress in this case of 85 kN/cm^2 (123 ksi). The loss of an airfoil will not cause the subsequent loss of adjacent blades through failure of the disk post.

The blade attachments were designed so that the blade airfoil is the weakest link in the airfoil, dovetail, and disk post system to minimize the size of the piece that will detach in event of a vibratory failure. The resulting design is such that when the airfoil is operating at its maximum allowable vibratory stress, the blade dovetail is at 98% of its maximum and the disk post is at 92% of its maximum. Figures 7.10 and 7.11 illustrate this design concept.

Figure 7.10 shows the points of maximum stress on the blade dovetail and the disk post for which stresses are calculated in the dovetail computer program. The ratio of the vibratory stresses at these points to the vibratory stress in the airfoil is shown in the fatigue limit diagram (Figure 7.11).

With the airfoil at its maximum allowable stress, all of the maximum stress points on both the blade and disk dovetails are at less than their allowable stresses.

7.4 FAN DISK DESIGN

The OTW fan disk is machined from a 6-Al-4V titanium forging. An integral cone attaches the ring disk to the main reduction gear shafting. Slots machined into the forward and aft ends of each disk post provide attachment for individual blade retainers. The rotor is required to have low-cycle fatigue (LCF) capability for 48,000 mission cycles and 1,000 ground cycles. To achieve this requirement, disk extensions were provided for the attachment of adjacent shell members. This, in addition to scalloping the flanges, lowered the stresses at the flanges sufficiently to meet the LCF requirements. Stresses in the disk and shells were calculated using a shell and ring program in the computer library. A finite element program was used to calculate stress in the disk dovetail post and in the bottom of the dovetail slot.

The total dead load supported by the disk is 18.5×10^6N (4,150,000 lb). This includes the centrifugal weight of all nonself-supporting parts (blades, retainers, disk dovetail posts, etc.) as well as side loads imposed by adjacent members. Maximum permissible stress in the disk including stress concentrations was limited to 51 kN/cm^2 (74 ksi) to meet the LCF life requirements. Calculated stresses (105% N) including local stress concentrations are shown in Figure 7.12 for various parts of the disk and shaft. Crack propagation calculations indicate the LCF life in excess of 16,000 cycles with an initial 0.0254 - 0.0762 cm (0.01 × 0.03 inch) defect.

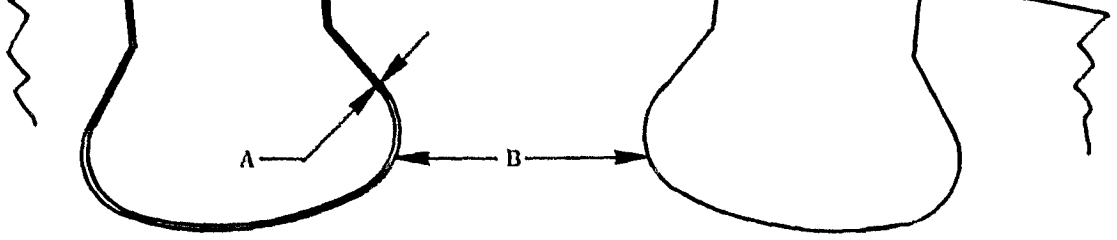

(A) Dovetail Crush Stress - 51 kN, cm^2 (74 ksi) at 105% Speed

(B) Maximum Stress on Disk Post Due to Blade Out - 44.1 kN/cm^2 (64 KSI)

Figure 7.9. OTW Fan Blade Dovetail.

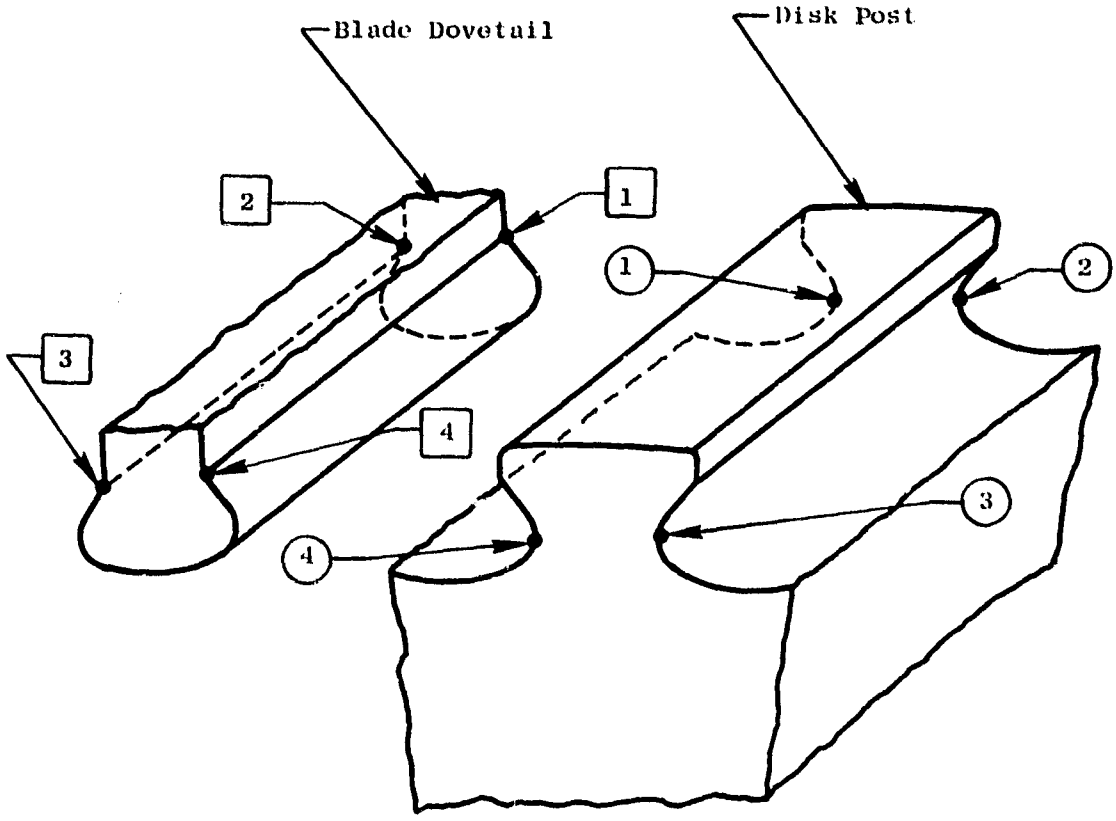

Figure 7.10. Stress Points on Blade and Disk Dovetails.

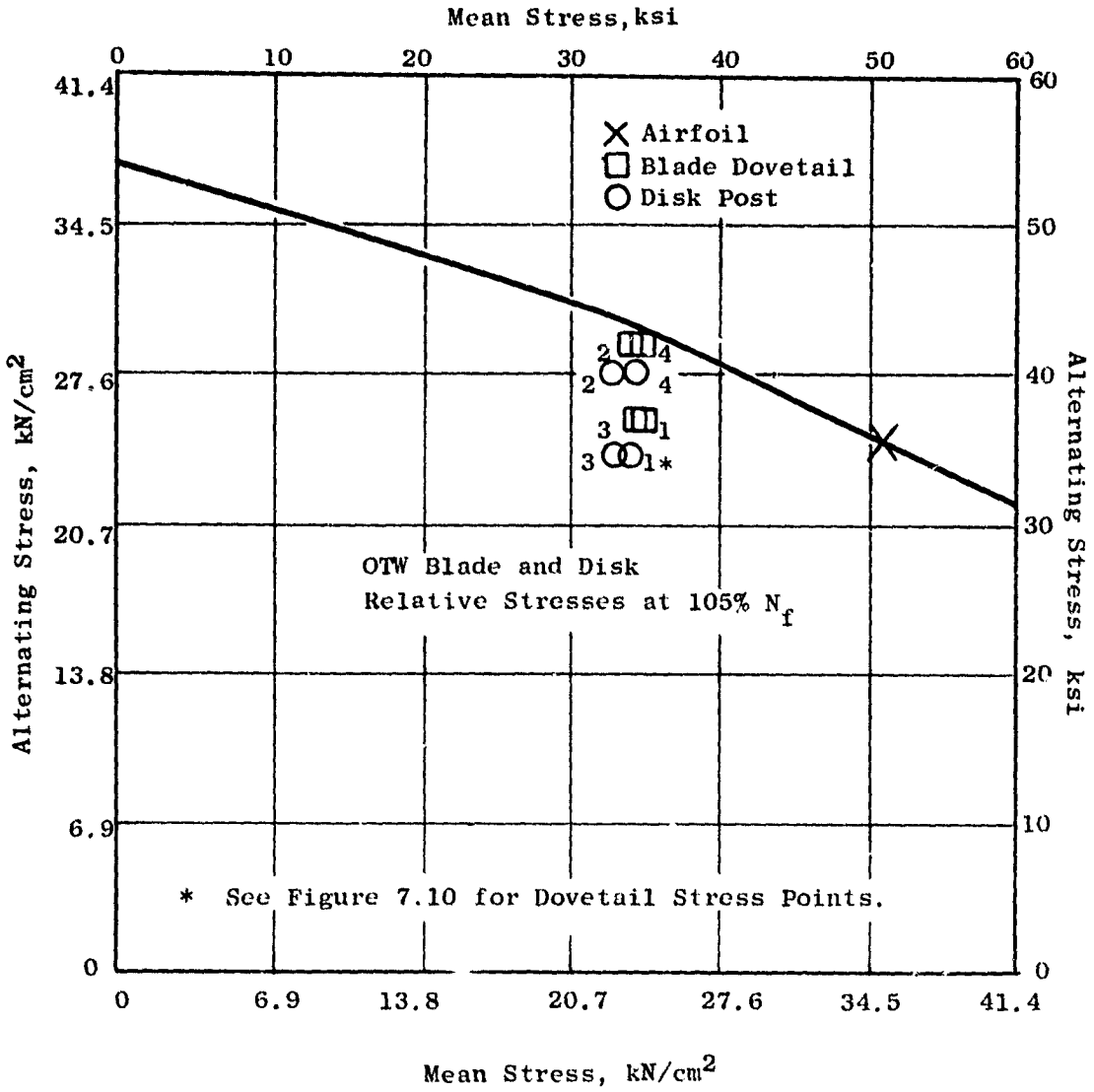

Figure 7.11. Room Temperature Fatigue Limit.

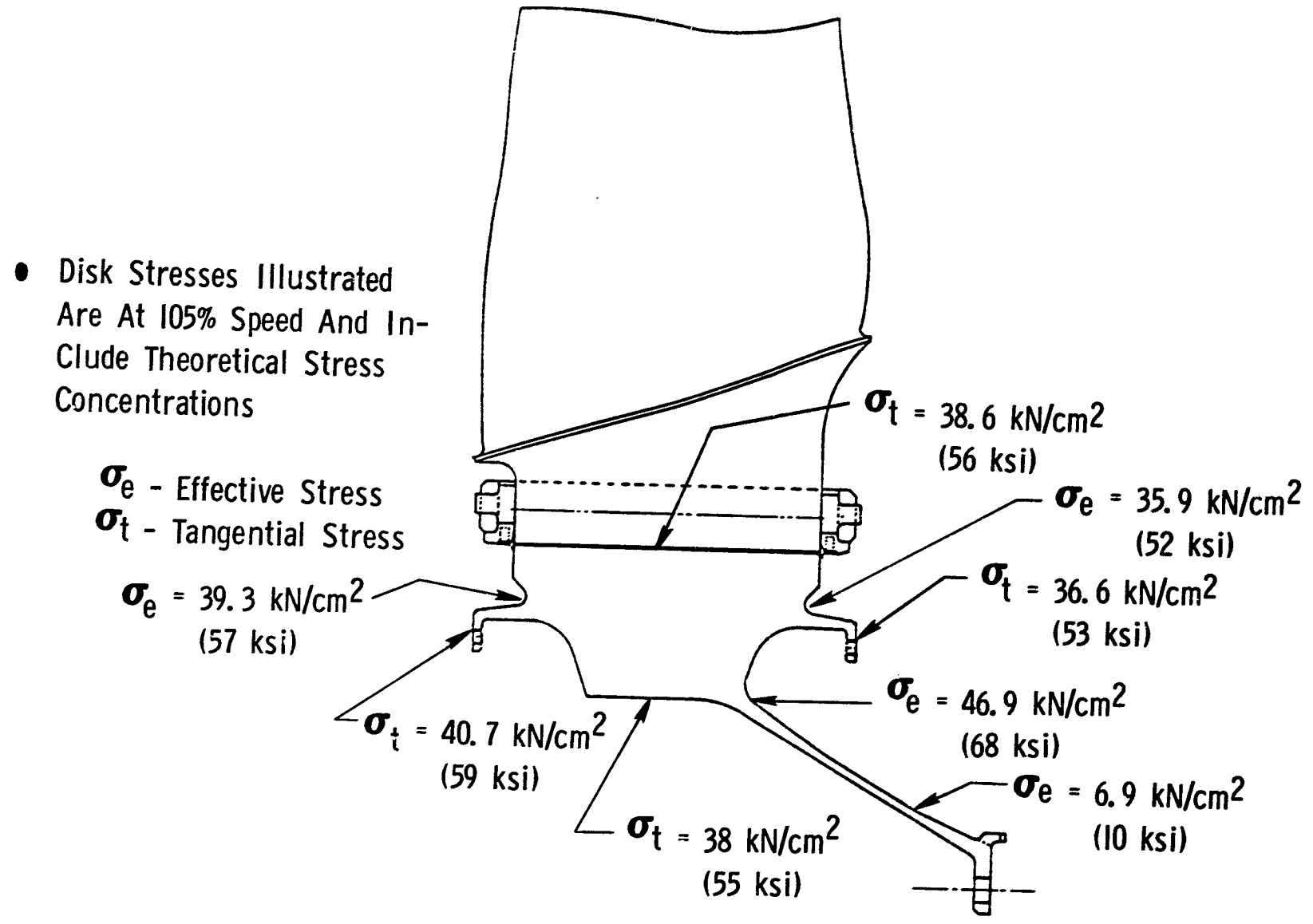

Figure 7.12. OTW Disk Stresses.

The disk is designed as a prime reliable component, capable of withstanding a stress twice that at the maximum cycle speed without bursting. This requires a special capability of 141% of the maximum cycle speed or 5615 rpm. The calculated burst speed of the disk as designed is 6260 rpm or 157% of maximum cycle speed.

The additional burst margin is available because the disk was not sized solely on burst considerations, but also on the need to reduce dovetail stresses, meet low-cycle fatigue requirements, stiffen the disk to avoid blade frequency problems, and provide capability for reslotting for possible future testing of composite blades.

7.5 BLADE RETAINERS

The blade retainers are blocker plates at the ends of each dovetail slot held in place by slots at the ends of the dovetail post. Radial movement of the plates is restricted by tapering the slots and providing load points against the disk. Figure 7.13 illustrates the design. The plates are held in place during buildup by individual clips and are finally locked in place by installation of the coupling. This design permits individual blade change by removal of the spinner, coupling, and individual blocker plate.

To prevent the axial shifting of the blades under unusual load conditions, the retainers are designed to withstand thrust loads of up to 30% of the blade centrifugal force. This results in a possible axial load of 167 kN (37,500 lb) that must be restrained without failure of the retention system. At this maximum load condition, calculated stresses in the retainer are at or near the ultimate strength of the material. However, under normal operating conditions, stress in the retainer does not exceed 14 kN/cm^2 (20 ksi).

7.6 ROTOR SHELL MEMBERS

The forward spinner is machined from a 6061 Al forging and forms the forward inner flowpath of the fan. It is attached to the forward coupling which isolates it from the higher stresses of the disk. Scalloping between attachment bolt holes and contouring of the counterbore reduces stress concentrations such that the spinner meets life requirements.

On the experimental engine, the spinner will have a nose cap to provide access to the interior of the rotor. The opening is also available for instrumentation lead-in and slipring support.

Permanent two-plane balance of the spinner will be obtained by attachment of balance weights to the flange at the nose cap and a flange at the rear of the spinner. Rotor field balance capability is built into the spinner by the inclusion of a series of bolts of variable weight into the rear of the spinner.

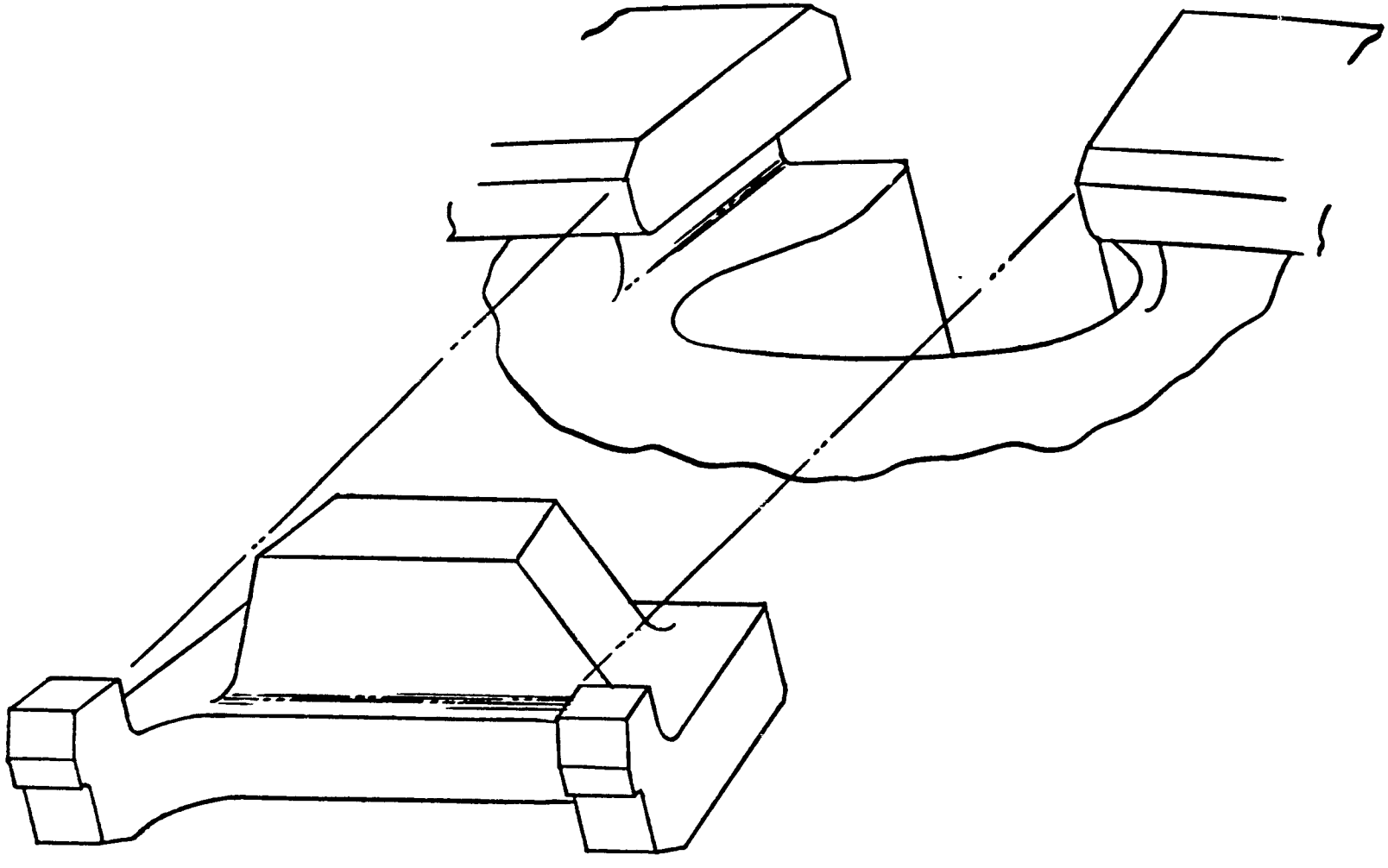

Figure 7.13. OTW Fan Blade Retainer.

The aft spinner is machined from a 6061 Al forging and continues the inner fan flowpath from the blade exit to the fan core OGV's. A flow discourager seal inhibits air recirculation at this point. Openings in the support member of the aft spinner provide access to fan frame bolts to allow removal of the fan package.

Titanium couplings at the front and rear of the disk provide transition members from the disk to the aluminum spinners and isolate the aluminum parts from the relatively high stresses in the disk. The couplings also lock the blade retainers in place. The fore and aft coupling designs are interchangeable and may be used on either side of the disk. Jack points are provided at rabbeted joints to aid in separating the rotor parts.

Stresses in the rotor shells were calculated using a shell and ring program in the computer library. The stresses are shown in Figure 7.14 and include stress concentrations. Allowable stresses were determined by low cycle fatigue considerations and are limited to 51 kN/cm^2 (74 ksi) in the titanium parts and 17 kN/cm^2 (25 ksi) in the anodized aluminum parts.

Rotor deflections are given on Figure 7.15. Axial movements shown are relative to the shaft flange. The platform of the blade and the contours of the forward and aft spinners are dimensioned so that the operating deflections and dimensional stackups will not cause forward facing steps at the interfaces between these parts. The contours that form the flowpath are dimensioned to be on the aerodynamic flowpath at the fan design point.

7.7 FAN HARDWARE

All structural joints in the fan except the nose cap use 0.794 cm (5/16 in.) diameter Inco 718 bolts and Waspaloy nuts. The rotor joint at the fan stub shaft uses 18 1.27 cm (1/2 in.) diameter MP159 bolts and heavy walled Waspaloy nuts to permit higher loading of the bolts. The threads at all the joints are lubricated with MIL-T-5544 lubricant. A summary of design data on the stub shaft flange bolts is shown in Table 7-IV.

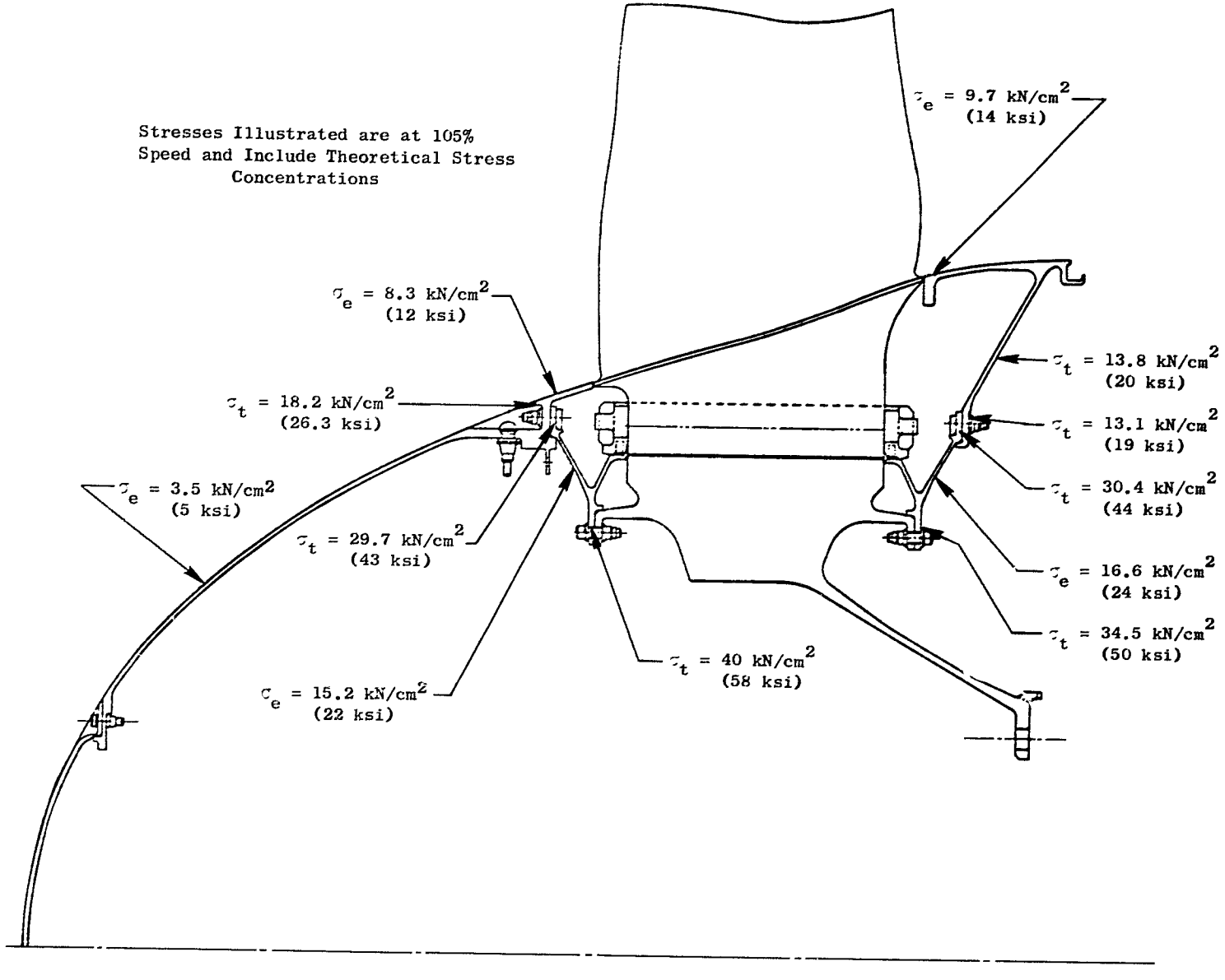

Figure 7.14. OTW Fan Rotor Shell Stresses.

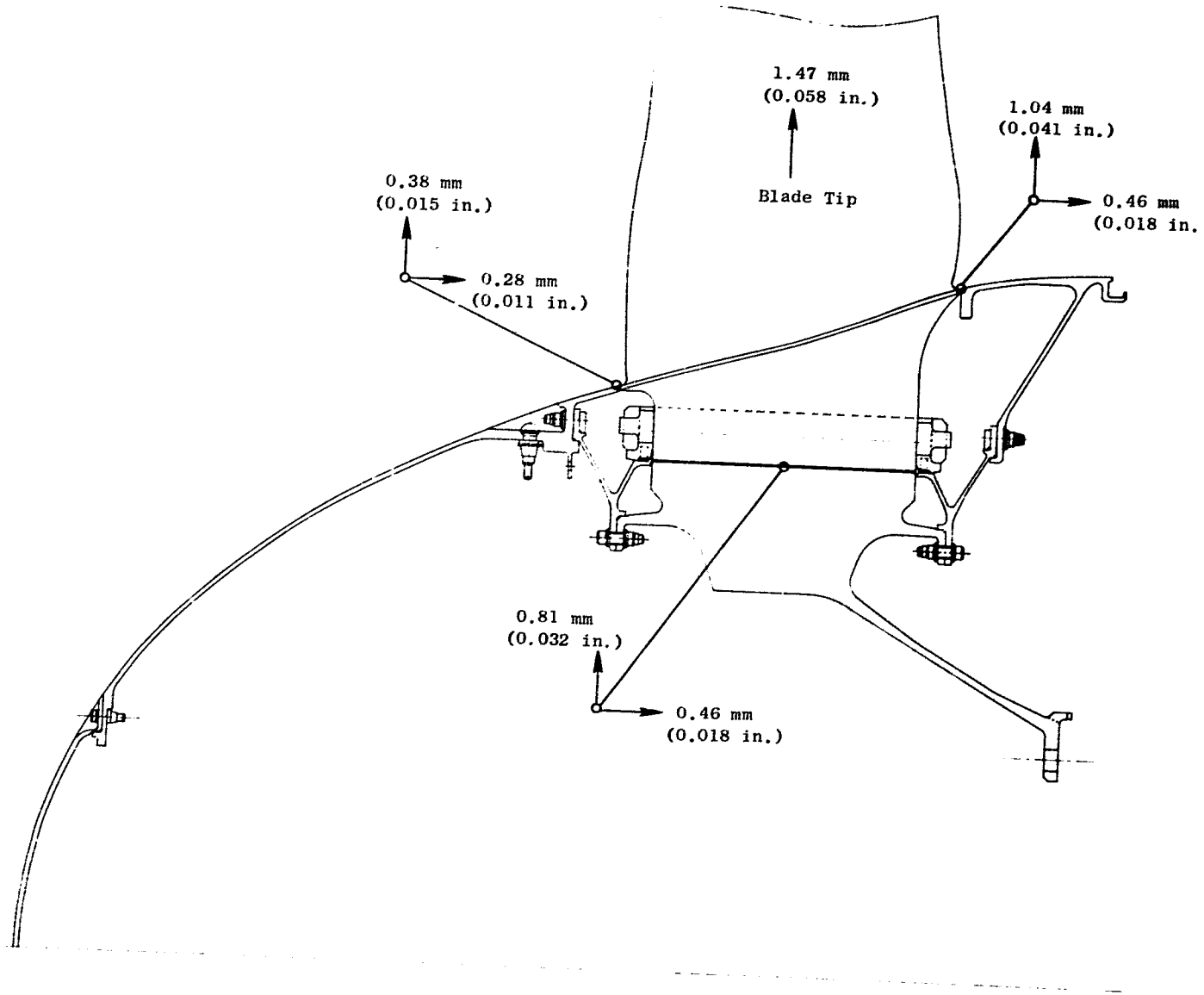

Figure 7.15. Rotor Deflections.

Table 7-IV. Stub Shaft Flange Bolts.

- Number of bolts = 18
- Size = 1.27 cm - 7.87 thd/cm (1/2 in. - 20 thd/in.)
- Material = MP159
- Assembly torque = 176 N-m (130 ft-lb)
- Minimum preload = 95,230 N/Bolt (21,400 lb/bolt)
- Total preload = 1.714×10^6 N (385,000 lb)
- Minimum bolt preload stress = 92.3 kN/cm^2 (134 ksi)
- Percent fan torque carried by friction (for f = 0.15) = 105%
- Bolt tensile stress (1 metal airfoil out) = 25% of ultimate
- Bolt shear stress (1 metal airfoil out) = 31% of ultimate

SECTION 8.0

FAN FRAME MECHANICAL DESIGN

8.1 SUMMARY

The OTW fan frame is a flight-weight, integrated design constructed of advanced composite materials and is identical to the UTW frame except for several minor differences not connected with the structural integrity. Design integration is achieved by combining the functions of the fan stator vanes, fan outer casing, and fan frame into one unitized structure, as shown in Figures 8.1 and 8.2. This approach saves considerable duplication of structure, resulting in a significantly lighter weight design. This unitized approach is particularly suited to the use of composite materials, since these materials are more efficient when employed in large bonded structures rather than small structures which must be bolted together.

The composite material system selected as the basic material for the frame is Type AS graphite fiber in Hercules 3501 epoxy resin matrix. This material was selected based on the rather extensive data base for the material, its good mechanical properties, cost, and its ready availability.

The frame was analyzed using a finite element digital computer program. This program was run a number of times using different material property inputs for the various elements in order to arrive at practical thicknesses and ply orientations to achieve a final design that met all strength and stiffness requirements for all of the critical conditions. Using this information, the detail design of each of the individual parts of the frame was completed and released. On the basis of these designs, the tooling required to fabricate the various component parts of the frame was designed.

To verify the structural integrity of the critical joint areas, a subcomponent test program is now being carried out, and partial results are reported herein. In addition, an element test program was conducted to verify predicted mechanical properties for specific orientations required for the frame.

8.2 DESIGN REQUIREMENTS

8.2.1 Loads

In addition to the normal range and combination of steady-state pressure, thermal, thrust, and torque loads, the engine has been designed to withstand the loads defined in Table 8-I. Table 8-II summarizes the engine bearing loads on the frame for 1g down, 1 radian/sec, and one composite fan blade-out conditions. The OTW frame is designed for five composite blades out even

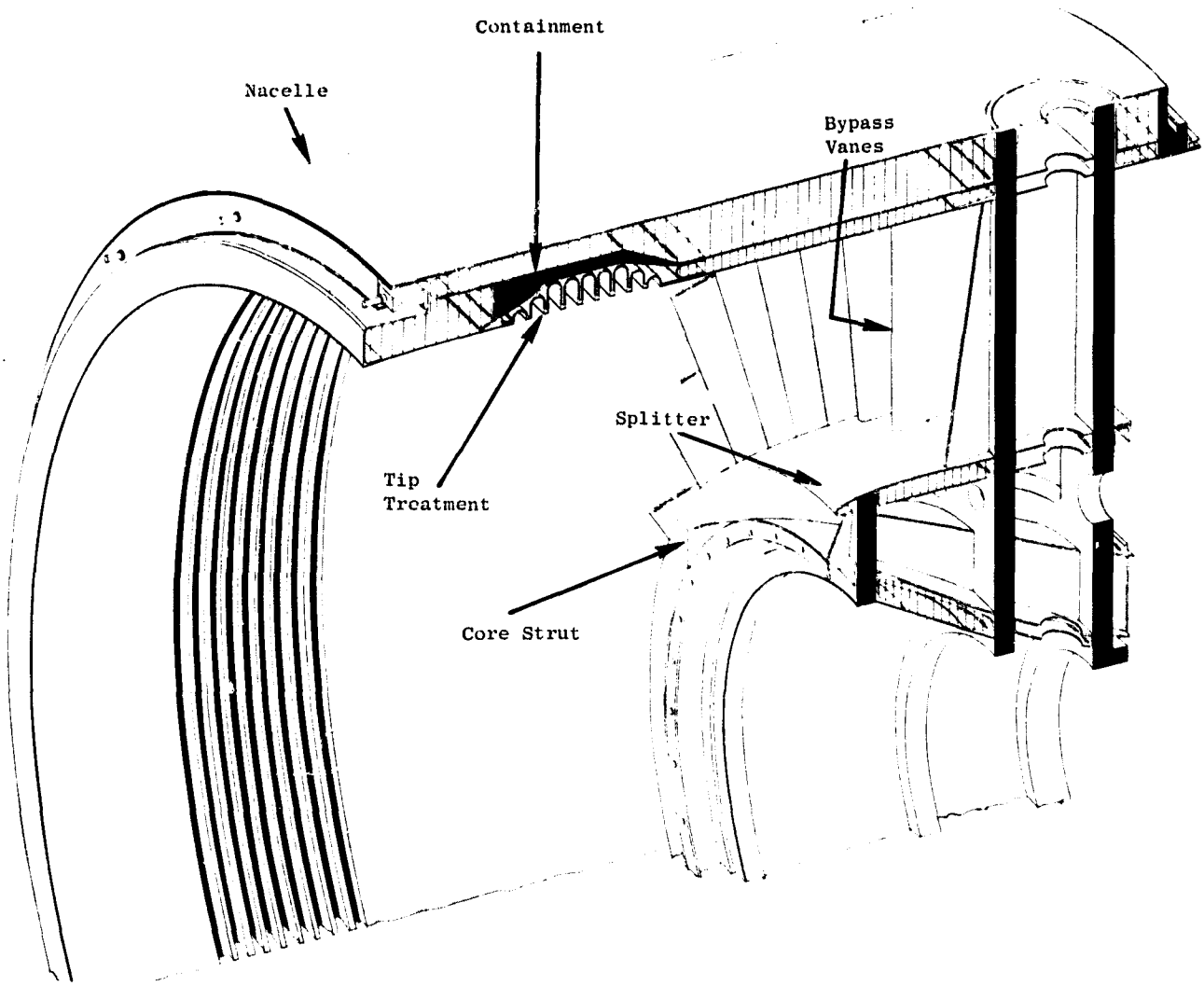

Figure 8.1. OTW Fan Frame.

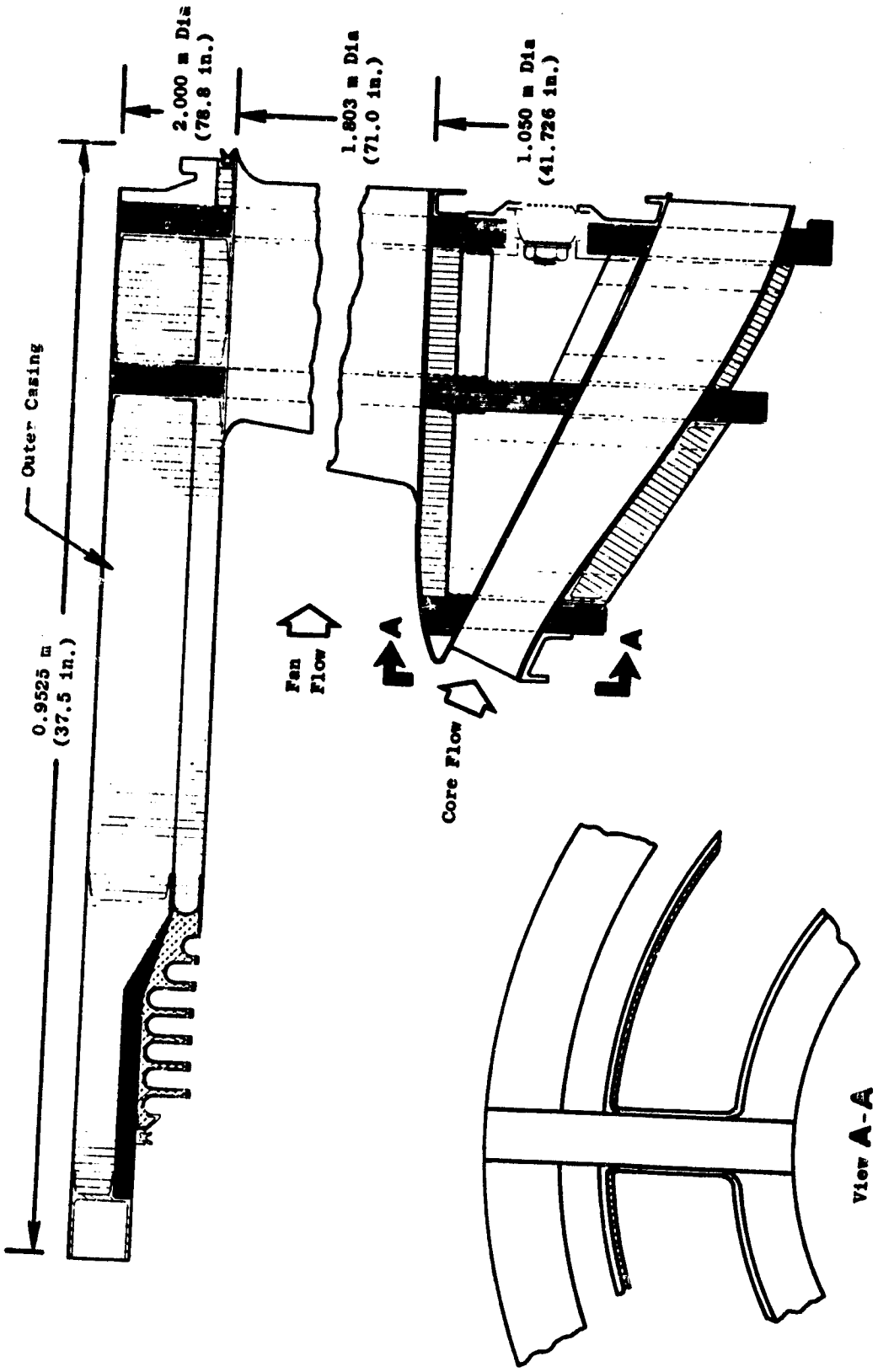

Figure 8.2. QCSEE Composite Frame.

Table 8-I. QCSEE Engine Loads.

Limit Loads

For any one of the following load conditions, all stresses shall remain within the material elastic limits.

Condition I: (Flight and Landing) - See load diagram, Figure 2.2.
Condition II: (Gust Load) - An equivalent load from a 51.44 m/sec (100 knot) crosswind acting at any angle within a plane 1.5708 radians (90 degrees) to the axis of the engine, zero-to-maximum thrust.

Condition III: (Side Load) - A 4g side load combined with 1/3 the equivalent load as defined in Condition II, zero-to-maximum thrust.

Ultimate Loads

The engine shall not separate from the aircraft when subjected to Conditions IV, V, and VI and for static loads equivalent to 1.5 times the loads specified as limit loads in metal parts, and 3.0 times the loads specified as limit loads in composite parts.

Condition IV: (Flight-Engine Seizure) - The seizure loads are due to the fan and engine basic gas generator decelerating from maximum to zero engine speed in one second.

Condition V: (Crash Load) - The crash load is defined as 10g forward, 2.25g side, and 4.5g down at maximum thrust or up to zero thrust.

Condition VI: (5 blades out) - The engine shall be capable of withstanding unbalance loads caused by the loss of 5 adjacent fan blades at maximum rpm (composite blades only).

Table 8-II. QCSEE Frame Radial Bearing Loads.

Condition	Radial Bearing Load	
	Newtons	Pounds
1 g Down		
Bearing No.*		
1B	3425	770
1R	1099	247
2	364	82
3	823	185
1 Radian/Sec		
Bearing No.*		
1B	27397	6159
1R	27397	6159
2	1699	382
3	9559	2149
1 Fan Blade Out		
Bearing No.*		
1B	175468	39447
1R	144295	32439
2	16182	3638
3	32494	7305

*See Figure 11.17 for a schematic of the engine bearing locations.

though the OTW expeimental engine has metal blades. This was done to maintain structural commonality with the UTW frame. The loads caused by five composite blades out are slightly greater than a two OTW metal blade-out condition. Air loading on the bypass vanes is shown in Figure 8.3.

8.3 STRUCTURAL DESCRIPTION

The OTW frame is an all-composite, static structure formed from integration of several separate structures. As seen in Figure 8.1, the outer casing of the frame is an integration of the nacelle with the frame outer shell. This casing provides part of the external nacelle flow lines as well as the internal fan flow lines. Fan blade tip treatment and containment are provided by the grooved and felt-filled structures integrated into the forward portion of the outer casing. The same basic fan tip treatment is used for both the UTW and OTW. Due to the different stacking axis and the fact that the OTW blade tip is cylindrical rather than spherical, minor modifications were made to the rub material and several of the circumferential grooves were filled in the OTW frame. The differences in this area between the UTW and OTW configurations are shown in Figure 8.4. Positioning of the fan and core engine relative to the integral nacelle/outer casing is provided by 33 bypass vanes which also serve as the fan bypass stator vanes; therefore, the vanes serve as structural supports and provide flow turning of the fan flow discharge. The hub of the frame is connected to the frame splitter through six equally spaced struts.

Areas of the inner shell of the outer casing, the bypass duct and core duct surfaces of the frame splitter, and the pressure faces of the bypass vanes are perforated to provide acoustic suppression within the frame structure. Flow turning of the fan flow into the core is provided by an independent set of outlet metallic guide vanes (OGV's) attached to the forward flange of the frame hub with a nonstructural fairing extending back to, and resting on, the leading edge of the flowpath splitter. The fairing closes off the gap between these guide vanes and the splitter that existed in the UTW to help provide core air during reverse pitch operation. The fan core OGV design is a brazed and machined fabrication. The splitter is formed sheet metal with the stator vanes penetrating and brazed to the skins.

Oil containment has been achieved by closing all strut ends and forming the sump wall at the frame hub. Major interfaces for all penetrations into the fan sump area are achieved by forming local bosses at all penetration points. These penetrations include oil in, oil scavenge, power take off shaft (PTO), fan speed sensor, seal drain lines, and the scavenge pump drive shaft, as shown in Figures 8.5, 8.6, and 8.7. Provisions are also made for the $T_{2.5}$ temperature sensor, six total-pressure and -temperature rakes and several static pressure taps.

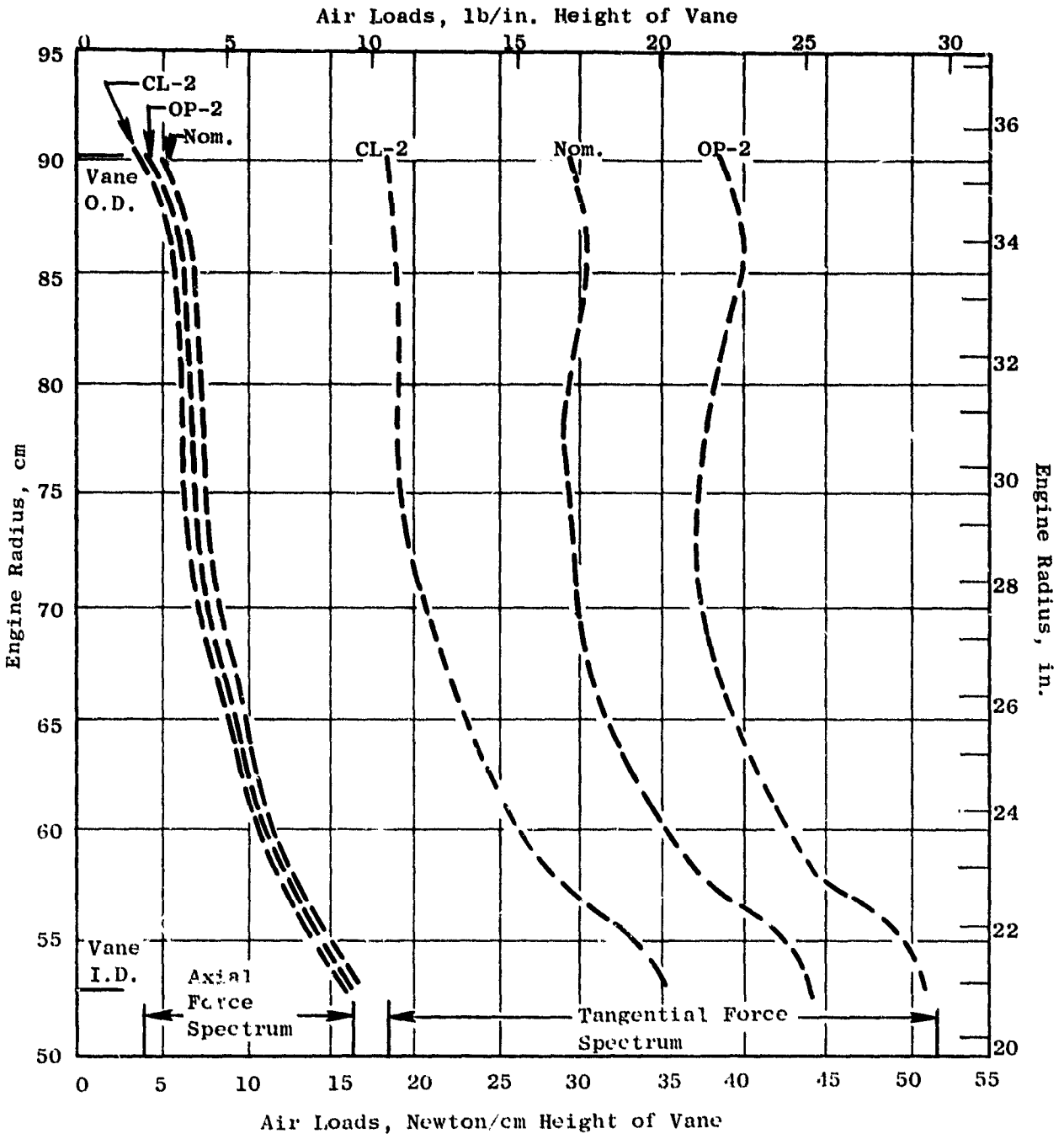

Figure 8.3. OTW Fan Design Bypass OGV/Frame Aero Design Air Loads, Closed 2°, Open 2°, and Nominal Vanes, 3793 rpm.

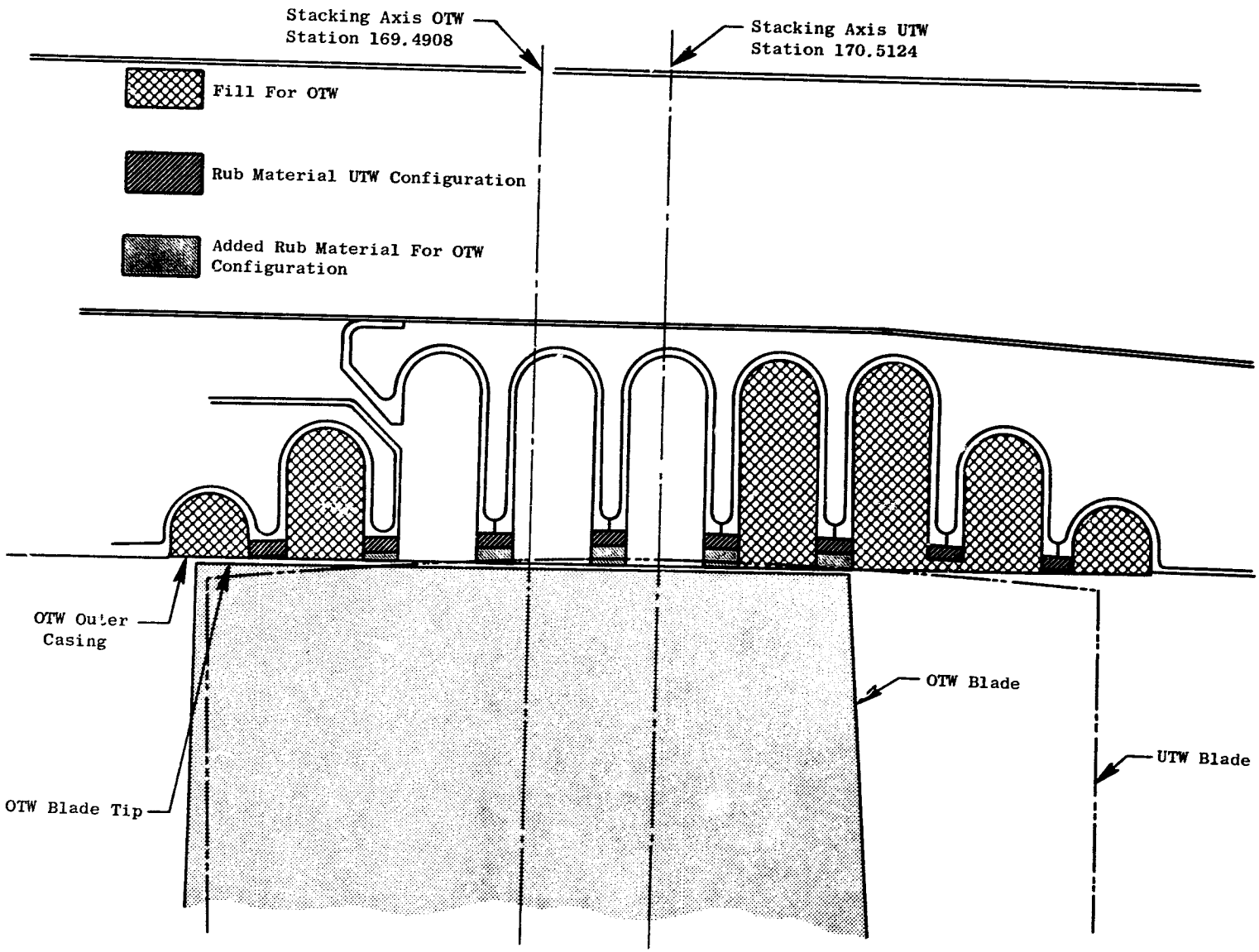

Figure 8.4. QCSEE Fan Tip Treatment.

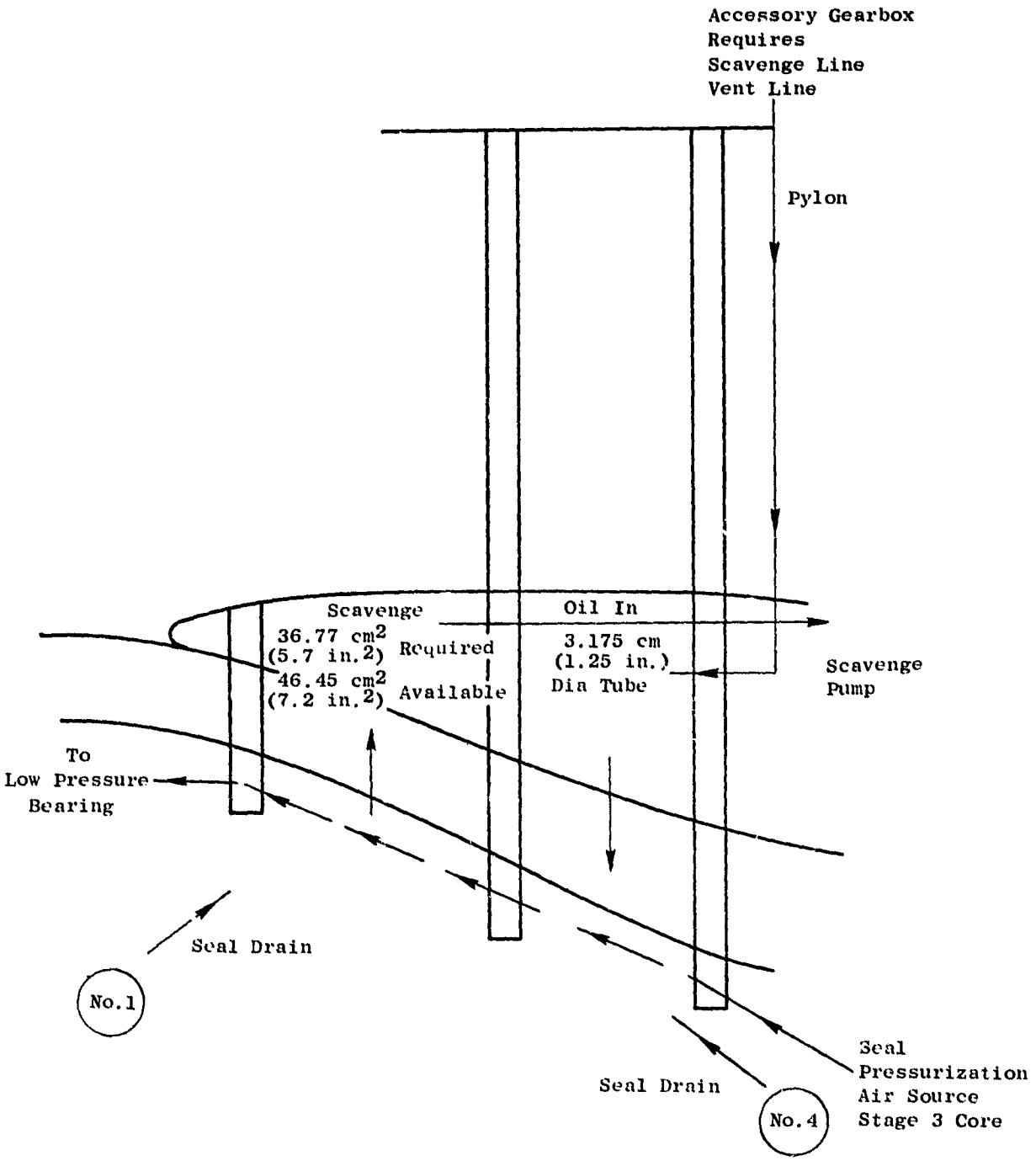

Figure 8.5. Fan Frame Service Areas.

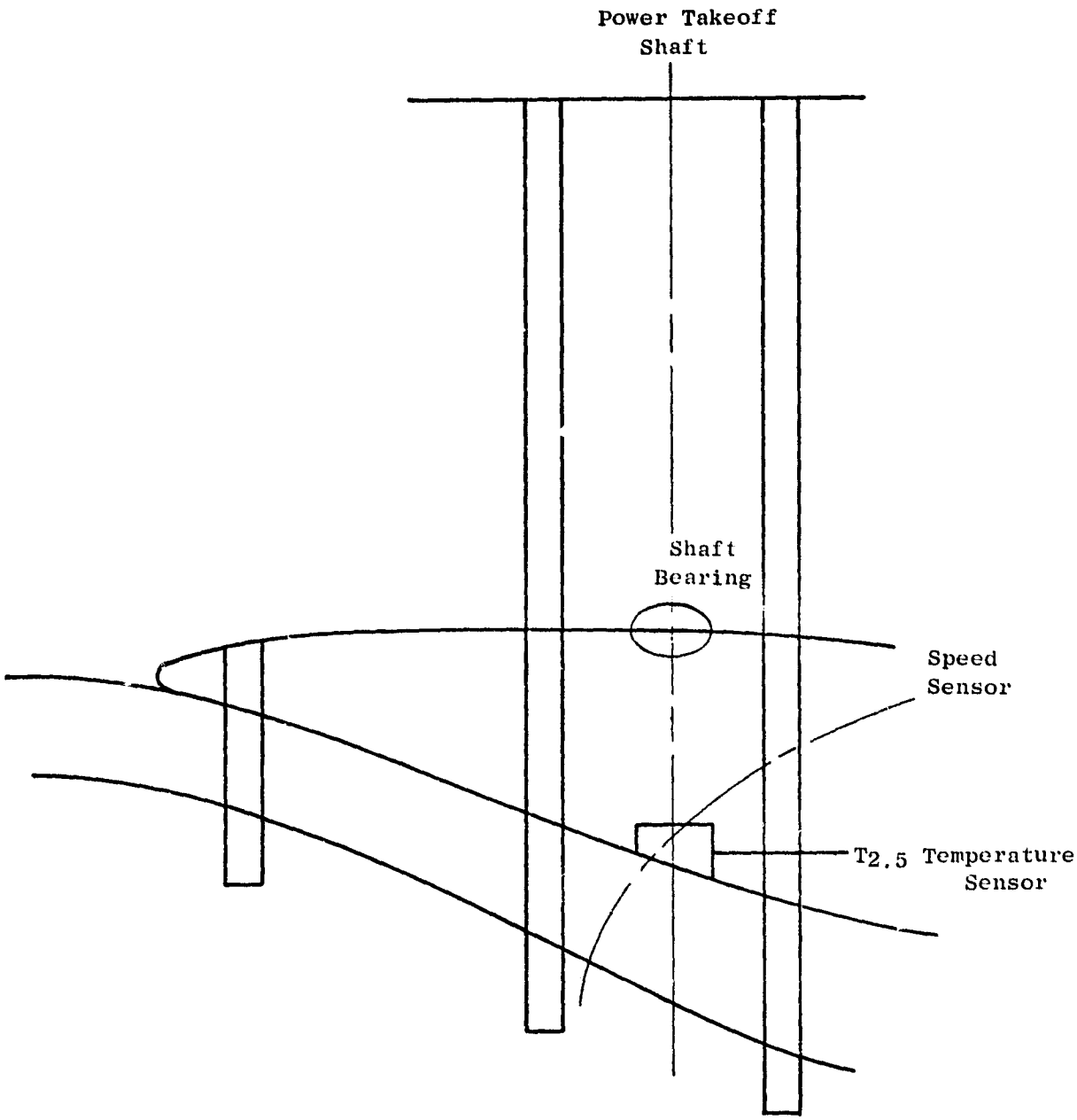

Figure 8.6. Fan Frame Service Areas.

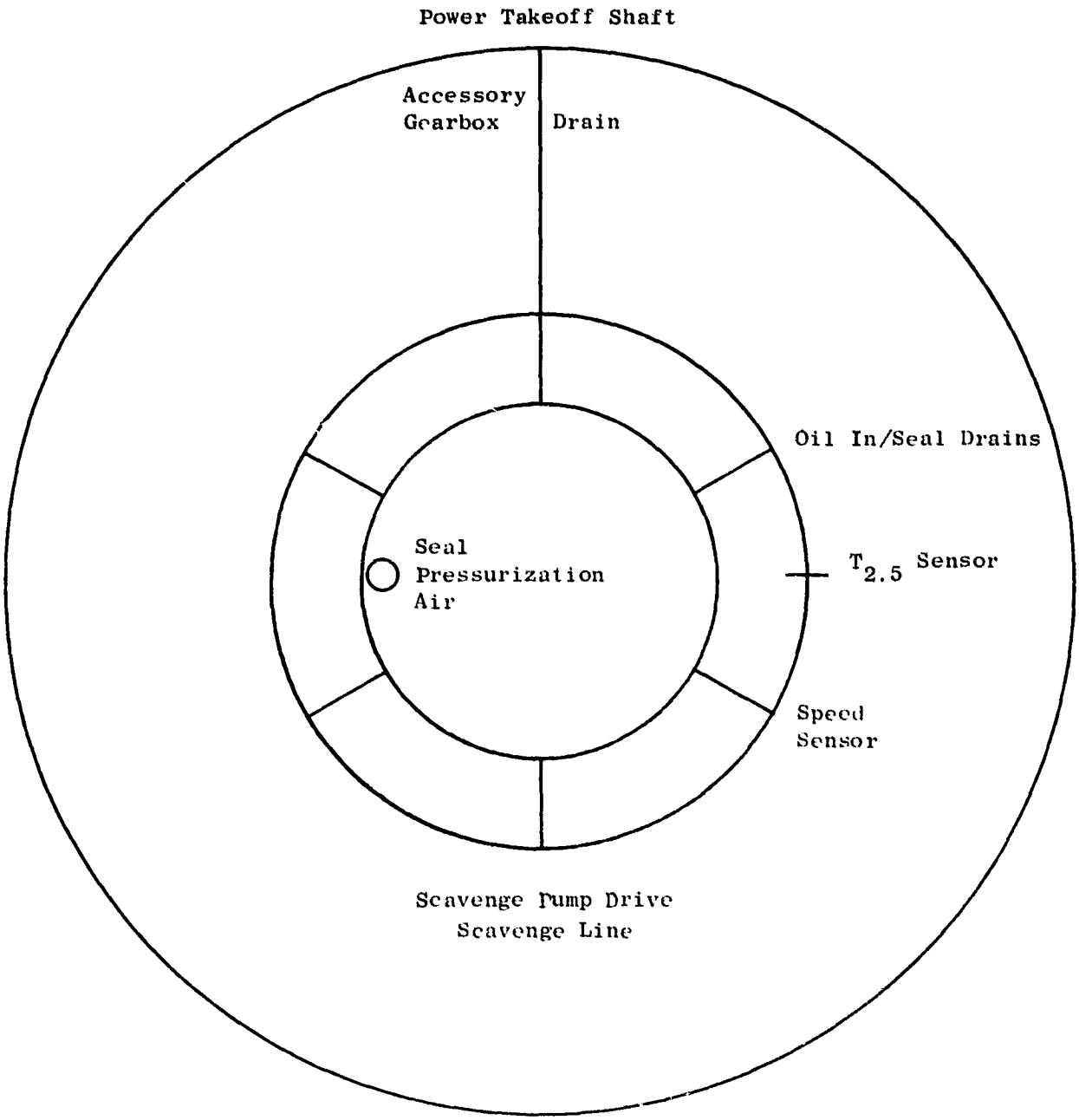

Figure 8.7. Fan Frame Service Areas (Forward Looking Aft).

Fan frame fabrication will be tailored to include the numerous penetration lines at specified steps in the manufacturing cycle. The lines are of a sheet metal and machined ring welded fabrication with local bosses at each O-ring to support the required clamping force. The scavenge tube and the other penetration lines are welded sheet metal or formed tubing fabricated with the required end connections for the O-ring seals.

Since the composite frame hub forms the sump walls, the original plan was to have a 360° metal liner to protect the composite material from exposure to the hot sump oil; however, a series of exposure tests showed that the composite material suffered no degradation when exposed to hot oil. Supporting test data are presented in Section 8.7. As a result of these tests, the liner was eliminated.

8.4 STRUCTURAL FUNCTIONS

The QCSEE frame is required to perform the following major structural and aerodynamic functions:

- Provides the main engine forward attachment points for thrust, vertical, and side loads sustained during flight and ground handling.
- Supports the fan thrust bearing.
- Supports the fan radial load bearing.
- Supports the reduction gear.
- Supports the compressor thrust bearing.
- Supports the aft inner fan cowl.
- Supports the core compressor at the forward casing flange.
- Supports the fan hub outlet guide vanes.
- Provides the mounting position for the accessory gearbox.

8.5 STRUCTURAL CONCEPT

The overall structural concept used in the frame consists of three basic elements (i.e., structural wheels, shear panels, and reinforcing flanges) with each element designed to perform specific load-carrying functions. The large wheel-like structures are joined together with shear panels which form the bypass and core flowpaths. The frame is then locally reinforced with flanges in the outer casing, splitter, and hub areas as needed.

The structural wheel satisfies several load transfer requirements. First, it transfers tensile and compressive radial loads through the struts from one casing ring to another. Second, it transfers both normal and bending ring loads throughout the ring structure. Third, it transfers any forward overturning bending moments that exist in the strut from one casing shell to another. An example of this type of structure is the frame mid-wheel shown in Figure 8.8.

The shear panels are bonded to the four sides of each wheel cavity and serve as the basic load-carrying members between wheels. The panels perform the following functions. First, they transfer shear forces between wheels imposed on the frame by a forward overturning bending moment. Second, they transfer radial tensile and compressive forces between casings imposed on the struts by a tangential bending moment. Third, they transfer axial tensile and compressive forces between wheels. Fourth, they serve as the airflow surfaces within the frame cavities. Examples of these types of panels are presented in Figures 8.9 and 8.10 which show the nominal bypass vane and the core strut skin, respectively.

The reinforcing flanges located at either end of each strut or vane perform two basic load-carrying functions: first, they transfer tangential bending moments out of the struts and into the forward and aft rings, and second, they transfer tensile and compressive axial loads between wheels.

Analyses have shown that, for the QCSEE frames, a three-wheel frame concept is adequate to carry all imposed loads. The forward wheel is a flat-spoked wheel composed of splitter ring, a hub ring, and six spokes. The middle and aft wheels are flat-spoked wheels composed of an outer casing ring, a splitter ring, a hub ring, six spokes integrally connecting the hub and the splitter rings, and 33 spokes integrally connecting the outer casing and the splitter rings. The shear panels are bonded to the interior of each wheel cavity, and the panels form the airflow surfaces. "L" flanges are bonded to the inner and outer rings and flowpath panels. This structural concept not only provides a frame with highly efficient joints, but also results in a structure which should facilitate fabrication and repair. Structural soundness is enhanced by transferring loads by bonding in many small increments rather than in a few large increments.

Metal engine mount parts and metal brackets are attached to the composite structure by bonding and mechanical fastening. The aft splitter ring contains three engine-mount attachment points. The first attachment point is located at the 0° (12 o'clock) position on the aft splitter ring and consists of a metal uniball which supports vertical and side loads. At 45° down from either side of the metal uniball are metal brackets which support all thrust loads of the engine. The inner hub of the frame has flanges for attachment of fan rotor bearing supports, stationary reduction gear bearing supports, the low pressure turbine shaft forward bearing support, and the core rotor forward bearing support.

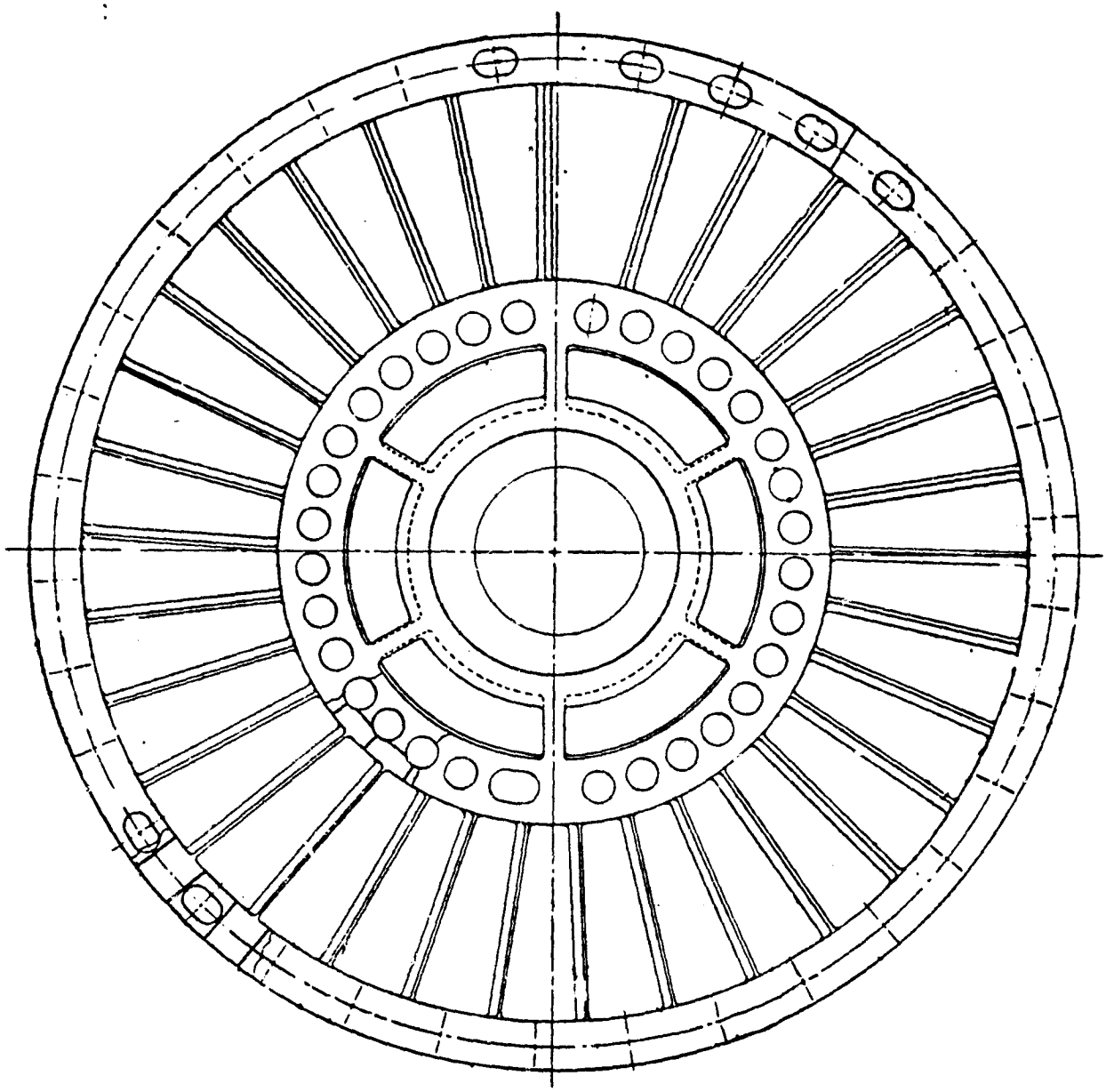

Figure 8.8. Frame Midwheel.

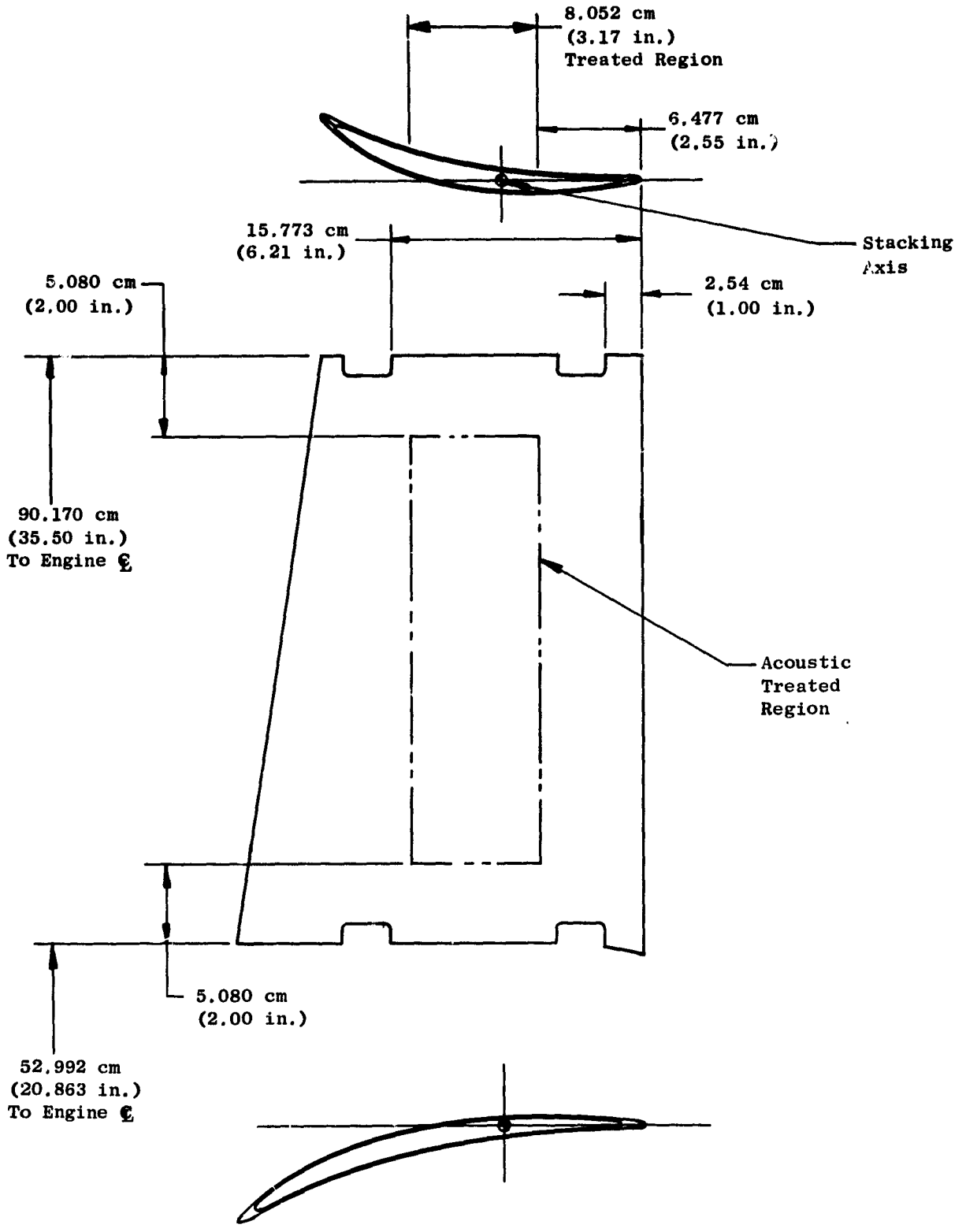

Figure 8.9. Nominal Bypass Vane Skin.

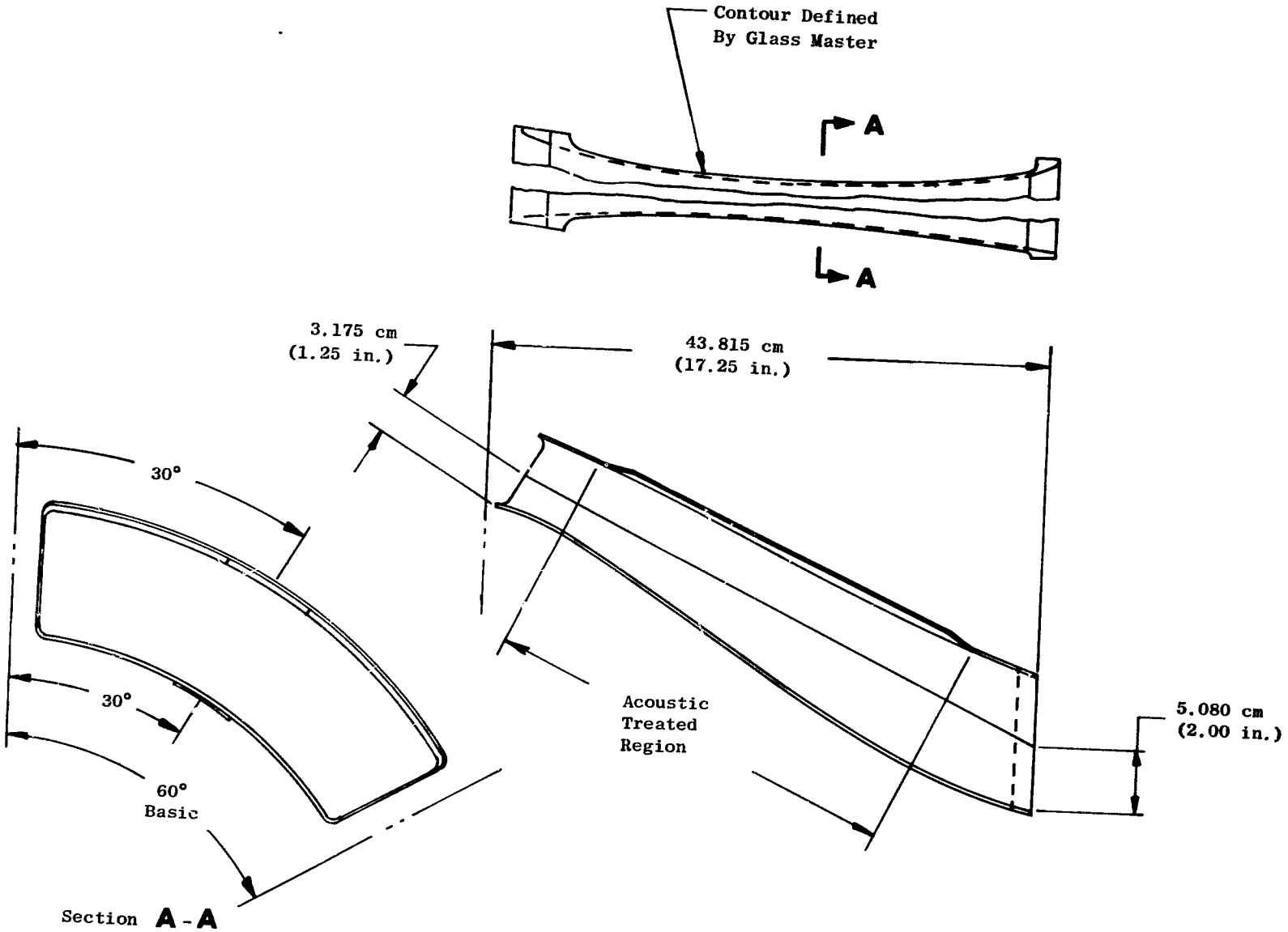

Figure 8.10. Core Strut Skin.

The nacelle and fan casing are integral with the frame from the bypass vanes forward to the inlet. The high strength and stiffness in the frame provide the necessary supports for the stator, radial drive gearbox, and other equipment. The entire wall thickness of the fan case and nacelle is utilized to provide fan shroud stiffness and to support the blade containment member. The full-depth honeycomb is lighter and less expensive to fabricate compared to the conventional double structure. The joints normally required in a metal frame design are minimized, which reduces weight, tooling, and fabrication costs. This concept is particularly well suited to composite materials due to their low density and easy "bondability." Slotted tip treatment and a small area of frangible honeycomb are provided over the fan blade.

8.6 DESIGN ANALYSIS

The integral load distribution for the frame was determined using a finite element computer program which represented the frame structure as a combination of curved beams, straight beams, and plates, all capable of having orthotropic material properties.

In the core region of the frame, the struts were modeled as three straight beams (representing the spokes of the wheels) connected to curved beams in the hub and splitter region (rims of the wheels), all tied together by plates representing the flowpath and splitter walls. The fan flowpath area was represented by radial beams representing the bypass vanes (wheel spokes and flowpath panels were lumped together and appropriate section properties used for these pseudo beams) tied to plates representing the outer casing forward to the inlet. Appropriate structure also was included to represent the mount structure and the compressor case back to the turbine frame; although this structure is not shown in the accompanying figures. The basic mathematical model is shown, superimposed on the frame trimetric in Figure 8.11. Computer generated views of the model are shown in Figures 8.12 and 8.13.

A number of iterations were made on thicknesses and orientations of the various constituent elements of the mathematical model to arrive at an efficient structure, which would satisfy the most severe loading conditions. The frame structure, in conjunction with the engine mounts, must withstand the maneuver loads as imposed by the conditions defined in Table 8-I. The frame must withstand these loads and maintain structural integrity without permanent deformation. In addition, this structure must be capable of transmitting mount loads equivalent to 3.0 times the worst possible combination of maneuver loads without experiencing collapsing, even though the members may acquire permanent deformation. All ultimate load conditions are calculated under a room temperature environment. Investigation of the mission requirements yielded two critical loading cases.

The first case is Condition II (gust loading). Design conditions require the frame to withstand three times the loads of a 51.44 m/sec (100 knot) crosswind acting at any angle within a plane perpendicular to the axis of the engine at zero-to-maximum thrust. This condition was used to size the outer

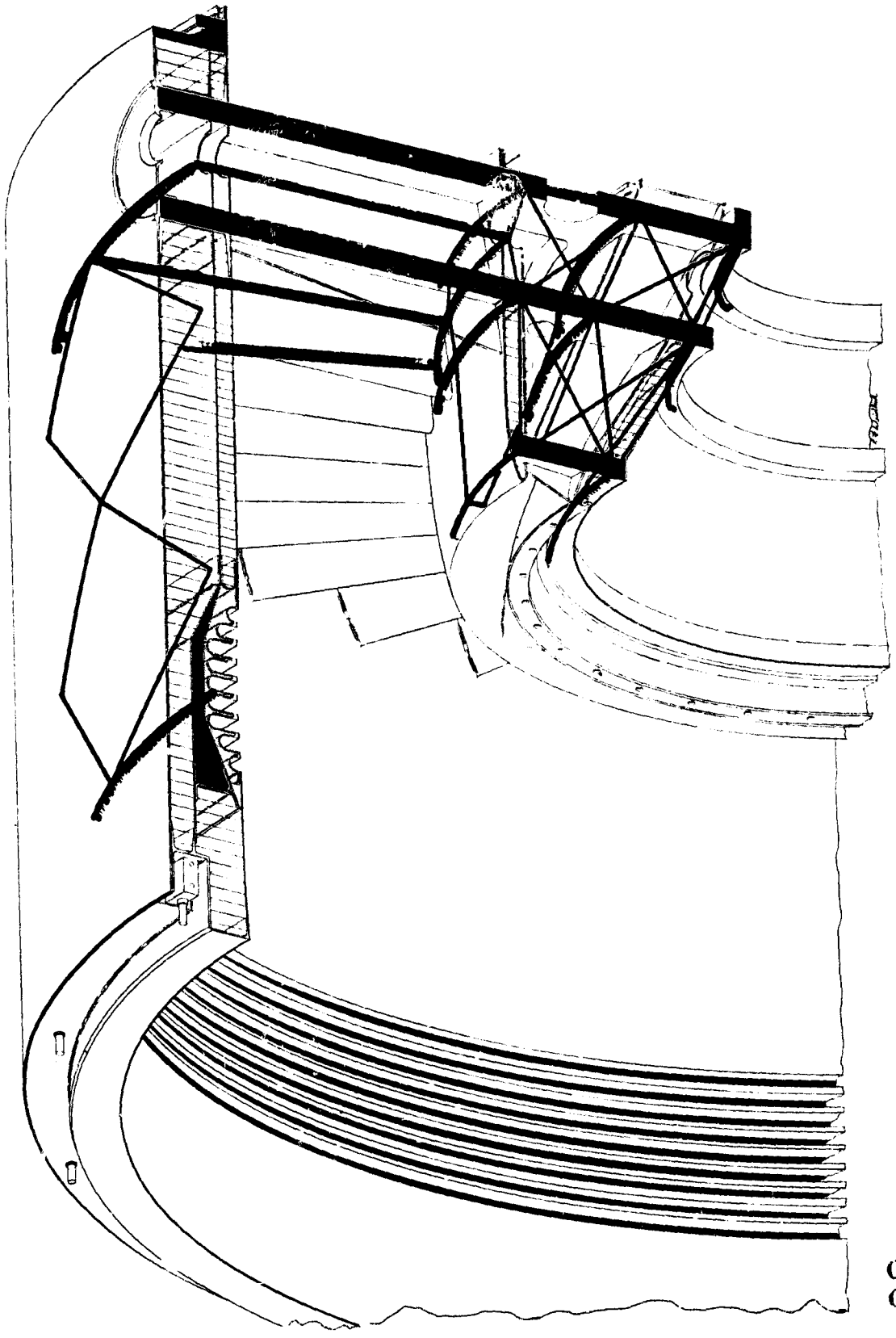

Figure 8.11. Computer Analytical Model of Composite Frame.

C-3

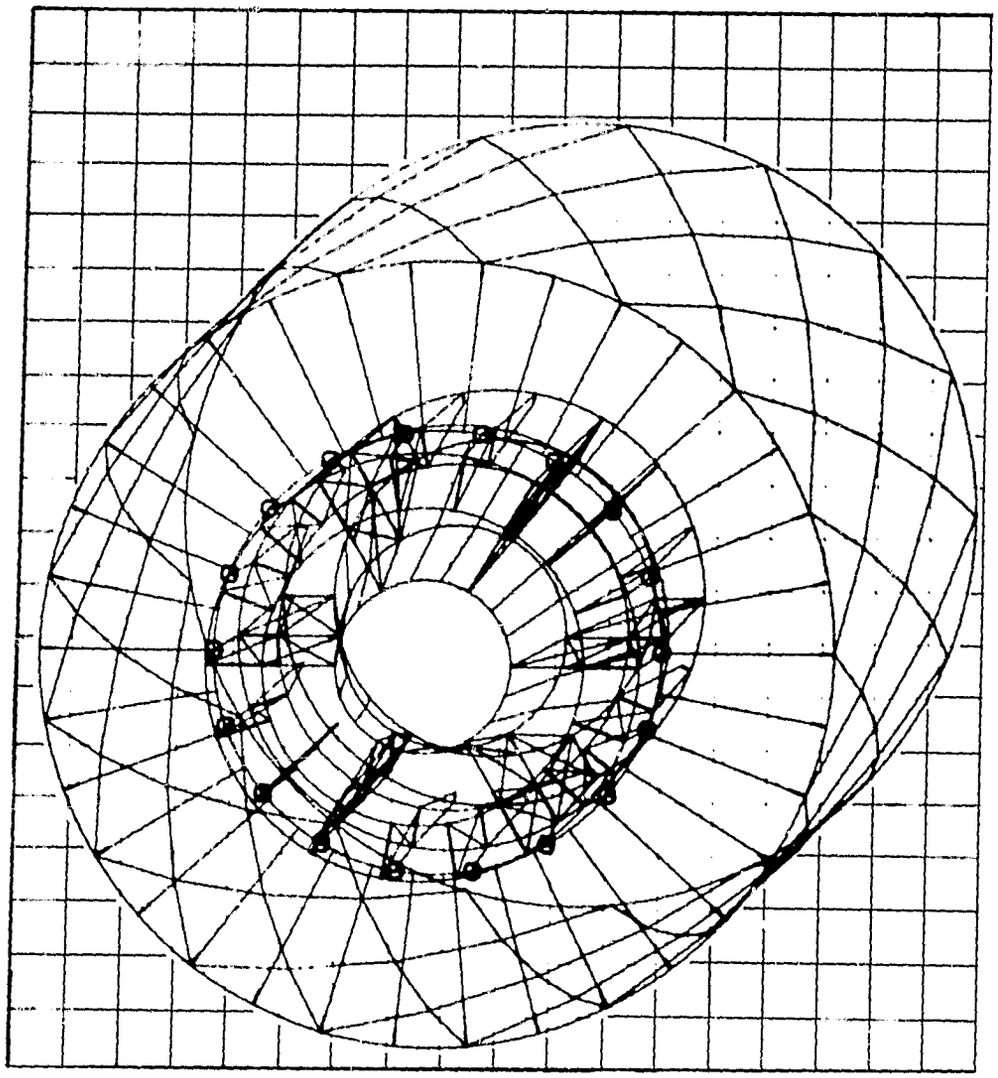

Figure 8.12. Computer Generated 3-Dimensional Finite Element Model - Composite Frame.

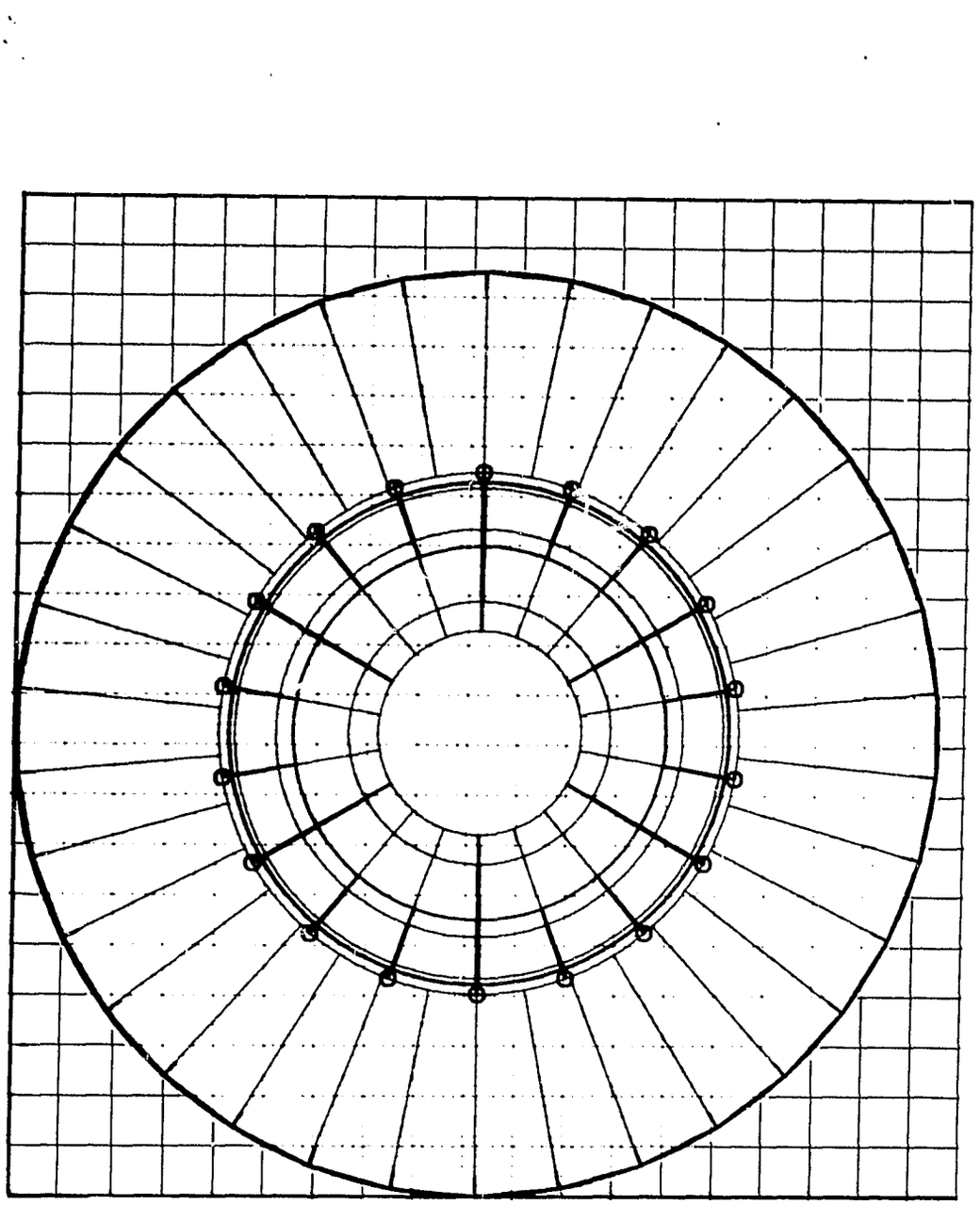

Figure 8.13. Computer-Generated End View Finite Element Model - Composite Frame.

nacelle shell and bypass vanes even though the inlet will not be rigidly attached in the experimental OTW engine configuration.

The second case is the Condition VI five-blade-out condition which requires the frame to withstand the unbalance load resulting from a five composite blade-out condition (UTW engine) on the fan rotor which causes a dynamic, 1/rev radial load on the No. 1 bearing support. This condition sized the core struts, hub, and splitter.

The final sizing for all the major frame structure is shown in Table 8-III, which gives both thicknesses and material configuration. The internal loads, stresses, and deflections associated with this configuration were computed by the program. The critical stresses, along with the predicted allowables for the major structural members, are shown in Table 8-IV. The allowables are taken from the Advanced Composites Design Guide. A comparison of these predicted allowables with coupon test data is presented in Section 8.7. The critical bond stresses calculated from the computer model output are shown in Table 8-V. The maximum radial deflection of the fan casing over the fan was 0.086 cm (0.034 in.). Running clearance is 0.254 cm (0.1 in.).

8.6.1 Thermal Analysis

Due to the low thermal coefficient of expansion that is characteristic of graphite/epoxy composites, an analysis of the critical interface areas, where metal structure is attached to composite structure and subjected to thermal changes, was performed. The only areas where this occurs to any significant extent is in the hub region where the titanium bearing cones are bolted to the composite rings and are subjected to a ΔT of 366° K (200° F). Applying the entire $\alpha\Delta T$ stress to the composite structure results in the stresses shown in Table 8-VI. This table also shows the summation of the static stress and the thermal stress versus the allowable stress. As can be seen, the thermal stresses are relatively low and had little or no effect on the sizing of the composite structure.

8.6.2 Dynamic Analysis

Since the fan stator vanes are an integral part of the fan frame, a dynamic analysis was performed to determine the relationship of the vane first flexural frequency to fan speed for the critical 28 per revolution (28 blade) excitation. The first flexural frequency of the composite vane was estimated by making an empirical correction to a theoretically calculated value. This correction was determined by actually measuring the frequency response of a very similar vane in the composite simulated F101 front frame which was available as a result of a previous program. This measured value was compared to the theoretical value for this vane and the correction factor thus obtained. Using this method, the first flexural frequency of all five of the OTW bypass vane configurations was obtained. These show as a band in Figure 8.14 which shows that first flexural excitation of the vanes will occur between 62% and 84% of the maximum normal fan speed. Although this indicates that the first

Table 8-III. Geometry of Composite Frame Components.

Material: Type AS Graphite/3501 Epoxy

Item	Thickness		Layup Configuration			0° Datum
	cm	Inches	0°	± 45°	90°	
Forward "Wheel"	2.54	1.000	50%	20%	30%	Radial
Middle "Wheel"	2.87	1.130	30%	20%	50%	Radial
Aft "Wheel"	2.87	1.130	30%	20%	50%	Radial
Nacelle Panel	.089	.035	28.5%	57%	14.5%	Axial
Bypass Vane Panel	.127	.050	40%	40%	20%	Radial
Bypass Vane Spoke	2.54	1.000	80%	20%	0%	Radial
Bypass Vane Outer Ring	2.54	1.000	30%	20%	50%	Radial
Core Vane Panel	.203	.080	25%	50%	25%	Axial

Table 8-IV. Frame Component Stresses.

Load Condition	Location	Calculated Stress N/cm^2 (psi)	Mode (1)	Direction (2)	Stress Allowable N/cm^2 (psi)	Temperature ° K (° F)
Ground Test	Forward "Wheel" Hub Ring	17906 (25970)	T	C	42749 (62000)	406 (270)
5 Airfoils Out	Forward "Wheel" Hub Ring	37233 (54000)	T	C	42749 (62000)	406 (270)
Ground Test	Forward "Wheel" Spoke	19805 (28723)	C	R	65503 (95000)	294 (70)
5 Airfoils Out	Forward "Wheel" Spoke	53574 (77700)	C	R	65503 (95000)	294 (70)
Ground Test	Bypass Vane Panel	4208 (6103)	C	R	57229 (83000)	294 (70)
Critical Flight	Bypass Vane Panel	40921 (59349)	T	R	57229 (83000)	294 (70)
Ground Test	Bypass Vane Spoke	2742 (3977)	C	R	93083 (135000)	294 (70)
Critical Flight	Bypass Vane Spoke	34938 (50671)	C	R	93083 (135000)	294 (70)
5 Airfoils Out	Core Panel	8599 (12471)	S	---	17238 (25000)	294 (70)
Ground Test	Nacelle Panel	2803 (4065)	T	A	27580 (40000)	294 (70)
Critical Flight	Nacelle Panel	12699 (18417)	T	A	27580 (40000)	294 (70)

(1)T - Tension, C - Compression, S - Shear. (2) C - Circumferential, R - Radial, A - Axial

Table 8-V. Bond Shear Stresses.

Load Case (1) No.	Location	Design Stress (2)		Allowable Stress	
		N/cm^2	psi	N/cm^2	psi
2	Vane/Splitter	605	878	1034	1500
6	Panel/O.R. Fwd "Wheel"	748	1085	1034	1500
6	Panel/Spoke Fwd "Wheel"	806	1169	1034	1500
6	Panel/I.R. Fwd "Wheel"	481	698	1034	1500

(1) Case 2 - 154.33-m/sec^2 (100-knot) crosswind gust load + maximum maneuver.

Case 6 - 5 composite blades out + maximum maneuver.

(2) Design stress - 3 × actual for flight and actual for emergency conditions.

Table 8-VI. Effect of Different Thermal Coefficients.

Ring	Thermal Coefficient Graphite Epoxy Ring cm/cm/° K x 10^{-6} (in./in./° F x 10^{-6})	Bearing Number	Thermal Coefficient Bearing - Ti6-4 cm/cm/° K x 10^{-6} (in./in./° F x 10^{-6})	Thermal Stress N/cm^2 (psi)	Static Ring Stress N/cm^2 (psi)	Total Stress N/cm^2 (psi)	Allowable Stress N/cm^2 (psi)
Forward Hub	4.5 (2.5)	1a, 1b	8.46 (4.7)	2069 (3000)	37233 (54000)	39302 (57000)	42749 (62000)
Mid Hub	2.34 (1.3)	2	8.46 (4.7)	4827 (7000)	20685 (30000)	25512 (37000)	59987 (87000)
Aft Hub	2.34 (1.3)	3	8.46 (4.7)	4827 (7000)	13790 (20000)	18617 (27000)	59987 (87000)

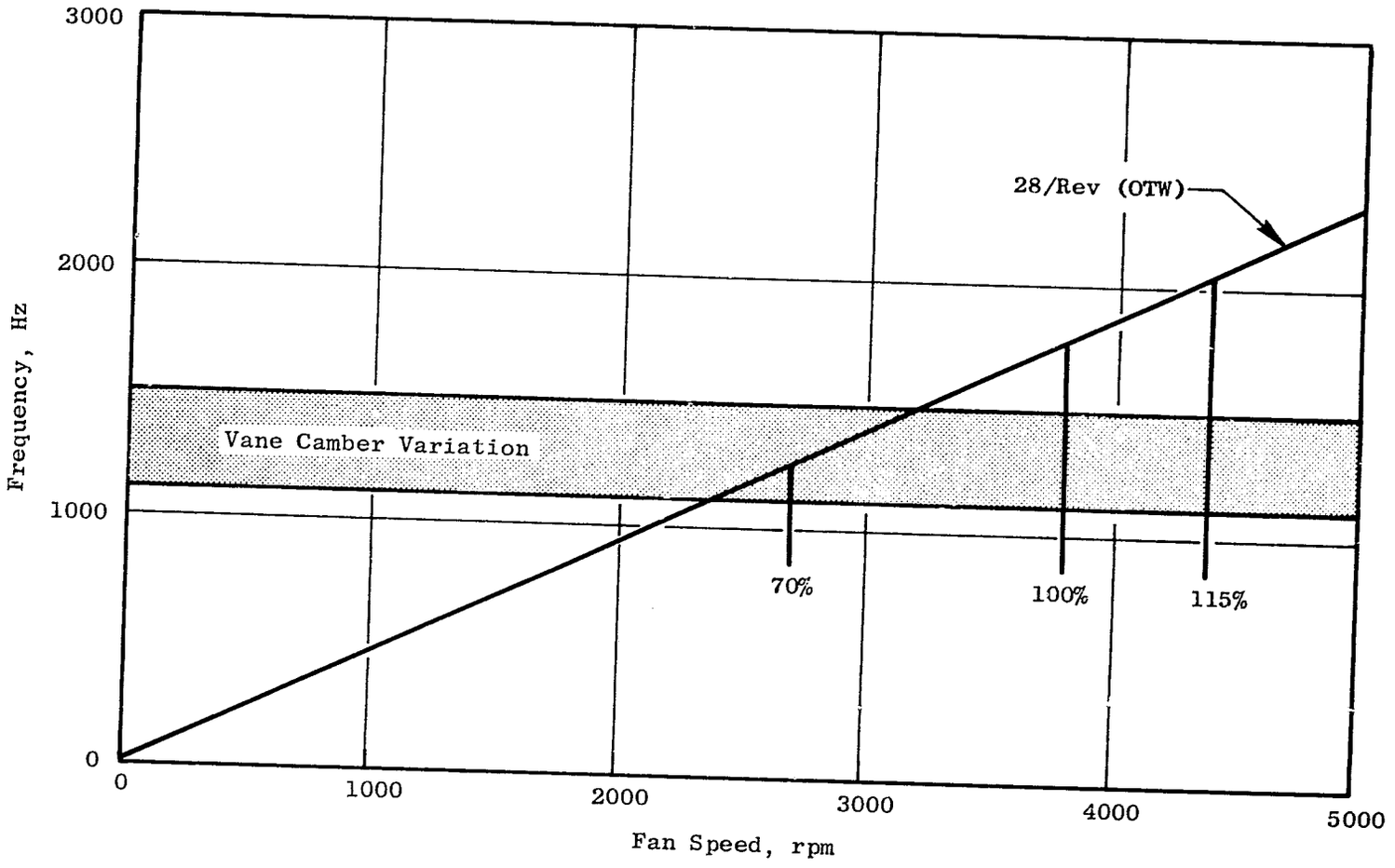

Figure 8.14. First Flexural Mode of Composite Frame Bypass Vanes

flexural frequency falls within the fan operating range, this should not be a problem since a relatively low rpm range is involved, the rotor vane spacing is large, the fan pressure ratio is low, the fan Mach number is less than 1, and the composite structure has good damping characteristics. Some vanes will be instrumented with strain gages during initial engine testing to ensure that vibratory stresses do not exceed safe levels.

8.6.3 Weight Analysis

A weight analysis was made based on the structure described in Section 8.3 and the sizing determined from the structural analysis. Results of this analysis are shown in Table 8-VII. These weights , however, do not include the weight of instrumentation or auxiliary items, even though they will become an integral part of the frame.

8.7 SUPPORTING DATA

The composite frame must attach to (and be detachable from) various structures at a large number of locations. Also, the composite frame employs a large number of structural joints that are integrally bonded rather than mechanically fastened together. Component tests were conducted using specimens and subcomponents representative of various critical areas of the frame to verify the effect of geometry, fiber orientation, and environmental exposure on the allowable design stress levels in these specific components.

8.7.1 Element Test Program

The material properties used in the design and analysis of the composite fan frame were taken from the Advanced Composites Design Guide, third edition. A limited element test program was conducted to verify that the processing techniques to be used on the frame would produce adequate results, and also to provide a check on the data obtained from the Design Guide. The test program is summarized in Table 8-VIII. Four critical areas of the frame were selected and preliminary material configurations were defined. Since the purpose of the test program was to verify the processing techniques and not to produce specific design data, it was not necessary to delay the test program until the final material configurations were determined. The test results for the tension, compression, shear, and bolt hole testing are shown in Tables 8-IX through 8-XII. Configurations 101 and 102, as defined in Table 8-IX were relatively thin [0.127 cm (0.050 in.)] and several tab failures occurred during the IITRI (Illinois Institute of Technology Research Institute) type tensile testing. Comparable sandwich beam tests indicated that the tensile values obtained from the tests in which tab failures occurred were not representative. Configurations 103 and 104 were relatively thick [0.0254 cm (0.100 in.)] and sandwich beam data could not be obtained due to shear failure of the core-to-face bond, as indicated in Tables 8-IX and 8-X. The only test

Table 8-VII. Composite Frame Weight Breakdown.

	Weight	
	kg	lb
Composite "Wheels," Rings, and Panels	120.2	265
Honeycomb	13.2	29
Composite Reinforcing Flanges	21.8	48
Adhesive	4.5	10
Inlet Flange	8.6	19
Sump Shield	2.7	6
Containment	20.9	46
TOTAL WEIGHT	191.9	423
Mounts	10.4	23

Table 8-VIII. Test Specimen Configurations.

Serial Identification	General Configuration Representation	Material	0° Datum	Test Dir.	Test Temp.	Test Mode (2)									
						IITRI (3) Tensile	Sandwich Beam Tensile	Sandwich Beam Compression	Rail Shear (Flat Panel)	Rail Shear (Sandwich Panel)	Interlaminar Shear	Bolt Hole Bearing	Bolt Hole Shear-[illegible]	Bolt Hole Net Tension	Clamping
101	Outer Nacelle Shell	Boron-Graphite/ Epoxy	Axial	0°	R.T.	X	X	X	X	X					
				90°	R.T.	X	X	X	X	X					
102	Bypass Vane Panels	Graphite/Epoxy	Radial	0°	R.T.	X	X	X	X						
				90°	R.T.	X		X	X						
		Graphite/Epoxy (10% Open Area)	Radial	0°	R.T.	X	X	X	X	X					
103	Bypass Spoke	Boron-Graphite/ Epoxy(1)	Radial	0°	R.T.	X		X			X				
104	Forward Core Spoke and Rings	Graphite/Epoxy	Radial	0°	R.T.	X	X	X	X		X	X	X	X	
				0°	406° K (270° F)	X		X				X	X	X	X
				90°	R.T.	X		X	X		X	X	X	X	
				90°	406° K (270° F)	X		X				X	X	X	

(1) 0° Plys - Boron
± 45° and 90° plys are graphite

(2) Each test mode consists of 3 replicates

(3) IITRI - Illinois Institute of Technology Research Institute

Table 8-IX. Tensile Test Results.

Basic Material - Graphite/Epoxy

Serial Identification	Laminate Configuration % Fiber at 0°	45°	90°	Load Direction (degrees)	Temperature ° K (° F)	Predicted Stress N/cm^2 (psi)	Avg. Test Results: IITRI[4] N/cm^2 (psi)	Avg. Test Results: Sandwich Beam N/cm^2 (psi)	Average % Difference
101	14[1]	57	29	0	Room Temperature	23305 (33800)	23395 (34800)	24408 (35400)	+4
				90	Room Temperature	39439 (57200)	32682 (47400)[2]	40405 (58600)	+2
102	40	40	20	0	Room Temperature	56539 (82000)	53919 (78200)	51575 (74800)	-7
				90	Room Temperature	37923 (55000)	27856 (40400)[2]	--- ---	--- ---
103	80[1]	20	0	0	Room Temperature	93083 (135000)	94875 (137600)	--- ---	+2
104	50	20	30	0	Room Temperature	64124 (93000)	51023 (74000)	(3)	-20
				0	406 (270)	59987 (87000)	69364 (100600)	--- ---	+16
				90	Room Temperature	44128 (64000)	51988 (75400)	--- ---	+18
				90	406 (270)	42060 (61000)	63020 (91400)	--- ---	+50

(1) Boron/epoxy

(2) Tab failures

(3) Excessive beam deflection failed core-to-face bond

(4) IITRI - Illinois Institute of Technology Research Institute

Table 8-X. Compression Test Results.

Sandwich Beam Tests

Serial Identification	Load Direction	Temperature ° K (° F)	Predicted Stress		Test Results		% Difference
			N/cm^2	psi	N/cm^2	psi	
101	0	Room Temperature	39370	57100	43645	63300	+11
	90	Room Temperature	40749	59100	37026	53700	- 9
102	0	Room Temperature	56539	82000	54195	78600	- 4
	90	Room Temperature	30338	44000	29580	42900	- 3
103	0	Room Temperature	144795	21000	*	---	---
104	0	Room Temperature	65503	95000	*	---	---
	0	406 (270)	48265	70000	*	---	---
	90	Room Temperature	43439	63000	*	---	---
	90	406 (270)	33786	49000	*	---	---

*Laminate did not fail - aluminum-to-honeycomb core bond failure.

Table 8-XI. Shear Test Results.

All Tests at Room Temperature

Serial Identification	Load Direction (degrees)	In Plane (Pail) Shear					Interlaminar (Short Beam) Shear Test Results	
		Predicted Stress		Actual Stress		% Difference		
		N/cm^2	psi	N/cm^2	psi		N/cm^2	psi
101 (Laminated)	0	16203	23500(1)	13928	20200	-14	---	---
	90	16203	23500(1)	18065	26200	+11	---	---
101 (Sandwich)	0	19306	28000	24133	35000	-25	---	---
	90	19306	28000	24133	35000	-25	---	---
102 (Laminated)	0	17238	25000	19651	28500	+14	---	---
	90	17238	25000	18410	26700	+ 7	---	---
103	---	---	---	---	---	---	8964	13000
104 (Laminated)	0	10687	15500	9860	14300(2)	- 8	5033	7300
	90	10687	15500	16962	24600	+59	6343	9200

(1) Buckling.

(2) Load deformation curve stepped at this value. Final failure at 17,376 N/cm^2 (25,200 psi).

Table 8-XII. Bolt Hole Test Results.

All Tests Done on Serial Number 104 Type Laminates

Temperature ° K (° F)	Load Direction (degrees)	Bearing Stress		Net Tension Stress		K_s	Shear Out Stress	
		N/cm^2	psi	N/cm^2	psi		N/cm^2	psi
Room Temperature	0	48058	69700	42266	61300	1.2	18823	27300
Room Temperature	90	48265	70000	43439	63000	1.2	19030	27600
406 (270)	0	53505	77600	43576	63200	1.6	16272	23600
406 (270)	90	55160	80000	39370	57100	1.6	16617	24100

value in the program that was significantly below predicted was the zero degree orientation at room temperature test of Configuration 104. Other tests of this configuration [90° orientation at 406° K (270° F) temperature] were considerably above predicted strength, indicating that the results for zero degrees orientation at room temperature were not valid. Based on these data, it was concluded that it was reasonable and valid to use information obtained from the Design Guide for the design and analysis of the frame.

To evaluate the effect of acoustic treatment holes in the vane skins, IITRI tensile tests were run using a 10% open area pattern of holes. The gross tensile strength was 29,650 N/cm^2 (43,000 psi) and the net tensile strength was 37,720 N/cm^2 (54,700 psi) compared to a baseline (no holes) value of 53,920 N/cm^2 (78,200 psi) as shown in Table 8-IX. This gives a stress concentration factor of 1.43. This information was taken into account in the stress analysis of the bypass vanes. The same stress concentration was assumed for the acoustically treated outer casing.

8.7.2 Fluid Exposure Tests

Two series of tests were run to evaluate the effect of elevated temperature exposures to aircraft fluids. The first series of tests evaluated the exposure to "Skydrol 500C." The exposure conditions were of an intermittent nature which left residual fluid on the composite material. The specific composite material system tested was the type AS graphite fiber in Hercules' 3501 epoxy resin matrix.

The degradation due to exposure was measured as changes in the compression and tension values of the exposed material. The composite material was molded and fabricated into individual test specimens. The tension specimens were of the IITRI type, while the compression specimens were modified ASTMD 695-69 specimens. The specimens, except for the control specimens, were exposed to "Skydrol 500C" hydraulic fluid for five minutes at 355° K (180° F) followed by an oven exposure (without wiping or drying the specimens) at 355° K (180° F) for time periods ranging from 0 to 15 days. Ultimate strength values were then obtained from the specimens.

The results of these tests are shown in Figure 8.15. Although there is some test scatter, it appears that the material system tested was not degraded by the exposure.

Another series of tests was made to determine if the hot sump oil could be in direct contact with the composite frame without causing degradation in the composite material properties. The primary purpose of these tests was to determine if a metal oil shield was required in the sump region.

Tensile test specimens (IITRI) were fabricated using the AS/3501 graphite epoxy system. The lay-up pattern was (45, 0, -45, -45, 90, 45, 45, 90, -45, -45, 0, 45), which is representative of the composite sandwich facing in the sump region which would be in contact with the hot oil. Several of the

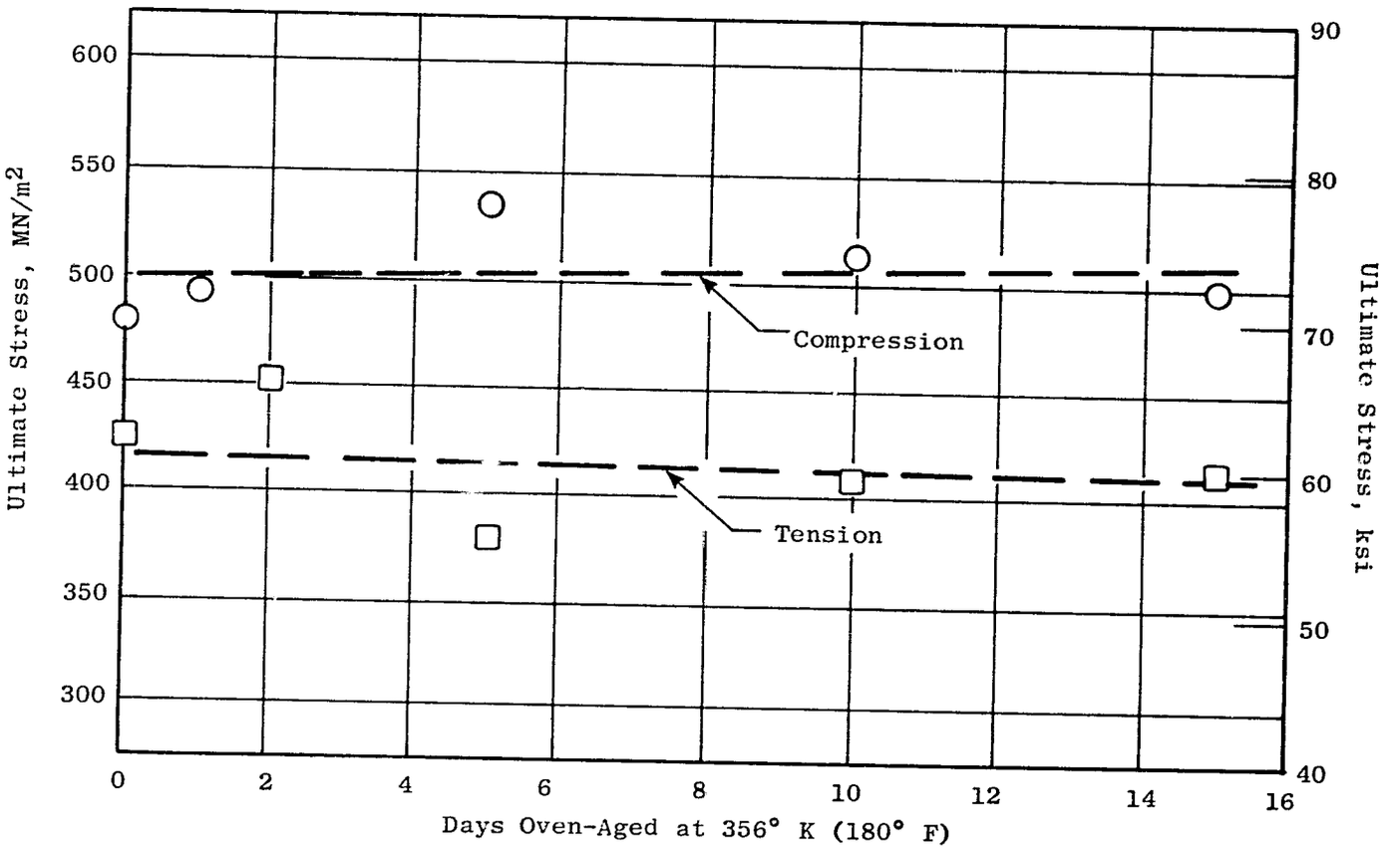

Figure 8.15. Graphite/Epoxy AS 3501 Exposed to Skydrol 500C for 5 Minutes at 356° K (180° F), Tested at 356° K (180° F).

specimens were coated with different coatings to see if they would provide any additional protection to the bare composite. The coatings used were Nubulan, Valspar, and Metlbond 328 adhesive. The specimens were soaked in hot MIL-L-23699 oil for one week at an oil temperature of 422° K (300° F). The specimens were then tested to failure at 405° K (270° F). In addition to the oil exposure specimens, several unexposed specimens were tested at 405° K (270° F) after 30 minutes in 422° K (300° F) air and several after one week in 422° K (300° F) air. The resulting test data are shown in Table 8-XIII. The predicted unexposed tensile strength, as obtained from the Design Guide for these specimens is 31,720 N/cm^2 (46,000 psi) at 405° K (270° F). Based on these data it was concluded that there was no degradation of the bare graphite/epoxy due to exposure to hot MIL-L-23699 oil, and neither the oil shield nor the protective coatings are required.

8.7.3 Subcomponent Tests

Since one of the most critical areas of composite structures is the joining of the individually molded pieces, either by bonding or mechanical fastening, the critical joint areas of the fan frame will be individually tested prior to the final frame assembly. This series of subcomponent tests are outlined in Figure 8.16 and listed in Table 8-XIV. The average results of these tests are shown in Table 8-XV along with the analytically predicted values and the values actually required by the frame design. As can be seen, the test results show that the specimens more than meet the requirements in all cases.

Table 8-XIII. Exposure Evaluation of MIL-L-23699.

Specimens	Exposure Environment	Coating	Stress	
			N/cm^2	psi
A	422° K (300° F) air for 30 min.	None	32173	46661
B	422° K (300° F) air for 1 week	None	33103	48010
C	Set 1 422° K (300° F) oil for 1 week	None	31758	46060
C	Set 2 422° K (300° F) oil for 1 week	None	33269	48251
D	422° K (300° F) oil for 1 week	Nubulan	33765	48970
E	422° K (300° F) oil for 1 week	Valspar	30283	43920
F	422° K (300° F) oil for 1 week	Metlbond	32949	47787

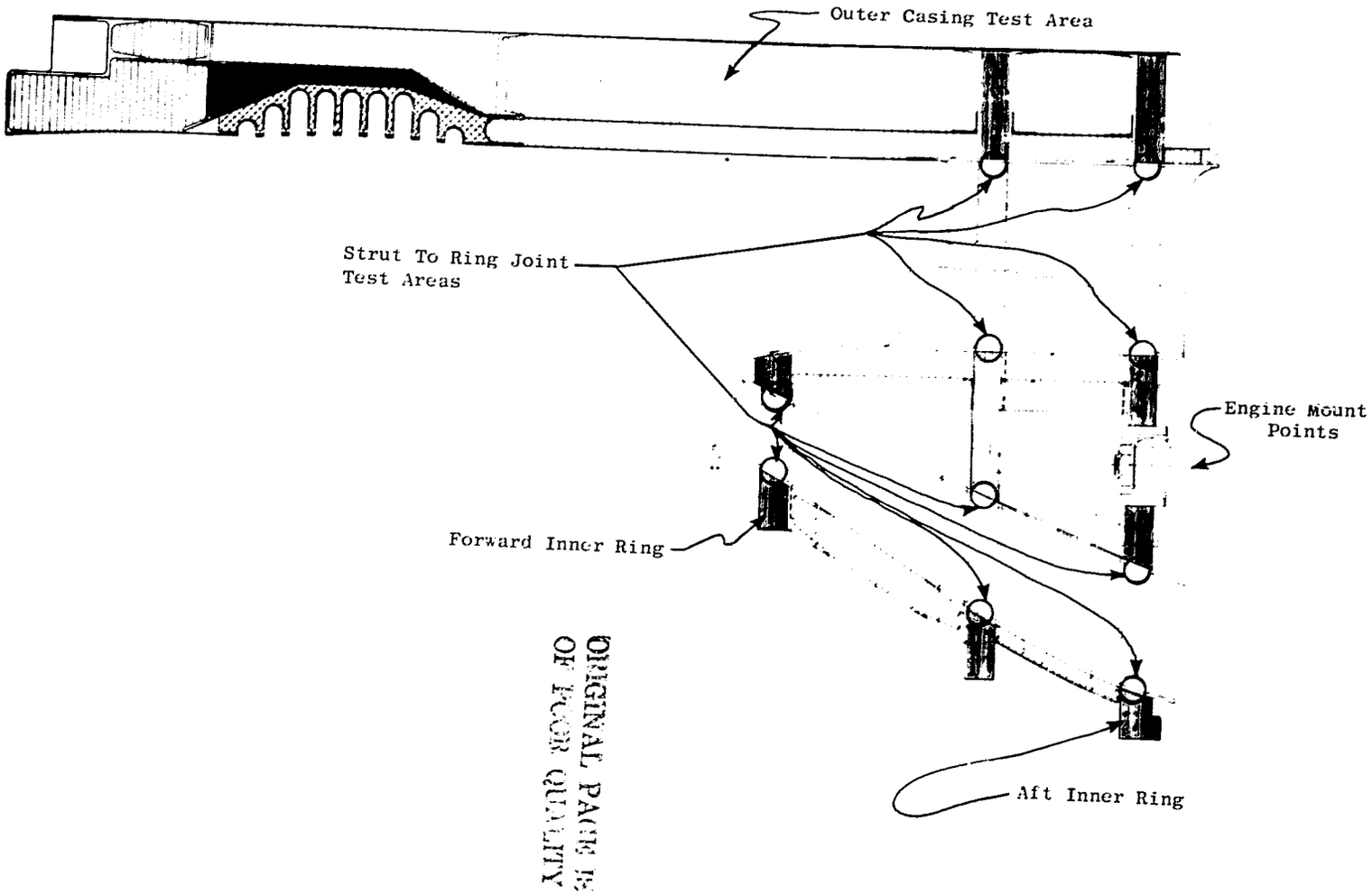

Figure 8.16. Frame Subcomponent Test Areas.

Table 8-XIV. Composite Frame Subcomponents Test Plan Summary.

Test Specimen Configuration	Test Temperature	Test Mode	No. of Replicates (Tests)
Ring structures			
Forward inner ring	Room temperature	Bend - I.D. tension	2
Forward inner ring	Room temperature	Bend - I.D. comp.	2
Aft inner ring	Room temperature	Bend - I.D. tension	2
Aft inner ring	406° K (270° F)	Bend - I.D. tension	2
Aft inner ring	Room temperature	Bend - I.D. comp.	2
Aft inner ring	406° K (270° F)	Bend - I.D. comp.	2
Strut-to-ring joints			
Core vane forward	Room temperature	Spoke tension	2
Core vane mid	Room temperature	Spoke tension	2
Core vane aft	Room temperature	Spoke tension	2
Core vane aft	406° K (270° F)	Spoke tension	2
Fan vane forward	Room temperature	Spoke tension	2
Fan vane aft	Room temperature	Spoke tension	2
Maximum moment joint	Room temperature	Spoke bending	2
Engine mount attachment			
Uniball attachment	Room temperature	Radial load	1
Uniball attachment	406° K (270° F)	Radial load	1
Thrust link attachment	Room temperature	Axial load	1
Outer casing			
Honeycomb sandwich panel	Room temperature	Bend - I.D. tension	2
Honeycomb sandwich panel	Room temperature	Bend - I.D. comp.	2
Inlet-to-frame attachment	Room temperature	Tension	1
Core Cowl Extension to Frame Joint	406° K (270° F)	Tension	1
Frame to Outer Cowl Door Joint	Room Temperature	Tension	1

Table 8-XV. Subcomponent Test Results.

Test Specimen Configuration	Test Temperature	Test Mode	Required for Safe Design	Failure Loads	
				Predicted	Test Average
Ring Structures					
Forward inner ring	Room temperature	Bend - I.D. tension	48590 cmN	257640 cmN	300580 cmN / 26600 in-lb
Forward inner ring	Room temperature	Bend - I.D. comp.	18080 cmN	298320 cmN	427140 cmN / 37800 in-lb
Aft inner ring	Room temperature	Bend - I.D. tension	59100 cmN	354140 cmN	297472 cmN / 26325 in-lb
Aft inner ring	406° K (270°F)	Bend - I.D. tension	59100 cmN	354140 cmN	312083 cmN / 27618 in-lb
Aft inner ring	Room temperature	Bend - I.D. comp.	59100 cmN	442734 cmN	498330 cmN / 44100 in-lb
Aft inner ring	406° K (270°F)	Bend - I.D. comp.	59100 cmN	442734 cmN	519303 cmN / 45956 in-lb
Strut-To-Ring Joints					
Core vane forward	Room temperature	Spoke tension	177920 N	273552 N	245530 N / 55200 lb
Core vane mid	Room temperature	Spoke tension	213950 N	269550 N	298016 N / 67000 lb
Core vane aft	Room temperature	Spoke tension	20016 N	114314 N	105418 N / 23700 lb
Core vane aft	406°K (270°F)	Spoke tension	20016 N	-	123210 N / 27700 lb
Fan vane forward	Room temperature	Spoke tension	34660 N	153130 N	105868 N / 23800 lb
Fan vane aft	Room temperature	Spoke tension	42667 N	108092 N	71172 N / 16000 lb
Maximum moment joint	Room temperature	Spoke bending	128820 cmN	160460 cmN	164980 cmN / 14600 in-lb
Engine Mount Attachment					
Uniball attachment	Room temperature	Radial load		230435 N	253015 N / 56880 lb
Uniball attachment	406°K (270°F)	Radial load		-	207732 N / 46700 lb
Thrust link attachment	Room temperature	Axial load	111206 N	182377 N	120102 N / 27000 lb
Outer Casing					
Honeycomb sandwich panel	Room temperature	Bend - I.D. tension	23906 N/cm^2	31164 N/cm^2	31268 N/cm^2 / 45350 psi
Honeycomb sandwich panel	Room temperature	Bend - I.D. comp.	23906 N/cm^2	31164 N/cm^2	36236 N/cm^2 / 52555 psi
Inlet-To-Frame Attachment	Room temperature	Tension	9341 N	28800 N	28636 N / 6438 lb
Core Cowl Extension To Frame Joint	406°K (270°F)	Tension	297.7 N/cm	774 N/cm	788 N/cm / 450 lb/in.
Frame to Outer Cowl Door Joint	Room temperature	Tension	446.5 N/cm	630.4 N/cm	446.5 N/cm / 255 lb/in.

SECTION 9.0

REDUCTION GEAR DESIGN

9.1 SUMMARY

A reduction gear is utilized in the OTW engine to provide a decrease in rotational speed between the low pressure turbine and the fan rotor. Application of the reduction gear permits the low-tip-speed fan to be driven by a two-stage F101 low pressure turbine. As shown in Figure 9.1, the main reduction gear which is located in the forward engine sump region has a gear ratio of 2.062 reducing the low pressure turbine speed from 7962 rpm to 3862 rpm for the fan. Input design power to be transmitted by the reduction gears is 12,813 kw (17,183 hp).

The main reduction gear is being designed and developed by the Curtiss-Wright Corporation, Wood-Ridge, New Jersey. The design is based on application of technology developed by Curtiss-Wright for the reduction gear set of the YT49 turboprop engine.

The OTW gear set is arranged in an epicyclic star configuration. The low pressure power turbine drives a sun gear which drives a ring gear through a set of eight star gears. These star gears are mounted on spherical roller bearings which in turn, are, mounted on a fixed carrier. This arrangement provides the required gear ratio and results in a compact lightweight design.

Design gear stresses have been maintained within industry-approved limits for the flight design. Somewhat higher stresses will be encountered during a limited part of the experimental testing. This higher stress level only occurs during fan mapping and is within limits previously found acceptable by both Curtiss-Wright and General Electric. Gear scoring will be prevented by controlling inlet oil temperatures and oil flows. The contact ratio of the gears is maintained at a value of 2, further reducing stress since two gear teeth per mesh are always in contact and sharing the load. This high contact ratio also reduces vibration and noise.

A bearing test program was conducted to ensure satisfactory star gear spherical roller bearing operation prior to testing in the gearbox. Results indicated the selected bearing design with reduced radial clearance would meet the requirements of the OTW experimental engine.

Back-to-back rig tests of two OTW reduction gear units are planned for the second quarter of 1976 to substantiate the design prior to engine test. A third OTW unit will be built expressly for engine use and will be tested prior to shipment.

- Gear Ratio - 2.062

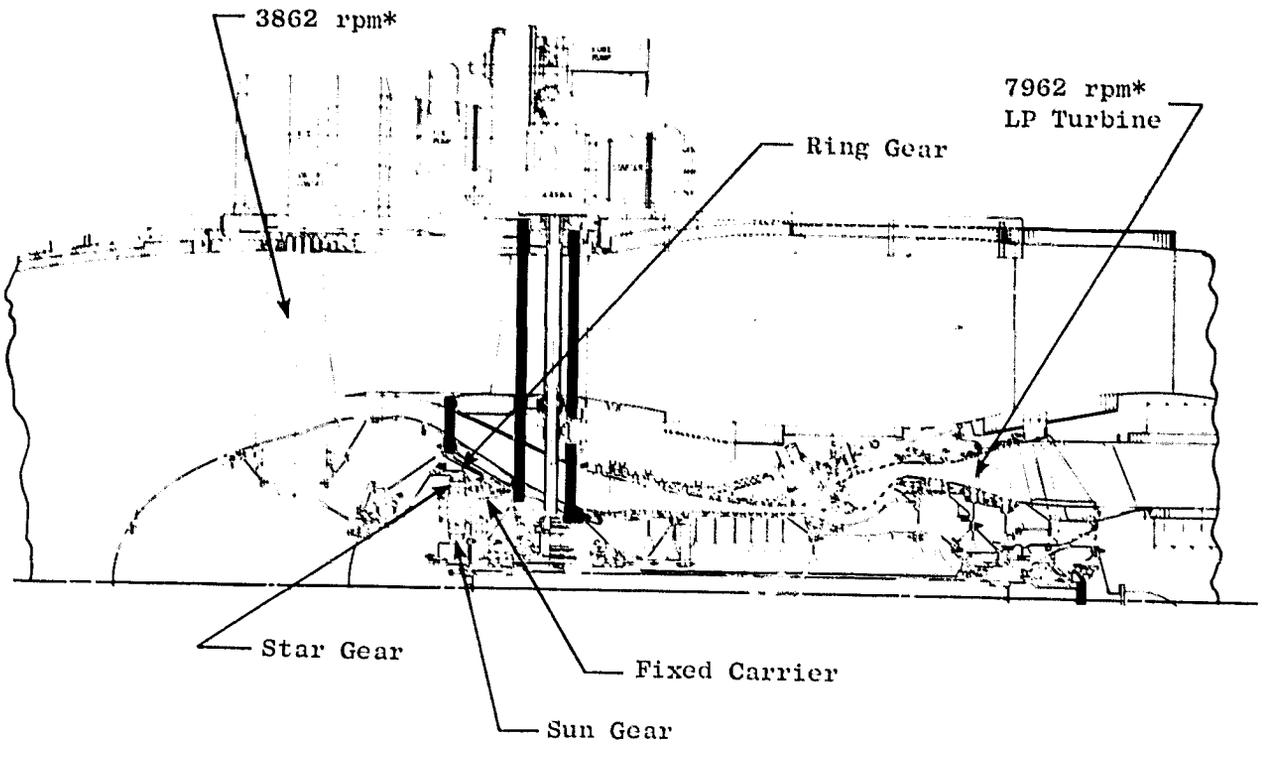

* Takeoff, 305° K (90° F) Day

Figure 9.1. Low Pressure Rotor Configuration.

9.2 DESIGN REQUIREMENTS

The OTW main reduction gear unit was designed to meet the following general requirements:

- 36,000 hours of life
- 6,000 hours time between overhaul (TBO)
- 6,000 hours minimum bearing B_1 life
- Flight weight design
- Minimum noise
- MIL-L-23699 or MIL-L-7808 oil
- Minimum efficiency of 99.2% (100% speed, 100% power)

The gear set has been designed to satisfy the above requirements in accordance with the Flight Duty Cycle specified in Section 2.0 of this report. The resulting design then was checked for satisfactory operation in the experimental engine ground test cycle.

A common set of engine/reduction gear interfaces was established for the UTW and OTW main reduction gears to permit commonality of the engine interface components (fan frame, engine bearings, shafting, etc.) between the UTW and OTW engines.

9.3 DESIGN DESCRIPTION

The OTW reduction gear is an epicyclic star gear arrangement, as illustrated in Figure 9.2. The star arrangement uses a concentric sun gear and ring gear with a set of idlers (star gears) between them. The star gears, which are mounted by spherical roller bearings on a fixed support (star gear carrier), distribute the load to many teeth in both the input sun gear and output ring gear members. Power input to the unit is transmitted from the low pressure turbine through a flexible coupling to the sun gear. Output power to the fan is transmitted from the internal tooth ring gear through a spline and cone shaft to the fan disk shaft. Design and configuration details are presented in Table 9-I.

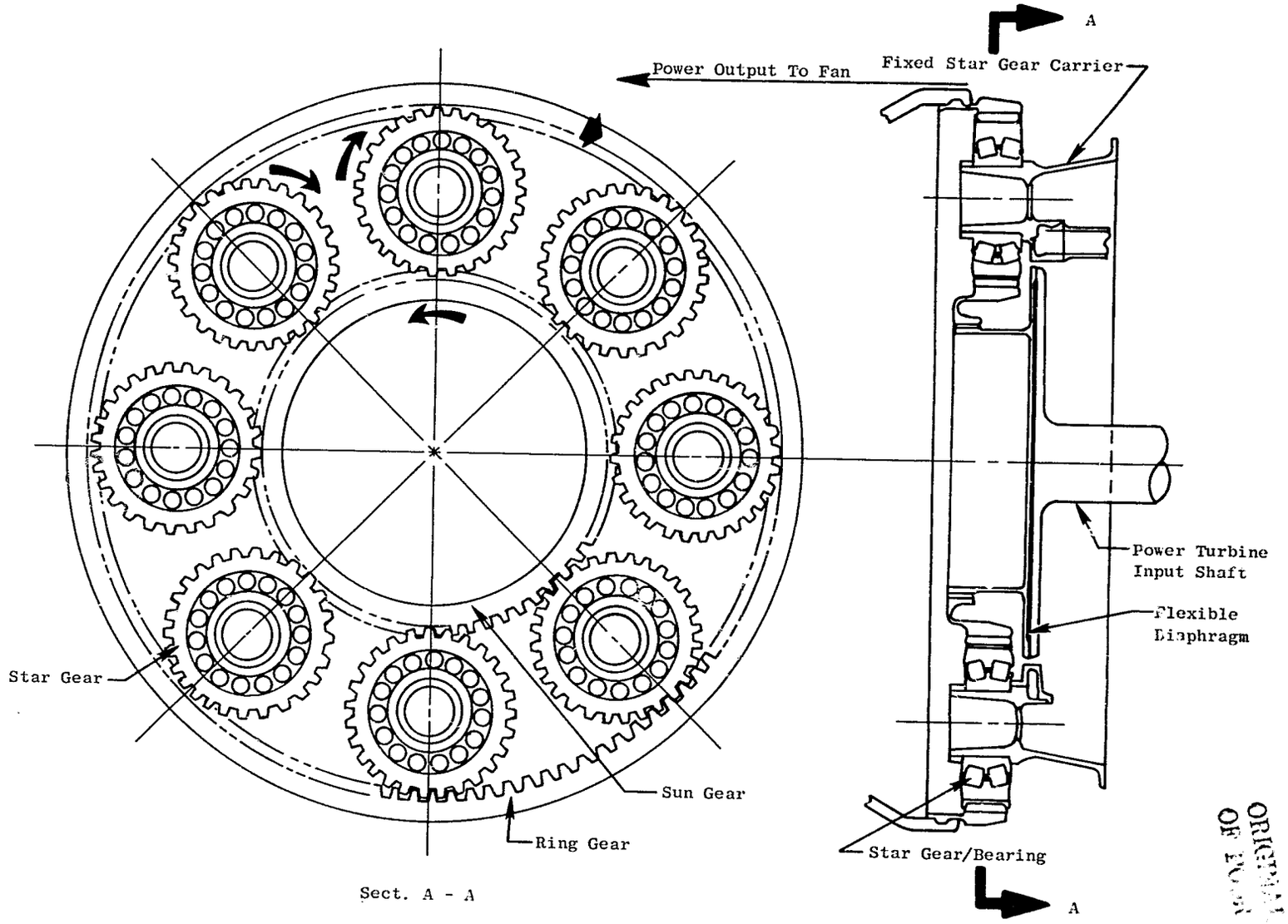

Figure 9.2. Main Reduction Gear Configuration.

Table 9-I. OTW Reduction Gear Design Details.

[Takeoff, 360° K (90° F) Day]
[100% Power, 100% Speed]

Gear ratio	2.062
Turbine power	12813 kw (17183 hp)
Turbine speed	833.8 rad/sec (7962 rpm)
Gear pitch line velocity	119.3 m/sec (23488 ft/min)
Star gear speed	1570.6 rad/sec (14998 rpm)
Bearing load	26,845N (6035 lbs)
Number of stars	8
Number of gear teeth	
Sun gear	81
Star gear	43
Ring gear	167
Hunting	Yes
Nonfactoring	Yes

9.4 DESIGN APPROACH

The selected OTW epicyclic star gear arrangement is very similar to the first stage of the YT49-W-1 reduction gear unit shown in Figure 9.3, which was developed for the Curtiss-Wright YT49 turboprop engine. The YT49 engine was designed, built, and tested during the mid 1950's. Listed below is a summary of the YT49 engine testing:

- Bench tests 290 hours
- Factory engine tests 1960 hours
- Flight test in B17 and B47 flight test beds 150 hours

A comparison of the principal design features of the OTW, UTW, and YT49 (1st stage) gear sets is presented in Table 9-II. As shown, the OTW design represents a somewhat greater departure from the YT49 design than does the UTW.

A star gear arrangement is the only epicyclic gear train capable of providing the selected OTW reduction gear ratio. In a star gear system the star gears distribute the load to many teeth in both the sun gear and ring gear members. This feature greatly reduces the face width required for each gear. Also, the star gears rotate about a fixed axis, unlike planetary gears which rotate about a sun gear as well as their own axis. This feature eliminates the centrifugal field created by rotation about the sun gear, allowing the star gears to utilize lighter bearings than a corresponding planetary gear arrangement.

Specific design approach features of the OTW reduction gear unit are as follows:

- Flexibility - Both the input and output members of the system are flexibly mounted to prevent engine deflections from influencing gear operation.
- Controlled Gear Deflections - Rims of the sun and ring gears are contoured so that their deflections match the deflection in the star gears.
- Self-Aligning Star Gears - Double-row spherical roller bearings are used to allow the star gears to align themselves with the sun and ring gears and thereby minimize the effects of carrier deflections. Bearing outer race is integral with the star gear to obtain maximum bearing capacity in minimum space.
- Nonfactoring Hunting Teeth - This combination of numbers of teeth results in minimum vibration, low noise, and long life.
- Modular Concept - Can be installed and removed as a unit.

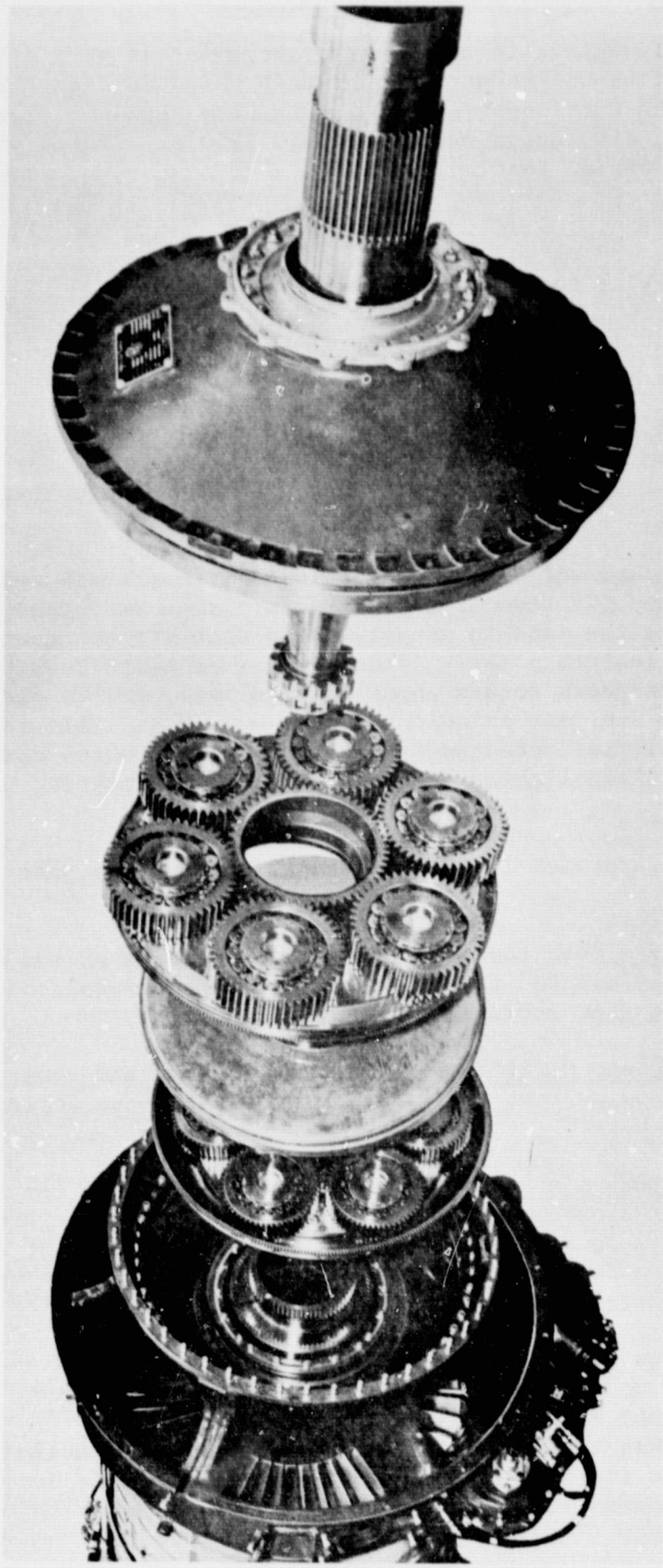

Figure 9.3. Curtiss-Wright YT49-W-1 Reduction Gear.

Table 9-II. Comparison of UTW, OTW, and YT49 (1st Stage) Reduction Gear Data.

	UTW	YT49	OTW
Turbine power	9802 kW (13,145 hp)	7457 kW (10,000 hp)	12813 kW (17183 hp)
Gear ratio	2.465	2.672	2.062
Sun gear rpm	7782	8000	7962
Star gear rpm	10689	9574	14998
Ring gear rpm	3157	2994	3862
Output torque	29641 MN (21,895 ft-lb)	23777 MN (17,535 ft-lb)	31026 MN (22918 ft-lb)
Gear contact ratio (Min.)	1.98	~1.6	2.05
Bearing DN × 10^{-6}	0.74	0.72	0.90

In addition to hunting teeth, the design approach includes the following low noise features:

- Precision AGMA quality 13 gears
- Contact ratio of 2
- Gear diametral pitch = 7.1884
- 21° pressure angle
- Modified involute at tip and root

9.5 DESIGN ANALYSIS AND RESULTS

9.5.1 Design Conditions

The detail design of the OTW reduction gear has been conducted in accordance with the operating conditions defined in Table 9-III for the Flight Engine Cycle. Upon completion of the design the stresses were evaluated at operating conditions established by the experimental engine duty cycle (Table 9-IV). Results indicated that, although the stress levels were highest during the fan mapping portion of the experimental engine cycle, they fell within operating limits previously found to be acceptable by both Curtiss-Wright and General Electric.

Table 9-III. OTW Reduction Gear Flight Cycle.

Flight Cycle

Condition	Fan Power %	Fan Speed %	Time %	Oil-in Temperature ° K	Oil-in Temperature ° F
Start	0	0-30	1.11	-	-
Idle	10	67	6.89	339	150
Takeoff	100	100	2.71	355	180
Climb	79.00	95	22.22	355	180
Cruise	57.00	94	31.11	375	216
Descent	3.34	35	22.22	396	254
Approach	54	82	6.67	385	180
Reverse	100	100	0.18	355	180
Idle	10	67	6.89	339	150

100% Fan power = 12,703 kw (17,035 hp)

100% Fan speed - 404.4 rad/sec (3862 rpm)

Table 9-IV. OTW Reduction Gear Experimental Engine Cycle.

Experimental Engine Cycle

Hours	% Time	% Turbine Speed	% Turbine Power
1	0.04	105	100
1	0.05	100	140
15	0.56	100	130
15	0.56	100	110
150	5.59	100	100
500	18.64	90	80
1000	37.28	75	50
1000	37.28	30	10
100% Turbine power = 12,813 kw (17,183 hp)			
100% Turbine speed = 833.8 rad/sec (7962 rpm)			

9.5.2 Materials

Table 9-V lists the materials used in the OTW gear set. The gear materials are the same as those utilized in the YT49 reduction gear design.

Table 9-V. Gear Set Materials.

- Sun gear — AMS 6265 - carburized - silver plate
- Star gear — AMS 6265 - carburized - shot peen
- Ring gear — AMS 6470 - nitrided
- Carrier support — AMS 6415 - RC32-36
- Bearing
  - Inner race — AMS 6490 - CEVM M-50 steel, R_c 60 min.
  - Rollers — AMS 6490 - CEVM M-50 steel, R_c 60 min.
  - Cage (steel) — AMS 6414 - silver plated
  - Outer race (integral with star gear) — AMS 6265 - carburized, R_c 60-63

9.5.3 Reduction Gear Geometry

Final OTW reduction gear geometry details are summarized in Table 9-VI. Without exception all resulting design details are consistent with good reduction gear design practice based on the experience of both Curtiss-Wright and General Electric.

9.5.4 Stress Analysis

The stress analysis approach and results are summarized in Figures 9.4, 9.5, and 916 for the sun, star, and ring gears, respectively. Conventional compressive and bending stress levels were calculated for the OTW flight duty cycle using the American Gear Manufacturing Association (AGMA) recommended procedure. Also shown in the figures are allowable compressive and bending stress levels based on AGMA and Curtiss-Wright experience. As shown, the calculated stresses fall well within the limits set by AGMA for infinite life.

In addition to the conventional gear teeth compressive and bending stresses, an attempt was made to combine the bending stresses with the rim stresses. Referring to Figure 9.4 for the sun gear, rim stresses were calculated at three circumferential locations, Stations I, II, and III. The sun gear teeth are in mesh with the star gear teeth at Stations I and II, but out of mesh at Station III. The tooth bending stress, ± 23,818 N/cm^2 (± 34,545 psi), was directly added to the rim stress at Stations I and II to determine the combined stress. It should be noted that this represents a conservative approach, since the maximum rim and bending stresses actually do not occur at the same location. As shown in Figure 9.4, the maximum positive, 45,420 N/cm^2 (65,874 psi), and negative -16,299 N/cm^2 (-23,640 psi), combined stresses occur at Stations I and II. These two numbers then were used to define the alternating stress, 35,668 N/cm^2 (44,757 psi), and the steady-state stress, 14,560 N/cm^2 (21,117 psi), plotted on the Goodman diagram. As shown, the resulting stress condition falls within the limit line for infinite life. The same procedure was used to substantiate the star gear (Figure 9.5) and the ring gear (Figure 9.6) designs.

9.5.5 Design Oil Flow Rates

The design oil flow rates based on the flight cycle conditions are presented in Table 9-VII. Oil inlet temperatures were defined by General Electric on the basis of overall engine heat balance studies. The maximum limit for the bearing outer race temperature was established at 422° K (300° F). As shown, the calculated maximum bearing outer race temperature occurs at the cruise operating condition. Available oil pressure at any given operating condition is a function of the core engine speed. The required bearing oil flow at the cruise conditions, together with the oil supply pressure, established the bearing oil flow orifice control size. The controlling operating condition for oil flow to the gears based on gear scoring criteria is takeoff. With the bearing and gear oil orifice control

Table 9-VI. OTW Reduction Gear Geometry.

	Sun Gear	Star Gear	Ring Gear
No. of teeth	81	43	167
Diametral pitch	7.1884	7.1884	7.1884
Pressure angle	21°	21°	21°
Pitch diameter	286.2 mm (11.268 in.)	151.9 mm (5.982 in.)	590.1 mm (23.232 in.)
Center distance		219.1 mm (8.625 in.)	219.1 mm (8.625 in.)
Base diameter	267.2 mm (10.520 in.)	141.8 mm (5.585 in.)	550.9 mm (21.689 in.)
Tooth thickness at P.D.	5.375 mm (.2116 in.)	5.725 mm (.2254 in.)	5.375 mm (.2116 in.)
Backlash	.102-.152 mm (.004-.006 in.)	.102-.152 mm (.004-.006 in.)	.127-.203 mm (.005-.008 in.)
Root radius (min.)	1.12 mm (.004 in.)	1.37 mm (.054 in.)	.864 mm (.034 in.)
Contact ratio (no edge break)	2.184	2.183	
(max edge break)	2.075	2.057	
Gear face width	37.6 mm (1.48 in.)	42.7 mm (1.68 in.)	37.6 mm (1.48 in.)

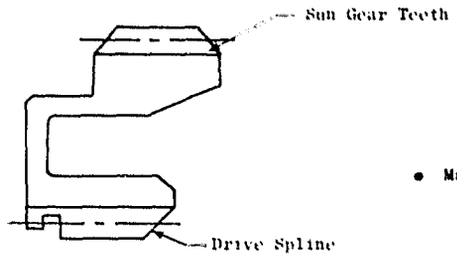

- Material: AMS 6265 Case Carburized Steel

Combined Rim and Gear Stresses

Station	I (Loaded Tension)	II (Compression)	III (Out-of-Mesh)
Rim Stress Incl SCF, N cm^2 (psi)	14,861 (21,553)	-766.4 (-1,111.5)	17,351 (25,165)
Combined Stress, N cm^2 (psi)	42,715 (61,951)	-28,620 (-41,509)	17,351 (25,165)

Conventional Gear Stresses

	Compressive Stress, N cm^2 (psi)
Flight	92,423 (134,044)
AGMA	102,570 (148,760)
C-W	110,320 (160,000)

	Bending Stress
Flight	27,854 (40,398)
AGMA	38,693 (55,250)
C-W	41,370 (60,000)

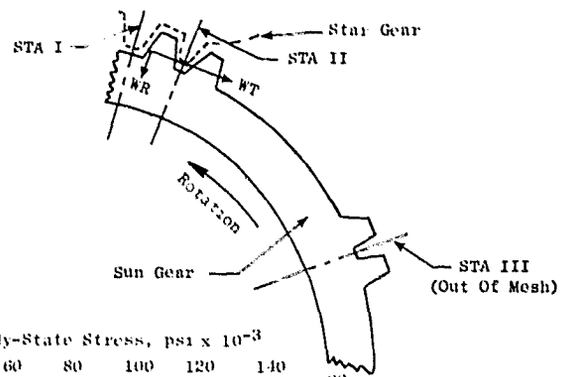

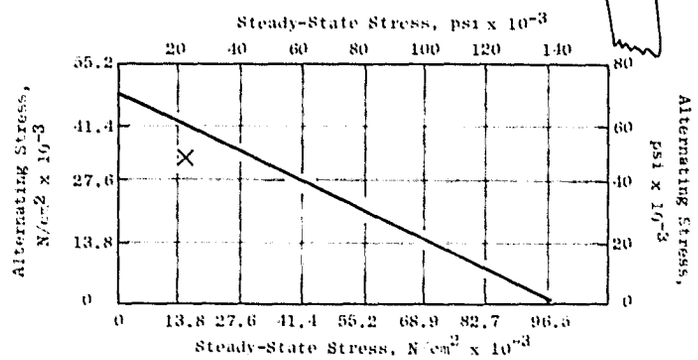

Figure 9.4. Sun Gear Stresses, Takeoff.

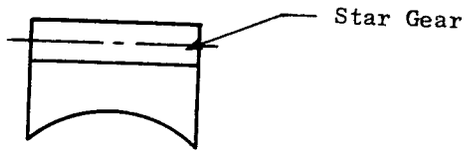

- Material: AMS 6265 Case Carburized Steel

Combined Rim and Gear Stresses

Station	I (Loaded Tension)	II (Compression)
Rim Stresses Incl SCF, N/cm^2 (psi)	9,315 (13,510)	-1,440 (-2,088)
Combined Stress, N/cm^2 (psi)	36,243 (52,564)	-28,367 (-41,142)

Conventional Gear Stresses

	Compressive Stress, N/cm^2 (psi)
Flight	92,423 (134,044)
AGMA	102,570 (148,760)
C-W	110,320 (160,000)

	Bending Stress
Flight	21,618 (31,350)
AGMA	26,928 (39,054)
C-W	38,693 (56,117)

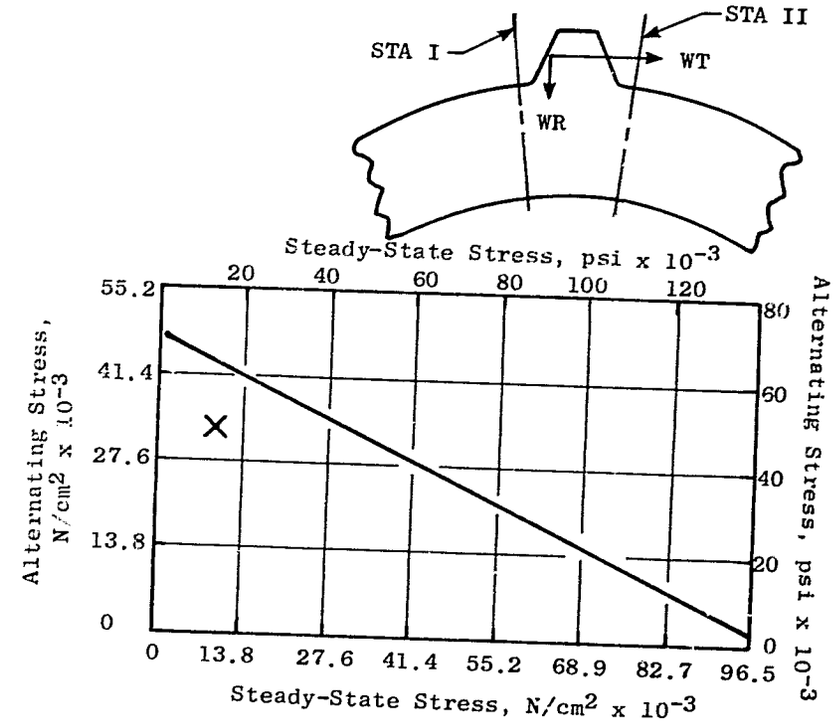

Figure 9.5. Star Gear Stresses, Takeoff.

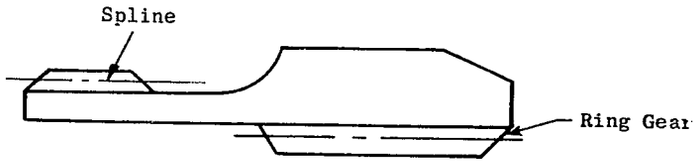

- Material: AMS 6470 Nitralloy

Combined Rim and Gear Stresses

Station	I (Loaded Tension)	II (Compression)	III (Out-of-Mesh)
Rim Stress Incl SCF, N/cm^2 (psi)	5,081 (7,369))	-11,516 (-16,702)	32,065 (46,504)
Combined Stress, N/cm^2 (psi)	27,028 (39,199)	-33,463 (-48,532)	32,065 (46,504)

Conventional Gear Stresses

	Compressive Stress, N/cm^2 (psi)
Flight	59,755 (86,664)
AGMA	102,570 (148,760)
C-W	110,320 (160,000)

	Bending Stress
Flight	21,947 (31,830)
AGMA	32,888 (47,699)
C-W	41,370 (60,000)

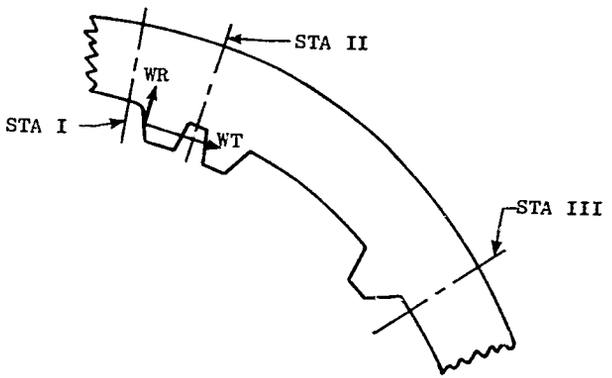

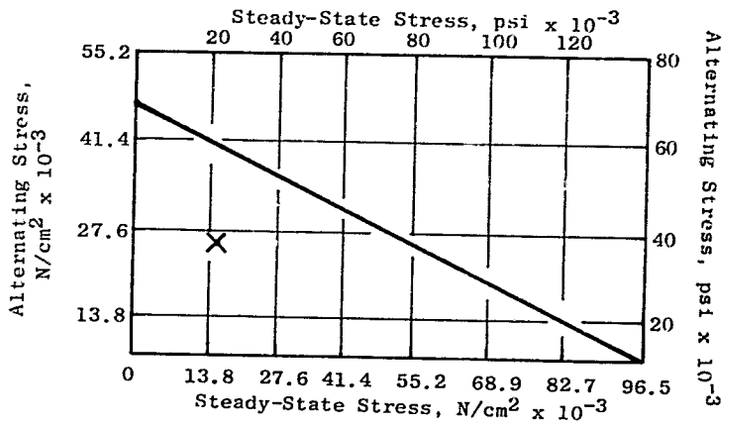

Figure 9.6. Ring Gear Stresses, Takeoff.

Table 9-VII. OTW Reduction Gear Total Oil Flows (SI Units).

Flight Cycle

Condition	Total Star Brg. Flow, cm^3/sec	Flow to Gears (Spray Bars), cm^3/sec	Total Oil Flow cm^3/sec	Oil in ° K	Brg. Outer Race Temp. ° K
Idle	381	630	1011	339	377
Takeoff	639	1208	1847	353	413
Climb	626	1172	1798	353	408
Cruise	622	1154	1776	375	422*
Descent	512	955	1467	396	406
Approach	586	1119	1705	353	398
Reverse	639	1208	1847	353	413
Idle	381	630	1011	339	219

*Controlling condition

Table 9-VIIa. OTW Reduction Gear Total Oil Flows (English Units).

Flight Cycle

Condition	Total Star Brg. Flow, gal/min	Flow to Gears (Spray Bars), gal/min	Total Oil Flow gal/min	Oil in ° F	Brg. Outer Race Temp. ° F
Idle	6.04	9.99	16.03	150	219
Takeoff	10.13	19.14	29.27	180	283
Climb	9.92	18.58	28.50	180	275
Cruise	9.87	18.29	28.16	216	300*
Descent	8.12	15.14	23.26	254	271
Approach	9.29	17.73	27.02	180	257
Reverse	10.13	19.14	29.27	180	283
Idle	6.04	9.99	16.03	150	219

*Controlling condition

sizes set, the resulting total oil flows at each operating condition were established. The engine will be capable of providing flow rates significantly higher than the design values, should component or engine tests indicate that increased oil flow rates are desirable.

9.5.6 Reduction Gear Efficiency

Overall reduction gear efficiency is determined by calculating losses for the spherical roller bearings, gear meshes, and for churning and windage. These losses are presented in Table 9-VIII. As shown at takeoff, the estimated reduction gear efficiency is 99.1%, which is slightly less than the objective level (99.2%). It should be noted that roughly half the losses are in the gears, while the bearings, churning, and windage make up the balance.

9.5.7 Heat Rejection

Total heat generated due to the losses in the gears, and the effect of this heat on the temperature of the oil supplied to the gears for the flight cycle, is shown in Table 9-IX. The resulting bulk oil temperatures do not exceed the capabilities of either MIL-L-7808 or MIL-L-23699.

9.5.8 Gear Scoring

Tabulated in Table 9-X are gear scoring index data based on the AGMA method of analysis. A maximum scoring index of 422° K (300° F) was used in the design. Although AGMA gear scoring data indicate this falls within the medium risk range, both General Electric and Curtiss-Wright experience indicate that scoring does not occur in high quality gearing at this scoring index. During the experimental engine ground test program, the oil inlet temperature to the gears will be maintained at a low level to minimize any risk of scoring. As shown in the table, the calculated maximum value of the AGMA gear scoring index occurs at the takeoff and reverse thrust operating conditions.

Table 9-VIII. OTW Reduction Gear Efficiency (SI Units).

Flight Cycle Power Loss - kw

Condition	Spherical Brg.	Gear Mesh	Churn & Windage	Total	Overall Efficiency %
Idle	11.46	4.62	1.52	17.60	98.63
Takeoff	26.32	49.97	37.72	114.01	99.11*
Climb	23.85	39.48	27.34	90.67	99.10
Cruise	20.60	28.49	18.94	68.03	99.07
Descent	3.46	1.84	0.13	5.43	98.73
Approach	18.31	26.99	13.77	59.07	99.15
Reverse	26.32	49.97	37.72	114.01	99.11
Idle	11.46	4.62	1.52	17.60	98.63
*Spec 99.20%					

Table 9-VIIIa. OTW Reduction Gear Efficiency (Engligh Units).

Flight Cycle Power Loss - hp

Condition	Spherical Brg.	Gear Mesh Gear Mesh	Churn & Windage	Total	Overall Efficiency %
Idle	15.37	6.19	2.04	23.60	98.63
Takeoff	35.30	67.01	50.59	152.90	99.11*
Climb	31.98	52.94	36.66	121.58	99.10
Cruise	27.62	38.20	25.40	91.22	99.07
Descent	4.64	2.47	0.17	7.28	98.73
Approach	24.55	36.19	18.46	79.20	99.15
Reverse	35.30	67.01	50.59	152.90	99.11
Idle	15.37	6.19	2.04	23.60	98.63
*Spec 99.20%					

Table 9-IX. OTW Reduction Gear Heat Rejection (SI Units).

Flight Cycle

Condition	Total Loss kw	Delta Rise in Bulk Oil Temp. ° K	Oil-in Temp. ° K	Bulk Oil Temp. ° K
Idle	17.60	8.63	339	348
Takeoff	114.00	31.20	355	386
Climb	90.62	25.47	355	381
Cruise	68.01	19.85	375	395
Descent	5.43	1.97	397	399
Approach	59.04	17.51	355	373
Reverse	114.00	31.20	355	386
Idle	17.60	8.63	339	348

Table 9-IXa. OTW Reduction Gear Heat Rejection (English Units).

Flight Cycle

Condition	Total Loss Btu/min	Delta Rise in Bulk Oil Temp. ° F	Oil-in Temp. ° F	Bulk Oil Temp. ° F
Idle	1001	15.53	150	166
Takeoff	6486	56.15	180	236
Climb	5157	45.85	180	226
Cruise	3870	35.73	216	252
Descent	309	3.54	254	258
Approach	3360	31.51	180	212
Reverse	6486	56.15	180	236
Idle	1001	15.53	150	166

Table 9-X. OTW Reduction Gear Scoring Index.

Flight Cycle

Condition	Oil In Temp.		AGMA XT		AGMA Scoring Index	
	° K	° F	° K	° F	° K	° F
Idle	339	150	268	23.17	351	173
Takeoff	355	180	321	117.88	420*	298*
Climb	355	180	311	100.03	410	280
Cruise	375	216	299	78.53	419	295
Descent	396	254	262	11.97	403	266
Approach	355	180	299	78.02	399	258
Reverse	355	180	320	117.88	421*	298*
Idle	339	150	268	23.17	351	173

*Controlling conditions

9.5.9 Star Gear Bearing

The selected star gear bearing configuration is illustrated in Figure 9.7. Bearing design features include:

- Double-row spherical roller bearing
- Integral star gear and outer race
- "Conventional" inner race, roller, and cage
- Oil feed through center of inner race

This spherical roller bearing was chosen as the prime candidate on past experience with similar bearings in the Curtiss-Wright YT49 turboprop engine first-stage reduction gears and the recommendations by the SKF Bearing Corporation.

Table 9-XI shows the average loads and speed used to determine the bearing B1 life of 6000 hours. The calculations indicate that the bearings can meet requirements. Details of bearing size, geometry, and the effect of radial looseness are discussed in Paragraph 9.6.1.

Table 9-XI. Bearing Life Prediction (Star Gear).

Flight Cycle

Cubic mean load	17534 N (3942 lb)
Mean speed (rpm)	10964
B1 life (hours)	6026

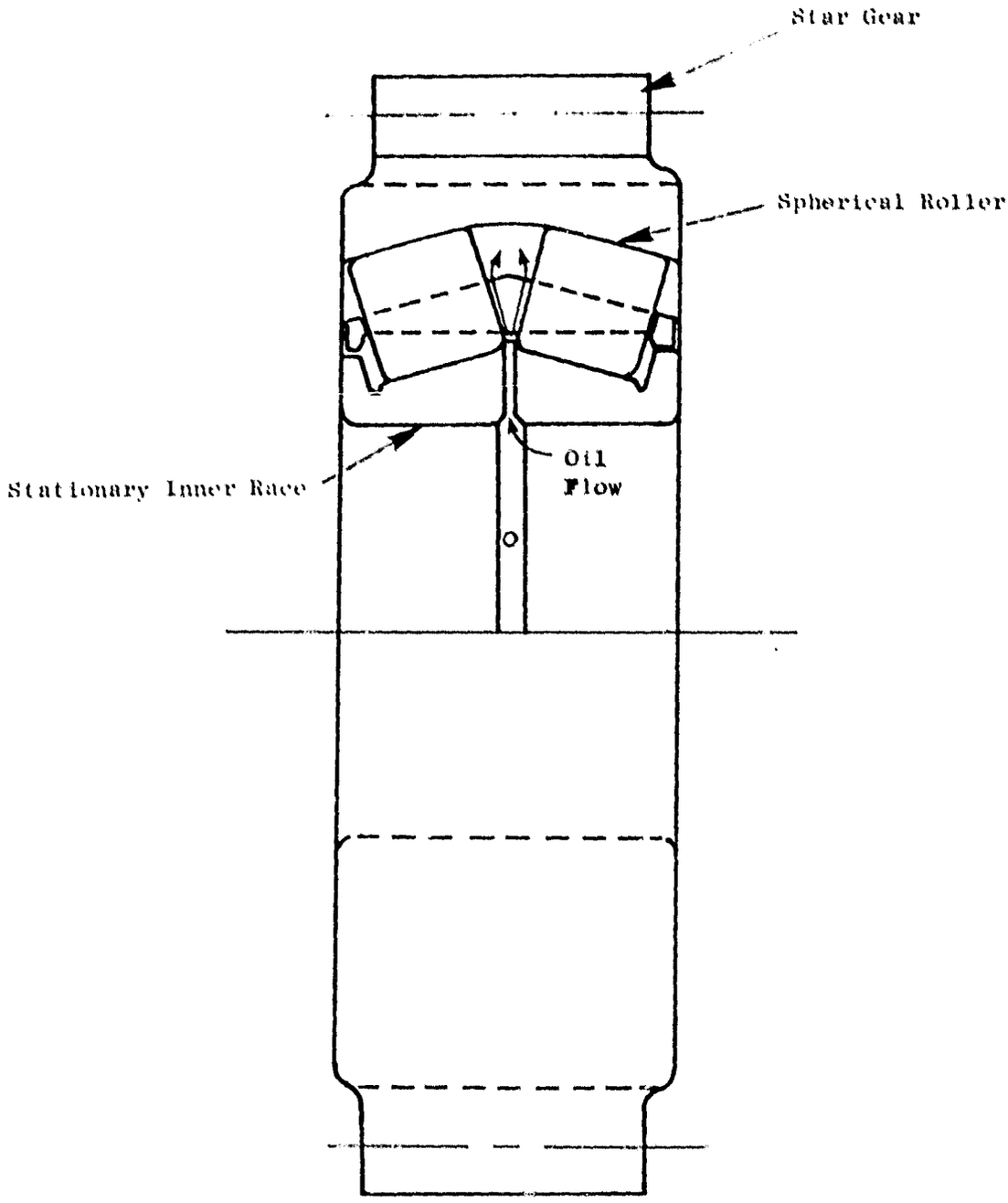

Figure 9.7. Star Gear Spherical Roller Bearings.

9.5.10 Weight

The weights of the reduction gear components and the overall gear weight for the OTW experimental engine are presented in Table 9-XII.

Table 9-XII. OTW Reduction Gear Weight Summary.

	kg	lb
Sun gear assembly	8.07	17.80
Ring gear	12.42	27.38
Star nuts	2.07	4.58
Carrier	23.00	50.70
Stars	37.26	82.14
Manifold	1.80	3.98
Spray bars	0.27	0.61
Misc.	4.99	11.00
Total	89.88	198.19

9.6 COMPONENT TEST PROGRAMS

9.6.1 Star Gear Bearing Tests

From the start of the QCSEE program the star gear bearing has been considered as the most critical reduction gear element. This is particularly true for the OTW engine where the bearing speeds are much higher than those of the UTW engine. To ensure successful operation of the bearings, a component test program was conducted by Curtiss-Wright. A schematic of the bearing test rig is shown in Figure 9.8, and a photograph of the rig is presented in Figure 9.9. The bearing tested was an available SKF bearing very similar in design, but slightly larger than the OTW bearing, and slightly smaller than the UTW bearing. Tests were conducted to simulate the more severe OTW operating conditions. The test results are summarized in Table 9-XIII. As shown, skidding was encountered at low-power, high-speed conditions during the first test. Evaluation of the data indicated that the large bearing clearance and a low oil flow rate resulted in the skidding problem. The clearance was reduced, and the tests were extended to cover all critical engine operating modes. No further problems were encountered. Based on these test results, it has been concluded that the selected OTW bearing design will perform satisfactorily during the engine test program.

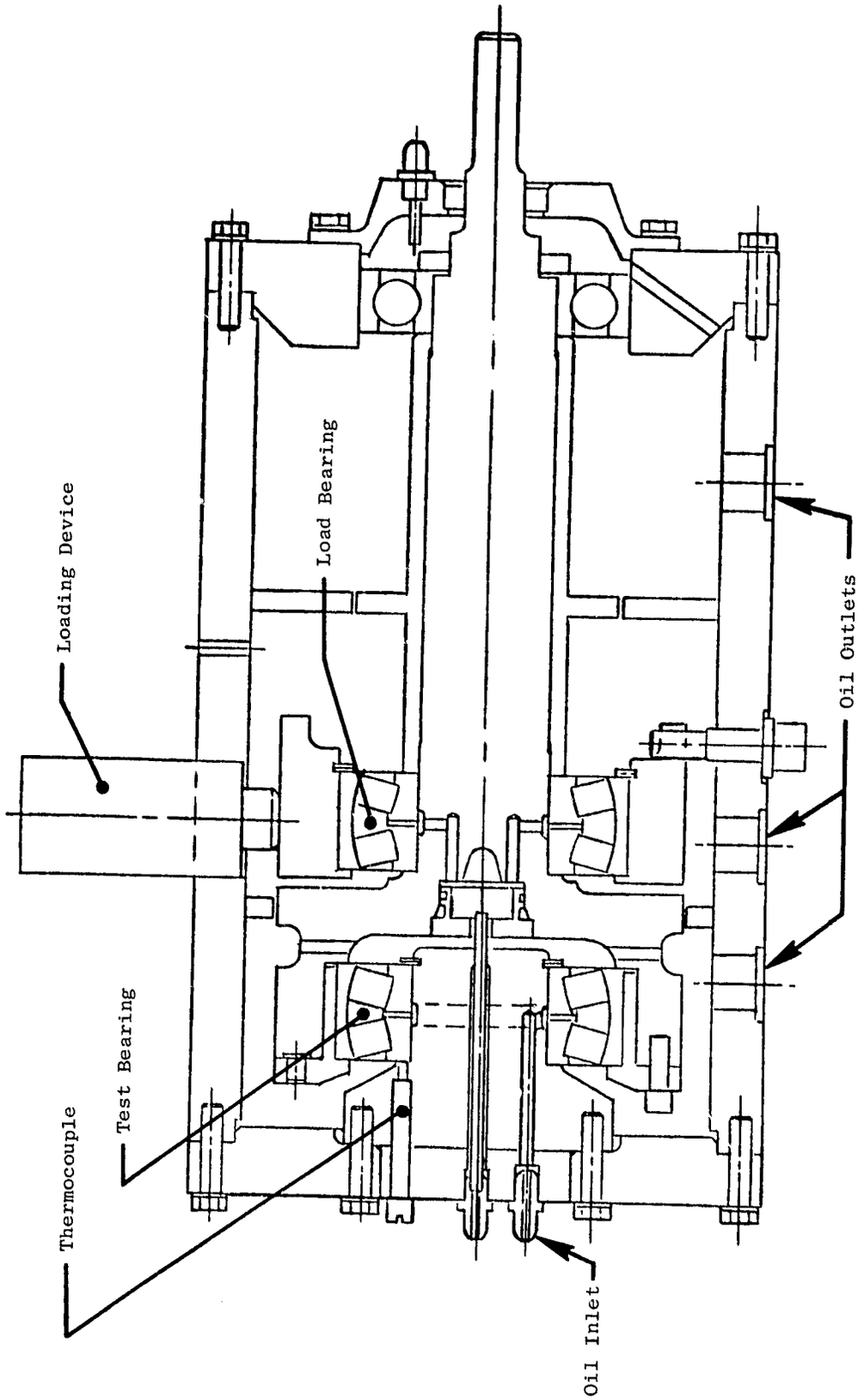

Figure 9.8. Bearing Test Rig Schematic.

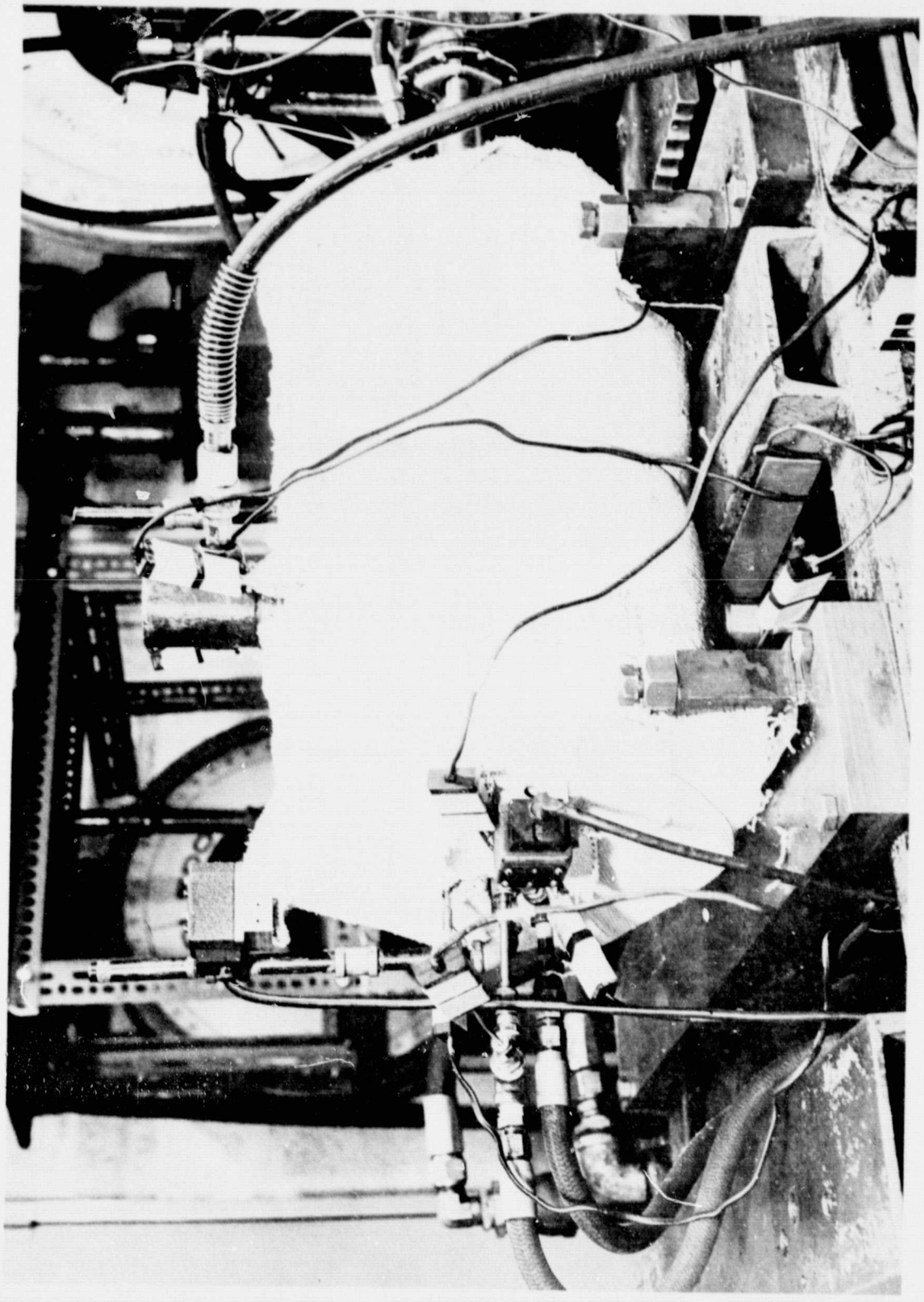

Figure 9.9. Bearing Test Rig.

Table 9-XIII. Star Gear Bearing Test Results.

SKF 22313 Double Row Spherical Roller Bearing

Test No.	Clearance		Test Conditions				Test Conditions	Test Results
			Oil-in Temp.		Oil Flow			
	cm	inch	° K	° F	kg/min	lb/min		
1	0.0178	0.007	356	180	2.99-4.99	6.6-11.0	Full range	Skidding at low-power, high-speed conditions
2	0.0064	0.0025	358	185	3.99-4.99	8.8-11.0	TO and climb	OK
3	0.0064	0.0025	358	185	4.49	9.9	Cruise and approach	OK
4	0.0064	0.0025	358	185	3.99	8.8	Idle descent	OK
5	0.0064	0.0025	358	185	2.49	5.5	SLS idle	OK

A comparison of the size and operation parameters of the SKF Double-Row Spherical Roller Bearing in different star gear bearing applications is presented in Table 9-XIV. Applications include the YT49 turboprop engine primary reduction gear, the UTW and OTW reduction gears, and the test bearing for the Curtiss-Wright evaluation.

9.6.2 Reduction Gear Back-to-Back Test

Back-to-back tests of the OTW reduction gear are planned during the second quarter of 1976. A schematic of the test rig is presented in Figure 9.10. As shown in the figure, two reduction gear units will be run back to back. Simulated loads will be applied by hydraulic cylinders at the torque plates. With this type of test setup, the input power requirement is only that required to overcome the losses in the system, which are only 2 to 3% of the design power transmission level of a single gear unit.

As indicated in Figure 9.10, the engine geometry and scavenge system will be simulated on the test gear set side of the rig. During the rig tests the reduction gear power levels, speeds, and oil-in temperatures will be simulated over the range of flight cycle operating conditions. Objective of the test is to verify operating characteristics, including oil flow, heat rejection, efficiency, gear tooth pattern, adequacy of gear lubrication (absence of scoring) and bearing performance. Satisfactory completion of these tests will provide the necessary confidence in the reduction gear design prior to engine test.

Table 9-XIV. Star Gear Bearing Application Comparison.

SKF Double Row Spherical Roller Bearing

	YT49 Turboprop. Eng. Primary Red. Gear	OTW	UTW	Rig Evaluation @ CW
SKF Bearing Designation	22315	22312	22314	22313
Bore, mm	75	60	70	65
O.D. mm	160	130	150	140
Width, mm	55	46	51	48
Operating speed, rpm	9,571	14,998	10,577	13,850
DN Value	0.72×10^6	0.90×10^6	0.74×10^6	0.90×10^6

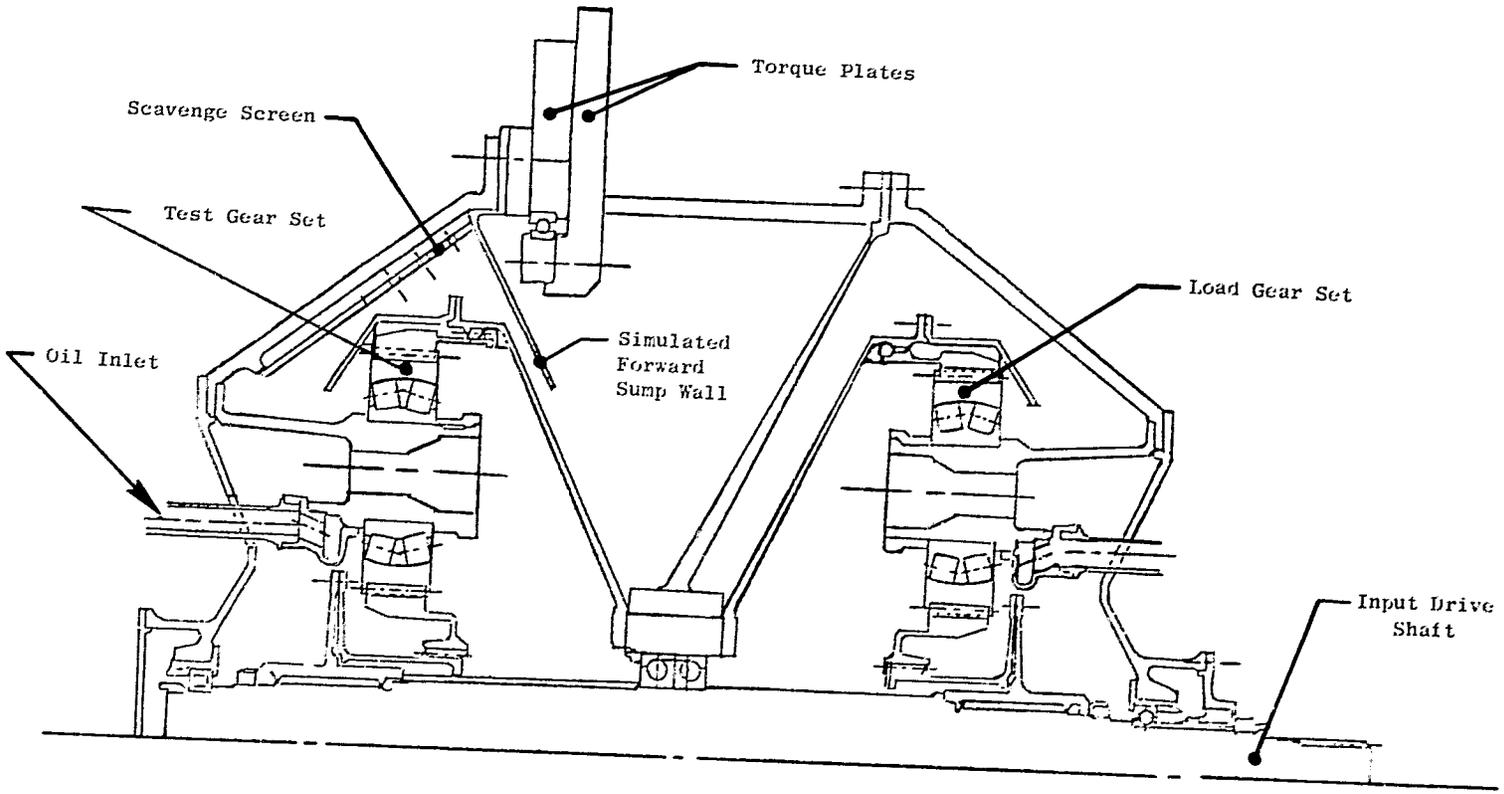

Figure 9.10. Main Reduction Gear Test Rig Schematic.

SECTION 10.0

ENGINE CORE AND LOW PRESSURE TURBINE DESIGN

10.1 SUMMARY

In order to minimize development risk and expense in the QCSEE program, the F101 core and low pressure turbine were selected. Moreover, to capitalize on the advanced state of development of these components, the qualified PFRT, or YF101, design was specified insofar as practical. Several exceptions to this approach exist. The following components are different from the PFRT configuration:

1. Accessory drive gear mount
2. Compressor IGV and inner flowpath
3. Compressor stator actuator and feedback
4. Compressor first stage rotor blade airfoil
5. Combustor
6. HP turbine diaphragm area
7. LP turbine diaphragm area
8. LP turbine No. 2 blade
9. Turbine frame
10. Balance piston arrangement
11. PV HP turbine shrouds
12. Warm bridge HP turbine blade

10.2 DESIGN REQUIREMENTS

The F101 core and low pressure turbine were proposed for the QCSEE engines, because, in addition to providing desirable cycle and thrust size, this core engine employs suitable advanced technology components.

A major consideration in the detail core selection has been the desire to retain as much "qualified" hardware as practical. Therefore, the PFRT configuration has been specified in all areas except those discussed in the following paragraphs.

10.3 ENGINE CORE MODIFICATIONS

The following specific deviations from the PFRT configuration are planned for the OTW engine.

10.3.1 Accessory Drive Gear Mount

The F101 internal accessory drive bevel gears are mounted in a 17-4PH steel casting. This casting is bolted to the aft inner flange of the fan frame. Because of the higher bypass ratio of the OTW engine, the aft ring of the composite frame interferes with this gear mount casting. The solution to this problem was to reverse the casting and bolt it to the forward ring of the frame as shown in Figure 10.1.

In addition, the OTW experimental engine will have two radial drive shafts; one driving the top-mounted accessories and another driving the scavenge pump, located in the lower core cowl region. This requirement can be readily satisfied by using two sets of bevel gears and two support castings in each engine. (The casting occupies less than 180° of the mounting flange.)

10.3.2 Compressor IGV and Inner Flowpath

In order to increase the margin between maximum core rpm and panel vibration in the first stage compressor blade, the 42-IGV F101 PV configuration has been substituted for the 48-IGV F101 PFRT configuration. This change is discussed further under paragraph 10.3.4.

The F101 inner flowpath in the IGV region is shown as a heavy line in Figure 10.2. Because of the higher bypass ratio and lower fan exit radius ratio in the OTW engine, difficulty was encountered in fairing into this flowpath contour from the fan frame with acceptable aerodynamic flow lines. Therefore, a modification was made to the inner ring of the inlet guide vane, as shown in the figure.

10.3.3 Compressor Stator Actuator

The F101 compressor has been developed to optimize efficiency and flow at reduced corrected speeds, as required by its higher-Mach-number mixed mission. For use in the OTW engine, higher airflow is desired, consistent with existing rpm and T_4 limits. Operation at greater than 100% corrected speed would result in a severe compressor efficiency loss.

Fortunately, as a part of the F101 compressor development, various other stator schedules have been tested. One of the demonstrated schedules delivers significantly higher corrected flow at high corrected speeds, which meets the OTW requirements.

The OTW stator schedule is shown in terms of IGV setting angle versus corrected core speed in Figure 10.3.

Increased vane travel is required to achieve the higher airflow, necessitating several minor modifications in the actuator and linkages.

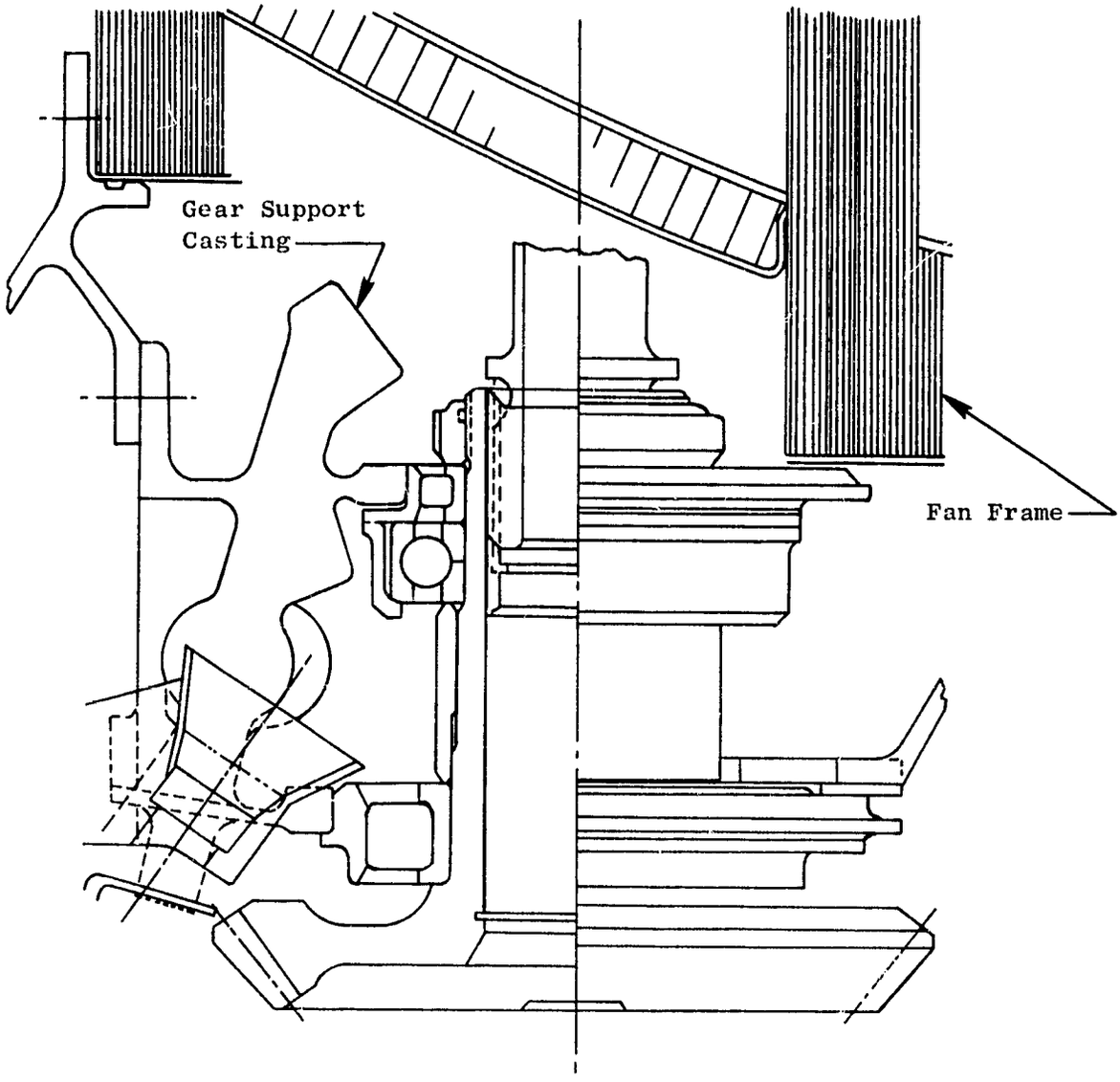

Figure 10.1. Accessory Drive Gear Mount.

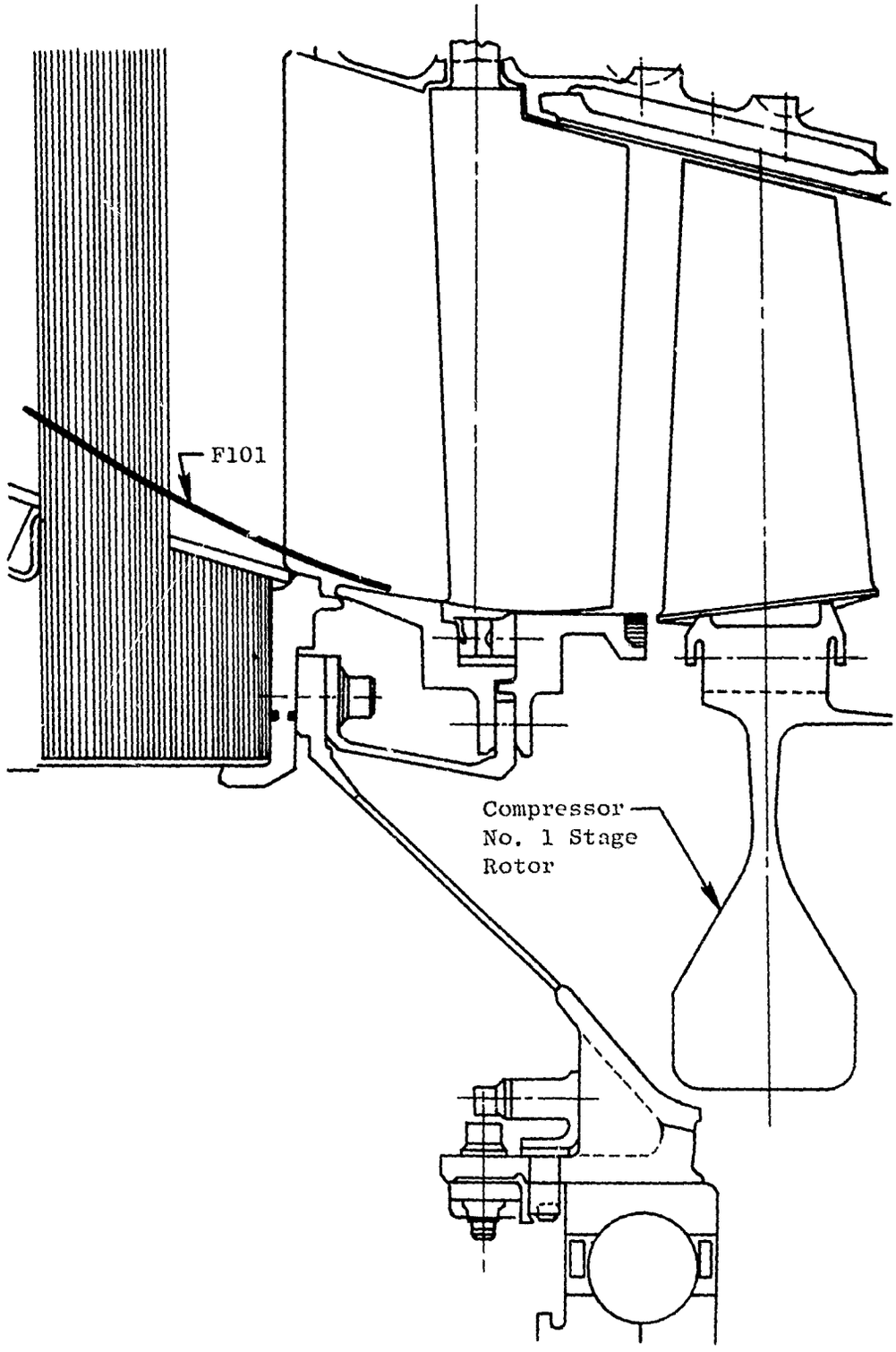

Figure 10.2. Compressor IGV Inner Flowpath.

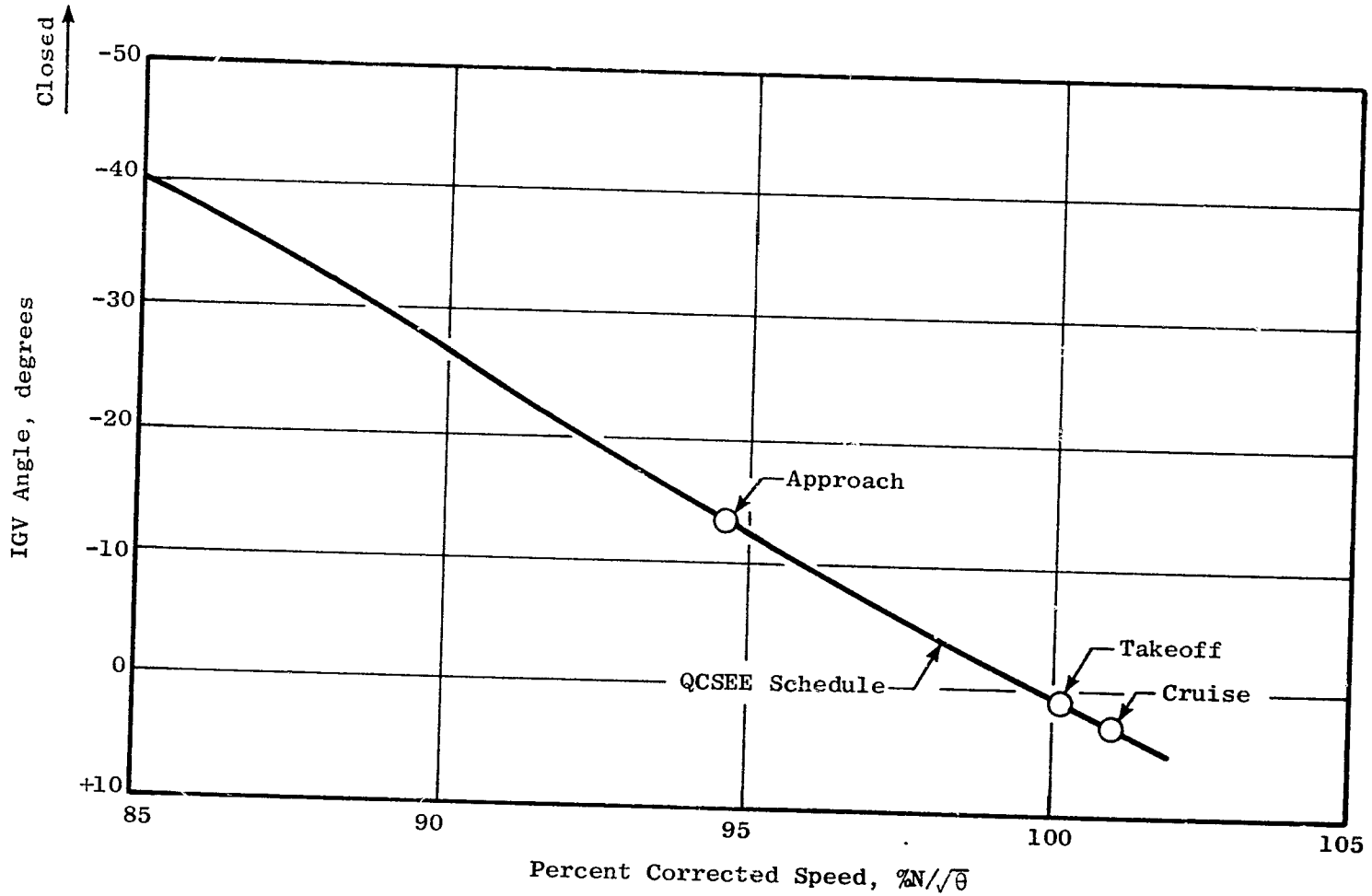

Figure 10.3. OTW Compressor Stator Schedule.

1. The vane actuator stroke must be increased from 7.747 cm (3.05 in.) to 8.89 cm (3.5 in.).

2. A new Stage 3 bellcrank must be provided.

3. The rod end of the Stage 3 linkage must be shortened about 0.127 cm (0.050 in.).

4. Bolts and nuts in the actuation assembly bellcranks must be replaced with flathead pins to permit them to pass between the actuation support members.

5. In the F101 engine, compressor stator angle is fed back to the control by means of a splined shaft. For use with the full authority digital control in the QTW engine, an LVDT electric feedback is substituted.

10.3.4 Compressor First Stage Rotor Blade Airfoil

Although the PFRT first stage compressor blade has proven satisfactory in the F101 engine, it has been found to exhibit aerodynamic instability in the part speed region if the stators are mis-rigged opened from the nominal schedule. To provide further assurance against operational problems, the F101 PV airfoil has been selected for the QCSEE engines. This airfoil is slightly thicker than the PFRT design and does not have the leading and trailing edges cropped at the tip.

Previous testing of the PV airfoil indicates no aerodynamic instability and no vibratory problems when run with the F101 PV 42-vane IGV. Therefore, this configuration has been selected for the QTW engine.

Figure 10.4 shows the engine speed margin provided for takeoff operation as a function of ambient temperature on the day of testing. Also shown are the other limits that would come into play only during fan mapping with elevated operating lines. Rotor speed limits will be set to ensure adequate frequency margin at all ambient temperatures.

10.3.5 Combustor

The selected F101 PFRT combustor, which incorporates a scroll carbureting dome, provides a substantial data base for the development of low emissions technology. Sector burning (fueling of only part of the fuel injectors) will be employed to reduce HC and CO emissions at idle, but these emission levels will not meet the QCSEE goals. The combustor will meet the NO_x goal; the smoke requirements, as determined by rig testing, will probably be met.

Although the PFRT combustor will be used in the QTW engine tests, additional work is under consideration to develop a new Double Annular Dome Combustor for QCSEE based on the NASA-GE Clean Combustor program.

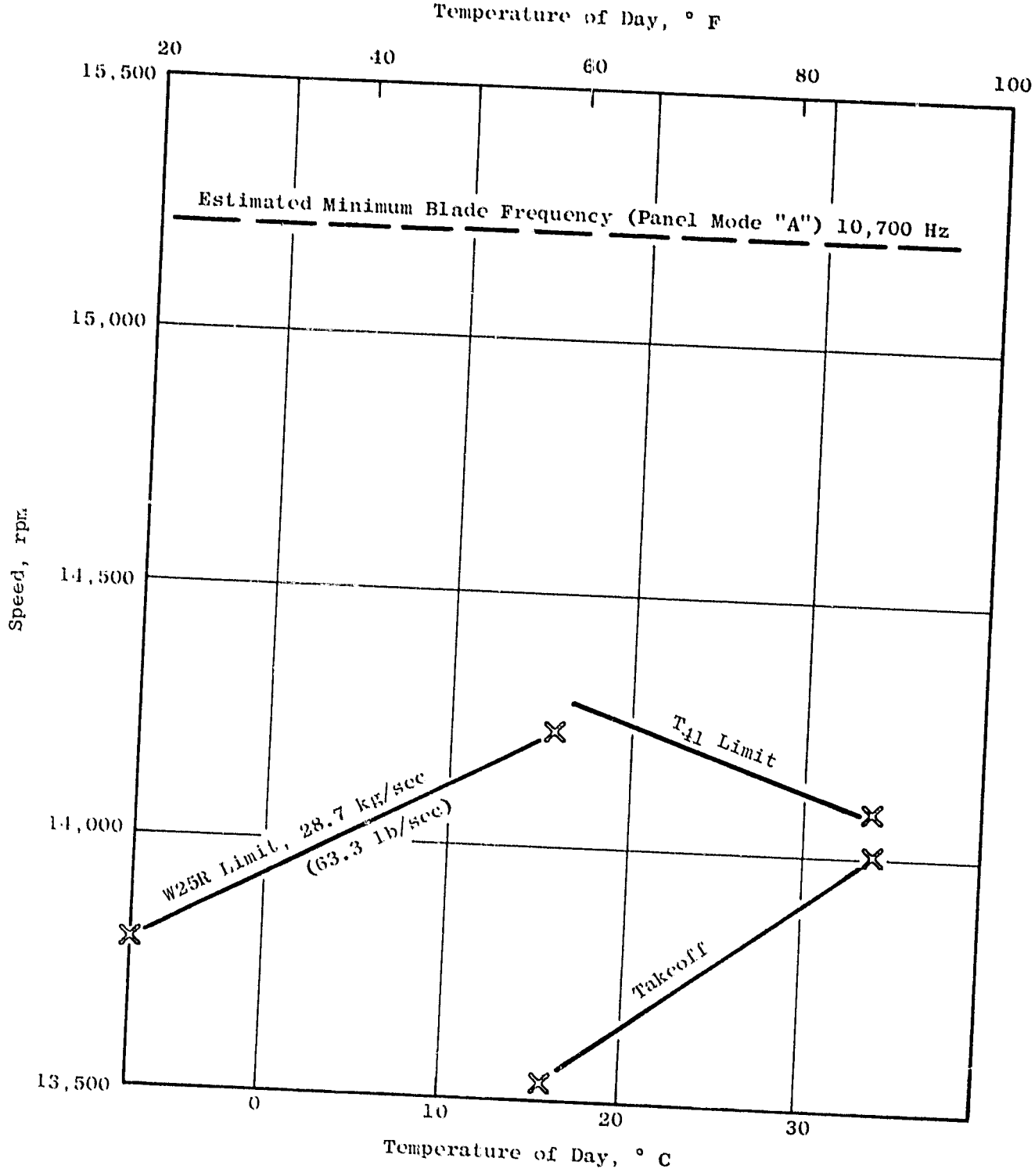

Figure 10.4. OTW First Stage Compressor Blade Frequency Margin.

10.3.6 HP Turbine Diaphragm Area

Figure 10.5 shows the compressor characteristic selected for the OTW engine. Because of the reduced cycle pressure ratio of the OTW engine compared to the F101 cycle, both the HP and LP turbine effective areas require adjustment to satisfy turbine flow function requirements.

By increasing the HP turbine effective area by 5% and decreasing the LP turbine effective area by 5%, the compressor can be made to operate at a more favorable point.

The means for adjusting turbine area is to rotate the vanes slightly to open or close the throat dimension. Figure 10.6 illustrates the degree of rotation needed for a 5% increase in HP turbine area. This will be accomplished by rotating the tool used to EDM the vane slots in the bands. Modified inspection fixtures are also required.

10.3.7 LP Turbine Diaphragm

In the case of the LP turbine, 5% reduction of area is accomplished by similar means. In either case the change in throat dimension (Do) is less than 0.05 cm (0.020 in.). Figure 10.7 illustrates this adjustment in the LPT stage one diaphragm.

10.3.8 Low Pressure Turbine Second Stage Blade

In the OTW engine, the higher energy extraction of the LP turbine results in an increase in exit swirl which will be removed by using longer straightening vanes in the turbine frame. However, to minimize the required turning in these vanes, and to provide more predictable angles of attack on the vanes, it was deemed advisable to incorporate a modified second stage LPT blade. This blade is slightly decambered in the vicinity of the pitch line and is the blade currently specified for the F101 PV configuration.

10.3.9 Turbine Frame

Modifications to the F101 turbine frame to extract greater swirl and to adapt the frame structurally to meet the OTW requirements are described in detail in Sections 10.4 and 10.5.

10.3.10 Balance Piston

Introduction of a reduction gear between the low pressure turbine and the fan of the OTW engine effectively cuts the load path normally used to balance fan plus LPT rotor net thrust force. Therefore, the rear sump area will be modified to incorporate a pneumatic piston to balance part of the turbine rotor thrust. The design of the balance piston is discussed in detail in Section 12.5.

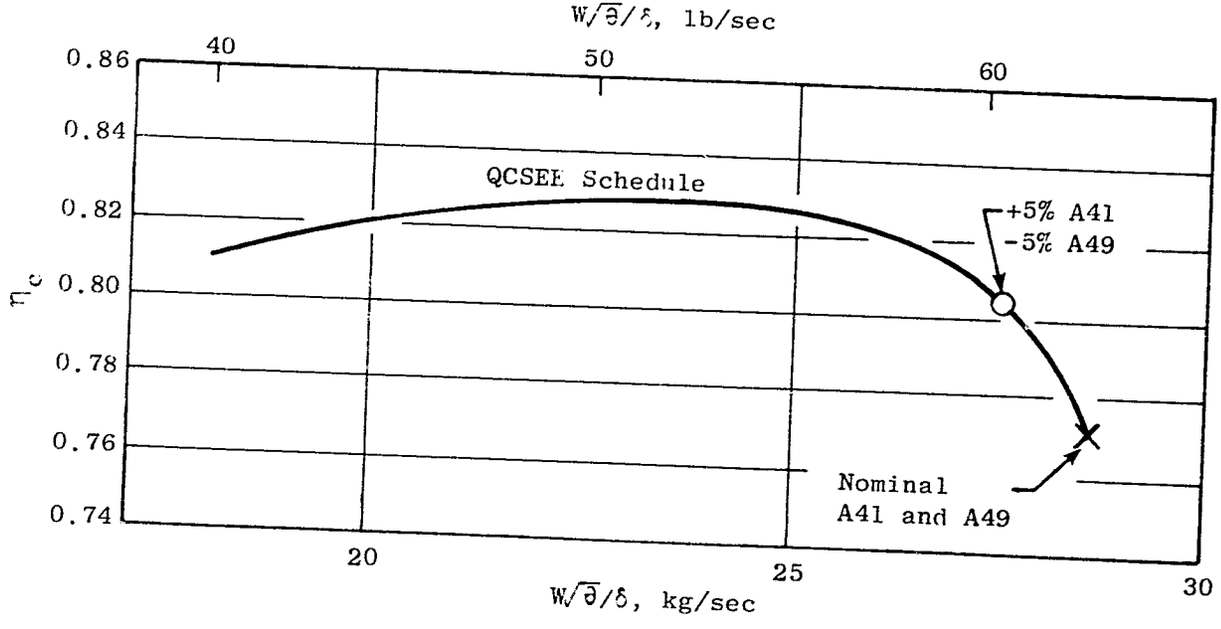

Figure 10.5. Compressor Characteristics.

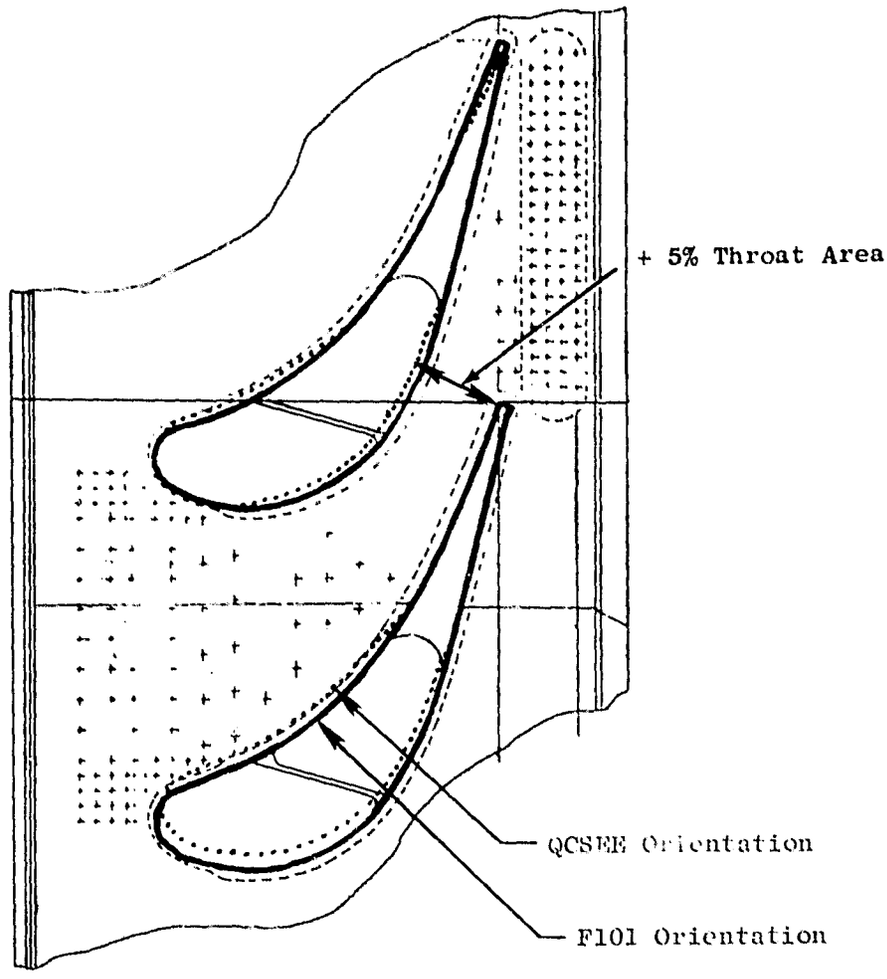

Figure 10.6. High Pressure Turbine Stator Assembly.

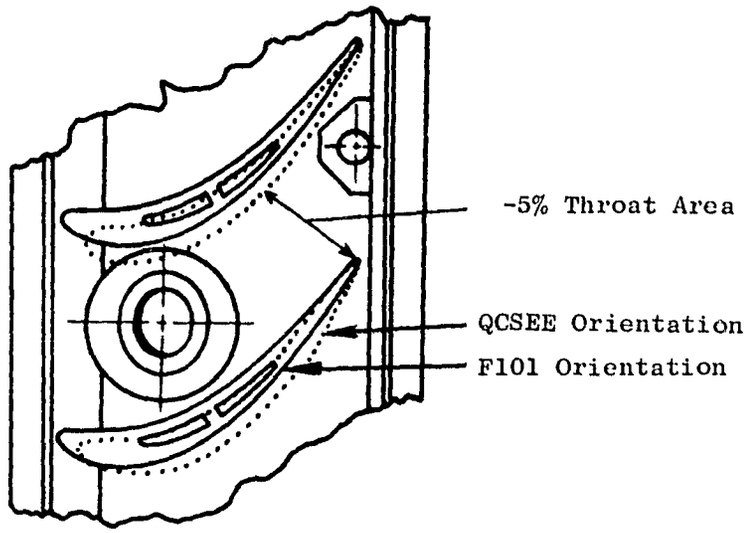

Figure 10.7. Low Pressure Turbine Stage 1 Stator Assembly.

10.3.11 PV Turbine Shrouds

The stationary shrouds at the tips of the high pressure turbine blades consist of Poroloy rub pads welded to structural support segments. Some shroud failures have occurred in F101 PFRT engines wherein the Poroloy pads crack and small pieces break out. Although no secondary damage has been observed, an improved shroud design has been released for the F101 QT (PV) engine. This design uses a coarser wire in the Poroloy, a revised layup pattern, and additional support points. Since the shroud is fully interchangeable with the PFRT design, it has been specified for the QTW core.

10.3.12 Warm Bridge HP Turbine Blade

Another change being introduced in the F101 PV engine is the warm bridge turbine blade. This design employs serpentine cooling air passages with leading edge film discharge, and trailing edge pin-fin cooling, in place of the impingement insert design used in the PFRT blade. Test experience has indicated a much superior endurance life with the warm bridge blade. The blades can be substituted in the same disk; however, minor modifications are required in the retainers to adjust axial blade clamping and in the cooling air inducer to increase airflow 0.5% of W25. These changes have been specified for the QTW engine.

10.4 LOW PRESSURE TURBINE FRAME AERODYNAMIC DESIGN

10.4.1 Introduction

The QTW low pressure turbine is a slight modification of the F101 low pressure turbine operating at an increased pressure ratio. The increased turbine exhaust swirl necessitated a modification to the present F101 frame/OGV aerodynamic geometry. The frame/OGV was redesigned for low noise and low loss characteristics.

A single-frame configuration has been designed to satisfy the requirements of both the UTW and QTW engines. Frame design modifications related to UTW engine requirements are, therefore, included in the following discussion.

10.4.2 Design

Design Point Selection

The turbine operating point for the frame/OGV aerodynamic design was selected to avoid off-design modes where separation and consequent core noise can occur at critical engine operating points. Based on initial cycle data, turbine off-design vector diagram studies were made at significant QCSEE operating points using the Multi-Sector NASA Turbine Computer Program (TCP). A summary of results is shown in Table 10.1. The QTW takeoff condition was

Table 10-I. Low Pressure Turbine Operating Point Data.

Engine Condition	UTW			OTW		
	TO	APPR	Max. Cruise[1]	TO	APPR	Max. Cruise[1]
$\frac{\Delta h}{T}$ ∿ Btu/lb° R	0.063	0.055	0.073	0.066	0.056	0.066
$\frac{\Delta h}{T}$ ∿ J/g ° K	0.264	0.230	0.306	0.277	0.235	0.277
$\frac{N}{\sqrt{T}}$ ∿ rpm/$\sqrt{°\ R}$	165	180	176	164	152	162
$\frac{N}{\sqrt{T}}$ ∿ rpm/$\sqrt{°\ K}$	221	241	236	220	204	217
$\Psi = \frac{\Delta Vu}{u}/2$	1.04	0.76	1.05	1.10	1.10	1.12
Swirl (degrees)	25.8	8.2	33.5	29.6	24.1	29.9
Mach Number	0.47	0.34	0.68	0.53	0.40	0.52
				▲ Design Point		

[1] Alt/Mach Number = 600 m/0.7 (20,000 ft/0.7)

chosen as the design point, as this case represented the highest turbine exhaust swirl and Mach number conditions (excluding maximum cruise points). Subsequent cycle data indicated somewhat higher swirl points, but the OTW takeoff case shown was still considered to be a reasonable design condition.

Axisymmetric Analysis and Flowpath Modification

Axisymmetric analysis of the frame/OGV was done using the CAFD computer program. This calculation accounts for streamline slope and curvature as well as lean and sweep effects. The analysis was set up with many intrablade calculation stations in order to analyze endwall Mach number distributions. First, the F101 frame flowpath with an additional 2.54 cm (1 in.) of axial width in the OGV was analyzed. Based on the results of this analysis, a modified flowpath was selected which was considered an aerodynamic improvement (with reduced diffusion) and also satisfied frame mechanical design and exhaust system requirements. This flowpath is shown in Figure 10.8.

The results of the axisymmetric analysis are shown in Figure 10.9. Plotted versus radial height at the OGV inlet are the gas angle, OGV design angle, and inlet absolute Mach number. Also shown is the absolute Mach number distributions on the inner and outer walls through the OGV. The NASA diffusion factors associated with this flowpath are:

$$D_{Root} = 0.316$$

$$D_{Pitch} = 0.440$$

$$D_{Tip} = 0.183$$

Vane Modification

The vane modification involved adding 2.54 cm (1 in.) of axial width to the present F101 OGV to remove the additional swirl. The change was made entirely in the false nose extension with the strut and aft strut extension remaining unchanged. Three vane sections at approximate root, pitch, and tip locations were designed and analyzed using both the CASC and CABIS programs. The CABIS (Cascade Analysis due to Beuckner, Isay, and Schnacker) program is an incompressible analysis while CASC (Cascade Analysis by Streamline Curvature) gives a compressible solution which accounts for radius change and streamtube thickness variation. The CASC Mach number distribution for the pitch section is given in Figure 10.10 for two different false nose extensions. Figure 10.10 shows that if the nose extension were designed to attach to the strut, as it presently does in the F101, there would be a distinct "bump" on the pressure surface. A smooth pressure surface was designed as shown, and both configurations were analyzed with CASC. The resulting Mach number distributions clearly indicate the effect of the bump. Consultation with experienced OGV designers indicated only a small decrement in performance associated with this. However, it was decided (with Mechanical Design concur-

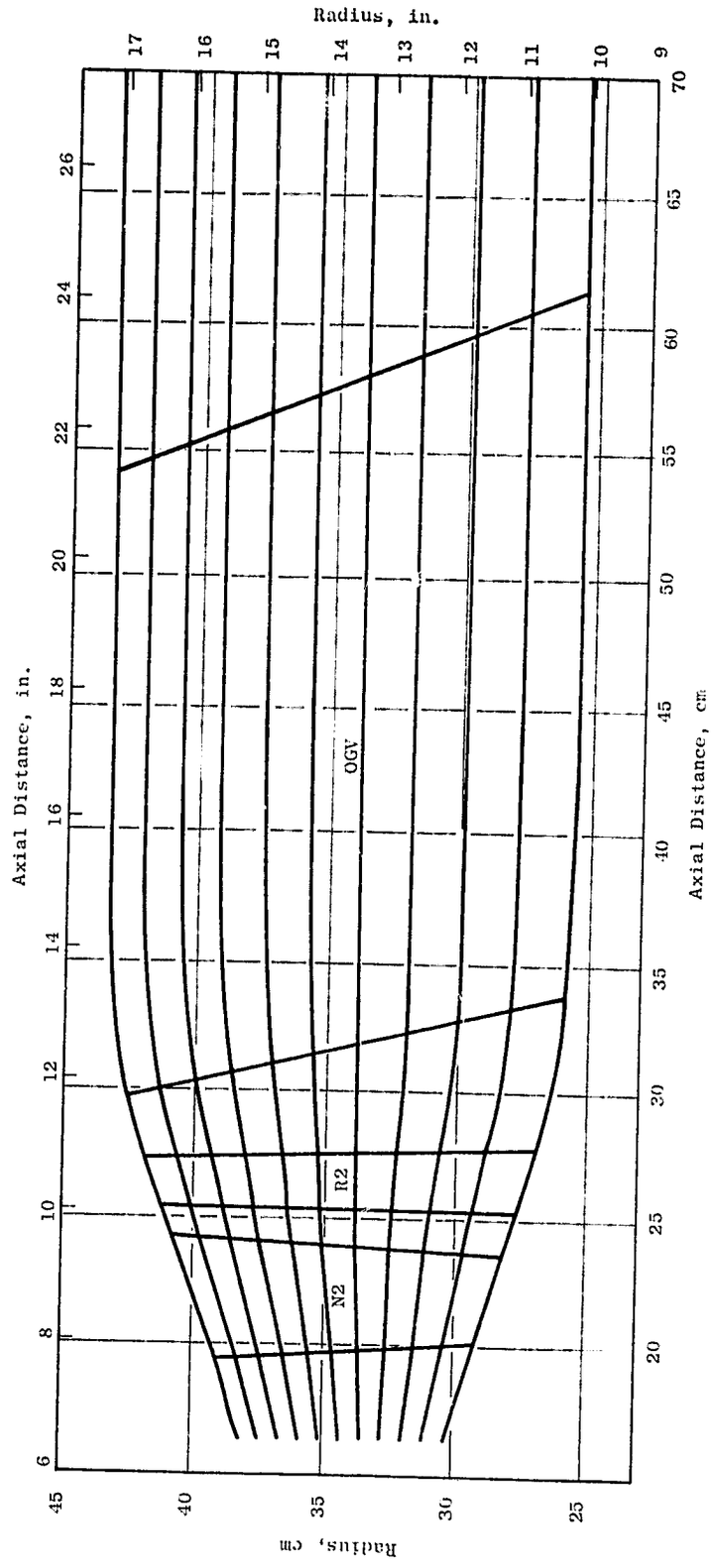

Figure 10.8. QCSEE OGV/Frame Flowpath.

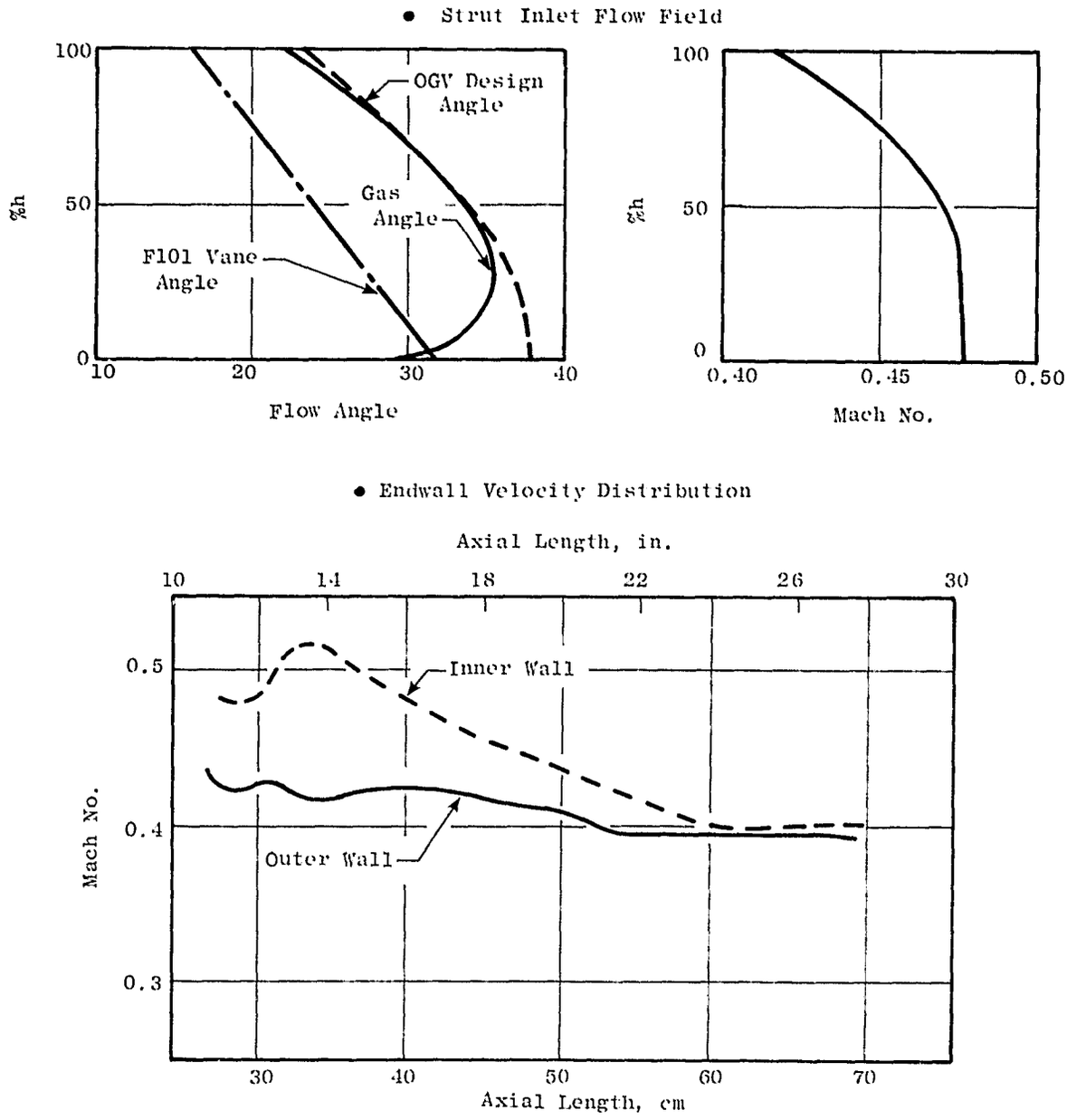

Figure 10.9. QCSEE Turbine Frame Axisymmetric Flow Analysis.

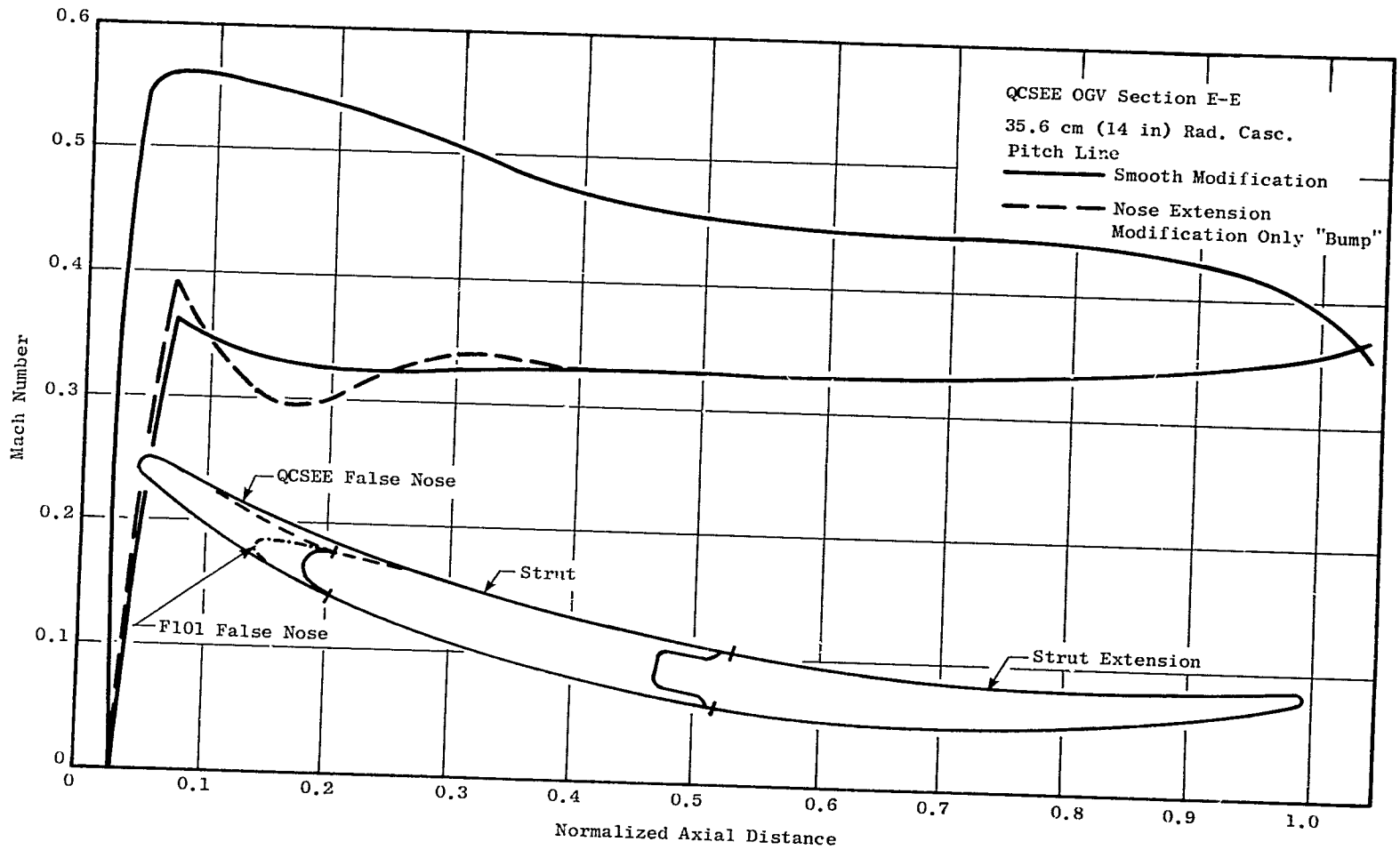

Figure 10.10. QCSEE Vane Modification.

rence) to modify the OGV smoothly as shown. CASC Mach number distributions for the root and tip are shown in Figures 10.11 and 10.12. Other intermediate sections were designed to yield a smooth stack-up.

10.4.3 Off-Design Study

Based on revised cycle data, an off-design study was undertaken to evaluate the OGV performance at several significant operating points. Vector diagrams for the low pressure turbine operating at the takeoff, approach, and maximum cruise points for both the UTW and OTW engines were calculated with the TCP program. A summary of these results was shown in Table 10.I. Axisymmetric analyses for the OTW takeoff case (design point) and the UTW approach and maximum cruise points (representing extremes in operation) were made using the CAFD program. These results are shown in Figure 10.13 plotted versus radial height at OGV inlet are the gas angle, OGV design angle, and Mach number. Also shown are the absolute Mach number distributions on the inner and outer walls through the OGV for the UTW approach and maximum cruise positions. Root, pitch, and tip vane surface Mach number distributions for these cycle points were obtained using the CASC program. These are shown in Figures 10.14, 10.15, and 10.16. At the OTW takeoff point, the Mach number distributions are satisfactory, and therefore they are satisfactory at the less severe approach and cruise points.

10.5 LOW PRESSURE TURBINE FRAME MECHANICAL DESIGN

10.5.1 Summary

The turbine frame used in the OTW engine is a modification of the F101 turbine frame. Figure 10.17 illustrates the major design features, and Table 10-II summarizes the differences from the F101 frame.

Table 10-II. Summary of Design Changes.

Item	Change	Reason
• Vane/Strut	Extended forward fairing	Reduce exit swirl
• Outer ring	Larger cross section	Change mounting system to accommodate pylon
• Flowpath liners	Recontour	Improve aero flowpath
• Outer casing	New structural part	Support exhaust nozzle
• Inner casing	Thickened and added flanges	Support centerbody

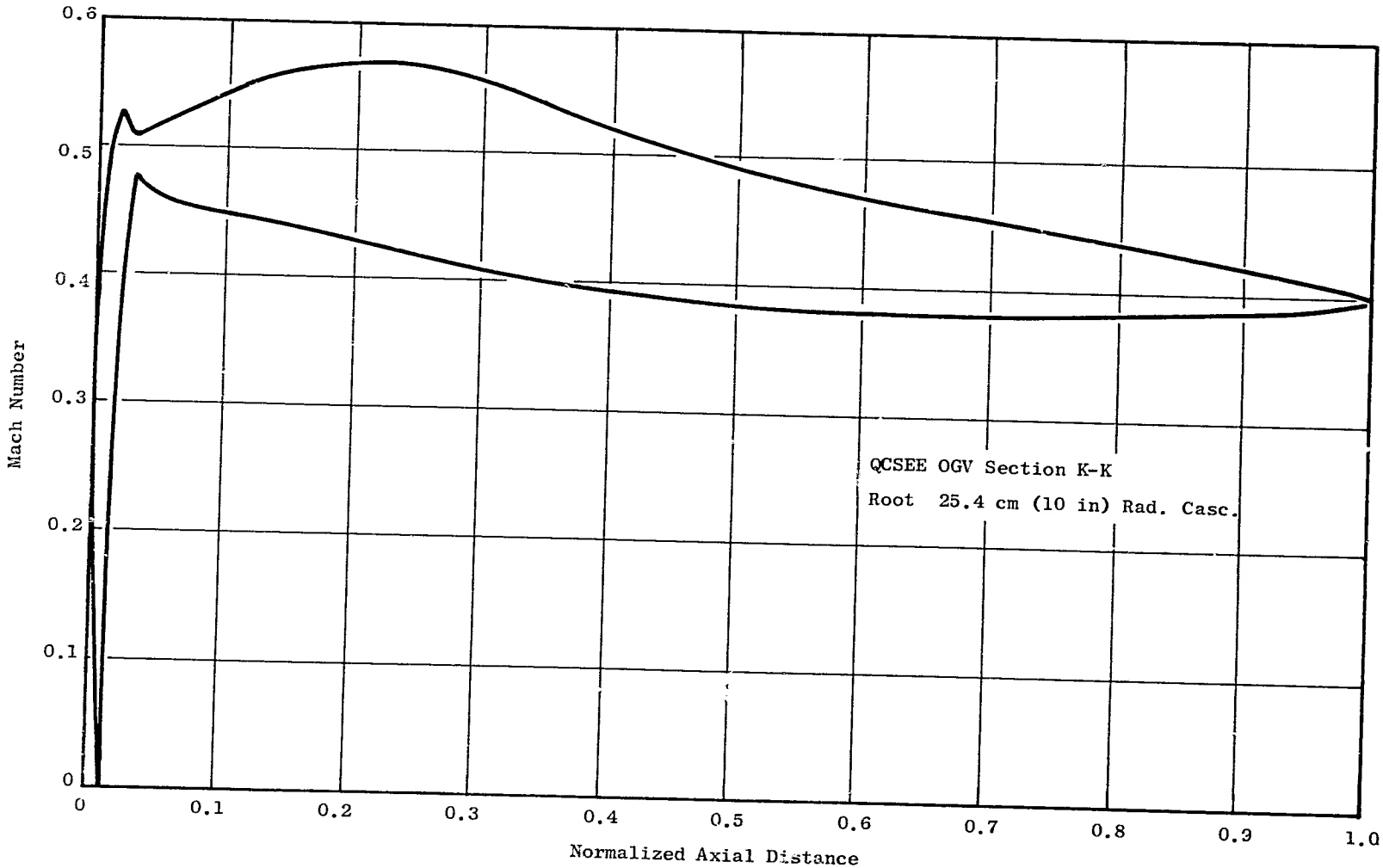

Figure 10.11. CASC Mach Number Distributions.

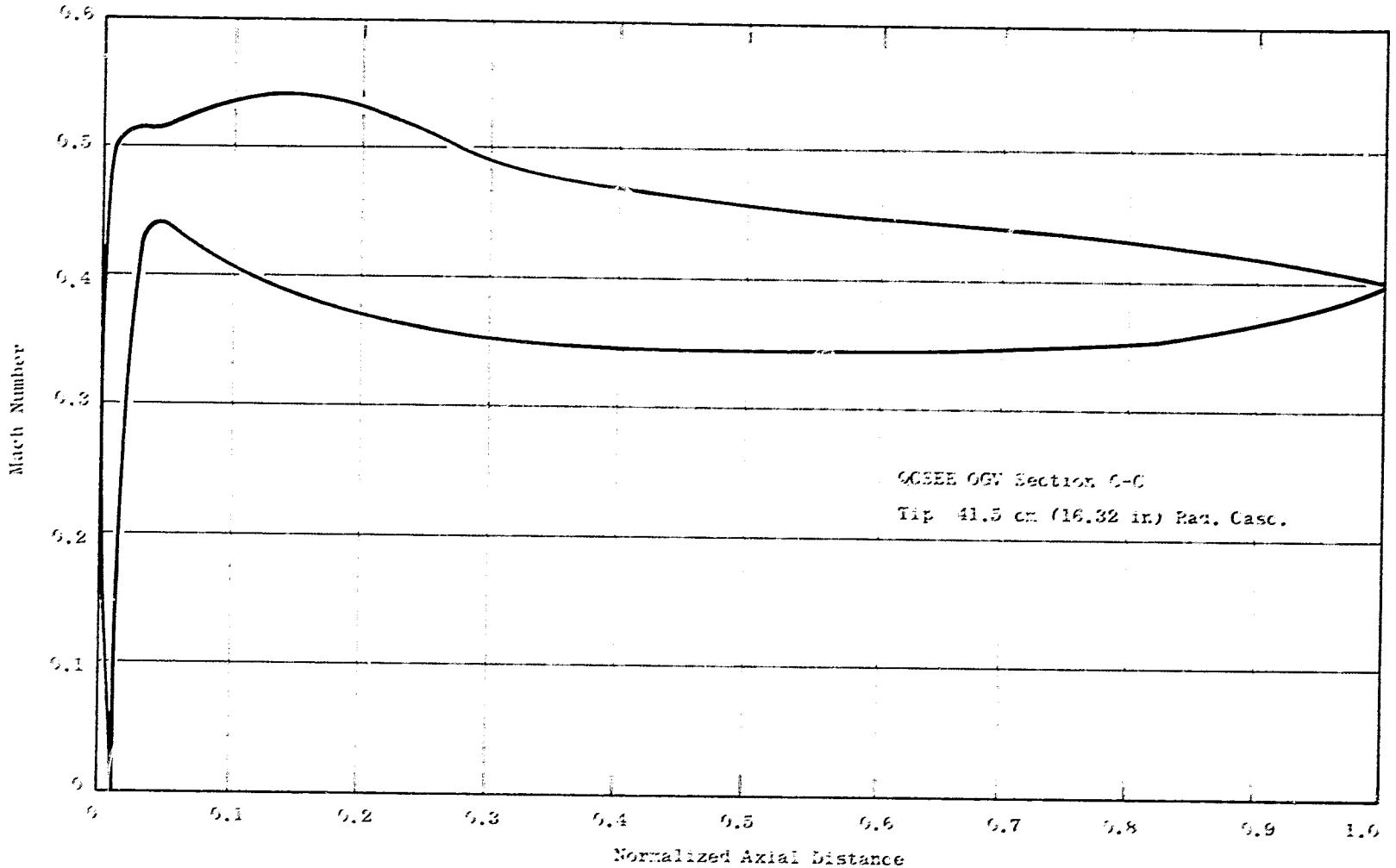

Figure 16.12. CASC Mach Number Distributions.

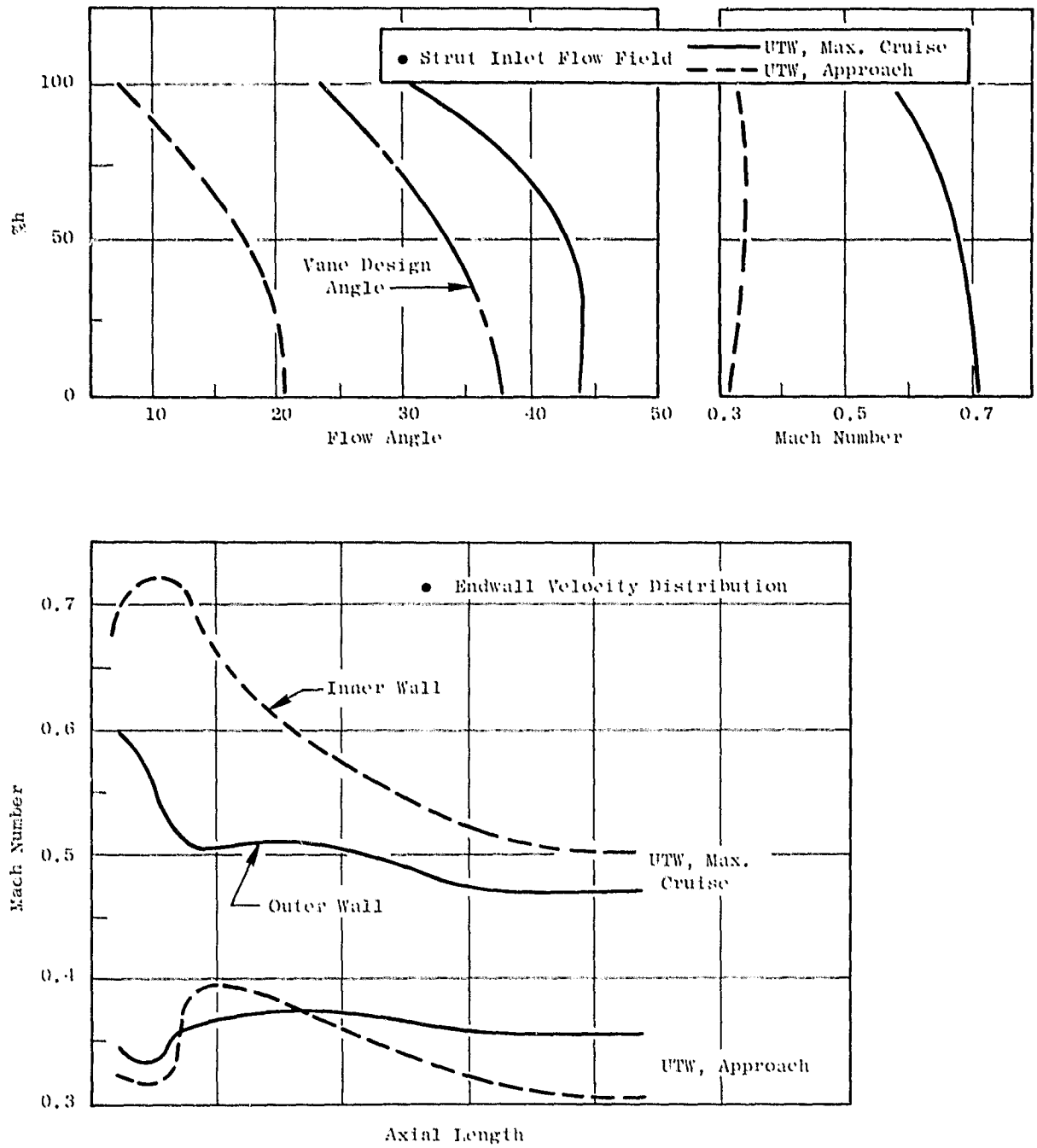

Figure 10.13. Turbine Frame Axisymmetric Flow Analysis, Off-Design Study.

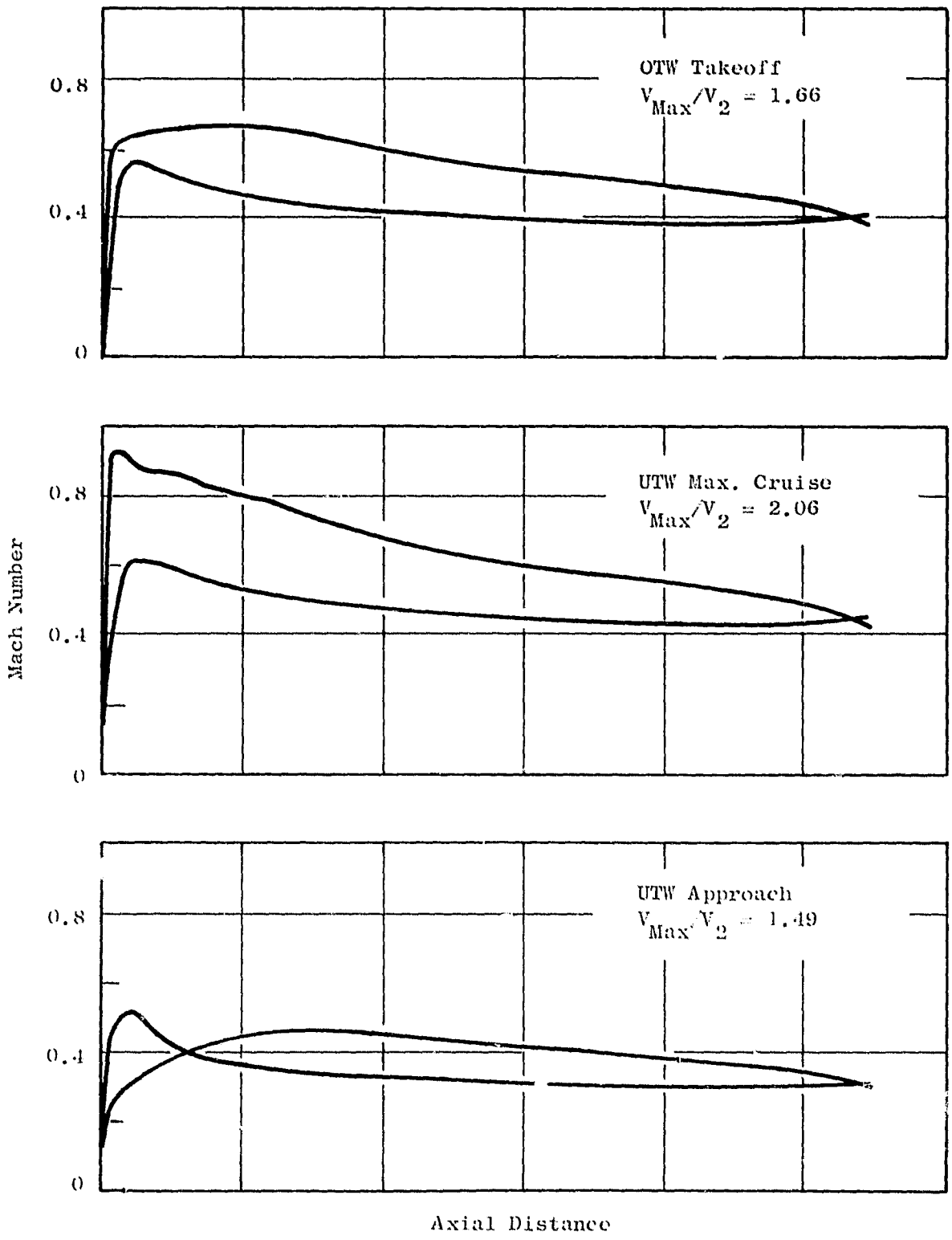

Figure 10.14. Off-Design Study, CASC Results, Root Section.

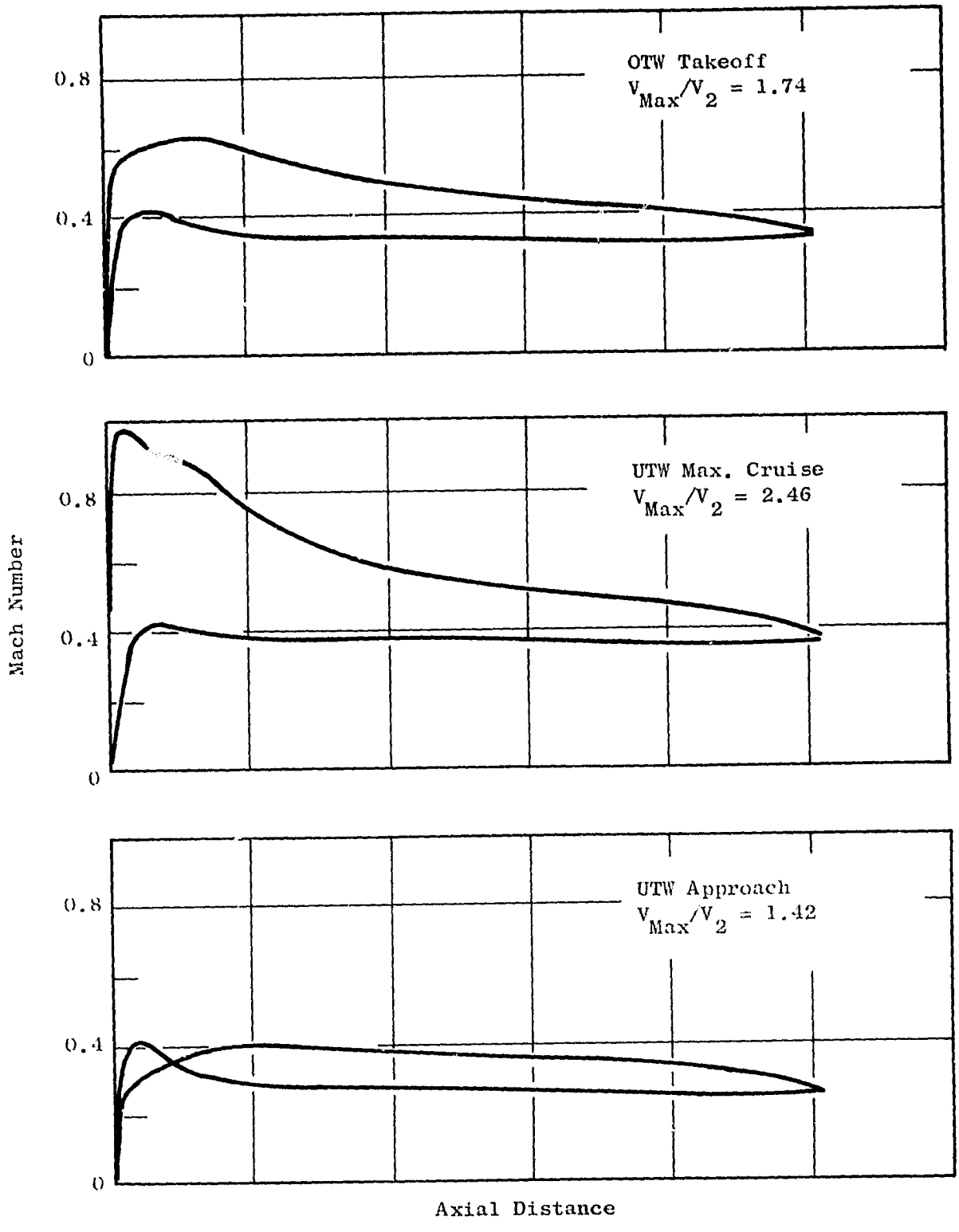

Figure 10.15. Off-Design Study, CASC Results, Pitch Section.

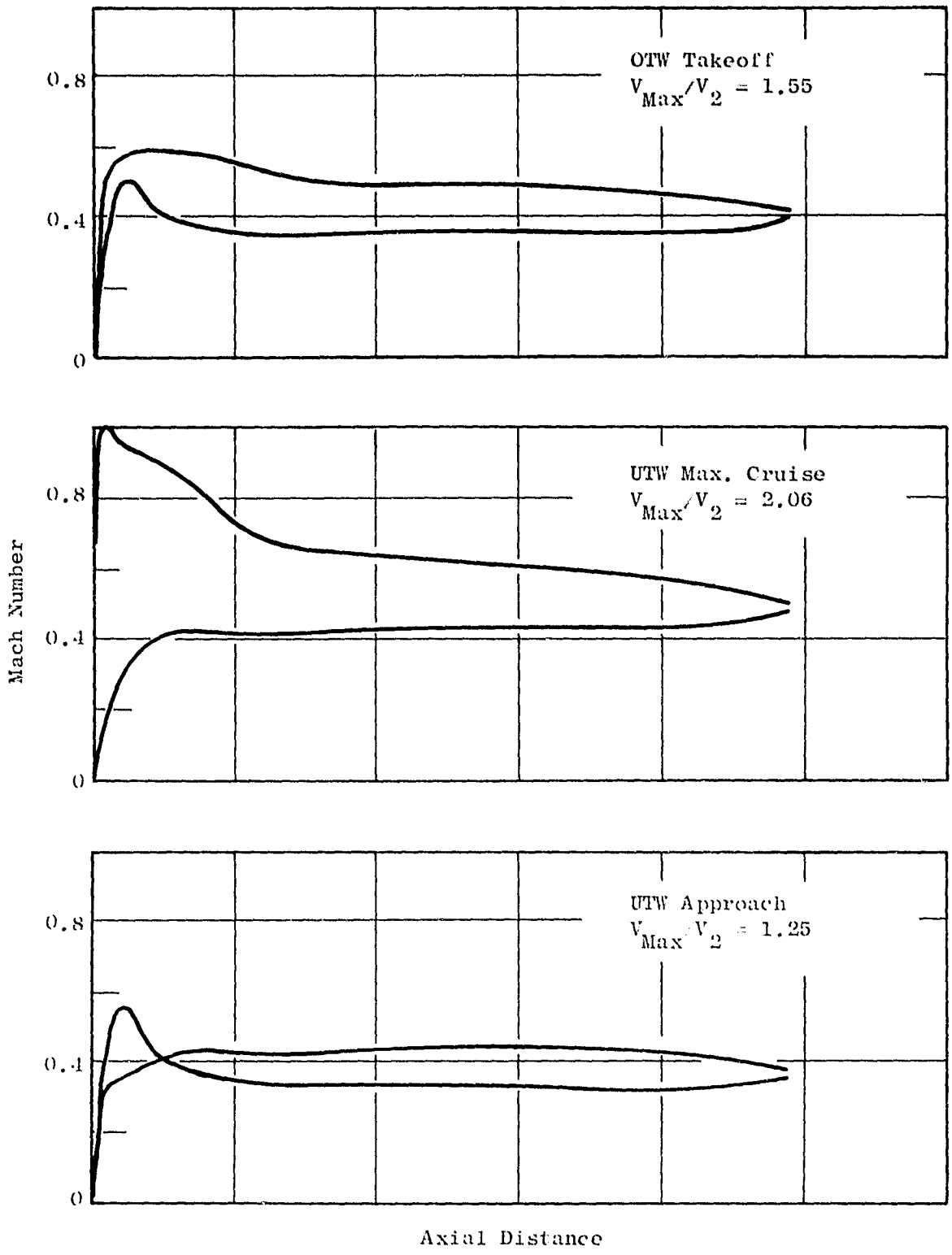

Figure 10.16. Off-Design Study, CASC Results, Tip Section.

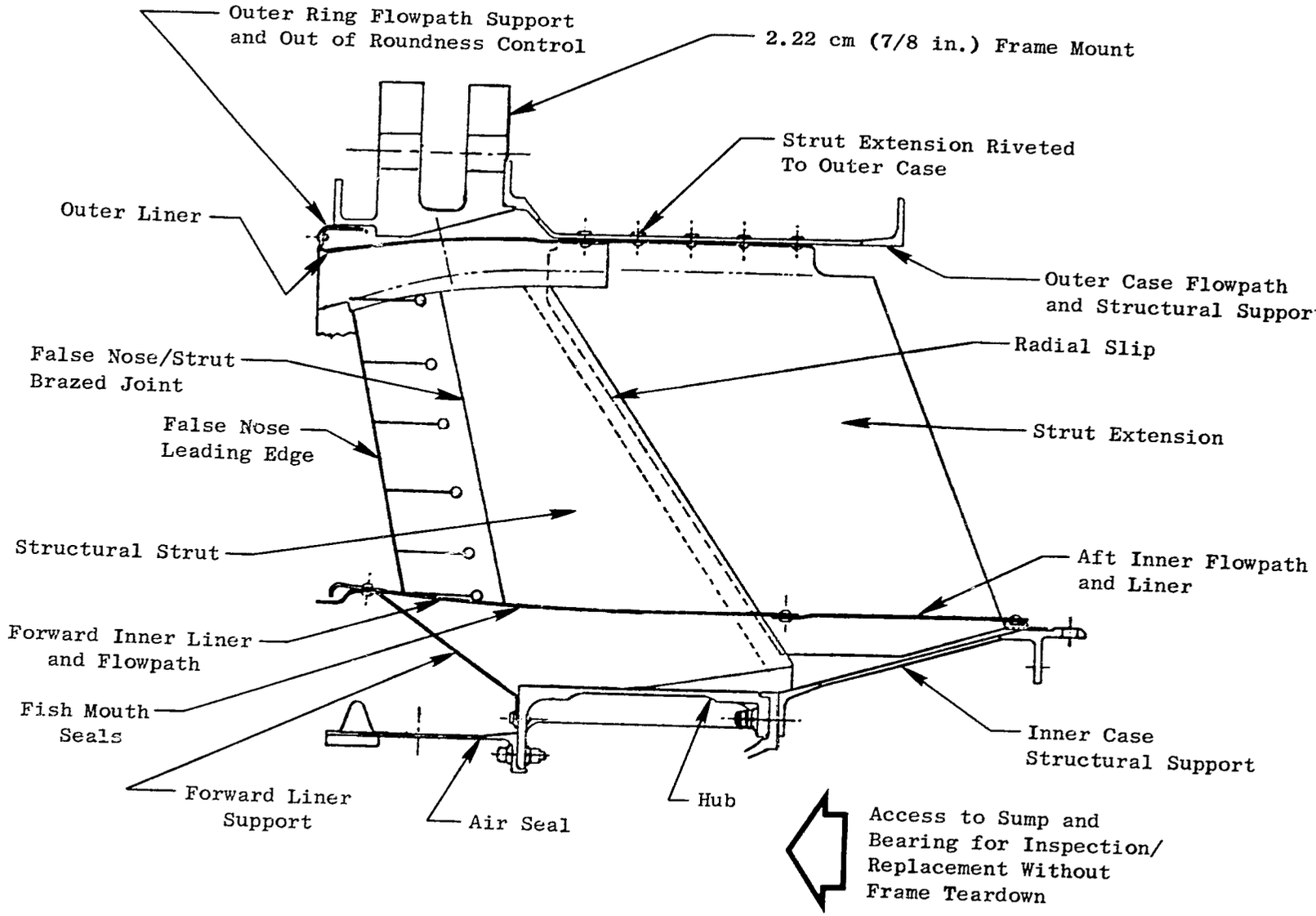

Figure 10.17. Turbine Frame Assembly Features.

10.5.2 Design Requirements

In addition to the maneuver loads shown in Section 2.0, the following specific design criteria were established:

Max. maneuver loads at operating temperatures	< 0.2% Y.S.
1-1/2 times max. maneuver loads at operating temp.	< UTS
Blade-out loads at operating temp.	Maintain engine support
1-1/2 times buckling loads at operating temp.	< 0.2% Y.S.
Transient thermal plus 1g load	< 0.2% Y.S.
4g vibratory load	< Goodman diagram

In conjunction with the above limit loads, the primary gas temperature profile used for frame analysis is shown in Figure 10.18.

10.5.3 Design Description

The OTW turbine frame consists of an outer frame, 14 aerodynamic vane/struts, flowpath liners, a hub structure, and inner and outer support casings. Figure 10.19 is a schematic of the OTW engine mounting system.

The outer frame structure consists of the outer casing with a three-link engine mount, flowpath lines, and support casing for exhaust system. Since the OTW pylon necessitates a top-mounted frame configuration, a three-link system has been employed. These links take vertical and side loads and rolling moments.

Since the three-link configuration concentrates the mount reactions at the top of the frame, the outer ring section properties must be increased. This results in a larger ring section as shown in Figure 10.20. Details of the revised outer ring are shown in Figure 10.21.

In addition to engine mounting provisions, the outer casing extends aft from the outer frame, to support the core exhaust nozzle.

In order to axially straighten the exhaust gas, greater turning must be provided through the 14 vane/struts. These vane/struts are assemblies consisting of a central structural section with leading and trailing edge fairings having the cross section shown in Figure 10.22. The fairings are nonload-carrying members, with the leading edge fairing sawcut at intervals to relieve thermal stress. The leading edge fairings are modified to accept the higher turbine exit swirl in the OTW engine.

Bearing loads are transferred through the central structural portion of the struts. The inner ends of the struts are bolted to the hub through foot pad extensions. The outer ends are assembled to the outer frame through uniball connections designed to carry loads (but not moments).

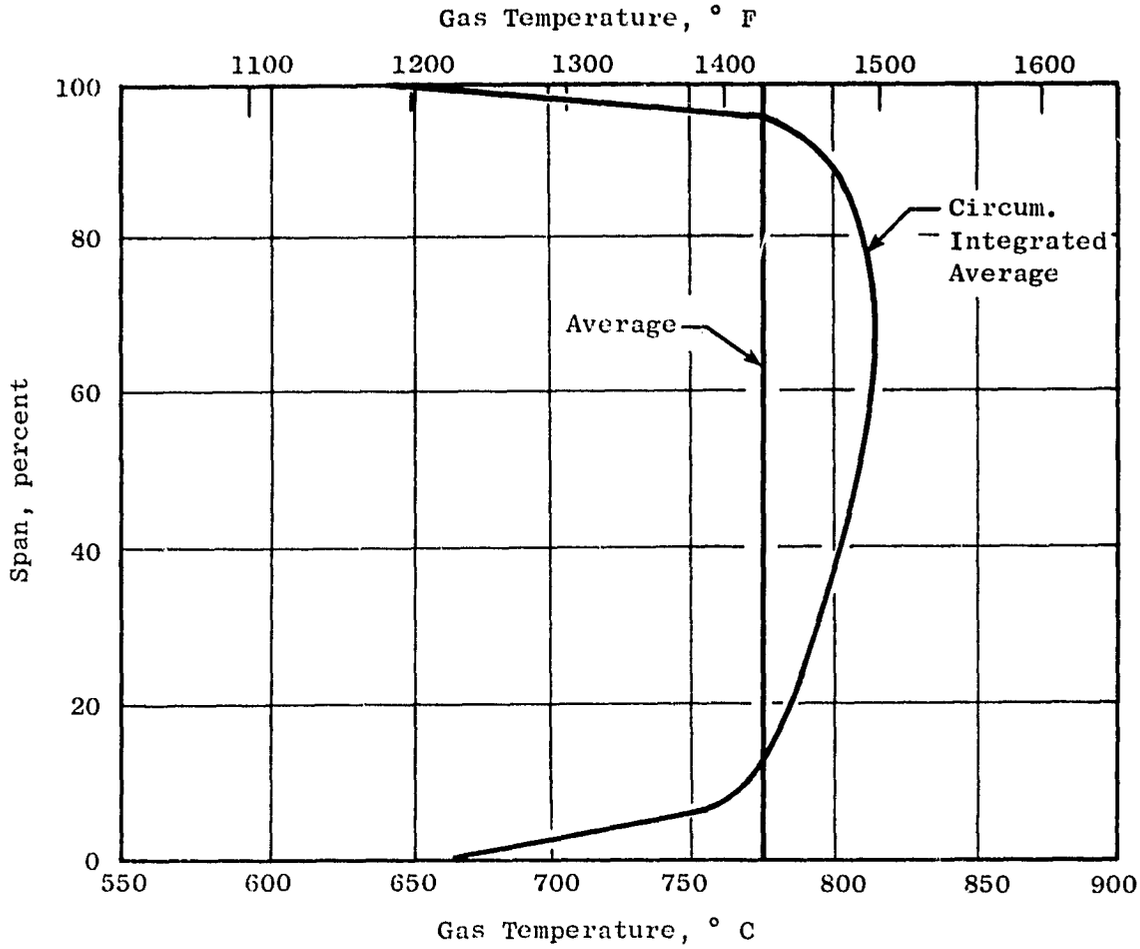

Figure 10.18. Turbine Exit Gas Profile (OTW).

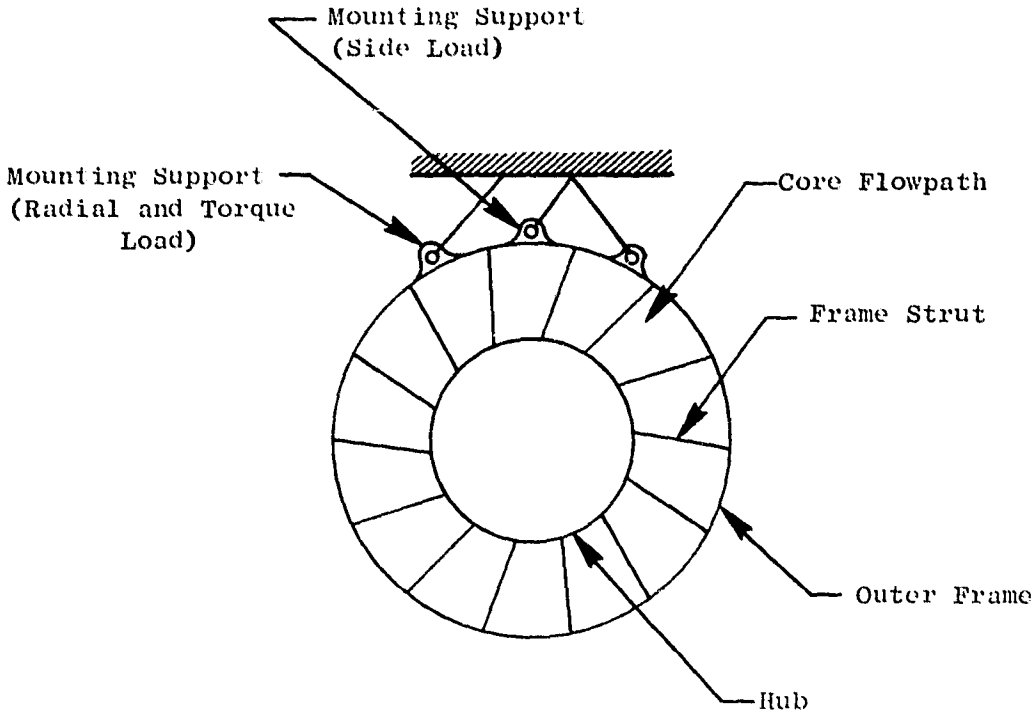

Figure 10.19. OTW Rear Mount System.

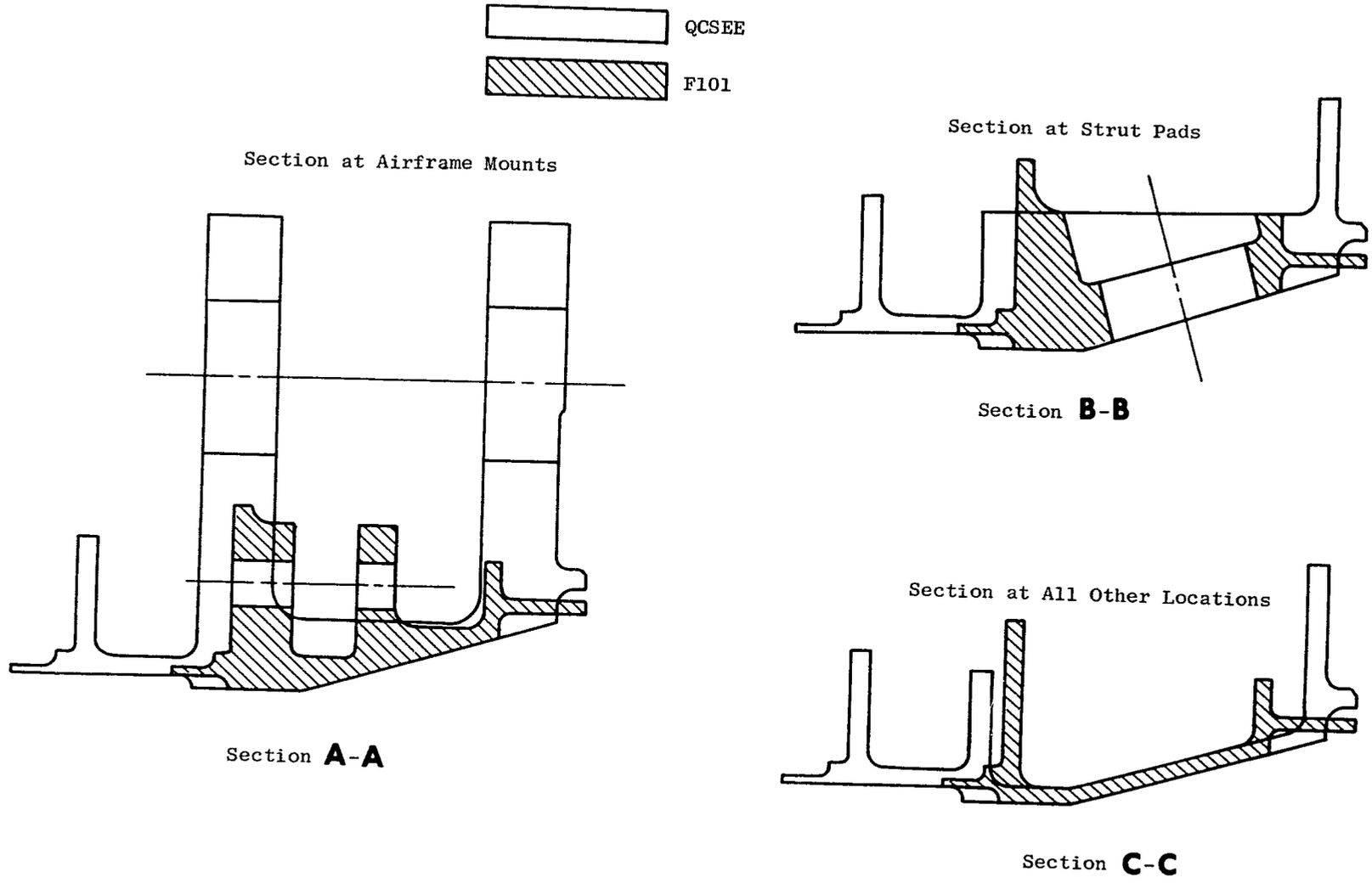

Figure 10.20. QCSEE and F101 Mounting System.

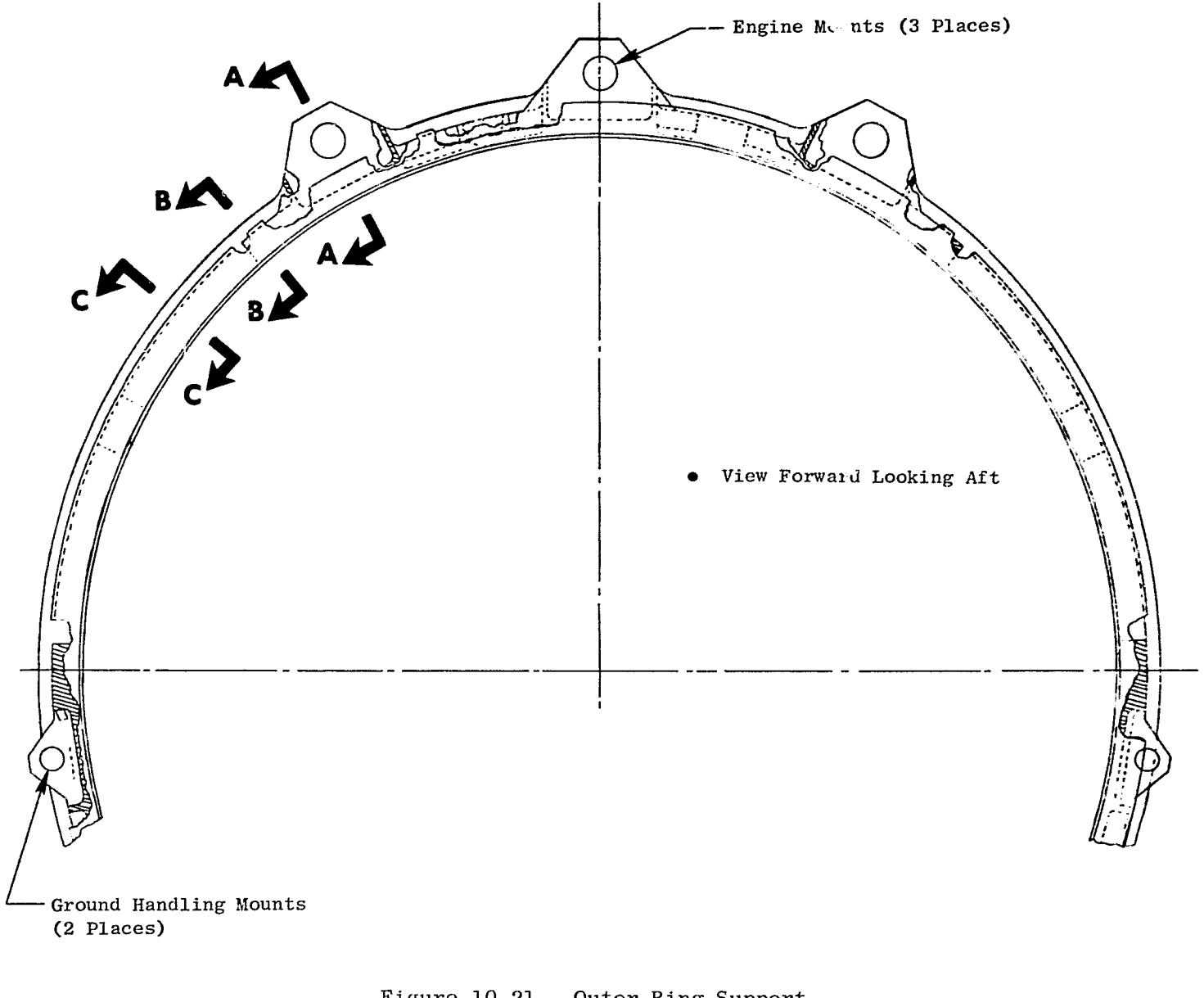

Figure 10.21. Outer Ring Support.

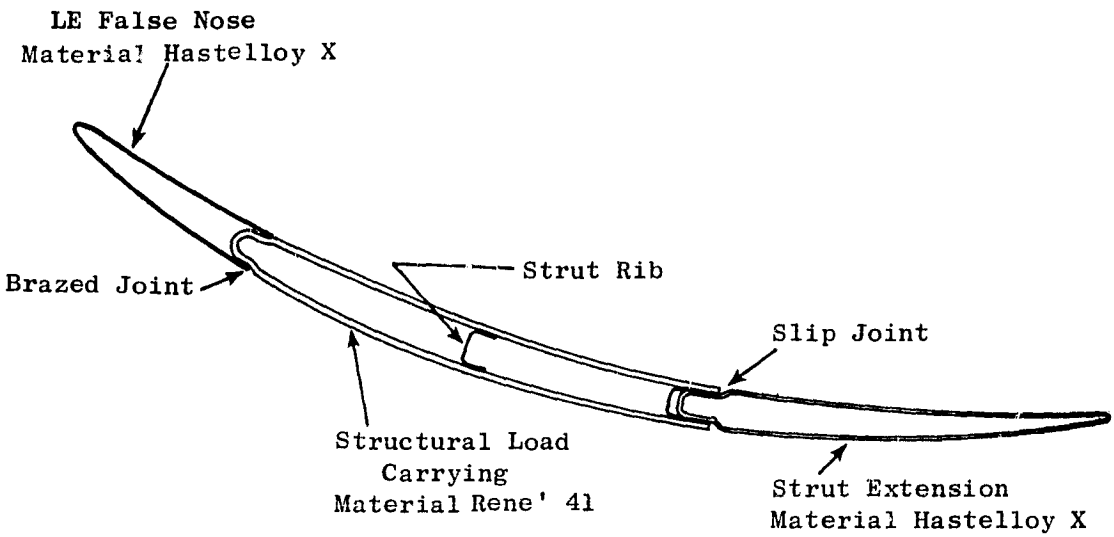

Figure 10.22. Turbine Frame Strut, Cross Section.

The rear fairings act as vane trailing edges and are attached to the central strut section by slip joints, providing for thermal expansion. The outer ends of the rear fairings are riveted to the exhaust support casing, and the inner ends are supported by pin joints which are attached to the structural strut.

As shown in Figure 10.17, a cast hub forms the inner structural member of the frame. It is composed of forward and aft flanges connected by a shear cylinder. Additional stability is provided by 14 gussets connected to the forward and aft flanges. Mounted off the forward flange are the forward liner support and inner turbine seals, while the aft flange supports the bearing and sump housing and the nozzle centerbody.

Inner and outer flowpath liners are contoured to provide a smooth aerodynamic passage from the turbine to the exhaust nozzle and centerbody. In addition, the liners protect the hub from contact with the hot gas, allowing improved thermal matching with the outer structure.

The inner liner is formed in segments between struts. The liner is supported along its axial length as shown in Figure 10.17. The outer liner is also segmented between struts, with the exhaust support casing forming a separate continuous part behind the liners. The outer liner is supported from the outer casing and outer ring flow path support, and is fabricated from Hastelloy-X material.

The space between the flowpath liners and structural struts is purged by turbine rotor cooling air. In order to minimize losses from purge air reentering the gas stream, a fishmouth seal is brazed to the strut along the inner flowpath as shown in Figure 10.23. The purge air reenters the gas stream aft of the strut extensions.

10.5.4 Design Analysis

An analytical model representing the turbine frame system was developed. The GE computer program "MASS" was used to determine loads, stresses, and deflections. The model consisted of plates in the form of rectangles and squares. These geometric sections were joined to form the cylindrical and conical surfaces of revolution. The struts were modeled as beams with variations of section properties along their length. The outer mount ring was modeled as curved beams. Variation of physical properties along the circumference was included in the analysis.

The forward and aft hub flanges were modeled as curved beams and connected to the shear cylinder which is modeled as curved plates. The axial gussets in the hub were connected to the hub flanges and to the shear cylinder plates. The outer strut ends were connected to the outer ring mount using a boundary condition that allows rotation with no moment transfer to the mount. The three locations at the outer mount system connect to ground through uniballs.

Results of the analysis were as follows:

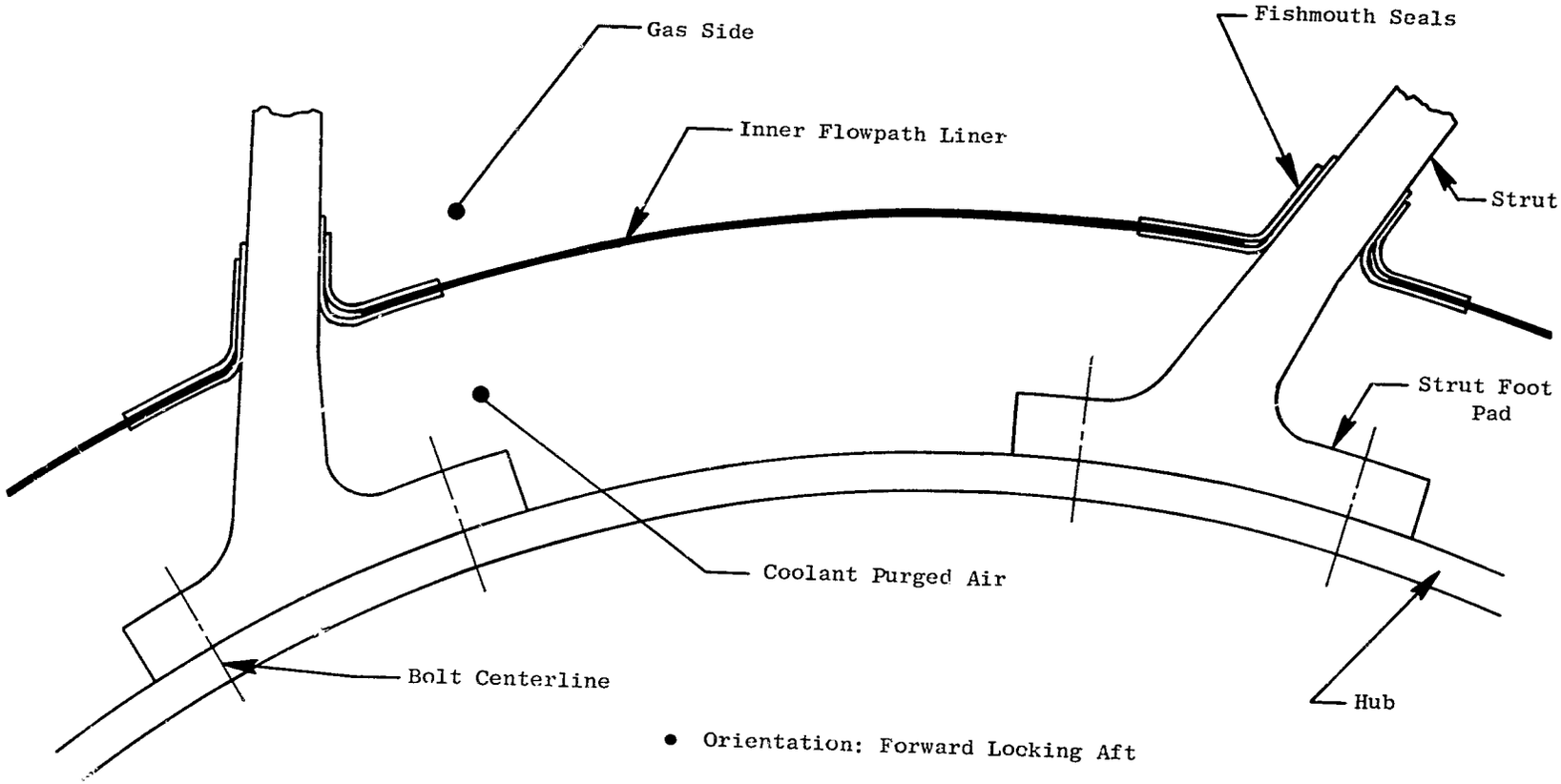

Figure 10.23. Turbine Frame Strut Fishmouth Seal, Forward Looking Aft.

Steady-State Plus 10G Landing at Temperature

Loading and stresses are shown in Figure 10.24. Table 10.III summarizes the maximum effective stresses for the various components. All parts meet the design criteria under this loading condition.

Strut Buckling

This condition was based on establishing the transient time under which the maximum strut combined stress due to compression and bending would occur. This was based on a 50-second excursion from start to maximum sea level thrust based on the temperatures shown in Figure 10.2 . The strut weld joint was found to be the most critical element, as defined in Figure 10.26. Interaction between the strut longitudinal compression and bending determined the effective buckling stress. The allowable stress in compression and bending established the margin of safety of 1.56.

Transient plus 1G Load

Using the 50-second transient condition, the effective stresses and loads are presented in Figure 10.27. Table 10.IV summarizes the maximum effective stresses for the components, together with the resulting margins of safety. Maximum steady-state plus 4g vibratory are the combined loads existing under normal operating conditions. The Campbell diagrams shown in Figures 10.28 and 10.29 reflect these combined loads for the hub and struts. Maximum combined loads under temperature for the struts were found to be at the inner strut weld line. Stress concentration factors (K_T) have been applied to the vibratory stress.

Pin Reaction and Link Attachment

Inco 718 mounting pins, 2.22 cm (7/8 in.) in diameter, have been selected for the OTW rear mount. Pin load reactions for OTW for the blade-out condition are shown in Table 10-V. Table 10-VI reflects the pin mount loads due to maneuvers. The frame loads shown in Table 10-VII reflect the OTW unit loadings. As can be seen from the tables, the pin diameter was determined by the blade-out condition.

Pin Reaction Mounting Lug Design

The mount lug design is based on withstanding the maximum load due to one blade out and maintaining engine support. Maximum stress levels occur due to shear tearout across the net section combined with bending. Under this condition the design strength far exceeds the limit imposed by the load. Figure 10.30 shows the blade-out lug margin of safety.

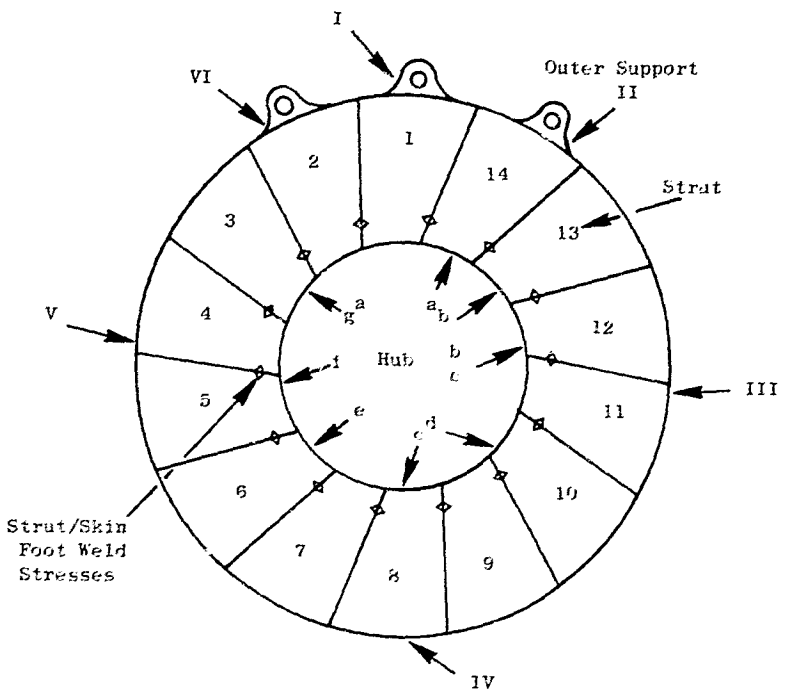

Note: Frame Orientation is Forward Looking Aft

Note: Max. Hub Moment/Stresses Occur at the Aft Hub Flange for this Condition.

Strut	Loads		Stresses	
	N	lb	kn/cm^2	ksi
1	17100	3845	13.6	19.7
2	18200	4098	4.4	6.4
3	20600	4636	6.2	8.9
4	1170	263	12.1	19.9
5	3380	762	14.2	20.6
6	4640	1044	13.1	18.9
7	5850	1318	11.1	16.1
8	6640	1492	12.9	18.7
9	6660	1484	11.2	16.2
10	6350	1437	15.4	22.3
11	3560	800	6.1	8.8
12	2940	660	16.0	23.2
13	-1510	-339	22.6	32.8
14	18500	4158	15.8	22.8
Outer Support				
I	14000	1239	15.5	22.4
II	75300	6659	49.4	71.5
III	-	-	4.3	6.2
IV	4950	437	10.0	14.5
V	-	-	8.0	11.6
VI	71900	6352	46.7	67.8
	Moment			
Hub	kNm	lb in.		
a	3.27	2893	18.0	26.0
b	3.22	2848	18.0	26.0
c	1.02	901	6.7	9.7

Figure 10.24. Turbine Frame Stresses and Loads - Max. Sea Level Steady State plus 10 G Landing.

Table 10-III. Turbine Frame Maneuver Stresses, Maximum Steady-State Plus 10 G Down Loading.

Item	Material	Eff. Stress/ys† $kN/cm^2/kN/cm^2$ (ksi/ksi)	Ult. Eff. Stress/ Ult. Stress‡ $kN/cm^2/kN/cm^2$ (ksi/ksi)	MS† 0.2% ys	MS‡ Ult.
Hub	Cast IN 718	17.9/53 (26/77)	24.1/66.2 (35/96)	1.96	1.74
Outer Support	Forge IN 718	49.3/81.4 (71.5/118)	89.5/124.1 (130/180)	0.65	0.38
Strut Foot/ Skin Weld	Cast René 41	22.6/58.5 (32.8/85)	31.3/63.5 (45.2/92)	1.35	1.03

† 0.2% yield strength at temperature

‡ • Ultimate stress is (1.5 X mech.) + thermal
• Ultimate strength at temperature

$$MS = \frac{\sigma_{all}}{\sigma_{eff}} - 1$$

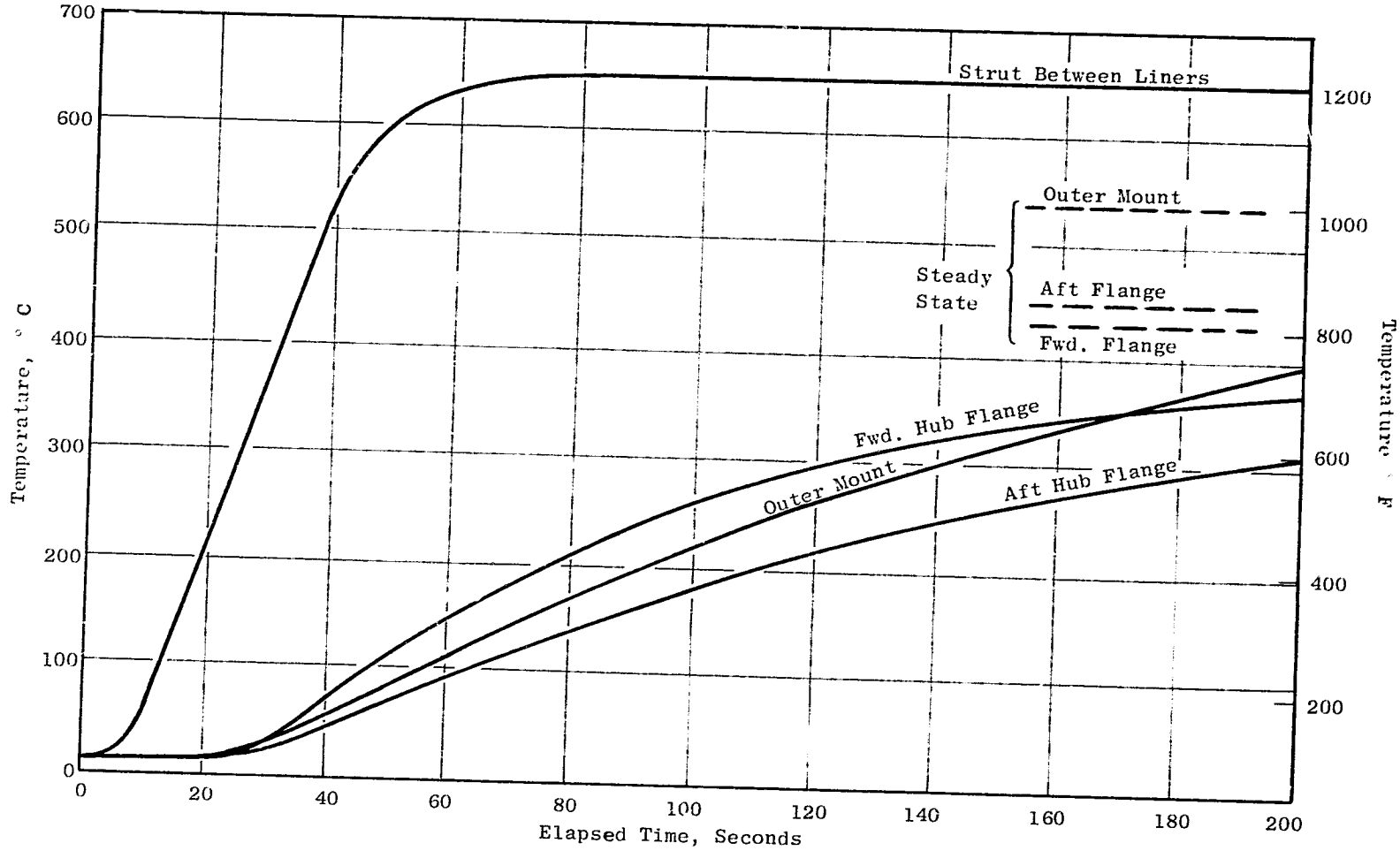

Figure 10.25. Turbine Frame Transient Average Temperatures for Start to Max. Sea Level.

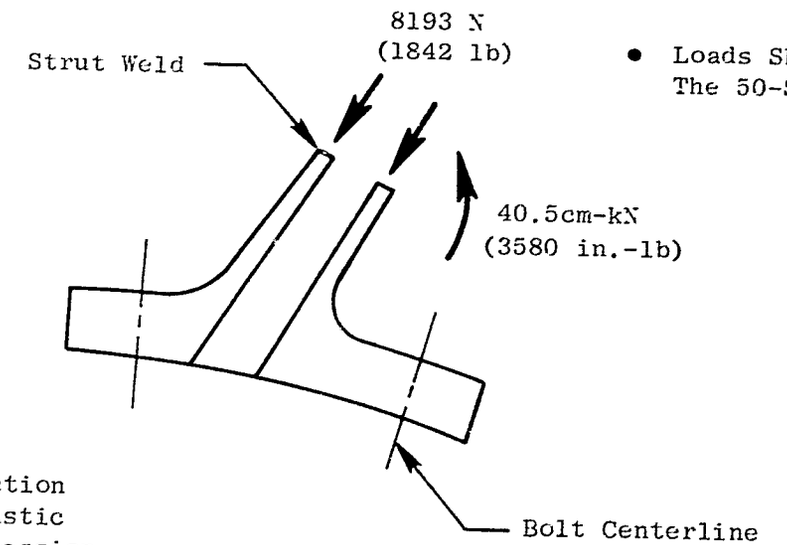

$\frac{L_{eff}}{L_{act}} \cong 1.20$

Assume Elliptical Section
Analysis Indicate Elastic
Buckling Due To Compression

Compression and Bending Interaction

$$R_c + R_b \leqq 1$$

$$R_c + R_b = 0.391$$

$$MS = \frac{1}{R_c + R_b} - 1 = 1.56$$

Buckling Meets Criteria of $\geqq 0.5$

Where $R_c = \frac{\sigma comp}{\sigma all}$

$$R_b = \frac{\sigma bend}{\sigma all}$$

Figure 10.26. Turbine Frame Strut Buckling.

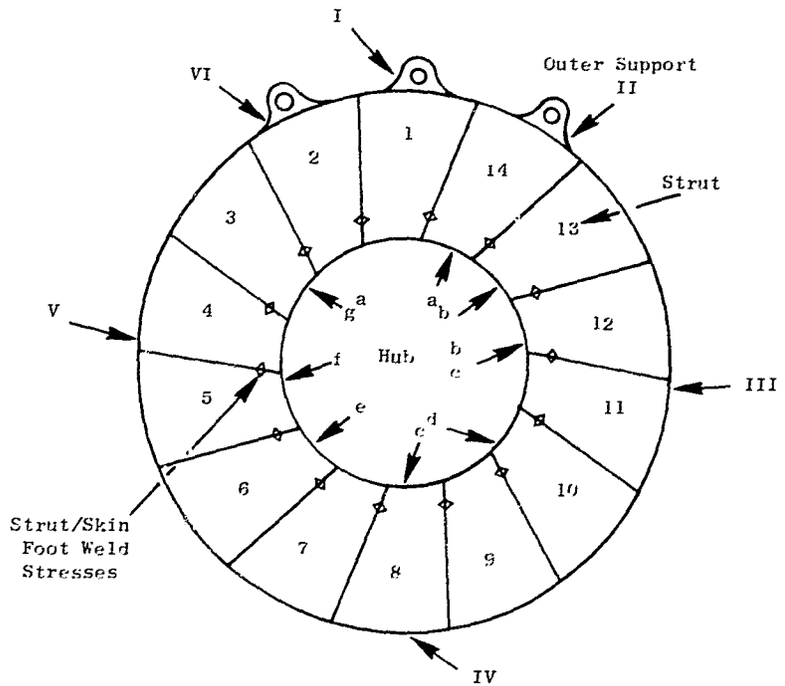

Note: Frame Orientation is Forward Looking Aft

Note: Max. Hub Moment/Stresses Occur at the Forward Flange for this Condition

Strut	Loads		Stresses	
	N	lb	kN/cm^2	ksi
1	-6085	-1368	30.2	43.7
2	-6032	-1356	29.7	44.0
3	-5764	-1296	30.7	44.5
4	-7460	-1677	31.1	45.0
5	-7264	-1633	30.9	44.7
6	-7028	-1580	30.8	44.6
7	-6912	-1554	30.8	44.6
8	-6872	-1545	30.8	44.6
9	-6899	-1551	30.9	44.7
10	-7273	-1635	30.9	44.7
11	-6828	-1535	30.7	44.5
12	-8193	-1842	31.2	45.1
13	-7513	-1689	30.2	43.7
14	-6041	-1358	30.1	43.6
Outer Support				
I	18553	4171	5.9	8.60
II	19359	4352	5.1	7.33
III	1 ;290	4112	8.1	11.70
IV	17246	3877	6.2	9.03
V	17388	3909	6.3	9.12
Hub	Moment			
	kNm	lb in.		
a	5.62	4974	17.8	25.7
b	5.70	5042	18.3	26.6
c	5.97	5282	19.1	27.7
d	5.70	5043	18.5	26.8
e	5.81	5139	18.6	26.9
f	5.92	5239	18.6	26.9
g	5.75	5090	17.8	25.7

Figure 10.27. Turbine Frame Stresses and Loads - 50 sec Transient plus 1 G Load.

Table 10-IV. Turbine Frame Stresses Thermal Loading and 1 G Engine Loading, Start to Maximum S.L. Thrust.

Component	Material	Temp, ° C (° F)	Stress/LCF Strength (1000 Cycles) $kN/cm^2/kN/cm^2$ (ksi/ksi)	K_t	% LCF Used at Transient Stress	Effective Stress, kN/cm^2 (ksi)	Buckling (Comb. Bend Plus Comp. Ratios)
Hub	IN 718 Cast	116 (240)	14.8/87.6 (21.4/127)	1.6	< 1	18.5 (26.9)	---
Outer Support	IN 718 Forge	88 (190)	5.4/151.7 (7.9/220)	1.35	< 1	8.1 (11.7)	---
Strut Skin	René 41 Sheet	621 (1150)	20.2/84.1 (29.3/122)	1	< 1	40.6 (58.6)	---
Strut Skin/ Foot Weld	René 41 Cast	316 (600)	34.7/51.7 (50/75)	2.2	10.5	30.7 (45.1)	0.391†
Strut Foot	René 41 Cast	288 (550)	28.7/51.7 (37.3/75)	1.6	2.2	32.2 (46.7)	---

† The margin of safety for strut buckling is $\frac{1}{.391} - 1 = 1.56$ (See Figure 10.26)

$$\sigma_{LCF} = \frac{\sigma_{eff} \times K_t}{2}$$

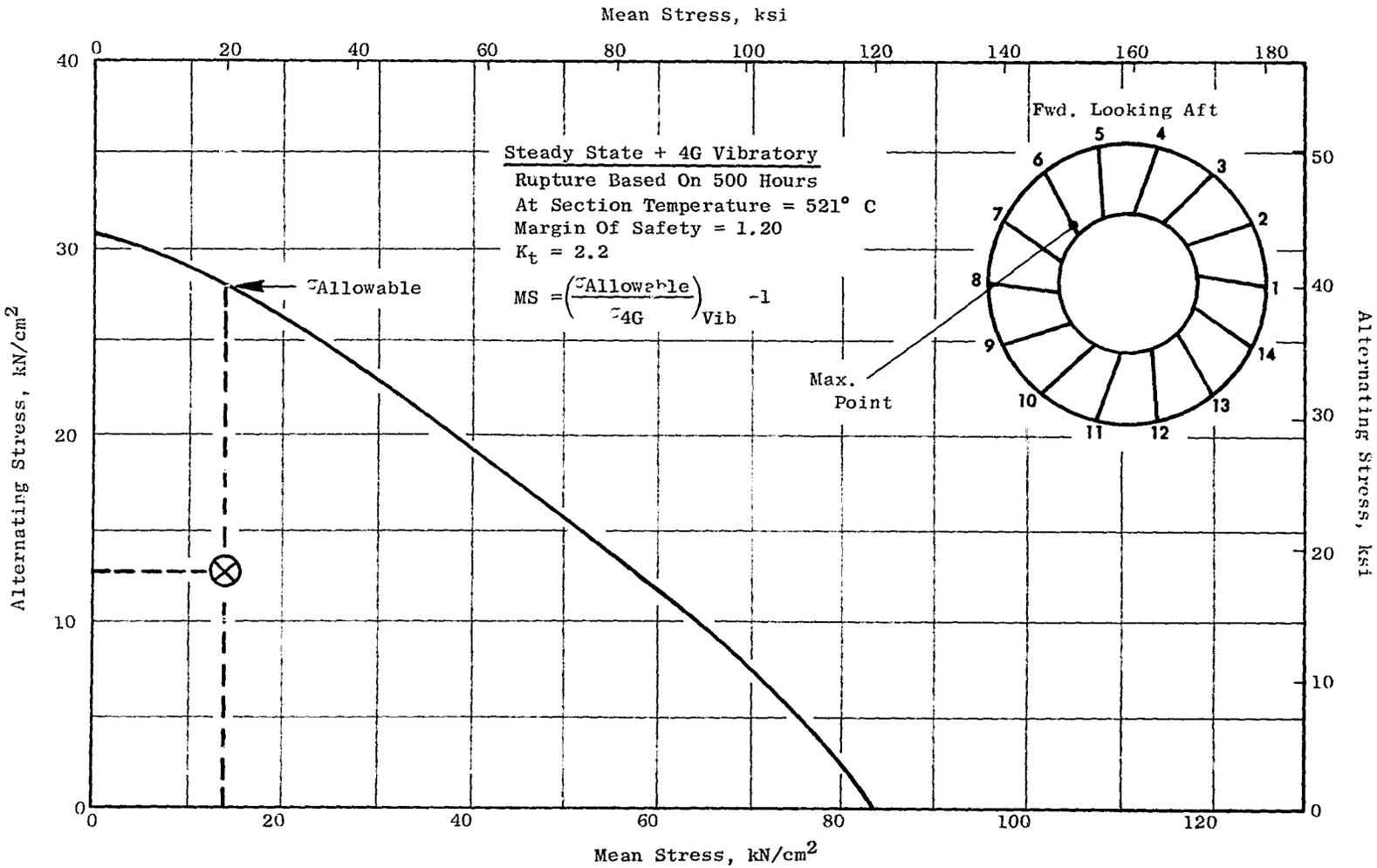

Figure 10.28. Frame Stress Range Diagram - Foot/Skin Weld Line.

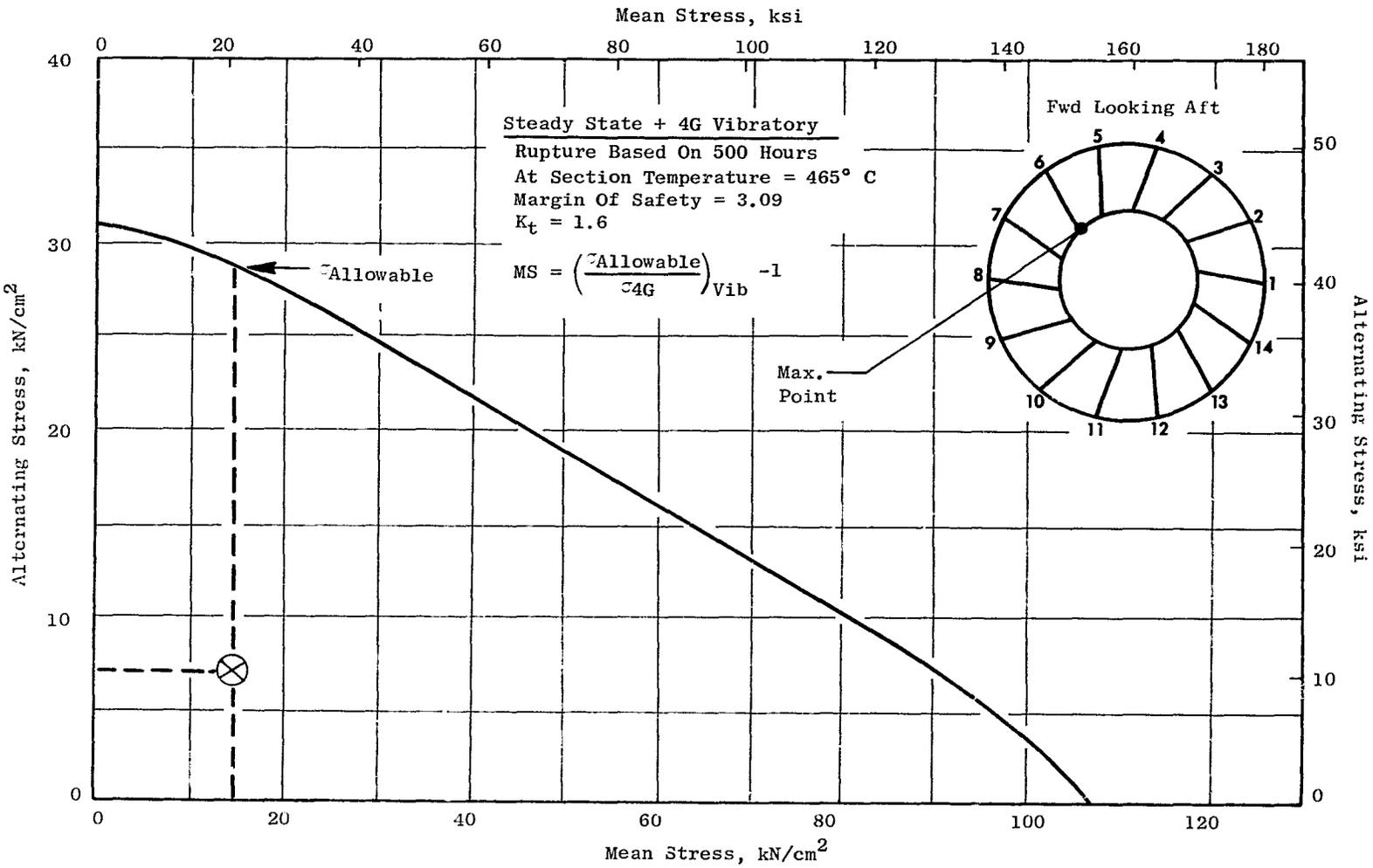

Figure 10.29. Frame Stress Range Diagram - Hub.

Table 10-V. OTW Turbine Frame 2.22 cm (7/8 In.) Pin Mount, 1 Blade Out.

	Load		Effective Stress		
	N	LB	kN/cm^2	ksi	MS
R_R	56047	12600	12.6	18.2	7.68
R_L	167070	37560	37.4	54.1	1.92
R_S	208620	46900	46.7	67.6	1.33

$$MS = \frac{\sigma_{ult}}{\sigma_{eff}} - 1$$

σ_{ult} - Ultimate strength of Inco 718 bar at 700° K (800° F)

σ_{eff} - Effective stress of 2.2 cm (7/8 in.) pin under double shear.

Table 10-VI. OTW Engine Mount Reaction Load Due to Maneuver, 2.22 cm (7/8 in.) Mount Pin.

Maneuver Condition [All conditions include 90,295 N, (20, 300 lb) Thrust]	R_L N (lbs)	R_R N (lbs)	R_S N (lbs)
10 G Down, 2 G Side	42,919 (9,649)	44,987 (10,114)	54,115 (12,166)
10 G Down, 1.5 G Side, 2 G Fwd	23,948 (5,384)	41,980 (9,438)	40,588 (9,125)
6 G Down, 4 G Side, 2 G Fwd	108,274 (24,342)	67,543 (15,185)	108,233 (24,333)
6 G Down, 4 G Side, 3 G Aft	118,900 (26,731)	56,917 (12,796)	108,233 (24,333)
4 G Side, 4 G Fwd	120,105 (27,002)	55,712 (12,525)	108,233 (24,333)
4 G Side, 3 G Aft	134,980 (30,346)	40,837 (9,181)	108,233 (24,333)
OTW engine weight used is 1,805 kg (3,980 lbs)			

Table 10-VII. OTW Engine Mount Reaction Loads for 2.22 cm (7/8 in.) Pin.

Maneuver	OTW		
	R_L, N (lbs)	R_R, N (lbs)	R_S, N (lbs)
1 G Down	$\pm$ 2,682 (603)	$\pm$ 2,682 (603)	--- ---
1 G Side	$\pm$ 29,441 (6619)	$\pm$ 14,509 (3262)	$\pm$ 27,057 (6083)
1 G Aft	$\pm$ 2.122 (477)	$\mp$ 2,126 (478)	--- ---
1 F Accel	$\pm$ 67 (15)	$\pm$ 67 (15)	--- ---
1 P Vel	$\mp$ 13,664 (3072)	$\pm$ 6,401 (1439)	$\pm$ 36,372 (8177)
1 Y Accel	$\pm$ 62 (14)	$\pm$ 27 (6)	$\pm$ 151 (34)
1 Y Vel	$\mp$ 15,679 (3525)	$\mp$ 15,679 (3525)	--- ---
1 Thrust (Aft)	$\pm$ 10,836 (2436)	$\pm$ 10,835 (2436)	--- ---
OTW engine weight = 1.805 kg (3,980 lbs).			

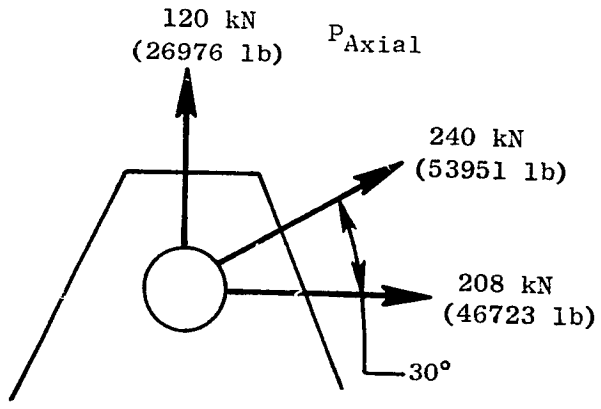

Detail **A-A**

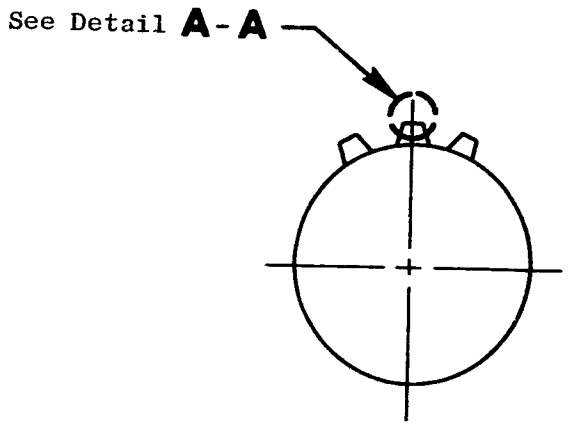

OTW 1 Airfoil-Out Load

- Design Includes Addition of 15% for Fitting Factor
- Shear Tearout Greater than Tension Across Net Section
- $MS = \frac{1}{(R_a^{1.6} + R_{tr}^{1.6})^{0.625}} - 1$

Where $R_a = \frac{P_{Axial\ Applied}}{P_{Ult\ At\ Temp}}$

$R_{tr} = \frac{P_{Transverse}}{P_{Ult\ At\ Temp}}$

$MS = 1.51$

- Reference: "Analysis And Design of Flight Vehicle Structures" by Bruhn.

Figure 10.30. Turbine Frame Ring Support Lug Analysis.

Blade-Out Load

The turbine frame was designed to meet UTW engine composite blade-out requirements. It was then analyzed for OTW loads, shown in Figure 10.31-A, representing the unbalance resulting from loss of one titanium airfoil. The analysis indicated that, at this load condition, the stress in the weld at the foot-pad/strut leading edge would reach 79 kN/m^2 (115 ksi). This would exceed the material ultimate strength less three standard deviations of 63.4 kN/m^2 (92 ksi). Furthermore, subsequent system studies have shown still higher blade-out loads as shown in Figure 10.31-B.

While the analysis indicated that the frame cannot withstand the blade loss without local failure, it is considered acceptable for the experimental program for the following reasons.

1. The analysis did not consider plastic deformation and the resulting stress redistribution.

2. Possible cracking in the foot pad/strut weld should not be catastrophic because sufficient rotor support remains to allow engine shutdown.

3. The titanium fan blades have been designed using an airfoil contour suitable for composite construction. This results in abnormally high loads in the very unlikely event of airfoil loss. Much greater blade-out capability would be available in a flight configuration using composite airfoils.

e-4

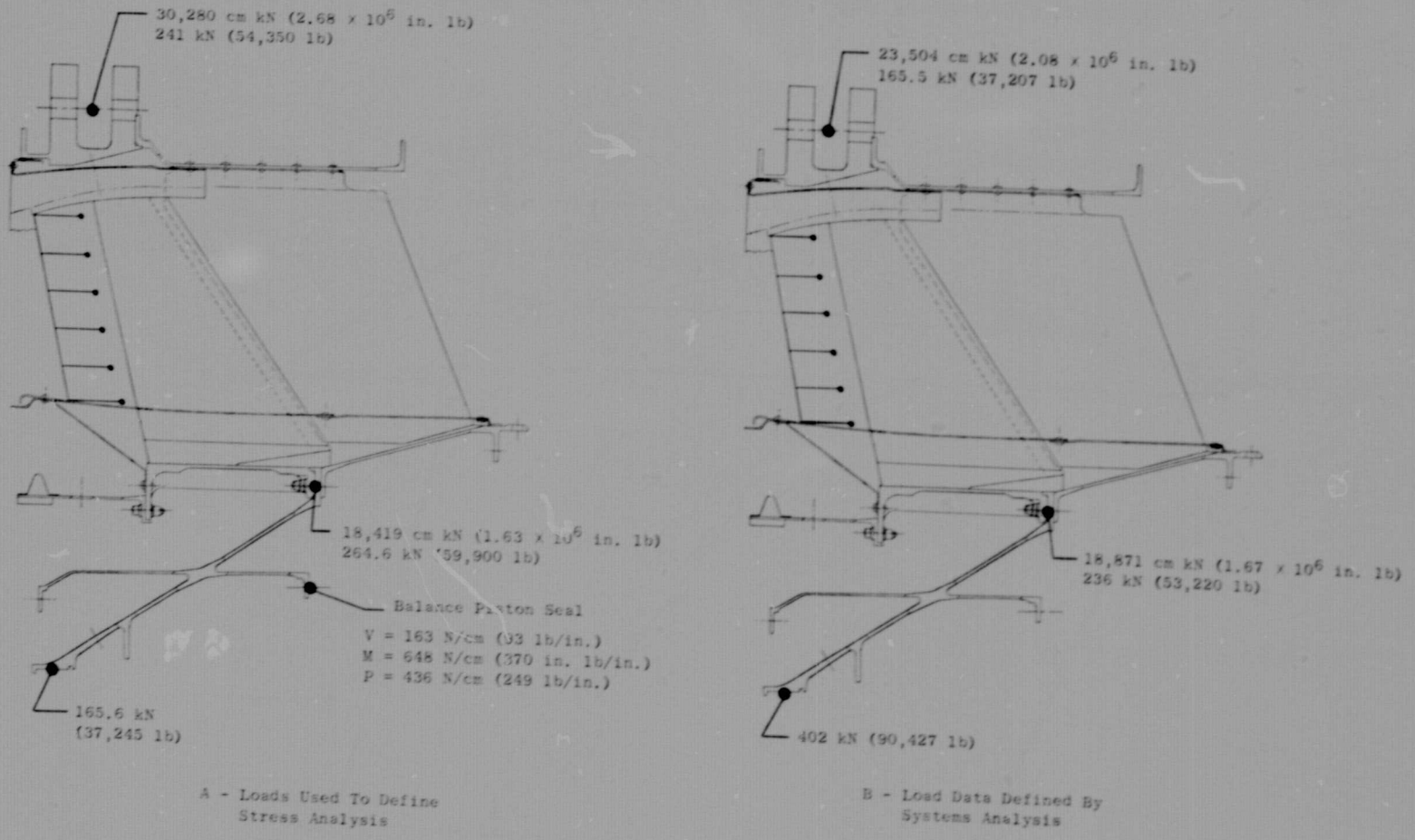

Figure 10.31. Turbine Frame External Loads, Blade Out.

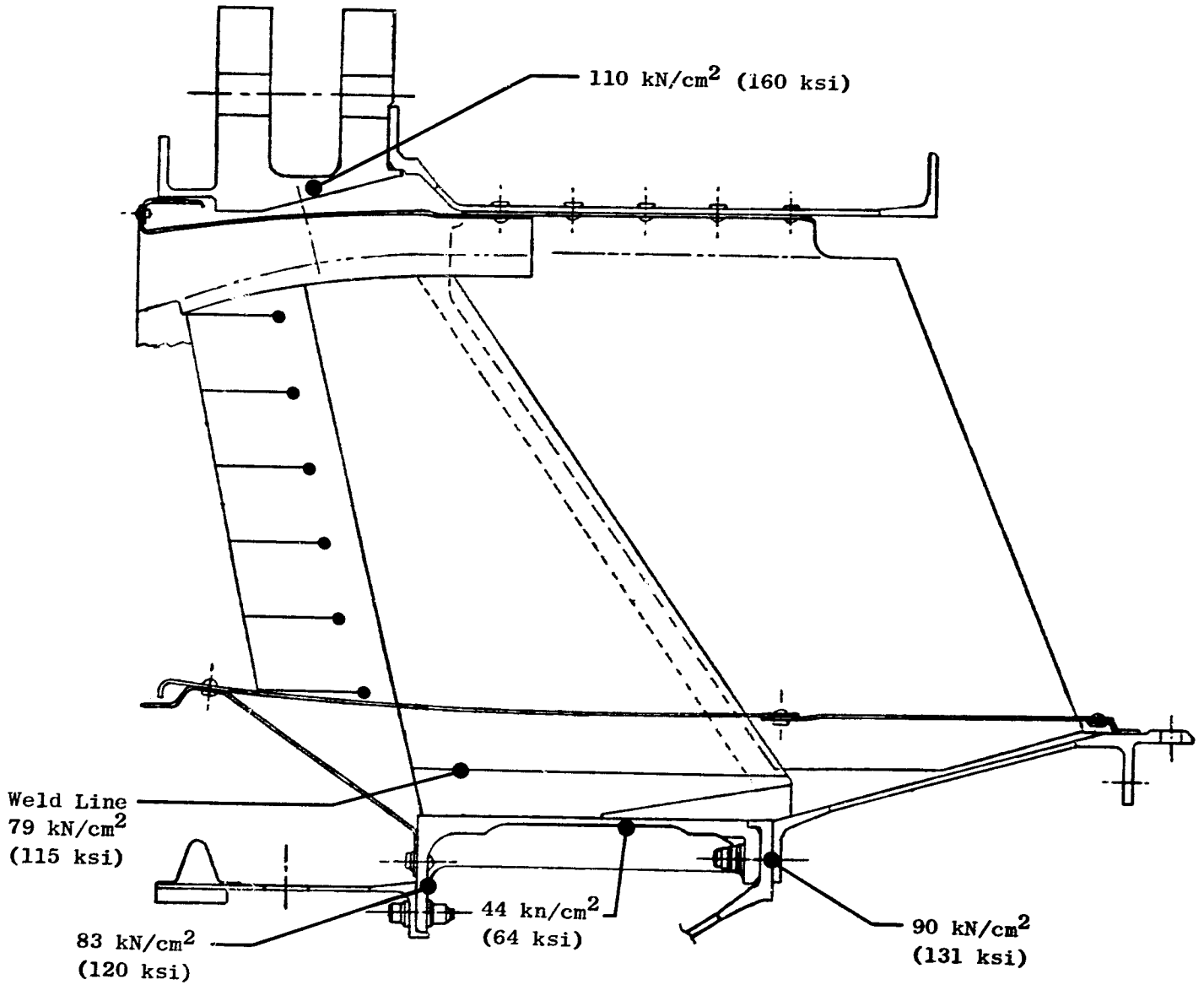

Figure 10.32. OTW Turbine Frame Stresses, One Blade Out Condition.

SECTION 11.0

BEARINGS AND SEALS DESIGN

11.1 SUMMARY

This section summarizes the detail design of the OTW bearings, seals, and accessory drives. The systems described in this section include the sumps, lube oil supply and scavenge, dynamic oil seals, venting and pressurizing systems, pump, oil coolers, filters, deaerators, magnetic chip detectors, static leak check valves, and the lube storage tank. Also included in this discussion is a review of the bearing and accessory lubrication and cooling systems and the rotor thrust balance provisions.

The OTW engine utilizes six main shaft bearings to support the rotating turbomachinery. The short construction of the concentric OTW rotors permits a two-bearing support system for each rotor. The No. 1B and 1R bearings support the fan rotor. The high pressure core rotor is supported by the No. 3 and No. 4 bearings. The No. 2 and No. 5 bearings support the low pressure turbine and power transmission shaft. Both the fan and low pressure turbine shaft are soft coupled to the engine main reduction gear to minimize induced loads on the gears. The thrust bearings have been located in the engine forward sump to provide more precise control of fan and compressor blade clearances.

Application of a main reduction gear between the fan and low pressure turbine requires that the normal axial load "tie" between fan and low pressure turbine components be severed. As a result, the No. 2 thrust bearing must react the full aft load of the turbine without any negating forward thrust from the fan. In order to reduce the bearing load to an acceptable level, a thrust balance cavity has been added to the rear sump. This cavity uses compressor discharge air to pressurize a balance piston, providing a forward compensating force on the turbine rotor. A high-load-capacity CF6 No. 1 thrust bearing is used in the design to react the fan axial loads.

A top-mounted accessory gearbox is driven from the core by an F101 internal bevel gearset and a long radial drive shaft. An additional F101 internal bevel gearset located in the bottom half of the engine is combined with a short radial shaft and a second bevel gearset located in the core cowl area to drive a vane-type pump that scavenges oil from both the forward and aft sumps. This pump also scavenges the top-mounted accessory gearbox which drains into the forward sump.

The lubrication system is designed on the basis of current dry sump technology utilizing a circulating oil system. Internal engine and gearbox passages are used wherever possible for oil delivery and return. Venting and pressurization functions also make use of internal engine passages when possible. The accessories and tube tank are located in the engine pylon area.

Careful attention has been given to fire-safe design features. Carbon seals are provided for minimal leakage of pressurization air into the sumps. During normal operation these seals also eliminate oil leakage from the sump and thus minimize oil consumption. Oil slingers or windbacks are provided with the objective of preventing coke formation in the moving parts of the seals. Each of the cavities adjacent to the sumps are pressurized with cool air to prevent the inflow of hot gases into the sumps. Adequate oil drains have been provided to remove inadvertent oil leakage and prevent fire damage. There are also no trapped oil pockets within the rotating hardware.

11.2 DESIGN REQUIREMENTS

The OTW engine sump and drive system components are designed to meet the following requirements:

- Design loads for sumps and drives components are derived from the duty cycles defined in Section 2.0. Design life, based on these loads, meets established life requirements.
- Sumps are designed to scavenge at all steady-state attitudes shown in Figure 2.3.
- The design is applicable to future airline use. Where slave hardware is utilized, no compromises have been made that would not allow future adaptability for airline application.
- The system is designed to operate with MIL-L-7808 or MIL-L-23699 oil.
- Gearbox and sumps are vented to areas where temperatures are less than 371° C (700° F).
- The design eliminates any possibility of trapped oil in the rotors.
- Where possible, the experimental engine system has been designed to meet maintainability criteria. Where exceptions occur, due to utilization of existing hardware and components, studies have identified changes necessary in the flight design to meet maintainability requirements.

11.3 LUBRICATION SYSTEM

The OTW lubrication system contains the following subsystems:

- Oil supply
- Oil scavenge

- Seal pressurization air
- Vent air

A conventional dry sump system similar to that used on other General Electric engines is provided. The lube system schematic is shown in Figures 11.1 and 11.2. The bulk of the system oil supply is retained in the oil tank. Oil is pressure fed to each engine component requiring lubrication and/or cooling, and is removed from the gearbox and rear sump by scavenge pump elements for return to the oil tank.

The entire lubrication system has been designed to ensure that there are no areas where oil can be trapped (i.e., rotors, gearboxes, shafts, etc.) which could be detrimental to the engine. Also, the system has been sized to prevent flooding of sumps and gearboxes during engine shutdowns and to limit excessive lube tank gulping during engine start ups.

11.3.1 Oil Supply System

The oil supply subsystem consists of the oil tank, gearbox-mounted oil supply pump, oil supply filters, static leak check valve, oil supply nozzles, and associated piping.

The basic lube supply system operates in the following manner: MIL-L-23699 oil is supplied by gravity to the inlet of the supply pump at all operating conditions. The oil is then pumped through two parallel-piped, 46-micron oil supply filters to protect the lube nozzles from contaminants. The oil then flows through the static check valve and is distributed to the desired areas in the engine. Presented in Table 11-I are the engine system oil flow requirements.

During engine shutdowns, sump and gearbox flooding are prevented by the static check valve located downstream from the lube supply filters. This valve, along with careful pipe sizing, also prevents lube flooding during engine startups.

To sense oil supply pressure during engine running, a port for a pressure sensor is provided immediately downstream of the static leak check valve. This pressure sensor, along with other pressure readings taken in the sumps and gearbox, provides a ΔP indication across the oil nozzles.

The following special oil supply features have been included in the system design:

- The constant-displacement supply pump has been modified to add a variable bypass orifice to increase engine oil flow.
- Pressure relief bypass valves have been added to the oil supply filter system. These valves open when the pressure across the

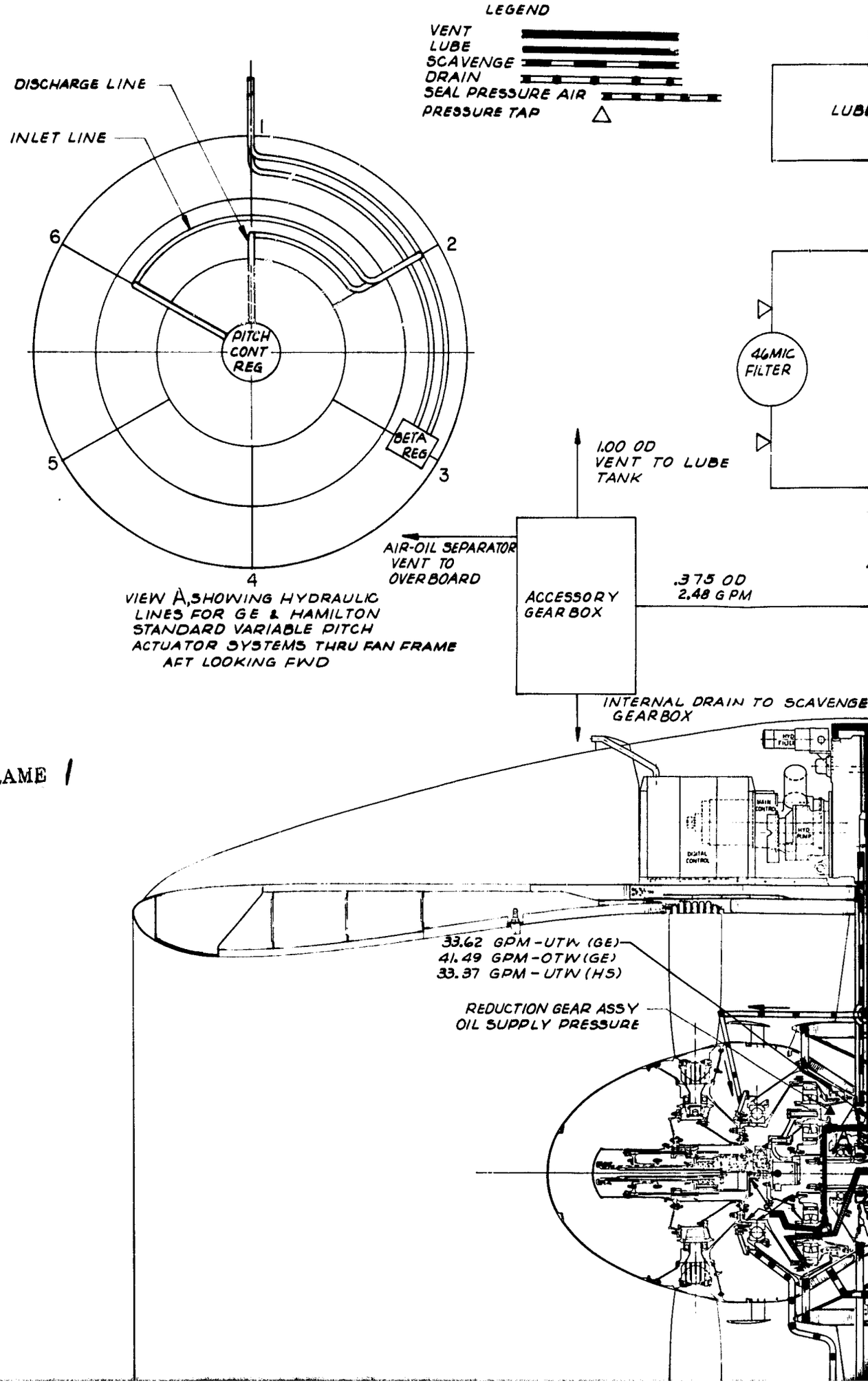

FOLDOUT FRAME 1

FROM SLAVE LUBE SYSTEM
SEE DWG 4013180-853
△ LUBE PUMP INLET PRESSURE

UMP DISCHARGE
DD
GPM - UTW (GE)
GPM - OTW (GE)
GPM - UTW (HS)

46MIC FILTER

FILTER DELTA P SENSORS

D

K VALVE
KING PRESSURE — 15 PSI DELTA

OD

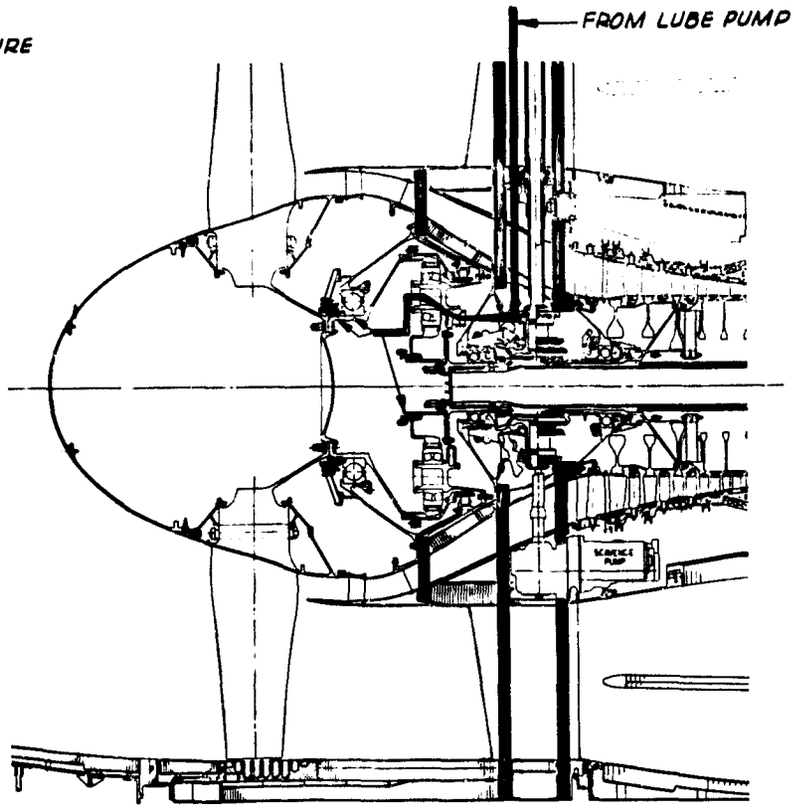

OTW CONFIGURATION, OTHERWISE SAME AS UTW WITH THE EXCEPTION OF: NO FAN ACTUATION SYSTEM & LINE FLOWS

FOLDOUT FRAME 2

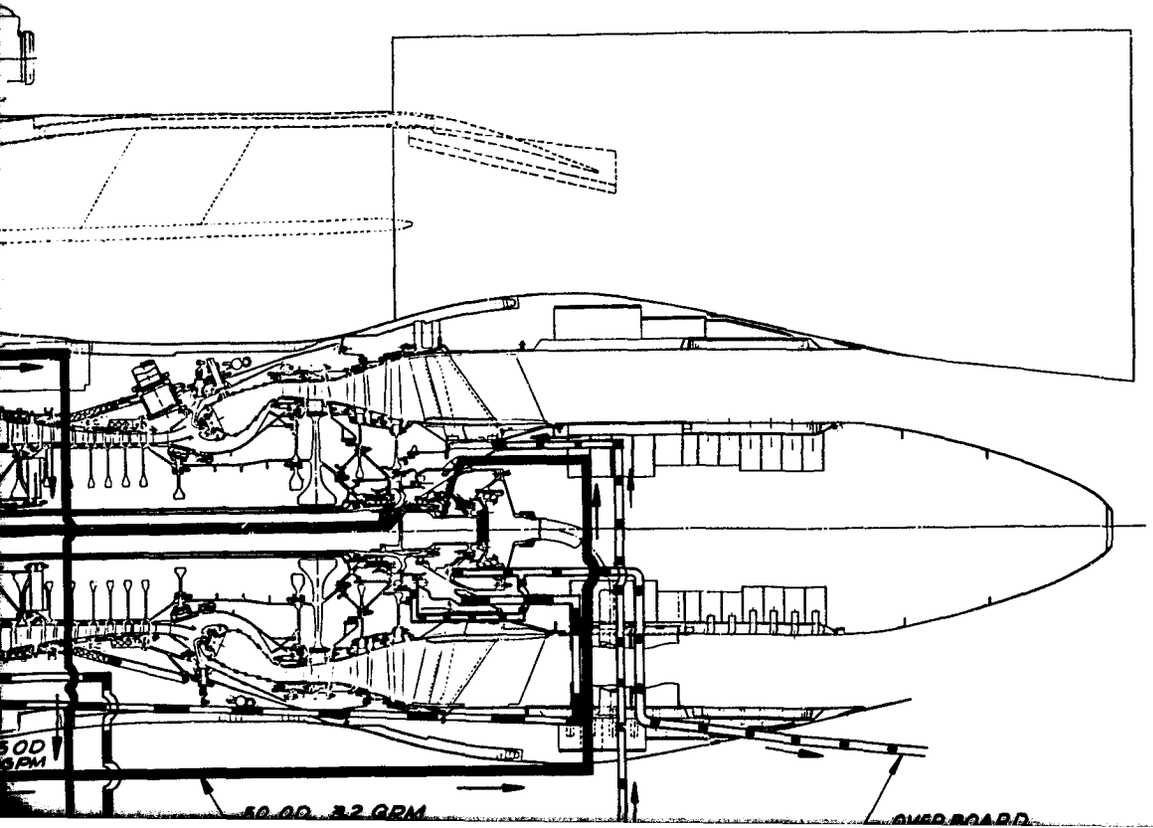

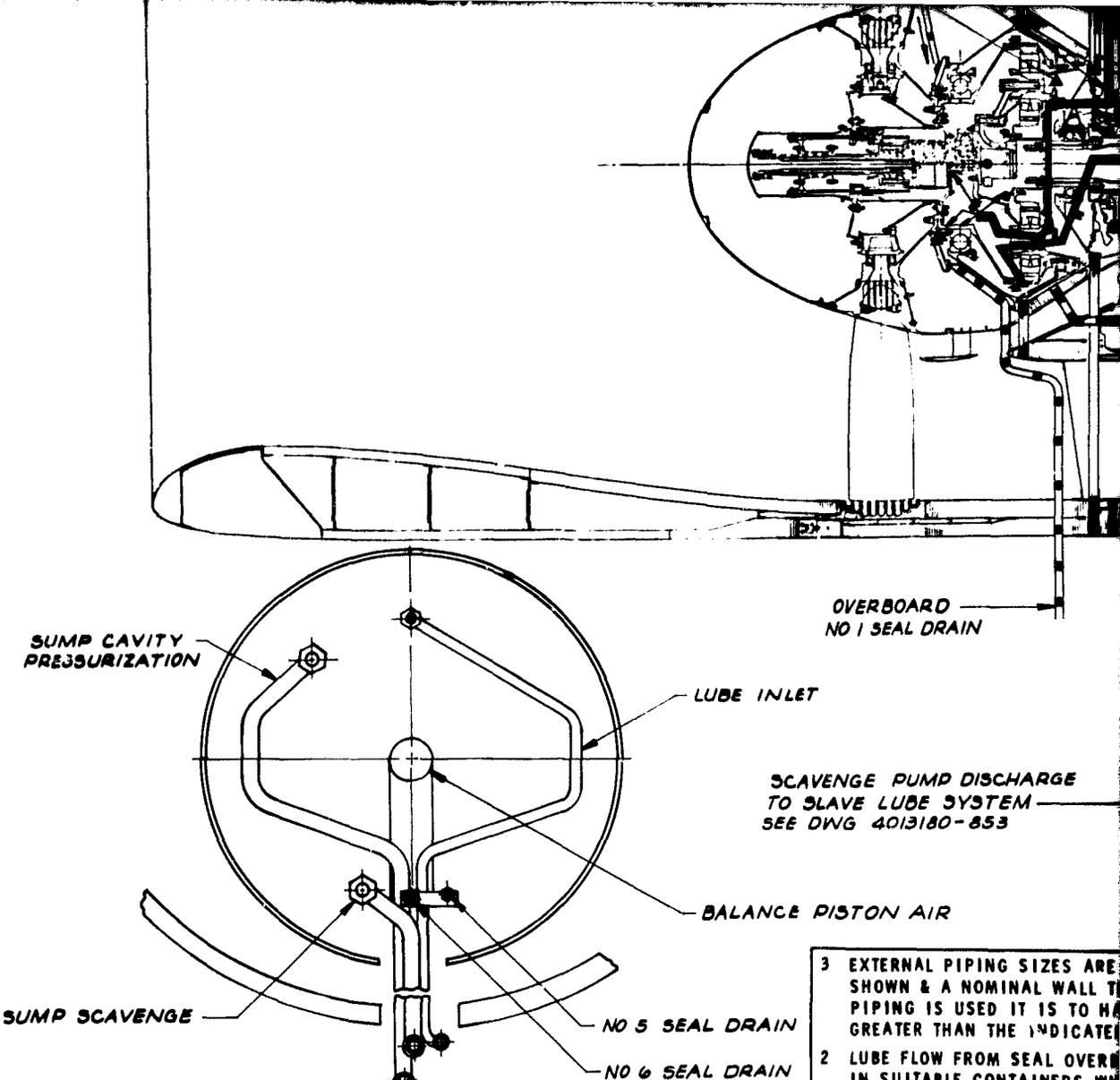

Figure 11.1. Eng

FOLDOUT FRAME 3

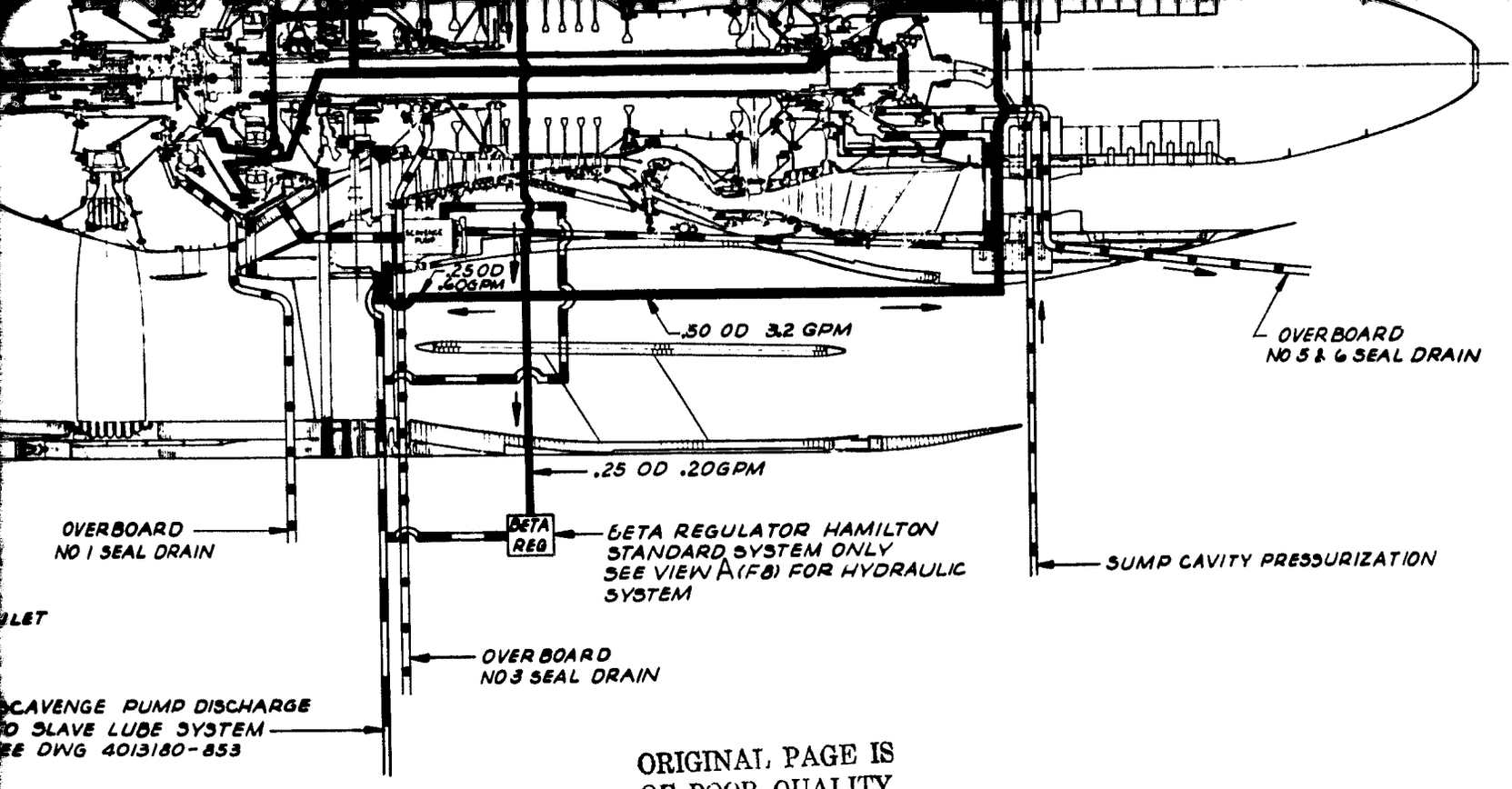

ORIGINAL PAGE IS
OF POOR QUALITY

3	EXTERNAL PIPING SIZES ARE BASED ON THE OUTSIDE DIAMETER SHOWN & A NOMINAL WALL THICKNESS OF .035 INCH. IF FLEXIBLE PIPING IS USED IT IS TO HAVE AN INSIDE DIAMETER EQUAL TO OR GREATER THAN THE INDICATED SIZE
2	LUBE FLOW FROM SEAL OVERBOARD DRAIN LINES TO BE COLLECTED IN SUITABLE CONTAINERS WHICH ARE VENTED TO THE TEST CELL
1	THE TABULATED OIL FLOWS ARE NOMINAL FLOWS OF MIL-L-23699 AT SLS13500 CORE R.P.M. 160°F OIL SUPPLY TEMPERATURE

Figure 11.1. Engine Lube System Schematic.

FOLDOUT FRAME 4

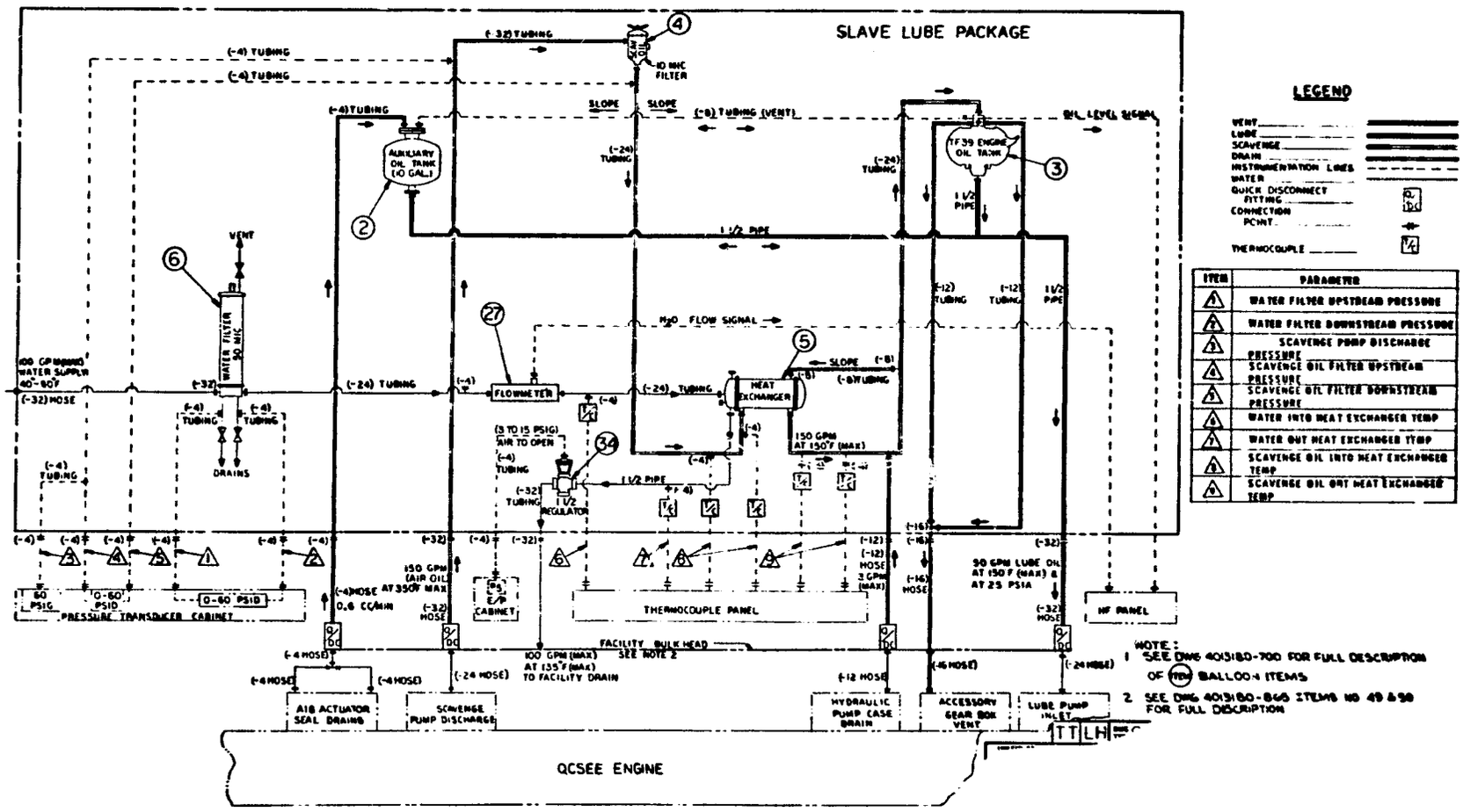

Figure 11.2. Facility Lube System Schematic.

Table 11-I. QCSEE Lube Flows - OTW.

	cm^3/sec	GPM
No. 1B Bearing	126	2.00
No. 1 Seal	63	1.00
No. 1R Bearing	94.6	1.50
No. 2 and 3 Bearing	137.5	2.18
No. 3 Seal	14.5	0.23
No. 1 and No. 2 Inlet G/B	148.9	2.36
Accessory G/B	156.4	2.48
Scavenge Pump G/B	31.5	0.50
Main Reduction Gears	2032.5	32.22
No. 4 and No. 5 Beaming	164.0	2.60
No. 6 Seal	37.8	0.60
Rad. Shaft Midspan Rig	9.5	0.15
	3016.6	47.82

Flows Referenced to 14,460 rpm Core Speed
(5977 rpm pump speed)

filters reaches 27.6 N/cm^2 (40 psid). Thus, if the filters become plugged, full oil flow is always supplied to the engine.

- The static leak valve, which is designed to crack and reseat at 10.3 N/cm^2 (15 psid) has been strategically placed to prevent flowing of oil engine sumps and gearboxes during shutdown.

- 37,850 cm^3 (10 gal) supplementary oil resevoir, which is vented to the oil tank and discharges directly into the line leading to the lube pump inlet. This resevoir is required to accomodate the volumetric expansion and contraction of the air/oil mixture in the large capacity slave lube system components.

Oil supply subsystem components selected for the experimental engine are defined in the following paragraphs:

Oil Tank - A TF39 oil tank has been modified for application in the OTW experimental engine oil supply system. Modifications include:

- A new vortex generator plate designed to accept two CF6 deaerators to handle increased oil flows.

- Addition of a level sensor similar to one used in the CF6 and F101 tanks.

- Replacement of the TF39 lube supply port by a larger port.

- Replacement of the TF39 filter caps with CF6 caps. A specially marked dip stick also has been provided that permits filling to the 37,850 cm^3 (10 gal) level. The supplementary resevoir provides an additional 37,850 cm^3 (10 gal) of capacity.

Shown in Figure 11.3 is a cross section of the modified TF39 tank.

Lube Supply Pump - A CF6 engine lube/scavenge pump is utilized in the OTW experimental engine oil supply system. Specific design features including necessary modifications are as follows:

- 5 CF6 Scavenge elements manifolded for OTW lube supply

- Lube bypass variable orifice added [2268 cm^3/sec (36 gpm) at 126 cm^3/sec (2 gpm)/turn]

- 276 N/cm^2 (400 psi) Lube relief added

- LM2500 tach pad cover and filter bowl plug

- F101 drive spline (to mate with gearbox)

- Gearcase bolts changed from AN4CH6A to MS9501-12 bolts to increase vibratory capability

- CF6 gask-o-seals, manifold bolts/washers, V-band, and seal.

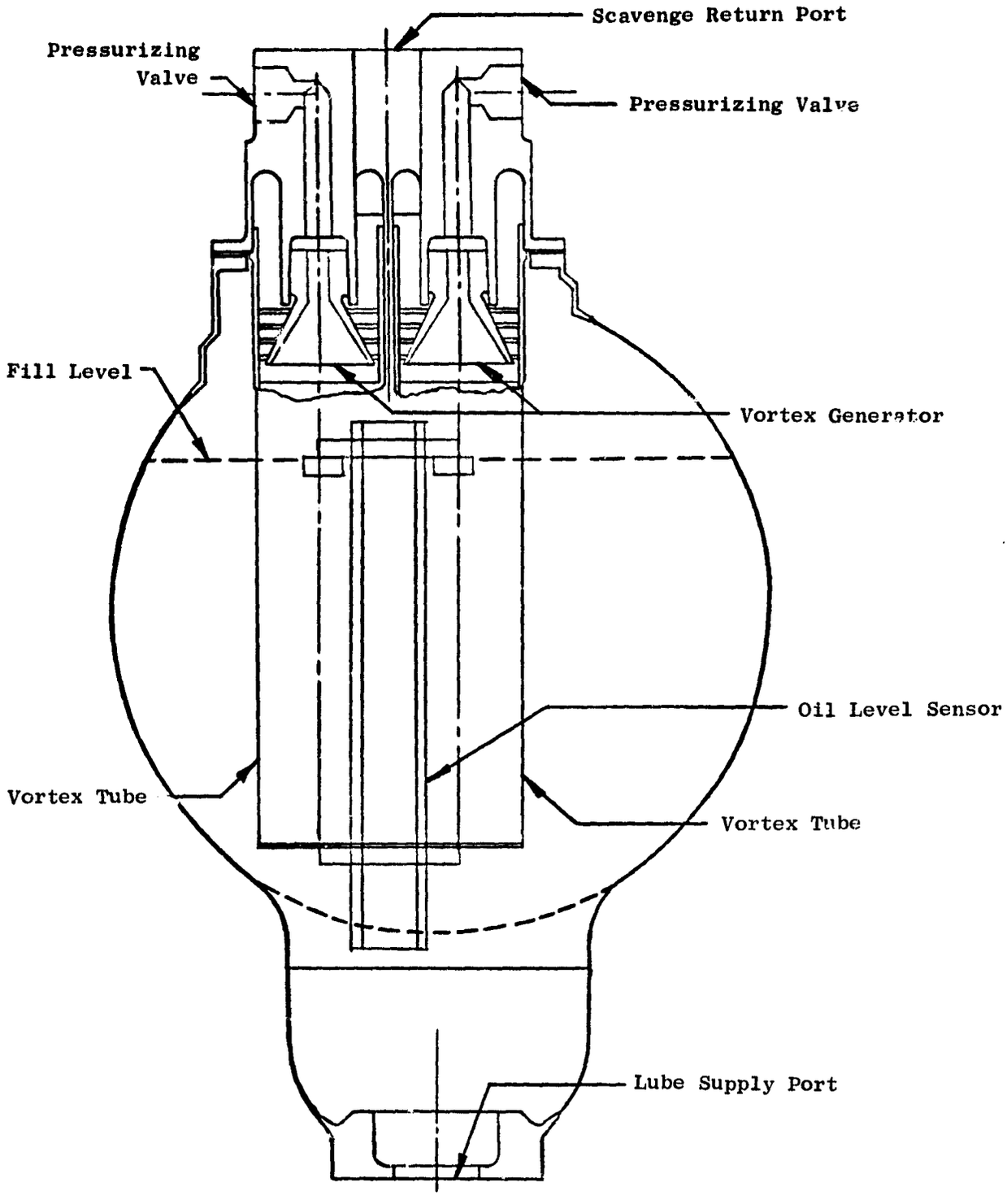

Figure 11.3. Lube Tank Cross Section.

Figures 11.4, 11.5, and 11.6 show demonstrated pump performance.

Lube Filter - Two CF6 scavenge filters will be connected in parallel and located downstream of the lube pump in the experimental engine oil supply system. Design features include:

- 46μ Nom/76μ Absolute
- 827 N/cm^2 (1200 psi) Proof Pressure
- 11.0 N/cm^2 (16 psi) ΔP @ 1512 cm^3/sec (24 gpm), 367° K (200° F)
- 27.6 N/cm^2 (40 psi) Minimum Bypass ΔP
- 46 cleanable water elements

A cross-section of the lube filter is shown in Figure 11.7.

Check Valve - The lube check valve located downstream of the lube filters has the following design features:

- Proof pressure 414 N/cm^2 (600 psig) without leakage or distortion
- Cracking and reseat pressure is 10.3 N/cm^2 (15 psid)
- Capability of operation with lube temperature range of 233° K (-40° F) to 450° K (+ 350° F) for either oils conforming to MIL-L7808 or MIL-L-23699.

11.3.2 Oil Scavenge Subsystem

The scavenge subsystem consists of a three-element pump, slave filter, slave oil cooler, oil deaerators in the oil tank, and other associated hardware.

The basic scavenge subsystem operates in the following manner: oil in the top-mounted accessory gearbox flows by gravity into the forward sump through drain pipes where it is combined with the forward sump scavenge oil. This combined oil is then scavenged by the bottom-mounted scavenge pump. Oil, which lubricates the scavenge pump drive system, is scavenged by a separate element located within the pump. Aft sump scavenge oil is piped forward to the bottom-mounted scavenge pump and scavenged by a third element. Each element is provided with an inlet screen and magnetic chip detector. The inlet screens catch any debris which is larger than can be passed through the pumping element without causing damage or excessive wear. The magnetic chip detectors collect ferrous particles to help condition monitor the sumps and gearbox components. More detailed information is available through spectrographic analysis of collected debris.

Total engine scavenge flow is discharged through a common port and routed through a static check valve (integral with the pump) into the 10-micron

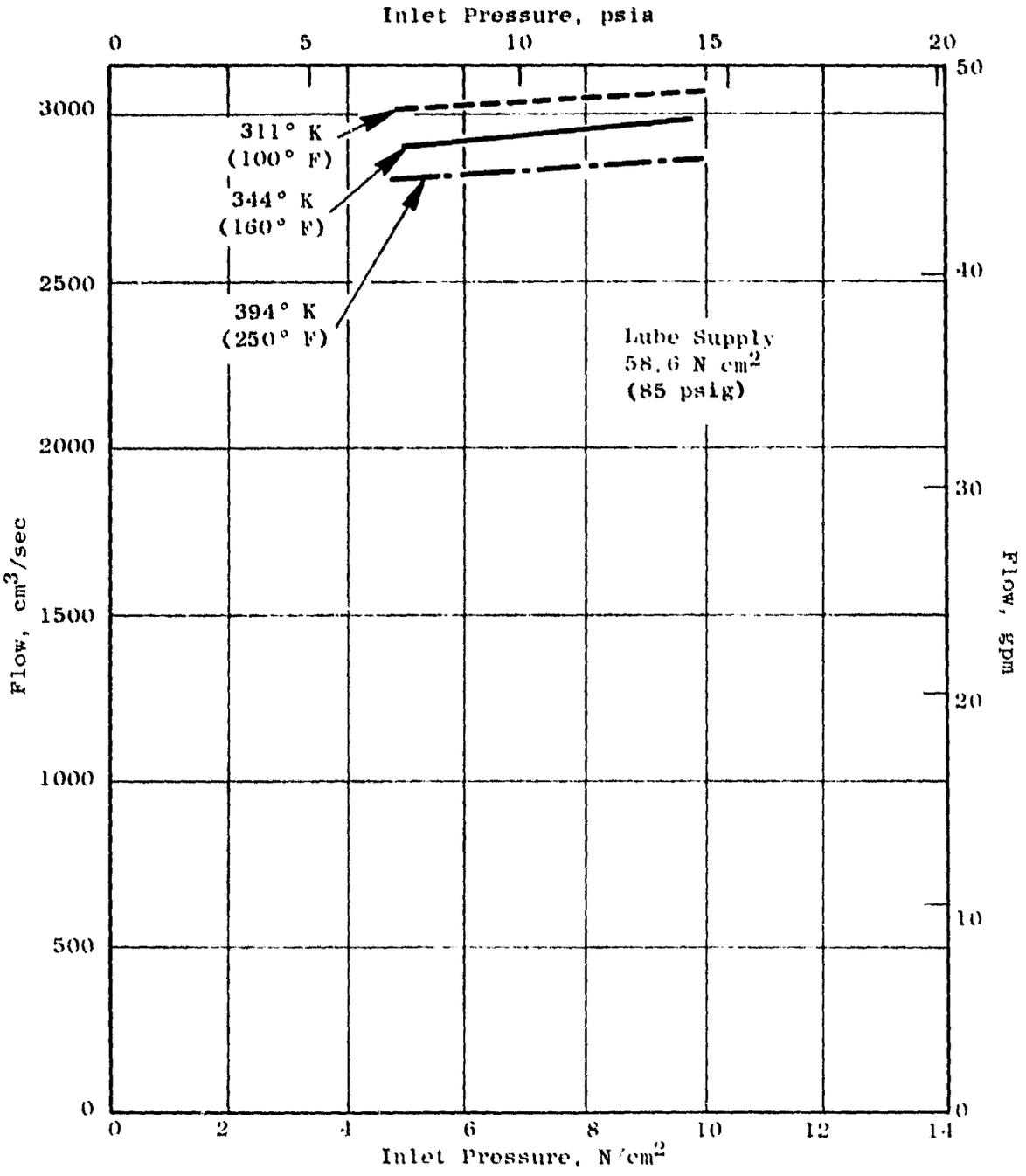

Figure 11.4. Lube Supply Pump Flow Vs. Pressure at 5977 rpm.

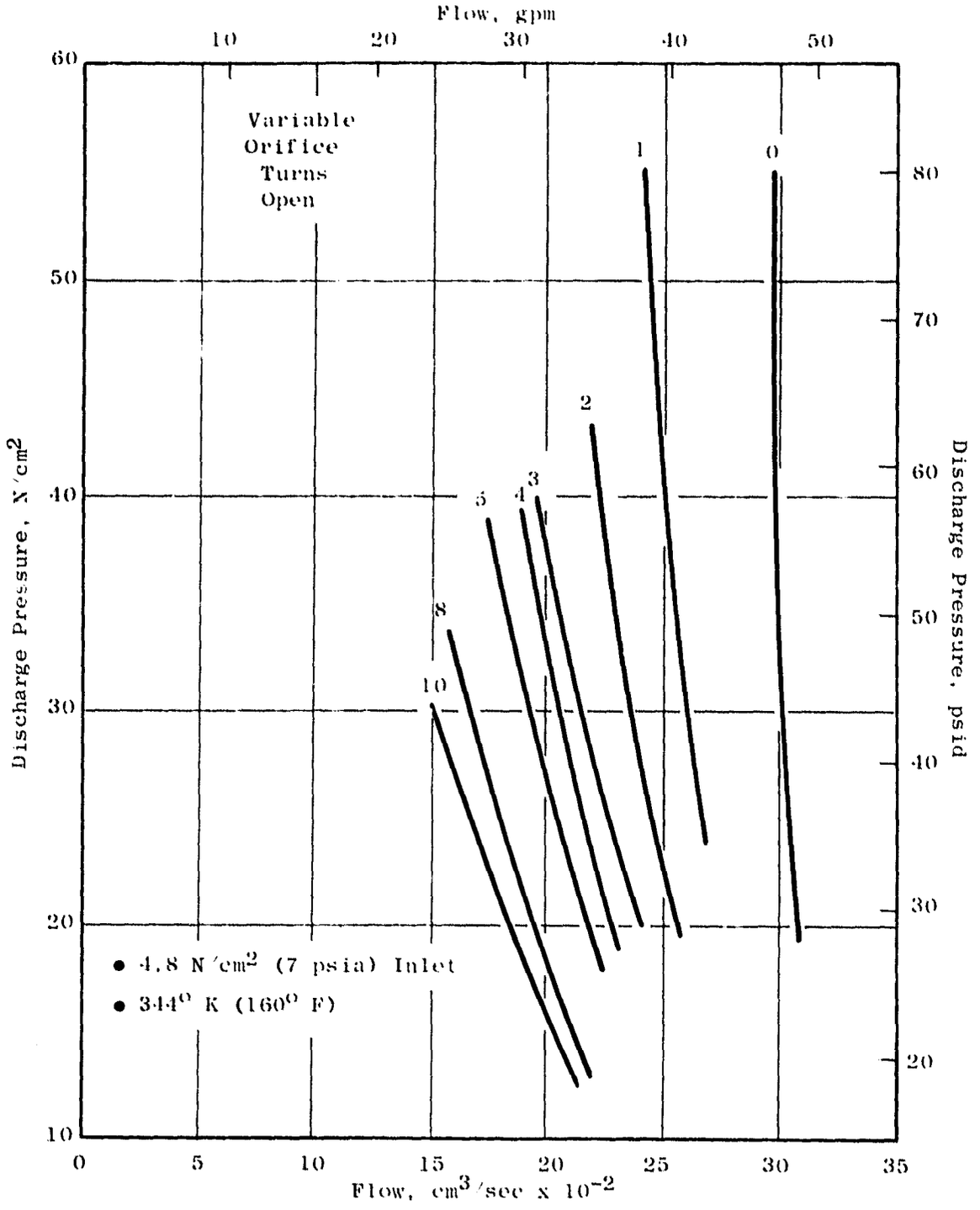

Figure 11.5. Lube Supply Pump Flow Vs. Discharge Pressure at 5977 rpm.

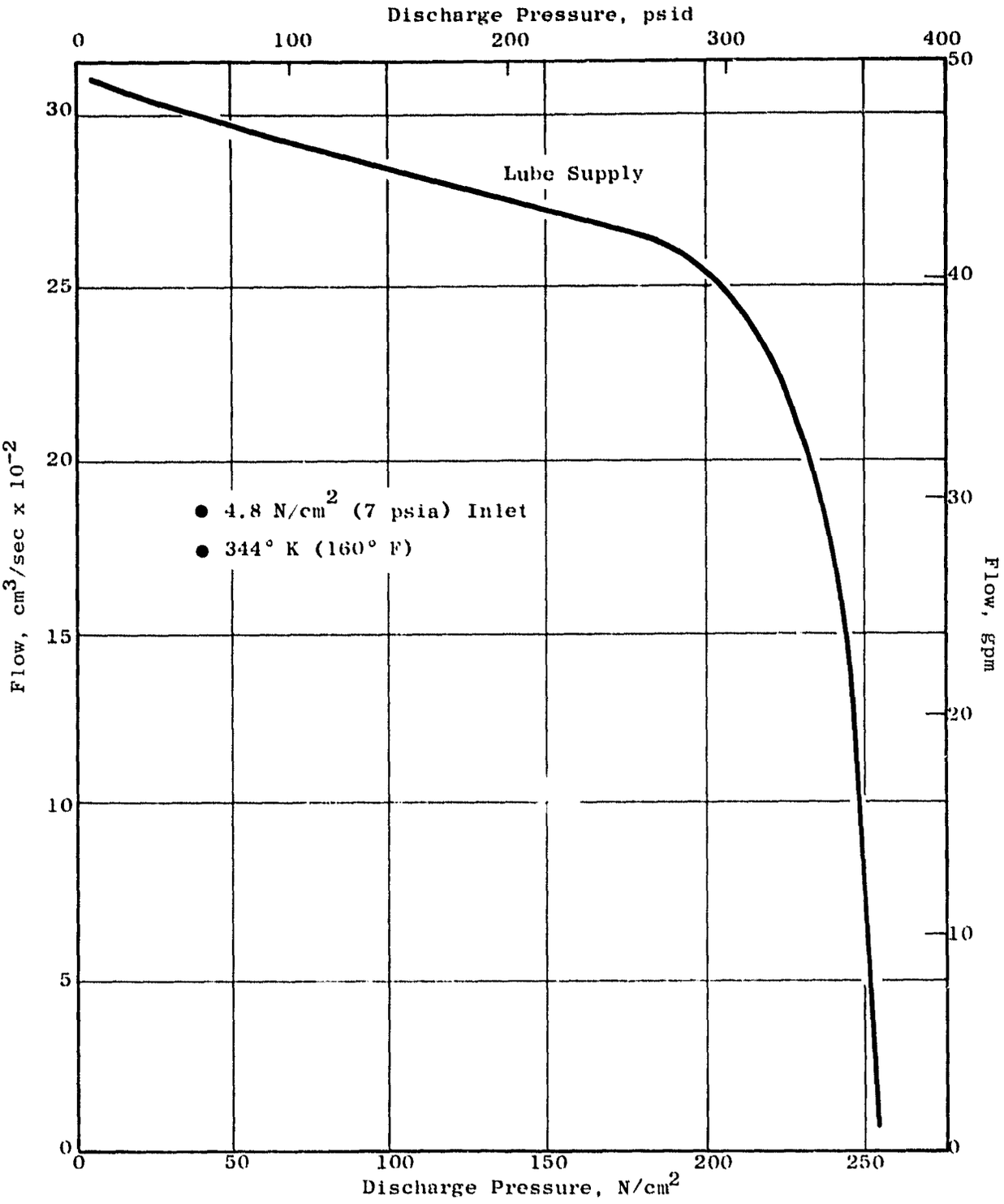

Figure 11.6. Relief Valve Flow Vs. Discharge Pressure at 5977 rpm.

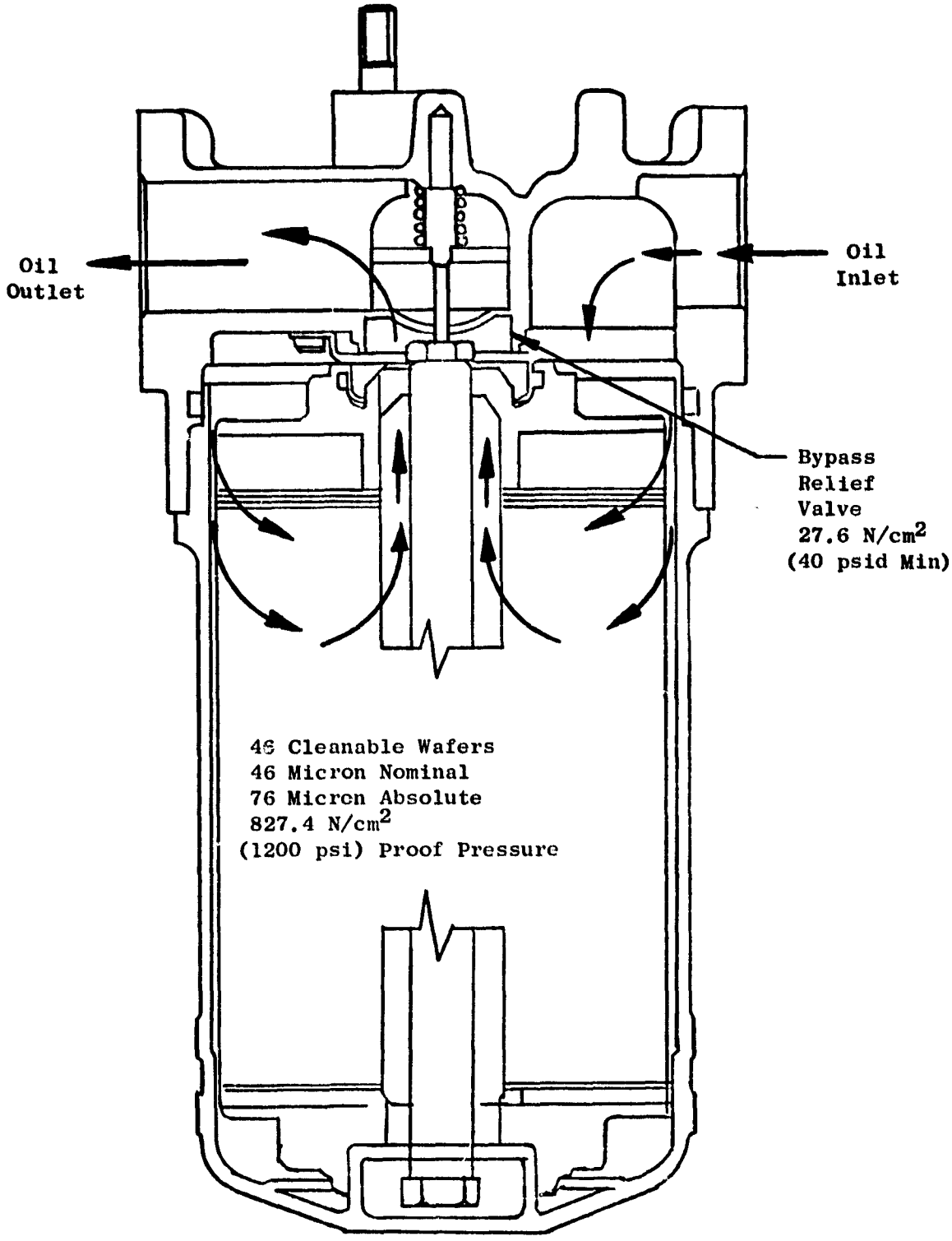

Figure 11.7. Lube Filter.

scavenge filter. The oil then flows to the system heat exchanger where the heat load of the main shaft bearings, seals, sump walls, gearboxes, and piping is transferred to the coolant. The oil is then returned to the tank where deaerators remove entrained air and condition the oil for reuse by the supply system.

Special features of the scavenge subsystem include:

- A static check valve in the discharge line to prevent flooding of the sump
- Chip detectors at all scavenge pump inlets for condition monitoring of accessory drives, sumps, and bearings
- A pressure relief bypass valve on the scavenge filter, which opens when the pressure across the filter reaches 27.6 N/cm^2 (40 psi), to ensure continuous flow to the tank
- A service shutoff valve in the filter to minimize oil loss during filter element changes

Major scavenge system component features are summarized in the following paragraphs:

Scavenge Pump - design features of the scavenge pump, shown schematically in Figure 11.8, are as follows:

- 3 Elements (main, rear sump, gearbox, scavenge) 5166, 473, 126 cm^3/sec (82, 7.5, 2.0 gpm) minimum, respectively
- 9144 m (30,000 ft) altitude design [3.0 N/cm^2 (4.4 psia) inlet]
- Inlet screens and push-turn magnetic plugs at all inlets
- Static leak check valve [1.36 - 2.76 N/cm^2 (2 - 4 psi) crack]
- Mini-element (gearbox scavenge) is metering element discharging into main inlet to prevent priming problems
- 6700 rpm input (rear and gearbox elements) geared to 2931 rpm for main element

Detail design information for the three scavenge pump elements is presented in Table 11-II. Test results are shown in Figures 11.9 and 11.10.

Scavenge Filter - specific design characteristics of the slave scavenge filter are:

- Pressure: rated 276 N/cm^2 (400 psi), proof 414 N/cm^2 (600 psi), burst 862 N/cm^2 (1250 psi)

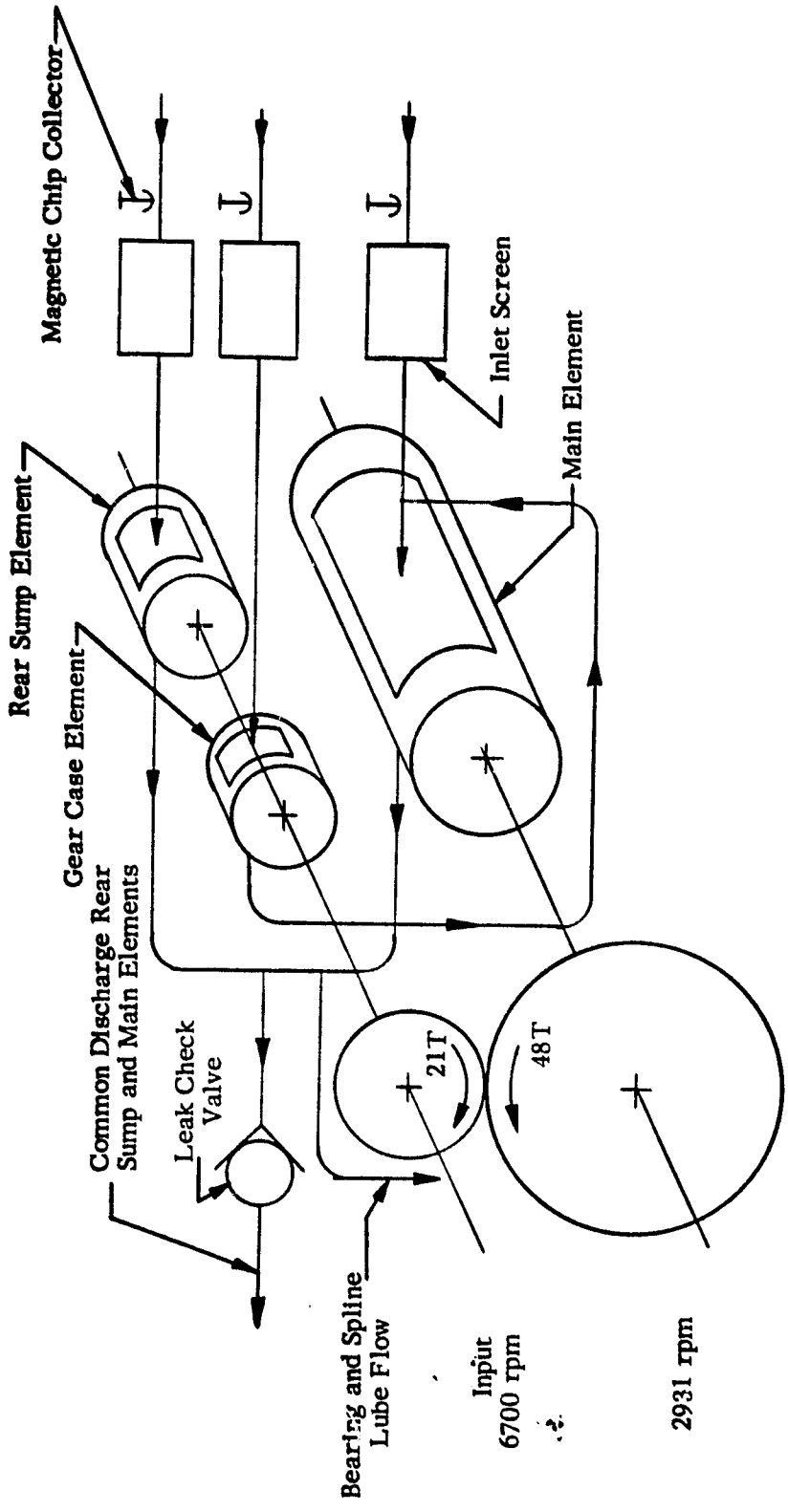

Figure 11.8. QCSEE Scavenge Pump Schematic.

Table 11-II. QCSEE Scavenge Element Predicted Performance.

	Main	Rear Sump	Gear Case
RPM	2931	6700	6700
Bore Dia.	4.72 cm (1.86 in.)	1.91 cm (0.75 in.)	1.91 cm (0.75 in.)
Elem. Length	9.65 cm (3.8 in.)	3.25 cm (1.28 in.)	1.17 cm (0.46 in.)
Elem. L/D	2.04	1.70	.61
Theor. Displ.	139.3 cm^3/rev (8.5 $in.^3$)	5.4 cm^3/rev (0.33 $in.^3$)	1.97 cm^3/rev (0.12 $in.^3$)
Theor. Flow	6804 cm^3/sec (108 gpm)	610 cm^3/sec (9.67 gpm)	223 cm^3/sec (3.53 gpm)
Est. Flow(1)	6248 cm^3/rev (99 gpm)	540 cm^3/rev (8.7 gpm)	217 cm^3/rev (3.5 gpm)
Est. Flow(2)	5774 cm^3/sec (93 gpm)	540 cm^3/rev (8.7 gpm)	217 cm^3/rev (3.5 gpm)
Theor. Cav. Knee	2.41 N/cm^2 (3.5 psia)	1.86 N/cm^2 (2.7 psia)	1.86 N/cm^2 (2.7 psia)
Flow In	2782 cm^3/sec (44.1 gpm)	233 cm^3/sec (3.7 gpm)	32 cm^3/sec (0.50 gpm)
Scavenge Ratio	2.1	2.3	6.8
Brg. P/A Loads	525 N/cm (300 lb/in.)	394 N/cm (225 lb/in.)	3.5 N/cm (2 lb/in.)

(1) Sea level, 394° K (250° F)

(2) 9144 m (30,000 ft) altitude, 394° K (250° F), 3.03 N/cm^2 (4.4 psia) inlet

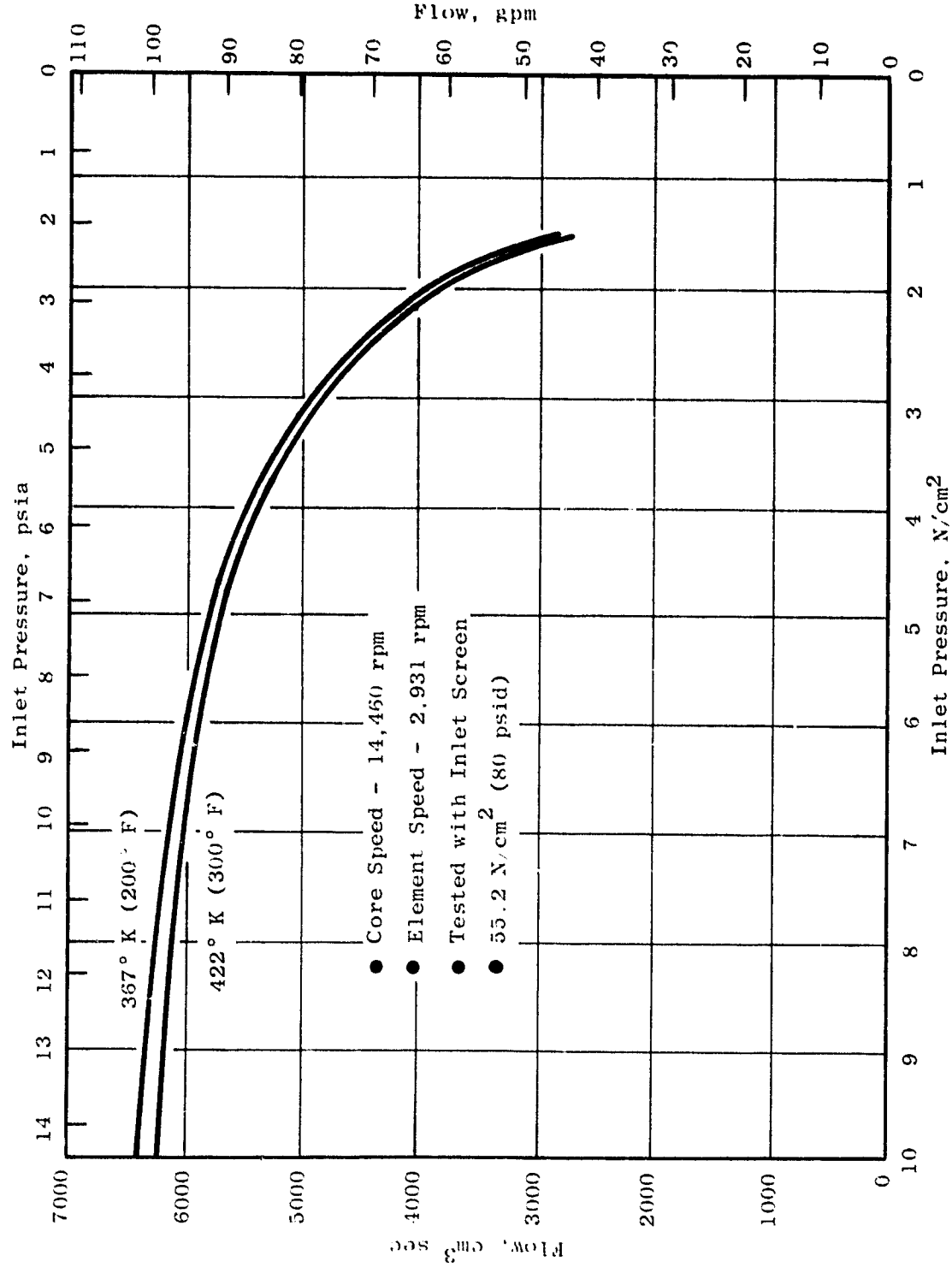

Figure 11.9. Scavenge Pump Main Element Flow Vs. Inlet Pressure.

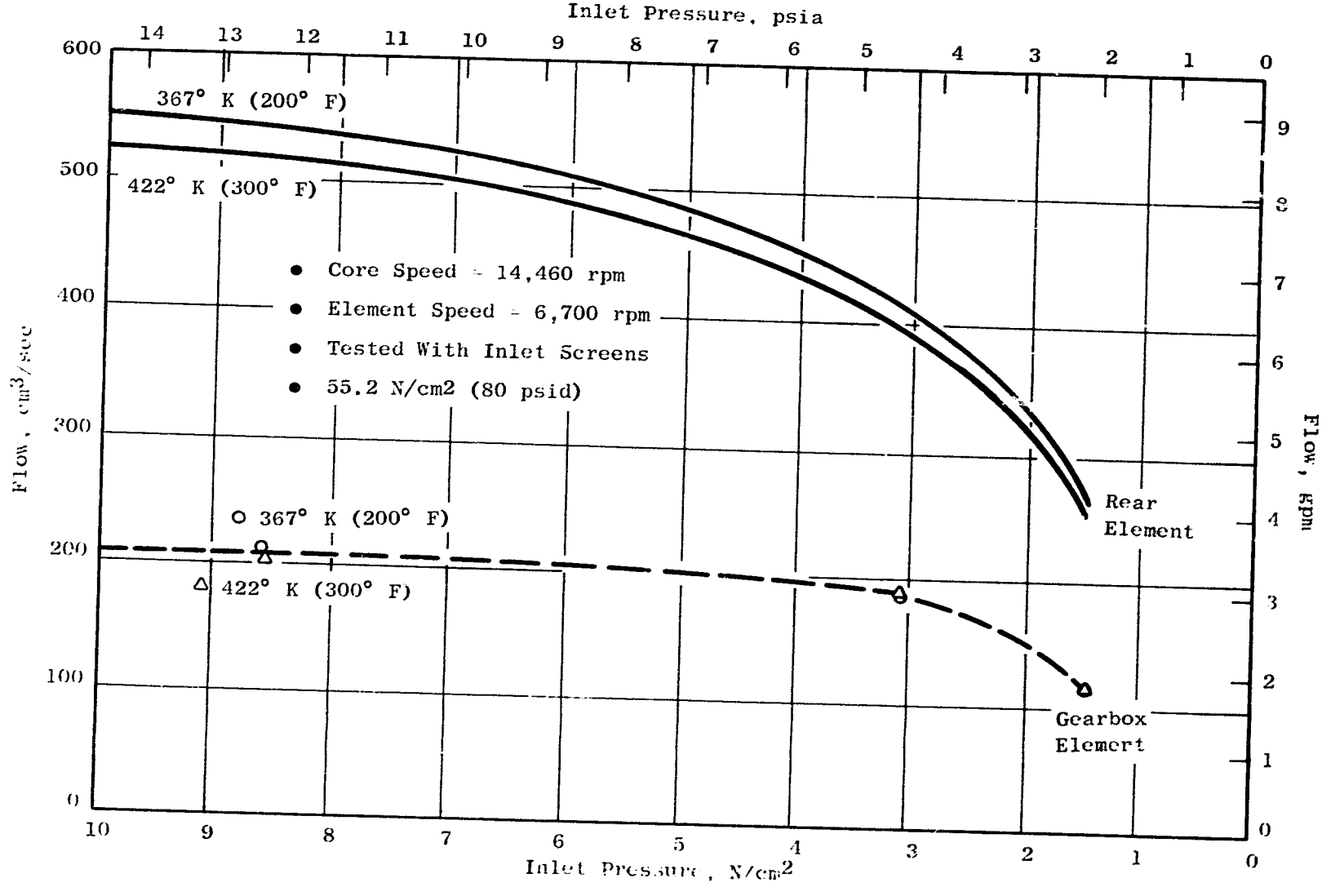

Figure II.10. Scavenge Pump Gearbox and Rear Element Flows Vs. Inlet Pressure.

- Temperature range: 233° to 810° K (-40° to + 350° F)
- Element collapse pressure: 103 N/cm^2 (150 psid)
- Bypass valve cracking pressure: 34.5 ± 3.4 N/cm^2 (50 ± 5 psid)
- Visual bypass indication: 27.6 ± 3.4 N/cm^2 (40 ± 5 psid)
- Pressure drop at 3150 cm^3/sec (50 gpm), MIL-L-7808

Housing: 2.07 N/cm^2 (3.0 psi)

Element: 2.07 N/cm^2 (3.0 psi)

Total 4.14 N/cm^2 (6.0 psi)

- Materials: Anodized Aluminum, AISI 1010 Carbon Steel, Epoxy Painted.

11.3.3 Vent Subsystem

Venting of the oil seal pressurization air from the sump cavities is accomplished through the gearbox. The rear sump is vented through the low pressure turbine shaft to the forward sump. The forward sump is vented to the accessory gearbox. The air in the gearbox is vented overboard through a rotating air/oil separator. Air which is separated from the scavenge oil in the lube tank is returned to the accessory gearbox. This air is required at all conditions to satisfy the scavenge ratio requirements of the scavenge pump.

The vent flow areas have been sized to:

- Maintain the sump internal pressure below outside cycle air pressure
- Prevent reverse airflow across the oil seals during rapid power reductions
- Continue engine operation:
  - with one seal failed from any cause including coking
  - with the remaining seals at their maximum service leakage limit

11.3.4 Flight Engine Thermal Balance

The flight engine lube oil is cooled by transferring heat to the engine fuel as well as bypass fuel which is returned to the fuel tanks. The engine

heat balance study showed that, on a 32° C (90° F) day at 100% rates reduction gear power, this type of system will probably provide the required 82° C (180° F) oil needed to maintain 149° C (300° F) maximum gear temperature with 50° C (122° F) fuel inlet temperature. The fuel bypass will absorb the pumping temperature rise. The engine heat loads shown in Table 11-III were determined from the November 1, 1974 QCSEE Technical Requirements and the September 5, 1974 Curtiss-Wright Gearing Data. Heat loads from the reduction gearbox and the engine lube systems have been calculated for each flight condition and are tabulated in Table 11-IV.

Additional studies, outside the QCSEE work scope, are required to obtain a total system understanding of a recirculating fuel system for future aircraft application. These studies must include fuel cooling, wing tank cooling, flight envelope considerations, and the impact of circulating and storing heated fuel.

11.3.5 Heat Exchanger

A General Electric LM2500 engine lube oil heat exchanger module has been selected as a slave heat exchanger for the OTW experimental engine. This heat exchanger is an all-stainless-steel heat exchanger offering 527,950 J/sec (30,000 Btu/min) with 6300 cm^3/sec (100 gpm) of 200° K (80° F) water. Oil side pressure drop of the heat exchanger is less than 6.9 N/cm^2 (10 psi) at 3024 cm^3/sec (48 gpm). Water side pressure drop is less than 6.9 N/cm^2 (10 psid). Table 11-V and 11-VI show predicted bearing race and AGMA scoring temperatures for estimated and derated reduction gear efficiency. All temperatures are below the limit of 148.9° C (300° F) of 9310 steel.

11.3.6 Seal Pressurization Subsystem

Oil leakage can potentially contribute to seal coking and contamination of compressor bleed air, as well as increasing the engine oil consumption. In order to prevent oil leakage, the mainshaft oil seals are pressurized to force air to flow across the seals into the sumps at all operating conditions.

The compressor stage for extraction of seal pressurization air has been selected to have adequate pressure to prevent the hot engine cycle air from entering the sumps and yet low enough in temperature during higher-Mach-number, hot-day operation to permit the oil seals to meet their required life. Pressurization air is extracted at the hub of the third stage compressor rotor and routed internally within the engine to both the forward and rear sump oil seals. Air from the hub of the compressor is used because it contains the minimum contamination. For ground idle operation, shop air will be provided to the aft sump to ensure that hot gas will not back-flow into the system. A higher pressure source could be used in a flight engine if required.

Oil seal drains are provided in the forward sump oil seals to remove any seal leakage which could contaminate the compressor. Since these drains carry fluid only in the case of a seal failure, the forward sump seal drains are routed overboard. The aft sump seal drains are routed to the flowpath aft of the low pressure turbine.

Table 11-III. Heat Study Conditions*.

Condition	Case No.	Alt.	Flight Mach No.	Reduction Gear Efficiency, %	LPT kW/hp	Fan Speed, %	Core Speed, %
Gidle	111	SL	0	98.63	74.6/100	15.1	55.4
Takeoff	1	SL	0	99.11	12,526/16798	101.5	96.3
Climb	301	SL	.38	99.10	12,193/16351	94.5	95.4
Cruise	404	25K	.7	99.07	6529/8756	96.4	91.8
Descent	503	15K	.6	98.73	1593/2136	62.4	77.6
Approach	7	200 ft	.12	99.15	6718/9009	81.8	87.1
Max. Fan Torque	926 (revised)	SL	0	99.11	15,032/20158	97.8	97.4

*From Nov. 1, 1974 Tech. Req. and Sept. 5, 1974 C - W Data Selected on the Basis of Max. AGMA Scoring ΔT

Table 11-IV. Predicted Heat Loads and Oil Flows.

Condition	Reduction Gearbox kw/Btu/min	Engine Lube, kw/Btu/min	Total Q, kw/Btu/min	Oil Flow,* kg/min/lbs/min
Gidle	1.02/58	5.97/340	7.0/398	80.7/178
Takeoff	1.5/6345	68.2/3880	179.7/10225	140.6/310
Climb	109.7/6245	62.2/3542	171.9/9787	139.3/307
Cruise	60.7/3456	56.3/3203	117.0/6659	133.8/295
Descent	20.2/1151	24.4/1391	44.7/2542	113.4/250
Approach	57.1/3250	41.7/2374	98.8/5624	127.0/280
Max. Fan Torque	133.8/7614	68.1/3878	201.9/11492	142.0/313

*8.866×10^{-4} kg/cm^3 (7.4 lbs/gal)

Table 11-V. Predicted Temperatures - 6300 cm^3/sec (100 gpm) (80° F) Cooling Water.

Condition	AGMA ΔT, °C/°F	Bearing Race ΔT, °C/°F	Scav Oil, °C/°F	Lube Oil, °C/°F	Bearing Race,* °C/°F	AGMA Scoring Index,* °C/°F
Gidle	-15.5/4	-13.9/7	29.4/85	26.7/80	30.6/87	28.9/84
Takeoff	46.1/115	37.8/100	78.3/173	41.1/106	96.7/206	105.0/221
Climb	45.6/114	35.6/96	70.0/158	34.4/94	87.8/190	97.8/208
Cruise	21.7/71	19.4/67	61.7/143	36.1/97	73.3/164	75.6/168
Descent	-2.2/28	0/32	41.7/107	30.0/86	47.8/118	45.6/114
Approach	24.4/76	24.4/76	57.2/135	34.4/94	76.7/170	76.7/170
Max. Fan Torque	56.1/133	38.3/101	84.4/184	43.3/110	99.4/211	117.2/243

*9310 Steel 148.9° C (300° F) Limit

Table 11-VI. Derated Reduction Gear Efficiency 6300 cm^3/sec (100 gpm) (80° F) Water Cooling.

Condition	Red. Gear Efficiency %	Total Q kw/Btu/min	Lube Oil, °C/°F	Bearing Race,* °C/°F	AGMA Scoring Factor,* °C/°F
Gidle	96.63	8.49/483	27.2/81	31.1/88	27.8/85
Takeoff	97.11	430.2/24483	61.7/143	117.2/243	125.6/258
Climb	97.10	415.9/23666	60.0/140	113.3/236	123.3/254
Cruise	97.07	247.6/14091	46.7/116	83.9/183	86.1/187
Descent	96.73	76.5/4355	32.8/91	50.6/123	48.3/119
Approach	97.15	233.2/13271	45.6/114	87.8/190	87.8/190
Max. Fan Torque	97.11	502.6/28602	67.8/154	123.9/255	141.7/287

*9310 Steel = 148.9° C (300° F) Limit.

11.4 ROTOR THRUST BALANCE

In addition to the loads resulting from flight maneuvers and misalignment, the main shaft bearings of a turbofan engine are subjected to axial loads which are the result of the axial aerodynamic forces on the turbomachinery blading, plus pressure forces on the rotor components. Generally these thrust loads can be minimized by adjusting the radial location of one or more labyrinth seals.

The core engine (high pressure compressor and high pressure turbine) of the F101 uses a conventional method of thrust balancing, i.e., the forward compressor load and aft turbine load are balanced by radially adjusting the labyrinth seals to provide the balancing gas loads. The net axial thrust load is taken at the No. 3 ball bearing.

The rotor thrust balance situation for the low pressure rotor (fan and low pressure turbine) of a geared fan system is quite different from that of a conventional turbofan engine. This is illustrated in Figure 11.11. Loads shown are typical for the takeoff condition of the OTW engine. In the conventional engine, the low pressure midshaft ties the turbine rotor to the fan rotor so that the thrust bearing reacts only the difference in thrust between the rotors. The OTW engine has a reduction gear which axially disconnects the fan from the LP turbine. Therefore, each rotor system (fan and LP turbine) must have its own thrust bearing. Figure 11.11 shows schematically the difference between a conventional system and a geared system to support the OTW fan rotor thrust loads high load capacity ball bearing from the CF6 engine. This bearing is identified as the No.1 ball bearing in the OTW engine. A balance piston arrangement has been applied to the low pressure turbine rotor to minimize the axial thrust loads on the rotor thrust bearing (No. 2 ball bearing).

Rotor thrust bearing design conditions and loads are discussed for the fan, core, and LP turbine rotor systems in the following paragraphs.

11.4.1 Fan Rotor Balance

Thrust forces considered in determining the axial loads acting on the fan rotor thrust (No. 1B) bearing are identified in Figure 11.12. Results of the analyses, based on the OTW experimental engine duty cycle, are presented in Table 11-VII.

The No. 1 bearing cubic mean thrust load for the experimental duty cycle is 42.07 kN (9457 lb). Based on a specific dynamic capacity of 308.7 kN (69,400 lb) and a radial load of 4.002 kN (900 lb), this bearing has a calculated B_{10} life of 21,775 hours. A material life multiplier of 5 was used in this analysis.

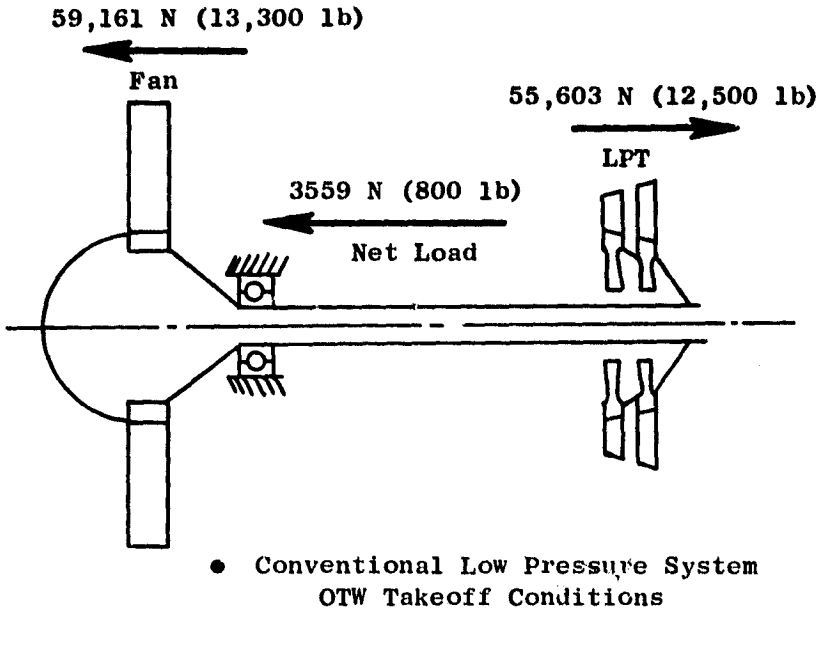

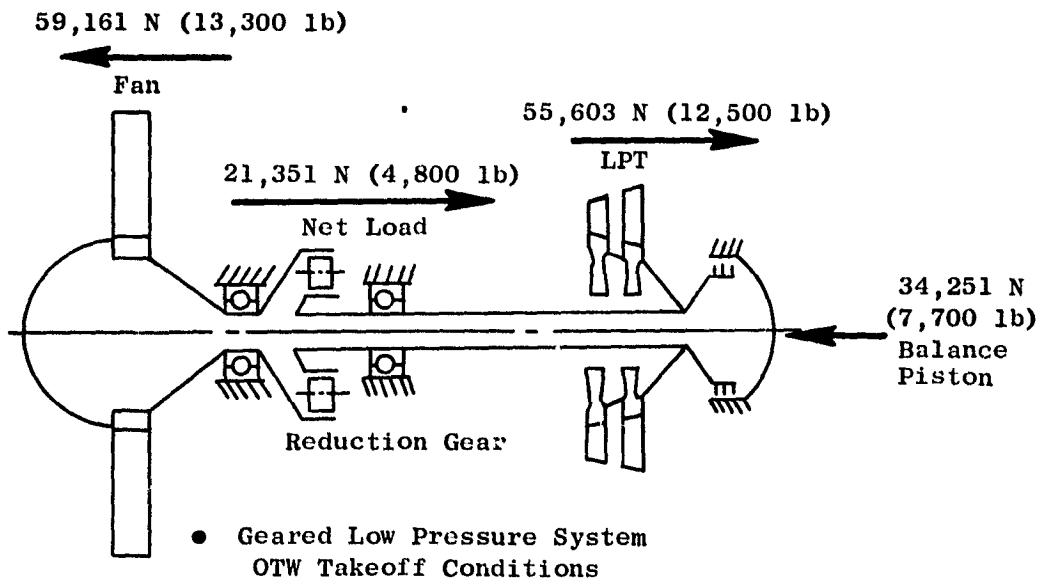

Figure 11.11. Schematic of Conventional and Geared LP Drive Systems.

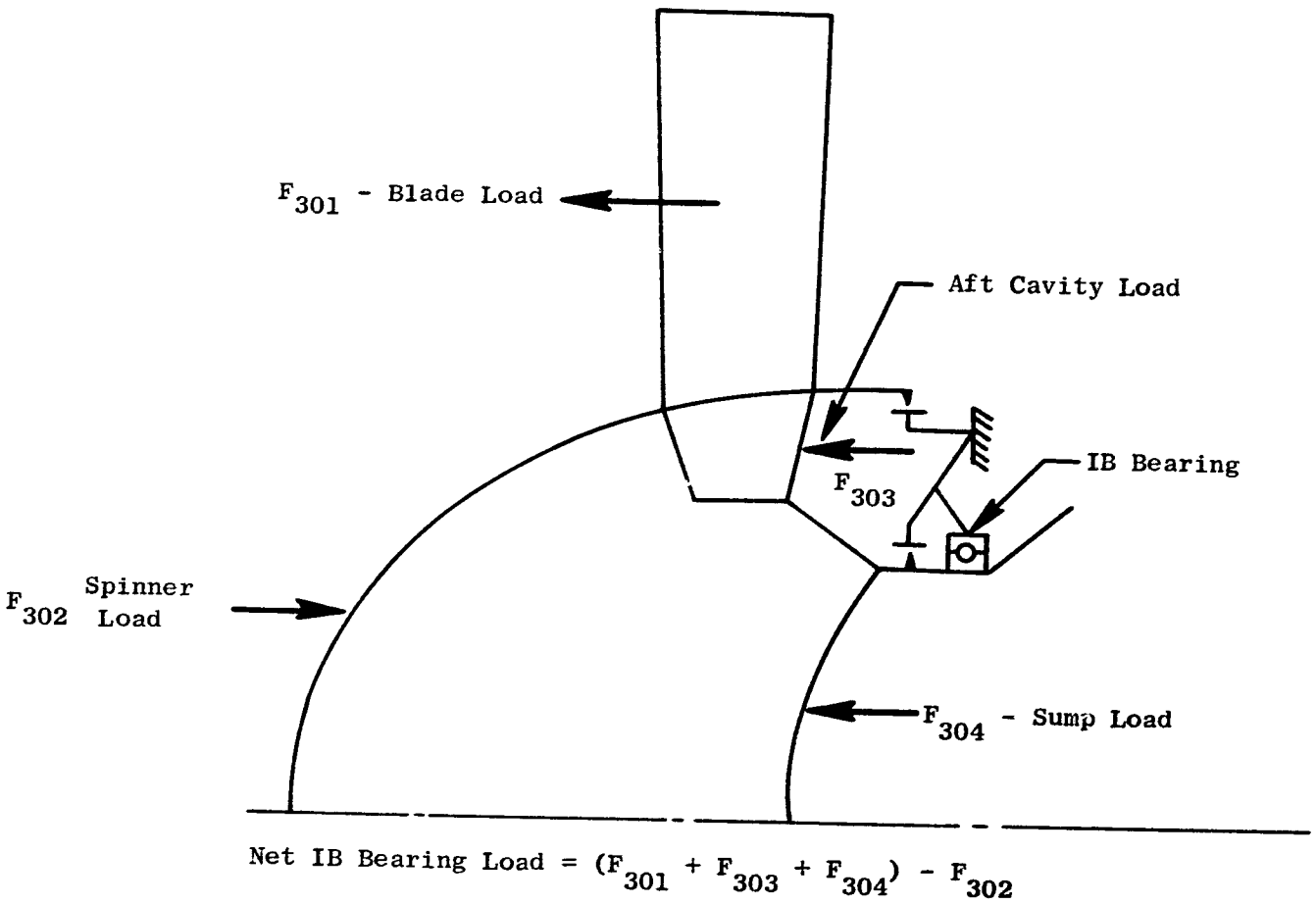

Figure 11.12. OTW Fan Thrust Load Vectors.

Table 11-VII. Fan Rotor Thrust (No. 1B) Bearing Axial Loads.

Item	Case No.	$\%N_f$	% Fan Power	Rpm	% Time*	kN**	lbs**
1	946	105	100	3982	.04	57.6	12,949
2	926	102.9	106.7	3904	.60	58.9	13,244
3	945	101.5	105.5	3848	.55	59.2	13,303
4	1	101.5	101.2	3848	5.59	56.2	12,635
5	947	90	82	3414	18.64	49.5	11,134
6	948	75	52	2845	37.29	36.7	8242
7	949	30	5	1138	37.29	9.4	2142

*Total operational time = 2682 hours

**Sign Convention: + = forward

Table 11-VIII. Core Engine Rotor Thrust (No. 3) Bearing Axial Loads.

Item	Case No.	% Time*	H.P. Spool (rpm)	kN**	lbs**
1	946	.04	13883	-7.6	-1717
2	926	.60	14078	-10.8	-2429
3	945	.55	14075	-7.0	-1580
4	1	5.59	13924	-8.5	-1902
5	947	18.64	13612	-7.0	-1584
6	948	37.29	12939	-7.6	-1718
7	949	37.29	10666	-1.4	-309

*Total Operational Time = 2682 hours

**Sign Convention: + = forward

11.4.2 Core Engine

High pressure rotor (HP compressor and HP turbine) thrust load vectors considered in the core engine thrust balance analysis are shown in Figure 11.13. The HP rotor thrust (No. 3) bearing net axial loads resulting from these vectors are presented in Table 11-VIII for the OTW experimental engine duty cycle.

The No. 3 bearing cubic mean thrust load for the experimental duty cycle is 6.67 kN (1501 lbs). Based on a specific dynamic capacity of 95.99 kN (21,580 lbs) and a radial load of 0.89 kN (200 lbs), this bearing has a calculated B_{10} life of 13,560 hours. A material life multiplier of 5 was used in this analysis.

11.4.3 Low Pressure Turbine Rotor

Low pressure turbine thrust balance load vectors considered in the rotor thrust balance analysis are shown in Figure 11.14. The turbine aft load is counteracted by the forward-acting balance cavity force. The balance piston seal is located in the aft sump area described in Section 11.5. The net load (aft LP turbine minus forward balance piston) acts on the No. 2 ball bearing. Thrust balance air is supplied from the high pressure compressor 9th stage rotor as shown in Figure 11.15. This compressor discharge (CDP) air is routed through a 5.09 cm (2 inch) pipe to the bottom vertical service strut. The pipe then passes through the strut and connects to the balance piston cavity.

CDP airflows required for the thrust balance cavity are: 0.272 kg/sec 0.60 lb/sec) for a 0.038 cm (0.015 inch) seal clearance. A 0.152 cm (0.060 inch) seal clearance requires 0.63 kg/sec (1.39 lb/sec).

Axial loads resulting from the LP turbine load vectors based on the experimental engine duty cycle are presented in Table 11-IX.

The No. 2 bearing cubic mean thrust load for the experimental duty cycle is 10.58 kN (2361 lbs). Based on a specific dynamic capacity of 84.20 kN (18,930 lbs) and a radial load of 2.67 kN (600 lbs), this bearing has a calculated B_{10} life of 31,700 hours. A material life multiplier of 5 was used in the analysis.

11.5 BEARINGS, SEALS, AND SUMPS DESIGN

The OTW engine bearing arrangement is shown schematically in Figure 11.16. As shown, the core is supported by a ball thrust bearing (No. 3) located at the forward end of the HP compressor and an intershaft roller bearing (No. 4) located at the HP turbine aft end. The ball thrust bearing, which reacts HP system unbalance thrust loads and radial component loads, is supported by a housing structurally identical to the housing used in the F101 engine. This housing is mounted on the aft inner flange of the composite

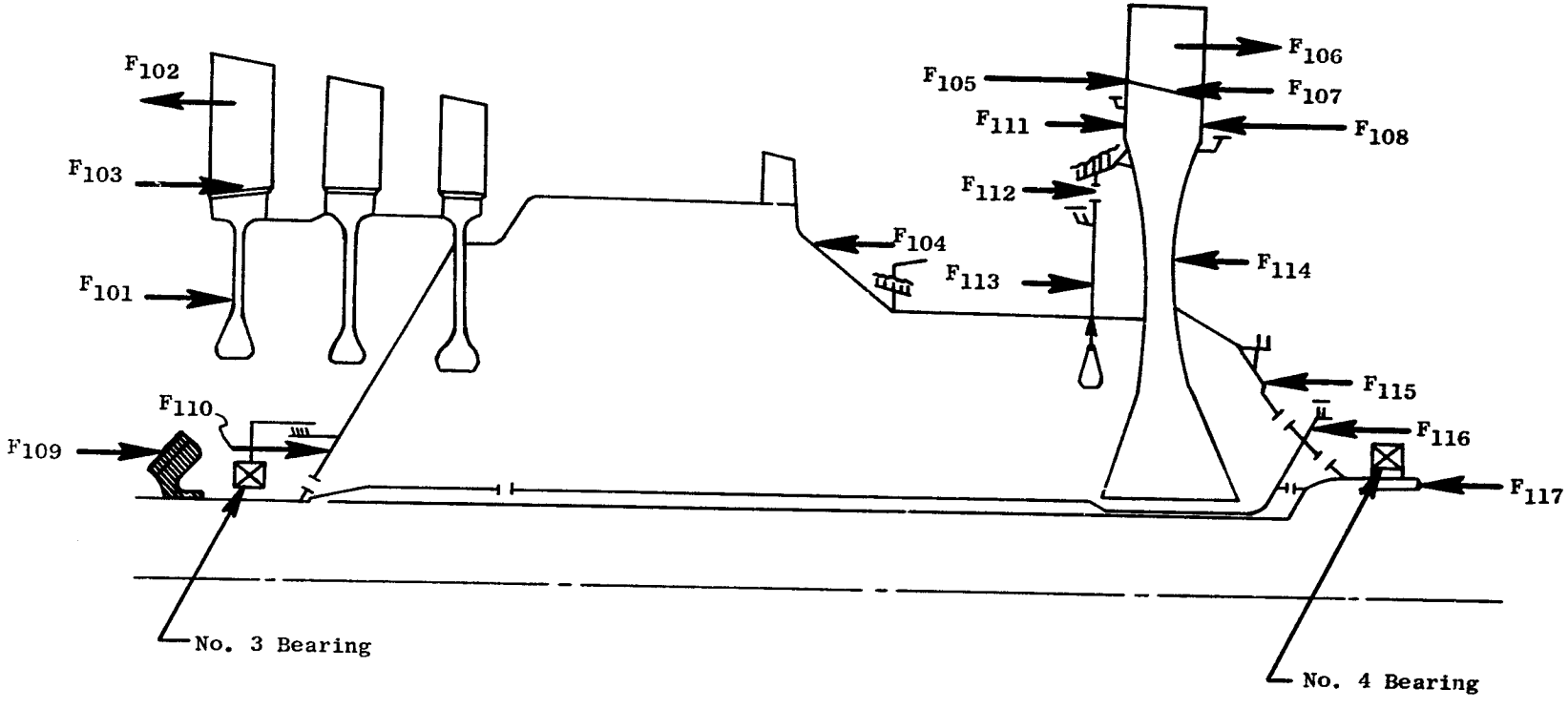

Figure 11.13. HP Spool Thrust Load Vectors.

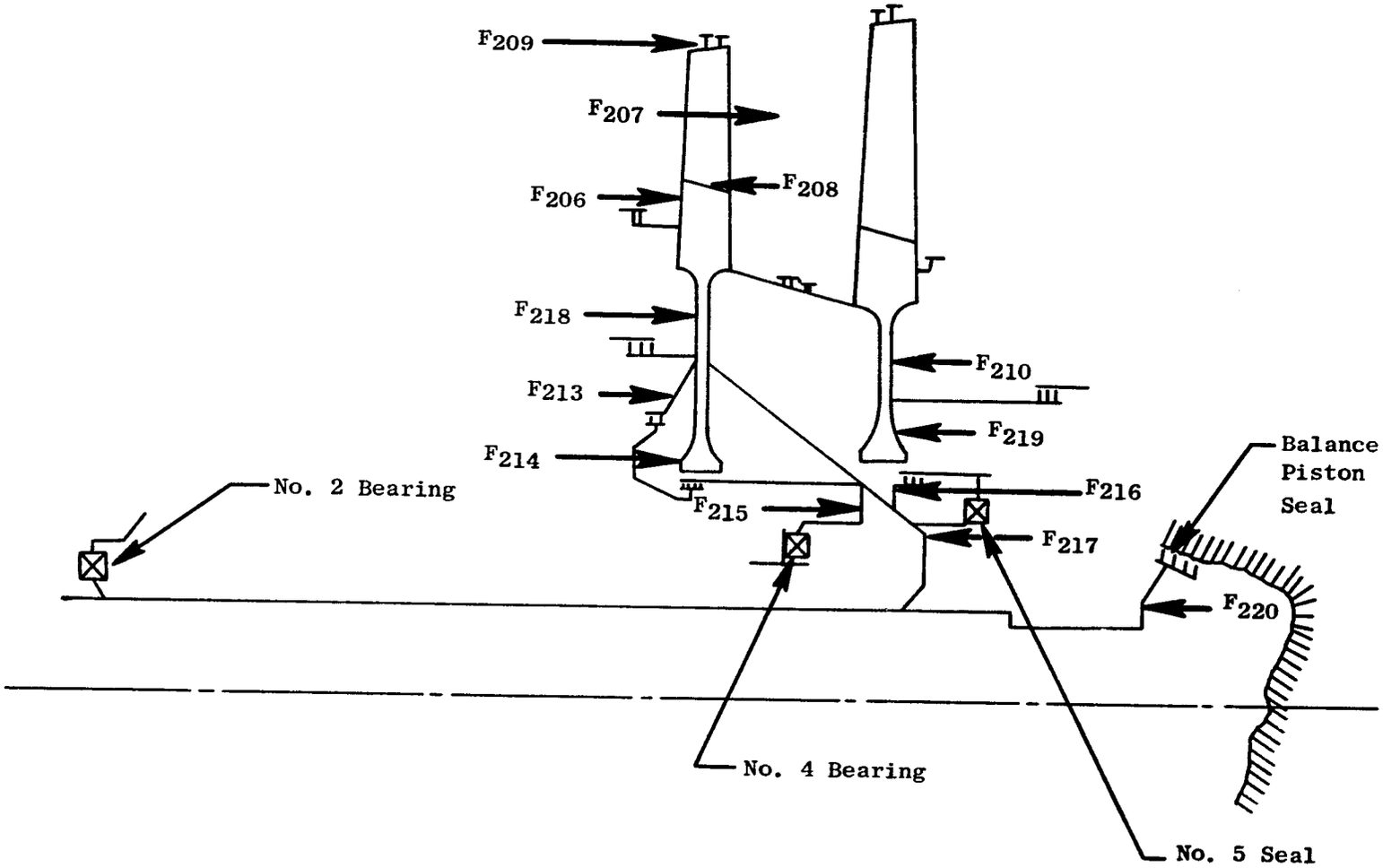

Figure 11.14. LP Turbine Thrust Load Vectors.

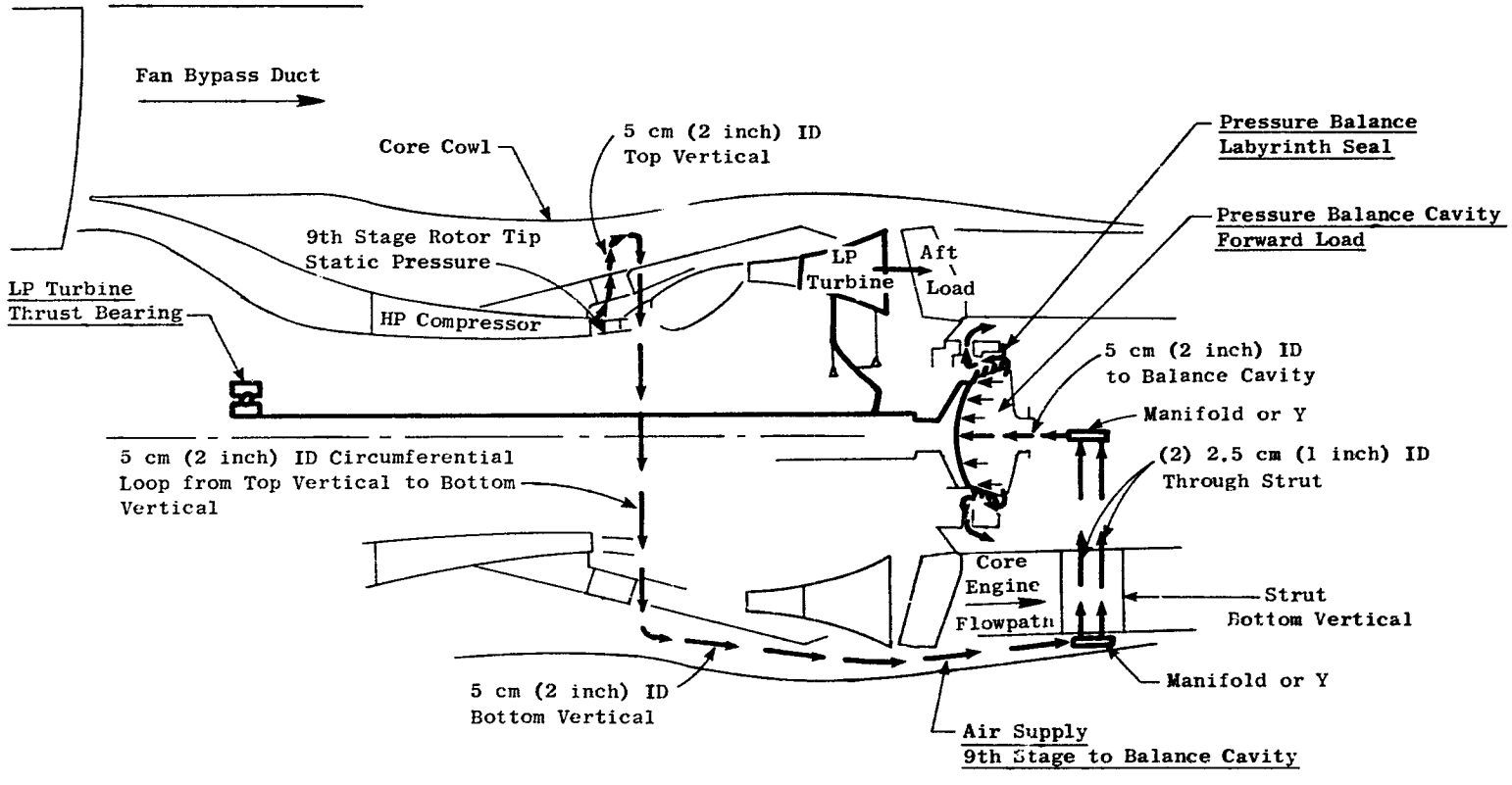

Figure 11.15. LP Turbine Thrust Balance System.

Table 11-IX. Low Pressure Turbine Rotor Thrust (No. 2) Bearing Axial Loads.

Item No.	Case No.	% Time[1]	% N_F	% Fan Power	LP Turbine (rpm)	kN[2]	lbs[2]
1	946	0.04	105	100	8211	-21.34	-4798
2	926	0.60	102.9	106.7	8050	-20.43	-4593
3	945	0.55	101.5	105.5	7934	-19.85	-4462
4	1	5.59	101.5	101.2	7934	-18.68	-4199
5	947	18.64	90	82	7038	-11.35	-2552
6	948	37.29	75	52	5865	-2.56	-576
7	949	37.29	30	5	2346	+4.13	+928

[1] Total operational time = 2682 hours.

[2] Sign conventions: + = forward, - = aft.

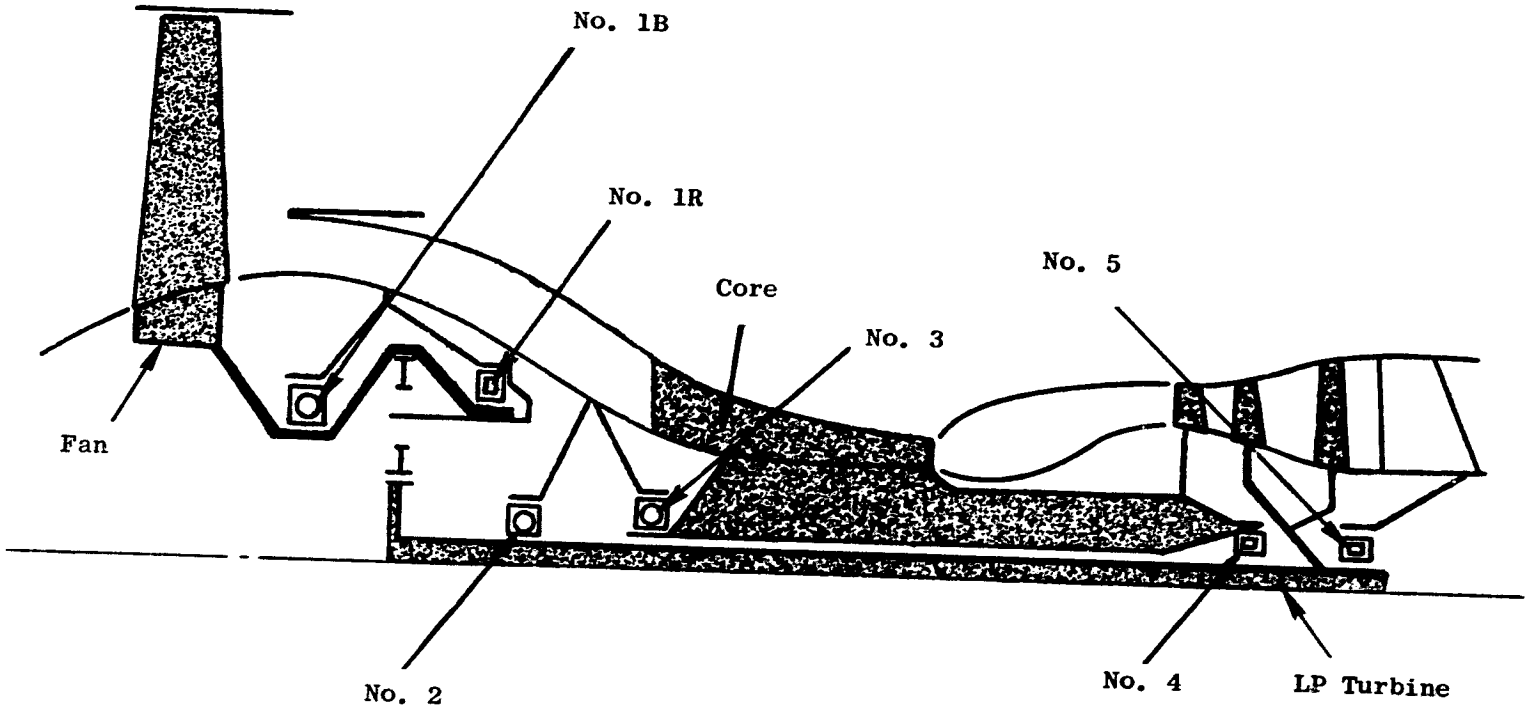

Figure 11.16. Schematic of OTW Engine Bearing Arrangement.

fan frame. The No. 4 roller bearing, which supports the aft end of the core rotor, is mounted between the HP and LP turbine shafts.

The low pressure system of the OTW engine is supported by four bearings. The main LP turbine shaft is supported by a ball thrust bearing (No. 2) at the forward end and a roller bearing (No. 5) at the aft end. The ball bearing is the same as the F101 fan thrust bearing. This bearing carries the net thrust load of the LP turbine rotor and thrust balance piston, and also a radial load component from the LP shaft. The No. 5 roller bearing, which is identical to the corresponding F101 engine bearing, carries radial loads from the LP shaft and the No. 4 intershaft bearing. Both the No. 2 and No. 5 bearings are supported by housings similar to the corresponding F101 engine housings. The No. 2 bearing housing is mounted to the mid-inner flange of the composite fan frame, and the No. 5 roller bearing support is mounted to the aft end of the turbine frame. The fan rotor is supported by two bearings: a ball thrust bearing (No. 1B) at the forward end, and a roller bearing (No. 1R) at the aft end. The ball thrust bearing carries fan thrust and radial loads. The roller bearing reacts only fan shafting radial loads. Ball bearing support is provided by a housing mounted to the composite fan frame forward flange. The roller bearing housing is mounted to the same forward flange of the composite frame.

A tandem circumferential carbon seal is positioned forward of the No. 1B bearing. It provides a seal between the fan rotor cavity and the forward sump. The No. 3 bearing is sealed from the HP compressor rotor cavity by a face-type carbon seal. The HP turbine rotor cavity is sealed from the aft sump by the No. 4 carbon piston ring seal located forward of the inner shaft bearing. Both the No. 3 and No. 4 seals and their associated parts are identical to F101 hardware. Another tandem circumferential carbon seal is placed between the No. 5 bearing and the balance piston cavity, sealing off the aft sump.

All structures such as shafting, seals, and housings were analyzed using a GE computer program capable of structural analysis with axisymmetric or discrete loading. Stresses were combined using Von Mises failure criteria with appropriate stress concentration factors. All combined stresses, under the most severe design conditions, are below material 0.2% yield properties.

Bolted connections were analyzed using a GE computer program (where applicable) for analyzing bolted flanges. This program includes thermal, centrifugal, torque, and all other flange-type loadings. Bolt materials were selected on the basis of strength and material compatibility with mating structures.

Interface connections were analyzed by evaluating structural component stiffness levels. These stiffness values were calculated using various analytical techniques for required directional loadings, and were then combined with appropriate mating structures to obtain stress resultants.

11.5.1 Forward Sump

The forward sump, shown in Figure 11.17, contains the internal accessory drive bevel gearsets, reduction gears, the No. 1B and No. 1R fan shaft bearings, the No. 2 LP shaft bearing, the No. 3 HP shaft bearing, and carbon seals forward of the No. 1B bearing and aft of the No. 3 bearing. The balls and cage of the No. 1 bearing will be the same as used in the CF6. The balls are M50 and the cage is silver-plated AMS 6414 (AISI 4340 steel). A new outer race, which will provide support over its entire length, is designed and fitted to the common CF6 parts. The outer race is mounted to the forward support housing by a flange that incorporates an anti-rotation device. The inner race is mounted on a chrome-plated fan shaft journal and is retained by a spanner nut common to the CF6 design. Lubrication is provided for this bearing by inner race slots and a groove that is positioned over oil holes that penetrate the fan shaft. The holes in the shaft are fed by two oil jets. Both inner and outer races are made of M50 material.

A tandem circumferential carbon seal forward of the No. 1B bearing is mounted in a 400 series stainless steel housing that is detachable from the No. 1B bearing support cone. The carbon rides on a fan shaft runner clamped between the No. 1B inner race and spanner nut. The runner is made from AMS 6322 with the sealing surface chrome plated. The seal is pressurized between the carbons by third stage air and is cooled by oil flowing against the underside of the runner. A seal drain is provided between the carbons to collect any incipient leakage and direct it overboard to prevent core engine contamination. Seal design information is presented in Table 11-X.

Table 11-X. No. 1 Seal Design Information.

Base Diameter	39.17 cm (15.42 in)
Rotational Speed	3900 rpm
Surface Speed	665.5 cm/sec (262 ft/sec)
Delta Pressure	6.21 N/cm^2 (9.0 psid)
Max Supply Air Temp	204.4° C (400° F)
Rubbing Surface Heat Generation	2128 J/sec (121 Btu/min)
Oil Flow Rate	63.1 cm^3/sec (1 gpm)
Projected Min. Seal Life	>6200 hrs

The No. 1R bearing has a flanged inner race which is mounted to the aft chrome-plated journal of the fan shaft. Rollers, cage, and outer race are mounted as an assembly to the reduction gear support housing. The bearing is lubricated by two jets mounted 180° apart in the reduction gear support on the aft side of the bearing. The bearing is preloaded with a radial interface to prevent skidding. Bearing race and roller material is AISI 52100. Bearing design information is presented in Table 11-X1.

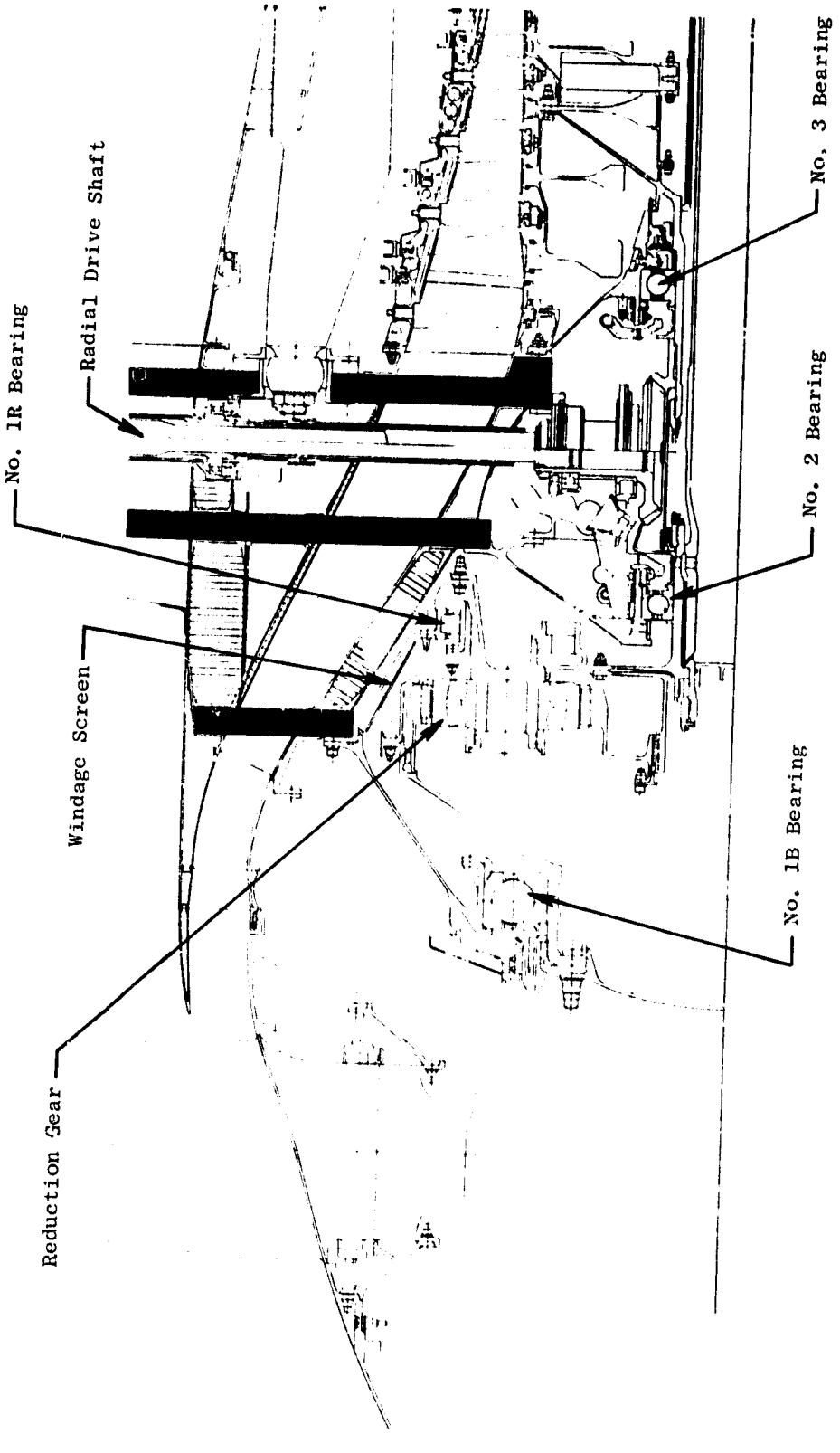

Figure 11.17. OTW Forward Sump.

Table 11-XI. No. 1R Bearing Design Information.

Base Diameter	518 mm (20.39 in)
Rotational Speed	3900 rpm
DN Value	2.02×10^6
No. of Rollers	60
Roller Diameter	18 mm (.7087 in)
Fatigue Life Exceeds	2×10^6 hrs

The LP turbine rotor No. 2 ball thrust bearing, which is identical to the corresponding bearing in the F101 engine, is made of M50 material and jet lubricated on both its forward and aft sides. The No. 3 HP rotor ball thrust bearing, identical to the corresponding F101 bearing, also is made of M50 material and jet lubricated on both sides. Oil from the aft jet cools the back face of the No. 3 carbon seal runner.

Fan shafting consists of two sections and is made of 17-4PH steel. The forward section is splined at its outer end to provide a torque connection between it and the main reduction ring gear. This shaft is flanged at the forward end to support the rotor disk. The shafting is supported at the forward end by the No. 1B bearing and at the aft end by the No. 1R bearing.

The outer cone that supports the star gear carrier of the main reduction gear is made of 17-4PH steel. This cone is bolted to the star gear carrier at its aft end, and is mounted to the forward inner ring of the composite frame at the forward end. This cone also supports the forward sump scavenge scoop/screen.

The No. 1B bearing support is made of 17-4PH steel. This housing supports both the No. 1B bearing and the No. 1 tandem carbon seal. Integral piping is incorporated in this housing to supply air to, and to drain leakage oil from, the carbon seal. The housing assembly is mounted to the forward inner ring of the composite frame.

The No. 2 bearing housing utilizes the inner casting from the F101 engine. A new conical shell and outer flange are required to mate with the composite frame. Two F101 internal bevel gear assemblies are mounted from the No. 2 bearing housing. Material for this housing is 6-4 titanium.

The No. 3 bearing housing is identical to that of the F101 with the exception that the extreme outer flange has been modified to accommodate a new fastener for mounting the housing to the aft ring of the composite frame. The housing, which is made from 6-4 titanium, provides support for the No. 3 carbon face seal and various lube jets.

Loading diagrams for the forward sump are presented in Figure 11.18, 11.19, 11.20, and 11.21 for both steady-state and blade-out conditions. Shafting was designed using maximum steady-state stresses combined with maximum blade-out loads. Steady-state loading included torque, centrifugals, thermals, and

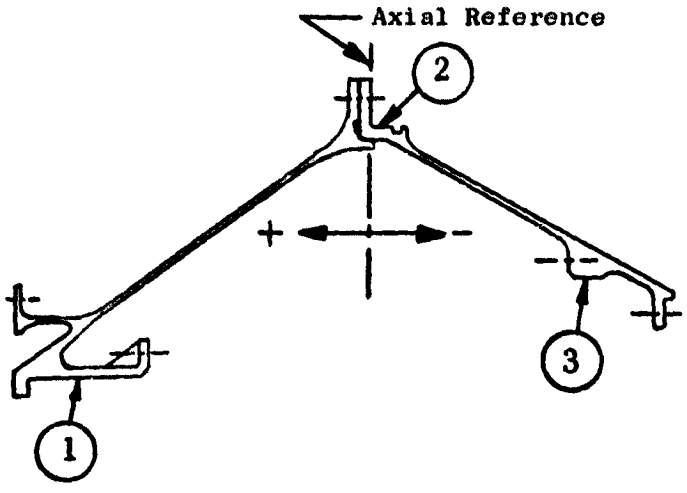

OTW Case 926

Steady State Loading

- Fan Torque 32,254 Nm (285,481 in.-lbs)
- Turbine Torque 15,644 Nm (138,469 in.-lbs)
- Fan Thrust 96,757 N (21,753 lbs)
- Temperature 121° C (250° F)

Deflections

Point	Axial	Radial ↑	Rotational Radians ↷ +
1	0.0442 cm (0.0174 in.)	0.0262 cm (0.0103 in.)	-0.0005
2	———	0.0008 cm (0.0003 in.)	———
3	-0.0348 cm (-0.0137 in.)	0.0320 cm (0.0126 in.)	-0.0012

Figure 11.18. Forward Sump Stationary Structure Deflections.

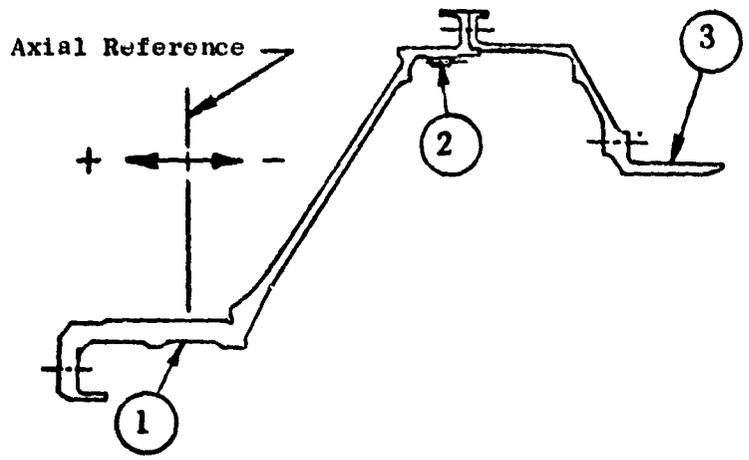

OTW Case 926

Steady State Loading

- Fan Torque 32,254 Nm (285,481 in.-lbs)
- Fan Speed 3904.5 rpm
- Fan Thrust 96,757 N (21,753 lbs)
- Temperature 121° C (250° F)

	Deflections		
Point	Axial	Radial ↑	Rotational Radians (+)
1	0	0.0191 cm (0.0075 in.)	0.0003
2	-0.0257 cm (-0.0101 in.)	0.0569 cm (0.0224 in.)	0.0006
3	-0.0401 cm (-0.0158 in.)	0.0246 cm (0.0097 in.)	0.0034

Figure 11.19. Forward Sump Rotating Structure Deflections.

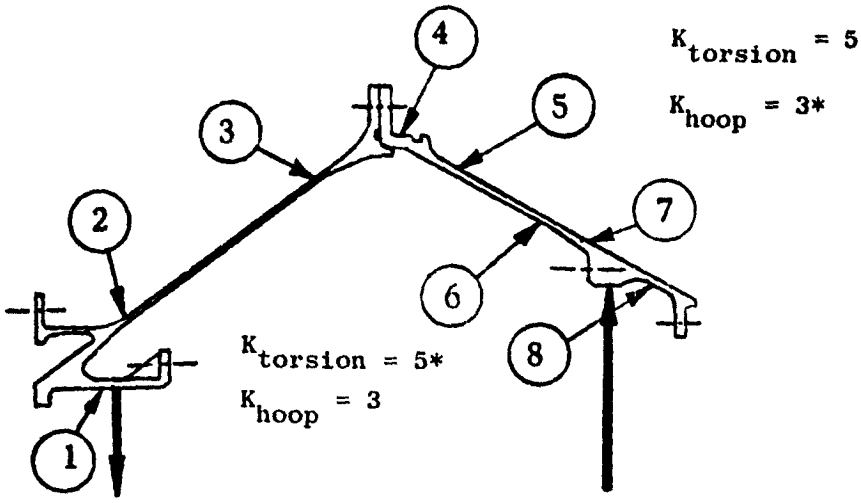

Point	Steady State Effective Stress kN/cm^2 (ksi)	One Metal Blade Out** Effective Stress kN/cm^2 (ksi)
1	2.76 (4.0)	24.5 (35.6)
2	2.07 (3.0)	47.7 (69.2)
3	27.6 (40.0)	57.0 (82.7)
4	21.4 (31.0)	23.2 (33.6)
5	32.2 (46.7)	37.8 (54.8)
6	30.9 (44.8)	39.7 (57.6)
7	7.58 (11.0)	10.1 (14.7)
8	10.3 (15.0)	12.3 (17.8)

17-4PH Steel - Rc 33/36

Min 0.2% Yield = 82.7 kN/cm^2 at 121° C (120 ksi at 250° F)

Min Ultimate = 95.8 kN/cm^2 at 121° C (139 ksi at 250° F)

* Stress Concentrations Included in Tabulated Stresses

Figure 11.20. Forward Sump Stationary Structure Stresses.

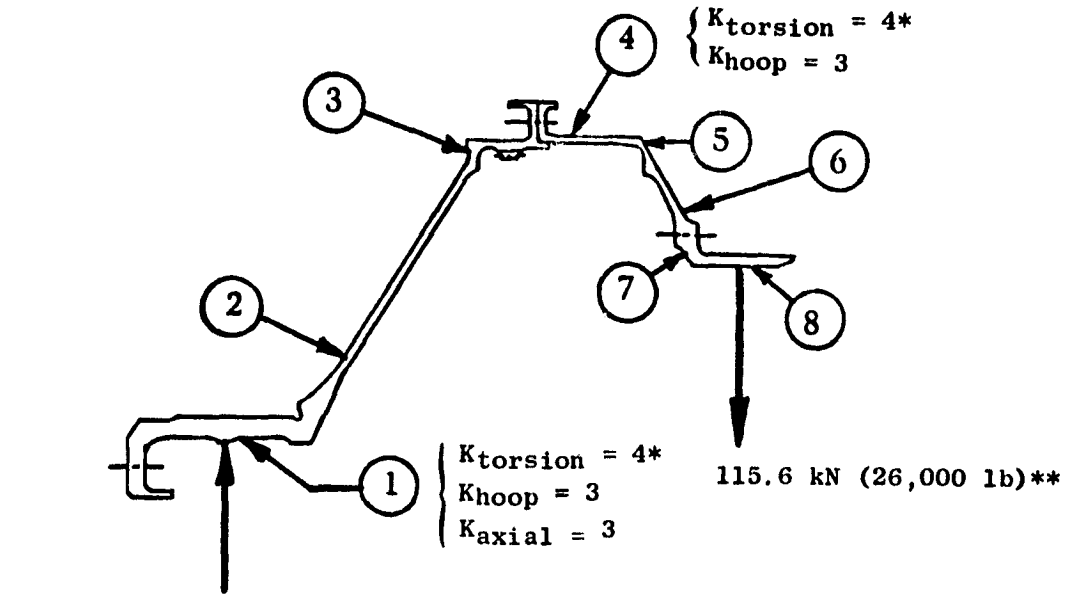

Point	Steady State Effective Stress kN/cm^2 (ksi)	One Metal OTW Blade Out** Effective Stress kN/cm^2 (ksi)
1	9.31 (13.5)	15.7 (22.7)
2	11.7 (17.0)	50.7 (73.6)
3	14.9 (21.6)	20.5 (29.8)
4	16.0 (23.2)	18.8 (27.2)
5	14.8 (21.4)	17.2 (25.0)
6	13.4 (19.5)	16.2 (23.5)
7	7.79 (11.3)	10.1 (14.6)
8	13.9 (20.1)	17.0 (24.6)

17-4PH Steel - Rc 33/36

Min 0.2% Yield = 82.7 kN/cm^2 at 121° C (120 ksi at 250° F)

Min Ultimate = 95.8 kN/cm^2 at 121° C (139 ksi at 250° F)

* Stress Concentrations Included in Tabulated Stresses

Figure 11.21. Forward Sump Rotating Structure Stresses.

thrust. The blade-out condition was one metal blade at maximum speed. Stresses in the No. 1B bearing housing were calculated from the resultant radial and axial load components transferred to the housing through the No. 1B bearing.

Star gear loads, as well as No. 1R bearing reactions, are carried by the reduction gear support housing. These loads were combined and used to calculate maximum stresses and deflections in this housing.

A flexible coupling is provided between the LP turbine shaft and the main reduction gear; the coupling is splined at the aft end to the LP turbine shaft and supported by the No. 2 bearing. The forward end is splined to the main reduction sun gear. This coupling is designed to accommodate misalignment between the reduction gears and the LP turbine shaft. The aft coupling section is made of 4340 steel. The forward coupling, which is mated to the reduction gear, is made of AISI 9310. Both the forward and aft sections are bolted together at the O.D. of the coupling diaphragms.

Stresses for this coupling are shown in Figure 11.22.

11.5.2 Aft Sump

The aft sump, shown in Figure 11.23 with maximum steady-state temperatures, contains the No. 4 intershaft roller bearing which supports the aft end of the HP turbine rotor on the LP turbine shaft and the LP turbine shafting which is supported by roller bearing No. 5. The F101 LP turbine shaft has been analyzed and is acceptable for QCSEE.

The aft sump cavity is sealed on the forward end by a carbon piston ring intershaft seal and on the aft end by a tandem circumferential carbon oil seal. A new bearing housing supports the No. 5 bearing, No. 5 seal, No. 6 seal, and the balance piston cavity stationary hardware. An extension of LP turbine shafting is mounted to the aft end of the F101 shaft. This new shaft supports the balance piston four-tooth labyrinth seal and also carries oil to the No. 4 bearing. Major modifications to the F101 aft sump hardware include the addition of a balance piston and the removal of the F101 aft sump metering/scavenge pump. The No. 4 intershaft roller bearing, which is made of M50 material, is lubricated through holes under the bearing inner race in the LP turbine shaft. The No. 5 bearing also made of M50 material, is jet lubricated from its aft side.

A tandem carbon seal is located between the No. 5 bearing and the balance piston cavity. The carbons are retained in a small support housing made of Inco 718 and mounted to the No. 5 bearing support cone. The seal runner is made of Inco 718, and coated with tungsten carbide to provide a hard running surface. This runner is integral with the new section of aft shafting and is cooled by oil dispersed from the aft side of the same jet assembly which feeds the No. 4 and No. 5 bearings. Seal design information is presented in table 11-XII.

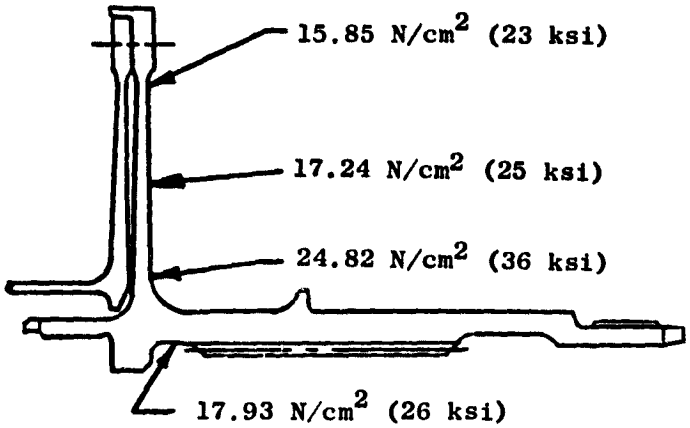

OTW Case 926

Steady State Loading

- LPT Speed 8049.9 rpm
- LPT Torque 15,644 Nm (138,469 in.-lb)
- Temperature 121° C (250° F)

AISI 4340 Steel

Min. 0.2% Yield = 68.9 kN/cm^2 at 121° C (100 ksi at 250° F)

For a 0.051 cm (0.020 in.) Offset Max. Alternating Stress is 12.4 kN/cm^2 (18 ksi)

Figure 11.22. Flex Coupling Stresses.

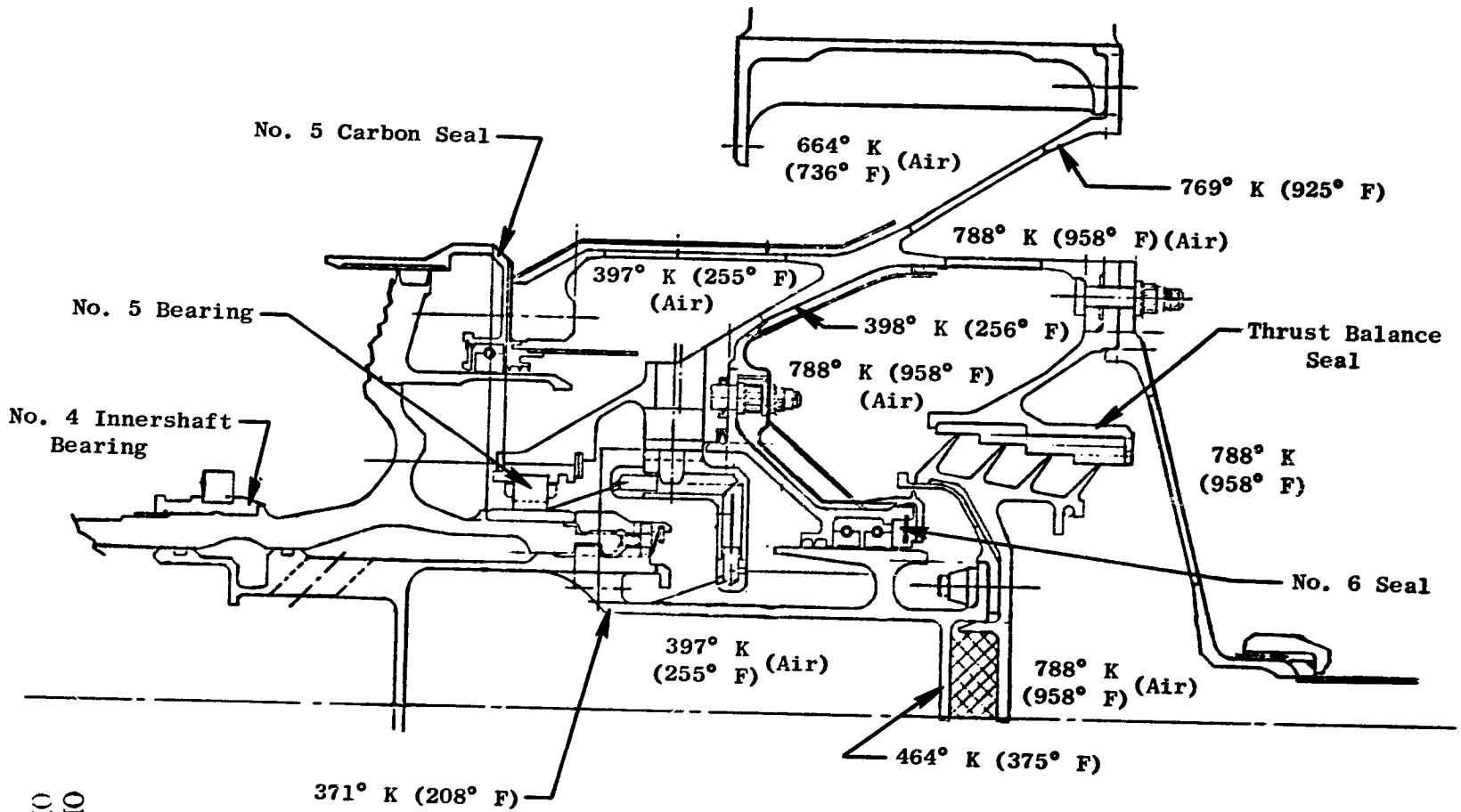

Figure 11.23. OTW Maximum Steady-State Temperatures.

Table 11-XII. No. 6 Seal Design Information.

Base Diameter	10.4 cm (4.1 in)
Rotational Speed	8040 rpm
Surface Speed	365.8 cm/sec (144 ft/sec)
Delta Pressure	4.14 N/cm^2 (6 psid)
Max Supply Air Temp	263° C (505° F)
Rubbing Surface Heat Generation	272.6 J/sec (15.5 Btu/min)
Oil Flow Rate	37.9 cm^3/sec (0.6 gpm)
Projected Min. Seal Life	>10,000 hours

The balance piston cavity is formed by a four-tooth, slant-stepped labyrinth seal made of Inco 718 and bolted to the aft end of the LP turbine shaft extension. Seal nominal diameter is 17.15 cm (6.75 in.). The seal teeth are designed for a one-to-one height-to-pitch ratio. This rotating seal is insulated from the shafting by a combination of insulating material and a metal heat shield. The seal teeth are coated with aluminum oxide to improve their ability to withstand a rub. The stationary rub surface for this seal is made of Hastelloy X abradable 1/32 hex cell honeycomb with a ribbon thickness of 0.0076 cm (0.003 inch). The honeycomb is brazed into an Inco 718 support. This support is mounted to a flange on the No. 5 bearing housing.

The No. 5 bearing, No. 6 seal, and balance piston stationary seal hardware are supported by a new Inco 718 housing which is mounted to the aft end of the turbine frame. This housing also provides a sump cavity with attachments for oil service lines.

All other aft sump hardware such as seals, spacers, and structural shafting are common between the F101 and OTW engines.

Loading diagrams for the aft sump are presented in Figures 11.24, through 11.27 for both steady-state and blade-out conditions. Maximum stresses for the aft sump were calculated using steady-state operating conditions combined with stresses resulting from one metal blade out. Steady-state loads are not as severe as those in the F101 engine due to reduced OTW horsepower requirements. The No. 5 bearing support housing stresses were calculated including resultant loads from the LP turbine frame assembly.

11.6 ACCESSORY DRIVE DESIGN

Engine accessory power is extracted from the core engine shaft through right angle bevel gearing, and transmitted through radial drive shafting to a top-mounted accessory gearbox and to a scavenge pump gearbox mounted in the core cavity area on the bottom vertical. To minimize frontal area projection of the engine, the accessory gearbox is configured to match the width of the pylon strut. Mounted to and driven from the accessory gearbox are the following components:

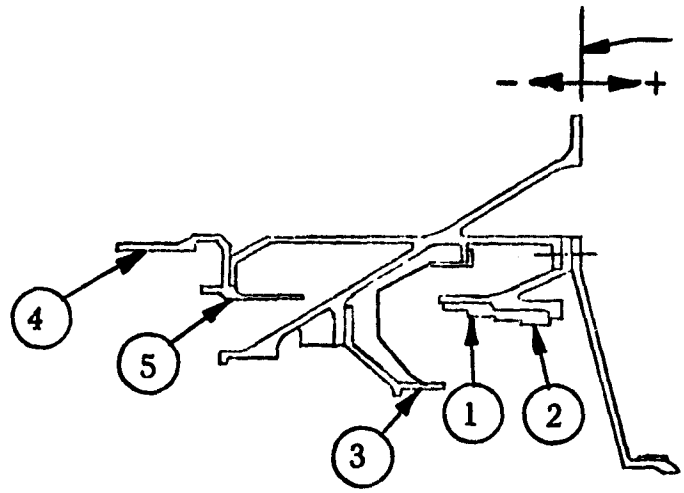

OTW Case 926

Steady State Loading

Deflections

Point	Axial	Radial ↑+	Rotational Radians (+)
1	0.0175 cm (0.0069 in.)	0.0654 cm (0.02576 in.)	0.000765
2	0.006 cm (0.00237 in.)	0.0622 cm (0.0245 in.)	-0.000615
3	0.0031 cm (0.00124 in.)	0.0155 cm (0.00609 in.)	-0.0194
4	-0.0269 cm (-0.0106 in.)	0.0544 cm (0.02142 in.)	0.00041
5	-0.0289 cm (-0.0114 in.)	0.0233 cm (0.00921 in.)	0.0046

Figure 11.24. Aft Sump Stationary Structure Deflections.

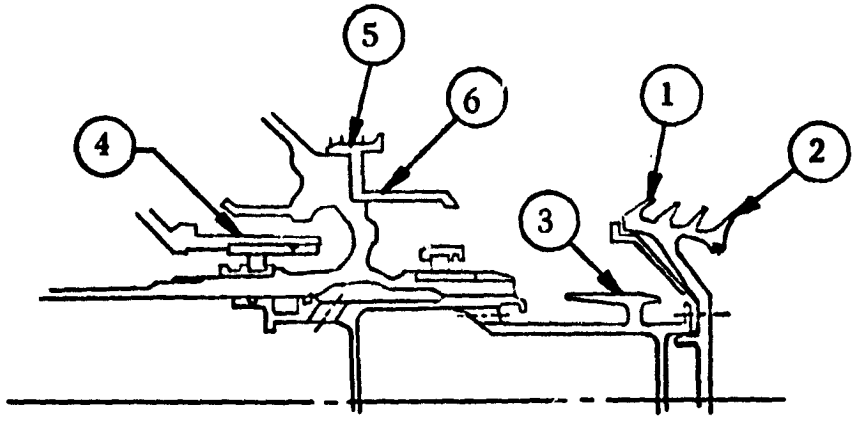

OTW Case 926

Steady State Loading

- Turbine Speed = 8050 rpm

Deflections

Point	Axial+ →	Radial+ ↑	Rotational Radians +
1	0.0549 cm (0.0216 in.)	0.0648 cm (0.0255 in.)	0.003
2	0.0820 cm (0.0323 in.)	0.0640 cm (0.0252 in.)	-0.0033
3	0.0587 cm (0.0231 in.)	0.0288 cm (0.01135 in.)	0.00429
4	0.0437 cm (0.01719 in.)	0.0500 cm (0.0197 in.)	0.0032
5	0.0734 cm (0.0289 in.)	0.0417 cm (0.0164 in.)	0.00486
6	0.0686 cm (0.027 in.)	0.0189 cm (0.00745 in.)	0.0039

Figure 11.25. Aft Sump Rotating Structure Deflections.

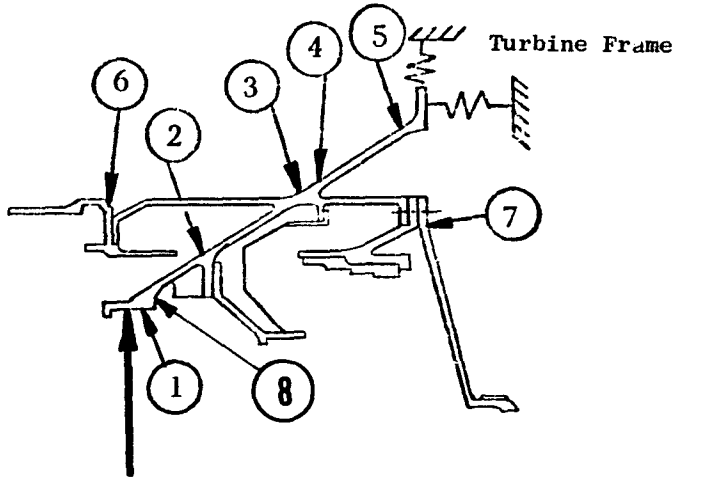

185.99 kN (41,500 lb)*

Point	Steady State Effective Stress kN/cm^2 (ksi)	One Metal OTW* Blade Out Effective Stress kN/cm^2 (ksi)	KT**	Temperature ° C (° F)	Min 0.2% Yield kN/cm^2 (ksi)	Min Ultimate kN/cm^2 (ksi)
1	0.43 (0.62)	43.5 (63.1)	--	123 (254)	97.6 (141.5)	120.0 (174)
2	12.4 (18)	50.5 (73.3)	3.0	139 (283)	96.9 (140.5)	119.3 (173)
3	6.9 (10)	19.4 (28.2)	--	276 (528)	93.7 (135.9)	113.8 (165)
4	7.7 (11.2)	52.0 (75.4)	1.6	320 (608)	87.6 (127.0)	112.4 (163)
5	7.7 (11.2)	72.1 (104.5)	1.6	495 (925)	82.0 (119.0)	105.5 (153)
6	15.2 (22)	15.2 (22.0)	--	276 (528)	93.7 (135.9)	113.8 (165)
7	6.2 (9)	6.2 (9)	--	514 (958)	89.6 (130)	110.3 (160)
8	11.0 (16)	73.8 (107.0)	--	134 (273)	97.1 (140.8)	120.0 (174)

- Material = Inconel 718

** Stress Concentrations Included In Tabulated Stresses.

Figure 11.26. Aft Sump Stationary Structure Stresses.

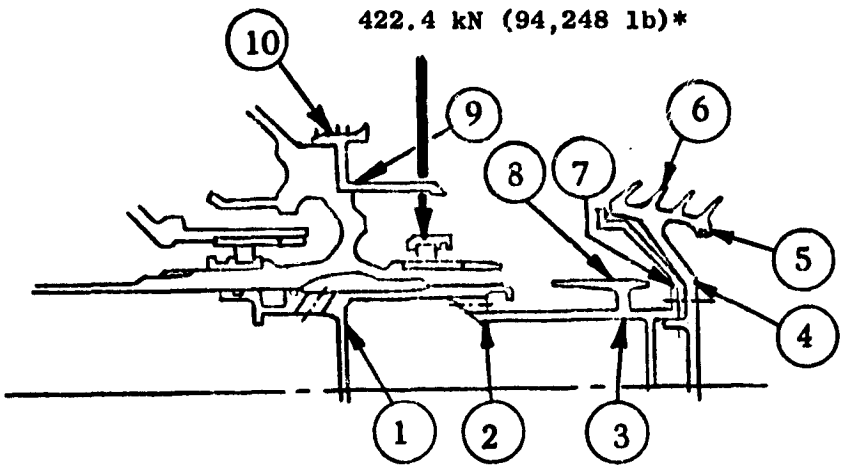

Point	Steady State Effective Stress kN/cm^2 (ksi)	One Metal OTW* Blade Out Effective Stress kN/cm^2 (ksi)
1	52.4 (76)	54.5 (79)
2	5.5 (8)	5.5 (8)
3	21.4 (31)	21.4 (31)
4	47.6 (69)	47.6 (69)
5	8.3 (12)	8.3 (12)
6	1.4 (2)	1.4 (2)
7	31.0 (45)	31.0 (45)
8	9.7 (14)	9.7 (14)
9	22.8 (33)	22.8 (33)
10	41.4 (60)	41.4 (60)

- Material = Inconel 718
- Minimum 0.2% Yield = 82.0 kN/cm^2 At 495° C (119 ksi At 925° F)
- Minimum Ultimate = 105.5 kN/cm^2 At 495° C (153 ksi At 925° F)

Figure 11.27. Aft Sump Rotating Structure Stresses.

- Fuel pump and control
- Lube supply pump
- Control alternator
- Starter

The drive system is shown schematically in Figures 11.28 and 11.29. The internal right angle bevel gearing utilizes two sets of F101 bevel gears. Splined to the main engine shaft is a 47-tooth gear which drives 35-tooth gears mounted in two individual gear housings. Figure 11.30 shows one of these gear housing assemblies. To utilize these gear assemblies, they are rotated about the vertical gear centerline to mount to the aft side of the No. 2 bearing housing instead of just forward of the No. 3 bearing housing, as is the case in the F101 engine. Larger moment loads associated with this system require a support between the fan frame aft flange and the bevel gear housing. The OTW engine design loads are presented in Table 11-XIII. Results indicate that adequate margin exists for the OTW engine test program.

Table 11-XIII. Inlet Gearbox Design Data.

Maximum started torque loads	339 mN (250 ft-lb)
Maximum accessory horsepower	125 kW (167 hp)
Equivalent horsepower (for bearing design)	53 kW (71 hp)
Calculated bearing design life[1]	750,000 hrs

[1]Based on an M50 material factor of five.

Gears and bearing materials are AISI 9310 and CEVM-M50, respectively, and the housing is investment-cast 17-4PH. The lubrication system is similar to that of the F101 engine with modifications to the internal lube manifold.

The bevel gears driving the bottom-mounted scavenge pump in the experimental engine are lightly loaded. Design optimization is required for the flight configuration. For the flight design, the 35-tooth gears driving the top accessory gearbox and the bottom scavenge pump are mounted in a common housing.

The one-piece radial drive shaft between the internal bevel gear and accessory gearbox has a central support bearing to keep the critical speed approximately 25% above shaft operating speed. The bearing is mounted in a machined housing which is bolted to the aft composite ring of the fan frame. Provisions are made in the top accessory gearbox for access to the radial drive shaft to raise it up approximately 3.81 cm (1.5 in.) so that the internal

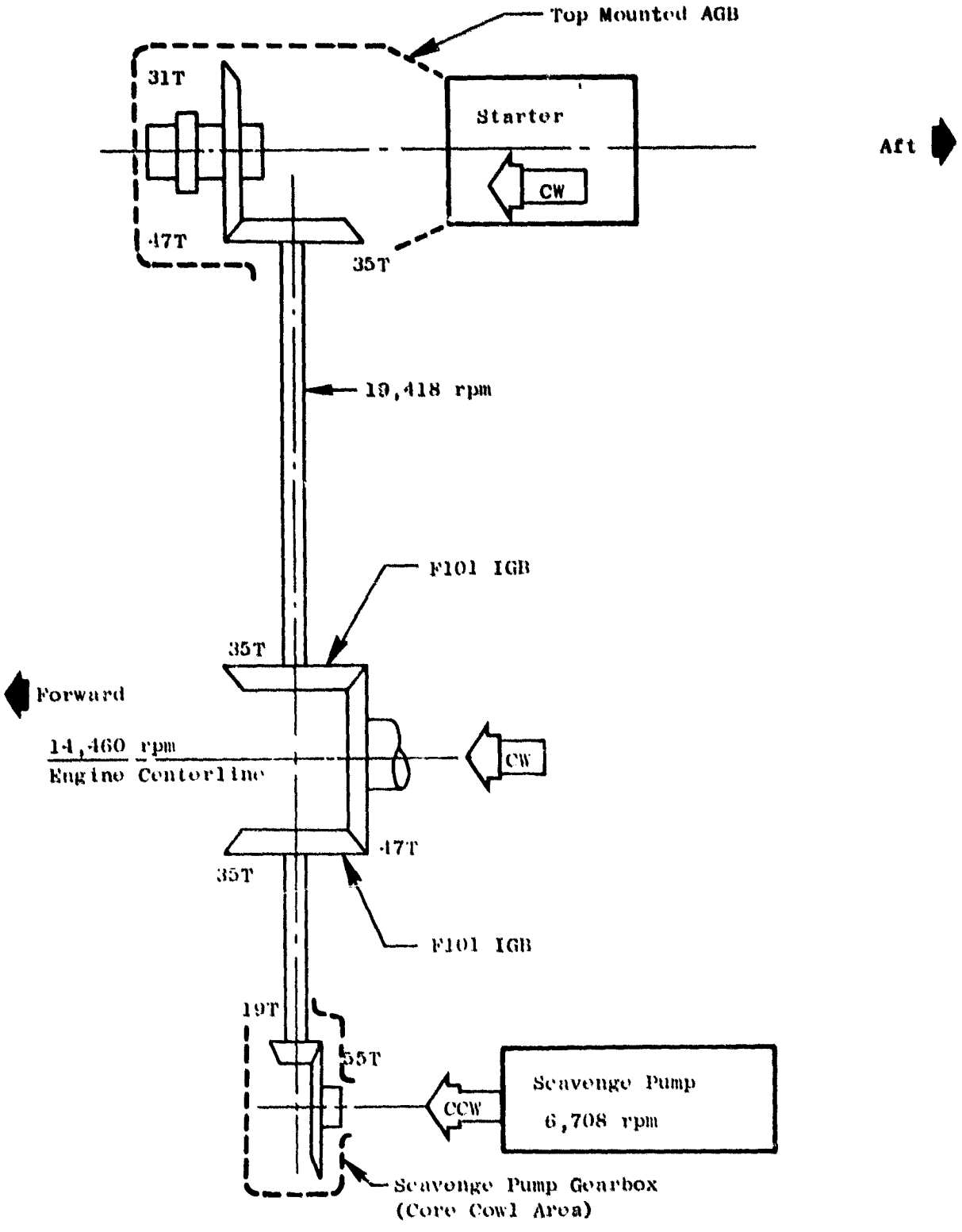

Figure 11.28. Accessory Drive System.

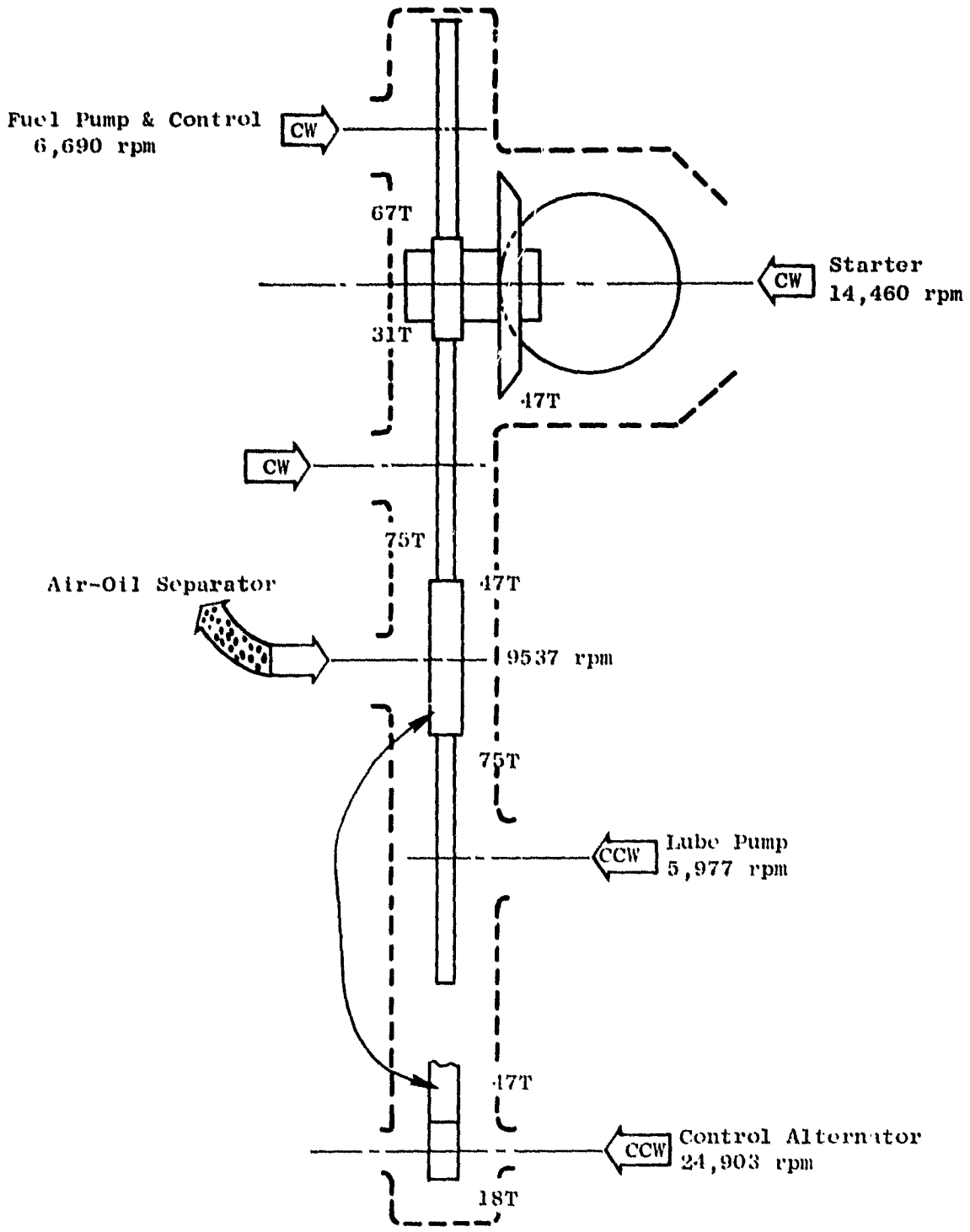

Figure 11.29. Accessory Gearbox System.

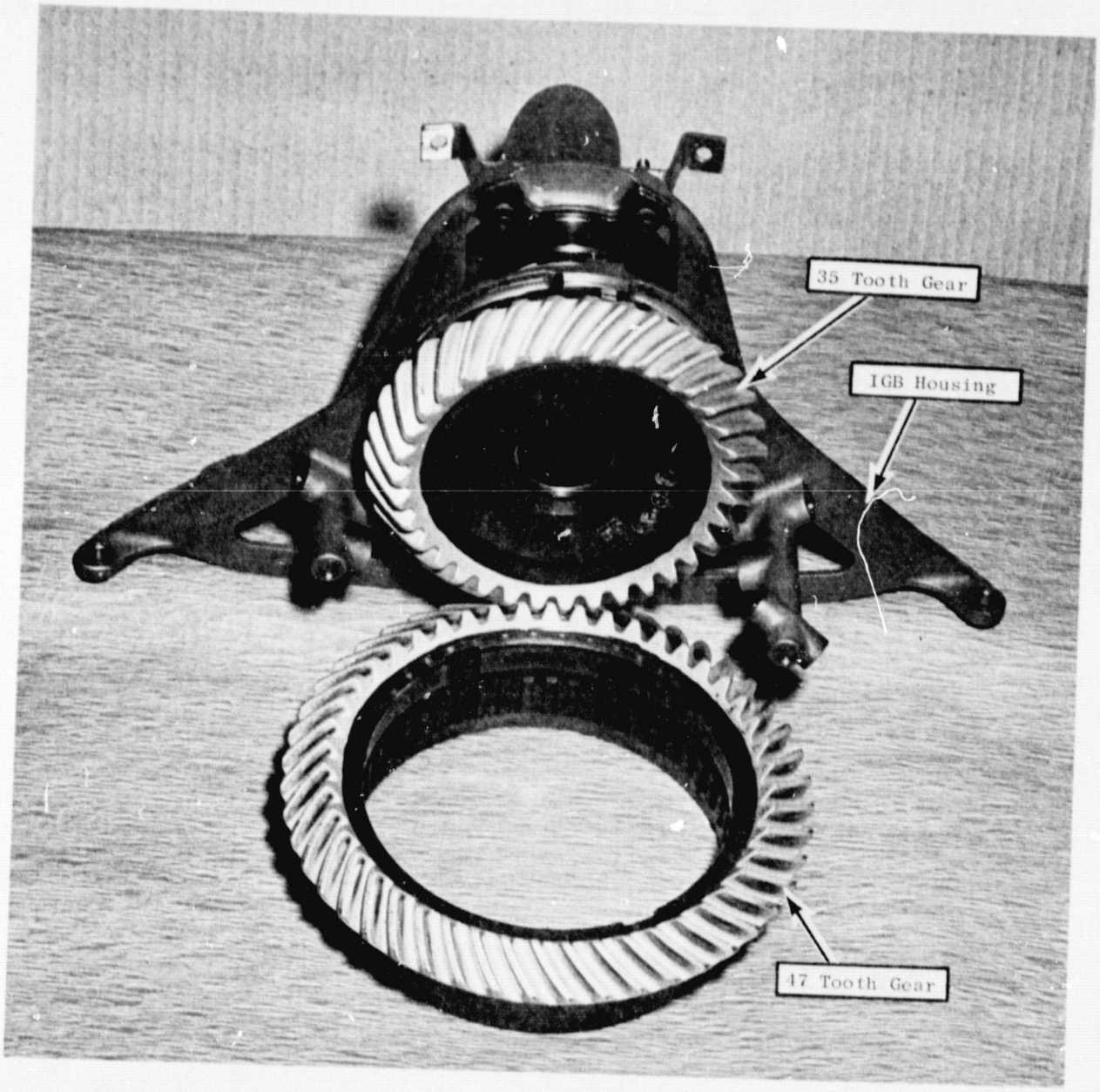

Figure 11.30. Inlet Gearbox Assembly.

gearboxes can be removed without removing the top accessory gearbox. The center hole of the shaft is used to vent the sumps to the accessory gearbox. The shaft material is AISI 4340 and the splines are induction hardened.

The shaft between the internal bevel gears and the bottom-mounted scavenge pump gearbox does not require a central support bearing because of its short length.

11.6.1 Accessory Gearbox

A cross section and external view of the top-mounted accessory gearbox are presented in Figures 11.31 and 11.32, respectively.

The accessory gearbox uses F101 bevel gears, spur gears, and bearings. One new bevel gear is required, and it will be made from an F101 forging. The spur and bevel gears are 10 and 7.100 diametral pitch, respectively, and are case-carburized AISI 9310 material. All bearings are CEVM-M50 material. The bearings are assembled in steel liners in the aluminum casing, and all outer races are keyed to prevent rotation.

F101 carbon face seals are used on the rotating gear shafts. Two new "gasko" seals have been designed to seal interfaces between the gearbox main housing and the adapters.

A new cast aluminum (AMS 4217) housing has been designed to fit in front of the pylon. The main casing is a one-piece design utilizing forward and aft adapters. These adapters also are cast aluminum (AMS 4217). A starter-mounting adapter and fan-frame adapter also have been designed. These are machined from forged aluminum bars.

Gear and bearing cooling and lubrication are accomplished in a manner similar to other General Electirc gearbox designs. The lower bevel gear is shrouded to facilitate scavenging of oil to the forward sump. An air-oil separator attached to the 47-tooth spur gear provides oil separation for the sump vent system before venting overboard. The air-oil separator is the same as that used in F101 MQT vent systems.

The maximum calculated gear tooth bending stress and compressive stress (Hertz) are 27,580 N/cm^2 (40,000 psi) and 113,078 N/cm^2 (164,000 psi), respectively. With applicable factors, the material allows tooth bending and compressive stresses of 33,096 N/cm^2 (48,000 psi) and 137,900 N/cm^2 (200,000 psi), respectively. The lowest calculated bearing life is 58,000 hours which is more than adequate for the OTW engine test program.

The accessory gearbox provides drive pads for the fuel pump/control, lube supply pump, control alternator, and starter. Provisions are made to hand crank the drive system through the 18-tooth gear shaft should that be necessary.

Pad	rpm
Starter	14,460
Fuel Pump	6,690
A/O Separator	9,537
Lube Pump	5,977
Alternator	24,903

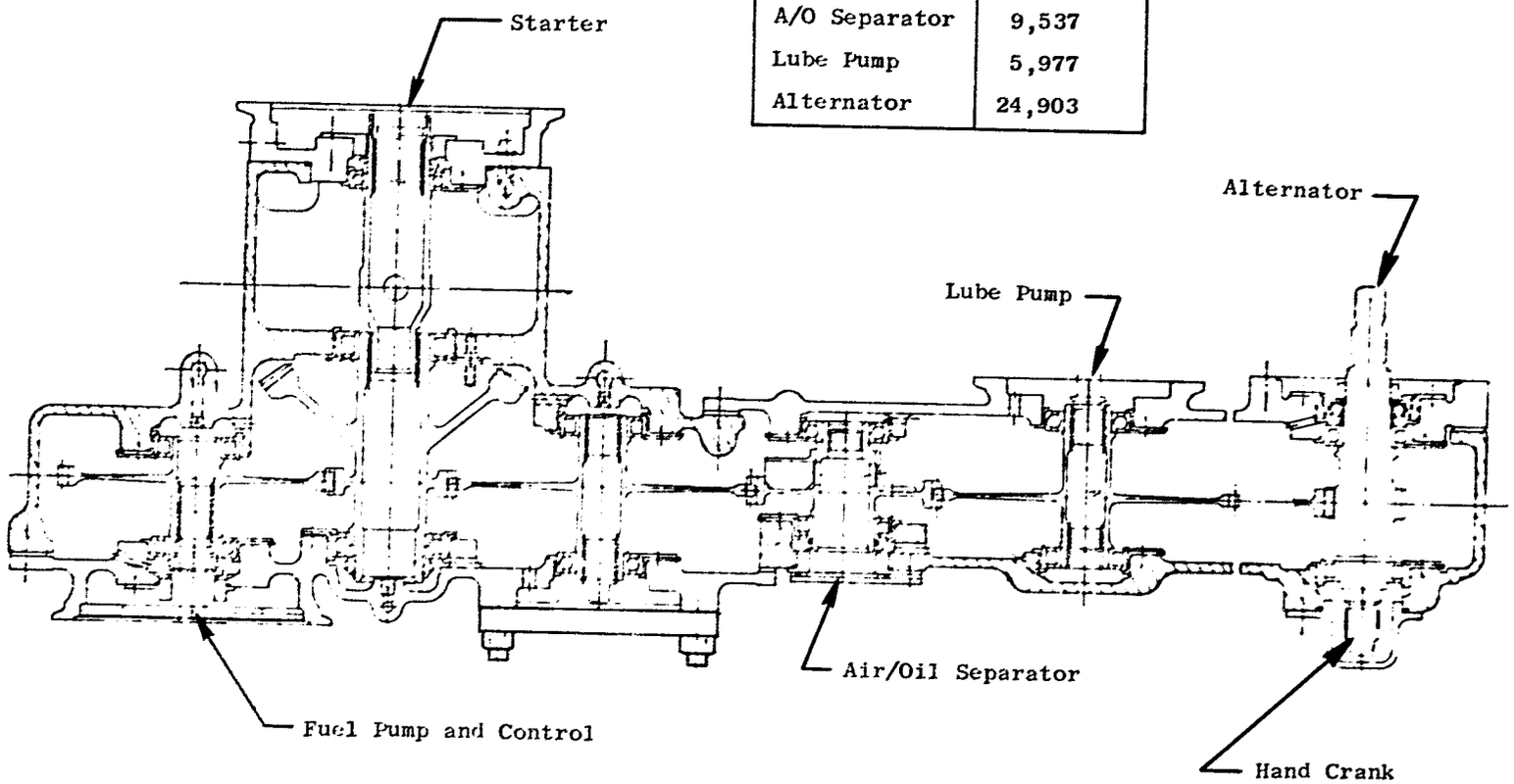

Figure 11.31. Accessory Gearbox.

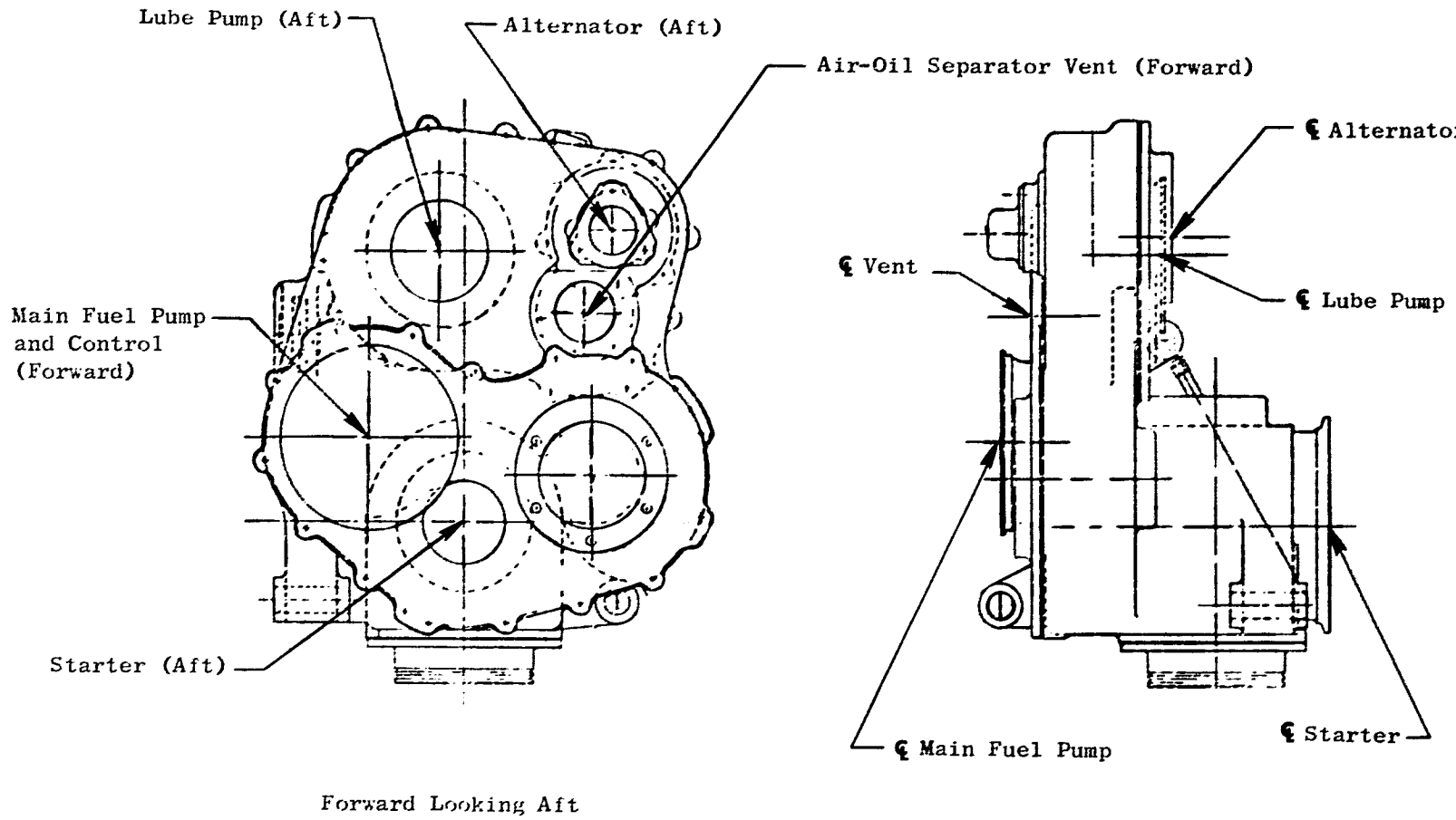

Figure 11.32. Accessory Gearbox Housing.

The fuel pump/control is the same as that of the F101 with the exception of some modifications in the control area. The lube pump is basically a CF6 lube pump with all its elements manifolded together, and a new quill drive shaft to fit the F101 gear shaft. The control alternator is adapted from the F101 engine.

The starter is based on an existing design modified to be compatible with the QCSEE accessory gearbox. These modifications include:

1. Provisions for a lubricated drive spline with oil being supplied from the accessory gearbox

2. The clutch has been adjusted to be compatible with the minimum engine idle speed

3. The QAD (quick-attach-detach) housing was eliminated from the starter and incorporated into accessory gearbox

4. The air inlet flange position has been made adjustable circumferentially

Design features of the starter include a single stage radial inflow turbine wheel, turbine nozzle, compound reduction gearing, pawl and ratchet - type engaging mechanism, and an output shaft splined to mate with the engine drive shaft.

The radial inflow turbine eliminates the need for an air access hole in the main engine mount located aft of the starter.

Shown in Figure 11.33 are the predicted starter torque characteristics at various pressure ratios. Starter torques at pressure ratios greater than 4 to 1 are above the anticipated engine lightoff point. Facility capability up to pressure ratios of approximately 5 to 1 is being provided. The program slope does not allow for optimization of starting time and it is anticipated that start time will be approximately 60 seconds.

11.6.2 Scavenge Pump

As shown in Figure 11.34, a short radial shaft connects the lower internal gearbox to a right angle drive to power the scavenge pump. This gearbox is located in the core cowl region between the fan frame mid- and aft composite rings. The gears have been selected to reduce the radial shaft speed from 19,418 rpm to the pump input speed of 6708 rpm. Radial access to the gears and shafting is accomplished by a plug in the bottom of the gearbox and an access panel in the fan flowpath liner between adjacent vanes.

The gears are carburized AISI 9310. Basic gear information is as follows:

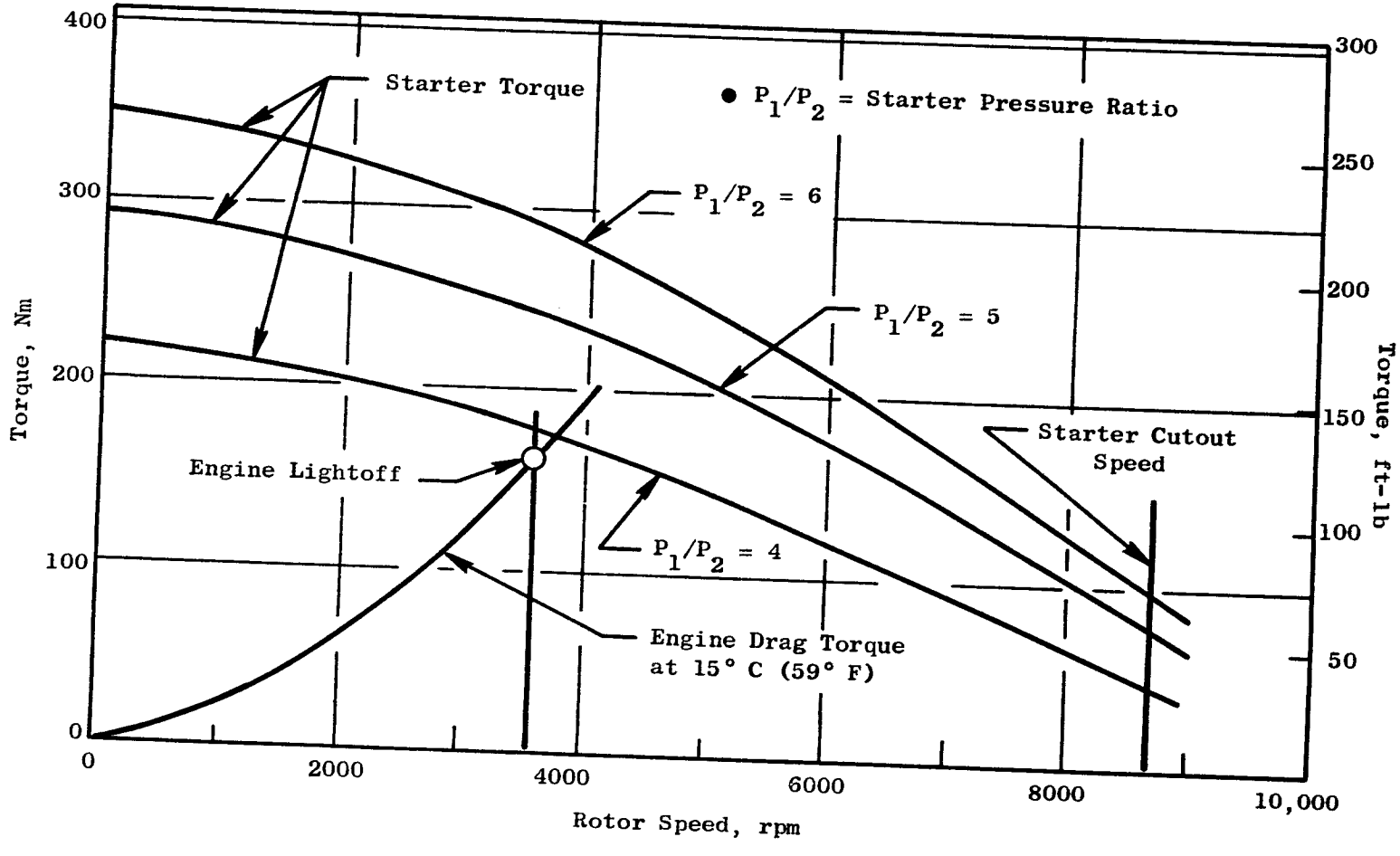

Figure 11.33. Starter Torque Vs. Rotor rpm at Various Starter Pressure Ratios.

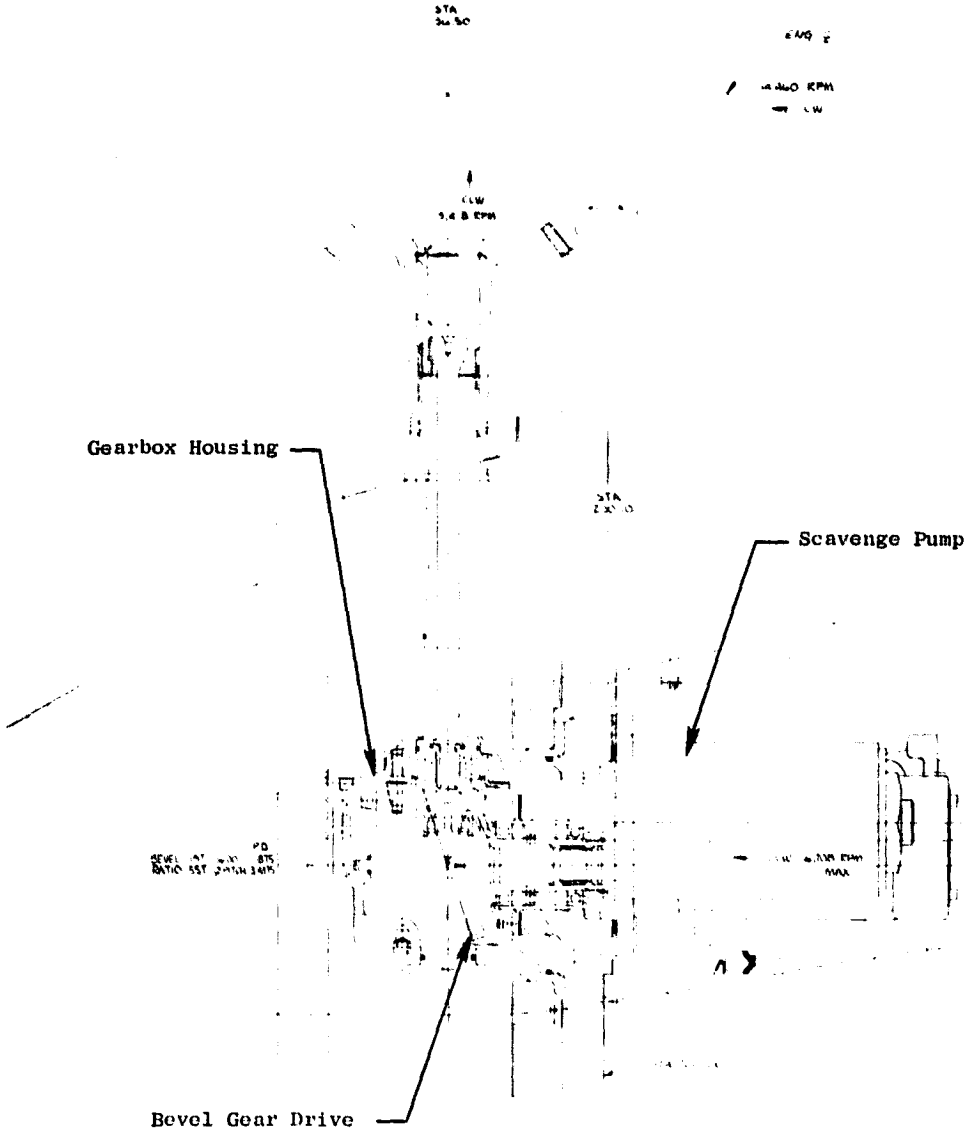

Figure 11.34. Scavenge Pump and Drive System.

	Gear Data	
	Pinion	Gear
Number of teeth	19	55
Diametral Pitch	16	16
Pressure angle	20°	20°
Spiral angle	35°	35°

The capacity of this gear set is calculated at 53 kw (71 hp), which greatly exceeds the maximum calculated pump requirements of 6.7 kw (9 hp).

Bearings are CEVM-M50 material. The lowest calculated bearing life of 52,000 hours is more than adequate for the OTW engine.

The housing and mounting adapter are case aluminum (AMS 4217).

The gear mesh and bearings are jet and splash lubricated, respectively, and the horizontal gear is shrouded to facilitate scavenging of the gear casing. Provisions are made to lubricate the pump spline.

SECTION 12.0

CONTROLS AND ACCESSORIES DESIGN

12.1 SUMMARY

The OTW experimental engine control system controls two variables: fuel flow and compressor stator angle. From a hardware viewpoint, the OTW system has been designed for maximum interchangeability with the UTW engine control system components. Both systems include a modified F101 hydromechanical fuel control and an engine-mounted digital electronic control specifically designed for QCSEE engines; however, the memory modules of the digital computer shall be unique to each engine.

New technology features to be demonstrated on the OTW experimental engine control system are:

1. Full Authority Digital Control - The OTW digital control will be programmed to provide steady-state control, transient fuel schedules, core stator schedules, and limiting fuel control functions, whereas the transient fuel schedules were performed hydromechanically on the UTW engine.

2. Failure Filter - A new Failure Indication and Corrective Action (FICA) scheme will be demonstrated on the OTW engine. The scheme employs a form of Kalman-Bucy filtering in which a model of the engine is included in the digital control program to estimate the control system sensor outputs. Model inputs are control outputs and the control system sensor outputs. If the sensors are functioning properly, the model outputs will be corrected to reflect the actual sensor outputs. But if a large error occurs between a model computed sensor value and the actual sensed value, a failed sensor is indicated and that sensor is no longer used in the control. However, the engine operation will continue with only a slight reduction in control accuracy.

To implement the electrical compressor stator control, a new fuel power servovalve assembly has been added to the control configuration as well as an LVDT to sense core stator position. The torque motor and LVDT have been designed for compatibility with the digital control circuitry from the UTW configuration so that, from an interface viewpoint, the digital controls for UTW and OTW are interchangeable.

Although the experimental engine will not include a variable exhaust nozzle, a flight-type engine would employ one; a variable nozzle was considered in the control mode definition studies. The design of a nozzle actuation system for a flight-type engine can be extrapolated from the current variable geometry actuation system design technology.

12.2 DESIGN REQUIREMENTS

The control system design is based on a number of requirements, some contractual and some resulting from the nature of the OTW engine designs. The major requirements are:

- Components - General - The system shall utilize existing controls and accessories components as applicable except it shall utilize digital electronics to perform all computational functions.

- Digital Control - General - The digital control shall be mounted on the engine and shall interface with a remotely located aircraft computer to provide selectable power management, failure indication, and failure corrective action.

- Control Variables - The OTW control system shall control fuel flow and core compressor stator vanes.

- Experimental Engine Flexibility - The system shall include the capability of making adjustments in the control strategy without hardware changes. The digital control shall be designed for ease of replacement of the control law memory modules.

- Control Capability - The system shall be capable of coordinated control variables so that STOL aircraft propulsion test investigations can be performed with the intent of achieving:

  - Thrust control throughout the specified flight map with minimum pilot workload.

  - Fast thrust response: 62 to 95% forward thrust in one second.

- Engine Protection - The system shall protect the engine from rotor overspeeds, turbine overtemperature, and excessive compressor or fan pressure.

12.3 ENGINE CONTROL SYSTEM

12.3.1 General Description

The requirements outlined in the previous section established the general structure of the control system, as shown in Figure 12.1. The digital electronic control is the heart of the system and controls the manipulated variables in response to commands representing those which would be received from an aircraft propulsion system computer. The system includes an existing (F101) hydromechanical control as called for in the program requirements. This control includes an electrohydraulic servovalve through which the digital control maintains primary control of fuel flow. The hydromechanical fuel control positions the metering valve and maintains a constant pressure drop across the metering valve to deliver the fuel flow required by the digital

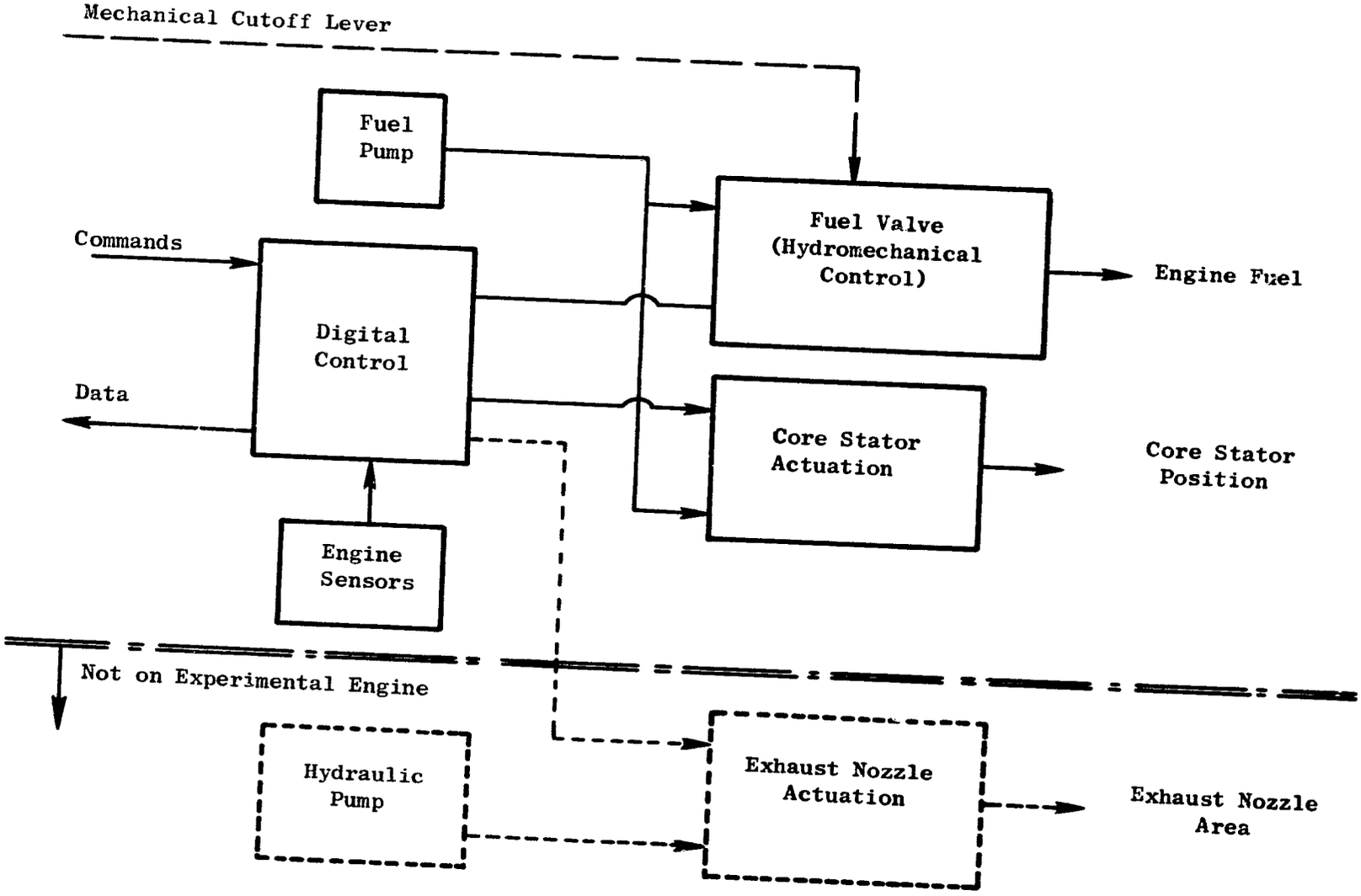

Figure 12.1. OTW Control System.

control. In addition, the fuel control provides the following: a backup core engine speed control, a positive metering valve shutoff, a metering valve position feedback to the digital control, a separate electrically operated emergency shutdown function, and a pressurized fuel output from the fuel pump to power the compressor stator servovalve and actuator assembly.

In order to achieve the operational flexibility required by the QCSEE program, the commands to the digital electronic control are being introduced through the control room elements shown on Figure 12.2. The interconnect unit, operator panel, and engineering panel are actually peripheral elements of the digital control. They provide means for the engine operators to introduce commands, to switch between available operating modes, to adjust various control constants, and to monitor control and engine data. The remote computer is a separate digital computer system supplied by NASA which can represent a typical aircraft computer, or can be used to provide other operating modes in addition to those stored in the digital control memory.

12.3.2 Automatic Control

General

The control system is designed for automatic modes in which operation of the controlled variables is integrated to respond to input demand signals simulating those which would exist in a STOL transport propulsion system. Studies have been conducted exploring a variety of potential methods for interrelating the controlled variables.

As a guideline for automatic mode studies, a list of general principles was established with advice from NASA, McDonnell-Douglas, and Boeing. The list is as follows:

1. A mechanical power lever link is assumed from the aircraft to the engine to be used to enable the fuel flow to be controlled by the digital control and for backup fuel control.

2. A digital demand signal is assumed from the aircraft computer to the engine digital control demanding percent of available thrust.

3. A digital mode signal is assumed from the aircraft computer to the engine digital control to select between available operating modes such as takeoff, climb, cruise, etc.

4. The engine digital control shall compute maximum available thrust at all flight conditions and shall be capable of setting this thrust or any portion of it as a function of a single-aircraft thrust-demand signal.

5. The engine control system shall provide selected engine safety limits, protecting against rotor overspeeds, fan or compressor stall, turbine overtemperature, and compressor discharge overpressure.

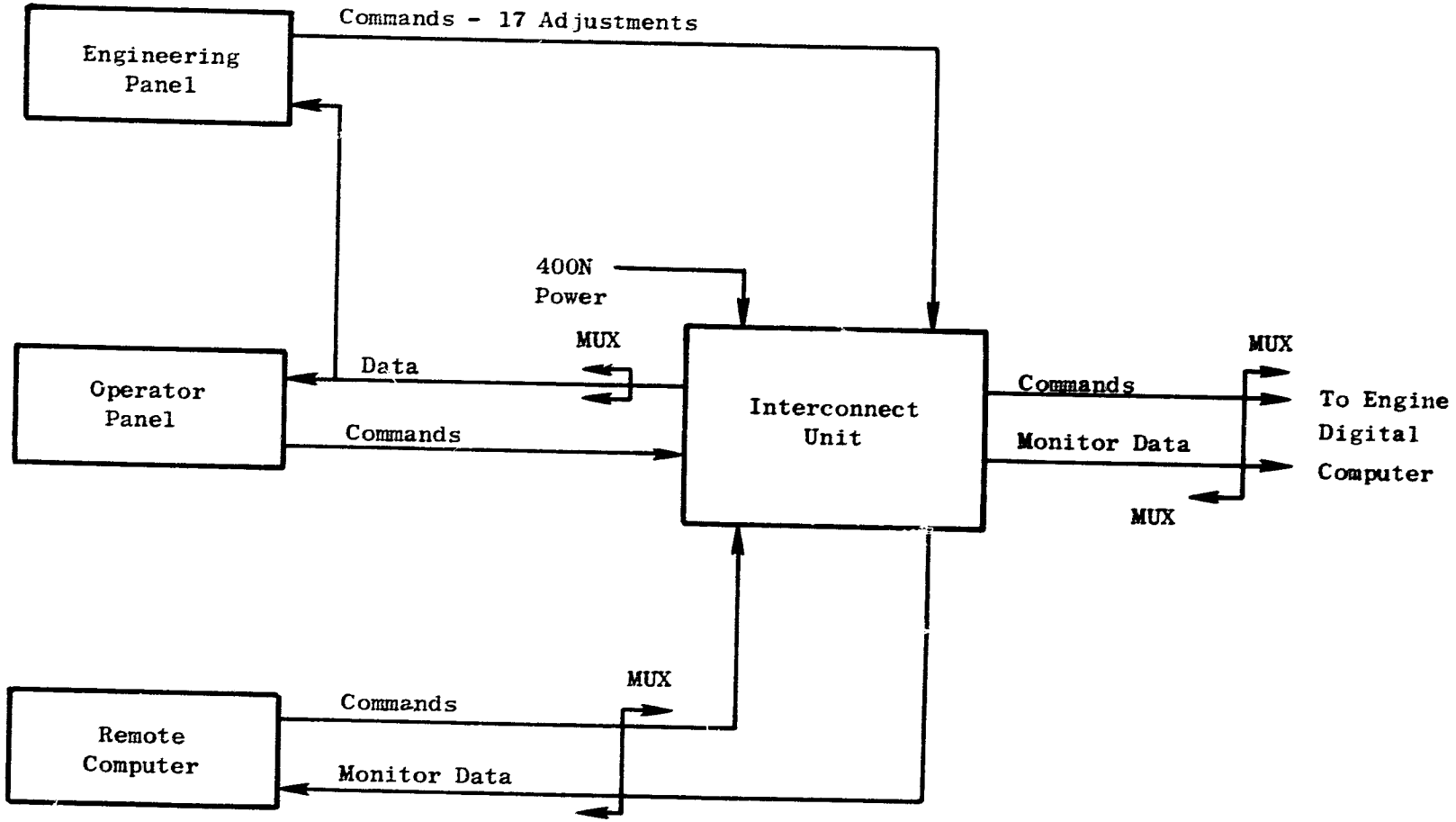

Figure 12.2. Overall Control Room Functional Block Diagram.

6. Manual control of thrust via the throttle shall be maintainable within safe limits if the engine digital control and/or aircraft digital control fails.

7. No throttle or thrust demand changes will be required during takeoff except in the event of an abort.

8. Detection of engine failure to produce commanded thrust shall be achieved through a combined indication from engine parameters in the engine digital control and a warning signal shall be transmitted to the aircraft.

Thrust Control Function

One fundamental factor in designing for automatic control is the choice of a thrust control and indication function. This function must be an accurate measure of thrust in the takeoff regime, and must be related to other sensed variables in such a manner that the engine digital control can compute and set maximum available thrust or any portion thereof anywhere in the flight envelope. A list of thrust functions evaluated for the OTW engine is given in Table 12-I.

To determine the thrust-setting accuracy of the various potential thrust control functions, tolerance studies were conducted. These studies were made up of a series of cases in which different sets of two independent variables were considered to be controlled by manipulation of fuel flow and nozzle area (it being assumed that the third OTW manipulated variable, core variable stators, will be scheduled as a function of core corrected speed as on the F101). One of the independent variables in each case was one of the candidate thrust functions. Each case was run through a computer program which combines typical control and measurement tolerances, engine component tolerances, and engine component deterioration with engine cycle characteristics to define expected variations in important characteristics such as thrust, turbine temperature, stall margins, etc. Typical results of such runs are shown in Table 12-II and the variations used in getting these results in Table 12-III.

For the experimental engine, fan speed (PCLNR) was selected as the thrust-setting parameter (fuel control) because it offers the best takeoff regime performance index established on the basis of thrust-setting accuracy and engine deterioration effects. In addition, none of the other mode selection criteria, such as stall margin variations or failure effects, are compromised with the selection of fan speed as the thrust control parameter. After experimental evaluation and development of the exhaust nozzle aerodynamics, the engine cycle will be evaluated to select the climb/cruise power-setting parameter.

One other factor to be considered in evaluating the potential thrust function is control loop stability when the function is combined with other manipulated variables in an automatic control system. This matter is discussed as a part of the next discussion.

Table 12-I. Thrust Functions Evaluated for QCSEE OTW Control.

Thrust Function	Basic Type
TP1 = P49/PTO	Core Power
TP2 = PS3/PTO	Core Power
TP3 = f(P14/PAMB) × (A18)	Gross Thrust
TP4 = f(P14/PTO) × (A18)	Gross Thrust
TP5 = f(XM11)/(A18)	Gross Thrust
TP6 = f(P14/PTO) × f_2(XM11)	Gross Thrust
TP7 = PCLNR	Gross Thrust
TP8 = T41C/T1	Core Power
TP9 = PCNHR	Core Power
TP11 = T8/T	Core Power
TP12 = [(T15 - T1)/T15] × f(XM11)	Fan Power
PT13 = WFM/PTO	Core Power

Note: Nomenclature is the same as used in the cycle and performance section with the following additions:

TP = thrust parameter

PTO = free stream total pressure

T41C = calculated T41

PS3 = the static pressure in the combustor

Table 12-II. Tolerance Study Results.

Variable controlled thrust variations* - % of Point

SLS Take-Off Power

1	2	P.I.**	FN	T41	SM12	XM11
WFM/PTO	PCNL	2.1	1.8	1.0	6.8	1.6
WFM/PTO	XM11	2.05	1.7	1.0	6.7	1.7
WFM/PTO	A8	1.7	1.4	1.0	4.6	2.2
WFM/PTO	XM15	1.9	1.5	1.0	8.8	1.6
P14/PTO	PCNL	2.2	2.1	2.0	7.3	1.4
P14/PTO	SM11	2.45	2.4	2.1	7.0	1.7
TP6	A8	2.15	2.1	2.2	4.7	2.7
TP6	XM15	2.25	2.2	2.2	8.8	3.7
TP6	XM11	2.4	2.4	2.1	7.9	1.7
TP6	PCNL	2.45	2.4	2.0	8.7	1.6
PS3/PTO	A8	2.25	2.0	2.5	4.7	2.5
PS3/PTO	XM15	2.5	2.2	2.5	9.1	3.4
PS3/PTO	XM11	2.7	2.4	2.5	8.3	1.7
PCNL	A8	1.65	1.5	1.9	5.0	1.1
PS3/PTO	PCNL	2.9	2.5	2.4	9.4	1.7
XM11	A8	2.4	2.2	2.2	5.0	1.7

*Variations are root-square-sum stackup of tolerances and variation listed in Table 12-VIII.

**Thrust performance indicator = FN variation + 1/2 deterioration effects.

Table 12-III. Tolerances and Variations Used.

(Note: All are ±% of point unless noted otherwiae)

Control Variables		Engine Characteristics	
Variable	SLS Takeoff	Characteristic	Variation
PCNLR	0.52	Fan airflow	0.5
A8	1.2	Fan eff.	0.5
XM11	1.65	Core compre. eff.	0.5
P49/PTO	1.07	P4/P3	0.5
PS3/PTO	0.97	Comb. eff.	0.3
TP3	5.5	HP turb. eff.	1.0
TP4	3.74	A49	1.0
TP5	1.74	LP turb. eff.	1.0
TP6	1.85	P18/P14	0.2
T41C/t1	1.04	P56/P5	0.5
T49/T1	1.05	Interstage Bld.	1.0
T8/T1	1.04	P3 Bld.	1.0
PCHHR	0.30	HP extract.	18.6 kw (25 hp)
TP12	2.41	Cooling Bld.	0.55
WFM/PTO	1.43	AE11	0.1
P14/PTO	1.11		
P14/PTO(P/P)	0.93		

Control Modes

Another task necessary in the definition of the automatic control was the identification and evaluation of control modes, that is, the interrelationships between manipulated and controlled variables.

Key operational requirements applicable to establishing automatic control modes at various conditions are:

- Takeoff - Set guaranteed maximum static thrust or percent thereof
- Climb - Set guaranteed maximum installed thrust or percent thereof
- Cruise - Attain minimum installed sfc at required thrust level.
- Descent - Maintain sufficient core speed for air conditioning and power extraction
- Approach - Fast thrust response at readily controlled level up to guaranteed maximum
- Ground Idle - Minimum thrust
  - Low exhaust pollution
  - rpm sufficient for centrifugal anti-icing

A simplified schematic of the fuel control system is shown in Figure 12.3. The fan speed (N1) demand to set percent of thrust is generated as a function of power lever angle, inlet temperature, and inlet pressure. The inlet temperature provides a corrected fan speed reference, and the inlet pressure resets the reference for altitude operation. The N1 demand then is compared with N1, and metering valve rate demand is generated. The rate demand is compared with the metering valve rate to generate a servovalve control signal that is used to position the metering valve. This interloop is employed to provide stable responsive control of the fuel metering section. Acceleration and deceleration schedules and temperature and pressure limits that bound the operation of the thrust-setting governor to achieve safe operation of the engine are input to the control strategy at the minimum and maximum selectors shown in Figure 12.3.

Core Stator Control - A simplified schematic of the core stator control is shown in Figure 12.4. The stators are scheduled as a function of corrected core speed. Core inlet temperature, T25, is calculated as a function of inlet temperature and fan speed. This eliminates the need for a separate T25 sensor.

One of the major requirements for this engine is to provide rapid thrust response during the approach phase of the flight profile. This will be accomplished through the use of stator reset logic as shown in Figure 12.5. When the reset is activated, the reset schedule will cause the stators to close as the power demand is reduced. This schedule will be designed to maintain the core speed at or near takeoff speed. Therefore, when the rapid

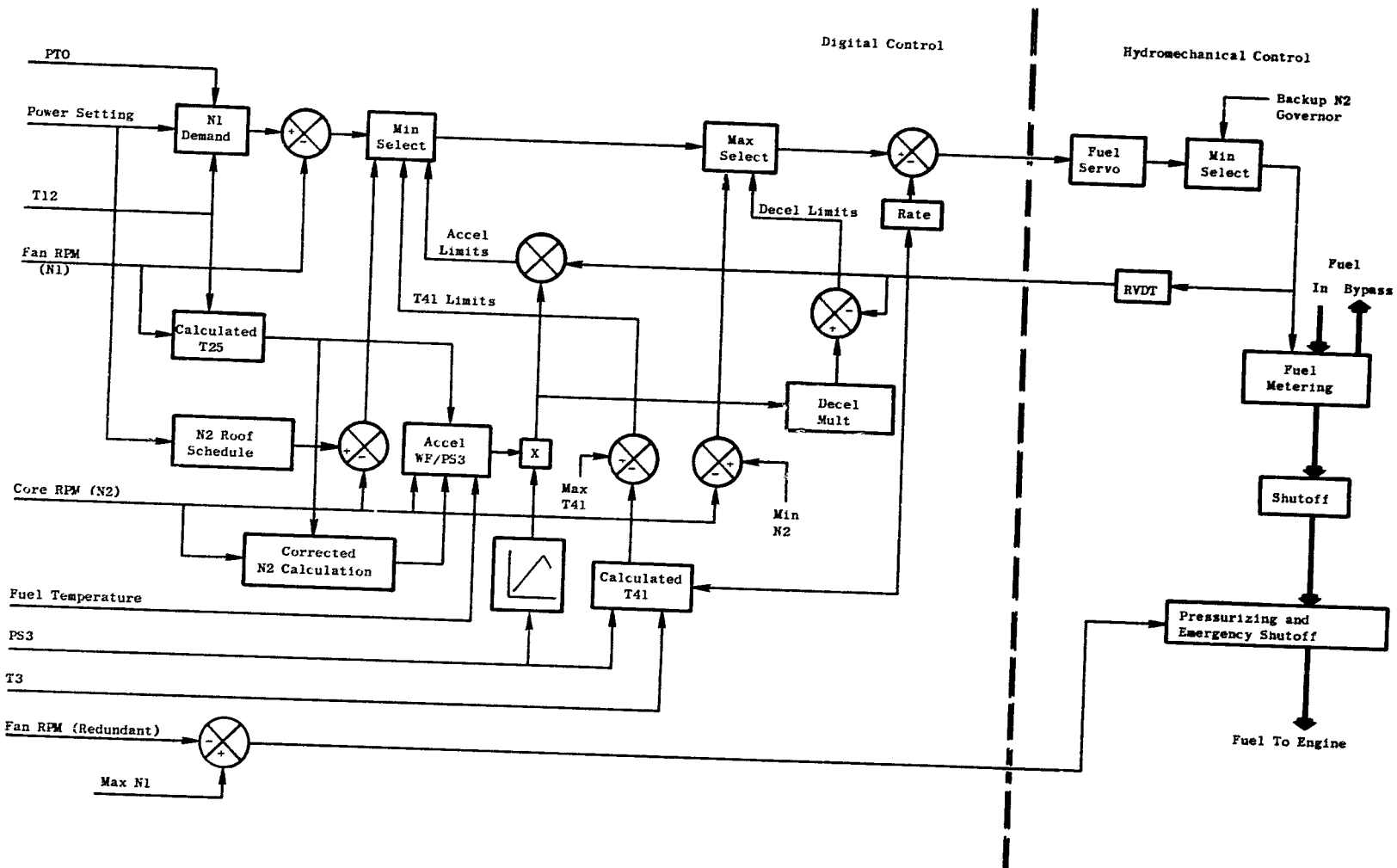

Figure 12.3. OTW Fuel Control Block Diagram.

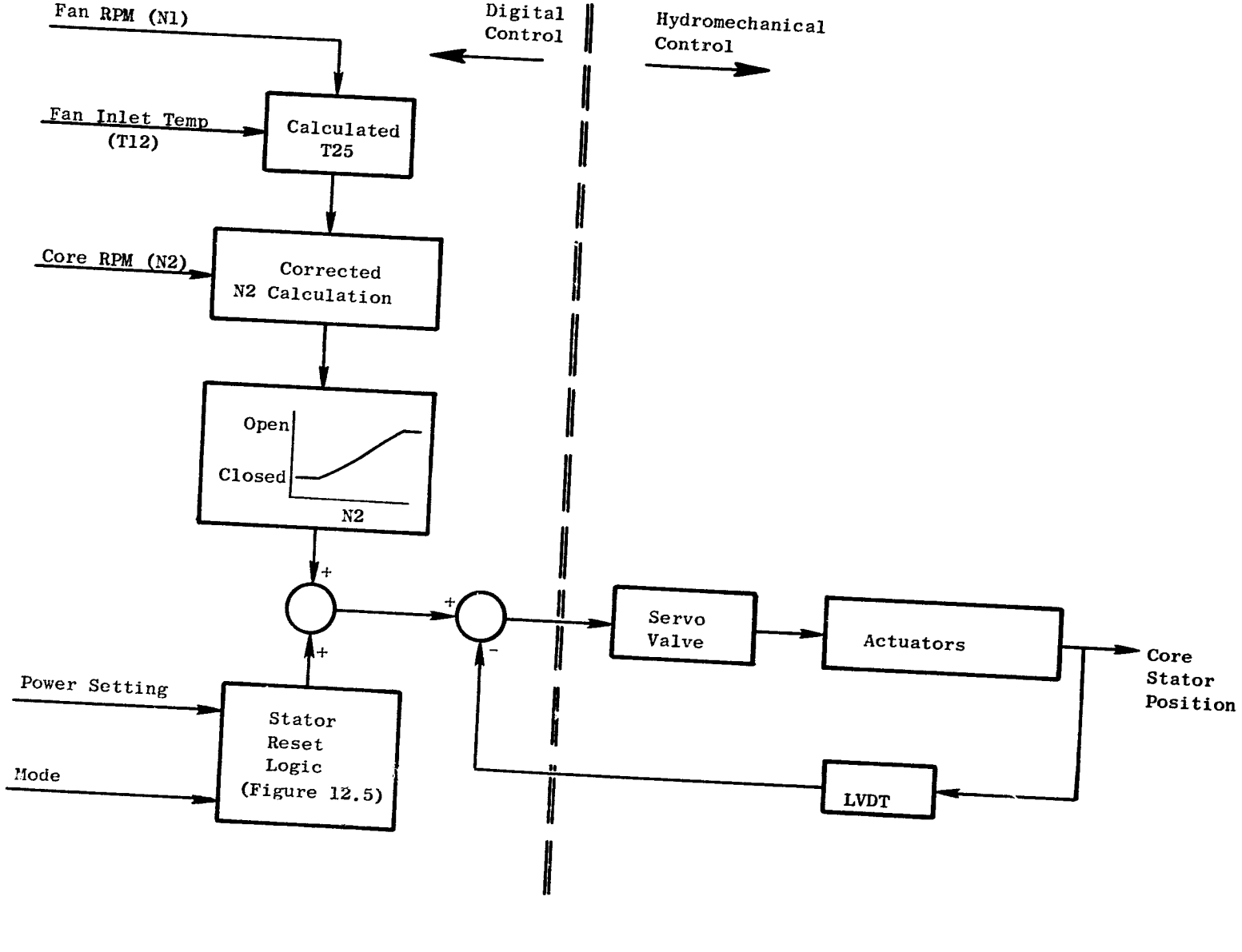

Figure 12.4. OTW Core Stator Control.

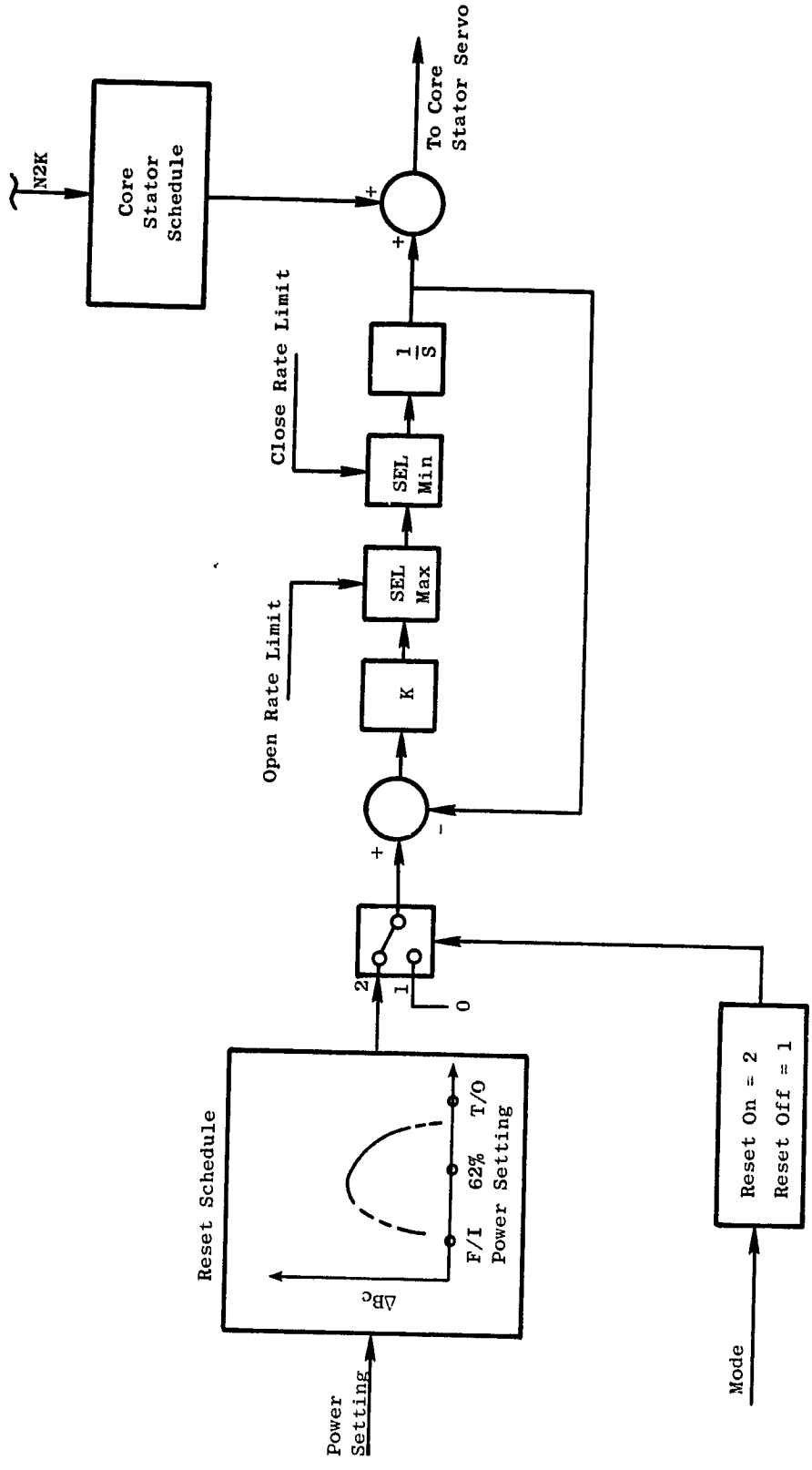

Figure 12.5. Core Stator Reset Logic.

thrust response is desired, only the fan will have to be accelerated, since the core will already be at full speed.

Transient Response - Once the basic control mode was defined, it was integrated into a hybrid computer model of the engine and control system in order to evaluate stability and response characteristics. Numerical values in the model were set in several ways, some being based on engine limits, some on linear stability analyses, and some on past experience. The model was run and adjustments were made as necessary to provide optimum stability. As a result of this process the model was refined to provide satisfactory steady-state and transient control.

After the numerical values in the model were refined for optimum stability, the model was run to explore the transient response characteristics of the chosen control mode, particularly at approach conditions, where fast response is most important. A typical data trace from one of these runs is shown in Figure 12.6. Figure 12.7 shows the engine response characteristics with and without stator reset as a function of control power setting. This figure also shows that the chosen control mode meets the QCSEE program goal of one second from 62 to 95 percent thrust at approach conditions. Figure 12.8 shows the predicted characteristics of thrust versus time for various control power settings. The transient response data indicates that a significant improvement in engine response time can be obtained using the stator reset technique discussed in the previous section.

Safety Limits

The control includes a number of safety limits which are briefly described below:

T41 Limit - Turbine inlet gas temperature (T41) is calculated in the digital control from the compressor discharge temperature (T3), fuel flow, and compressor discharge pressure; fuel flow is limited to prevent this calculated T41 from exceeding a predetermined limit.

Acceleration Limit - An acceleration fuel schedule (which is a function of core rpm, core compressor inlet temperature, and core compressor discharge pressure) is incorporated in the digital control, and fuel flow is prevented from exceeding this schedule. The schedule is designed to provide satisfactory starts and rapid acceleration without core compressor stall or excessive turbine temperature transients.

Deceleration Limit - A deceleration fuel schedule which is a fraction of the acceleration schedule is incorporated in the digital control, and fuel flow is not allowed to go below this schedule except in the case of operation of the emergency shutdown noted below. This schedule is designed to provide rapid engine deceleration without loss of combustion.

Fan Speed Limit (Normal) - The digital control senses low pressure turbine rpm and limits fuel flow to prevent exceeding a predetermined normal fan rpm limit.

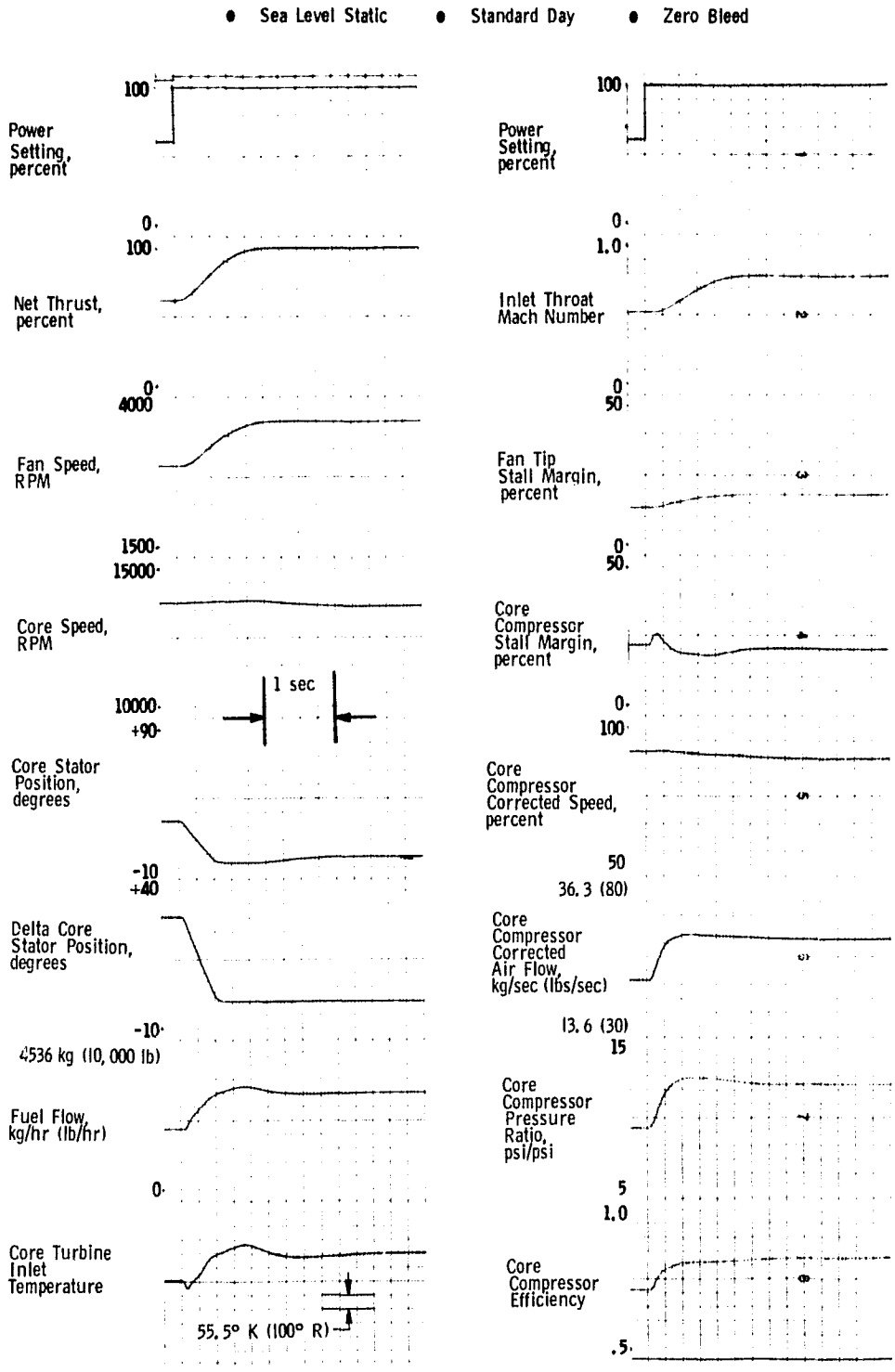

Figure 12.6. Typical Transient Response Data Trace.

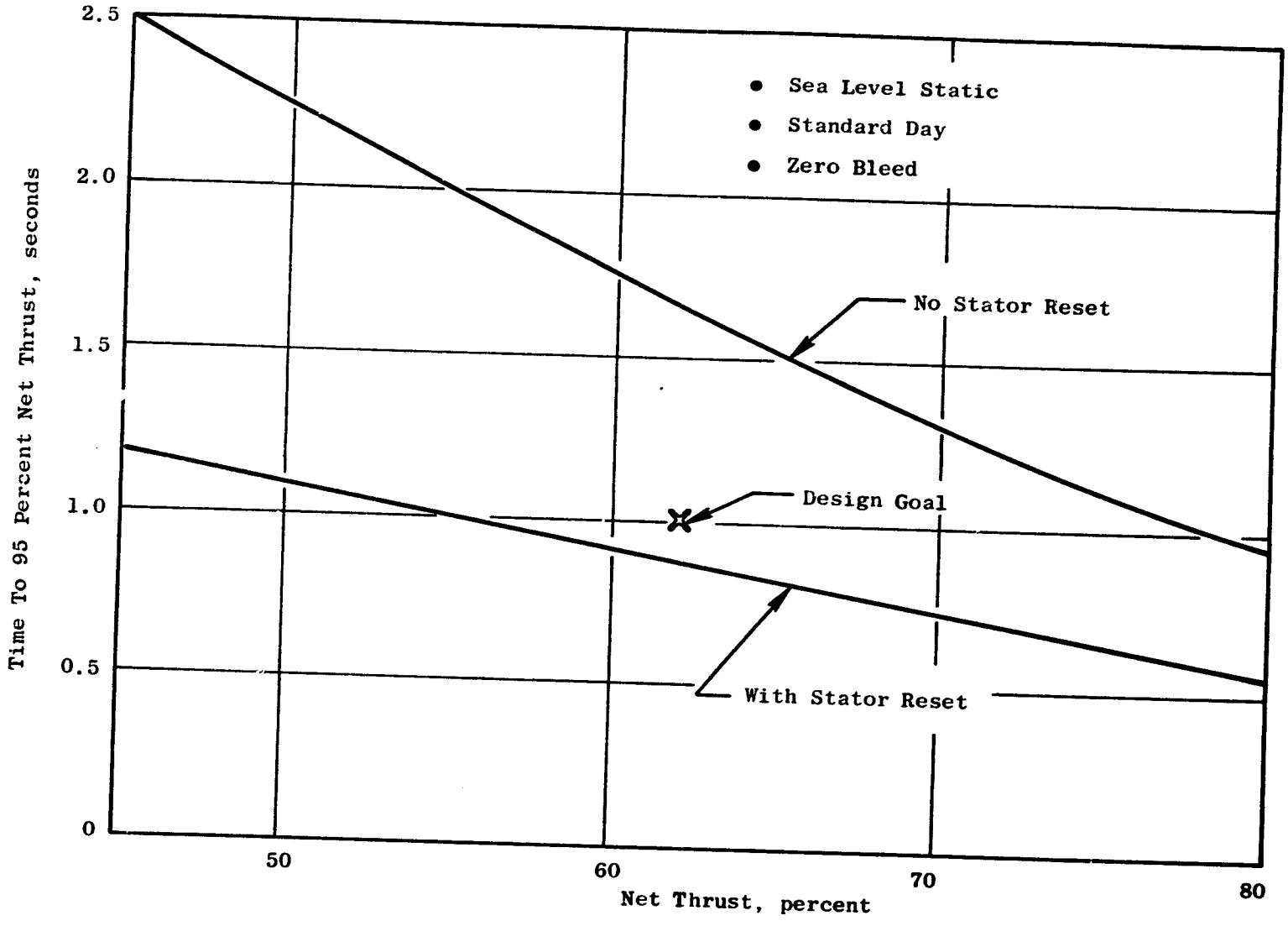

Figure 12.7. Transient Response.

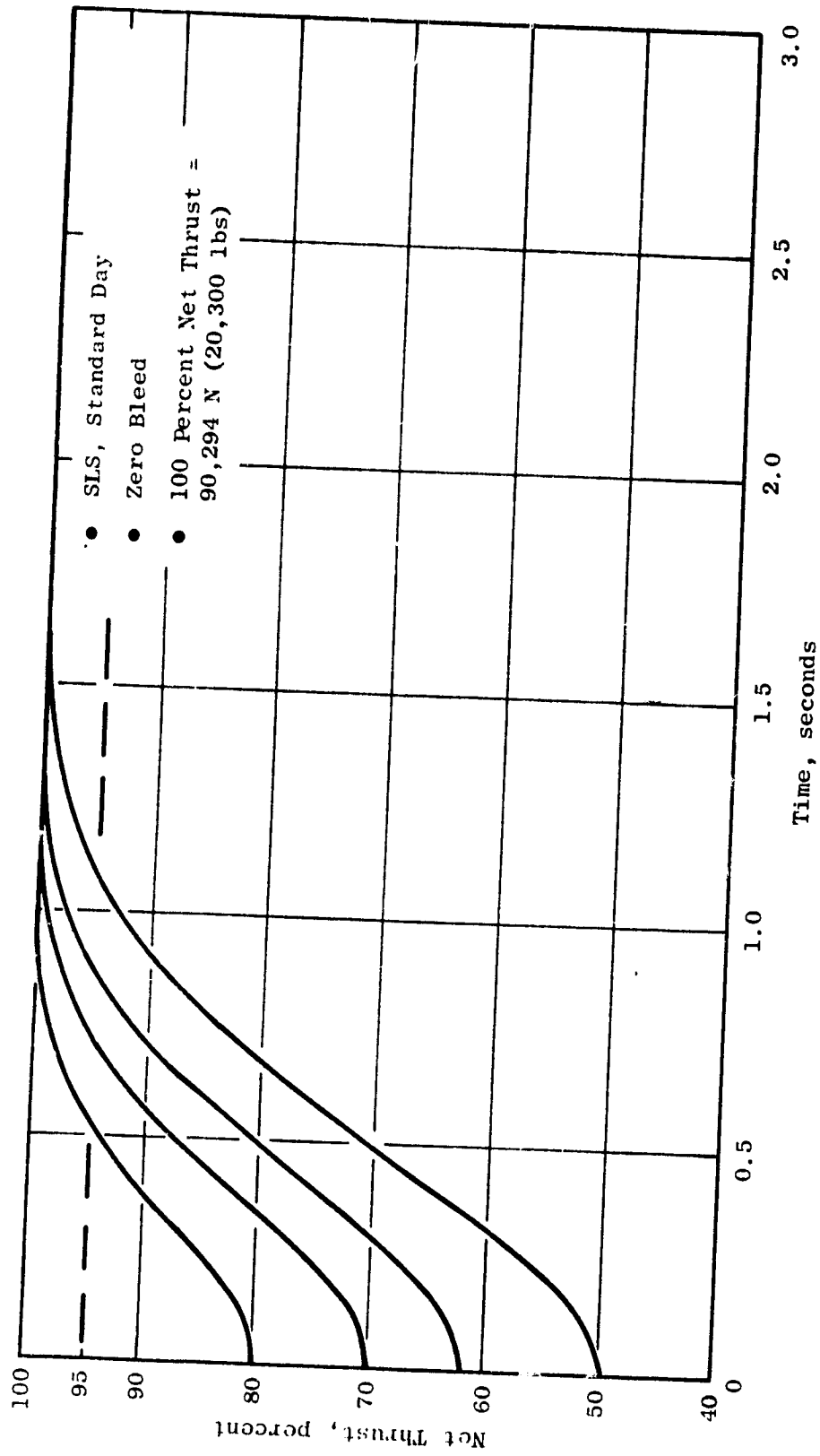

Figure 12.8. Transient Response with Core Stator Reset.

Core Speed Limits - Both the digital and hydromechanical controls sense core speed and provide fuel flow limiting to prevent core overspeed.

Emergency Shutdown - This feature provides complete fuel shutoff in the event that low pressure turbine rpm exceeds an absolute maximum limit or a preset rate of change. All elements of this feature are electrically isolated from the remainder of the system so that it also protects against system fault which might cause fan overspeed.

12.3.3 Digital Control Subsystem

The digital control subsystem, shown in Figure 12.9, consists of an engine-mounted digital control and command and monitor peripheral equipment located in the control room.

The digital control performs the computational requirements for the overall engine control system based on the demands received from the command and monitor equipment and other parameters received from engine-mounted sensors. In addition to generating control signals to manipulate fuel flow and compressor vane angle, the digital control transmits engine and control data to the command-and-monitor equipment in the control room.

The command-and-monitor equipment has a number of features to provide flexibility in testing an experimental engine. These include the following (1) several modes of operation, (2) selected adjustment inputs to modify steady-state and dynamic characteristics of the control strategy, (3) a fault indication and corrective action program, and (4) a comprehensive control and engine parameter display system which provides conditioned-monitoring features for the experimental engine.

A comprehensive failure filter employing a form of Kalman-Bucy filtering technique will be demonstrated on the OTW for the first time. The scheme, shown in Figure 12.10, includes a model of the engine for the purpose of estimating control sensor outputs. The engine model operates on the fuel control and stator control drive signals (IWFTM and IβC) and the control sensor data to produce an estimate of the control sensor outputs. For small deviations, between the sensor outputs and the computed values, the computer values will be adjusted to reflect the value of the sensor outputs through the "K" matrix shown in Figure 12.10. If, however, the deviation becomes larger than some predescribed limit, a failed sensor is indicated; the computed value will be inserted into the program in place of the sensor value.

Fault indication is a part of the digital control strategy. Four fault tests are performed by the digital control. These are as follows:

1. Digital control fault test to check out the analog-to-digital and digital-to-analog converters and certain portions of the digital control associated with test.

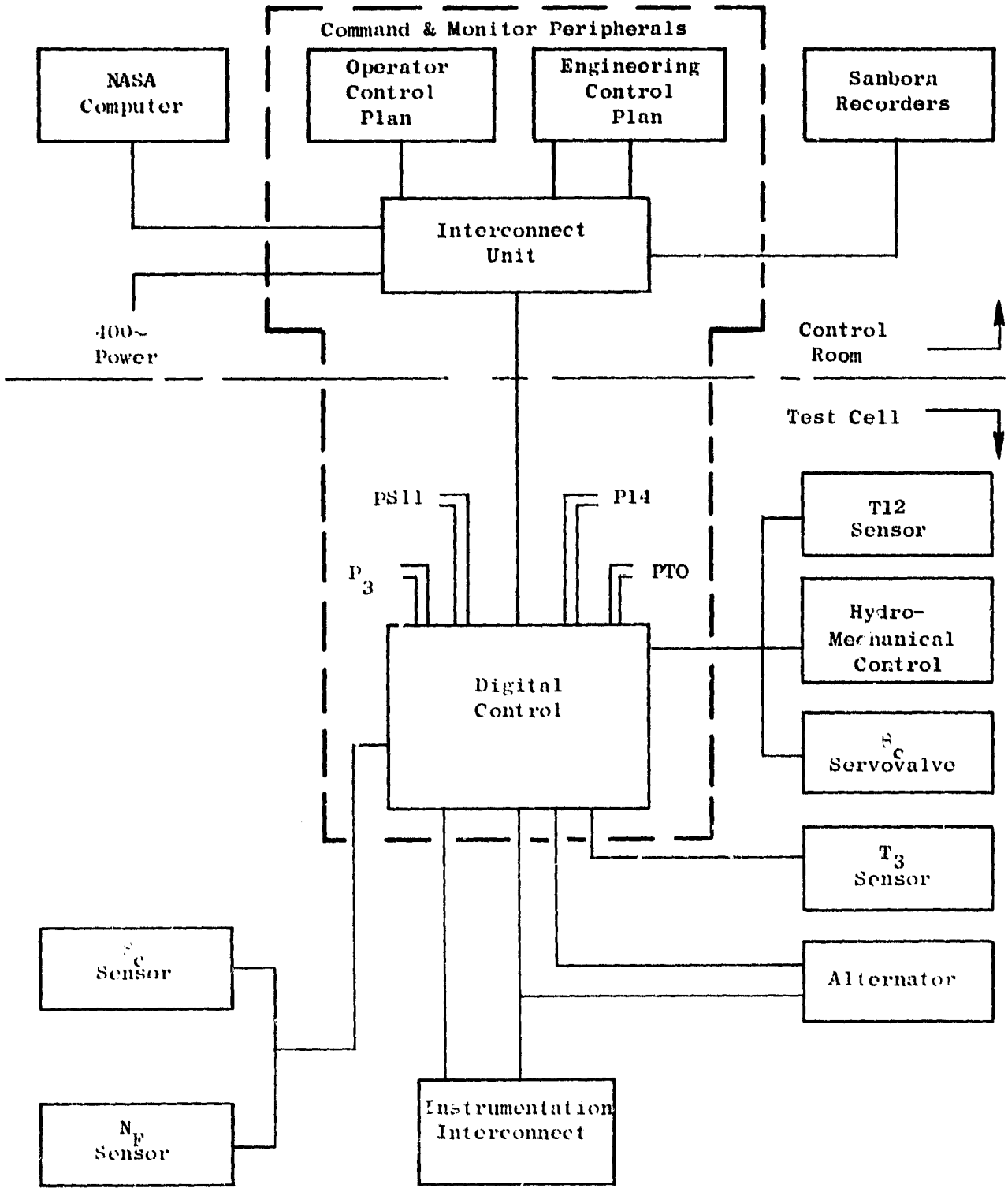

Figure 12.9. Digital Control Subsystem.

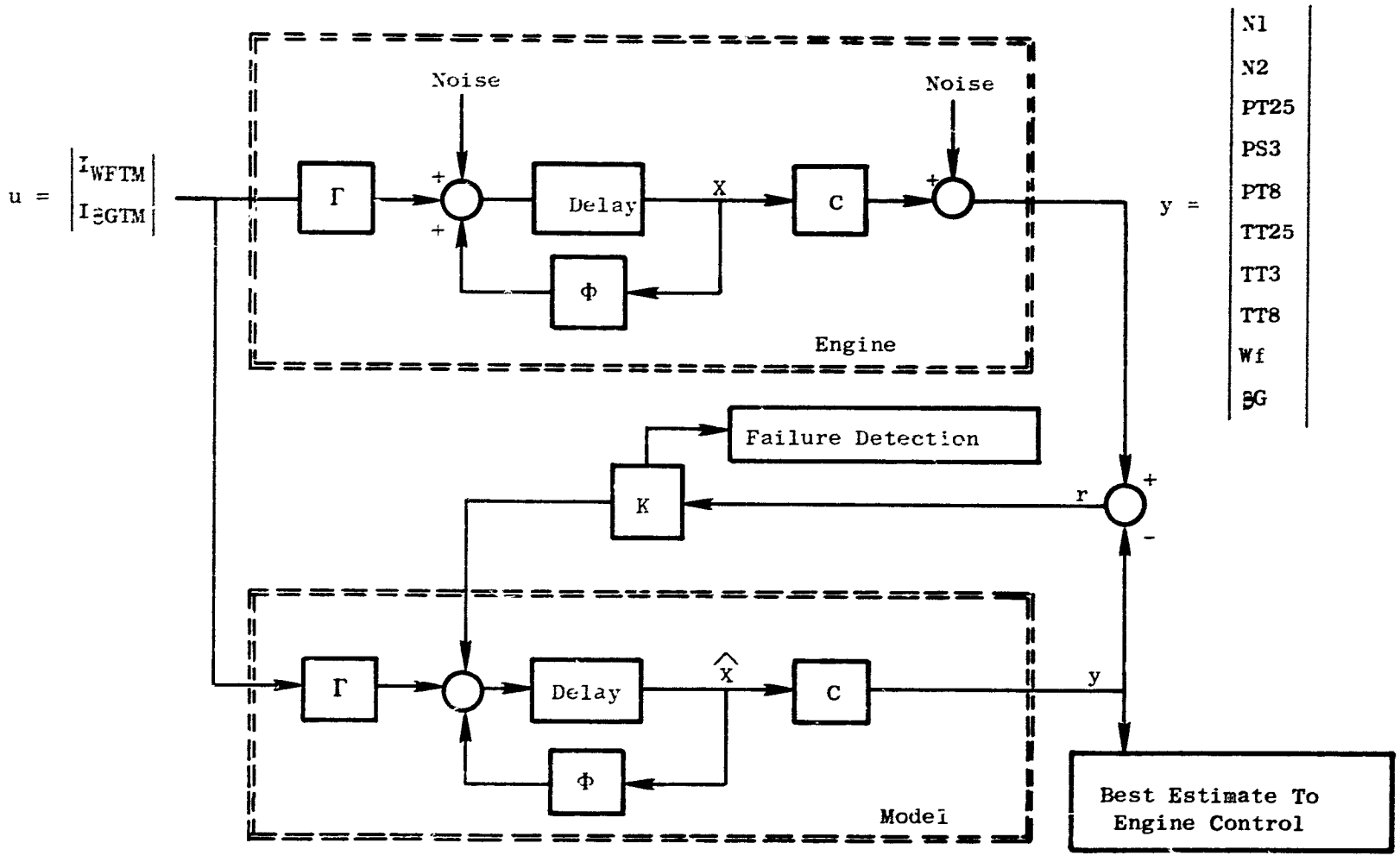

Figure 12.10. Failure Indication and Corrective Action.

2. High engine vibration levels.
3. Low pressure turbine rotor overspeed.
4. Loss of command data link.

For the experimental engine, the corrective action for the fault conditions No.'s 1, 2, and 3 is to reduce or shut down fuel flow, and the corrective action for fault condition No. 4 is to fail-fixed at the last true inputs. Fault status is part of the monitoring system. If a fault occurs, a fault discrete lights on the operator control panel and the fault condition may be uniquely identified on the engineering control panel.

The following listing contains 48 control and engine parameters and can be read out from the command-and-monitor equipment in the control room.

QCSEE OTW Monitor Data

1. Fuel control torque motor current
2. Compressor stator torque motor current
3. Fuel flow
4. Calculated turbine inlet temperature
5. Inlet Mach number
6. Compressor discharge to inlet pressure ratio
7. Electrical power demand
8. Fan speed
9. Core speed
10. Compressor stator angle
11-15. Fault identification data
16. Fuel mode control indication
17. Hydromechanical power lever angle
18. Inlet temperature
19. Inlet total pressure
20. Fan discharge to inlet differential pressure
21. Inlet total-to-static differential pressure
22. Compressor discharge pressure
23. Metering valve position
24. Compressor discharge temperature
25. Mode control demand input
26. Fuel temperature
27. Exhaust gas temperature
28. Engine oil inlet temperature
29. Scavenge oil temperature
30. Engine oil inlet pressure
31. Scavenge oil pressure
32. Fan discharge temperature
33. Low pressure turbine discharge pressure
34. Gearbox interrace bearing temperature
35. Engine horizontal vibration
36. Engine vertical vibration
37-48. Failure filter data

The above data may be read from a number of stations in the control room. Any of the 48 parameters may be selected for display on a Binary Coded Decimal readout on the engineering control panel, and all parameters are transmitted serially to the remote (NASA) computer binary form. Parameters 1 through 15 are available for real-time analog recording at the interconnect panel, and any of the 48 channels may be selected for analog recording as a 16th channel. Full parametric digital readouts of parameters 3 through 10 are displayed on the operator panel. Torque motor currents (items 1 and 2) are displayed on analog meters on the engineering panel.

Digital Control

The digital control accepts operational input demand and engine parametric information in the form of AC and DC analog and digital signals and uses this information to generate engine control signals and engine condition-monitoring data. A simplified block diagram of the control is shown in Figure 12.11. The analog signals are conditioned to a standard voltage range and then multiplexed to an analog-to-digital (A/D) converter. The output of the A/D converter is fed to the central processor unit (CPU) where all necessary calculations are performed. The CPU output is fed into two circuits. One circuit is a multiplexer that sends data out to the aircraft. The other circuit is a digital-to-analog (D/A) converter circuit. The output of the D/A converter is fed to sample and hold circuits and, subsequently, to the output drive circuits. The drive circuits provide signals to the torque motors that are used to provide engine control. Power to the control is provided by an engine-mounted alternator. The alternator AC signal is converted to the necessary regulated DC voltages.

Digital Control Inputs and Outputs

The QCSEE digital control inputs and outputs listed in Tables 12-IV, 12-V, 12-VI, and 12-VII are described below.

Inputs to the digital control consist of four classifications: (1) instrumentation signals, (2) sensor and transducer signals, (3) power signals, and (4) digital signals. Table 12-IV is a list of the instrumentation input signals. These signals are all 0-10 volt levels and the only signal conditioning required is an isolation amplifier in the digital control. Presently there are 15 instrumentation signals being used and there are four spare inputs that may be used if needed.

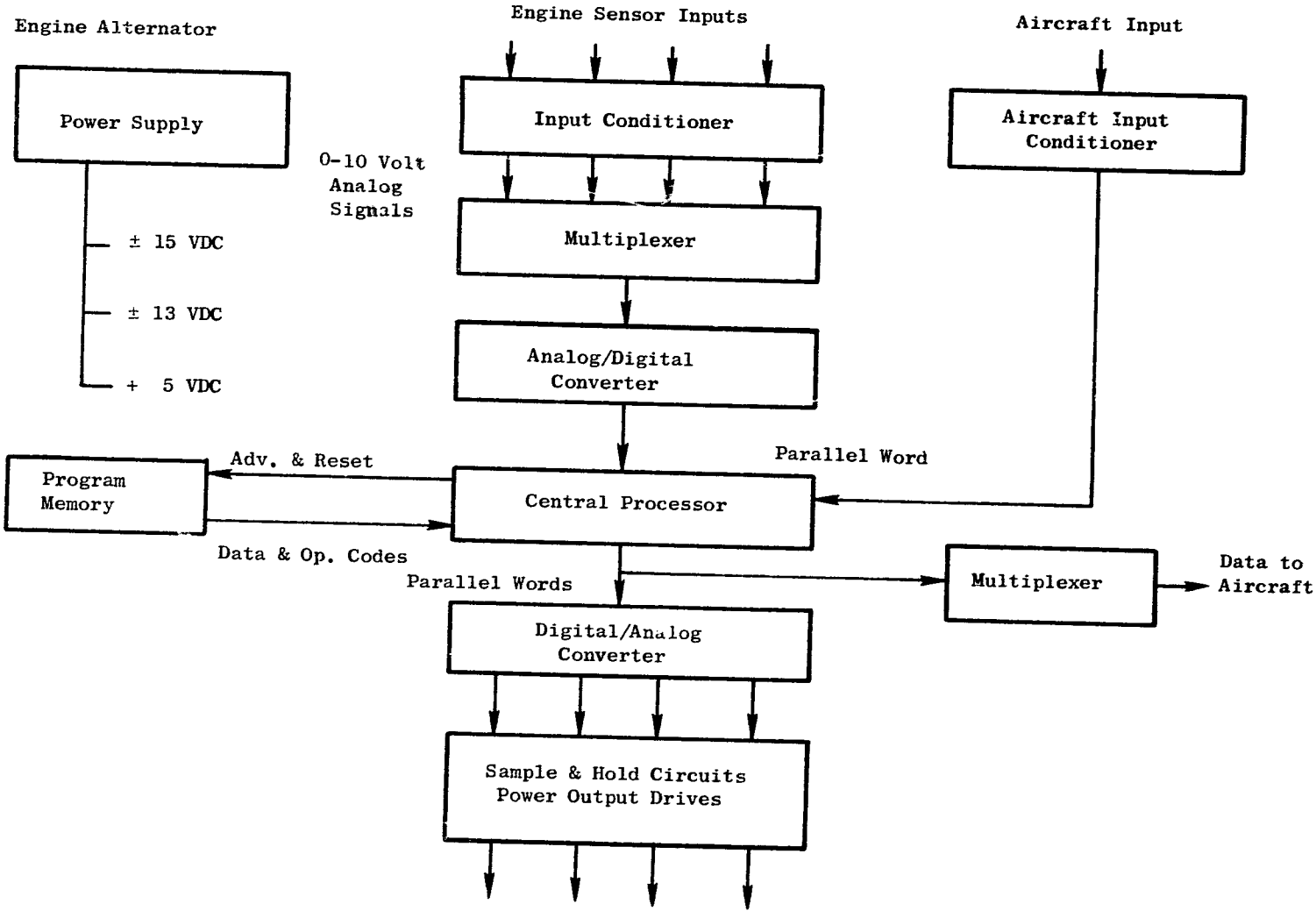

Figure 12-11. Digital Control Schematic.

Table 12-IV. Digital Control Instrumentation Input Signals.

1. Spare
2. Fuel temperature
3. WF manifold pressure
4. EGT
5. Fuel flow
6. Lube pressure
7. Lube scavenge pressure
8. Lube oil inlet temperature
9. Lube scavenge oil temperature
10. T25
11. P5 pressure
12. Gearbox inner race bearing temperature
13. Horizontal vib
14. Vertical vib
15. Core stator position
16. Spare
17. Spare
18. Spare
19. Spare

Table 12-V. Digital Control Engine Sensor and Transducer Signals.

1. Power lever RVDT (rotary variable differential transformer)
2. Fuel metering valve RVDT
3. Core stator LVDT (linear VDT)
4. N_{1T} (LP turbine rpm No. 1)
5. N_{1T} (LP turbine rpm No. 2)
6. T3 (compressor discharge total temperature)
7. T12 (fan inlet total temperature)
8. PS3 (compressor discharge static pressure)
9. PT0 (engine inlet total pressure)
10. PT0-PS11 (inlet static pressure)
11. P14 (fan discharge total pressure) - PT0

Table 12-VI. Alternator and Digital Signals to Digital Control.

1.	N2 alternator winding	
2.	N2 alternator winding	
3.	Command data	
4.	Command Sync.	Digital Signals - 3 twisted pairs to digital control
5.	Command clock	

Table 12-VII. Digital Control Outputs.

1.	Fuel metering valve torque motor current (TMC)	
2.	Core stator LVDT excitation	
3.	Fuel metering valve RVDT excitation	
4.	Power lever RVDT excitation	
5.	Fan nozzle LVDT excitation (flight version only)	
6.	Core stator TMC	
7.	Emergency shutdown TMC	
8.	Monitor sync.	
9.	Monitor clock	Digital Signals - 4 twisted pairs to control room interconnect unit
10.	Reset	
11.	T12 excitation	

The sensor signals are shown in Table 12-V and come from various transducers and sensors located on the engine. Some signals are AC and some are DC and have various voltage ranges. These signals are conditioned to a standard 0-10 volt level in order to be used by the digital control.

The remaining inputs are the alternator signals that provide the power to the digital control and the digital signals that feed digital data to the control. These are listed in Table 12-VI.

The QCSEE digital control outputs are of three types: (1) torque motor drive signals, (2) transducer and sensor excitation signals, and (3) digital signals. Table 12-VII lists these.

Digital Control Functional Description

Input Signal Conditioners

The input signal-conditioning circuits are of two types: (1) isolation amplifiers and (2) processing amplifiers. The isolation amplifiers isolate the instrumentation output amplifiers from the control. These amplifiers prevent loading problems.

The signal processing amplifiers differ in design depending on the type of input signal. These consist of demodulating circuits, frequency-to-DC converters, and straight gain-setting amplifiers. These circuits condition all input signals to a standard 0-10 volt level over the signal range of interest. The proper gains and offsets to accomplish this are set in these amplifiers. The outputs of both isolation amplifiers and processing amplifiers are fed into an analog multiplexer.

Analog Multiplexer

The analog mulitplexer circuit consists of three 16-channel multiplexer chips making a total of 48 signals which can be multiplexed. Each channel can be addressed separately depending on the signal needed by the digital control at any particular time. The outputs of the three multiplexer chips are connected together and are fed to a sample and hold circuit. The output of this circuit goes to an A/D converter circuit.

Analog-to-Digital (A/D) Converter

The A/D converter is a 12-bit successive approximation-type circuit with a conversion time of 24 microseconds. The input to the A/D converter is a 0-10 volt DC signal and is converted to a digital word that corresponds to the particular voltage at the converter input. For 12 bits, there are 4096 possible words. The output of the A/D converter is fed to a serial digital multiplexer and from there to the central processor unit (CPU).

Central Processor Unit (CPU)

The CPU along with the program memory form the digital computer of the digital control. This circuit contains the arithmetic logic unit, the control and timing unit, the scratch pad memory, the accumulator, and other logic circuits necessary to carry out all calculations to generate the engine control signals and other functions. This unit accepts the A/D converter signals and the aircraft digital signals via the serial digital multiplexer. A block diagram of the CPU is seen in Figure 12.12. The output of the CPU is fed to a digital multiplexer whose output transmits data to the aircraft. The CPU output also goes to a digital-to-analog converter.

Digital-to-Analog (D/A) Converter

The D/A converter has a 12-bit digital word as an input and the output is one of 4096 possible voltage levels corresponding to the digital input. The output of the D/A is bipolar and will be in the -5 volt to +5 volt range. The D/A output is fed to the output drive circuits.

Output Drive Circuits

The output drive circuits consist of sample and hold circuits and the output circuits needed to power the valves, torque motors, etc. As the digital control performs the programmed calculations, the output of the D/A converter is sampled at the proper time and stored in a sample-and-hold circuit. This value is held until the next time the program calls for this particular sample-and-hold circuit to be pulsed and the next value of the calculation to be stored. The output of each sample-and-hold circuit is fed to a driver amplifier. The outputs of the driver amplifiers are used to actuate the torque motors and the valves that provide engine control.

Other Circuits

Transducer excitation circuits also are provided in the digital control. A 2.048-mHz clock signal is used to generate a 3011-Hz, 20-volt, peak-to-peak sine wave signal. This signal is fed to two transducer driver amplifiers whose outputs are used to provide the excitation voltage for the position transducers (VDT's). The 3011-Hz signal also is used as a demodulate reference.

The emergency shutdown and overspeed circuit performs two functions: (1) detects a failure in the low pressure system through speed rate of change, and (2) detects a low pressure turbine overspeed. If either of these conditions exists, a fuel valve is closed to shut down the engine. This circuit is self-contained and has its own power supply.

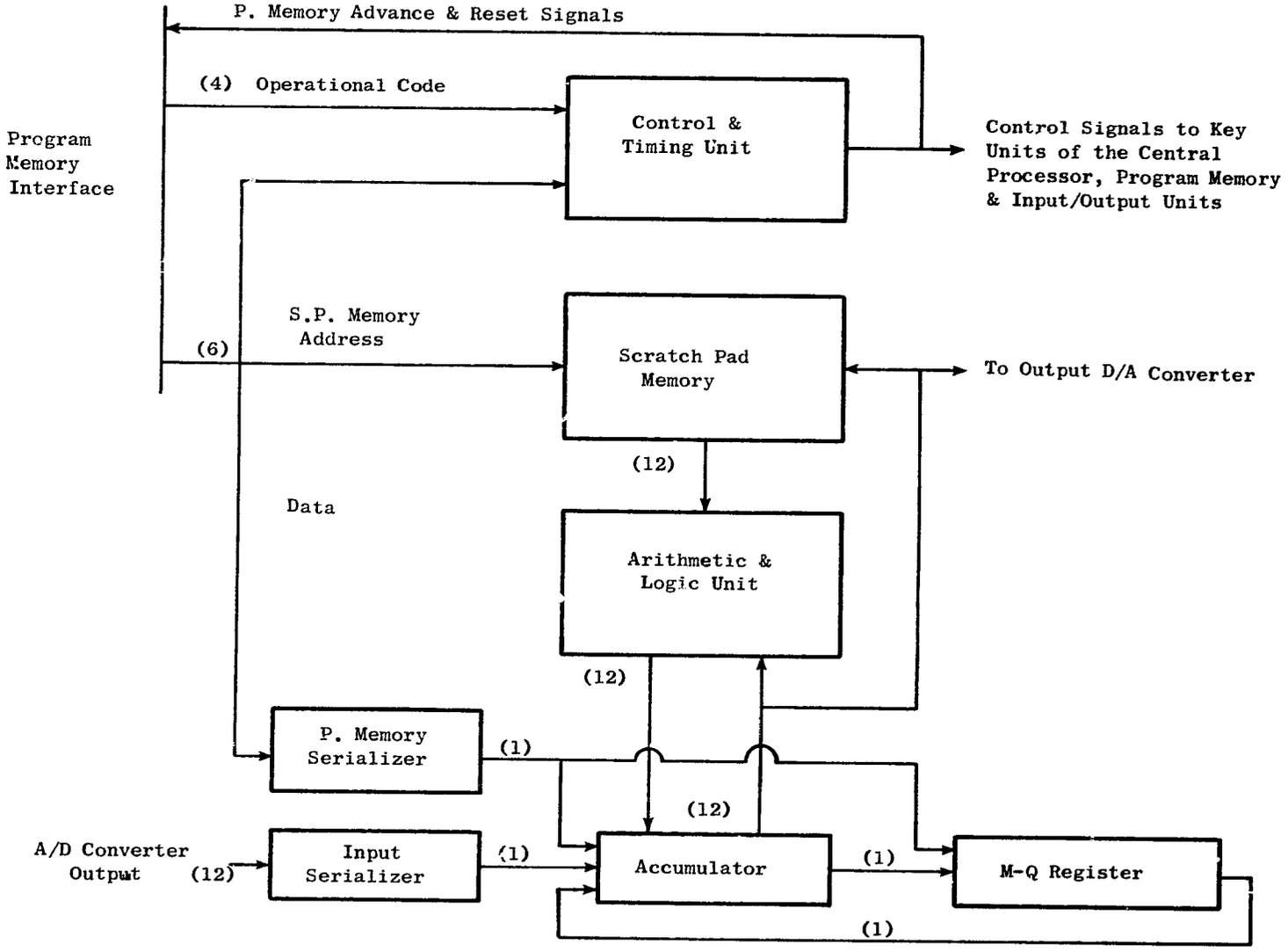

Figure 12-12. Central Processor Unit.

The QCSEE digital control power supply circuit accepts an AC signal from an engine-mounted alternator and converts it to the desired regulated voltages. There are three supplies: (1) a +15 and -15 volt supply, (2) a +11 and -11 volt supply, and (3) a +5 volt supply.

Mechanical Design

The engine-mounted digital control unit is made up of a chassis which provides mounting and which contains electrical connectors for external communications and a series of individual modules which contain the electrical components and circuits. A sketch of the unit is shown in Figure 12.13, and a typical module is shown in Figure 12.14.

The mechanical design and packaging approach for the digital control uses designs similar to existing on-engine electrical controls which have been proven on many military engine applications. To achieve the required reliability level, the control mechanical design must consider the unique turbine engine environment. Detail consideration is given to vibratory loads and cyclic temperature effects with respect to materials, mounting, potting, and interconnections. Structural integrity of the electrical components and interconnections is provided by installing the components in module cans which are filled with a resilient potting compound. This approach provides vibration damping. The digital control will be designed to meet a 10-g vibration level. The module cans are filled with potting material to a level covering the upper edge of the printed circuit boards (PCB's). Hookup wires are attached to the exposed pins at the upper edge of the PCB's, and a clear RTV is used to fill the module can. The above potted assembly is called a module. Each module is a functionally discrete portion of the control. It is tested as an individual assembly and is directly interchangeable with a like module should replacement become necessary.

Digital circuits, which use dual in-line package (DIP) components are mounted on wire-wrapped PCB's. These PCB's have terminal inserts. Interconnections are made by wire wrapping solid insulated wire as required for a point-to-point wiring arrangement on the inserts. These wire wraps and the DIP terminal interfaces are soldered to complete the electrical connections. The assembly for the wire-wrapped PCB's is the same as for the analog modules.

The chassis which contains the modules, the connectors, the electrical filters, and pressure transducers is a dip-brazed, aluminum, inseparable assembly. The chassis is supported on each end by a mounting bracket to the fan frame inside of the nacelle. Brackets are strengthened with a "T" sectioned brace between them. One of the connectors is mounted on the electrical filter housing which is needed for electromagnetic compatibility (EMC) purposes. Three of the pressure transducers are mounted on a single manifold which receives the necessary inputs through three pressure ports. The manifold is mounted to a support plate along with two connectors and a

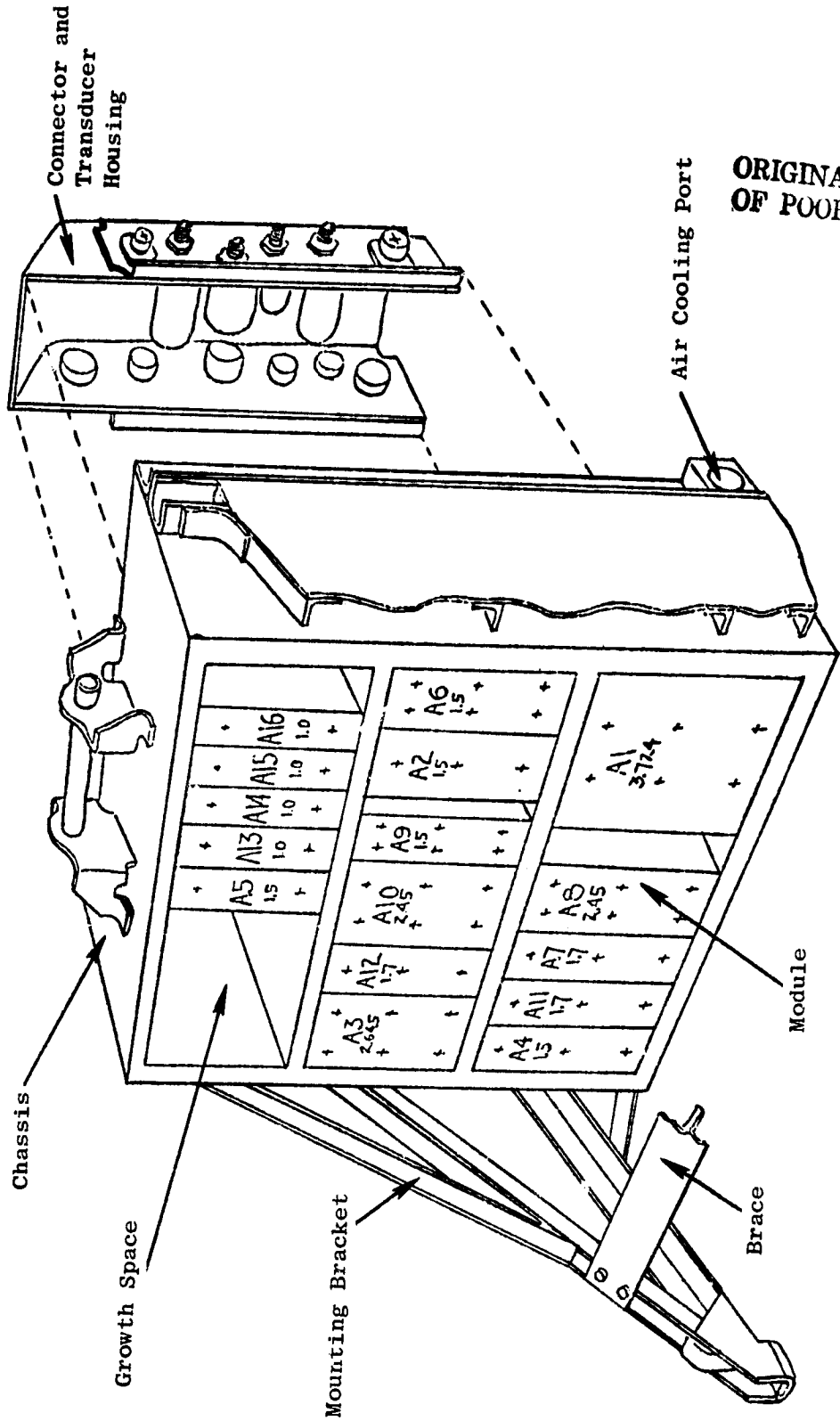

Figure 12.13. Digital Control.

C-5

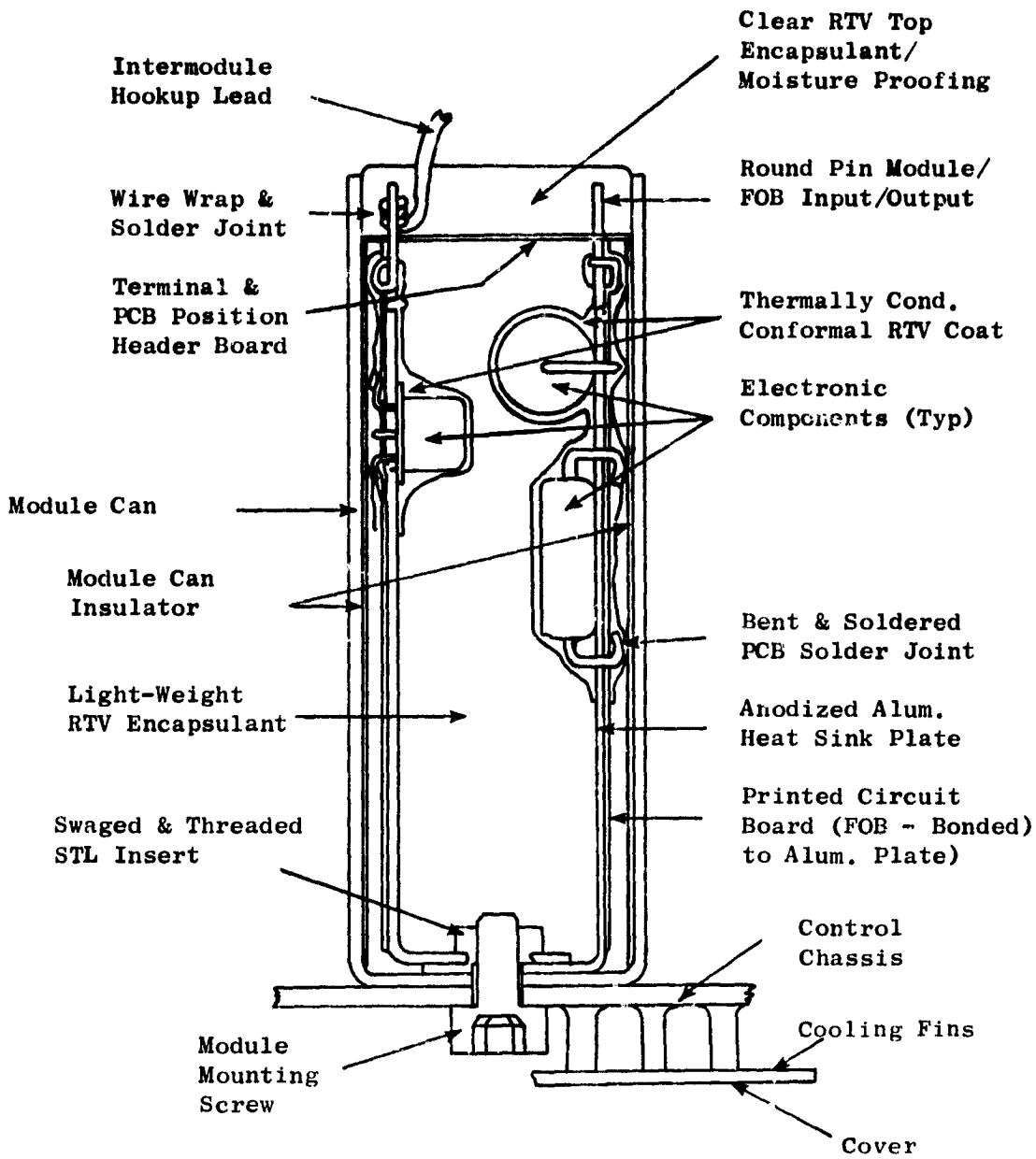

Figure 12.14. Typical Digital Control Module.

self-mounted transducer. Five connectors are mounted on a second support plate. These two connector supports and the filter housing help form the housing on the chassis. Internal to the chassis, two stiffening ribs are used to carry the module loads out to the sides of the chassis. Two flanges, stiffened with gussets, carry the loads from the chassis sides out to the mounting brackets. The transducer and connector mounting system is rugged enough to adequately resist the loads imposed by the electrical cables and the pressure lines. External surfaces of the chassis and covers are anodized to improve their resistance to handling. Chassis surfaces which interface with connectors, modules, transducers, covers, electrical filters, and ground paths are chemically treated to minimize electrical resistance.

The lower electrical resistance improves the EMC capability. The module mounting surface has finned passages for cooling air flow. These passages are located so as to maximize the conductive-convective relationships. The whole heat transfer system is designed to minimize the temperature difference between the cooling air and the electrical components.

Command and Monitor Peripheral Equipment

An overall function schematic of the command and monitor equipment is shown in Figure 12.15. The interconnect unit processes all of the command data received from the operator and engineering control panels and the remote NASA computer and transmits these data to the digital control in a time-shared serial format in a sequence prescribed by the digital control. Engine and control monitor data received from the digital control are processed in the interconnect unit and transmitted to the operator control panel, the engineering panel, the remote (NASA) computer, and to instrumentation. The following is a description of the input and output requirements of each of the command and monitor units.

Input and Output

The inputs and outputs to and from the interconnect unit are in the form of digital and analog signals.

Engineering Control Panel

From the Engineering Control Panel to the interconnect unit, analog signals of levels of 0 to 10 volts are used to transmit control demand and adjustment information. Mode information is transmitted in a parallel digital manner.

From the interconnect unit to the Engineering Control Panel, monitoring information is transmitted in a serial-digital form. The information transmitted is converted from binary to binary coded decimal and one selected word at a time may be displayed on a four-decade digital panel meter. Analog

C-5

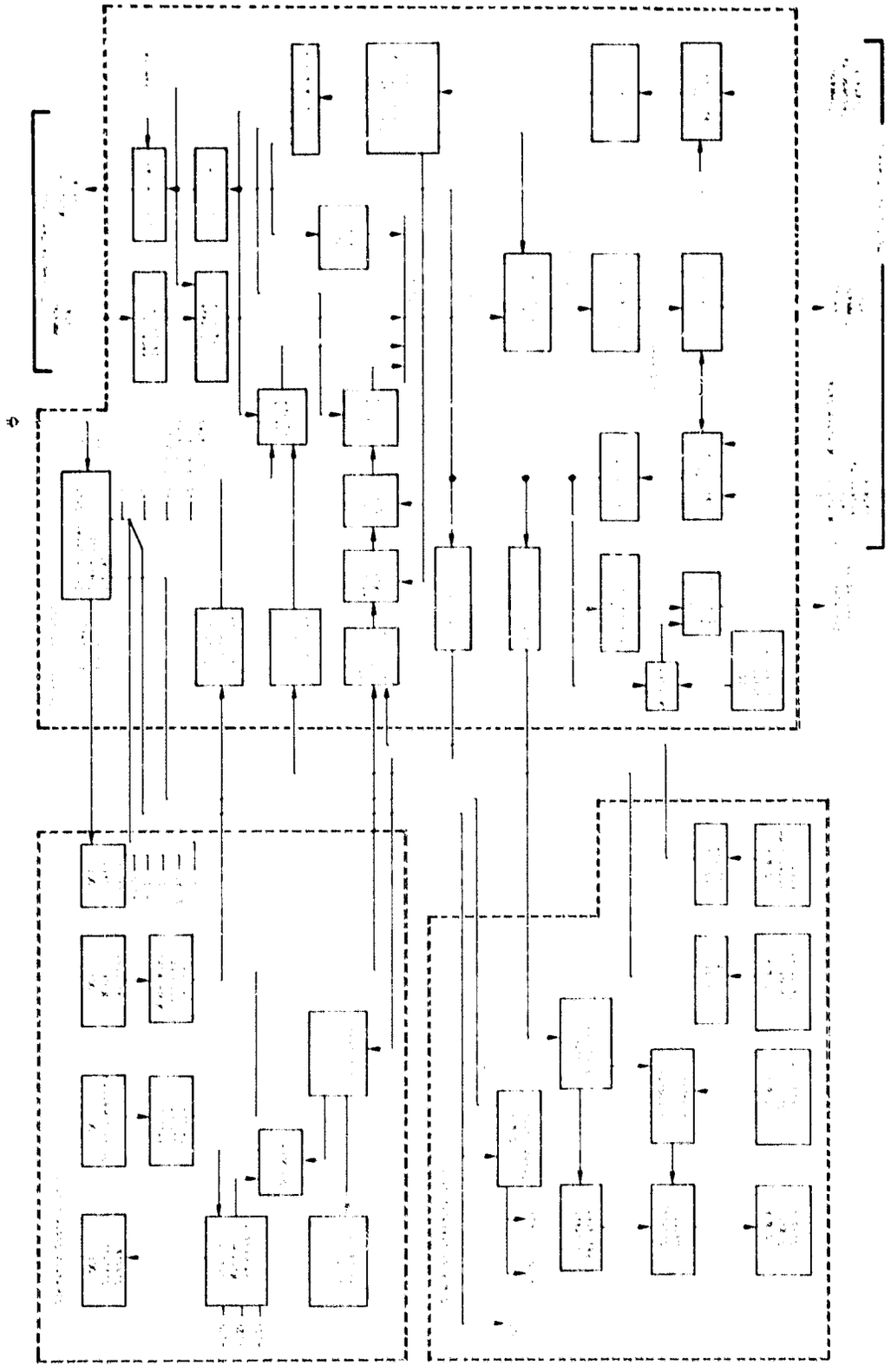

Figure 12.15. Digital Control Command and Monitor Equipment.

signals representing fuel metering, and core stator torque motor currents are transmitted to the Engineering Control Panel and displayed on three analog panel meters (Figure 12.16).

Operator Control Panel

From the operator control panel to the interconnect unit, analog signals (0 to 10 volts) are used to transmit control demand information. Mode information is transmitted in a parallel digital manner. The information transmitted is illustrated on the lower portion of the front panel display of Figure 12.17.

From the interconnect unit to the operator control panel, monitoring information is transmitted serially in a digital manner. The information is scaled by a microprocessor and displayed on nine 4-decade digital panel meters. The information displays are shown on the upper front panel as shown in Figure 12.17.

Remote Terminal Unit

From the Remote NASA Computer to the Interconnect Unit, four 16-bit data words are transmitted serially by bit. These words contain one mode word and three control command words.

From the interconnect unit to the Remote NASA Computer, monitoring information is transmitted serially by bit. The Remote Computer will accept this information and convert it to a form acceptable to the user.

Digital Control

From the interconnect unit to the digital control, all the information gathered from the peripheral units is transmitted to the digital control serially by bit upon demand from the digital control.

From the digital control to the interconnect unit, monitoring information is transmitted serially by bit and distributed to each peripheral unit in a suitable format acceptable to that unit.

Functional Description

Signal Conditioners

All digital signals are transmitted by differential line drivers and received by a differential line receiver over twisted wire pairs. All analog signals transmitted are buffered by low output impedance amplifiers and received by operational amplifiers in a differential configuration.

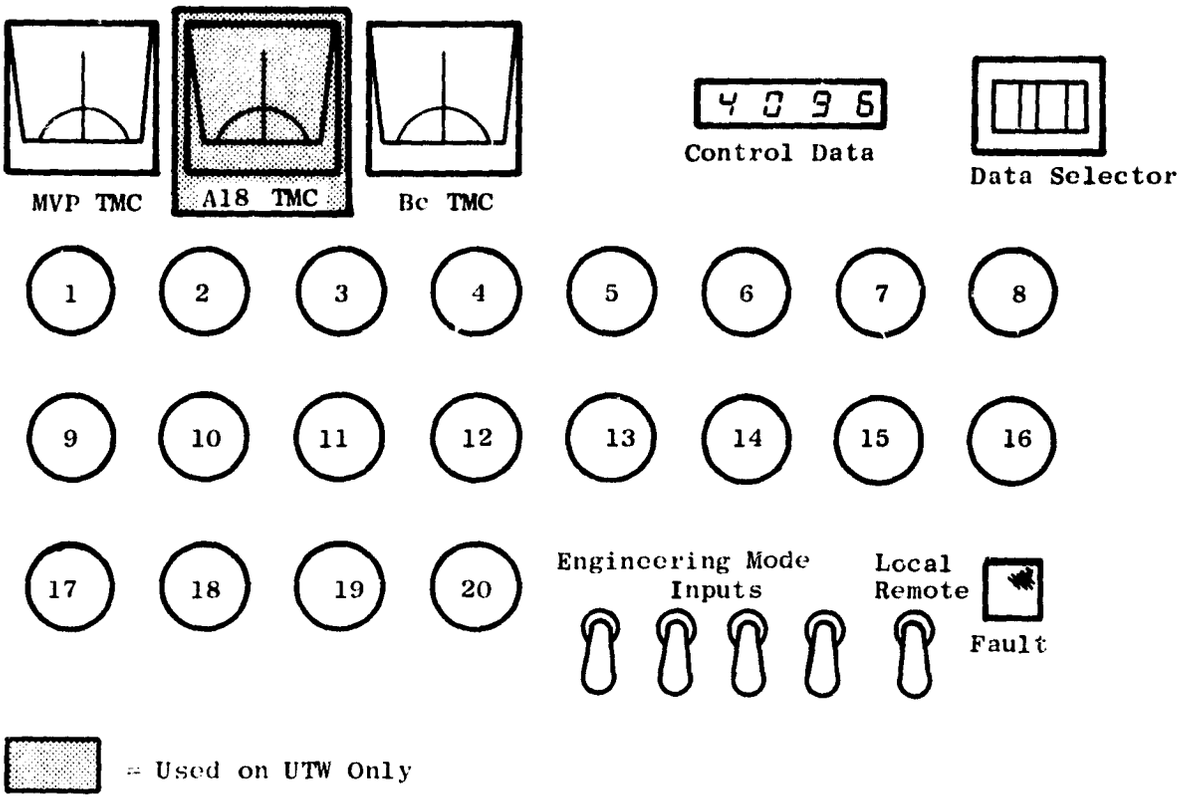

Figure 12.16. Engineering Control Panel.

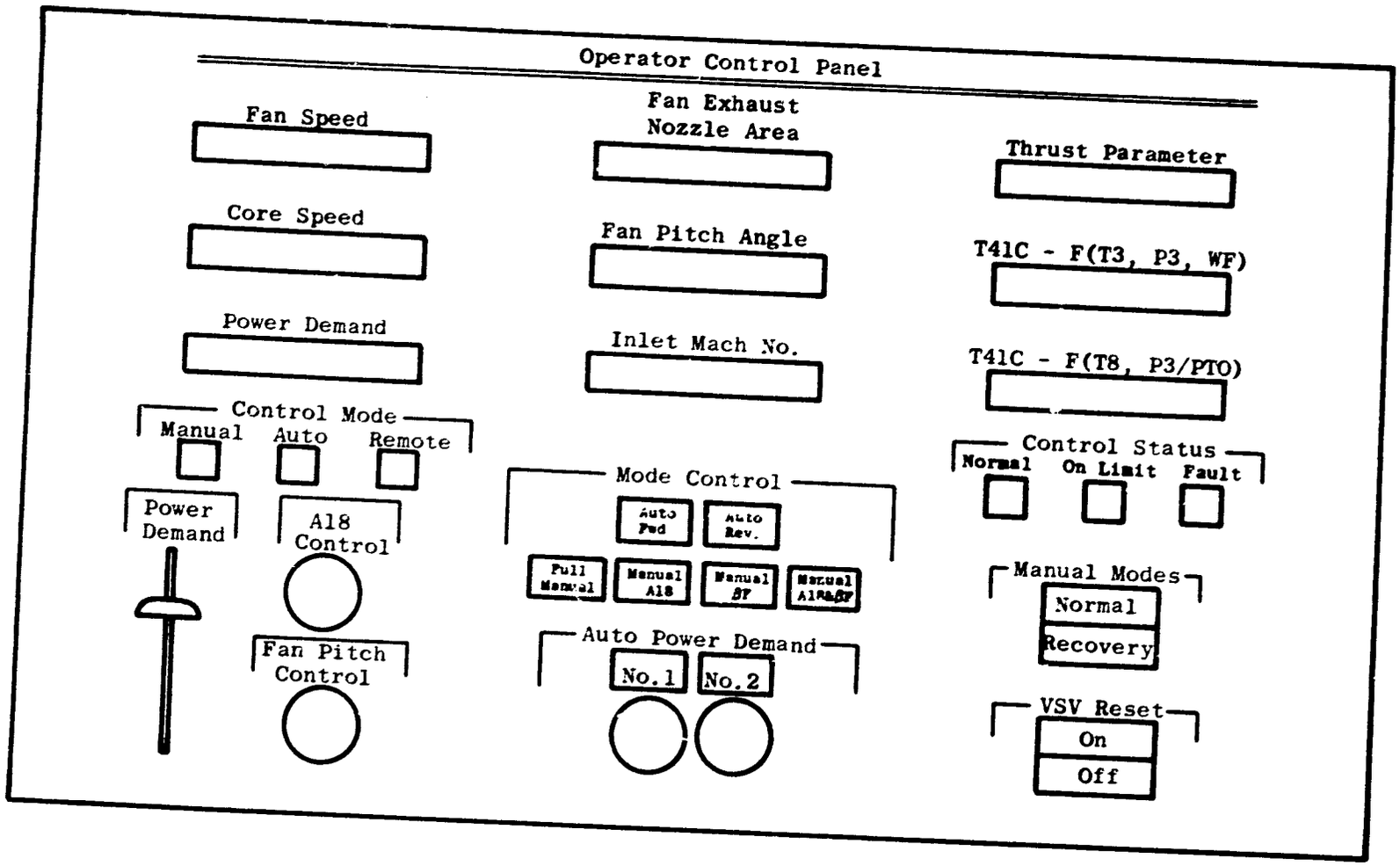

Figure 12.17. Operator Control Panel.

Analog Multiplexer

The analog multiplexer located in the Interconnect Unit consists of two 16-channel multiplexer chips capable of handling all the analog inputs from the Engineering Control Unit and the Operator Control Unit. Each of the 18 inputs is capable of being addressed separately in a predetermined sequence at a particular time determined by the digital control. The output of the multiplexer circuit goes to a sample-and-hold circuit and awaits A/D conversion.

Analog-to-Digital Conversion

All analog signals coming into the Interconnect Unit are converted to a digital word upon command from the digital control just prior to being transmitted to the digital control.

Data Bus

Digital multiplexing at the data bus is accomplished by employing tristate logic devices to provide inputs to the bus. The three states are high output, low output, and high impedance. Placed in the high impedance state, the devices can be essentially deactivated, while the other two states are used to define logic levels in the transmission mode. All but one of the devices whose outputs are connected to the data bus shown in Figure 12.15 are placed in the high impedance state, and the remaining device will be in the transmission mode. In this manner, a single input to the data bus is made available to the digital serializer as a 12-bit parallel data word.

Digital Serializer

The digital serializer is a 12-bit shift register which is parallel loaded upon command. Subsequently, the data are shifted one bit at a time into the transmission system.

Isolators

The isolation of signal and signal grounds is accomplished by means of optical isolators. These devices convert electrical signals into light, internally, and then reconvert the light signal back into electrical signals. This process breaks all electrical connection from input to output while maintaining the signal information. The purpose of the isolators is to assure that ground loops, power differences between systems, and signal noise are reduced to a minimum.

Power Supply System

The power supply for the peripheral units is derived from a 400 Hz source of 200 volt/amps or more. In the interconnect unit +15 and -15 volts are developed and routed to the Engineering Control Unit and the Operator Control Unit. Analog circuits requiring the use of ±15 volts in any of the three units use this regulated supply.

The +5 volts supply is generated separately and used as a logic supply in each of the three units.

There are two isolated +5 volt logic supplies in the interconnect unit derived specifically to be used in the isolation technique used in this system.

The Operator Control Unit develops -10v and -12v for the scaling microprocessor. The +5 volts is developed for a logic supply, and the 12 volts AC is used to light the front panel push button switches and indicators.

The Engineering Control Unit develops -10v to reference the potentiometers. The +5 volts is used as a logic supply while the 10 volts AC is the deriving source as well as the supplier of the one lighted indicator on the front panel. The +15 volts is used to derive the -10 volts as well as operating analog circuits.

Other Considerations

The packaging of the Off-Engine Control Peripheral Units (consisting of the operator control unit, the engineering control unit, and the interconnect unit) is designed to operate in a control room environment. Both mechanical and electrical systems are designed for control room use only.

12.3.4 Hydromechanical Control

General Description

The QCSEE hydromechanical control is an F101 main engine control which will contain appropriate modifications applicable to the unique requirements of the QCSEE control system and engine. The Woodward Governor Company is the vendor source for this control.

The modified F101 control will perform the following subsystem functions:

- Modulates core engine fuel flow to govern core speed as a backup to the digital control
- Provides positive fuel flow shutoff and limits core engine overspeed

- Reduces fuel flow in proportion to electrical signals from the digital control as the primary fuel control method
- Provides power lever position intelligence to the digital control
- Provides minimum fuel system pressurization
- Provides fuel flow shutoff to limit fan overspeed in response to electrical control signals from the digital control
- Provides electrical metering valve position intelligence to the digital control

Hydromechanical Control Inputs and Outputs

The inputs to and outputs from the hydromechanical control are listed below:

Inputs	Outputs
• Pump discharge	• Metered engine fuel flow
• Power lever angle	• Bypass fuel flow
• Core engine drive speed	• Stator vane actuator control supply pressure
• Electrical fuel flow limit signal	• Power level electrical position signal
• Electrical fan overspeed signal	• Metering valve electrical position signal

Hydromechanical Control Functional Description

A functional block diagram of the hydromechanical control is shown in Figure 12.18.

Fuel flow to the engine is set by controlling the area of the metering valve and maintaining a constant pressure differential across it by means of the bypass valve which returns excess fuel to the fuel return and thence to the fuel pump inlet.

Metering valve area is controlled by the metering valve actuator which is a fuel-operated piston that responds to the output of an electro-hydromechanical computer network within the control. One of the inputs to this network is an electrical signal from the digital control. This signal will normally be in command of the metering valve.

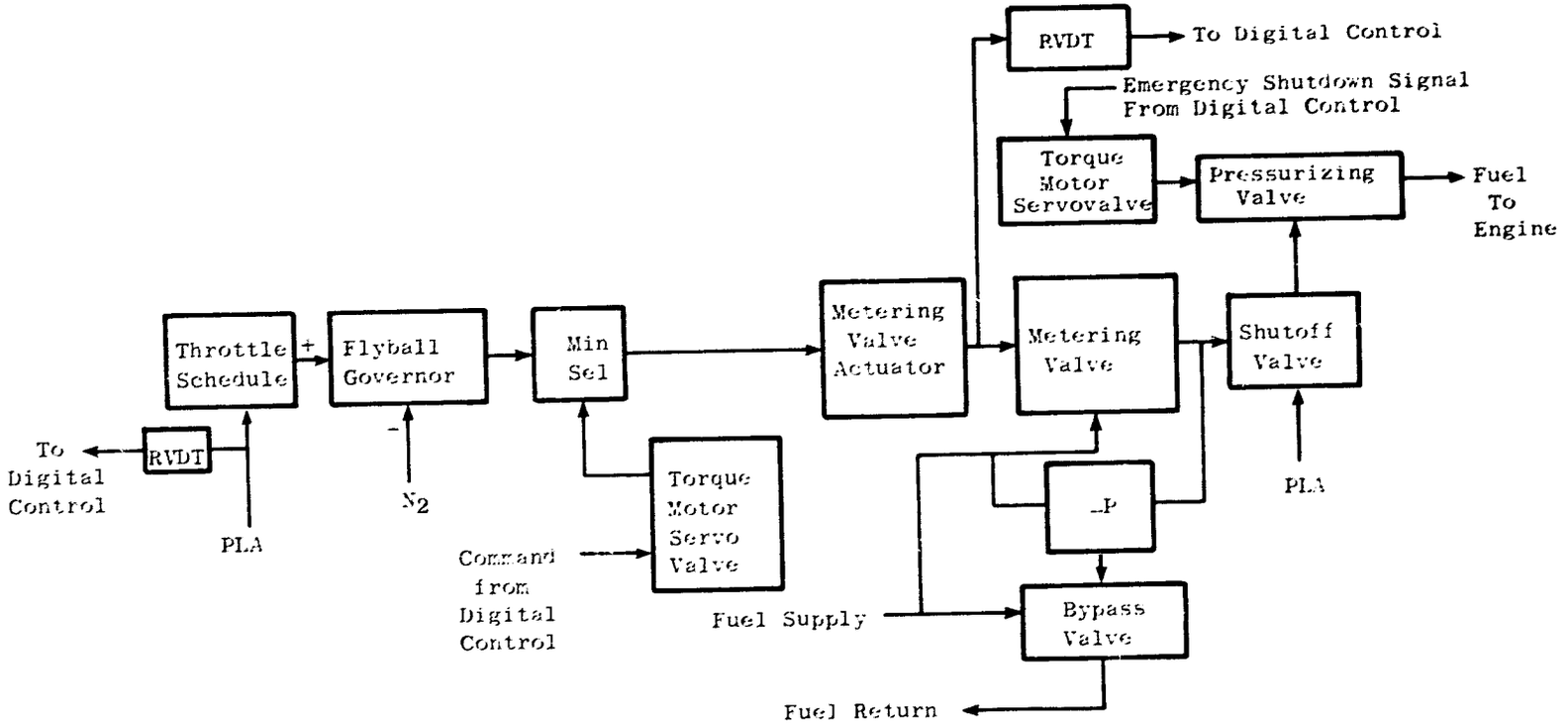

Figure 12.18. Hydromechanical Control Schematic.

The core speed governor receives an input demand by means of a cam that is scheduled as a function of mechanical power lever position. This demand is applied to a flyball governor rotated by the core engine rotor through the accessory gearbox and control drive shaft. If the demanded speed and actual speed do not correspond, the governor ports fuel servo pressure toward the metering valve actuator to change fuel flow and thus correct the difference. This pressure will only get through to the actuator, however, if the governor is calling for less fuel flow than the electrical command from the digital control.

The control includes two valves downstream from the metering valve, a power lever operated shut-off valve, and a pressurizing valve which operates to assure adequate fuel pressure at low-flow conditions to operate the core stator actuators and other fuel servomechanisms and which also serves as an emergency fuel shut-off valve, closing in response to a fuel servovalve operated by a signal from the digital control.

The hydromechanical control will be mounted on the F101 fuel pump similar to Figure 12.19. The pump is V-band flange-mounted to an F101 gearbox pump drive pad. Through shafting, it is used to provide core speed input to the control drive spline.

12.4 FUEL DELIVERY SYSTEM

The QCSEE fuel delivery system is primarily based on F101 engine main fuel system components including the hydromechanical control and temperature sensor described in Section 12.3.3. The fuel delivery system includes the following elements:

- Fuel control (metering section)
- Main fuel pump
- Fuel filter

These elements are interconnected as shown in the schematic of Figure 12.20.

The fuel pump is a standard F101 main fuel pump unmodified. It is a balanced vane design of fixed displacement and contains an integral centrifugal booster stage to charge the vane intakes.

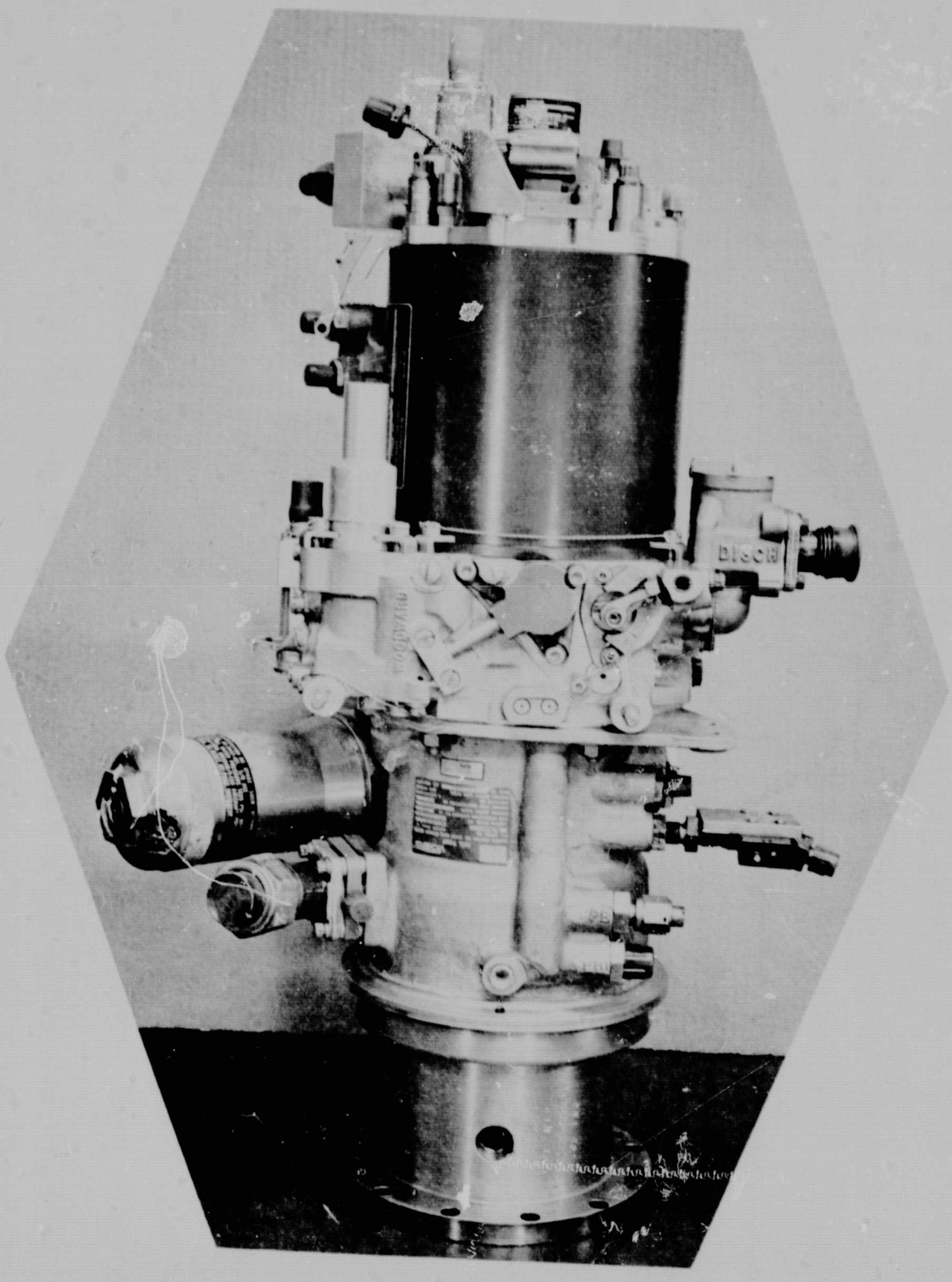

Figure 12-19. F101 Fuel Pump and Control.

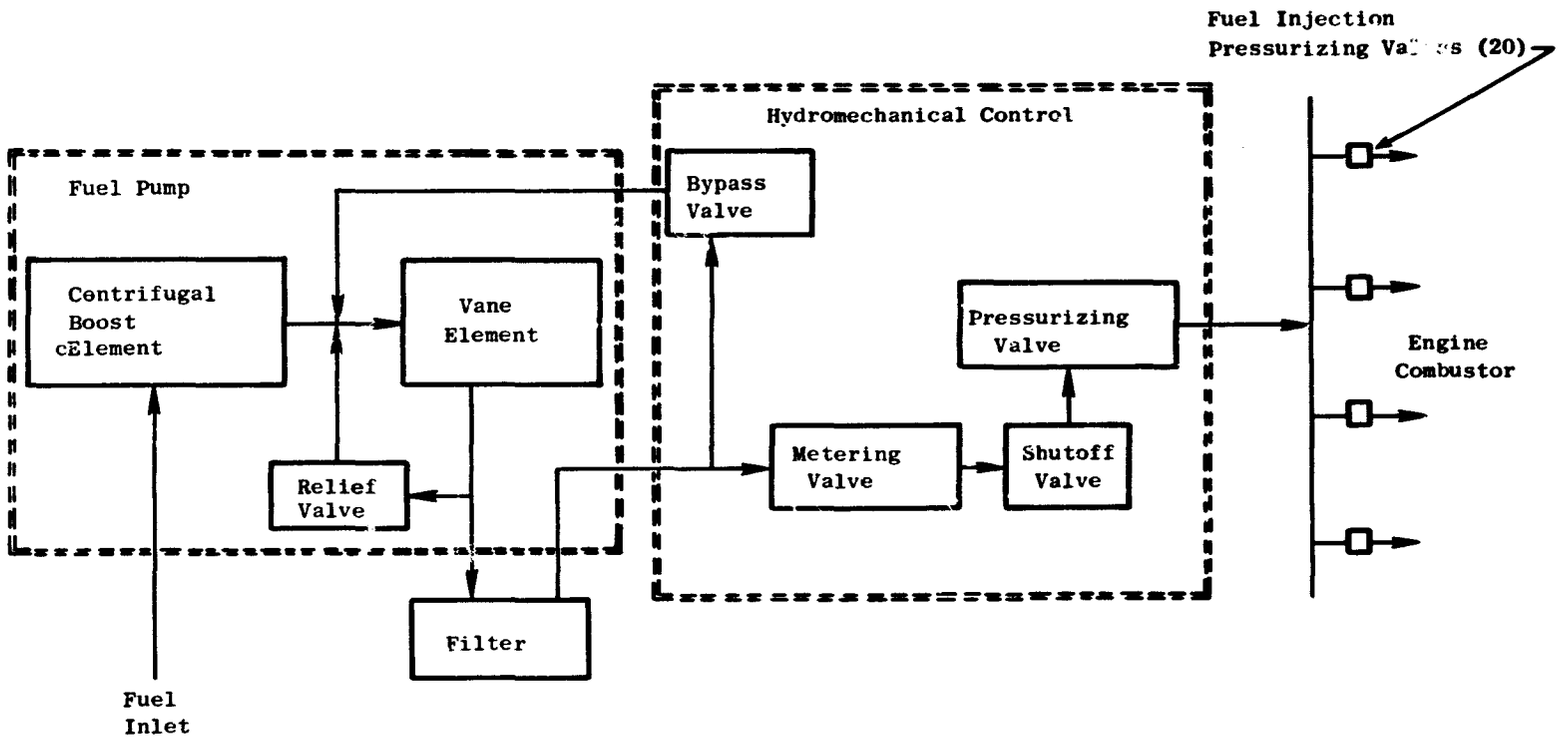

Figure 12.20. Fuel Delivery System.

12.5 COMPRESSOR STATOR ACTUATION SYSTEM

Actuation of the core compressor stators is accomplished by a pair of fuel-operated, ram actuators (Figure 12.21). Flow to the actuators is controlled by separate, 4-way, electrohydraulic, directional flow control valves mounted on a common manifold block which is mounted on the hydromechanical control. The valves control flow in response to a direct-current electrical signal from the digital control.

A schematic of the valve design is shown on Figure 12.22. The electrical signal is applied to parallel, redundant coils of the flat armature torque motor which applies torque to the jet-pipe causing it to deflect. This deflection unbalances the pressure on the opposite ends of the spool, causing it to move until the jet pipe is returned to its center position by the feedback spring, the force of the spring just counteracting the torque generated by the electrical signal. In this manner, spool position is made proportional to the electrical signal current. The position of the spool determines the porting between the high pressure supply from the hydraulic pump (P), the actuation ports (1 and 2), and the low pressure return (R).

The acutators are F101 components modified to increase the linear stroke by 5.08×10^{-3}m (0.2 inch). The modification is accomplished by shortening the piston head axial dimension to allow increased retraction when bottomed in the cylinder.

12.6 SENSORS

The engine sensors are devices which change the variable to be measured into a form that can be used as an input signal to the engine digital or hydromechanical control or as an input signal to an indicator gage. The sensors include the following:

Low pressure turbine speed sensor

Core engine speed sensor (AC generator)

Fan inlet temperature sensor

Static pressure and pressure ratio sensors

Position feedback sensors

12.6.1 Low Pressure Turbine (LPT) Speed Sensor

The LPT shaft speed sensor produces two electrical signals that represent the rotational speed of the low pressure turbine shaft. One signal will be used for engine fan speed governing. The other signal will be used to limit the rate of speed change and maximum speed in the event of a loss of fan load, overspeed, or control failure.

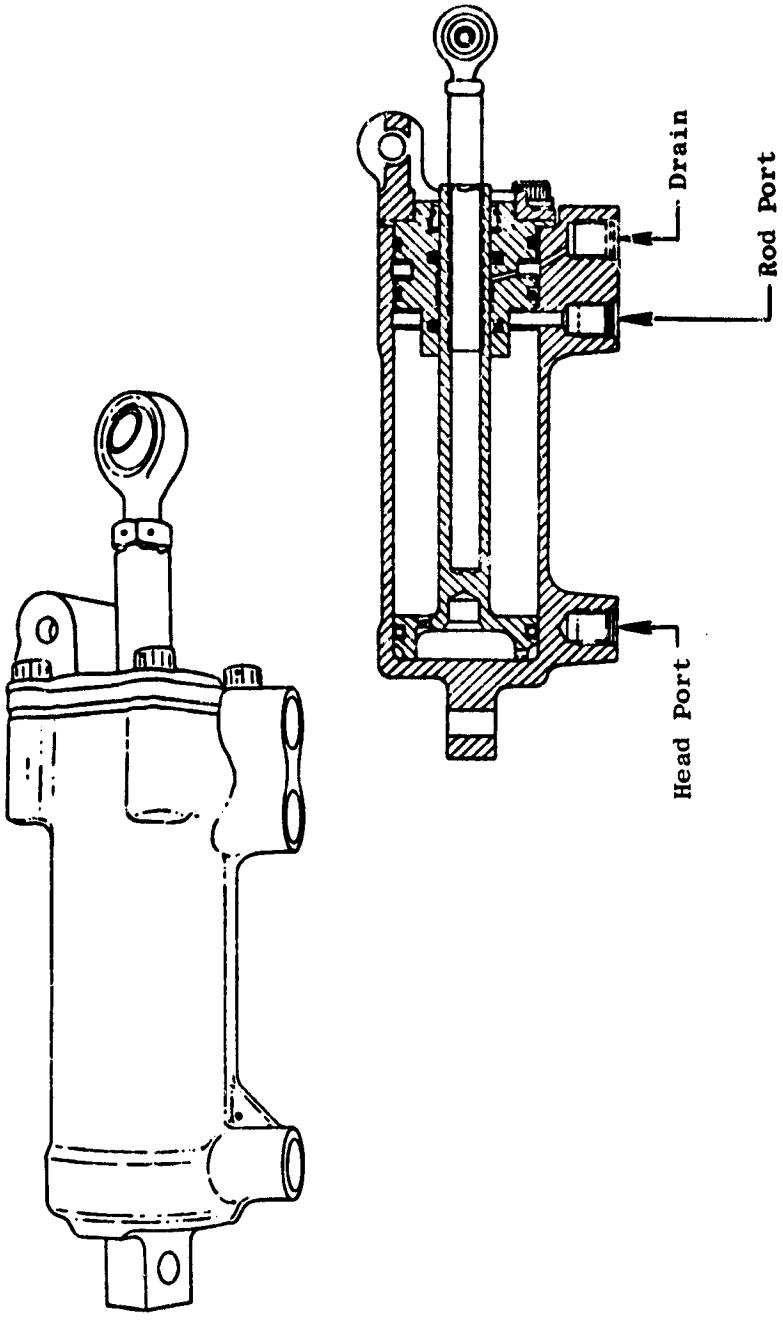

Figure 12.21. Variable Stator Vane Actuators.

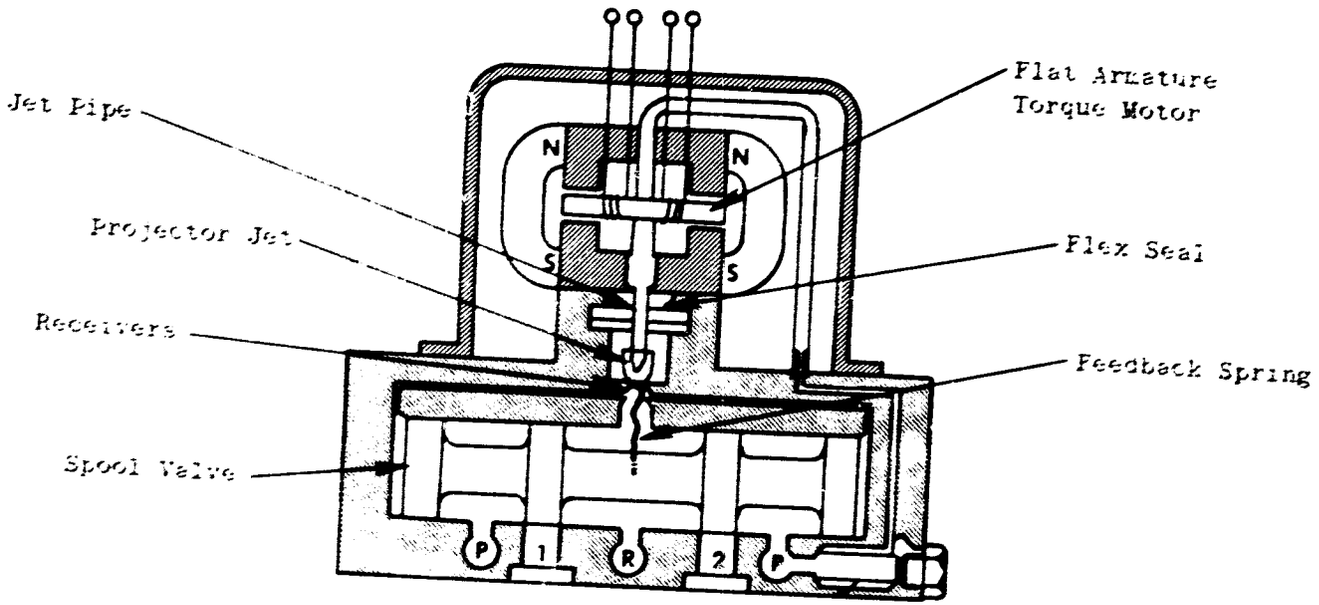

Figure 12.22. Electrohydraulic Servovalve.

The speed sensor is nearly identical to that used on the F101 engine, with a magnetic pickup at one end and an electrical connector at the other. The sensor is mounted within the fan frame; the pickup head and supporting tube extend through a fan frame strut to a point aft of the LPT shaft front bearing. The pickup is fixed in close proximity to a flanged ferromagnetic disk having 36 equally spaced teeth machined into the flange, 35 with the same air gap and one with less gap to provide a locating signal for use in rotor balancing.

The magnetic pickup consists basically of a permanent magnet behind a soft iron pole piece around which a coil has been wound. The magnetic flux linking the coil is high when a ferrous metal object (tooth) is placed in front of the pole piece and is low with no ferrous metal in front of the pole piece (slot). The generated voltage is proportional to the rate of change of flux in the pole piece, and the frequency of the AC signal is proportional to the speed at which the ferrous material (teeth) passes in front of the pole piece. The wave form of the electrical signal is nearly sinusoidal depending upon the relative width of slots and teeth on the rotating disk and also the width of the piece relative to the slots and teeth. Signal output from the speed sensor is routed to a conditioner device in the digital control which produces a uniform voltage amplitude and wave form at varying speeds so that ultimately the conditioned signal is interpreted in terms of frequency rather than voltage amplitude.

12.6.2 Core Engine Speed Sensor

An alternating-current-generator, driven by the engine gearbox, provides electrical power to the engine digital control. In addition, a signal source is generated which represents core engine speed and is used for engine control and indicating purposes.

The generator is a 12-pole, high-speed, four-winding, alternating-current-generator. The generator, shown in Figure 12.23, is identical to that used on the F101 engine. The generator rotor is mounted to a drive shaft which is supported by bearings in the accessory gearbox. Each winding on the stator functions as an independent power source with independent leads and pins in a single connector.

A shaft seal in the gearbox permits the rotor to run in an essentially dry environment, reducing heat generation and avoiding the possibility of metallic particle pickup on the Alnico-9 magnetic rotor. The rotor is shielded for retention of the magnetic segments and to provide a smooth, low disk friction surface.

The frequency of the sinusoidal wave form signal is used as an indication of core engine speed. The drive gear ratio is such that the rotor turns at 24,903 rpm at 100% engine speed which results in a frequency of 2490 Hz.

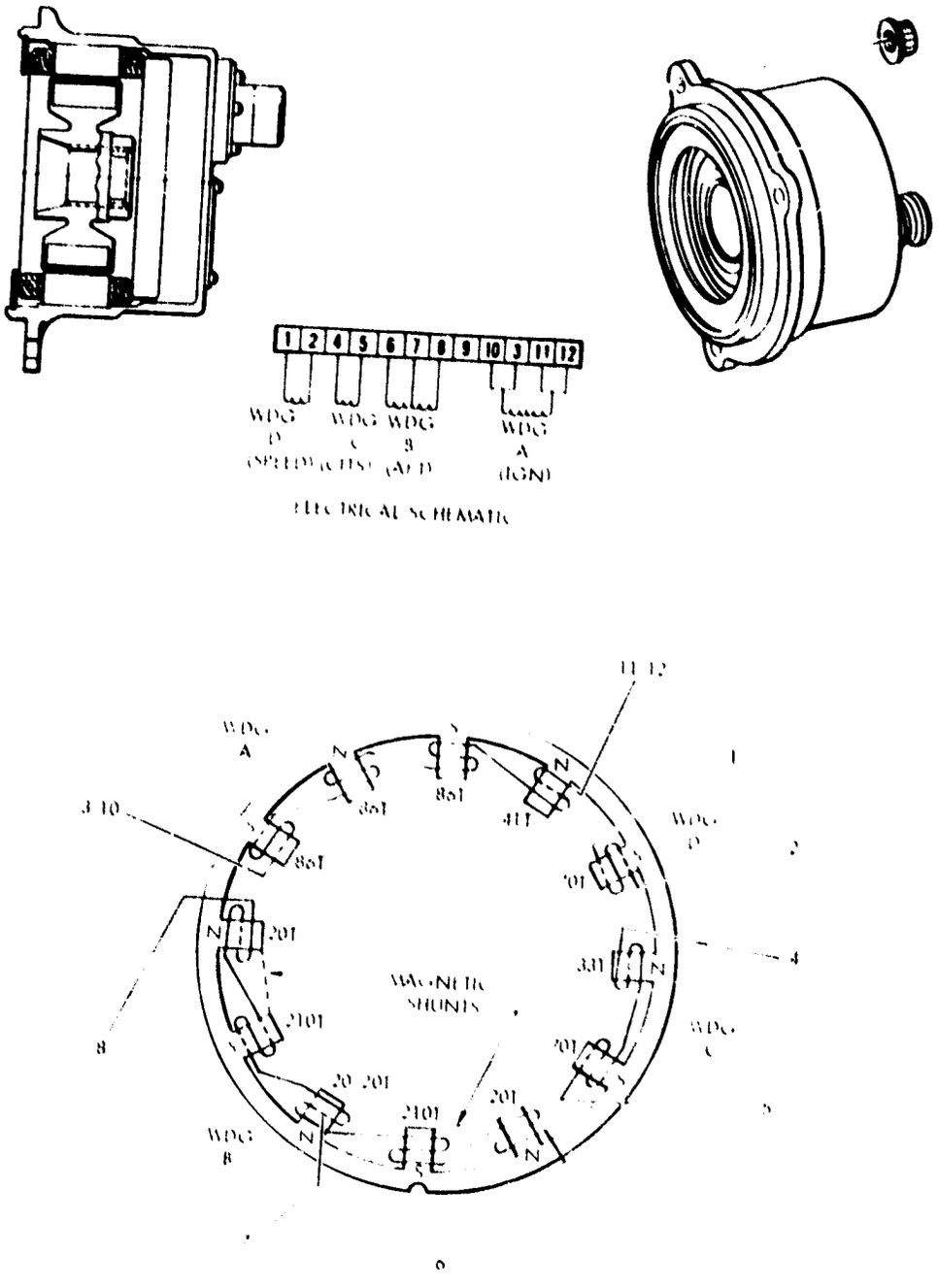

Figure 12.23. Alternating Current Generator.

12.6.3 Fan Inlet Temperature (T12) Sensor

The T12 sensor provides the engine control with an electrical signal representing the total temperature of the air entering the fan for use in scheduling and computing within the digital control.

The fan inlet temperature sensor shown in Figure 12.24 is identical to that used on the F101 engine. The sensor is a wire-wound resistance-type device mounted on and protruding through the front frame into the fan inlet air stream. The sensor consists of a sensing element and housing. The sensing element contains a platinum wire wound on a cylindrical platinum mandrel. The wires are insulated from each other and the mandrel by a ceramic insulant. The element is hermetically sealed in a capped platinum sheath and the connections are potted. The housing is a slotted airfoil which controls airflow so that the sensed temperature is that of the free stream. A series of small holes bleeds off the boundary layer and turns the stream, but not heavier particles, inward toward the sensing element. The boundary layer air is exhausted out the top. Some of the diverted air stream flows through the first slot and carries the lighter contaminants. The remaining portion of the diverted flow goes through the second slot and around the sensing element.

The T12 sensor operates on the principle that the resistance of the platinum wire is a predictable function of temperature. A constant direct current of 12.5 milliamperes is applied to the sensor coil, and the voltage is used as an indication of temperature.

12.6.4 Absolute and Differential Pressure Sensors

Fan inlet static pressure (PS11), fan discharge pressure (P14), free-stream total pressure (PT0), and core compressor discharge static pressure PS3) are sensed and used in the digital control for scheduling and computation. PS3 and PT0 are sensed as absolute pressures and (PT0-PS11) and (P14-PT0) are sensed as differential pressures.

The sensors are thin-film strain gage bridge transducers identical to those used in the F101 engine. A cross section of the sensor is shown in Figure 12.25. The sensors receive their electrical excitation from the digital control and change the ΔP and static pressure signals to electrical signals. They are located inside the digital control chassis.

In the thin-film resistance strain gage bridge transducer [below 6.89×10^5 N/m^2 (100 psia)], the strain member is a cantilever beam which provides a metal substrate on which a ceramic film is deposited for electrical insulation. For higher pressures, a diaphragm is used instead of the cantilever beam. The four strain gage resistors are then vacuum deposited on the insulator. The resistors are electrically connected into a bridge circuit using film-deposited interconnecting leads.

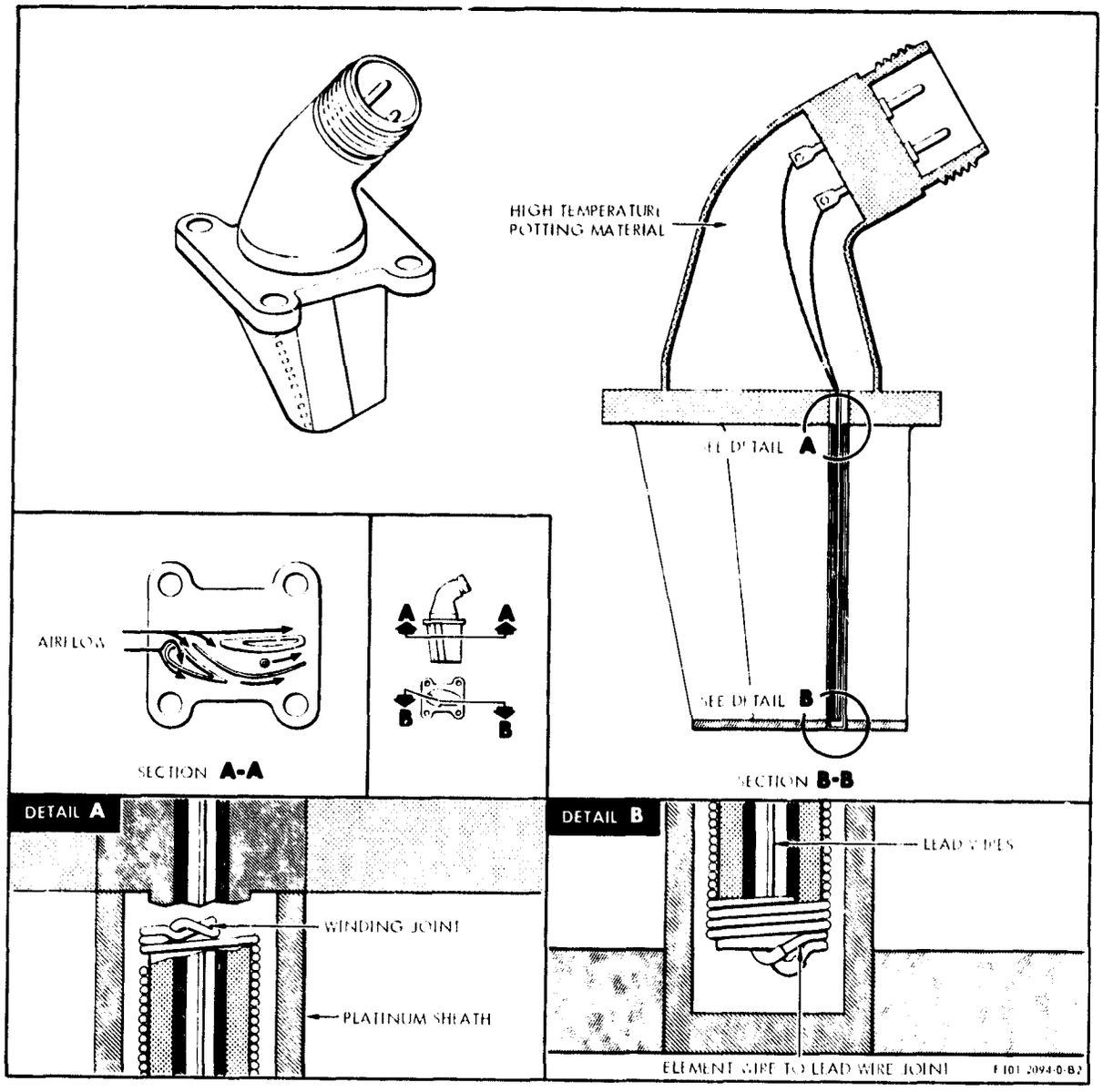

Figure 12.24. Fan Inlet Temperature (T12) Sensor.

ORIGINAL PAGE IS
OF POOR QUALITY

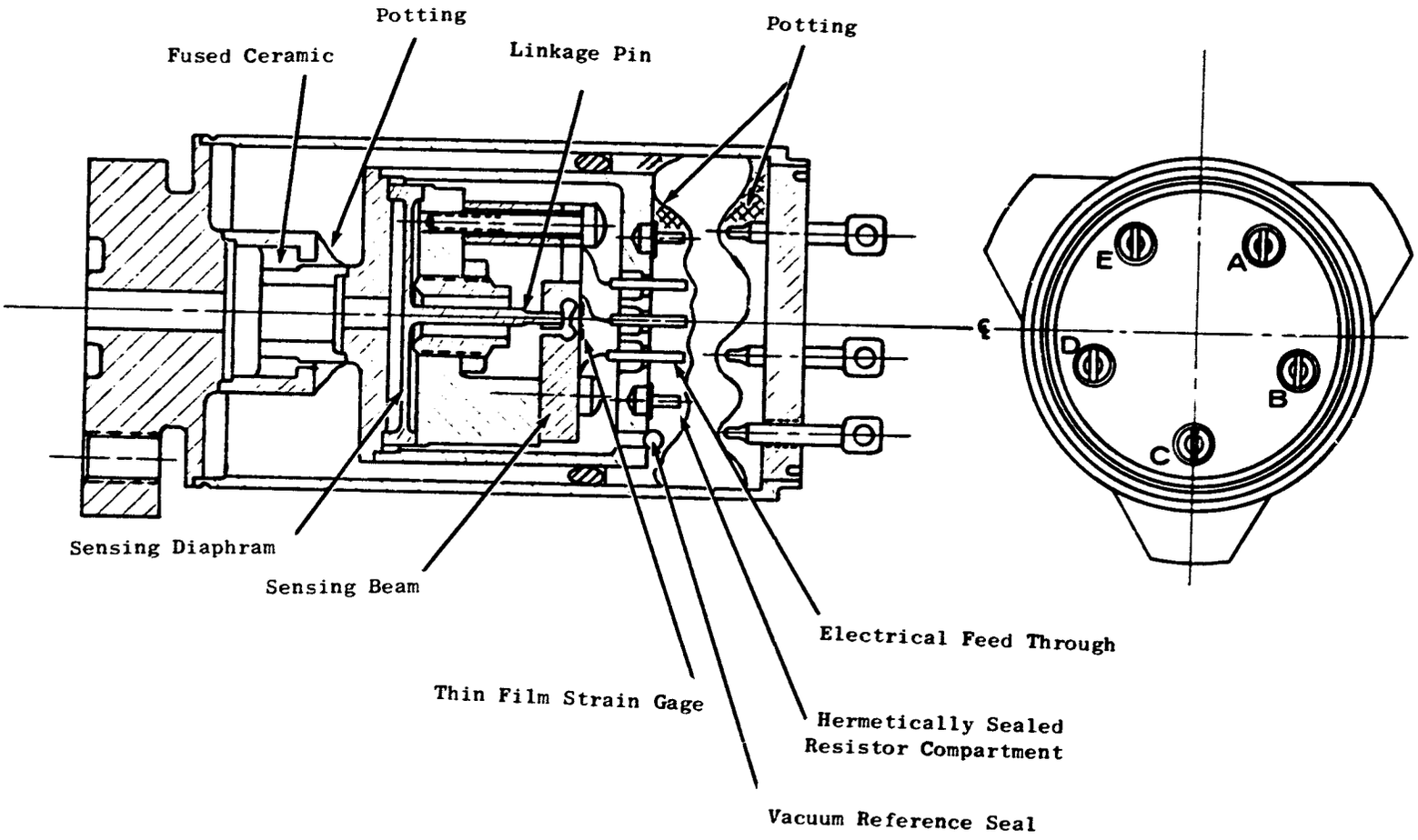

Figure 12.25. Pressure Sensor.

Operating ranges for the sensors are 0-206.9 N/cm^2 (0 to 300 psia) for PS3, 0-13.8 N/cm^2 (0 to 20 psia) for PT0, and 0-8.3 N/cm^2 (0 to 12 psid) for both differential sensors.

The sensors operate on the principle of a mechanical distortion producing a change in electrical resistance across a strain gage and, hence, a change in electrical current output from a bridge circuit. Referring to Figure 12.25, pressure is ported to the sensing beam. The beam is shaped such that it bends and causes "stretch" on the surface to which the strain gages are attached.

12.6.5 Position Feedback Sensors

Rotary and linear variable differential transformer transducers will be used to sense the position of various engine parts and components. These are:

	Type
Compressor stator vane actuator position	LVDT
Power lever position	RVDT
Fuel metering valve position	RVDT

The variable differential transformer translates the displacement of a magnetic core into an AC output voltage which is proportional to the displacement. Several different designs are used to obtain specific performance characteristics, but basically, these transducers are constructed of one primary coil and two secondary coils as shown in Figure 12.26.

An alternating current provided by the digital control (6.6 volts rms 3030 Hz) is fed through a primary winding. The magnetic core couples the primary and secondary coils by conducting the alternating field inside the coils. When the core is in the center position, an equal portion of the core extends into each of the secondary coils and affects an equal coupling between the primary and each secondary coil. An alternating voltage of equal magnitude is induced in the secondary coils. With the secondary coils connected in series opposed, the output is close to zero. As the probe is moved to either side, the coupling between the primary and one secondary coil is increased, while the coupling between the primary and the other secondary coil is decreased. A larger voltage is then induced in one secondary coil than in the other, and the output voltage will be the difference between the two voltages and linearily proportional to the position of the LVDT core rod.

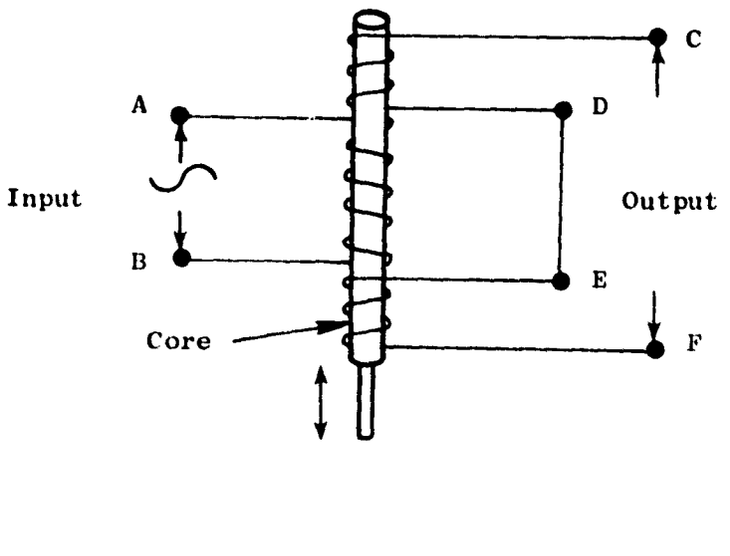

Figure 12.26. Variable Differential Transformer Schematic.

SECTION 13.0

NACELLE AERODYNAMIC DESIGN

13.1 SUMMARY

The QCSEE OTW propulsion system design requirements include exhaust area variation and flow turning exceeding any previous design data base. Therefore, in order to define an acceptable exhaust system for QCSEE, an experimental development program was conducted by GE and NASA at the Langley Dynamic Stability Branch facilities. Both static and low speed wind tunnel tests were conducted. As a result of this program, an exhaust system has been developed which meets the QCSEE OTW exhaust area variation requirements between takeoff and cruise; it provides excellent lifting capability at takeoff and approach wing flap settings, and it houses a target-type thrust reverser that meets the required reverse thrust objectives. Since the QCSEE program is a ground engine demonstration program only and no aircraft geometry was defined, the program did not have any high speed cruise drag test program.

The nacelle external geometry was designed for an aircraft cruise Mach number of 0.72. The nacelle external lines were defined to maintain a maximum diameter of 200.2 cm (78.8 inches) with a balanced design considering aerodyanmic, acoustic, and mechanical requirements. The fan discharge duct was designed to provide a low Mach number flow over the acoustically treated panels to optimize the attenuation effectiveness without adversely affecting aerodyanmic performance.

The upper portion of the exhaust nozzle houses the thrust reverser which is designed to provide reverse thrust equivalent to 35% of takeoff thrust. The sides of the nozzle contain movable doors which open up at takeoff and landing to provide approximately 25% more flow area than the closed cruise position. These doors were designed not only to effect this area requirement but also to enhance flow spreading and thereby improve powered lift operation.

An accelerating inlet with a high throat Mach number and acoustic treatment in the diffuser was selected to meet the engine noise suppression requirements. The design objective was to achieve the highest practical throat Mach number consistent with high levels of fixed-geometry inlet performance across the assumed aircraft operating envelope. The design throat Mach number of 0.79 was based on studies of available inlet data. The inlet was to be as short as possible consistent with acoustic treatment needs and required aerodynamic performance at all aircraft/propulsion system operating conditions. These system operating conditions included inlet operation without separation at 50° angle of attack at an aircraft speed of 41.18 m/sec (80 knots) and 90° crosswind at velocities of 18 m/sec (35 knots).

Scale model inlet tests of several inlet configurations conducted in the NASA Lewis 9 by 15-ft VSTOL Wind Tunnel resulted in the selection of an inlet geometry capable of meeting all requirements. The selected inlet configuration has a highlight diameter to throat diameter ratio of 1.21 and a highlight to maximum diameter ratio of 0.900.

13.2 DESIGN REQUIREMENTS

The primary system design requirements defining the OTW propulsion system were the following:

- System to be representative of a four-engine aircraft installation.
- Engine installation to be designed for a symmetrical configuration, not tailored to a specific aircraft design.
- System to have external flow lines representative of an installation having low drag at cruise Mach number = 0.72.
- System to provide upper surface flow attachment for all flap positions.
- Aircraft cruise/takeoff thrust = 0.21 for nozzle sizing purposes.
- Approach flap chord line angle = 60°.
- Takeoff flap chord line angle = 30°.
- Reverser to provide reverse thrust equivalent to 35% takeoff thrust for ground use only with operational capability down to 5.1 m/sec (10 knots) without exceeding engine limits.
- Inlet to have no separation at angles of attack to 50° with 41.1 m/sec (80 knots) free stream velocity, and up to 18 m/sec (35 knots) at crosswind angles of 90°.
- Exhaust system to provide about 25% area variation as required by the engine cycle between takeoff and cruise operating conditions.

13.3 COMPONENT DESIGN

13.3.1 Exhaust System

The exhaust nozzle was designed to achieve the desired flow characteristics specified in the design requirements using the data base established by NASA Langley. These data, shown in Figure 13.1 from SAE Paper 740470 define the unique relationship of the aerodynamic turning and geometric nozzle and flap parameters.

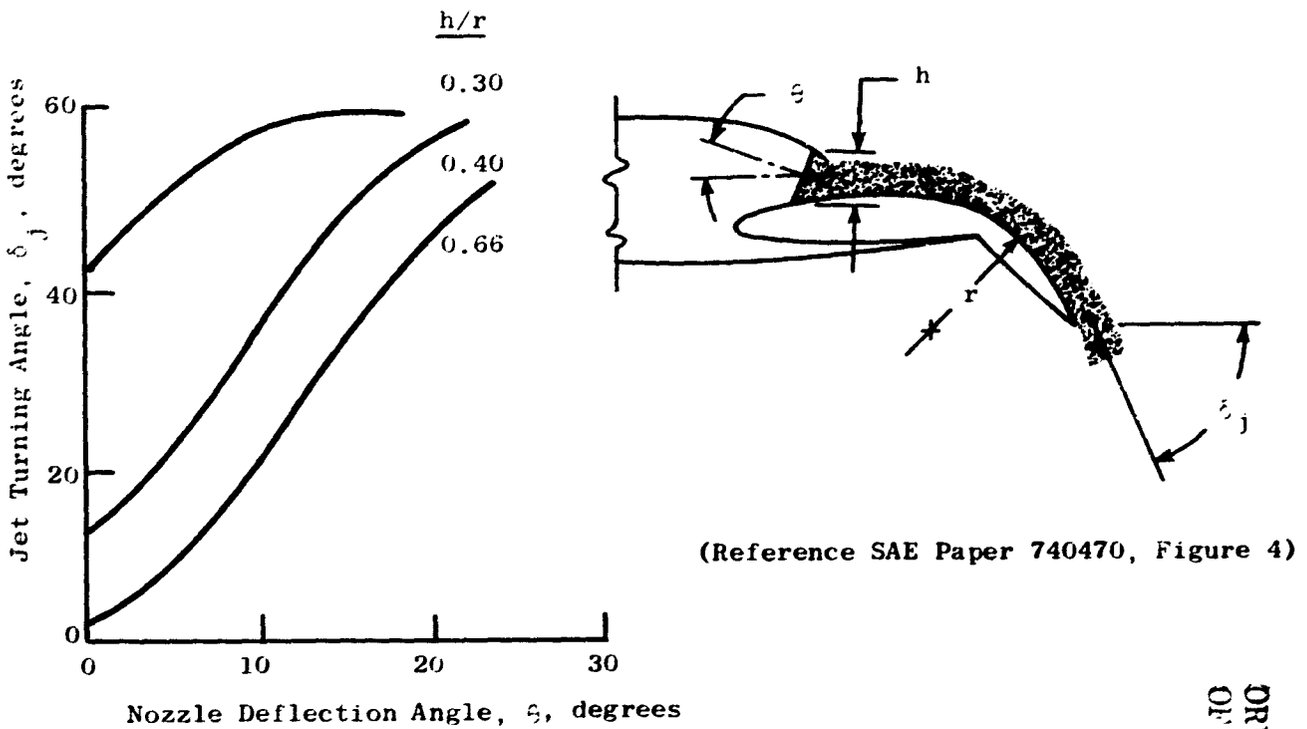

(Reference SAE Paper 740470, Figure 4)

Figure 13.1. Effect of Nozzle Deflection on Jet Turning Angle.

The design evolved from the preliminary flowpath definition shown in Figure 13.2 to the Baseline QCSEE OTW exhaust system configuration illustrated in Figure 13.3. The design incorporated two side doors for the 25% area variation requirement and a target-type thrust reverser. The Baseline design appeared to be aerodynamically and mechanically feasible but lacked a specific data base to launch any full-scale hardware design.

The inadequate data base was due largely to the innovation of the two-door concept which was unlike any other design available, and the difficulty in determining what the exit area characteristics were in terms of flow coefficient and velocity coefficient. A joint GE, NASA Lewis, NASA Langley program was established to obtain the required data base for the QCSEE nozzle and to define the forward and reverse nozzle geometries to satisfy the design requirements previously stated. It was also desirable to confirm that the flap flow attachment achieved at static conditions would be maintained during wind-on conditions.

The nozzle development effort commenced by establishing a general maximum area available for side door arrangements since the specific door design was not yet known. This area is shown in Figure 13.4. A brainstorming session by GE and NASA resulted in the concepts for consideration shown in Figure 13.5. The plan was to start with the baseline nozzle shown in Figure 13.5 and, if the test results so dictated, to proceed to investigate each concept in a designated order of priority. However, satisfactory baseline configuration performance made it unnecessary to pursue testing the remaining concepts.

The internal performance (flow coefficients, velocity coefficients) test setup is shown in Figure 13.6. The model is shown with a bellmouth installed on a 14 cm (5.5 inch) diameter tip turbine driven fan and round calibration nozzles at the exit. Also shown on the test bench in Figure 13.6 is the QCSEE OTW baseline nozzle with side doors open to the takeoff position. This model was designed to allow ready interchangeability of the aft ducting. The model was pressure instrumented and thrust was measured using a two-component force balance mounted beneath the floor plane. After round nozzle calibration runs were completed, QCSEE OTW nozzle thrust, airflow, and pressure ratio were obtained for takeoff and cruise side door settings. These data were taken with nozzle alone and with small and large flat plate wing upper surface simulations as shown in Figure 13.7.

For wing/flap static turning performance, the OTW scale model and fan assembly were taken off the force balance and a wing, which was configured for the 60° approach flap setting, installed. The QCSEE nozzle was positioned over the wing upper surface and mounted to the test bench in a manner which did not ground the wing/force balance system, see Figure 13.8. With the propulsion simulator and QCSEE nozzle supplying airflow to the wing upper surface, the resultant wing lift and drag forces were measured on the force balance. These data were combined with nozzle alone axial and vertical force data to obtain propulsion system/wing/flap static turning angle and turning efficiency (relative to the takeoff nozzle with large plate).

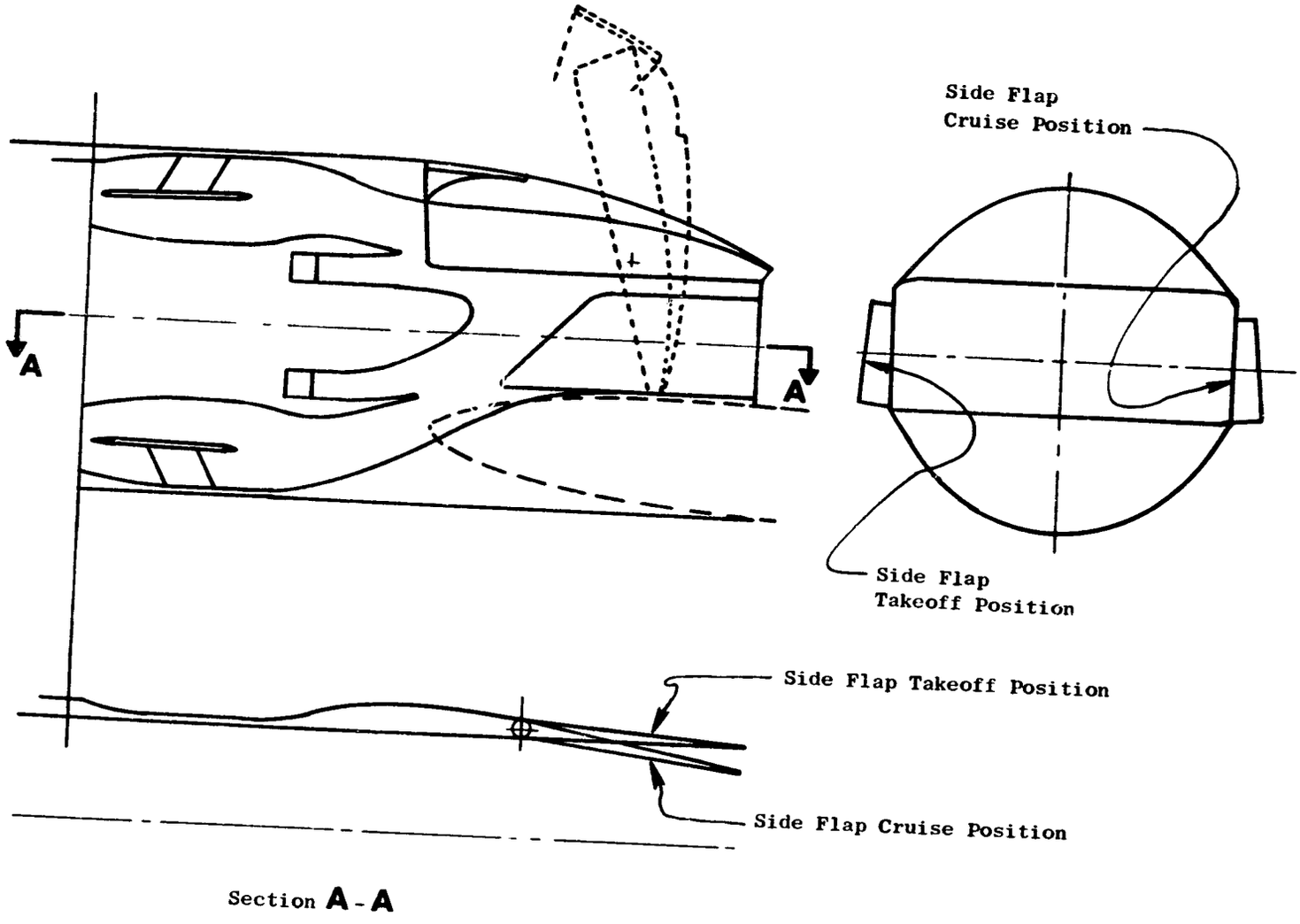

Figure 13.2. Preliminary Propulsion System Design.

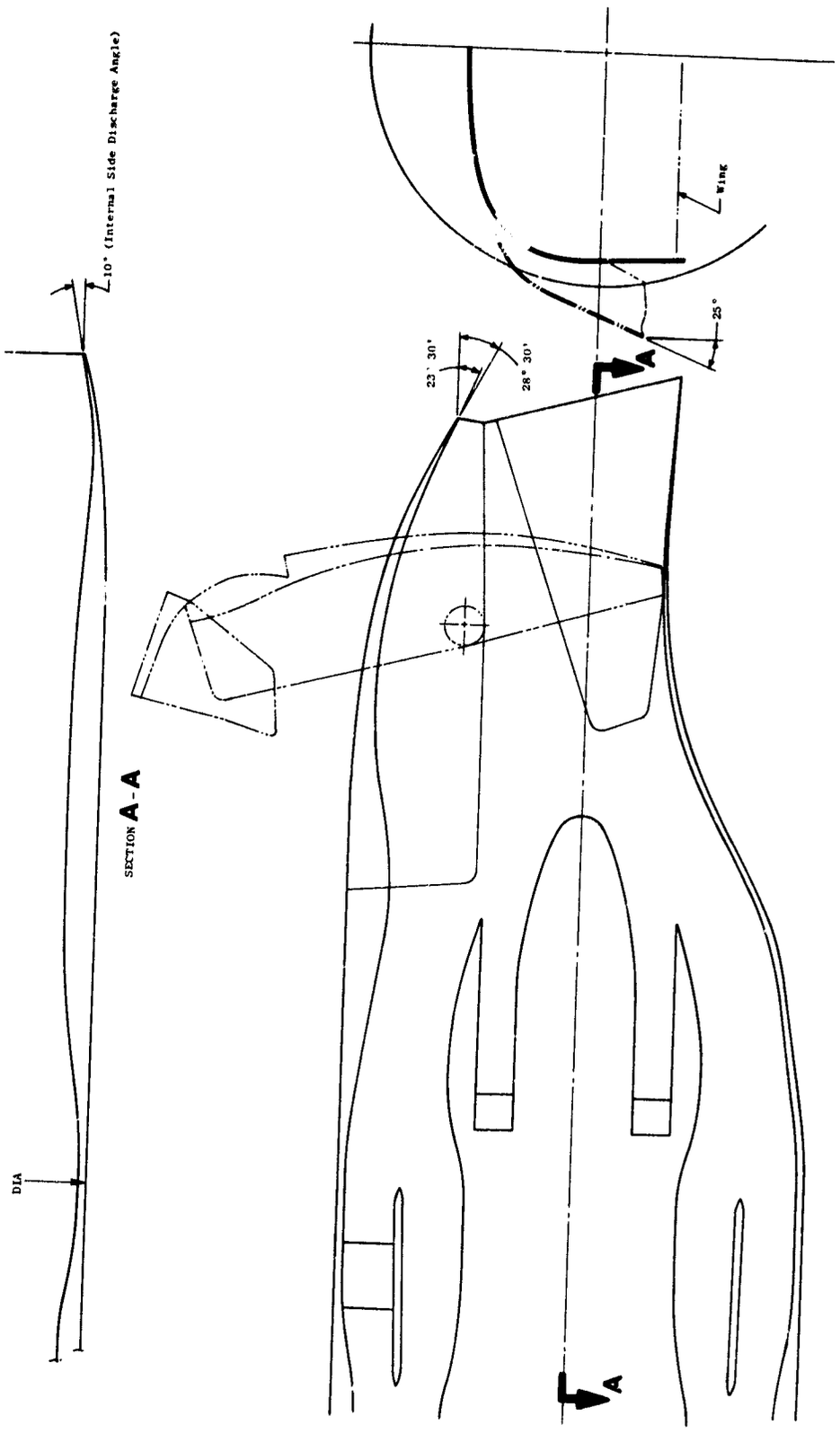

Figure 13.3. Baseline Propulsion System Design.

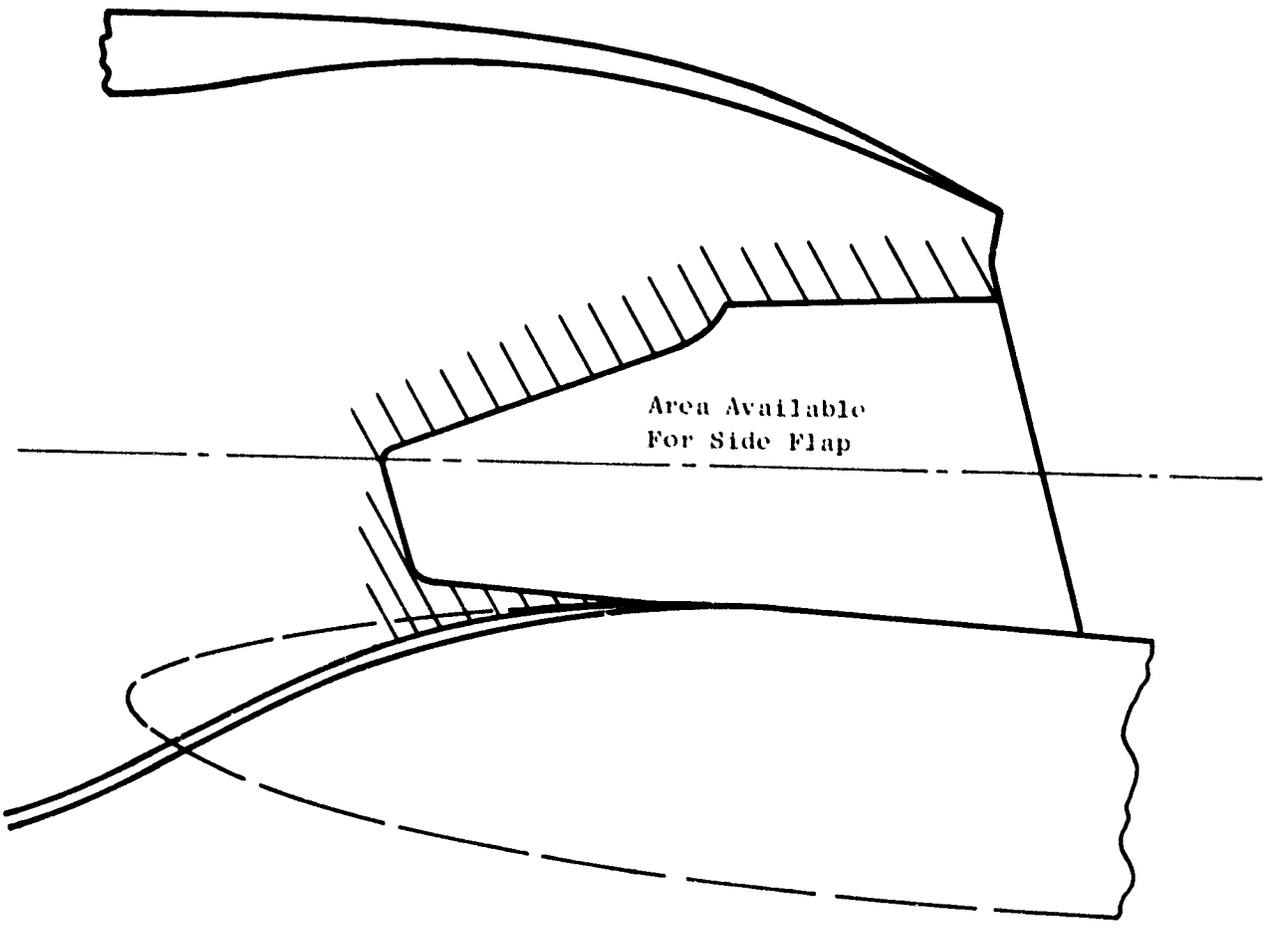

Figure 13.4. Exhaust System Side Door Geometry.

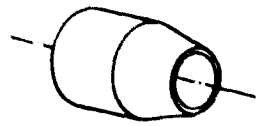

(1) Axisymetric Calibration Nozzle

(2) Baseline
(Reference GE Drawing 4013174-198,
Design "B")

(3) Horizontal Hinge Line

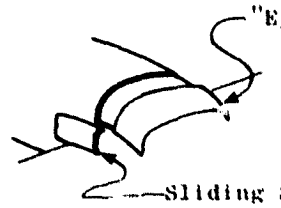

(4) Sliding Side Door and Deflector

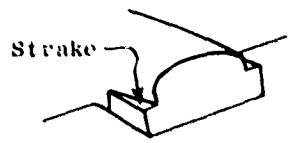

(5) Vertical Hinge Line Strake

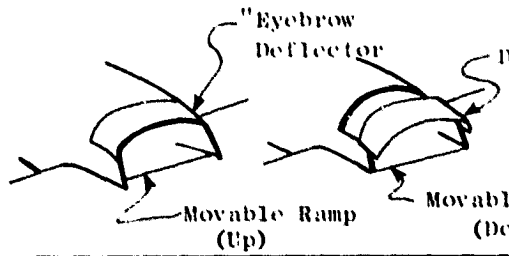

(6) Movable Ramp and Deflector

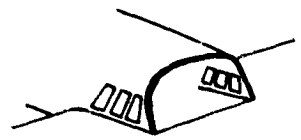

(7) Louvers

Figure 13.5. OTW Exhaust Nozzle Concepts.

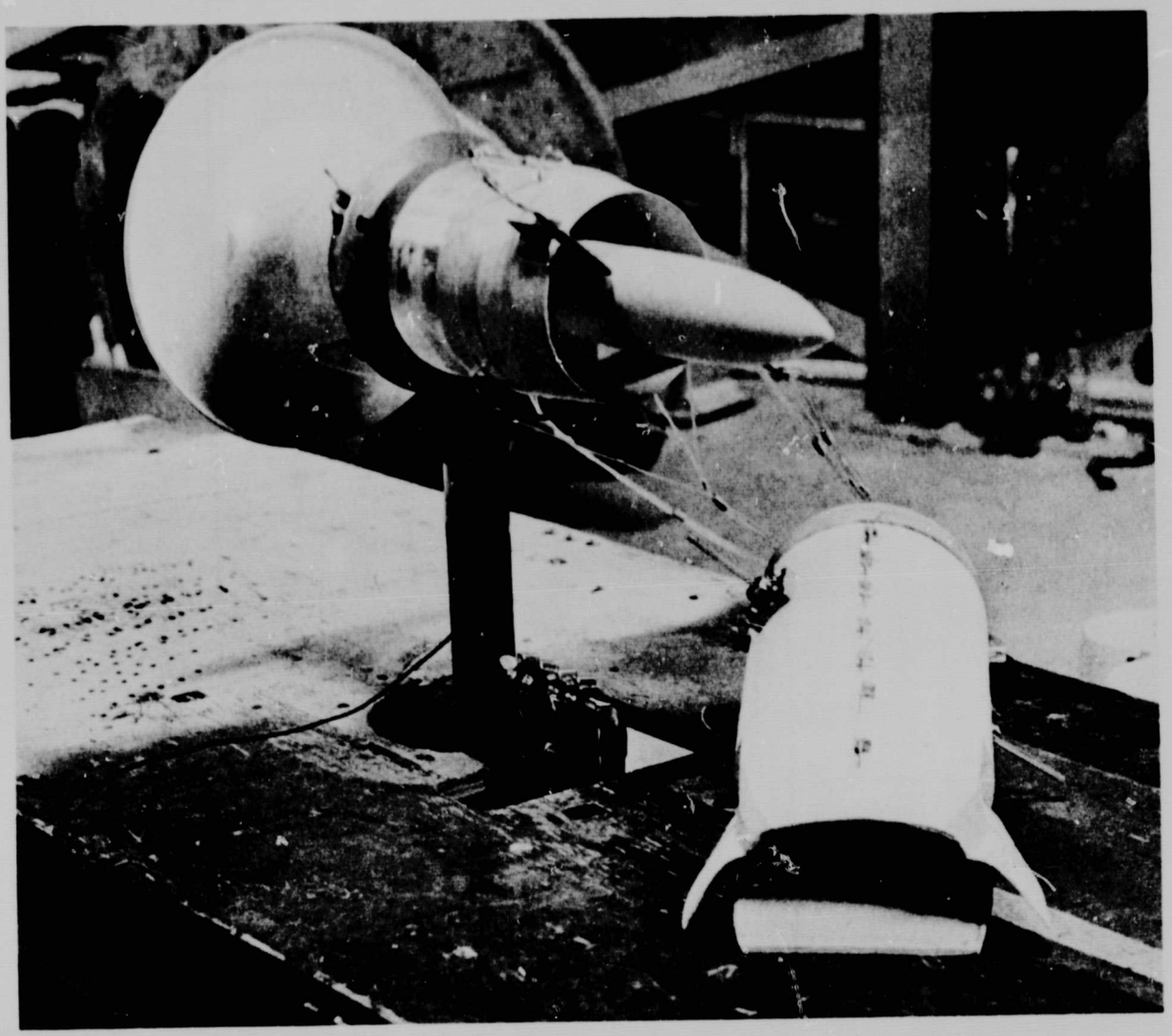

Figure 13.6. Nozzle Bench Test Setup.

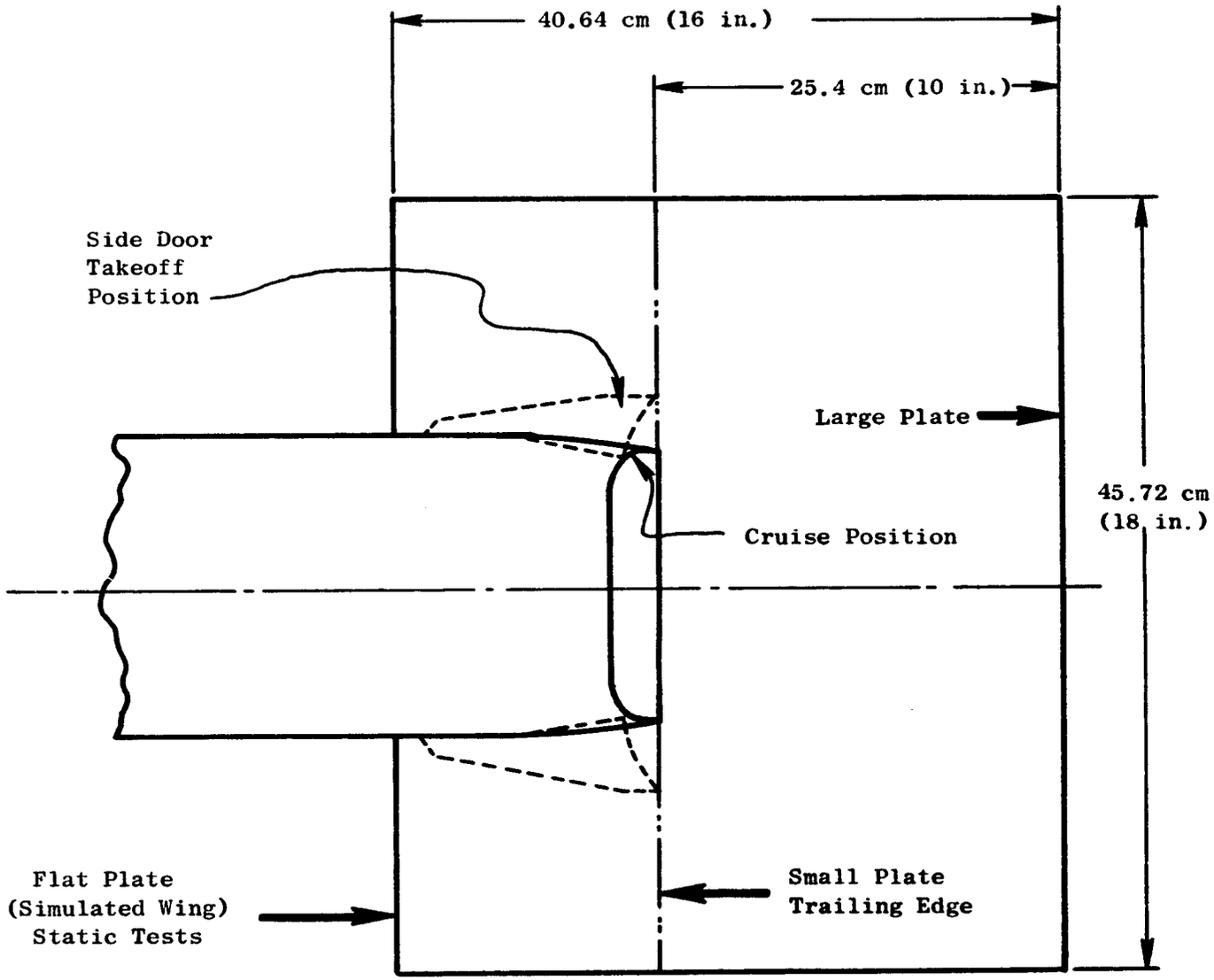

Figure 13.7. Langley Scale Model Bench Test Configuration.

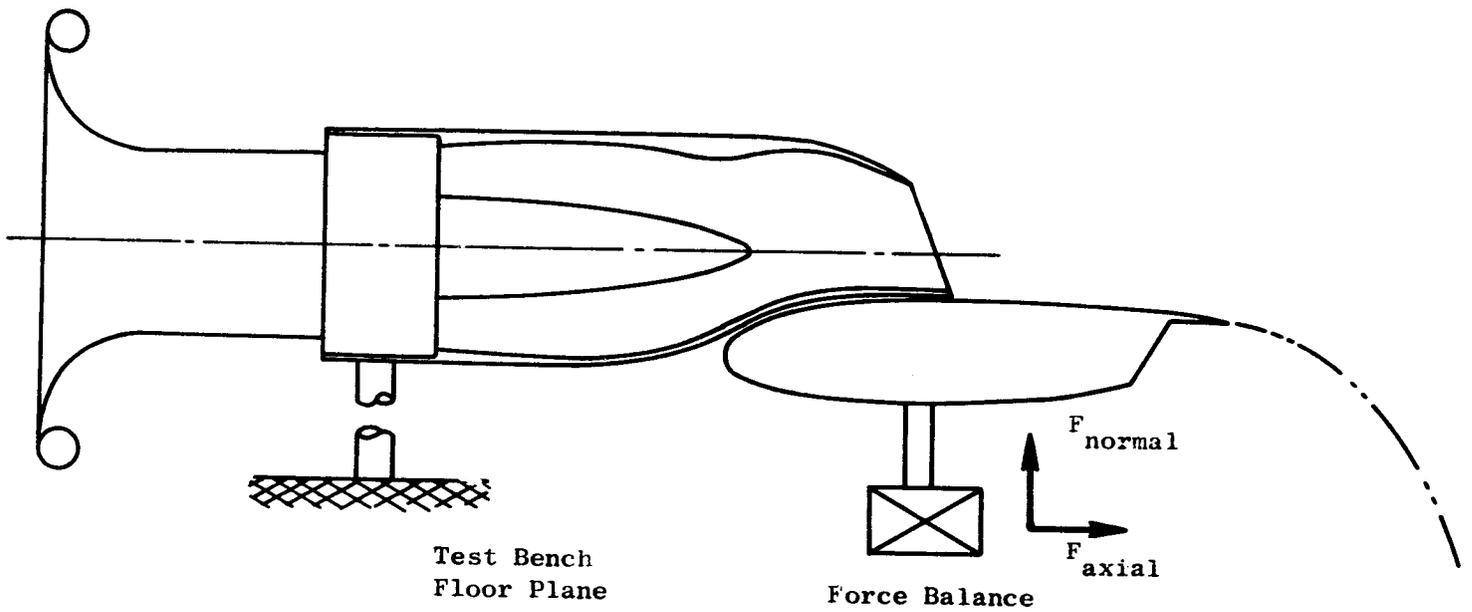

Figure 13.8. Wing Static Turning Test Configuration.

While the initial static turning test results of the baseline nozzle were very encouraging, and in general agreement with the Langley data base in Figure 13.1, the measured static turning angle (48°) did not meet the QCSEE objective of 60°. Variations of the baseline nozzle were then made and tested in the program as shown in various views on Figure 13.9 through 13.14. The nozzle arrangements depicted respectively as the Baseline, recontouured number 1, and recontoured number 2, reflected technical insight into the flow turning mechanism and the direction to proceed for improving static turning with some attention to the impact on external drag. Two side door arrangements were included in the experimental evaluation, a small door with angle of 60° and large door with angle of 25° described in Figure 13.10.

The resultant turning data for RC-1 and Baseline nozzles is shown in Figure 13.15. The recontoured RC-1 nozzle produced significantly better turning data than the baseline with relatively insignificant difference between the large and small door designs. RC-2 data indicated the same degree of static turning, but these results are not shown because of suspected force balance measurement errors.

The recontoured RC-1 nozzle performance with large nozzle side doors was considered very satisfactory, meeting all turning objectives, and all consideration for alternate concepts was dropped at this point. Only the wind-on test was required to ensure that the flow attachment was not affected by freestream effects.

The initial static tests were conducted at Langley using a single-fan propulsion simulator. With this configuration, the maximum nozzle exit pressure ratio obtainable was in the order of 1.15, whereas the QCSEE demonstrator engine nozzle pressure ratio was approximately 1.3 at the takeoff power setting. In order to avoid having to extrapolate scale model flow and velocity coefficient data from 1.15 up to the 1.3 nozzle pressure ratio region, the test set up was converted to a higher pressure ratio tandem fan arrangement as shown in Figure 13.16. Total pressure measurement instrumentation is also shown in this figure. All final calibration nozzle and QCSEE Baseline and RC-1 nozzle data presented on Figures 13.17 through 13.25 were obtained with this tandem fan configuration.

Figures 13.17 and 13.18 show the flow coefficient and velocity coefficient characteristics of the four round calibration nozzles. These data were adjusted to agree with reliable flow coefficient data which were obtained by NASA Lewis on similar nozzles (reference NACA Report 933). The adjustment was made by applying a total pressure bias correction to computation of model ideal weight flow and ideal velocity (both functions of measured nozzle pressure ratio) to effect a match between calibration nozzle flow coefficient data and the referenced NACA data at the respective nozzle cone half angles, θ. The bias correction was rationalized on the basis that simulator total pressure was measured from a manifolded single reading and did not compensate for significant total pressure profile effects which should have been mass weighted in favor of the higher fan pressures found at the fan tip and turbine drive air regions. Without this

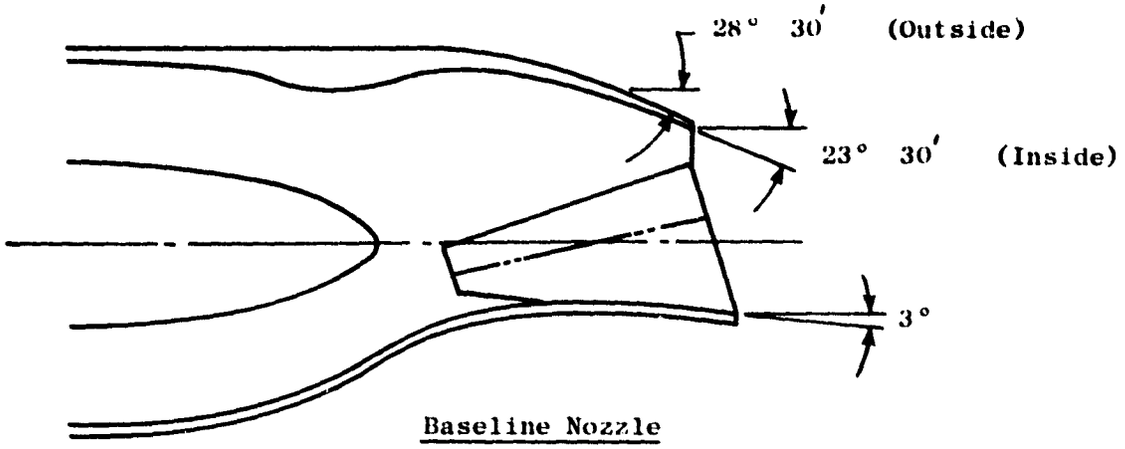

Baseline Nozzle

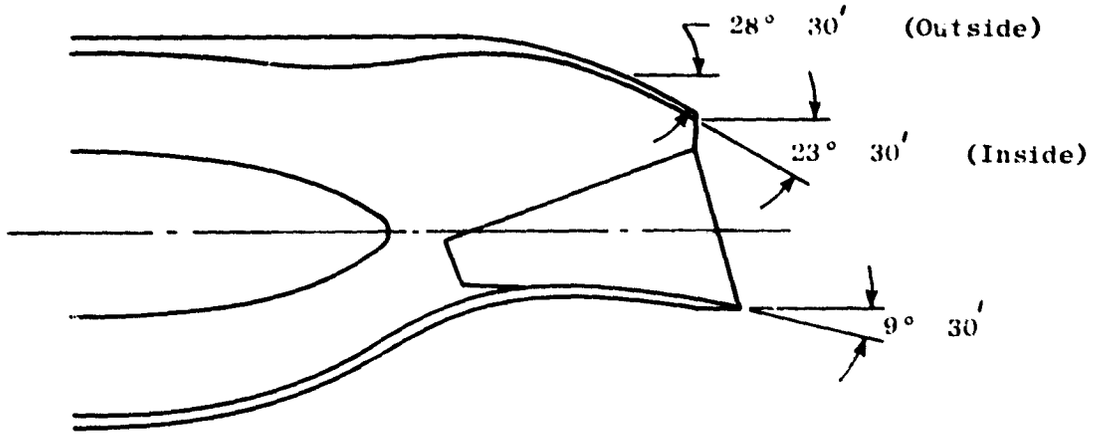

Recontoured No. 1

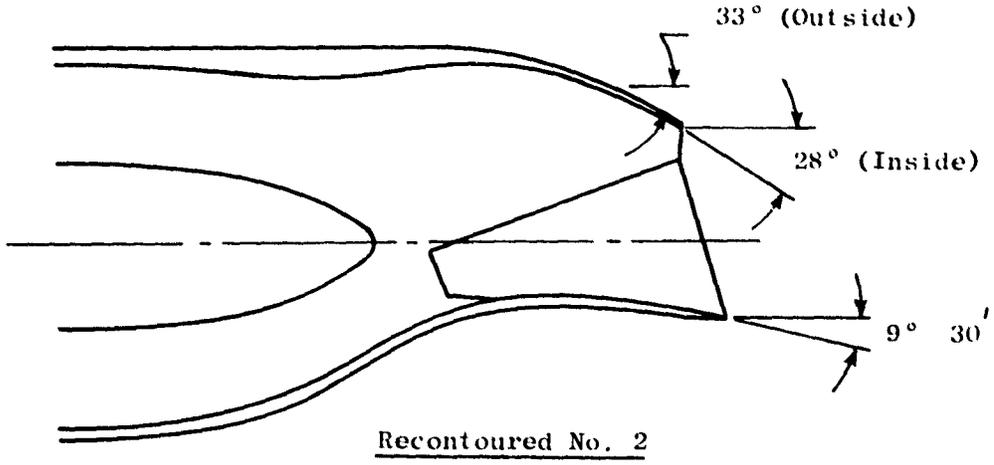

Recontoured No. 2

Figure 13.9. Baseline Nozzle Variation.

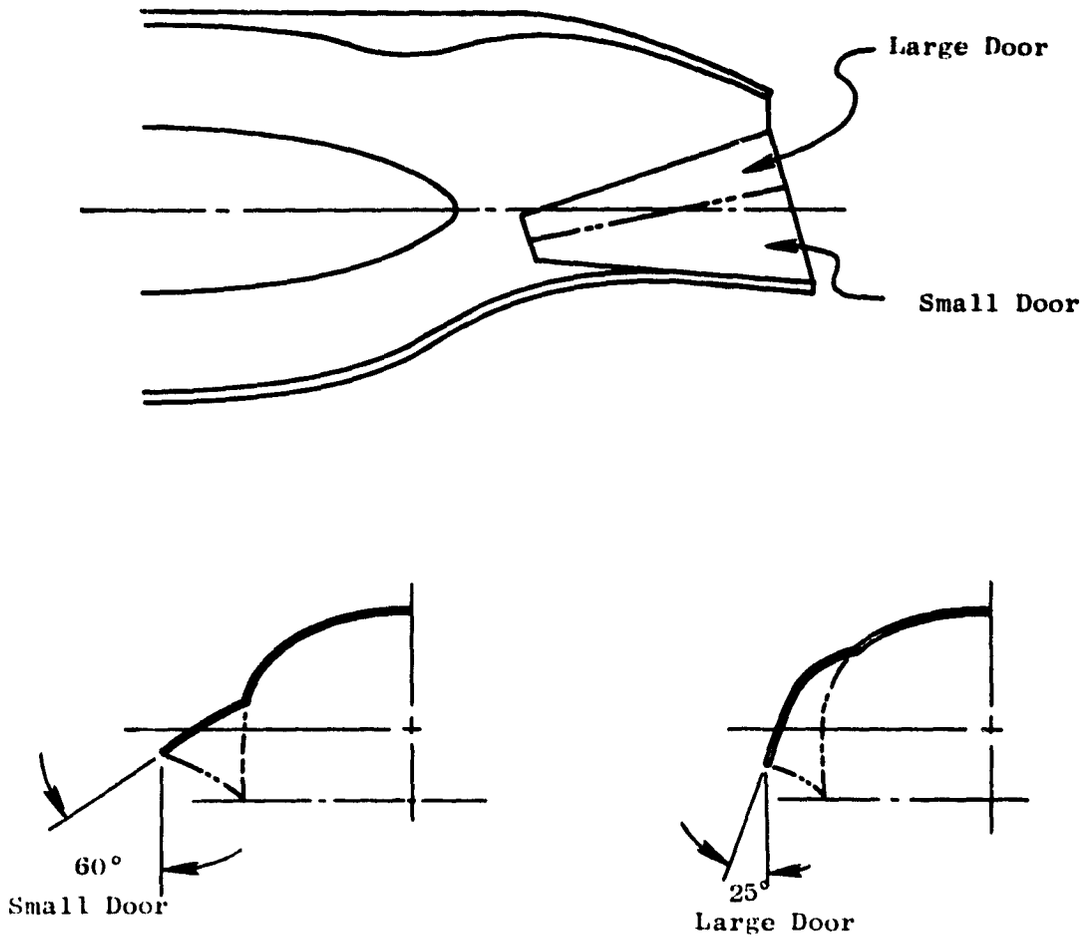

Figure 13.10. Baseline Door Designs.

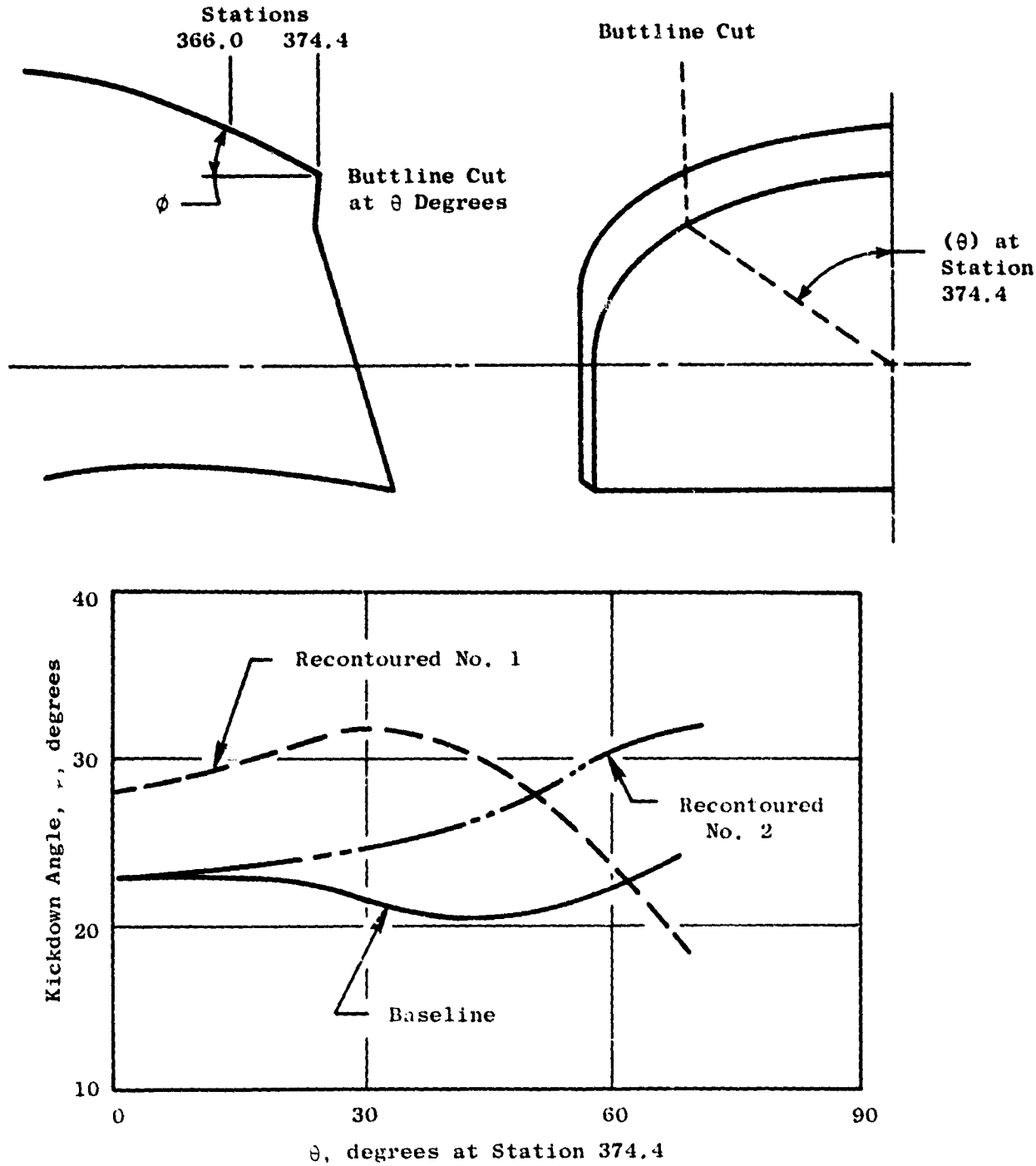

Figure 13.11. Nozzle Kickdown Angles.

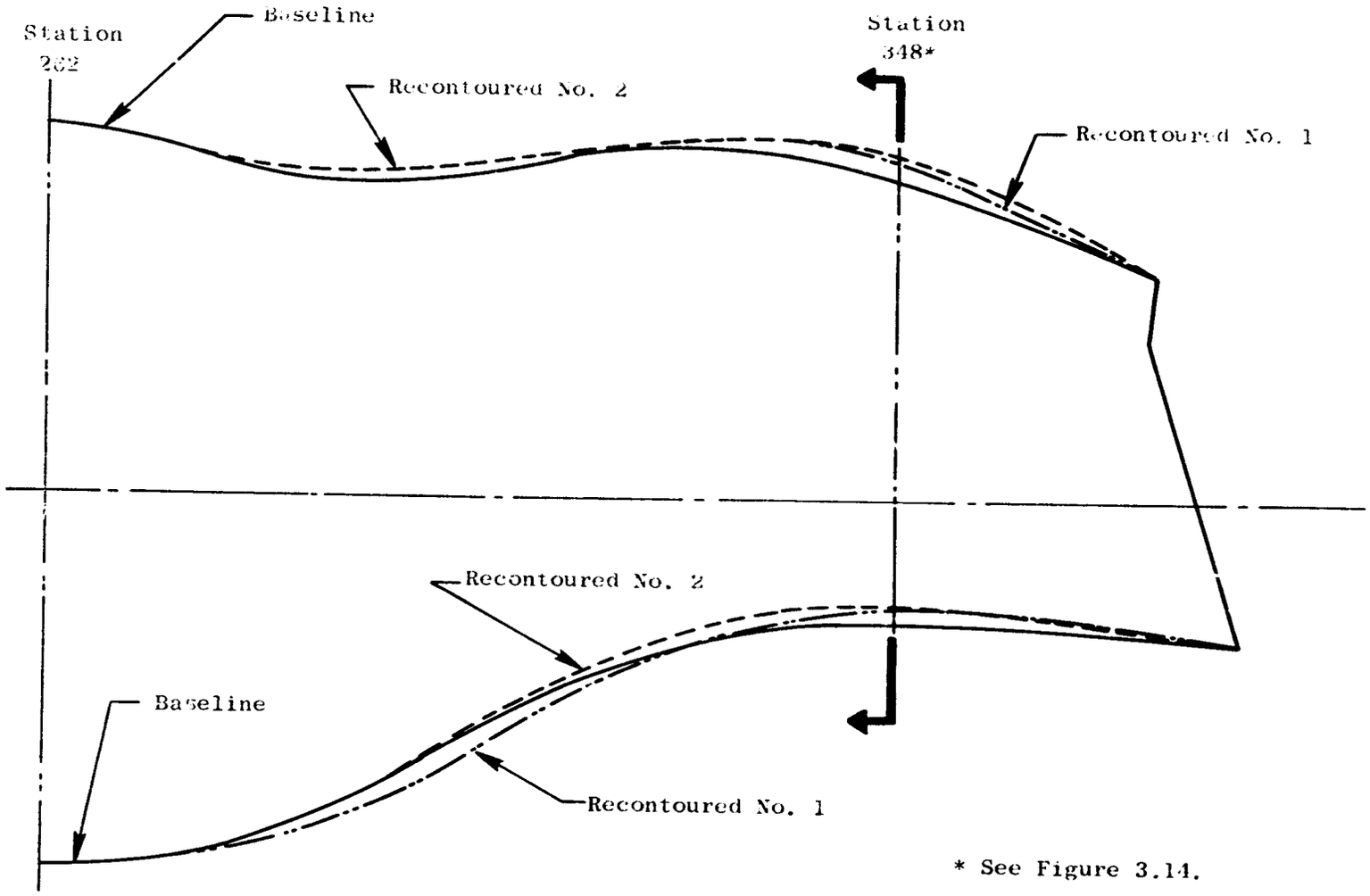

Figure 13.12. Nozzle Internal Flowpaths.

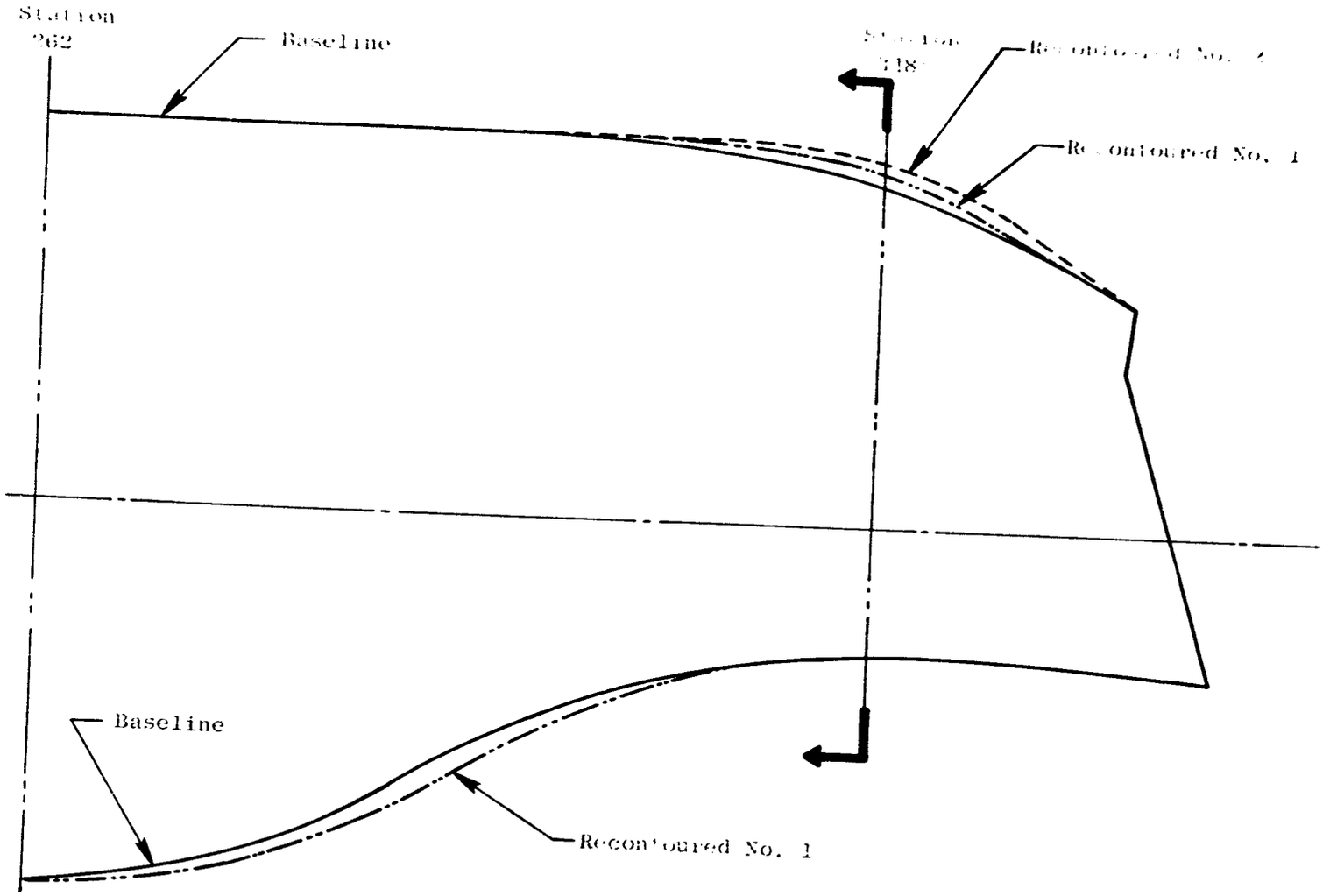

* See Figure 13.11.

Figure 13.13. External Nacelles.

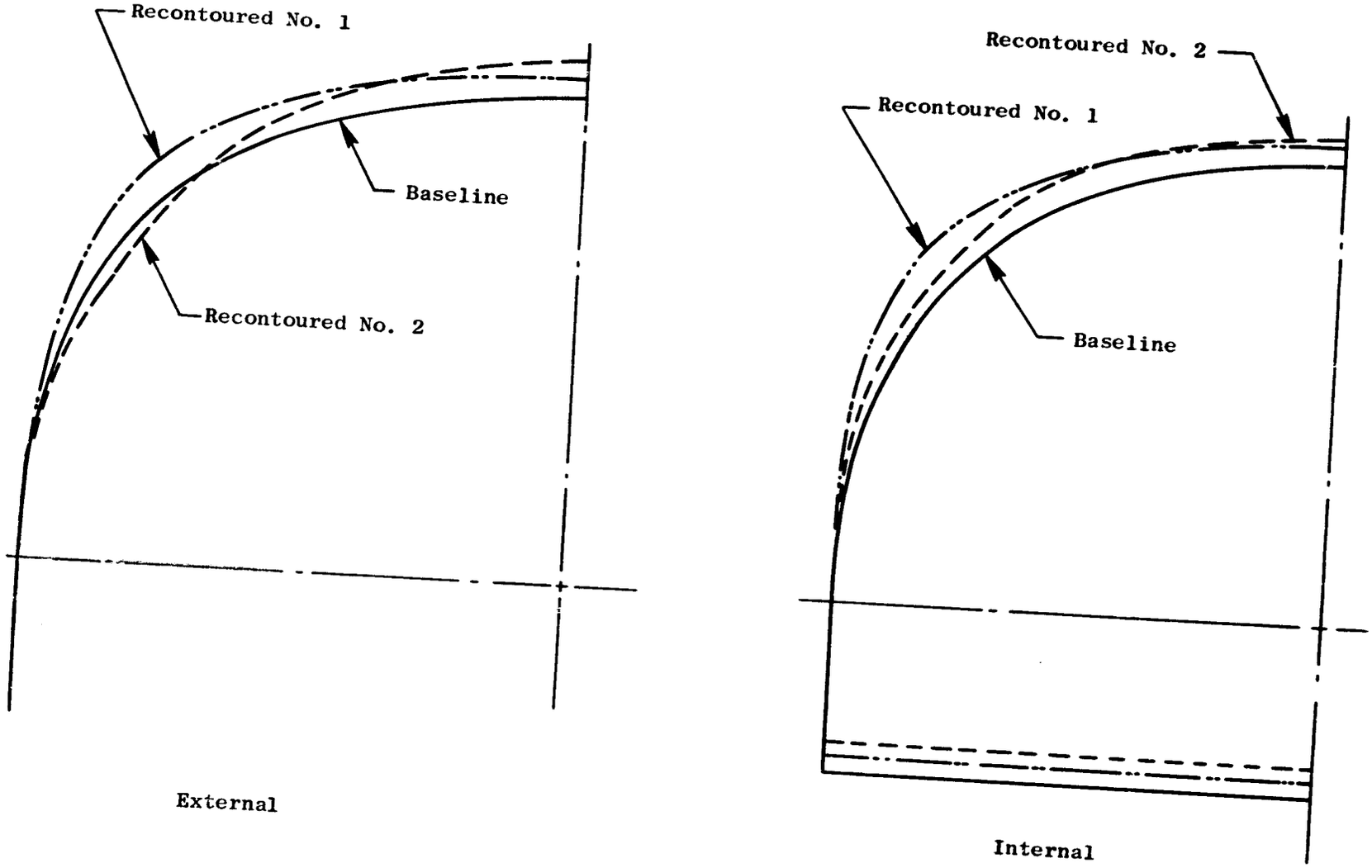

Figure 13.14. Nozzle Station 348.

Symbol	Nozzle	Side Doors
◇	Baseline	Large, 25°
△		Small, 60°
▮	RC-1	Large, 25°
		Small, 60°

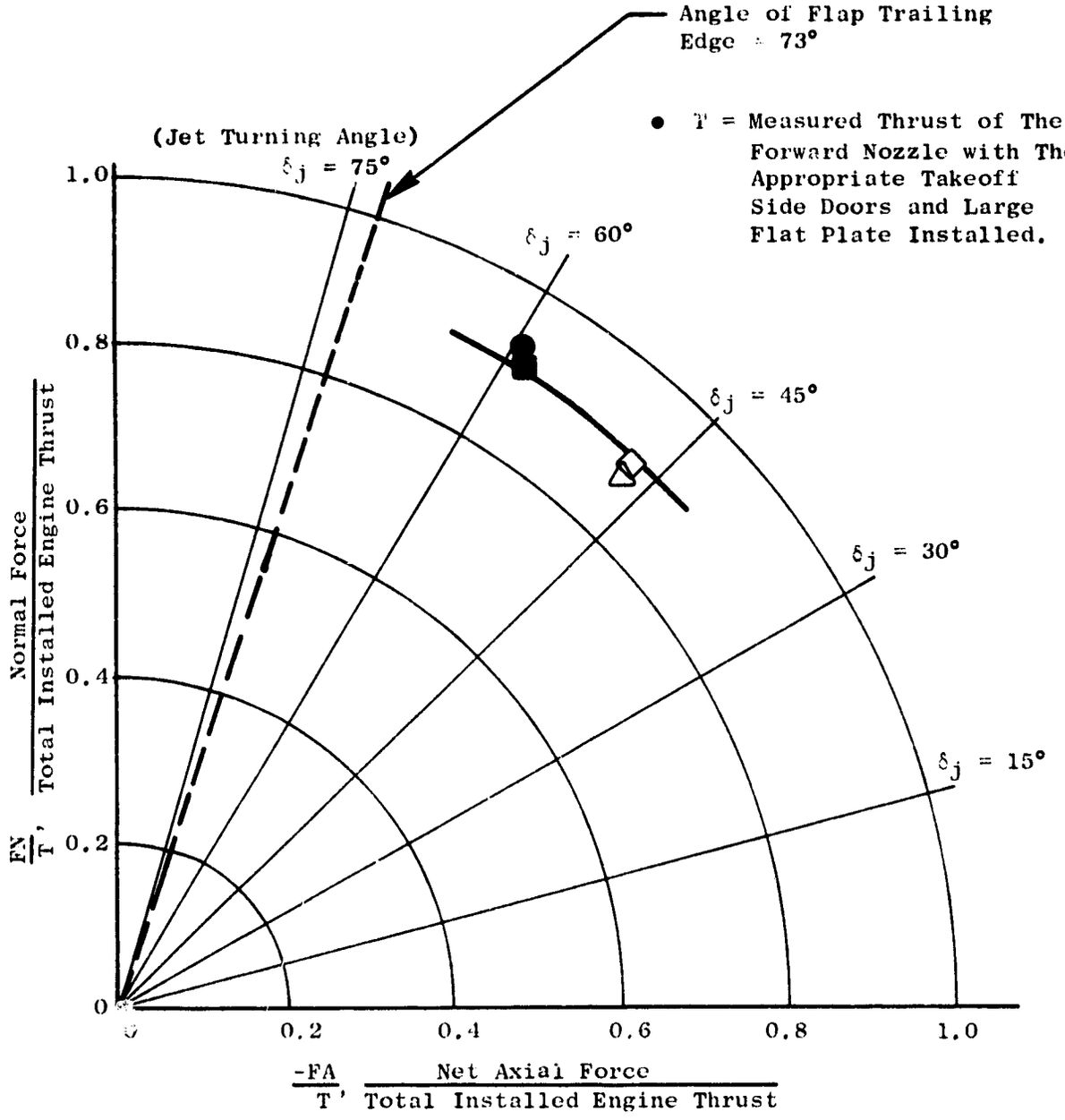

Figure 13.15. Baseline/Recontoured Nozzle Static Turning.

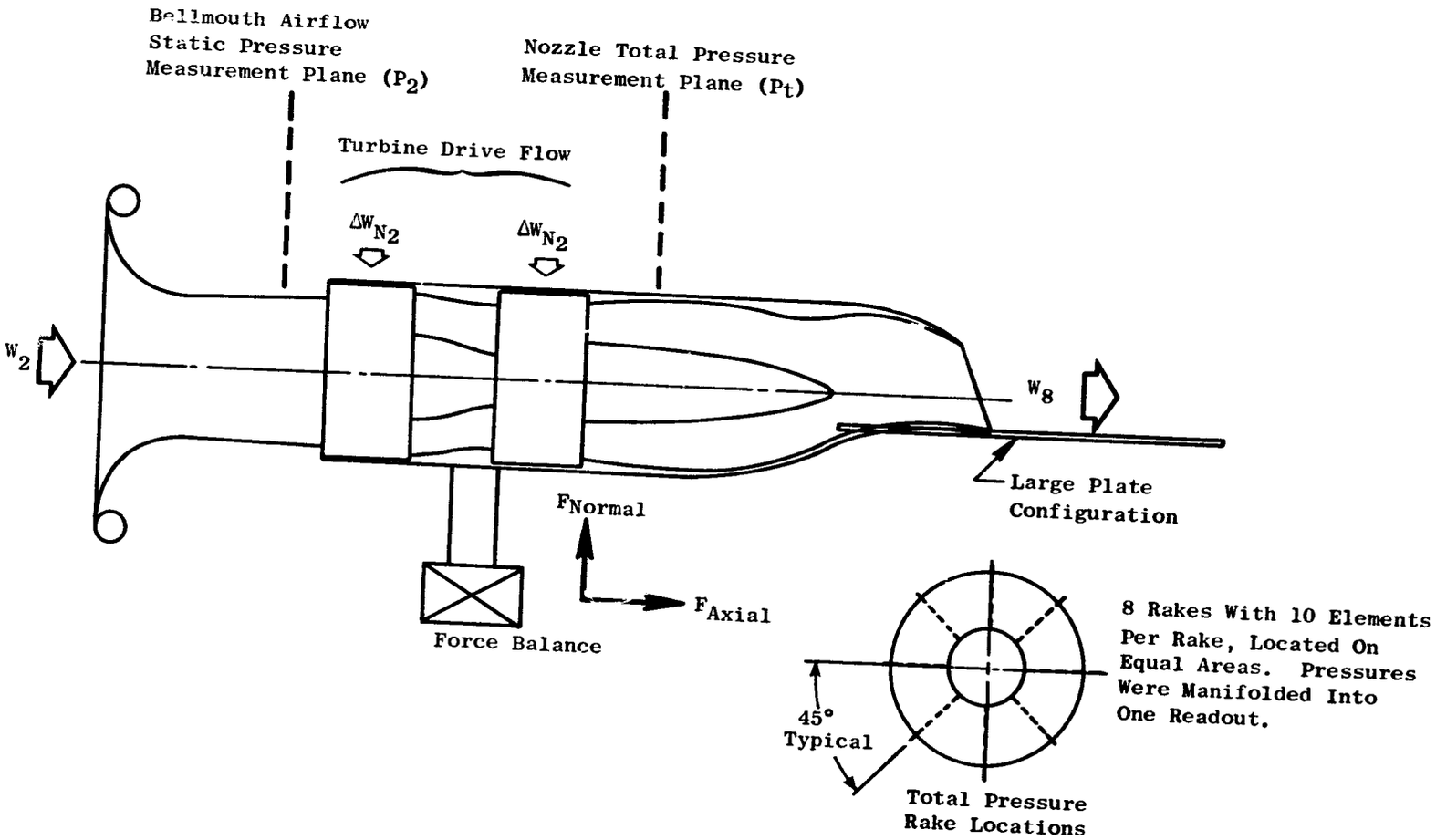

Figure 13.16. Forward Thrust Static Test Configuration, Tandem Fan.

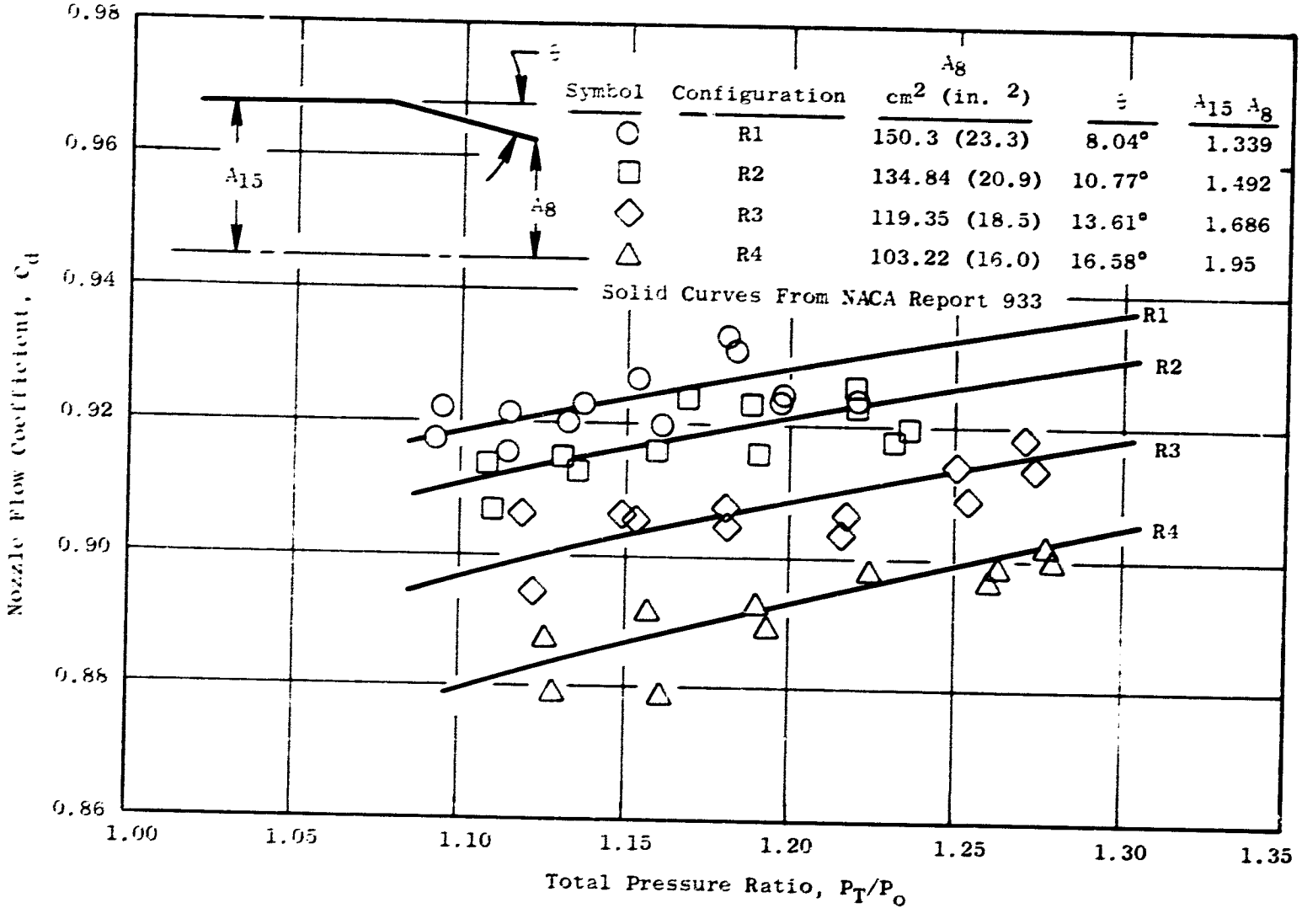

Figure 13.17. Calibration Nozzle Flow Coefficients.

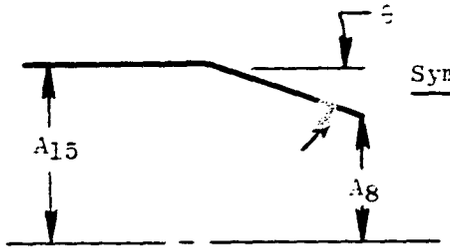

Symbol	Configuration	A_8 cm^2 (in. ^{2})	ε	A_{15}/A_8
○	R1	150.3 (23.3)	8.04°	1.339
□	R2	134.84 (20.9)	10.77°	1.493
◇	R3	119.35 (18.5)	13.61°	1.686
△	R4	103.22 (16.0)	16.58°	1.95

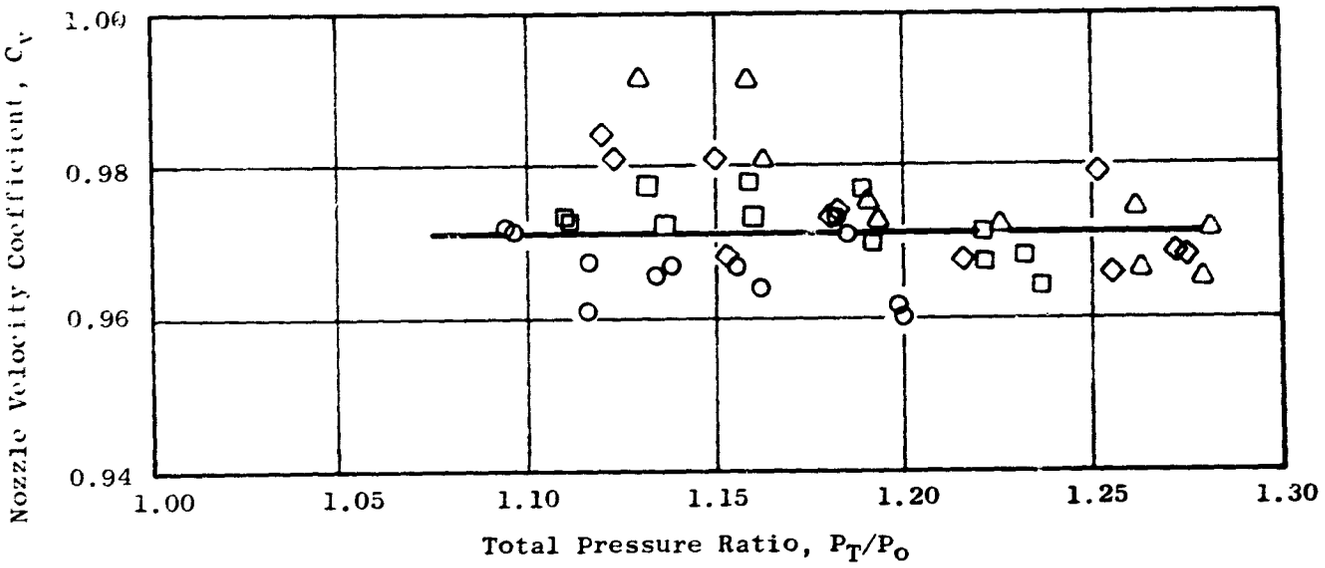

Figure 13.18. Calibration Nozzle Velocity Coefficients.

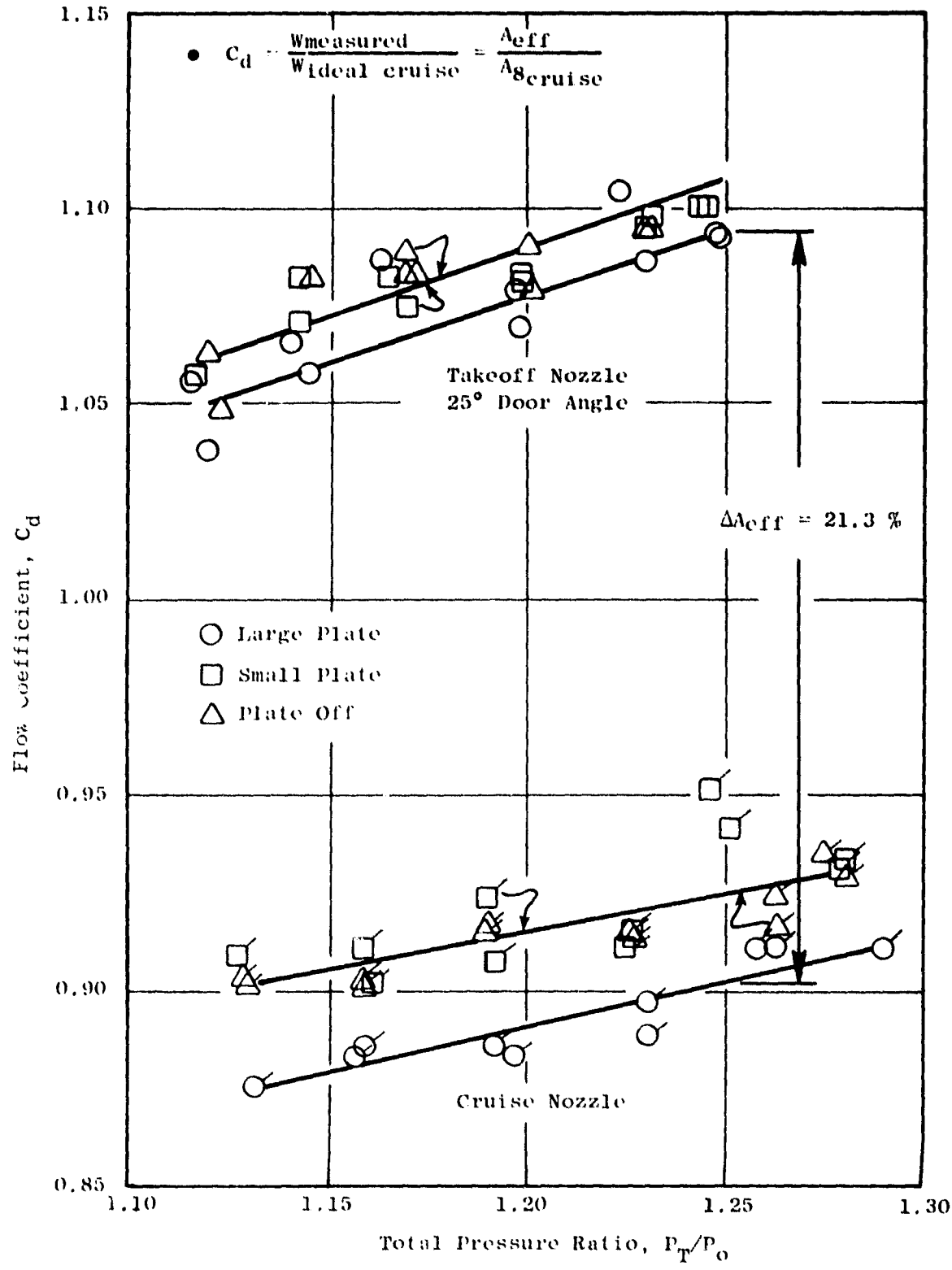

Figure 13.19. Recontoured No. 1 Nozzle Flow Coefficients.

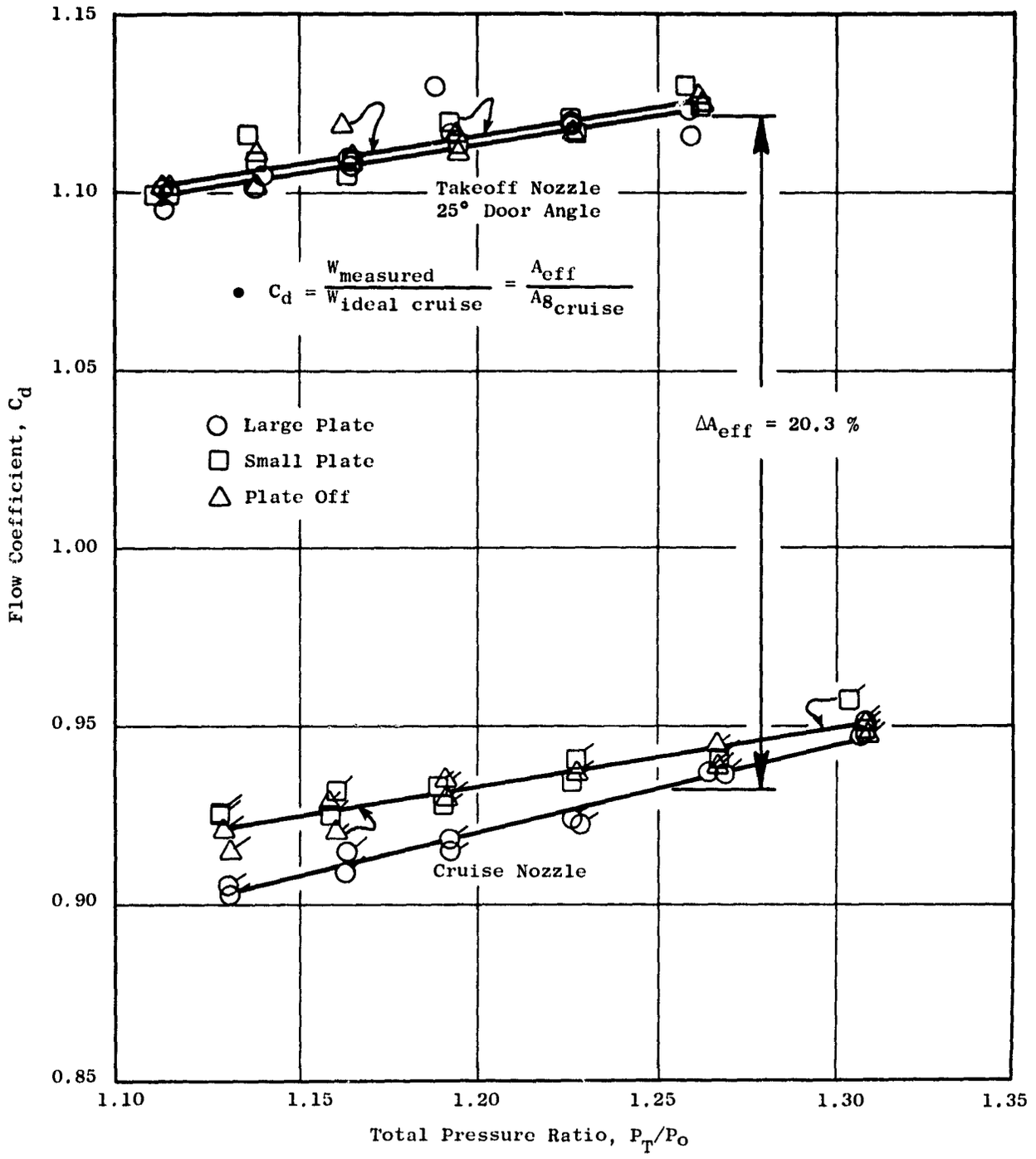

Figure 13.20. Baseline Nozzle Flow Coefficients.

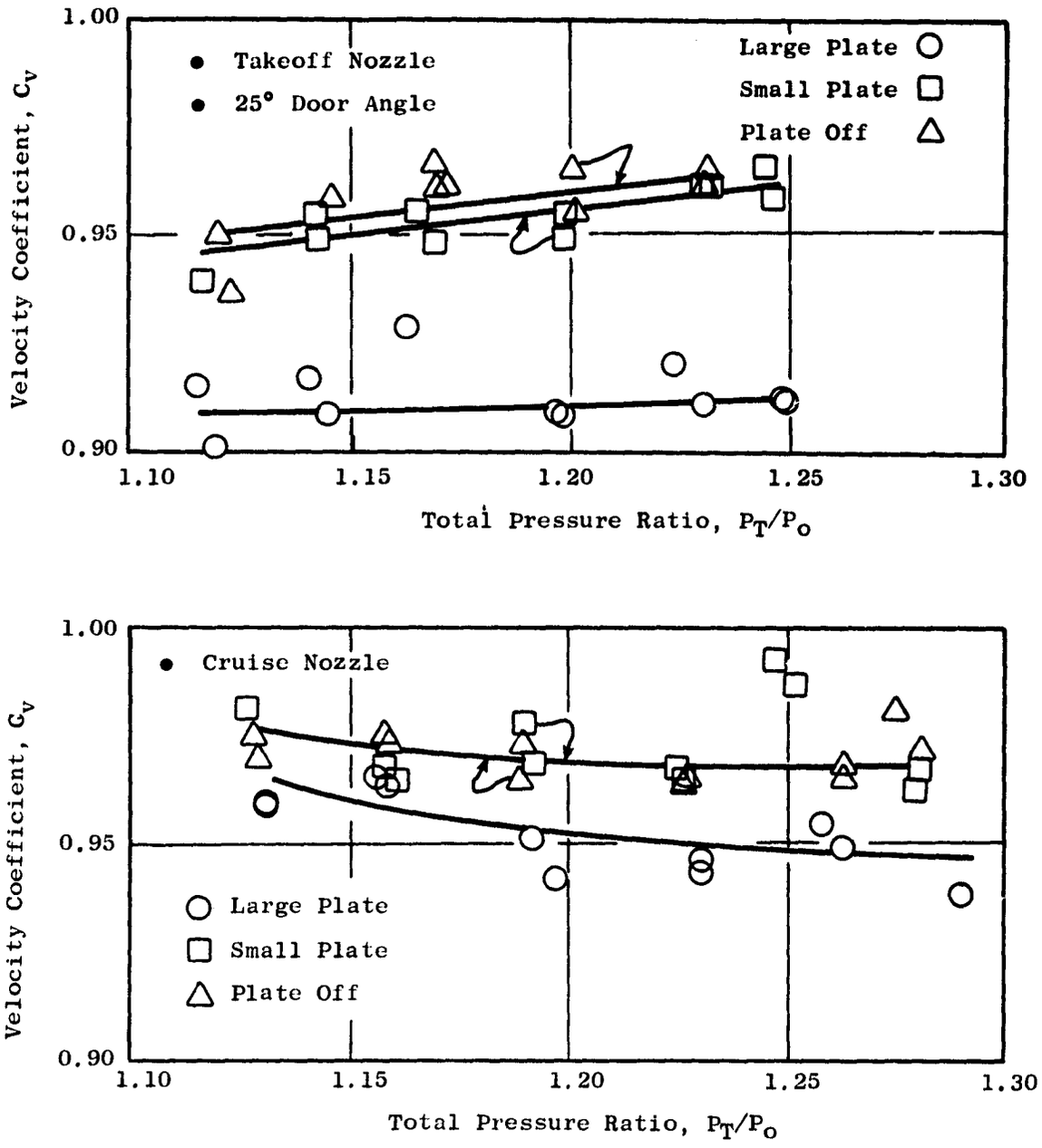

Figure 13.21. Recontoured No. 1 Nozzle Velocity Coefficients.

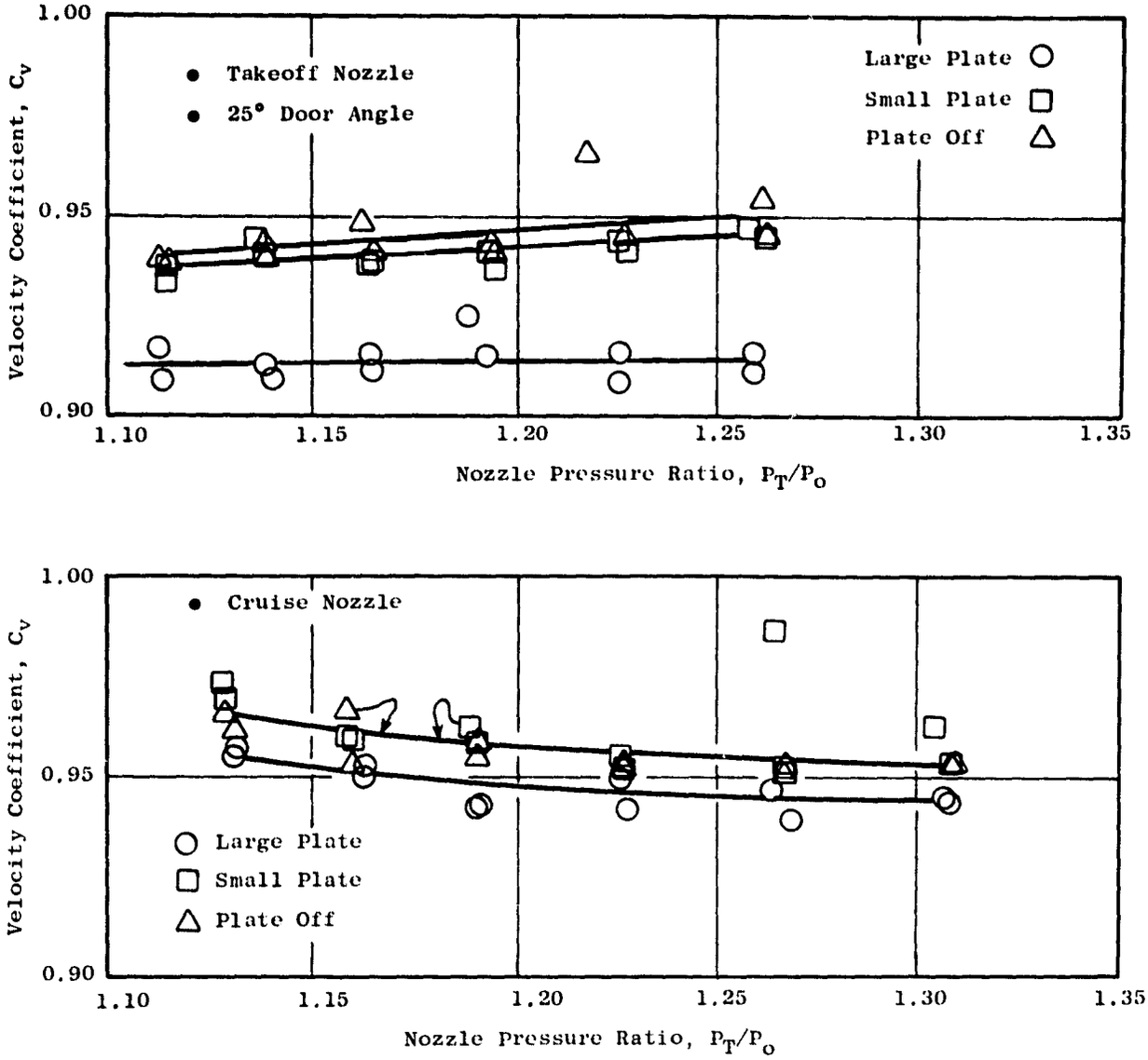

Figure 13.22. Baseline Nozzle Velocity Coefficients.

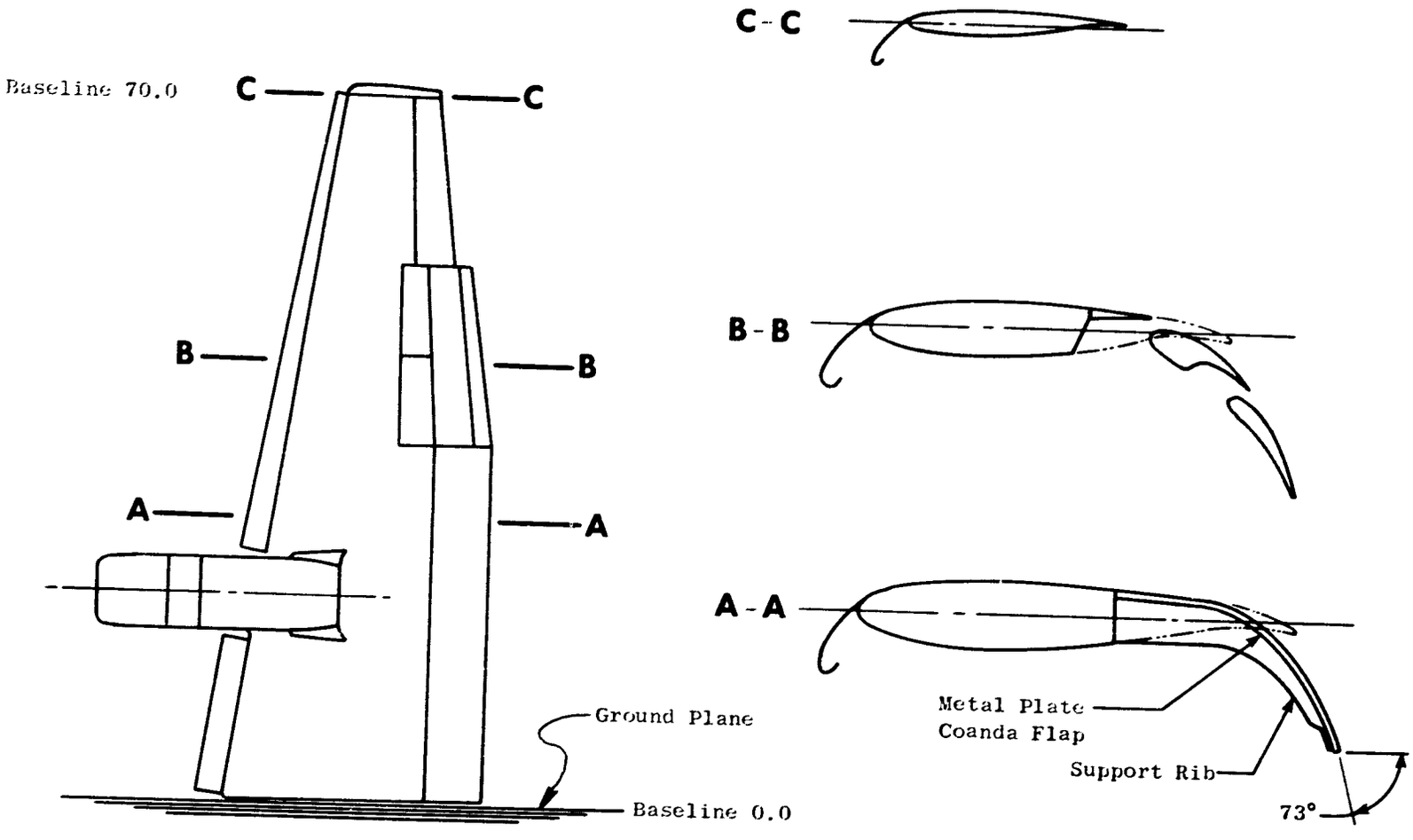

Figure 13.23. Model Used in Wind Tunnel Investigation (Schematic).

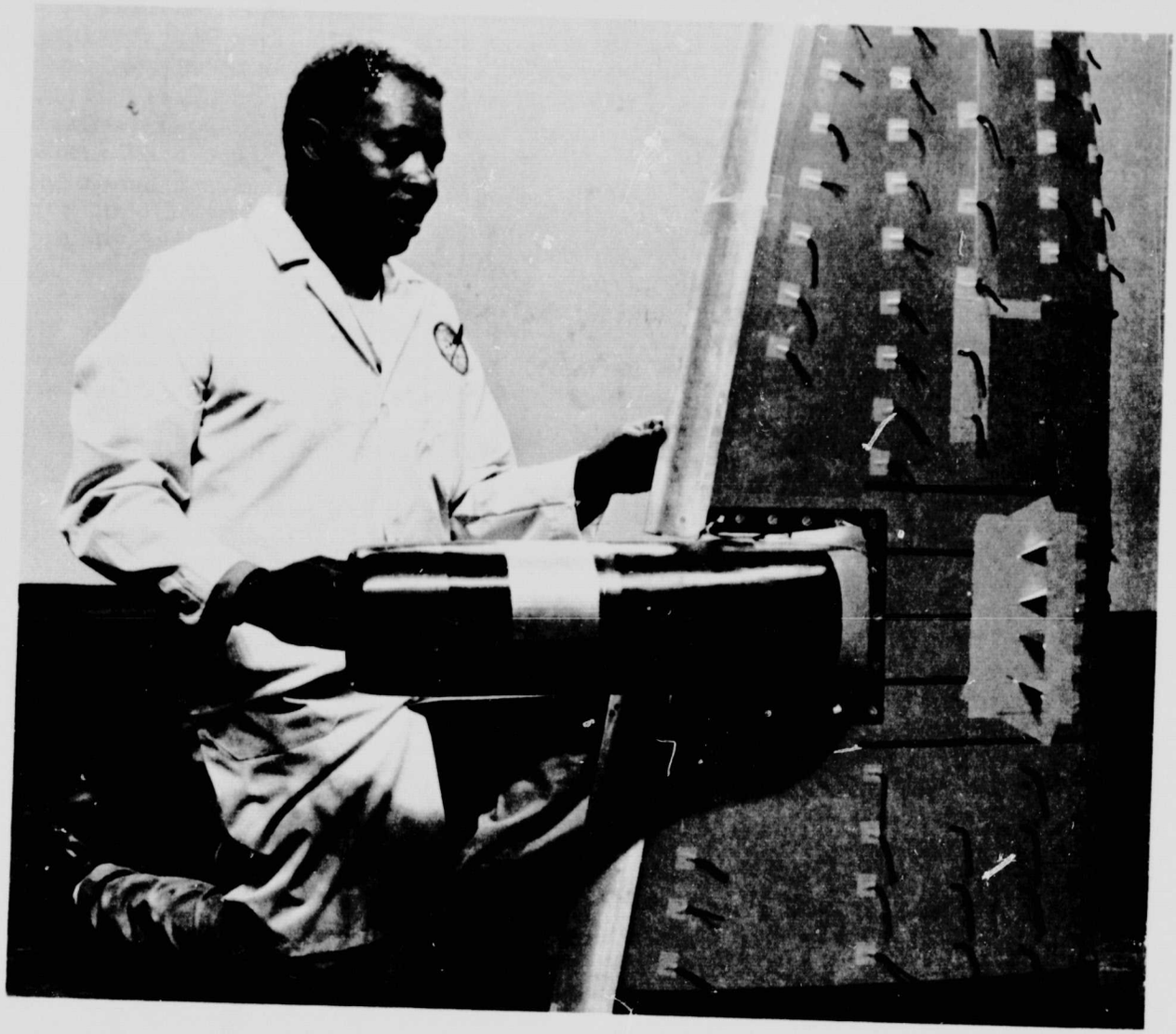

Figure 13.24. Model Used in Wind Tunnel Investigation.

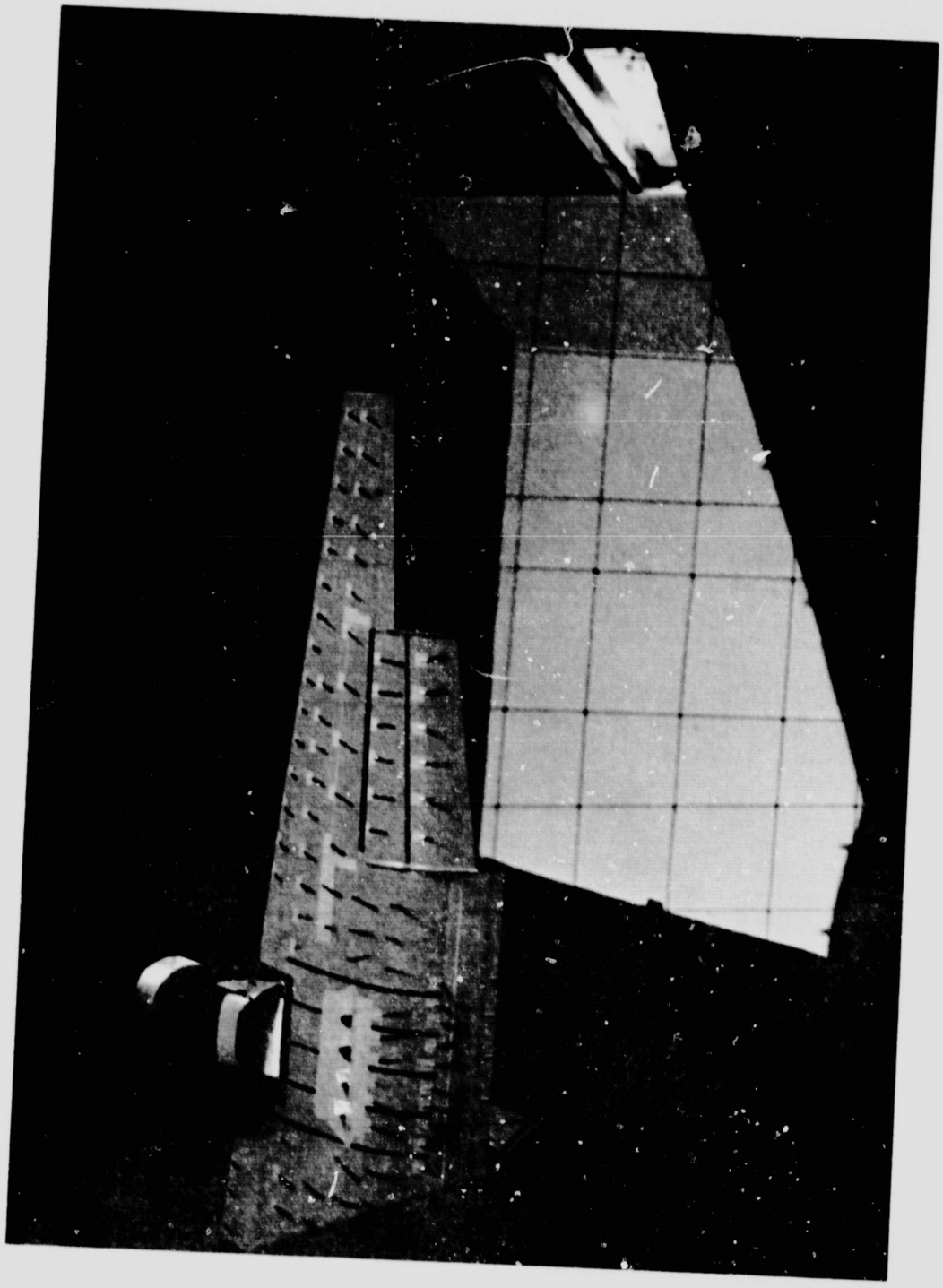

Figure 13.25. Model Used in Wind Tunnel Investigation.

mass weighting, measured total pressure was erroneously low and resulted in velocity and flow coefficient levels above unity with increasingly higher values occurring as model pressure ratio was decreased. The total pressure bias correction amounted to nominally 0.9 percent at a measured pressure ratio of 1.10 and 1.3 percent at measured pressure ratios of 1.25. The resultant round nozzle flow and velocity coefficient trends and level with the adjusted pressure ratio are reasonable and justify the method used to correct the data. All scale model coefficient data contained in this report have been adjusted using the corrections determined from analysis of the round nozzle data.

Figures 13.19 and 13.20 present flow coefficient data for the baseline and RC-1 Nozzles. Both nozzles show essentially the same area change between takeoff and cruise effective areas with relatively small changes in effective areas attributed to flat plate configuration. The cruise to takeoff area change measured is considered acceptable for the QCSEE OTW demonstrator engine cycle needs.

Nozzle velocity coefficient data are shown on Figures 13.21 and 13.22 for the baseline and RC-1 nozzle configurations. These velocity coefficients are defined as the resultant thrust (determined from vertical and axial force balance readings) divided by the calculated ideal thrust (function of pressure ratio). The results show that RC-1 and baseline takeoff velocity coefficients are essentially the same (~0.91 to 0.915) with the large plate installed, with RC-1 performance for the small plate and plate off approximately 1.0 to 1.5 percent better than the baseline. The difference in performance between the large plate and either small plate or plate off configurations is attributed to a combination of (1) large plate skin friction, (2) nonaxial velocity components (flow angularity loss) which arise from the side door flow spreading, and (3) jet impingement losses associated with turning the exhaust flow axially along the large plate.

Cruise nozzle velocity coefficient data indicate RC-1 and baseline nozzles have comparable performance with the large plate installed and for plate off conditions. As with the takeoff nozzle, the difference in performance between large plate and plate off configurations is attributed to large plate friction and jet impingement turning losses; angularity losses are considered to be essentially eliminated when side doors are closed.

The wind-on evaluation was conducted in the NASA Langley 3.65 m (12 ft) pressure tunnel. The test wing and flap arrangement is shown in Figure 13.23 schematically and installed in the wind tunnel in Figure 13 24. Illustrated in Figure 13.25 is the model with tufts under actual freestream conditions. The tufts show excellent flow attachment and confirm that the excellent static flow attachment characteristics are retained with wind-on.

The Langley program also evaluated the addition of vortex generators. The data shown in Figure 13.26 with the baseline nozzle show a slight improvement with the vortex generators but the system lift was still less than the recontoured nozzles and therefore the recontoured nozzle was selected as the QCSEE design. Another factor in the selection was the unknown impact of vortex generators on noise generation.

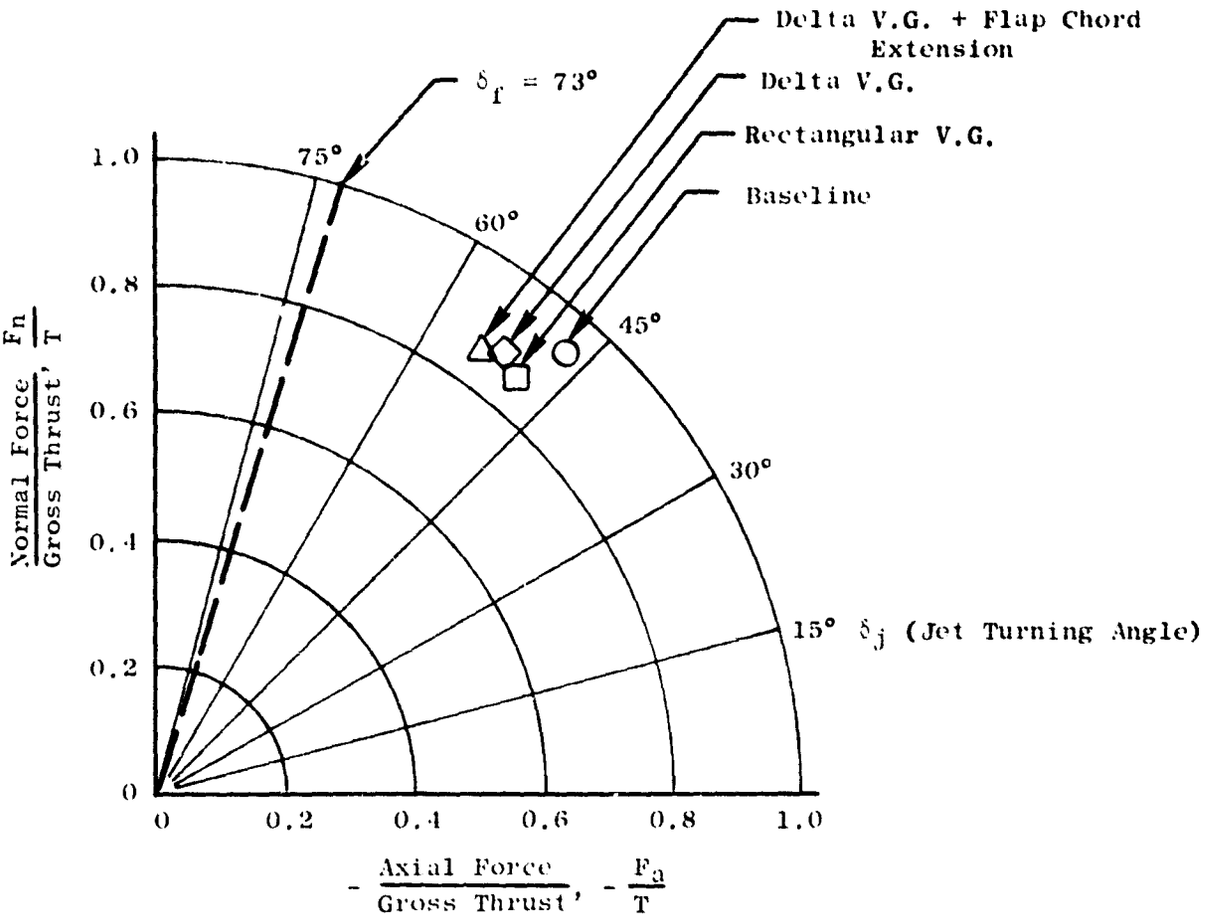

Figure 13.26. Effect of Vortex Generators (VG) On Static Turning with Baseline Nozzle.

The QCSEE OTW propulsion system final flow path design which evolved from the Langley development tests is shown on Figure 14.5 (Section 14.0). This configuration is designated RC-1A, being derived from the roof lines from RC-1 and the floor lines of RC-2 (see Figure 13.12). Roof lines from RC-1 were selected because of potentially higher cruise performance with the shallower 28°30' boattail angle versus 33° for RC-2, as shown on Figure 13.9. The floor lines from RC-2 were selected because the curvature was more moderate and, therefore, more conducive to flow attachment inside the nozzle.

13.3.2 Thrust Reverser

The OTW thrust reverser configuration was established from 1/12 scale model tests at the NASA Langley Research Center. The test setup shown schematically on Figure 13.27 consisted of two 13.97 cm (5.5 inch) diameter tip turbine driven fans coupled in tandem, a bellmouth for airflow measurement, and a force balance having both axial and normal (relative to model centerline) force measurement capability. Reverser configurations were attached to the aft portion of a single-stream simulation of the QCSEE OTW fan duct and "D" nozzle model which was modified to form the basic reverser opening and blocker door assembly. A typical scale model installation in the static facility is shown on Figure 13.28. This figure also shows the blast shield used to prevent reingestion.

Reverser geometry investigated included blocker axial spacing (X) blocker height (H_B), lip length (L) and lip angle (β), blocker door inclination angle (α), and skirt geometry and rotation angle (ϕ). Figure 13.29 further describes the geometric parameters evaluated. Forty-three configurations were tested in all, with reverser pressure ratios ranging between 1.12 and 1.32.

Initial informal testing at Langley showed that the baseline reverser geometry (refer to Figure 13.29) performed poorly relative to the 35% of takeoff thrust required. Also, the reverse airflow level was 15 to 20% below forward thrust takeoff values at the same pressure ratio. Some additional informal exploratory tests (many not recorded) were then conducted in an attempt to establish the direction for further development effort. Significant reverse thrust improvement was noted with extended lip length (up to $L/D_{TH} = 0.8$) and by extending the side skirt forward (including one configuration which totally blocked off the two sides) and rotating the skirts outward to capture flow which was observed to be spilling out the sides. Increasing the blocker door inclination angle (α) was also found to substantially increase reverse thrust level.

The final test matrix shown in Tables 13-I and 13-II was established on the basis of results obtained from the preliminary investigations. Lip angle (β) variation was included in the final matrix along with blocker door height (H_B) and the tabbed skirt configuration. The tabbed skirt concept evolved from the extended skirt in order to eliminate skirt and nozzle side door interference which would otherwise occur with stowing the

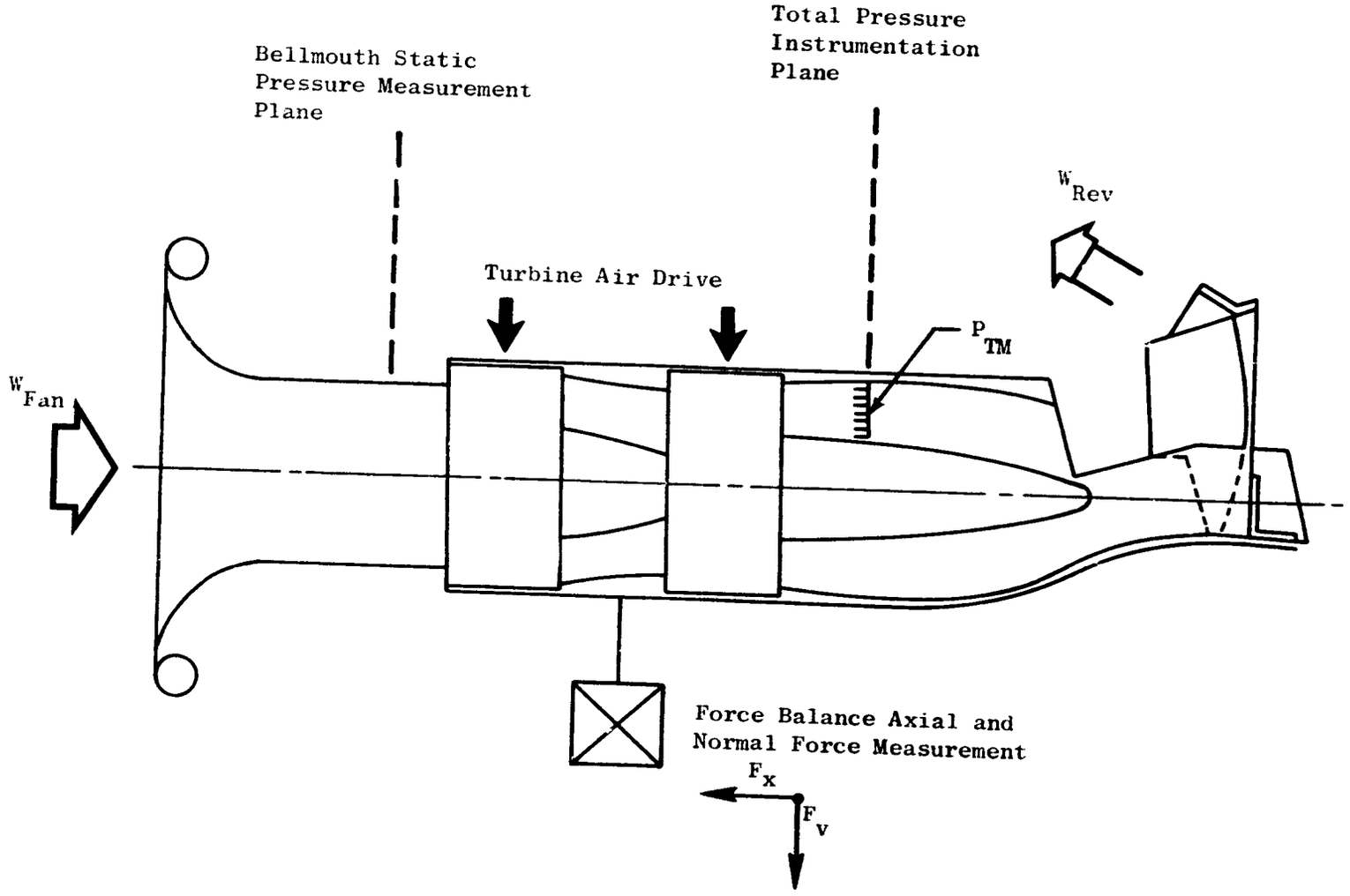

Figure 13.27. Reverse Thrust Static Test Configuration Schematic, Tandem Fan.

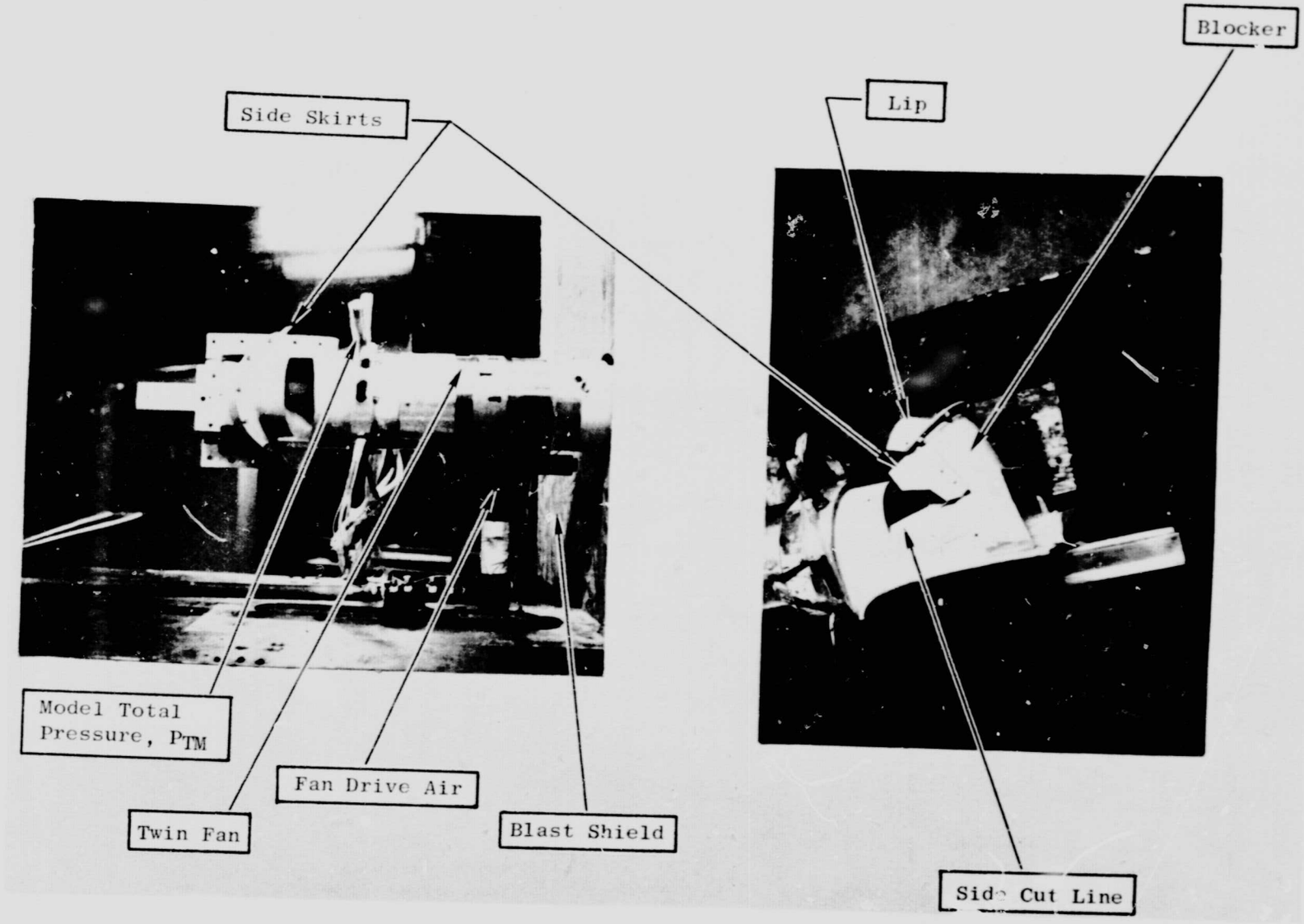

Figure 13.28. OTW Thrust Reverser Static Test Installation.

Figure 13.29. Thrust Reverser Scale Model Geometry.

Table 13-I. Reverser Test Matrix.

Untrimmed Cut Line										
Run No.	$\frac{X_P}{D_{TH}}$	α	β	$\frac{H_B}{D_{TH}}$	$\frac{L}{D_{TH}}$	Inlet	Blast Shield	Skirt	Skirt Angle ϕ	Date Tested
9	0.915	95	25	1.63	0.8	Bellmouth	On	Full	0	Dec, 75
10	0.915	95	25	1.63	0.8	Bellmouth	On	Nominal	0	Dec, 75
11	0.915	95	25	1.63	0.4	Bellmouth	On	Nominal	0	Dec, 75
12	0.915	95	25	1.63	0.4	Bellmouth	On	Extended	45	Dec, 75
13	0.915	95	25	1.63	0.4	Bellmouth	On	Extended	25	Dec, 75
14	0.915	95	25	1.63	0.4	Bellmouth	On	Nominal	45	Dec, 75
15	0.915	95	25	1.63	0.8	Bellmouth	On	Extended	45	Dec, 75
16	0.915	95	25	1.73	0.8	Bellmouth	On	Extended	45	Dec, 75
17	0.915	95	25	1.73	0.4	Bellmouth	On	Extended	45	Dec, 75
18	1.017	95	25	1.63	0.4	Bellmouth	On	Extended	45	Dec, 75
19	0.823	95	25	1.63	0.4	Bellmouth	On	Extended	45	Dec, 75
20	0.790	105	25	1.63	0.4	Bellmouth	On	Extended	45	Dec, 75
21	0.790	105	25	1.63	0.4	Bellmouth	On	Nominal	45	Dec, 75
22	0.790	105	25	1.63	0.4	Bellmouth	Off	Nominal	45	Dec, 75
23	0.790	105	25	1.63	0.4	Flight	Off	Nominal	45	Dec, 75
24	0.790	105	25	1.63	0.8	Bellmouth	Off	Nominal	45	Dec, 75
25	0.790	105	25	1.63	0.8	Bellmouth	Off	Extended	45	Dec, 75
26	0.790	105	25	1.63	0.8	Bellmouth	On	Extended	45	Dec, 75

Table 13-II. Reverser Test Matrix (Concluded).

Trimmed Cut Line, QCSEE Pivot										
Run No.	$\frac{X_P}{D_{TH}}$	α	β	$\frac{H_B}{D_{TH}}$	$\frac{L}{D_{TH}}$	Inlet	Blast Shield	Skirt	Skirt Angle ϕ	Date Tested
40	0.865	95	25	1.63	0.4	Bellmouth	On	Nominal	45	Jan, 76
41	0.865	95	25	1.63	0.4	Bellmouth	On	Tabbed	45	Jan, 76
39	0.865	95	25	1.63	0.4	Bellmouth	On	Tabbed	0	Jan, 76
42	0.865	95	25	1.63	0.2	Bellmouth	On	Tabbed	45	Jan, 76
43	0.865	95	25	1.63	0.8	Bellmouth	On	Tabbed	45	Jan, 76
46	0.865	95	35	1.63	0.4	Bellmouth	On	Nominal	45	Jan, 76
45	0.865	95	35	1.63	0.4	Bellmouth	On	Tabbed	45	Jan, 76
44	0.865	95	35	1.63	0.2	Bellmouth	On	Tabbed	45	Jan, 76
37	0.865	105	15	1.63	0.4	Bellmouth	On	Nominal	45	Jan, 76
36	0.865	105	15	1.63	0.4	Bellmouth	On	Tabbed	45	Jan, 76
38	0.865	105	15	1.63	0.4	Bellmouth	On	Tabbed	0	Jan, 76
35	0.865	105	15	1.63	0.2	Bellmouth	On	Tabbed	45	Jan, 76
32	0.865	105	25	1.63	0.4	Bellmouth	On	Nominal	45	Jan, 76
33	0.865	105	25	1.63	0.4	Bellmouth	On	Tabbed	45	Jan, 76
31	0.865	105	25	1.63	0.4	Bellmouth	On	Tabbed	0	Jan, 76
34	0.865	105	25	1.63	0.2	Bellmouth	On	Tabbed	45	Jan, 76
51	0.865	105	35	1.63	0.4	Bellmouth	On	Tabbed	45	Jan, 76
50	0.865	105	35	1.63	0.4	Bellmouth	On	Tabbed	0	Jan, 76
29	0.865	115	15	1.63	0.4	Bellmouth	On	Nominal	45	Jan, 76
27	0.865	115	15	1.63	0.4	Bellmouth	On	Tabbed	45	Jan, 76
28	0.865	115	15	1.63	0.4	Bellmouth	On	Tabbed	0	Jan, 76
30	0.865	115	15	1.63	0.2	Bellmouth	On	Tabbed	45	Jan, 76
48	0.865	115	25	1.63	0.4	Bellmouth	On	Nominal	45	Jan, 76
47	0.865	115	25	1.63	0.4	Bellmouth	On	Tabbed	45	Jan, 76
49	0.865	115	25	1.63	0.4	Bellmouth	On	Tabbed	0	Jan, 76

reverser. Blocker door axial spacing (X_F/D_{TH}) was also included in the matrix because of its potential for increasing the airflow level in reverse, since none of the other parameters previously investigated were totally effective in this regard.

Langley scale model test results are presented in Figure 13.30 through 13.39. Airflow ratio data (W_{REV}/W_{FWD}) contained on each figure is defined as the measured reverse mode flow at the test pressure ratio (P_T/P_O) divided by the forward takeoff nozzle airflow at the same pressure ratio. Reverse thrust data shown is defined as the measured reverse mode thrust at pressure ratio (P_T/P_O) divided by the resultant forward thrust at the QCSEE takeoff pressure ratio (about 1.29 on the model pressure ratio basis). Forward thrust and airflow characteristics were obtained from previous static tests (Section 13.3.1) of the RC-1 model configuration with nozzle area control doors in the 25° position and with the small plate attached; the resultant thrust was calculated from normal and axial force balance readings from the equation.

$$F_{FWD} = \sqrt{F^2_{AXIAL} + F^2_{NORMAL}}$$

Performance trends for the baseline reverser blocker door inclination angles with varying side skirt geometry and lip length are given in Figure 13.30. This figure shows that a very long (and mechanically impractical) lip (L/D_{TH} = 0.8) in combination with a tabbed side skirt rotated outward to 45° (ϕ) is required to meet the QCSEE 35% reverse thrust objective. The figure further points out the relative insensitivity of reverser airflow ratio (0.82 to 0.875) to these parameters compared to the large reverse thrust changes observed.

The effect of increasing the blocker door inclination angle (rotation of the door forward at the top) on performance is presented on Figure 13.31 and 13.32. These data show that reverse thrust requirements can be met at both 105° and 115° (ϕ) blocker door setting with a practical lip length of 0.4 L/D_{TH}. Again, side skirt geometry must be the tabbed configuration, rotated outward 45°. Note that the increased blocker door inclination angle caused a further reduction in flow ratio compared with values in Figure 13.30.

The effect of blocker door axial spacing was investigated to establish the effect on airflow matching characteristics and reverse thrust. The test results shown on Figure 13.33 indicate only 0.005 increase in reverse flow ratio for a large increase (1.06 to 1.20) in blocker spacing (X_F/D_{TH}), and that this flow increase was offset by a comparable reverse thrust loss at the 1.3 pressure ratio condition. Considering the results of QCSEE OTW engine stall margin studies with reduced exit area (described in a subsequent paragraph) and the level of reverse thrust demonstrated from the Langley reverser test, it was concluded that there was no reason to change the baseline QCSEE reverser pivot point from its current location (X_P/D_{TH} = 0.865).

Sym	Run	H_B/D_{TH}	L/D_{TH}	X_p/D_{TH}	Side Skirt	Skirt Angle ϕ	α	β	Cut Line
△	40	1.63	0.4	0.865	Nominal	45°	95°	25°	Trimmed
○	41	1.63	0.4	0.865	Tabbed	45°	95°	25°	Trimmed
□	39	1.63	0.4	0.865	Tabbed	0°	95°	25°	Trimmed
◇	42	1.63	0.2	0.865	Tabbed	45°	95°	25°	Trimmed
⌂	43	1.63	0.8	0.865	Tabbed	45°	95°	25°	Trimmed

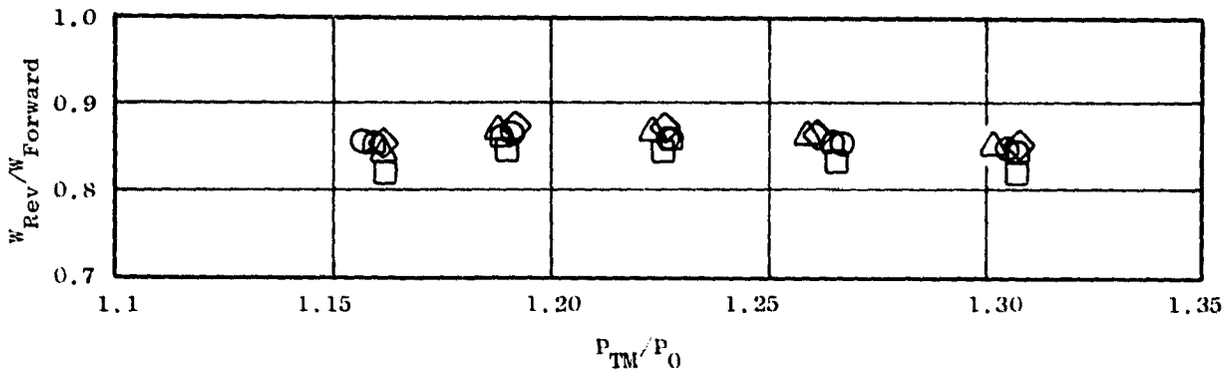

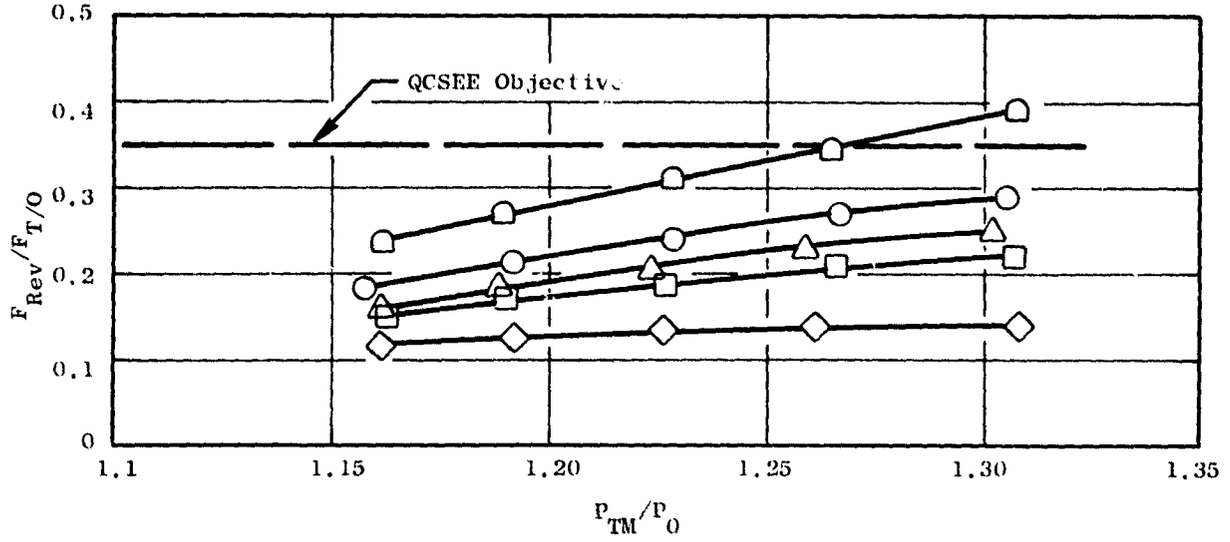

Figure 13.30. Effect Of Lip Length, Side Skirt Geometry and Skirt Angle on Reverse Thrust and Airflow; $\alpha = 95°$, $\beta = 25°$.

Sym	Run	H_B/D_{TH}	L/D_{TH}	X_P/D_{TH}	Side Skirt	Skirt Angle ϕ	α	β	Cut Line
△	32	1.63	0.4	0.865	Nominal	45°	105°	25°	Trimmed
○	33	1.63	0.4	0.865	Tabbed	45°	105°	25°	Trimmed
□	31	1.63	0.1	0.865	Tabbed	0°	105°	25°	Trimmed

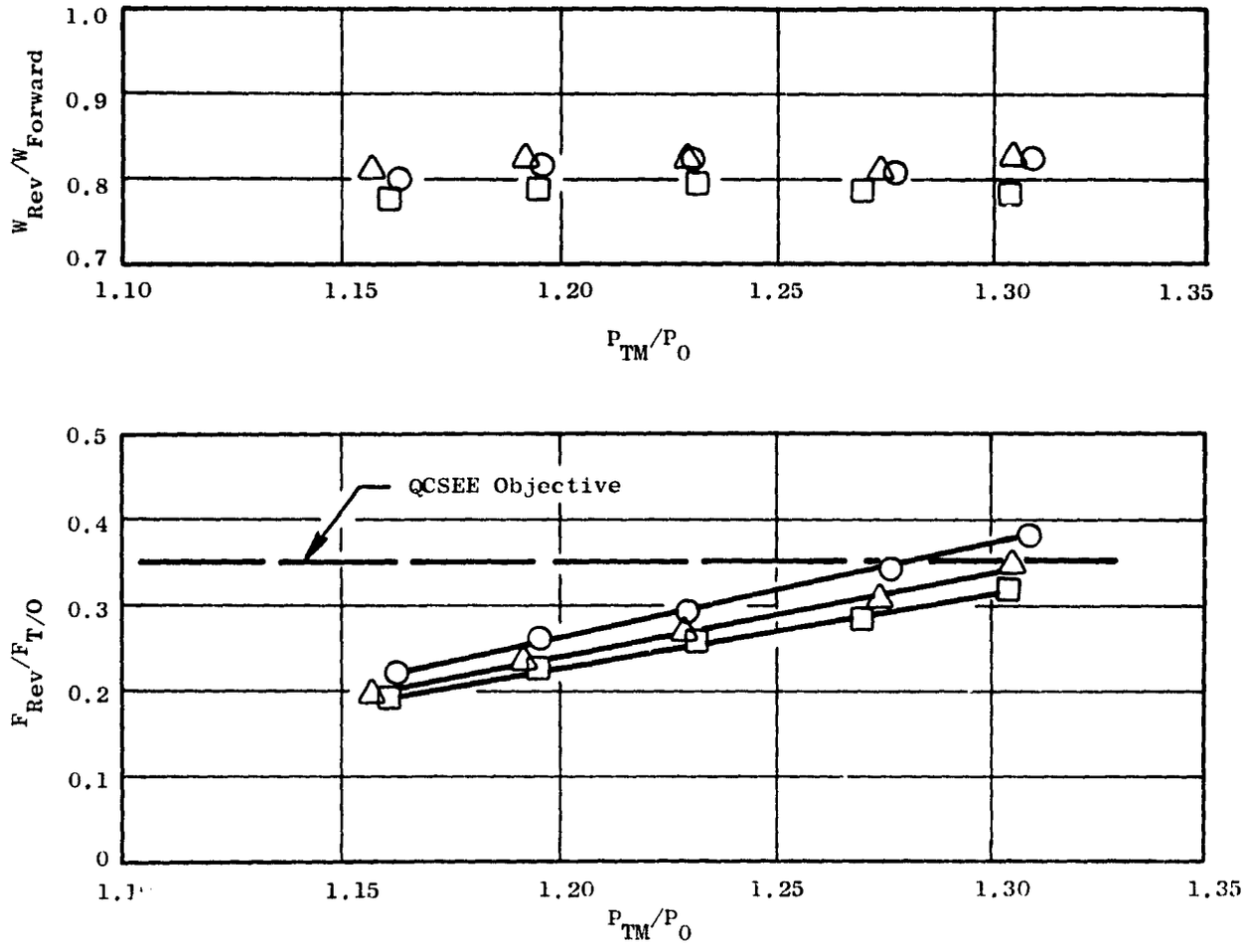

Figure 13.31. Effect of Side Skirt Geometry and Skirt Angle on Reverse Thrust and Airflow; $\alpha = 105°$, $\beta = 25°$.

Sym	Run	H_B/D_{TH}	L/D_{TH}	$X_{P'}/D_{TH}$	Side Skirt	Skirt Angle δ	α	β	Cut Line
△	48	1.63	0.4	0.865	Nominal	45°	115°	25°	Trimmed
○	47	1.63	0.4	0.865	Tabbed	45°	115°	25°	Trimmed
□	49	1.63	0.4	0.865	Tabbed	0°	115°	25°	Trimmed

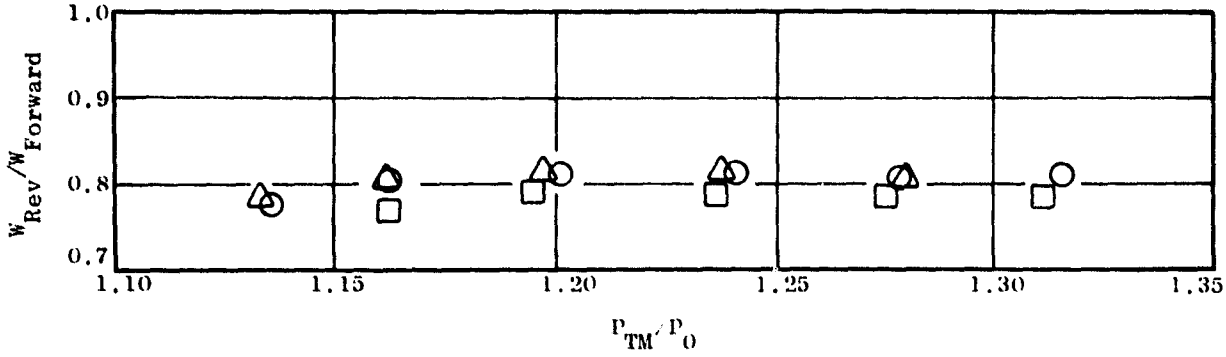

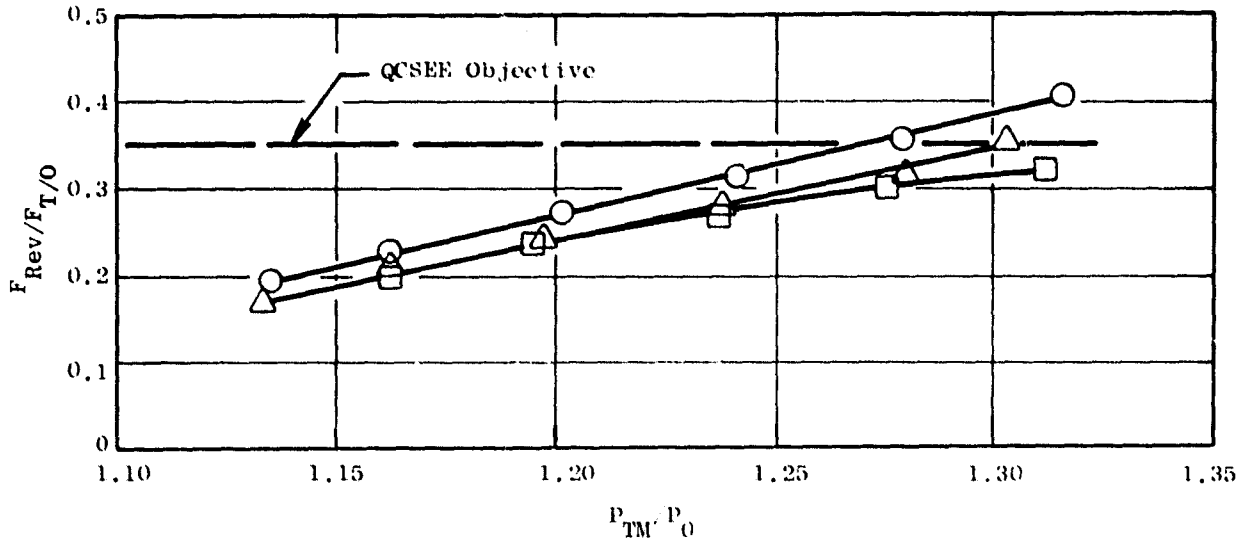

Figure 13.32. Effect of Side Skirt Geometry and Skirt Angle on Reverse Thrust and Airflow; $\alpha = 115°$, $\beta = 25°$.

H_B/D_{TH} = 1.63, Extended Side Skirt @ 45°
L/D_{TH} = 0.4, Untrimmed Cut Line
α = 95°
β = 25°
Runs 12, 18, 19

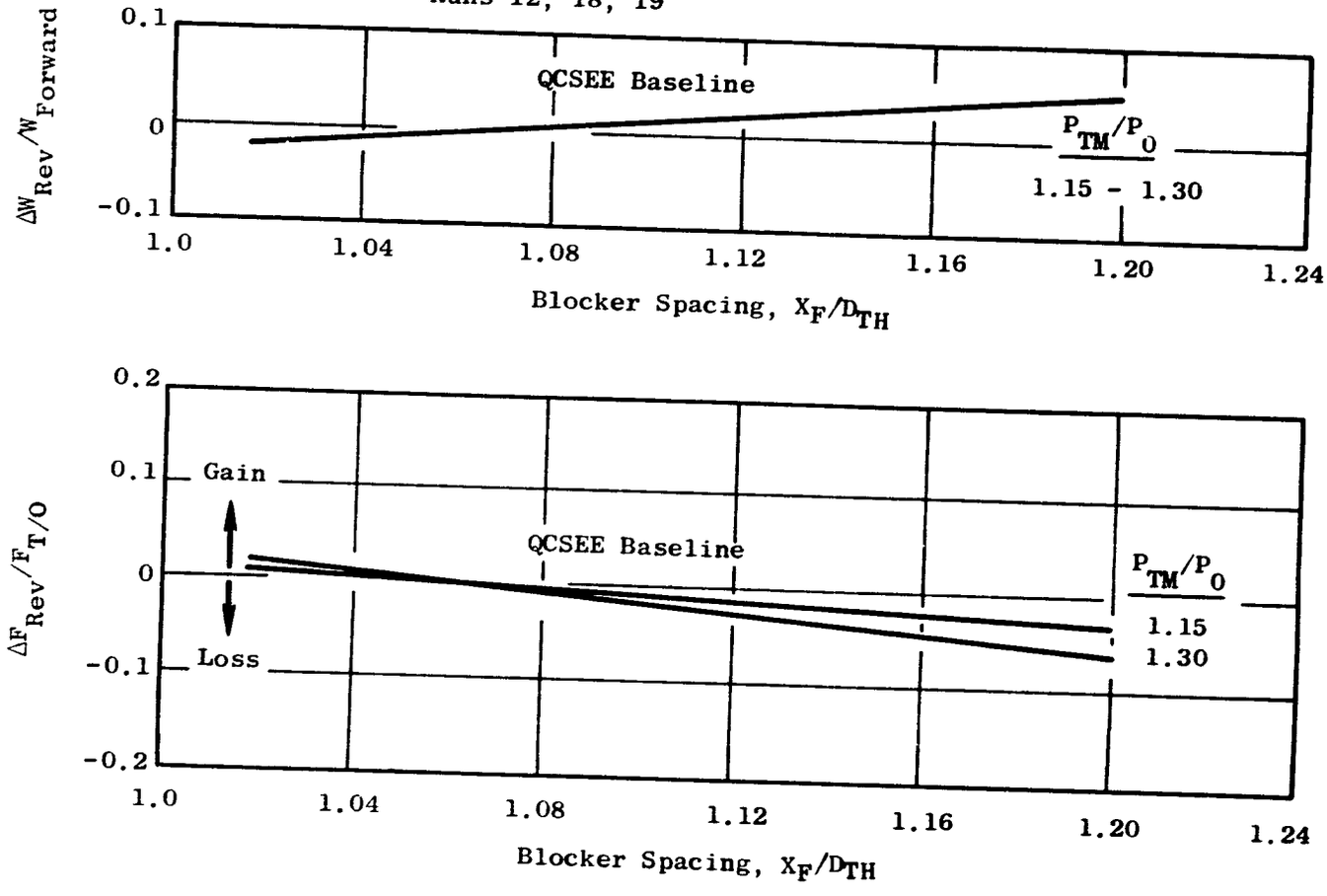

Figure 13.33. Effect of Blocker Spacing on Reverse Thrust and Airflow Relative to X_F/D_{TH} = 1.06.

The reverser side cut line was trimmed off at an angle (see Figure 13.29) to provide a smoother flow path for reverser efflux in the region where the side skirt is joined to the blocker door. The trimmed cut line also raises the reverser side walls and provides additional spillage control. The beneficial effect of the trimmed cut line is shown in Figure 13.34. At the takeoff pressure ratio level (P_T/P_0 = 1.3) an improvement in reverse thrust ratio of about 0.025 was measured; reverse airflow ratio was not affected.

Figures 13.35 through 13.39 present airflow and reverse thrust parametric derivatives obtained from cross plotted matrix data. Significant observations to be made from these data are:

1. Lip length (Figure 13.35) has a powerful effect on reverse thrust, particularly in the region from L/D_{TH} = 0.2 to 0.4. While gains in reverse thrust are significant all the way up to L/D_{TH} = 0.8, mechanical design constraints on an engine configuration would limit the lip length. Lip length has little influence on airflow capacity.

2. Lip angles (Figure 13.36) lower than 25° (relative to the engine centerline) are ineffective in increasing reverse thrust while significant improvement in reverse thrust was observed between 25° and 35° settings. Airflow capacity was little influenced by lip angle in the range tested (15°-35°).

3. Blocker door inclination angle (Figure 13.37) in the range 95° to 105° was found to significantly affect both reverse thrust and airflow capacity, while little change was noted for the increment between 105° and 115°.

4. Outward rotation of the side skirts (angle ϕ) had a strong favorable effect on reverse thrust with a moderate increase in airflow as shown on Figure 13.38. Some informal exploration of angles above the 45° shown on this figure indicated no additional performance benefit.

5. Blocker door height variation in the range of H_B/D_{TH} between 1.63 and 1.73 proved to have little effect on either reverse thrust or airflow capacity as indicated from Figure 13.39.

The OTW reverser configuration selected from analysis of the scale model data is shown on Figure 13.40. The configuration has an increased lip length (L/D_{TH} = 0.4) and the lip angle was reduced to 25° (δ). The reverser blocker door is rotated forward 10° (representative of the 105° scale model setting) and tabbed side skirts rotated outward 45° (ϕ) are incorporated. The reverser side cut line is also trimmed to take advantage of the performance gain indicated from scale model tests. The blocker door pivot point remains unchanged at X_P/D_{TH} = 0.865, since axial spacing test results showed no significant gains in airflow capacity could be made by moving the blocker aft any reasonable amount.

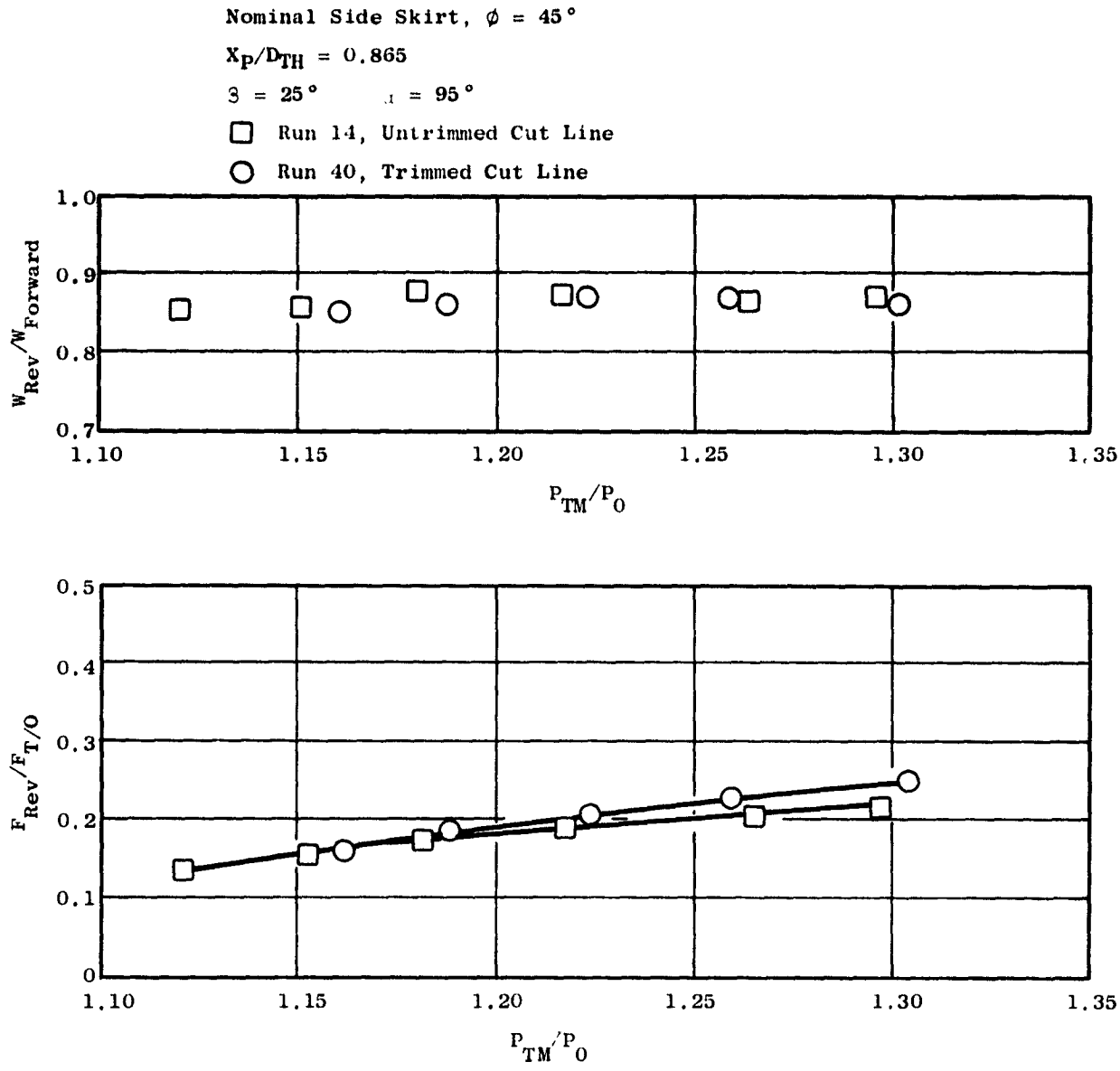

Figure 13.34. Effect of Reverser Cut Line on Reverse Thrust and Airflow.

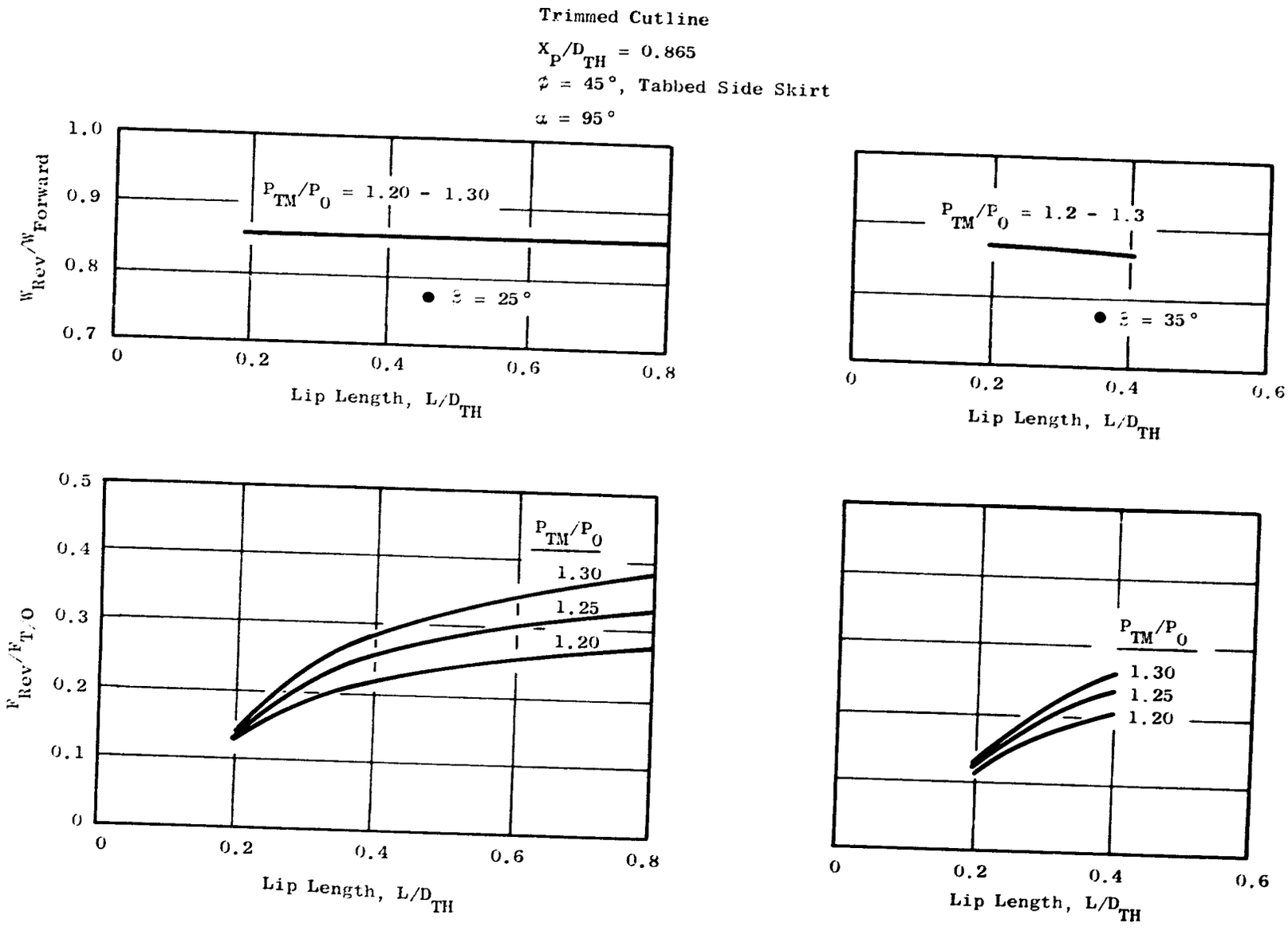

Figure 13.35. Effect of Lip Length on Reverse Thrust and Airflow.

Trimmed Cut Line

X_P/D_{TH} = 0.865

Tabbed Side Skirt

ϕ = 45°

L/D_{TH} = 0.4

α = 105°

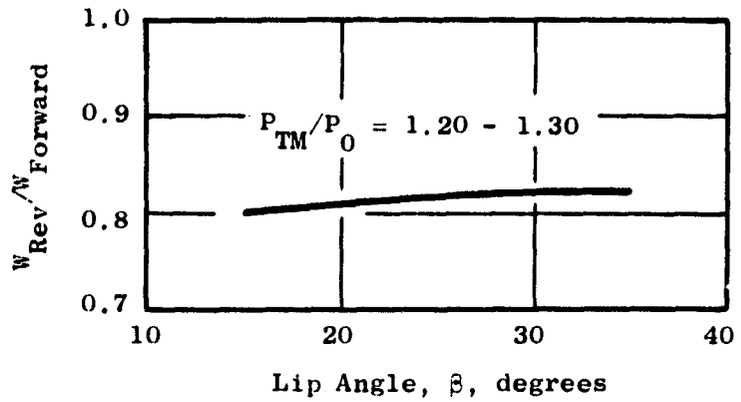

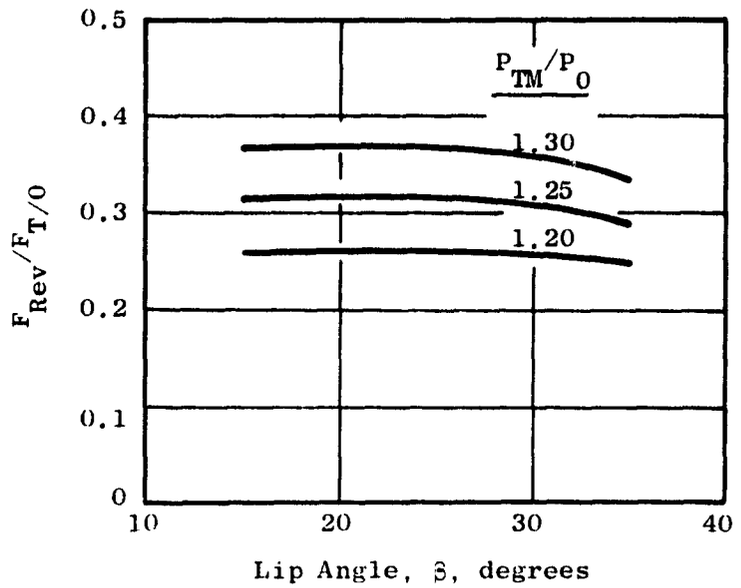

Figure 13.36. Effect of Lip Angle on Reverse Thrust and Airflow.

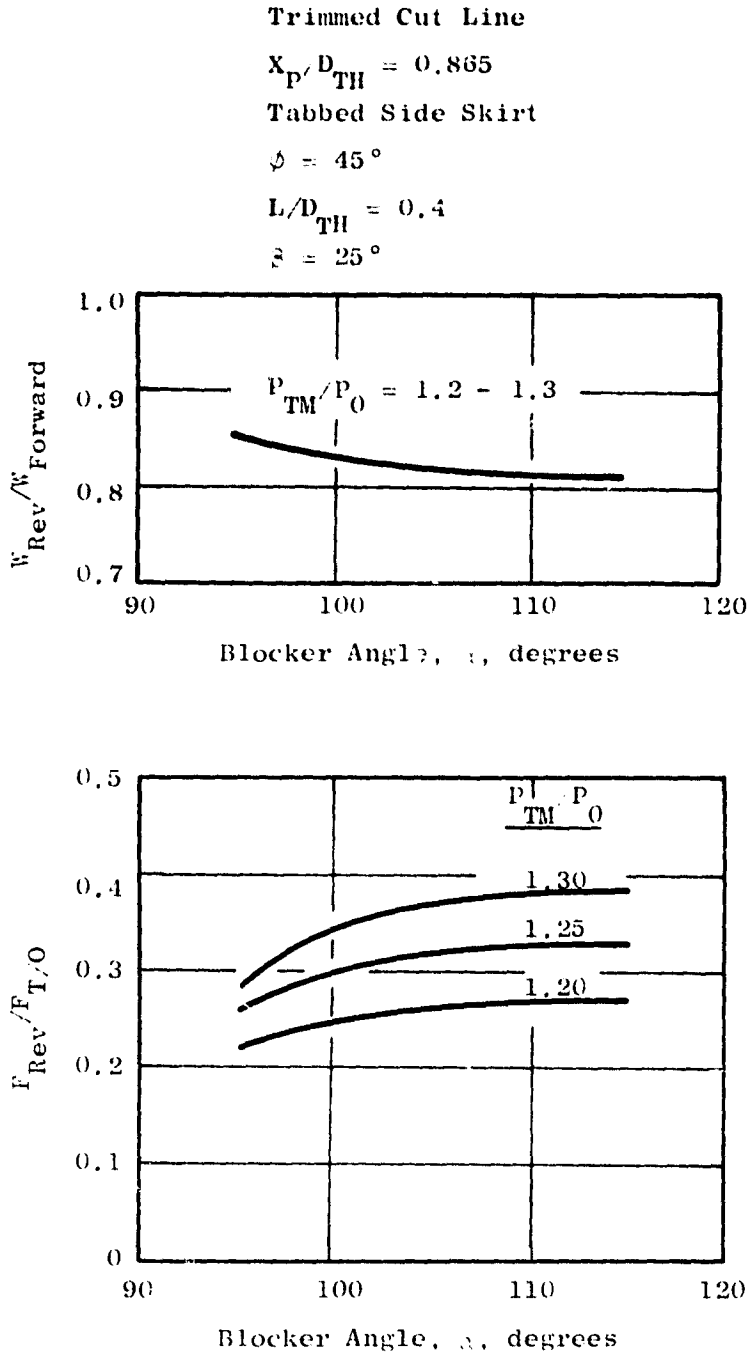

Figure 13.37. Effect of Blocker Angle on Reverse Thrust and Airflow.

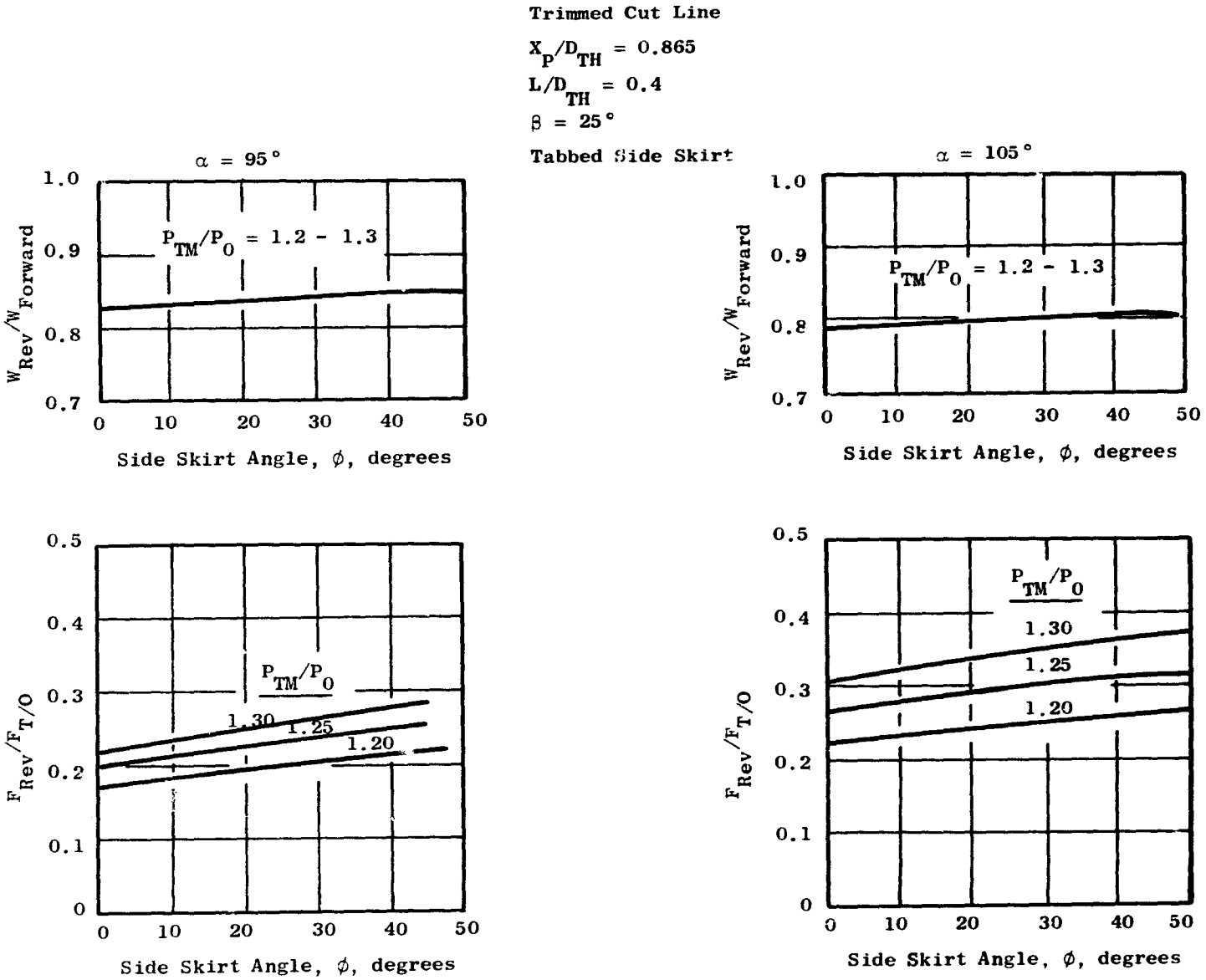

Figure 13.38. Effect Of Side Skirt Angle on Reverse Thrust and Airflow.

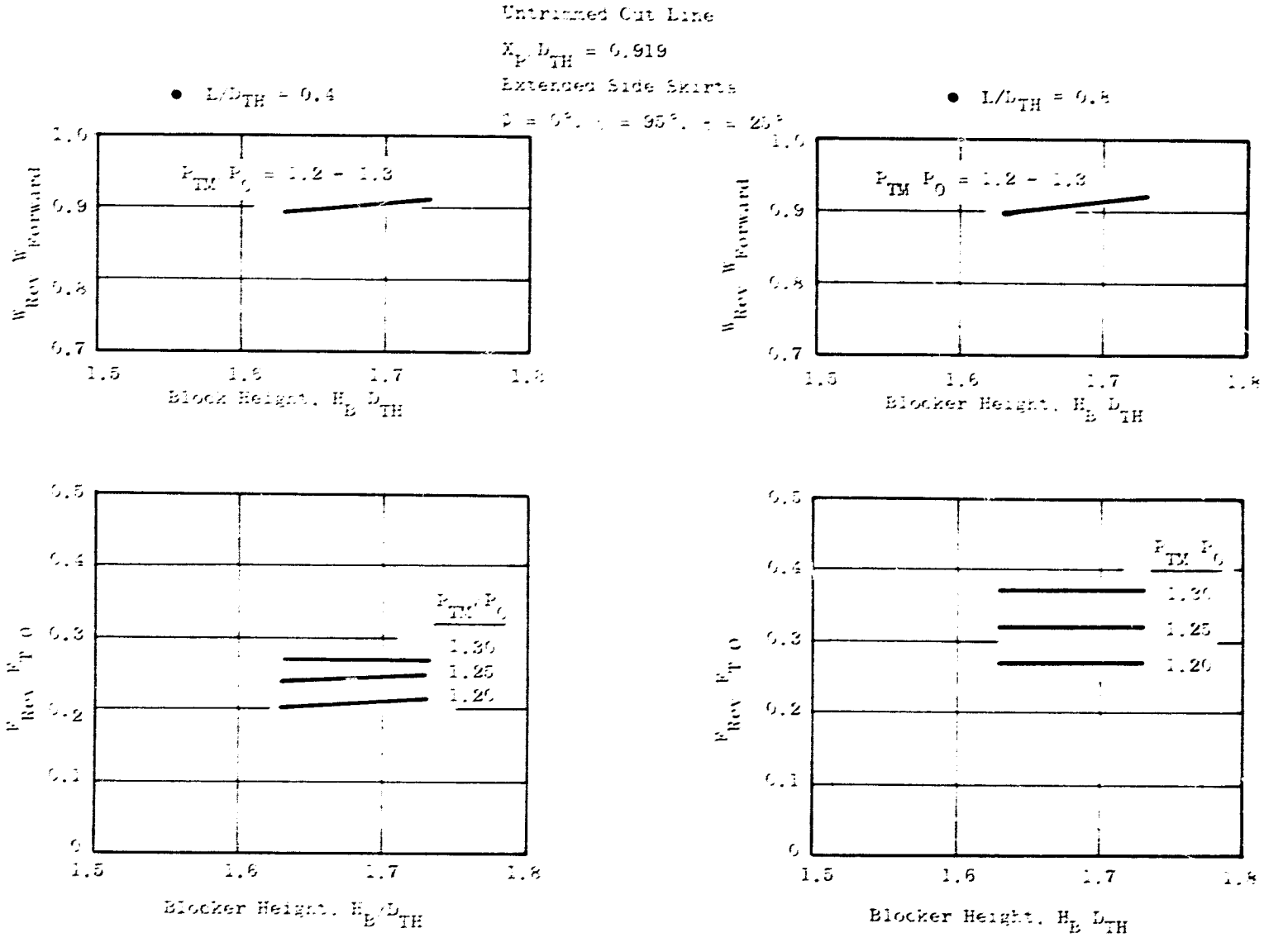

Figure 13.39. Effect of Blocker Height on Reverse Thrust and Airflow for L/D_{TH} = 0.4 and 0.8.

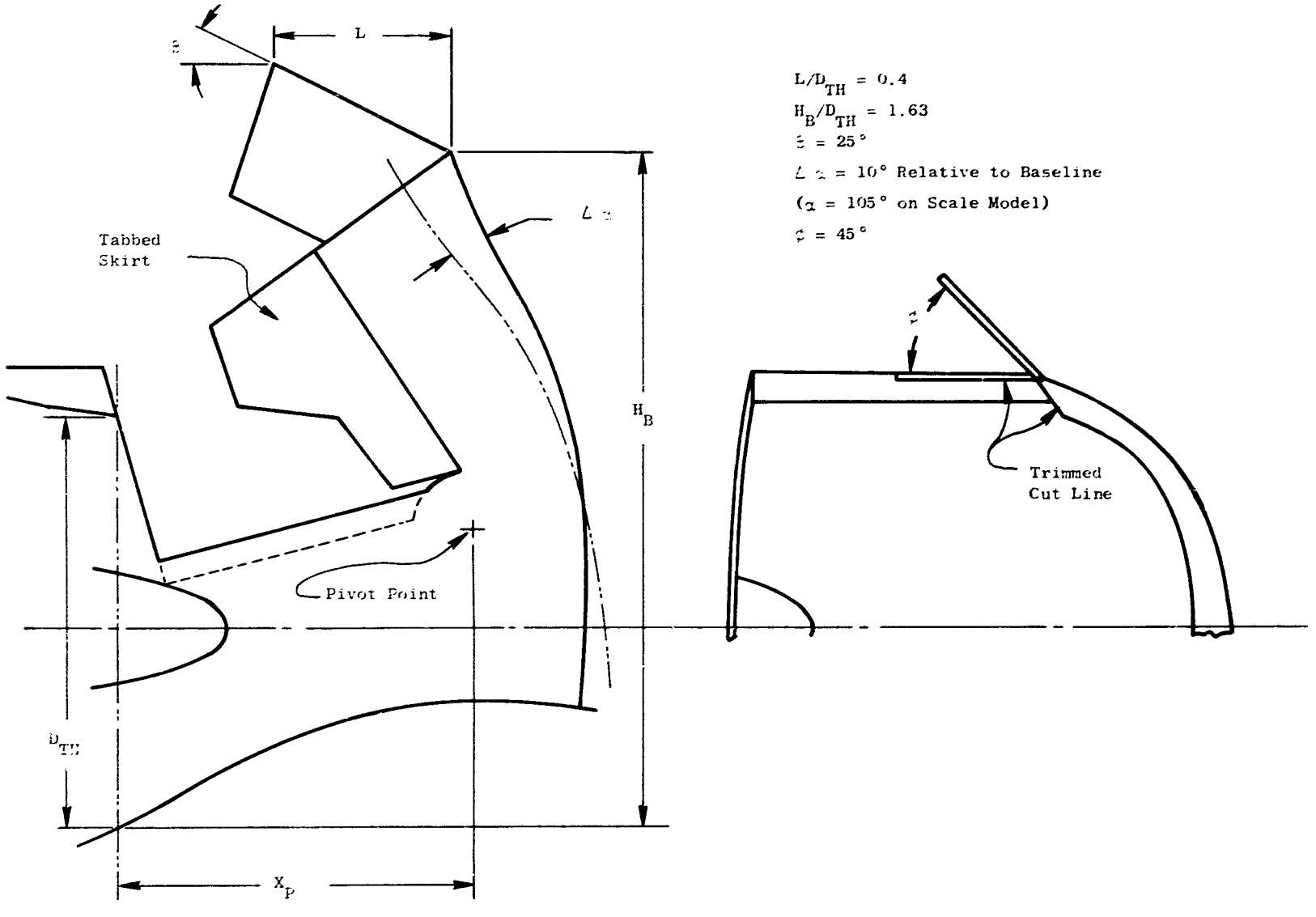

Figure 13.40. OTW Reverser Configuration.

The selected reverser configuration was evaluated in the test matrix (Table 13-II) was run 33. Scale model performance data from this configuration (see Figure 13.31) was adjusted to account for blocker door leakage expected on the full-scale reverser. Airflow ratio and reverse thrust characteristics with leakage effects included are presented on Figure 13.41. A blocker door leakage effective area of 770 cm^2 (119 $in.^2$) was used based on a physical leakage area of 1020 cm^2 (158 $in.^2$) and a flow coefficient of 0.75. The calculated full-scale reverser performance data from Figure 13.41 shows the 35% reverse thrust goal is met at a pressure ratio slightly above the takeoff value. These data also show that the QCSEE engine is backpressured 15% (W_{Rev}/W_{Fwd} = 0.85) in reverse mode relative to the forward thrust takeoff conditions.

Because of concern for the impact of 15% backpressure on the fan stall margin, a brief check was made using the fan map (Figure 13.42). The OTW cycle deck was used to generate a sea level static operating line with 82% of the nominal takeoff exhaust nozzle effective area. This operating line is the upper dashed line on the map. The operating line was then adjusted to reflect 3% leakage area resulting in the 85% operating line. The expected reverse thrust rating point is the intersection of this line with the required 1.34 fan pressure ratio (1.31 nozzle pressure ratio). This point indicates 14% stall margin, considered adequate for experimental engine testing.

13.3.3 Fan Discharge Duct

The fan discharge duct for the OTW propulsion system was designed to maintain low wall Mach numbers for maximum acoustic suppression objectives. The duct flow Mach number distribution is shown in Figure 13.43 as calculated using a one dimensional Mach number type of analysis.

The exit nozzle flow area distribution characteristics are shown in Figure 13.44 for the nozzle in the cruise and takeoff positions.

13.3.4 Inlet

The initial design objective for the QCSEE inlet was to achieve the highest practical throat Mach number consistent with inlet/engine operation across the assumed aircraft operating envelope using a fixed geometry inlet. As shown in Figure 13.45, based on representative subsonic inlet test results, a large degradation in inlet recovery is encountered at one-dimensional throat Mach numbers in excess of M = 0.82, due to effects of radial throat velocity gradient and boundary layer growth along the inlet lip. Consequently, to provide margin for effects such as engine-to-engine flow variation, flow variation due to operational effects on engine tolerances, and inlet-to-inlet throat area variation, a maximum practical design throat Mach number of 0.79 was selected.

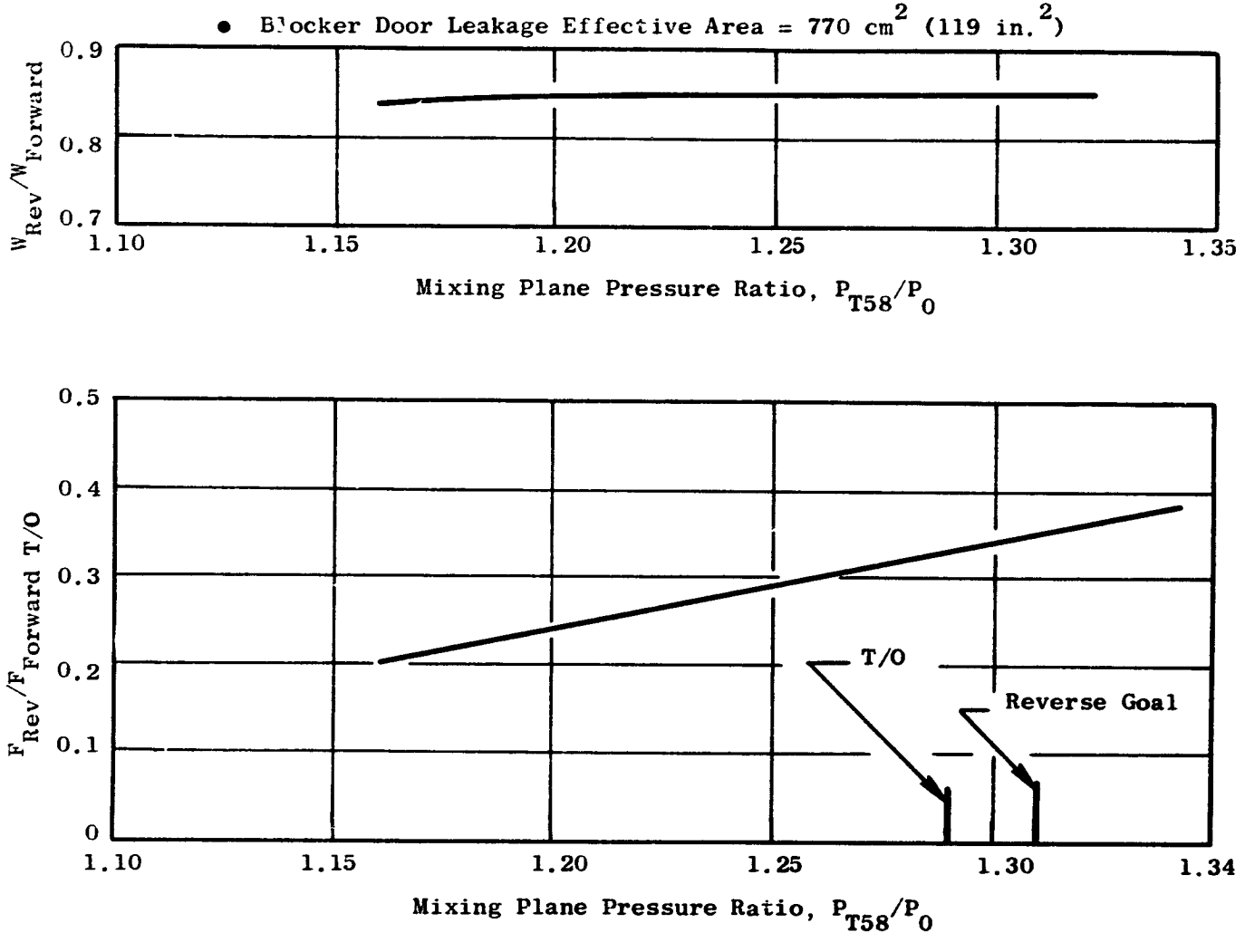

Figure 13.41. Estimated Reverse Thrust and Airflow Characteristics for the OTW Reverser.

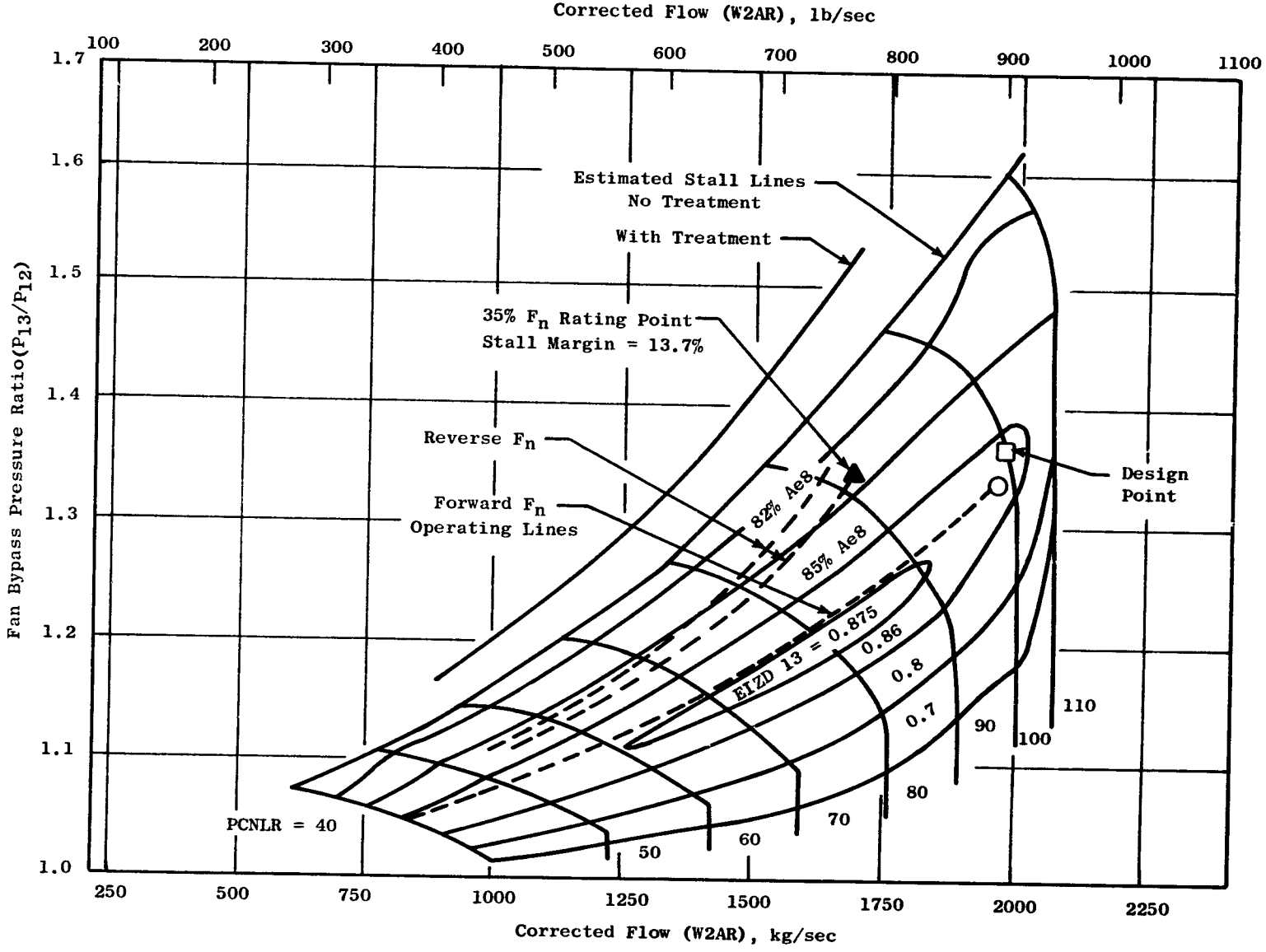

Figure 13.42. Predicted OTW Fan Performance.

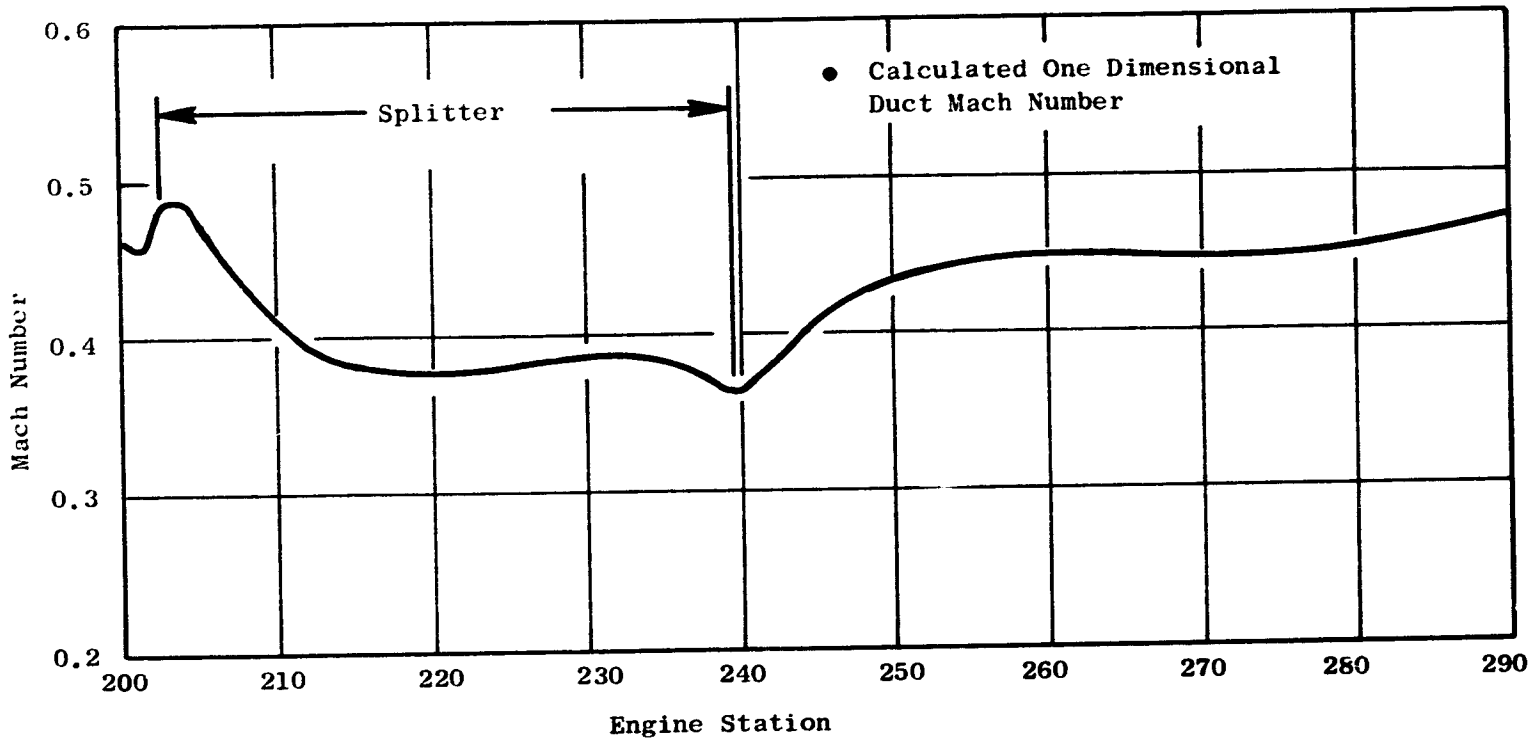

Figure 13.43. Fan Discharge Duct Mach Distribution, Boilerplate Nacelle.

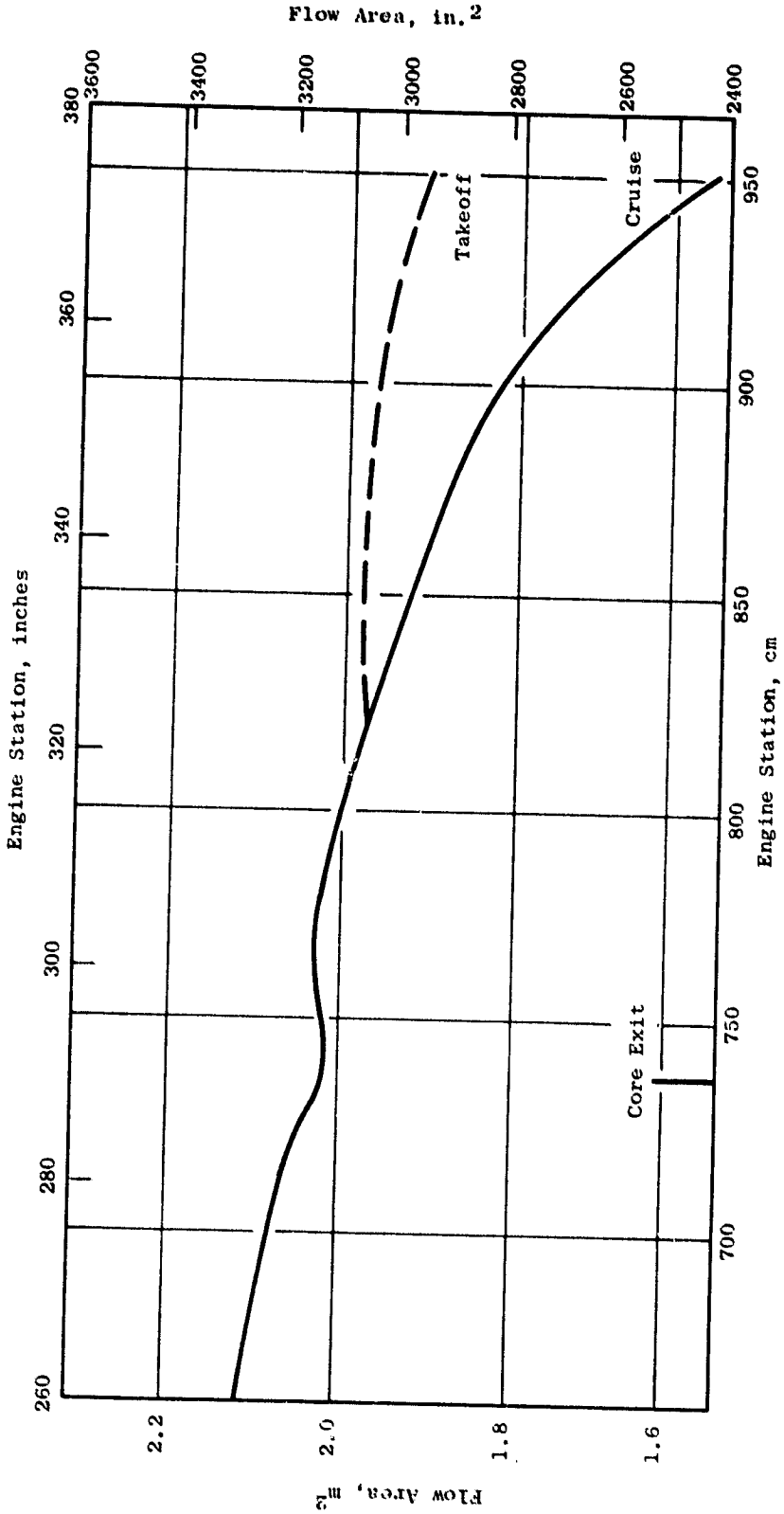

Figure 13.44. Exhaust System Area Distribution.

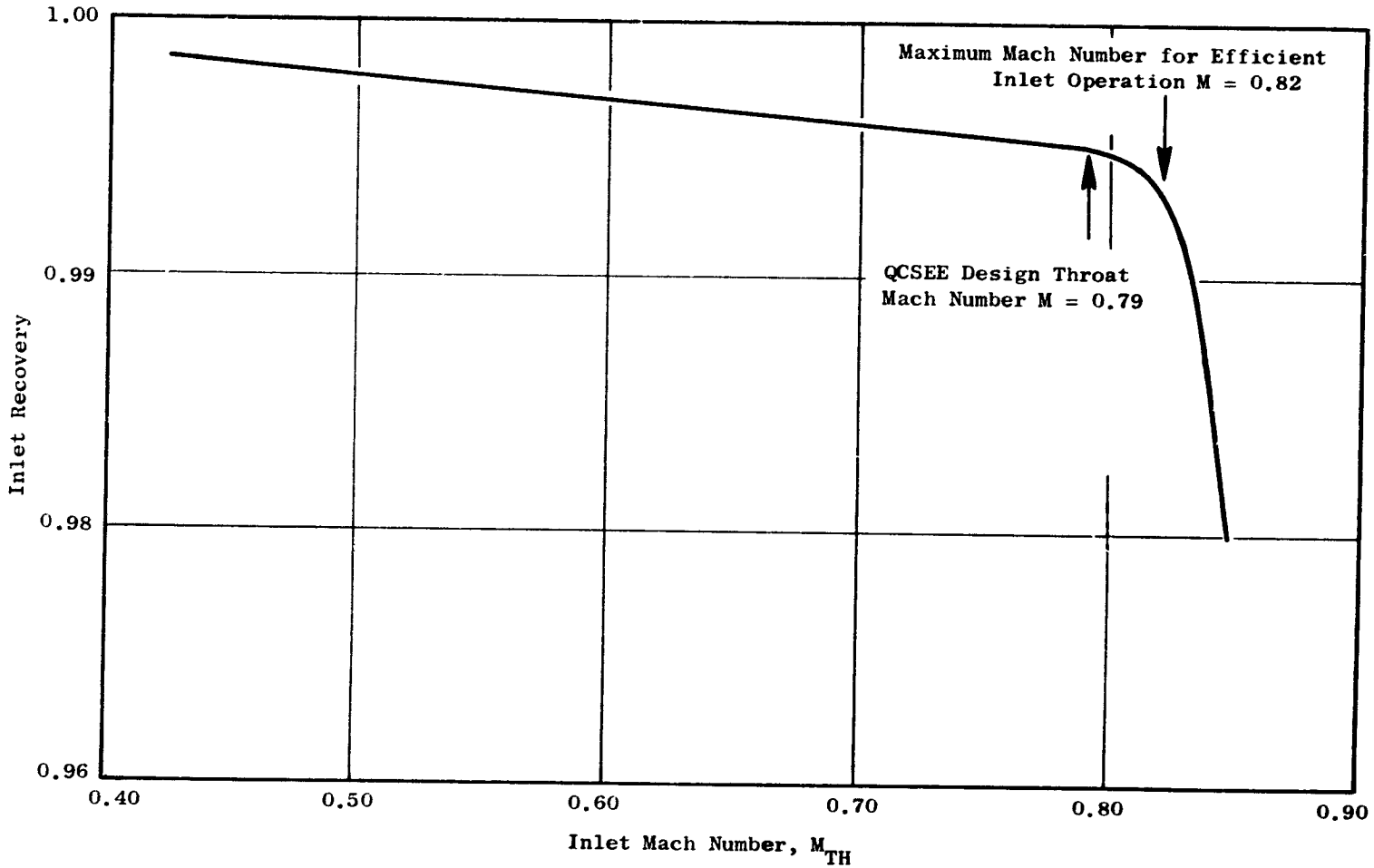

Figure 13.45. Inlet Throat Mach Number Selection.

The inlet aerodynamic design requirement was to achieve a high level of recovery at the high throat Mach number with the shortest possible length acoustic treatment in the diffuser. A scale model inlet program was conducted at the NASA-Lewis 9 x 15 Foot VSTOL Wind Tunnel. The scale model installed in the wind tunnel is shown in Figure 13.46. The 30.48-cm (12-inch) model represents a 17% scale of the full-size inlet. Test data in terms of inlet recovery as a function of angle-of-attack are presented in Figure 13.47 for four different inlet configurations. As shown, two of the configurations exceeded the 50° angle of attack objectives and two failed to meet the objectives. On the basis of the test results, a 1.21 diameter ratio (D_{HL}/D_{TH}) inlet with an external diameter ratio of 0.900 (D_{HL}/D_{MAX}) was selected as the best overall balanced design for angle of attack, crosswind, and cruise operation. Test results indicated that the selected configuration achieved all of the design objectives. The geometry of the selected inlet is presented in Figure 13.48. Additional inlet information is available in NASA CR-134866.

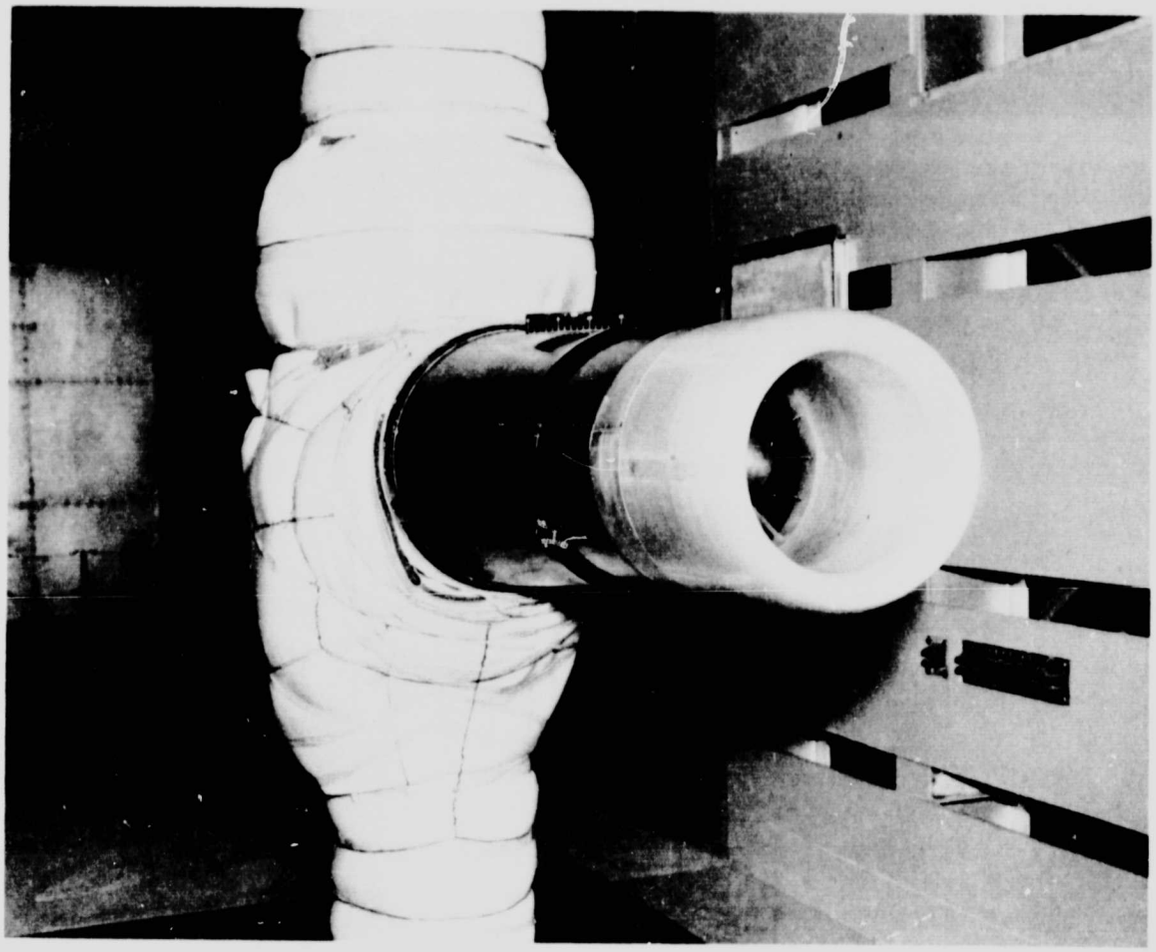

Figure 13.46. QCSEE 30.48 cm (12 in.) Inlet Model in NASA Lewis 9 x 15-foot VSTOL Wind Tunnel.

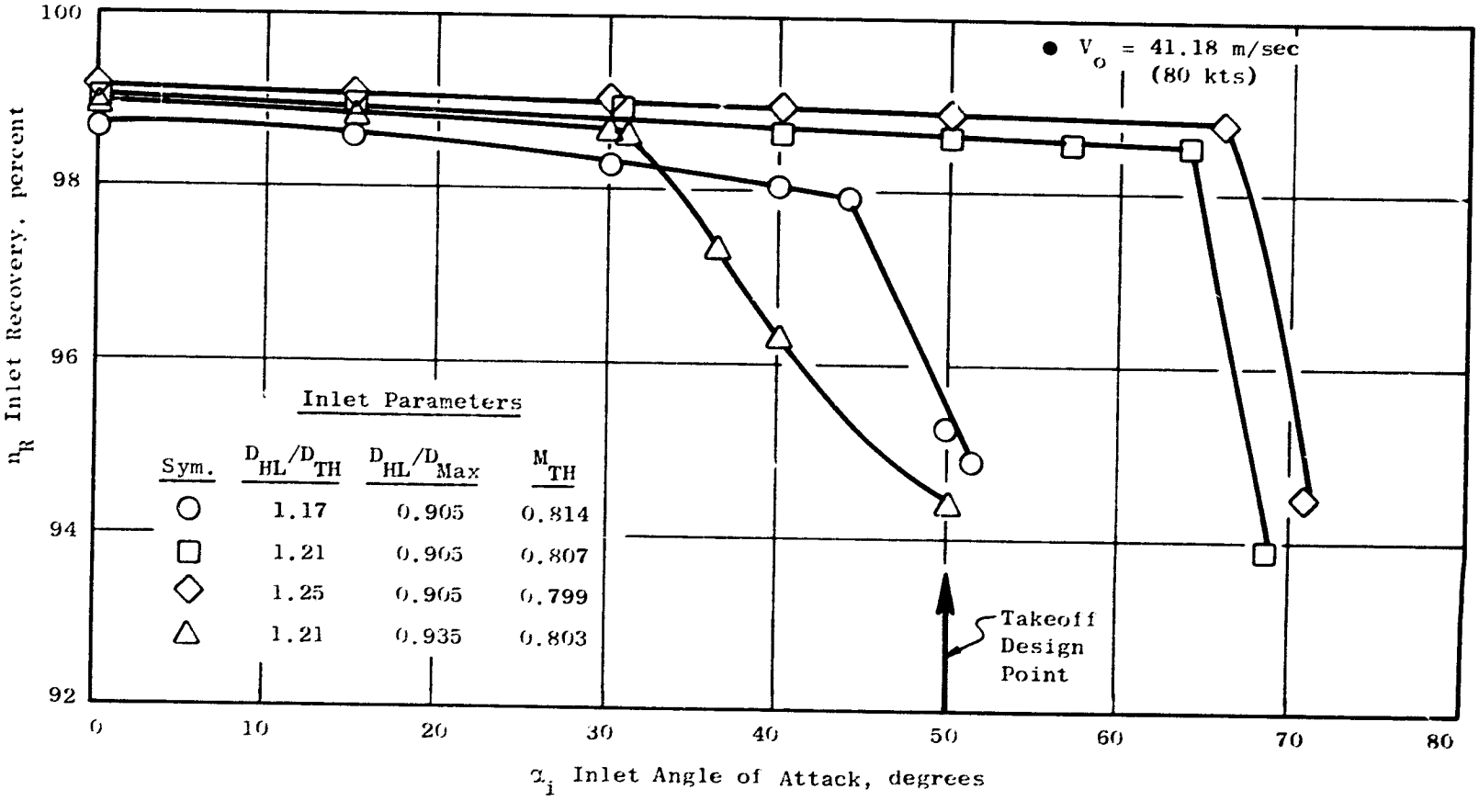

Figure 13.47. Inlet Performance Comparison Versus Angle of Attack.

- Experimental and Flight Nacelles - Same Aero Geometry

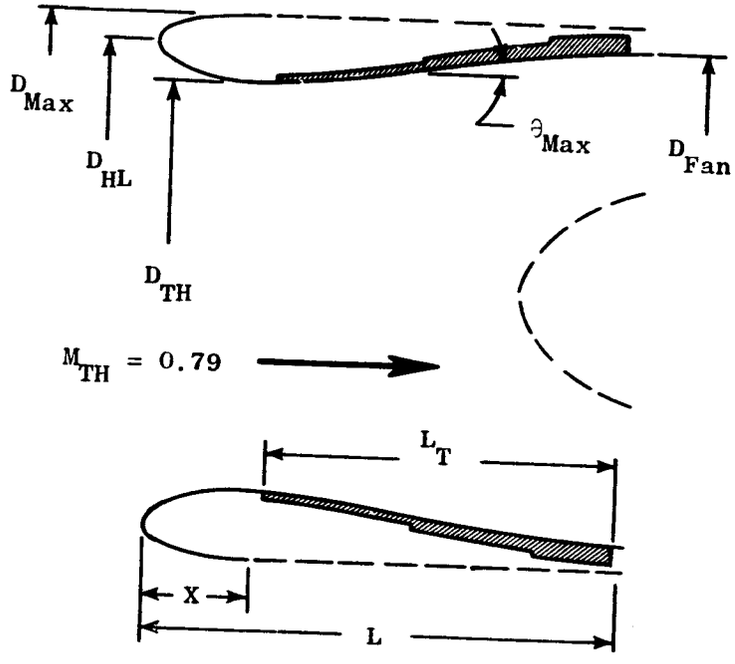

$L/D_{Fan} = 1.0291$

$D_{HL}/D_{TH} = 1.21$ Symmetrical

$D_{HL}/D_{Max} = 0.900$

$X/D_{Max} = 0.219$

$\theta_{Max} = 8.7°$

Diffuser Area Ratio = 1.466 (W/) Spinner

$L_T/D_{Fan} = 0.74$

- Angle of Attack [50° at 41.18 m/sec (80 kts)] and Crosswind [90° at 18 m/sec (35 kts)] Capability Confirmed by 30.5 cm (12 in.) Inlet Tests

Figure 13.48. Inlet Aerodynamic Design.

SECTION 14.0

PROPULSION SYSTEM AND NACELLE MECHANICAL DESIGN

14.1 SUMMARY

14.1.1 Flight Propulsion System

The over-the-wing flight propulsion system shown in Figure 14.1 is designed for installation on a high-wing, short-haul aircraft utilizing upper-surface-blown (USB) flaps to provide powered lift. Major features of this propulsion system include: a high throat Mach number inlet; full authority digital control; integrated aircraft, nacelle, and engine structure; composite acoustic panels and nacelle structures; a variable area "D"-shaped exhaust nozzle; and a single-door target reverser.

The engine accessory package is mounted on the bottom of the fan casing with a separate aircraft gearbox mount at the rear of the engine. The shaft-driven aircraft gearbox carries an air turbine starter, a 60 kVA integrated-drive generator (IDG), a hydraulic pump, and a fuel/oil cooler to dissipate heat generated by the gearbox and IDG. This arrangement has the unique advantage of eliminating all hydraulic and lube interconnections between the engine and aircraft. Thus on engine installation or removal, the only liquid disconnects would be the fuel lines. In this concept, the target reverser and the exhaust nozzle area control doors would be operated by the aircraft hydraulic system.

These features in combination with the integrated nacelle concept yield the following significant advantages when compared with current, conventional aircraft/propulsion system installations.

- Reduced Frontal Area - The high Mach inlet requires a small throat diameter than does a conventional low Mach inlet. This allows a smaller highlight diameter while maintaining the lip thickness required for operation at angle of attack or with a crosswind. Performance requirements at the low QCSEE cruise Mach number permits a high value of highlight-to-maximum nacelle diameter ratio which results in a relatively small frontal area.

  Separation of the engine and aircraft gearbox reduces the size of the conventional bottom bulge which also contributes to reduced frontal area.

- Shorter Pipes and Wires - Location of the accessories on the bottom results in shorter "runs" from the engine to the accessories and to the aircraft wing, reducing system weight and improving maintainability. On conventional propulsion system installations, pipes are routed around the fan casing. In the QCSEE design the exterior of the casing is clean permitting the engine fan casing to serve also as a part of the nacelle.

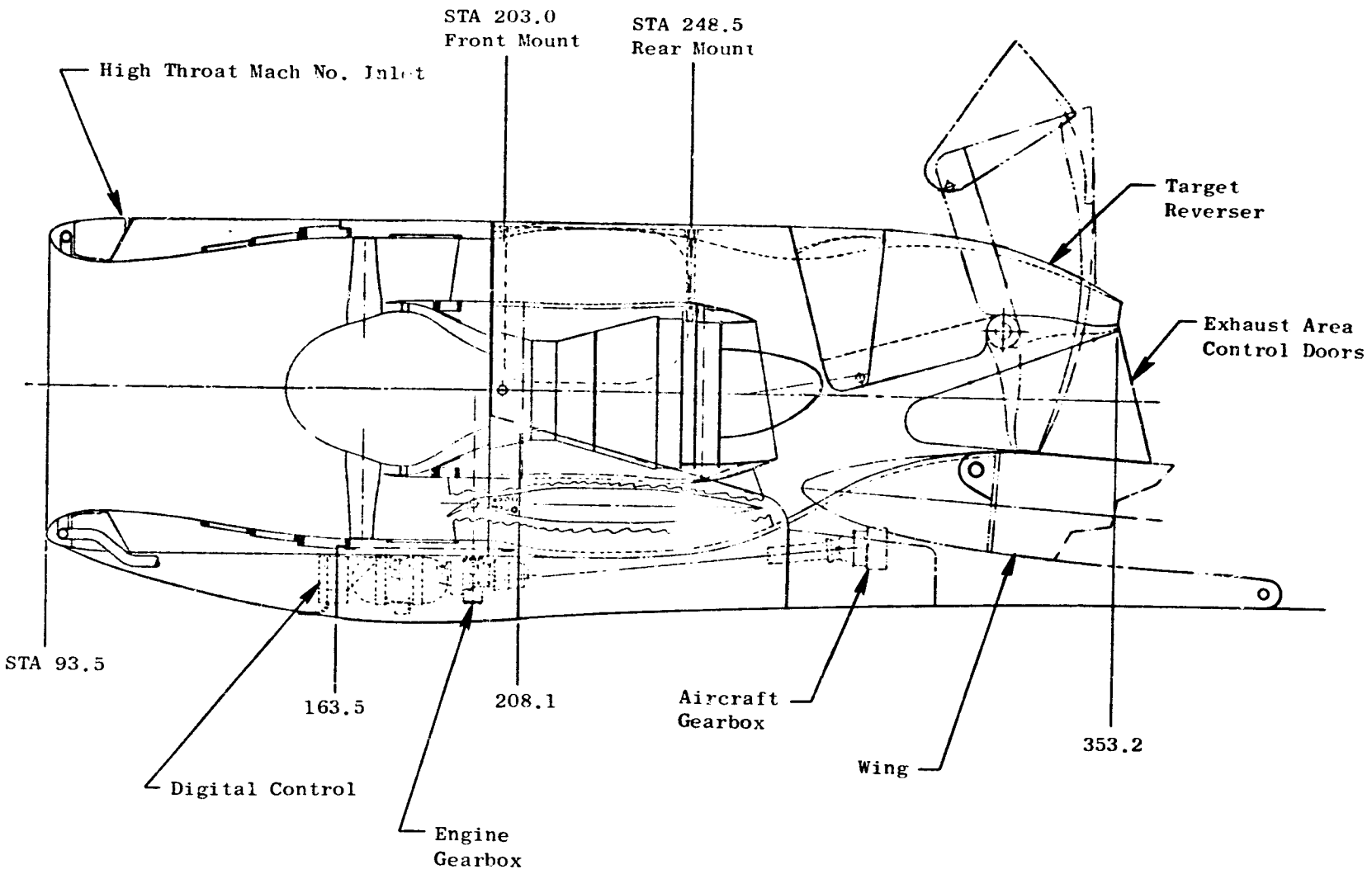

Figure 14.1. OTW Flight Propulsion System.

- Reduced Internal Losses - The engine mounting concept in the over-the-wing installation eliminates the need for an upper pylon. The bottom pylon can be reduced in size because it houses only the engine-to-gearbox piping and the aircraft bleed systems. The smaller pylon reduces bypass duct blockage and resultant internal pressure losses.

- Integrated Engine/Nacelle Structure - The small throat diameter of the high Mach inlet permits a significant reduction in nacelle maximum diameter while maintaining the required aerodynamic contours to assure good installed performance. This combination of diameters results in a substantial reduction in nacelle thickness and allows the fan cowl to be combined with the fan casing/frame into one integral structure.

The integrated engine/nacelle design approach results in thin nacelle walls of approximately 9.9 cm (3.9 in.) at the top and 35.6 cm (14.0 in.) at the accessory bay at the bottom. The walls of this configuration are 20 to 40% thinner than walls on current aircraft nacelles. The resulting nacelle maximum diameter is 198 cm (78.8 in.), and the overall length is 660 cm (259.7 in.).

The propulsion system installation over the wing results in a height from the ground to the bottom of the nacelle of approximately 4.6 m (15 ft). A maintenance stand therefore is required to reach the engine accessories. The accessory cowl doors are hinged to the fan casing and swing out to expose the engine accessories as shown in View A of Figure 14.2. This permits direct access to install or remove any component and allows visual inspection of accessories and piping joints while the engine is operating. Core engine access provisions are shown in View B. Opening this door also exposes the "power-take-off" drive shaft from the engine to the aircraft gearbox. A rear door opens for access to the aircraft gearbox and accessories as shown in View C. Fan and core cowl doors open to permit vertical installation of the engine, with the cowl doors and aircraft gearbox remaining "on-the-wing."

Nacelle cross sections showing the transition to the "D"-shaped exhaust nozzle exit are shown in Figure 14.3. These cross sections show how the reverser blocker door forms the top of the "D" nozzle in the forward thrust mode. The blocker in the reverse thrust mode is shown in phantom in Figure 14.1 and in the trimetric Figure 14.4. The side nozzle area control doors are shown in Figure 14.3. These doors open to enhance flow spreading over the upper surface of the wing for maximum propulsive lift on takeoff (if required) and at approach. The OTW cycle requires a range of forward thrust nozzle areas from 15,613 to 18,452 cm^2 (2420 to 2860 in^2) between cruise and takeoff operating conditions.

The OTW "flight" propulsion system installation gives a unique opportunity to combine several functions into a single structure. In the proposed configuration the aft outer fan duct serves as the aircraft support pylon, thus integrating engine, nacelle, and aircraft structure into a semicomposite unit. This system results in substantial weight savings. Figure 14.4 shows

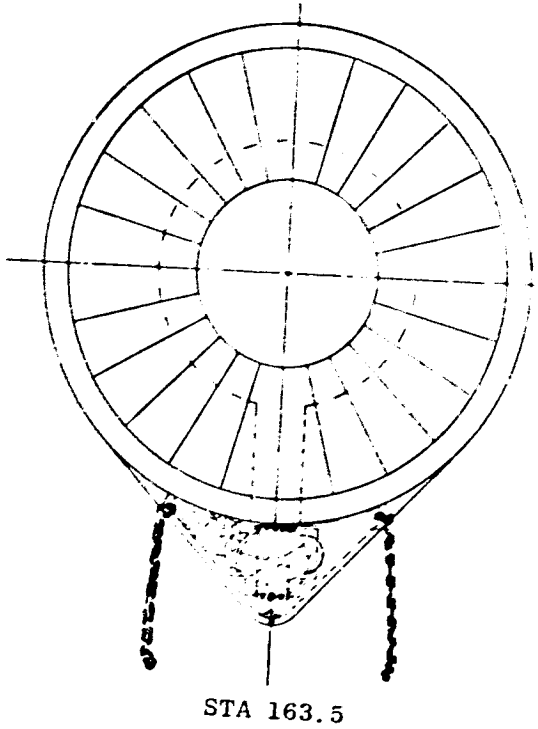

View A - Engine Accessory Access

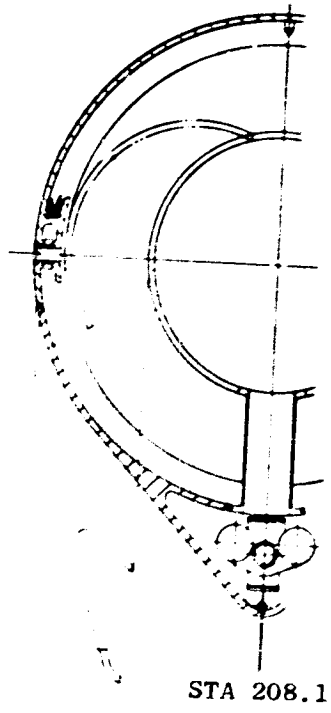

View B - Core Access

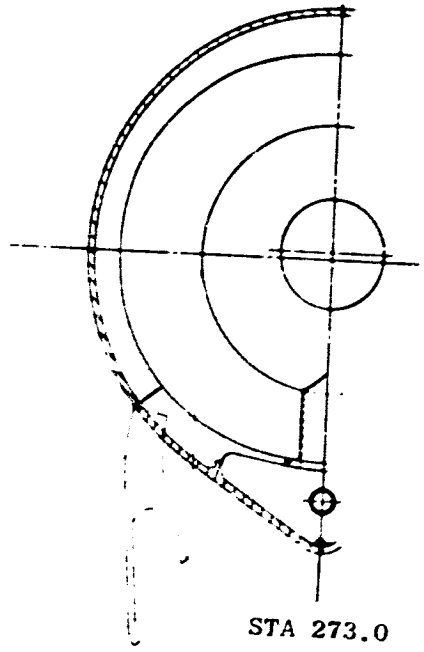

View C - Aircraft Accessory Access

Figure 14.2. Accessibility, Cowl Doors.

Figure 14.3. Nacelle Cross Sections, Exhaust.

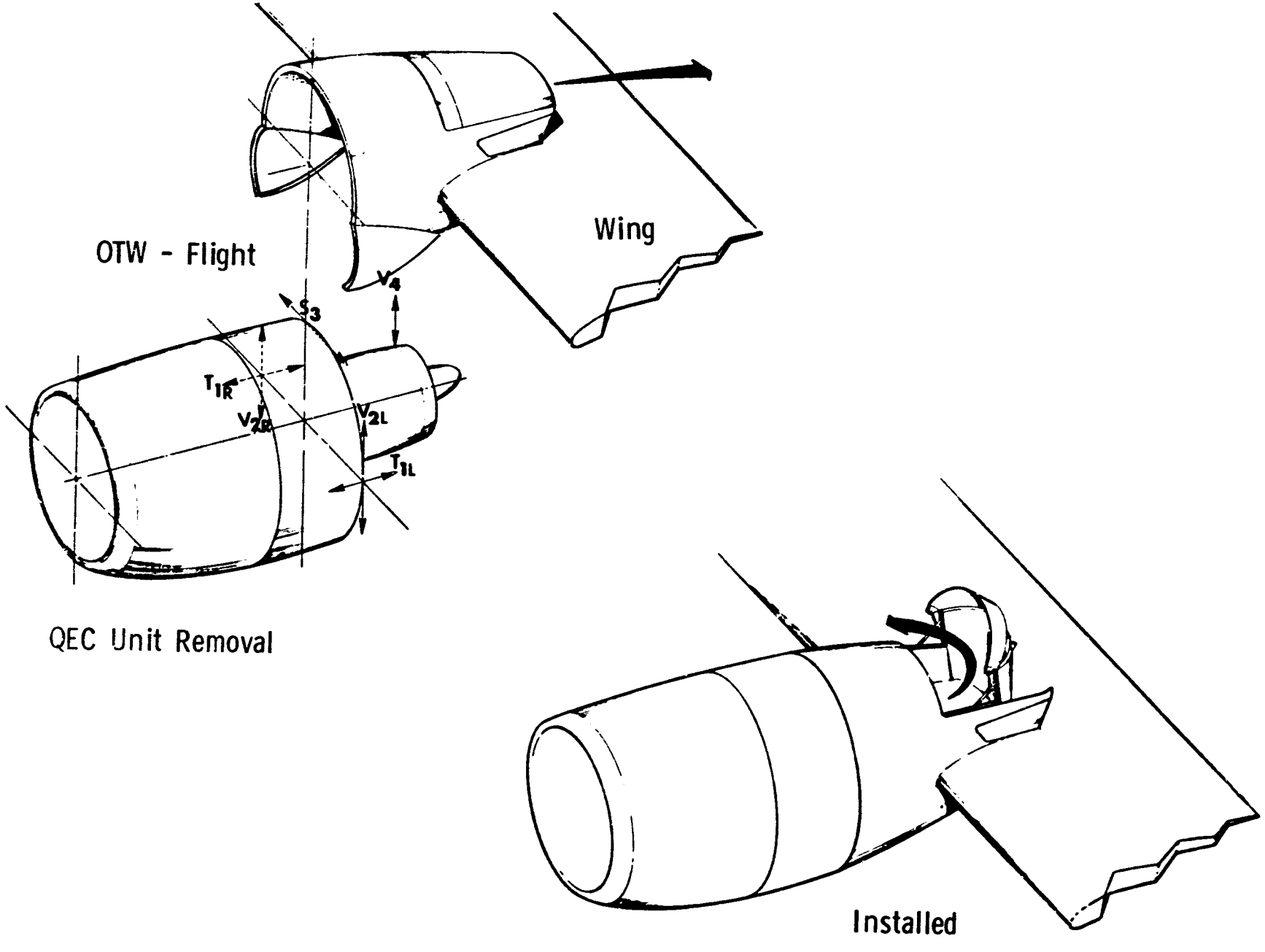

Figure 14-4. Flight Propulsion System Installation.

a typical flight quick engine change (QEC) unit or neutral engine system. The change unit includes the inlet, the engine accessories and piping, and the core cowl, bottom pylon, and the basic fan engine and core exhaust system.

The mount system shown in Figure 14.4 takes thrust loads (Vectors T_{1R} and T_{1L}) through uniballs on the horizontal centerline on both sides of the casing. These uniballs are oriented to also take vertical loads (Vectors V_{2L} and V_{2R}). Side load is reacted at the top (Vector S_3) with the induced moment due to side load/torque taken in the vertical mounts (Vectors V_{2L} and V_{2R}). To complete the determinant mount system, the sixth and final load vector (V_4), is an airfoil shaped vertical load link attaching the turbine frame to the nacelle at the top vertical centerline. Unit maneuver and blade-out loads at the mount points are shown in Table 14-I.

14.1.2 Experimental Propulsion System

The over-the-wing experimental propulsion system is shown in Figure 14.5. The experimental system will be mounted from an overhead facility, and will therefore be run in an inverted position. The overall configuration basically is the same as the flight system except that the exhaust nozzle plug is not canted, and a fan exhaust duct splitter has been added to meet the experimental engine acoustic objectives. The nacelle maximum diameter could be the same as in the flight installation, but the overall length is 54.1 cm (21.3 in.) greater to provide common core exhaust system hardware with the under-the-wing (UTW) experimental engine system. The overall length is 713.7 cm (281.0 in.) to the confluent flow exhaust nozzle exit plane. Comparative outlines of the "flight" and experimental systems are shown in Figure 14.6. Other specific design differences between the "flight" propulsion system and the experimental engine design are summarized in Table 14-II.

The test configuration of the OTW experimental engine will incorporate boilerplate nacelle components. Internal flow lines are similar to the "flight" lines; however, changes have been made to reduce overall program cost by maintaining commonality with the UTW experimental system and by eliminating hardware that is not essential to demonstrating the system statically.

The OTW system includes the following features/components:

- Boilerplate inlet from UTW program with one set of hardwall and one set of SDOF acoustic treatment panels. One set of bulk absorber panels and materials for an additional set of SDOF panels will be procured.

- Boilerplate fan and core cowls from UTW program with hardwall and one set of SDOF acoustic panels. Materials for an additional set of SDOF panels and two bulk absorber panels will also be procured.

Table 14-I. OTW Flight Propulsion System Mount Loads.

Maneuver		T_{1R}	T_{1L}	V_{2R}	V_{2L}	S_3	V_4
1 G Down	N	-	-	8,230	8,230	-	2,625
	(lb)	-	-	1,850	1,850	-	590
1 G Side	N	2,450	2,450	-	-	19,080	-
	(lb)	550	550	-	-	4,290	-
1 θ Pitch	N	9,650	9,650	-	-	-	-
Velocity	(lb)	2,170	2,170	-	-	-	-
1 ψ Yaw	N	-	-	8,985	8,985	-	17,970
Velocity	(lb)	-	-	2,020	2,020	-	4,040
1 θ Pitch	N	-	-	710	710	-	1,425
Acceleration	(lb)	-	-	160	160	-	320
1 ψ Yaw	N	755	755	-	-	-	-
Acceleration	(lb)	170	170	-	-	-	-
1000 lbs Thrust	N	2,225	2,225	-	-	-	-
	(lb)	500	500	-	-	-	-
1 Composite	N	46,260	46,260	104,080	104,080	148,120	356,280
Blade Out †	(lb)	10,400	10,400	23,400	23,400	33,300	80,100

† Vertical and Side Loads do not act simultaneously

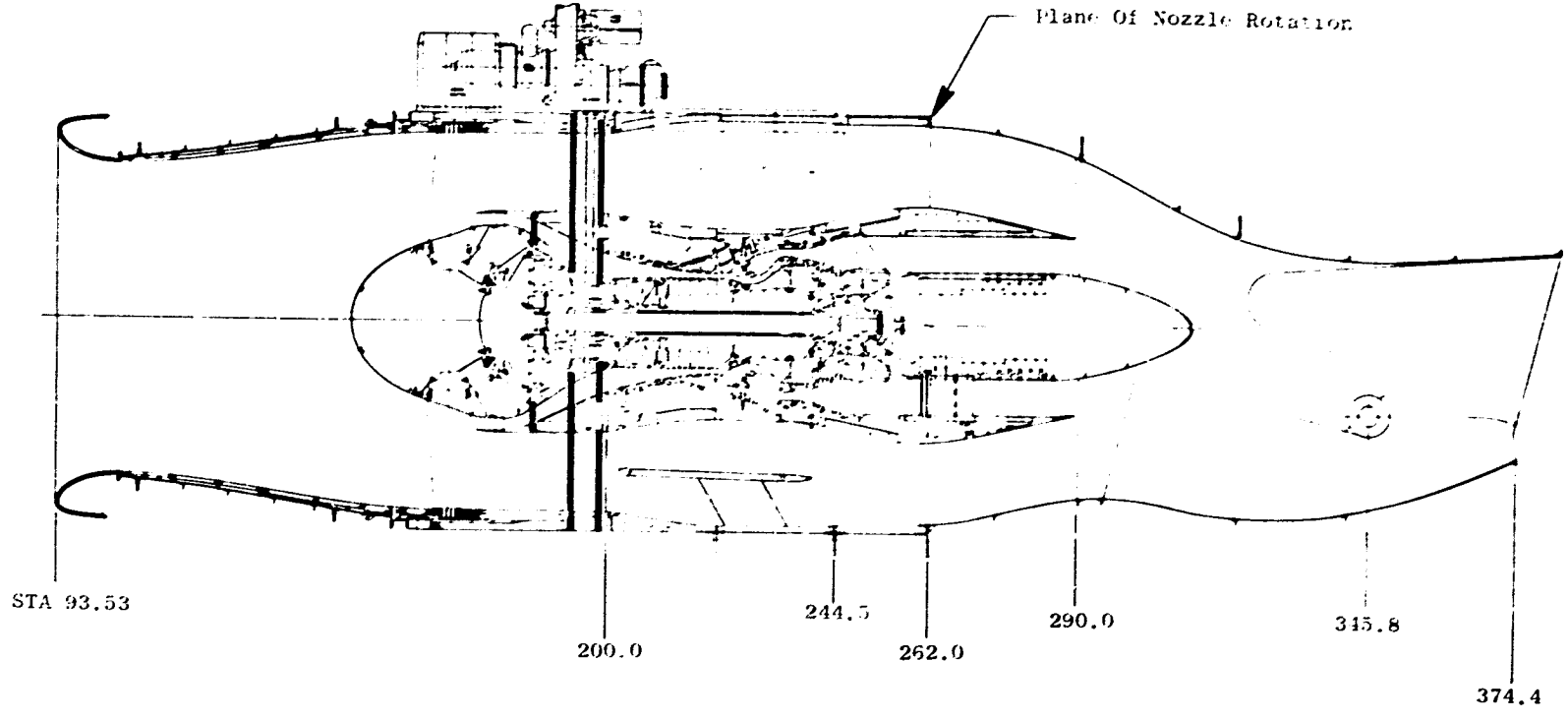

Figure 14.5. OTW Experimental Propulsion System, Installation.

Experimental

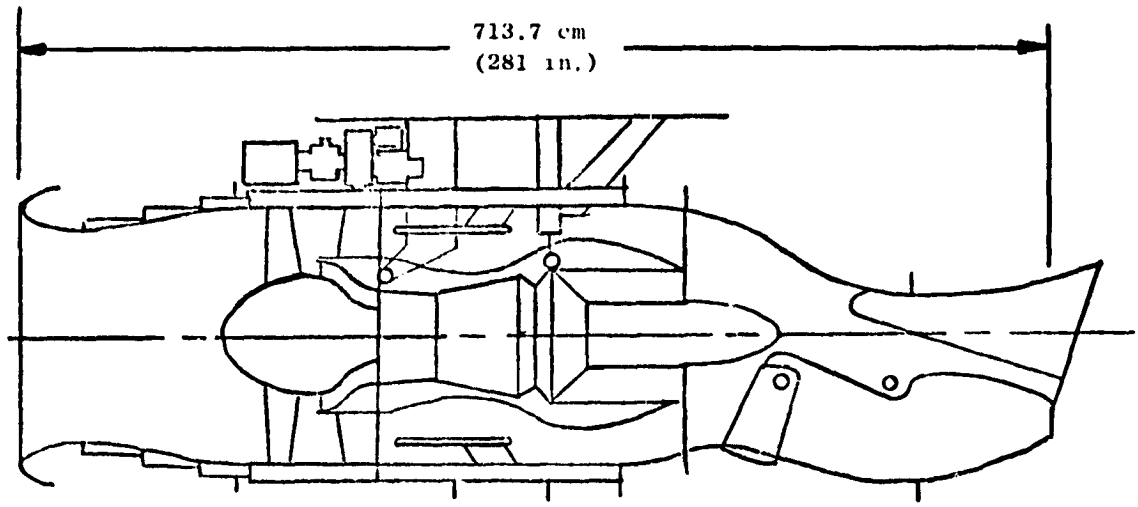

Flight

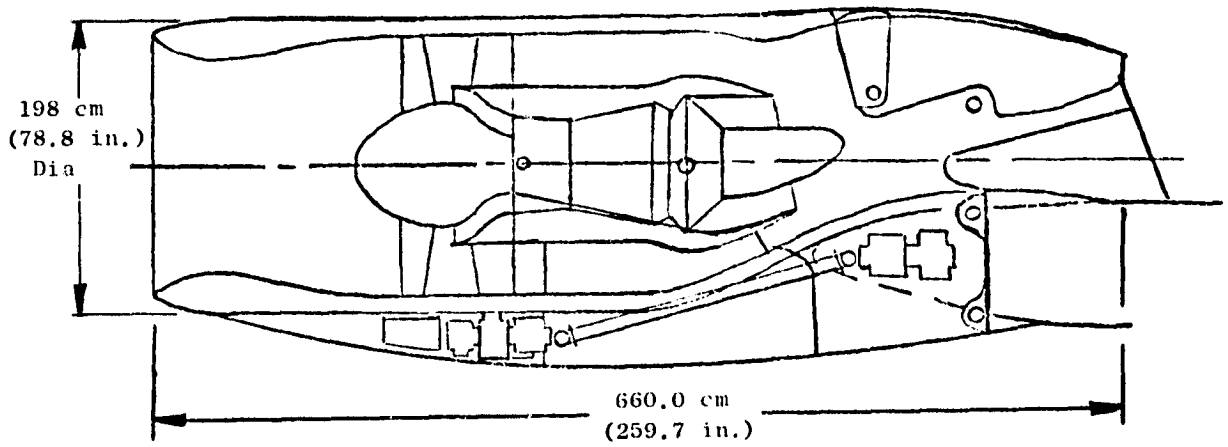

Figure 14.6. OTW Flight Versus Experimental System Outlines.

Table 14-II. Experimental Versus Flight Propulsion System, OTW

Areas of Difference	Experimental	Flight
Accessories		
Accessory gearbox case	Cast aluminum	Optimized design
Oil tank	TF39 Mod (Facility)	Shape to installation
Heat exchanger	Water/oil (LM2500-facility)	Fuel/oil (engine)
Fuel delivery system	F101 modified	Resized
Control system	Digital	Optimized digital
Lube filters	CF6/industrial	Flight design
Accessory placement	Test	Aircraft
Hydraulic system	None	Aircraft only
Nacelle		
Acoustic design	609.6 m (2000 ft) Takeoff	914.4 m (3000 ft) Takeoff
Fan exhaust system	Baseline	54.1 m (21.3 in.) shorter
Core exhaust system	Boilerplate	Optimized (unsuppressed)
Accessory cover	None	Hinged
Maintainability and Flight Safety		
Anti-icing	No	Yes
Fire det. and extinguishing	Test-type	Flight-type
Fuel system	Single-wall	Double-wall

- A boilerplate acoustic splitter from the UTW program will be adapted to the OTW engine by substituting a shorter tail piece.

- The core exhaust nozzle and plug from the UTW program will be used. These components incorporate interchangeable hardwall or stacked acoustic treatment.

- A lengthening of the OTW experimental system was required to use the core exhaust hardware from the UTW program and to provide the capability of rotating the OTW "D"-shaped nozzle for testing in either the horizontal or vertical planes.

- The experimental system is inverted relative to its normal position. This permits common facility mounting hardware for both the OTW and UTW test systems.

- The external flow lines and the accessory cover have been eliminated. If used, the radius would be approximately 8.9 cm (3.5 in.) larger than the flight configuration. This increase in external dimensions is required for the structure to support the replaceable acoustic panels.

- The boilerplate inlet, fan cowl, and exhaust nozzle/reverser will be supported from the test stand to prevent overloading of the composite fan frame. Primary component attachment joints will be the same as in the flight configuration to assure normal flange air and noise leakage. Secondary joints will be provided to "break" the load path between the engine and the test-stand-mounted boilerplate components (i.e., normal engine thrust and other operating loads will be carried through the main engine mounts to the test stand).

14.2 DESIGN CRITERIA

All components have been designed consistent with the requirements specified in Section 2.0. Additional specific nacelle component design criteria are as follows:

Inlet

- No anti-icing system components or inlet metal leading edge are included in the design.

- Design is a one-piece structure with quick disconnect-type fasteners. The experimental engine does not include the forward extension of the external pylon/accessory cover.

- Boilerplate hardware will be supported from the facility.

- Boilerplate inlet will have an aero-acoustic leading edge lip. The lip is contoured to simulate Mach number distribution for 80 knots forward aircraft velocity at static operation conditions.

Fan Cowl

- No power opening devices are included for either flight or boilerplate propulsion system hardware.

- Aft cowl to fan frame attachment is quick disconnect type similar to DC-10/CF6 design.

Exhaust Nozzle

- The variable-area exhaust nozzle is designed to spread the flow over the wing when propulsive lift is required. Exhaust area varies from 15,613 cm^2 (2420 $in.^2$) at cruise operating condition, to 18,452 cm^2 (2860 $in.^2$) at takeoff condition.

Thrust Reverser

- The target reverser in the flight configuration must be capable of withstanding inadvertent deployment to the reverse thrust position under the following operating conditions:

  - At speeds up to 154 m/sec (300 knots) from 0 to 3048 m (10,000 ft) altitude at cruise power without damage.

  - At speeds up to 193 m/sec (375 knots) above 3048 m (10,000 ft) altitude at maximum power without separation from the aircraft.

Core Cowl

- Must provide access to core and core-mounted accessories without engine removal.

Maintainability

- The engine is capable of removal from an aircraft wing and/or facility:

  - Without disconnecting engine-to-engine configuration hardware or accessory components (except for facility-mounted components and connecting hardware on the experimental engine).

  - Vertically downward (after uncoupling facility-mounted components on the experimental engine).

  - Without removal of fan cowl doors or exhaust nozzle.

- Access to boroscope ports is possible without removal of engine components or disconnecting piping.

- Engine accessories have been located for easy inspection and maintenance. In the experimental engine configuration some compromise has been made to facilitate use of existing component hardware.

14.3 BOILERPLATE NACELLE DESIGN

Presented in this section is a discussion of the conceptual design of the "boilerplate" nacelle hardware that will be used for testing of the OTW propulsion system. The preliminary design review of the boilerplate nacelle and facility hardware for the OTW system was held in September of 1975. Completion of the detail design is scheduled for the second quarter of 1976.

14.3.1 Inlets

Planned testing of the OTW engine will require three boilerplate inlet configurations. The NASA Quiet Engine "C" bellmouth inlet will be utilized for aerodynamic engine mapping and baseline acoustic evaluation. The bellmouth inlet package consists of a fiberglass/honeycomb bellmouth and a cylindrical casing that satisfied the aerodynamic requirements for a low-Mach-number inlet (Figure 14.7).

A massive inlet suppressor will be utilized to isolate aft end noise and provide additional information for acoustic evaluation. The four-ring splitter shown in Figure 14.8 from the Quiet Engine "C" satisfies the requirements for a massive inlet suppressor.

An accelerating inlet (Figure 14.9) will be employed for the aero and acoustic evaluations. It includes a fiberglass/honeycomb lip and a fiberglass structural shell that provides the attachment bosses for interchangeable sets of acoustic treatment panels and hardwall panels. A typical single-degree-of-freedom (SDOF) acoustic panel will consist of an aluminum perforated face plate stretch-formed to the correct contour and bonded to a honeycomb panel, which, in turn, is bonded to a fiberglass backing sheet.

A typical inlet-to-test-stand mounting system at the Peebles test site is shown in Figure 14.10. As a result of their non-flight-weight construction, all inlets will be mechanically decoupled from the engine to prevent overload of the composite fan frame flanges due to excessive engine motion and/or vibration. A typical decoupled or "loadbreak" joint is shown in Figure 14.7. The air seal is provided by a open-cell foam bonded to one-half of the flange and pressed against the other. The two seals aerodynamically and acoustically simulate the hard-joint condition of the final composite "flight" propulsion system assembly.

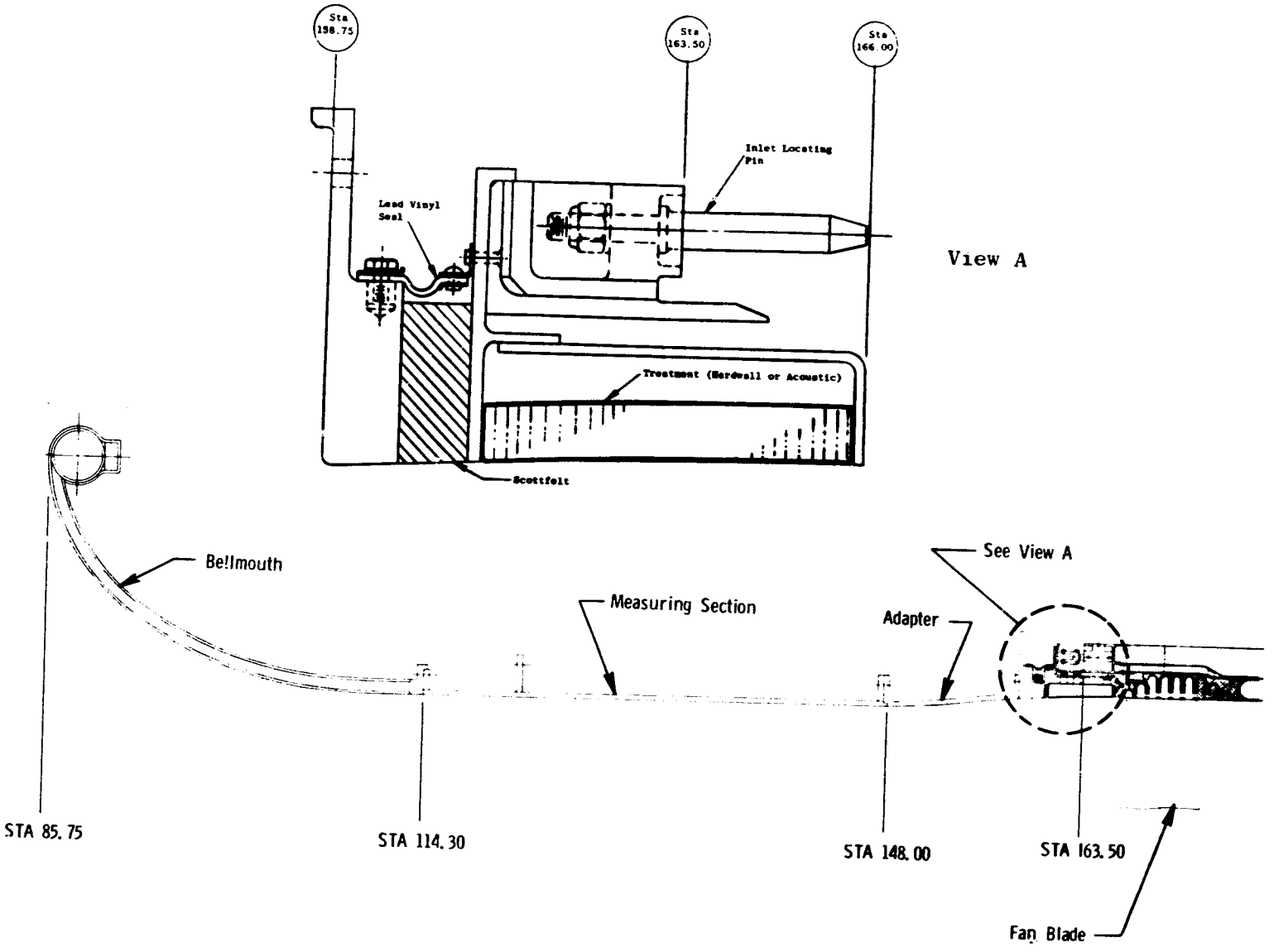

Figure 14.7. Boiler Plate Inlet, Bellmouth.

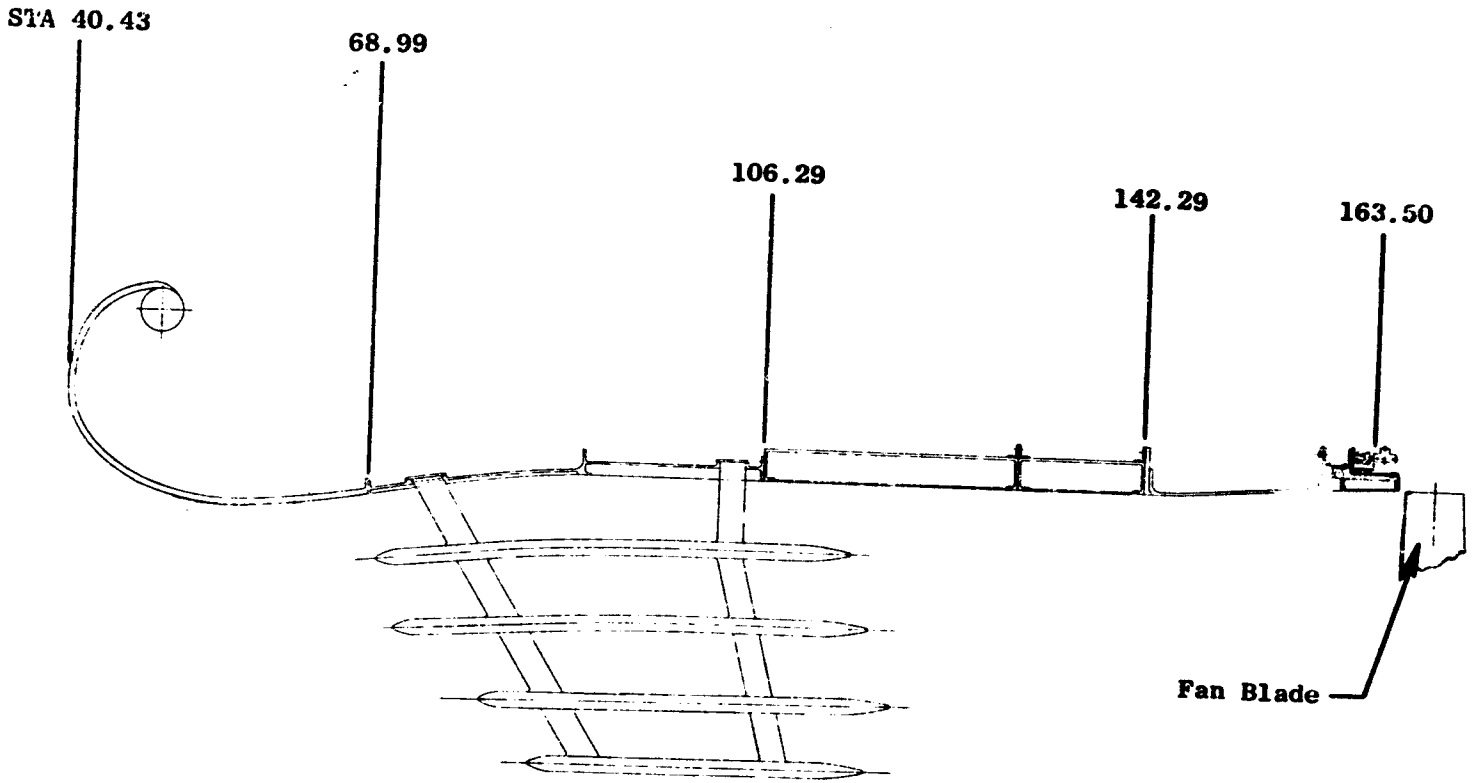

Figure 14.8. Massive Suppressor Inlet with Four Ring Splitter.

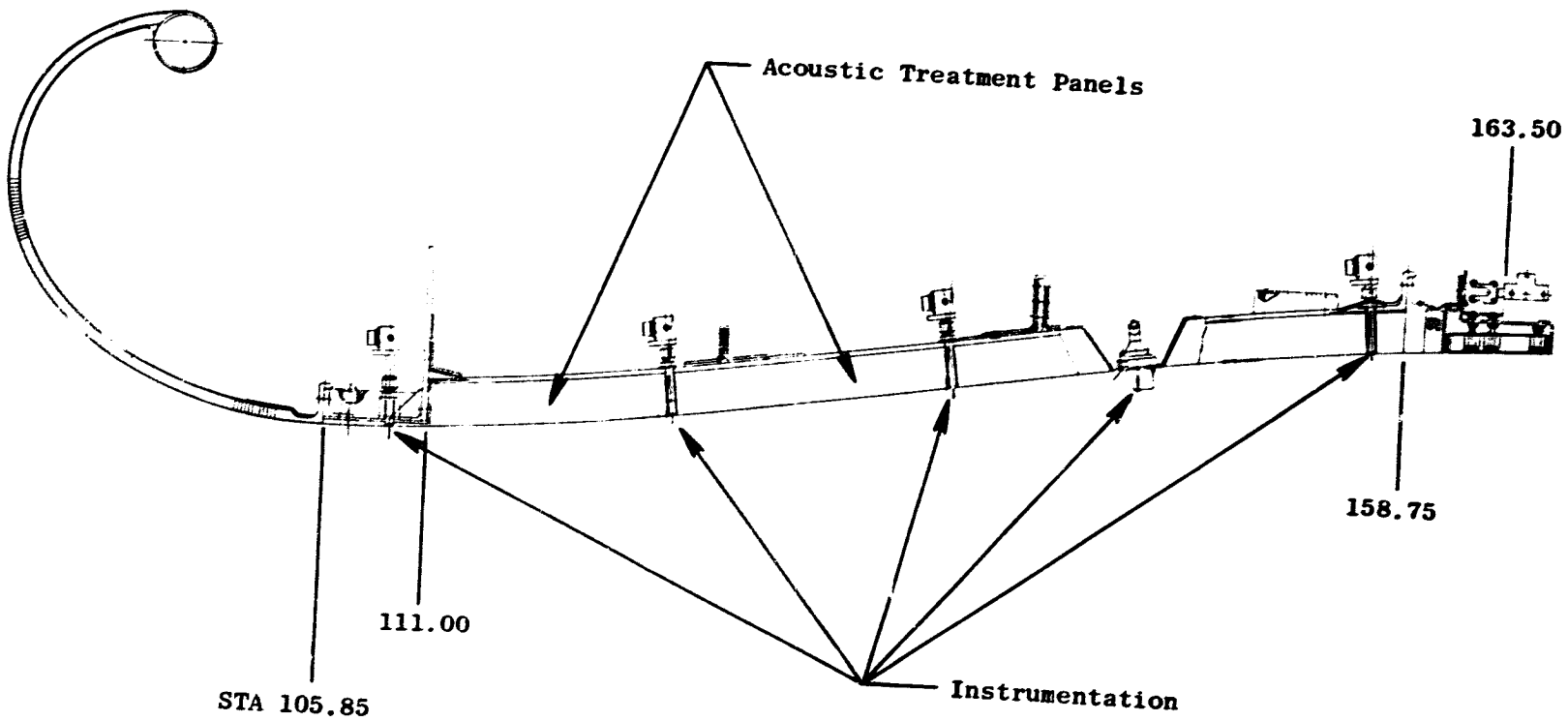

Figure 14.9. Boiler Plate High Mach Accelerating Inlet.

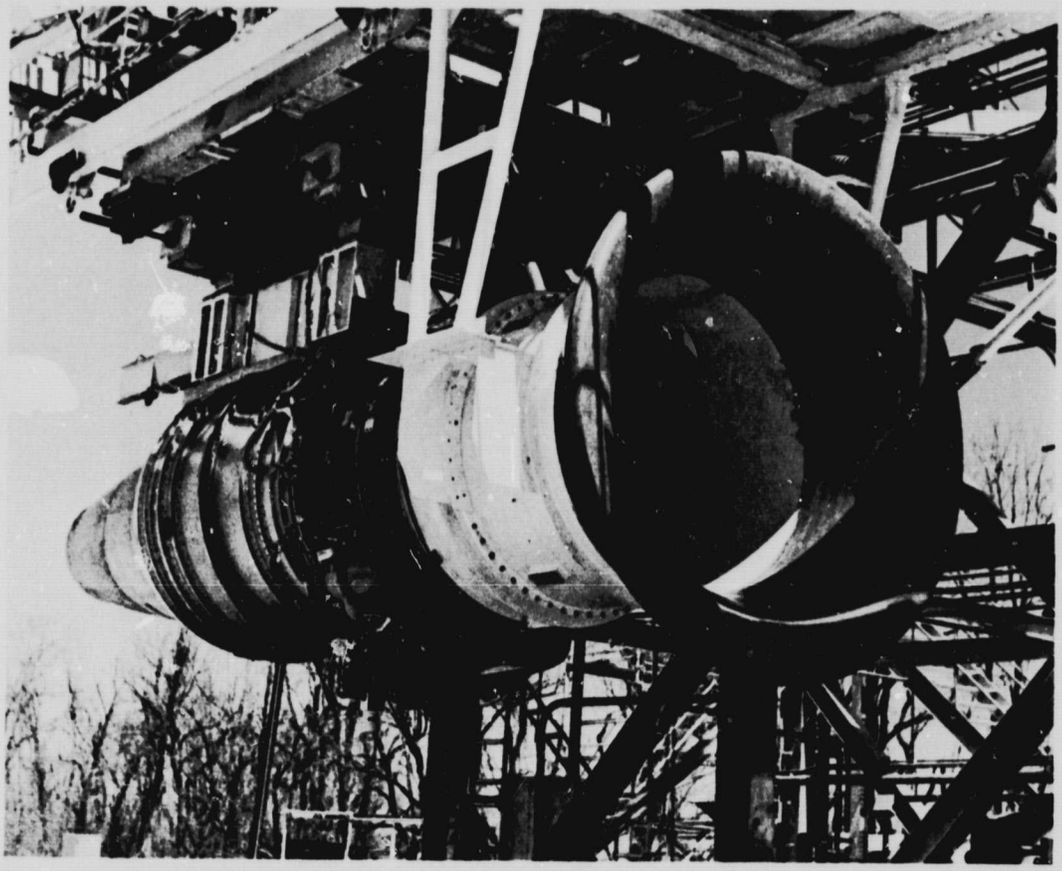

Figure 14.10. Inlet on Test Stand at Peebles Proving Grounds.

ORIGINAL PAGE IS
OF POOR QUALITY

14.3.2 Fan Cowl

The OTW fan cowl from the composite fan frame to Station 244.5 is a fabricated structural shell that provides the attachment capability for interchangeable sets of acoustic treatment panels. This hardware will be tested first on the UTW engine.

A splitter tailpiece, capable of converting the 101.6 cm (40 in.) UTW splitter to a 76.2 cm (30 in.) OTW configuration, will be procured. In addition, a new splitter assembly will be procured in the OTW program for use in the UTW composite configuration. This delay in building the second splitter provides additional acoustic design flexibility to define the final UTW splitter configuration. Both splitter assemblies will be supported by the duct through six airfoil-shaped struts (see Figure 14.11).

A new section of OTW fan cowl will be designed and built to extend from Station 244.5 to Station 262. This structure will be a fabricated shell and will accommodate one new set of acoustic treatment panels and one matched set of hardwall panels. This structure is supported at Station 244.5 and becomes part of the fan door assembly. Station 262 represents the last circular section and the end of acoustic treatment. It also is the plane of rotation for the nozzle which can be rotated 90° during NASA testing, so that the "D"-shaped nozzle will match with a vertical segment of an aircraft wing. The outer fan doors can be decoupled from the fan frame and supported from the facility through the pylon and a set of telescoping beams to gain access to the core engine.

14.3.3 Exhaust Nozzle and Reverser

The OTW fan bypass duct from Station 262 to Station 290 features a removable structural shell that is decoupled from the fan door system and provides the aerodynamic section that transitions from circular cross sections to the "D"-shaped thrust reverser and nozzle assembly. Core cowl access is accommodated by opening the hinged fan doors and removing this transition piece.

This section will include a pylon close-out piece that can be modified to accommodate the Peebles testing and the 90° rotational requirement for NASA testing. In all cases this structural shell is supported from the thrust reverser which has its own mount system to the facility thrust frame.

The "D" nozzle and thrust reverser assembly is a structural fabrication composed of contoured shells and rings that provides multipositional nozzle area control, and a two-position thrust reverser as shown in Figure 14.12. The control is maintained by two multipositional side doors and is accomplished by making adjustments during engine shutdown. The two-position thrust reverser will be bolted in either the closed or open position. Bolt-on side skirts and lip extension will simulate the configuration of the flight reverser in its fully deployed position. This assembly incorporates

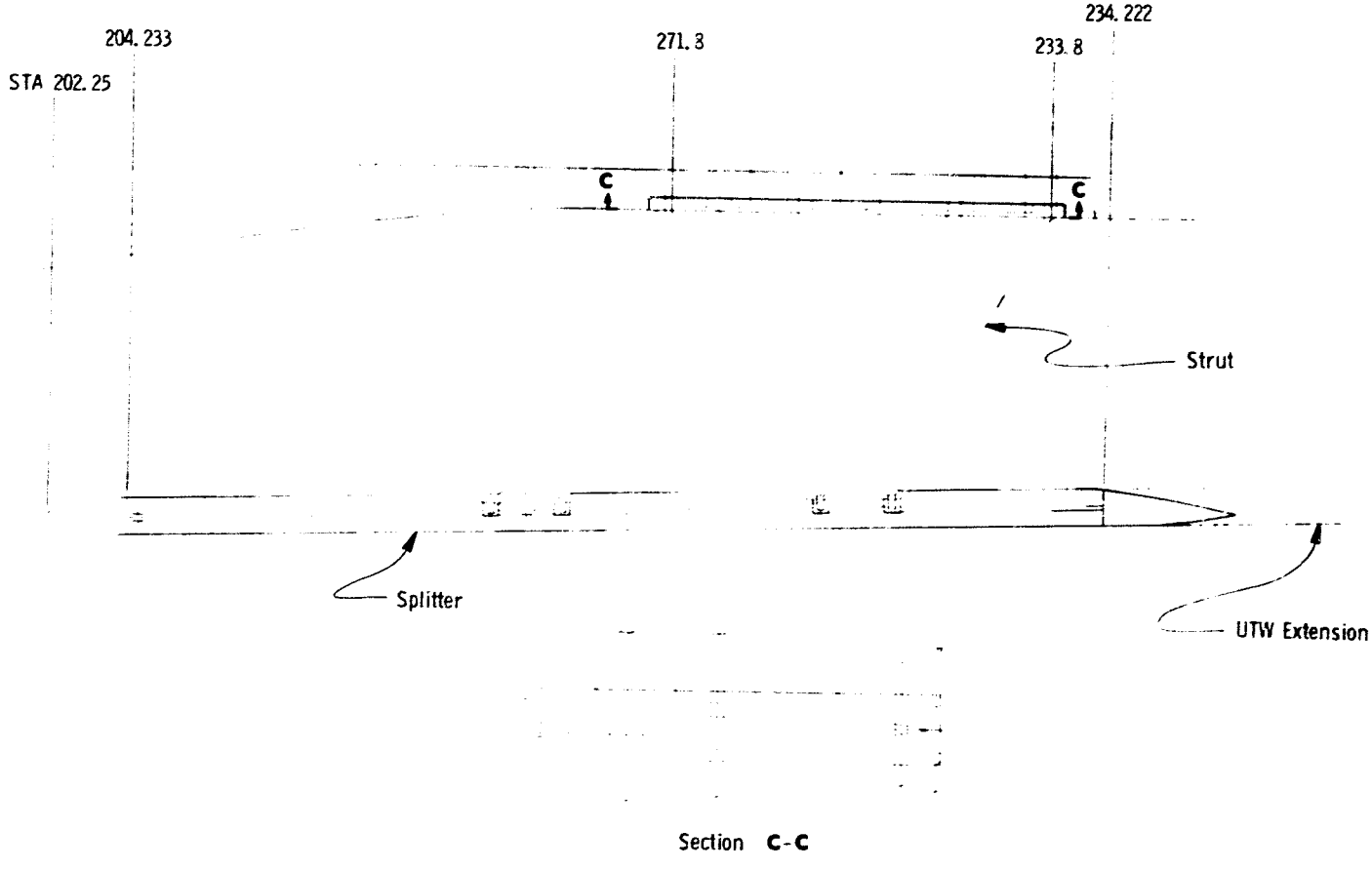

Section C-C

Figure 14.11. Acoustic Splitter, Fan Exhaust.

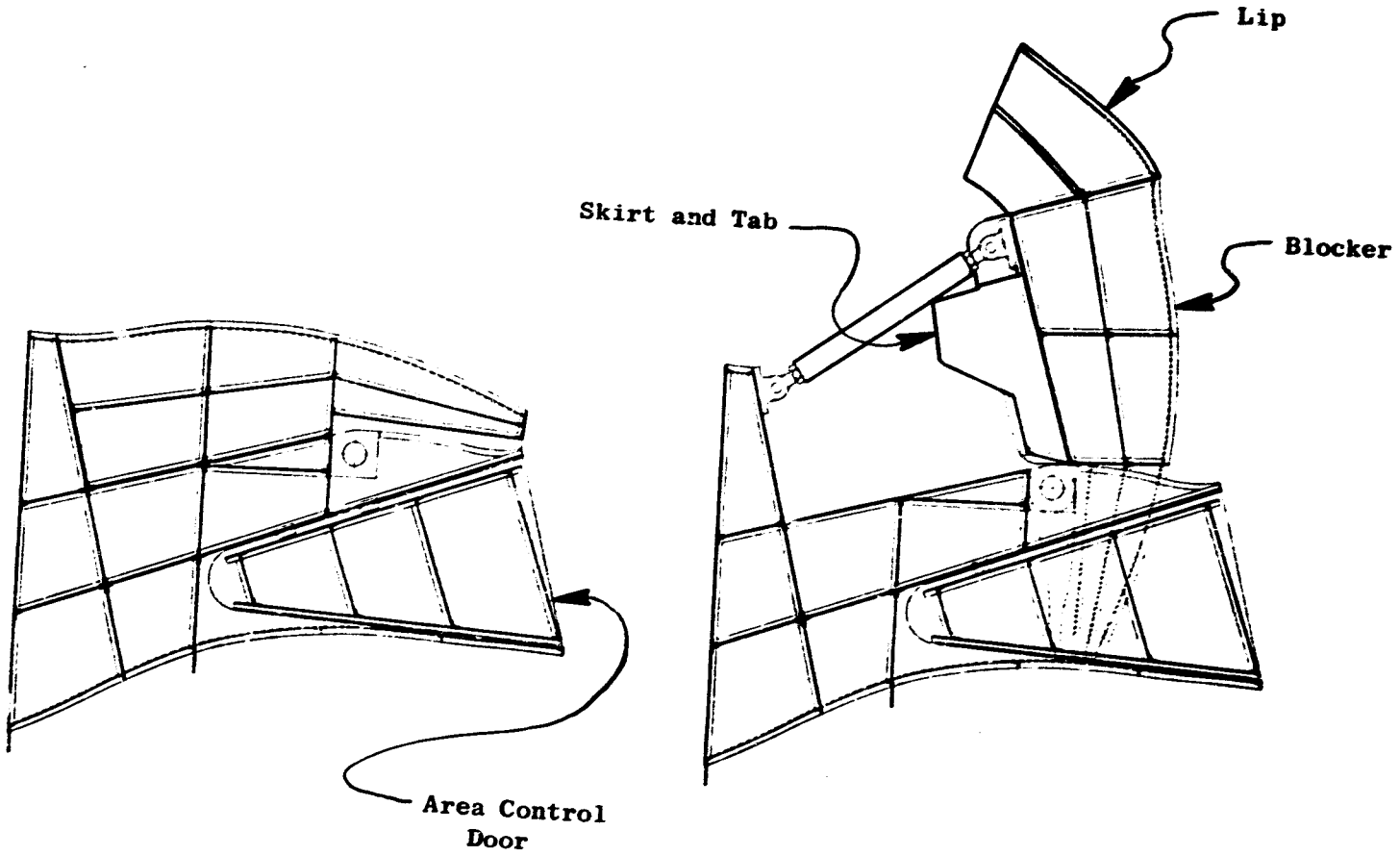

Figure 14.12. Exhaust System and Target Reverser.

its own mount system and will accommodate either the Peebles test system or the NASA 90° rotated test position. The mounting concept is shown in Figure 14.13.

14.3.4 Core Cowl

The OTW core cowl (see Figure 14.14) embodies the same design philosophy established for the fan duct. Since the core cowl flowlines are identical for both UTW and OTW systems, the UTW acoustic and hardwall panels can be utilized in the OTW system. The core cowl has a forward interface (Marman-type joint) with the fan frame and an aft interfacing slip joint with the core nozzle. Access to the compressor and turbine is provided by the hinged door construction of the core ducting. This is accomplished by attaching the core door and skirt system to structural stringers extending down within the pylon through a set of pins.

Temperature considerations were of primary importance in determining the core cowl configuration. The inner surfaces of the doors are exposed to radiant and convective heat from the core engine. Heat transfer analysis established the requirement for a radiation shield plus auxiliary cooling air to protect the cowl acoustic panels and ensure a safe operating environment for the epoxy resins that will be used in their construction. Two stainless steel radiation shields are mounted off the cowl door on each side of the fire wall. The auxiliary "shop" cooling air is bled in between the core cowl wall and the radiation shield and exhausted through the pylon. The total amount of cooling air required to keep the maximum temperature at the desired level is approximately 0.4536 kg/sec (1 lb/sec). In a "flight" configuration, the core cowl would be nonmetal/composite construction using a higher temperature resin such as polyimid. With this construction, the radiation shield would still be required, using fan discharge air between the cowl and the radiation shield and discharging back to the fan stream at the slip joint between the cowl and the core exhaust nozzle at engine Station 274.

On the experimental engine, the core cowl is drawn in as close to the core engine case as possible. This was done to give the required fan exhaust flow area with an acoustically treated splitter in the stream and to maintain the 78.8-inch maximum diameter consistent with the "flight" configuration.

14.3.5 Pylon-Skirt Assembly

The pylon assembly for the boilerplate nacelle is the primary structural support system for the fan doors and the core cowl doors. The pylon is bolted directly to the main engine mount suppports. In this manner, the outer door loads are transmitted directly to the facility for all conditions. The inner skirt and hinge is decoupled from the pylon during engine operation and attached to the pylon prior to opening the core doors. Core door loads are transmitted to the fan frame, radial fire wall, and outer core exhaust nozzle slip joint during engine testing. The aerodynamic contour of the

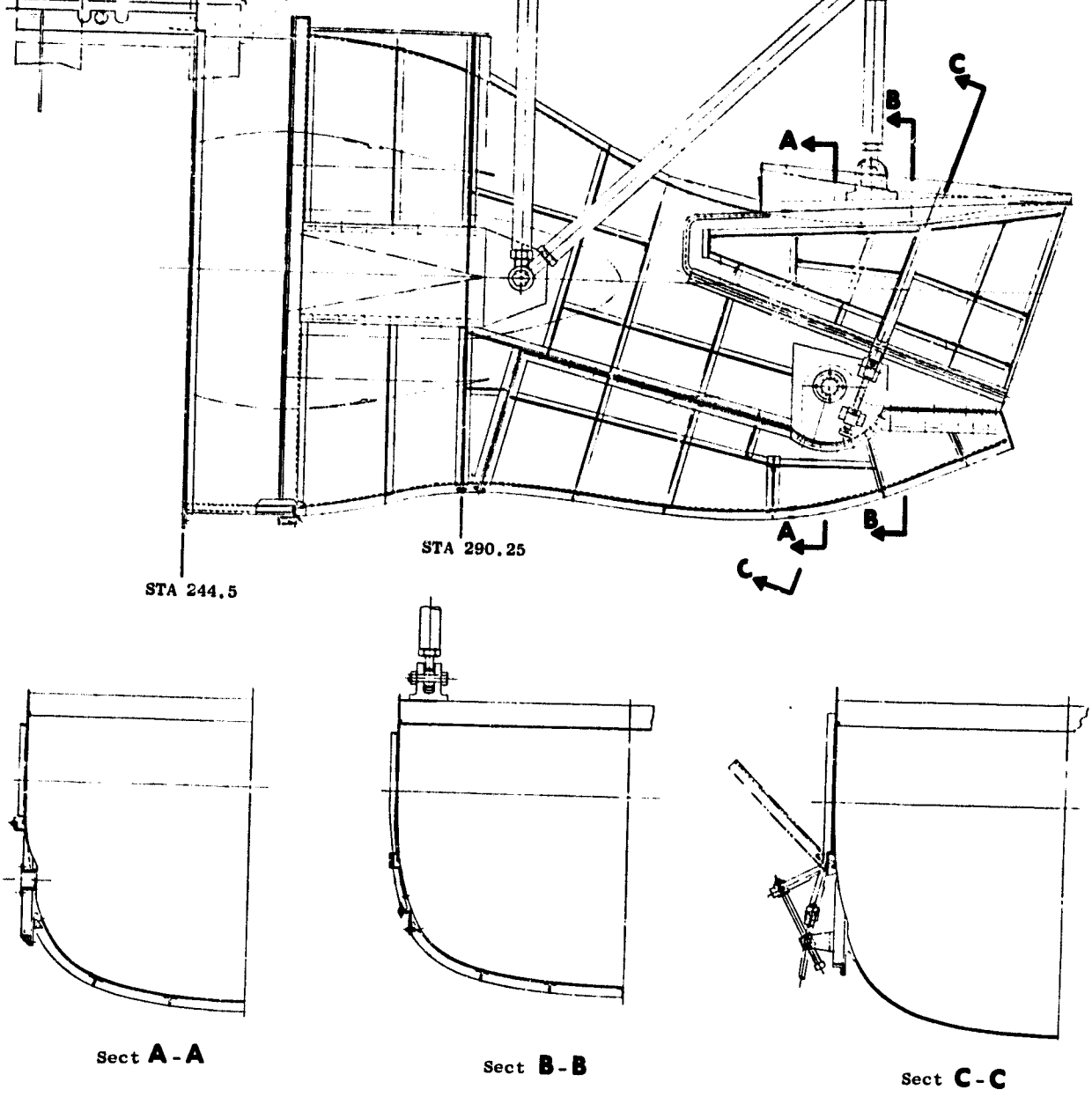

Figure 14.13. Boiler Plate Exhaust System - Support.

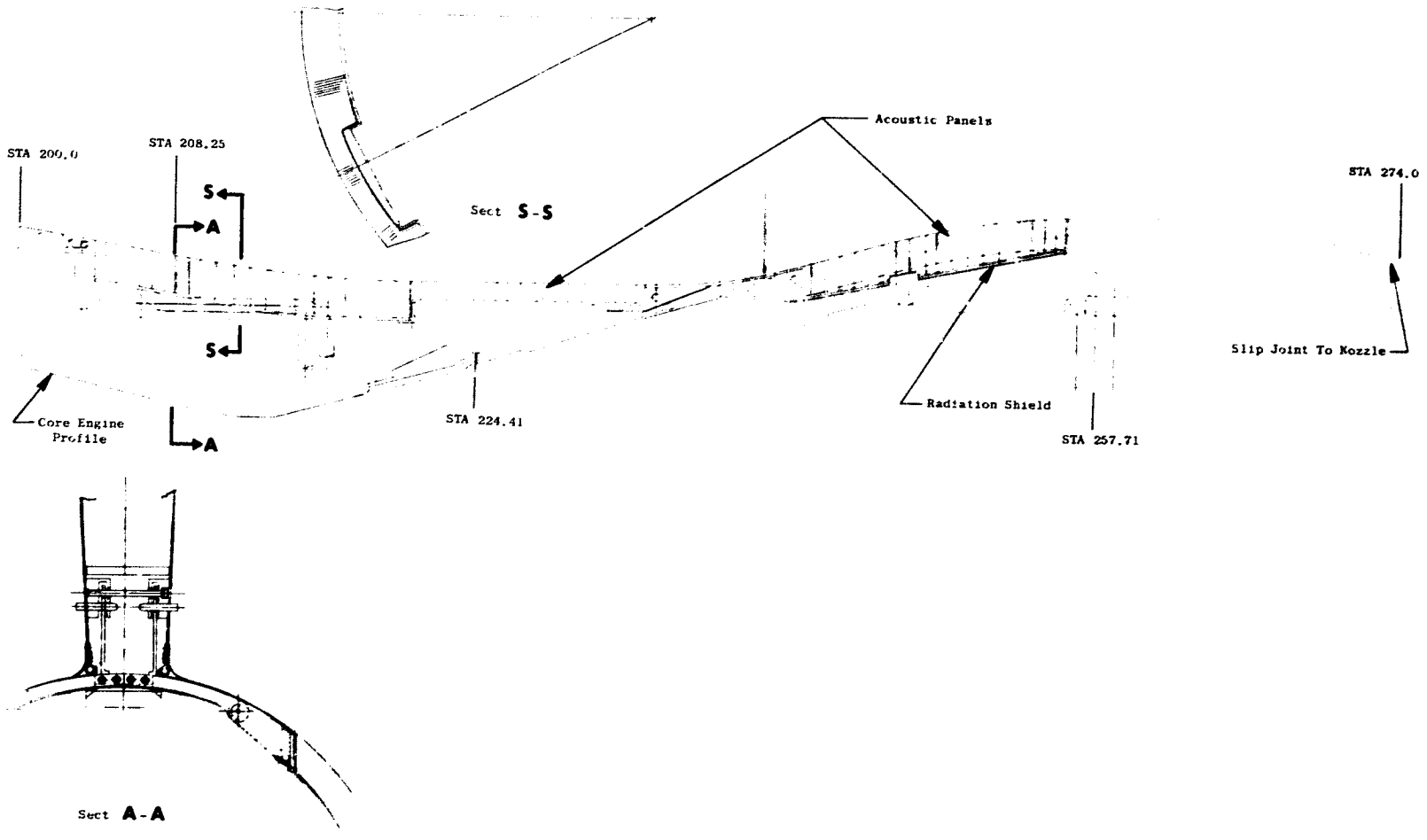

Figure 14.14. Core Cowl.

pylon is provided by removable nonstructural fairing panels bolted to the structural beam. The removable fairing provides accessibility for core inspection.

Figure 14.15 is a roll-out view of the fan cowl showing the top pylon transition into the top, "fat" strut of the fan frame forward of engine station 200. The gearbox radial drive is enclosed in this section of the frame strut/pylon leading edge. Just aft of Station 200 is the "Pylon Service Area" housing the engine-to-gearbox piping, cables and wires. An enlarged section of this area is shown in Figure 14.16. Figure 14.17 is a radial cut showing the piping span across the fan flowpath in the service area of the pylon. The combination tube supports and firewalls are drained to ensure no accumulation of flammable fluids. Present plans do not include acoustic treatment of the pylon walls and core skirt.

14.4 CORE EXHAUST NOZZLE

14.4.1 Core Exhaust Nozzle Design - Experimental

The non-flightweight OTW core exhaust nozzle is shown in Figure 14.18. The centerbody consists of a 61.0 cm (24 inch) long acoustically treated cylindrical section attached to a nontreated sheet metal cone with the radial bolts. This assembly then is attached to the turbine frame inner support with radial bolts. The outer flowpath also has a 61.0 cm (24 inch) long acoustic section attached to the core exhaust nozzle. The exhaust nozzle area control conical section will be trimmed to set the required area. At the forward end, this assembly is attached to the turbine frame outer casing flange with bolts. A single strut assembly located on the bottom centerline of the core exhaust nozzle provides an aerodynamic fairing around the aft sump service lines that penetrate the core nozzle flowpath. Cross flow between the plug cavity and outer core cowl cavity is prevented by inner and outer blank-off plates. The bolted construction permits interchangeability between the acoustic sections and the instrumented inner and outer hardwall assemblies required for performance and baseline acoustic testing. All sections of the core exhaust nozzle are interchangeable between the UTW and OTW engine systems.

The stacked acoustic treatment is designed to attenuate both high frequency turbine noise and low frequency combustion noise. The high frequency treatment consists of a welded honeycomb cylinder 2.16 cm (0.85 inches) thick with a perforated face sheet on the flowpath side. The outer face sheet has no perforations. The low frequency noise is attenuated as it passes through the 1.59 cm (0.625 inch) diameter tubes through the honeycomb into the resonating chambers which are 7.0 - 9.4 cm (2.75 - 3.7 inches) deep. Each section is designed for a specific frequency by varying the length of the tube and the volume of the resonating chamber.

During engine start-up, large thermal gradients exist across the honeycomb structure as shown in Figure 14.19. To minimize the thermal stress, the inner surface of the inner duct treatment and the outer surface of the outer

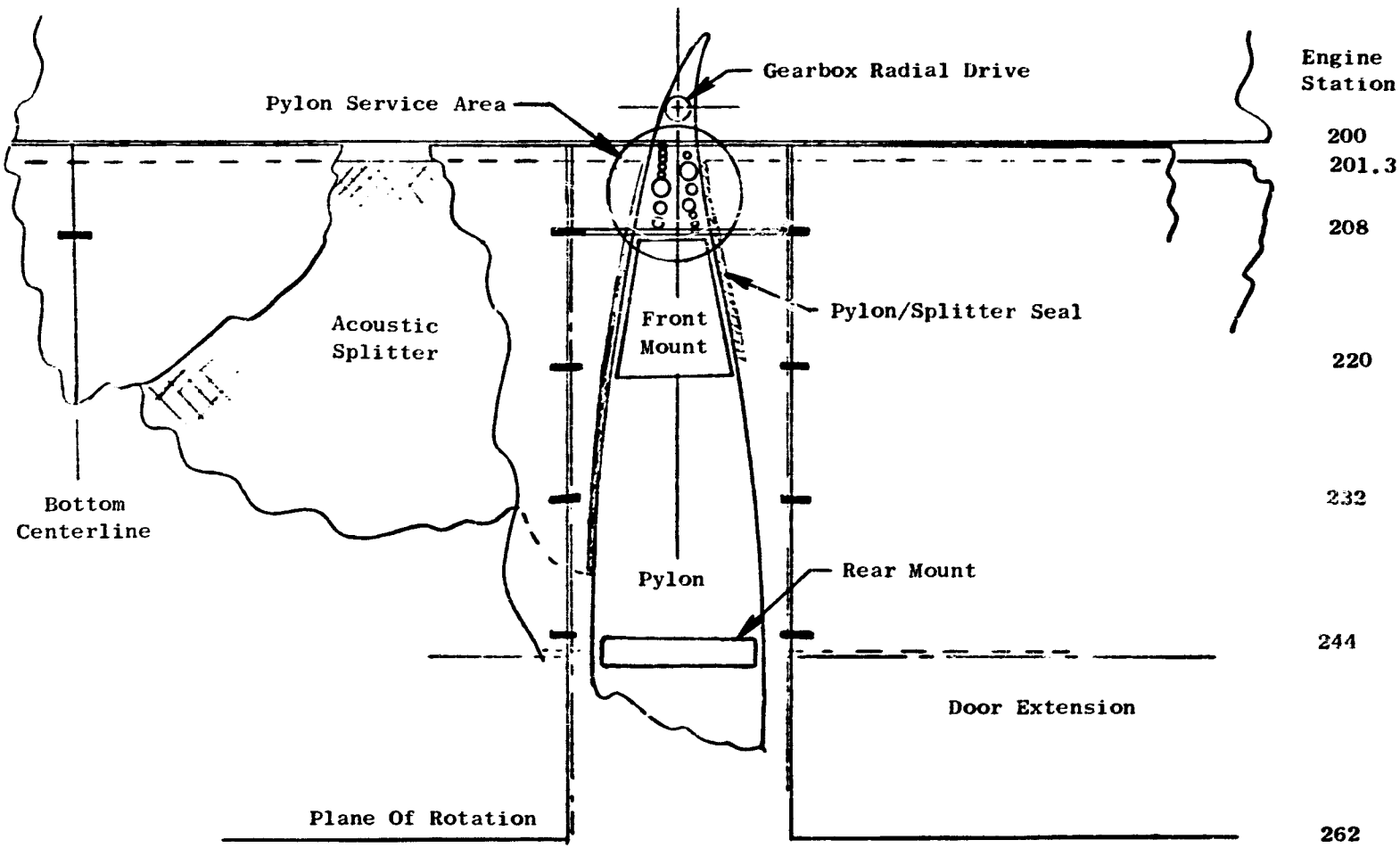

Figure 14.15. Fan Cowl Rollout.

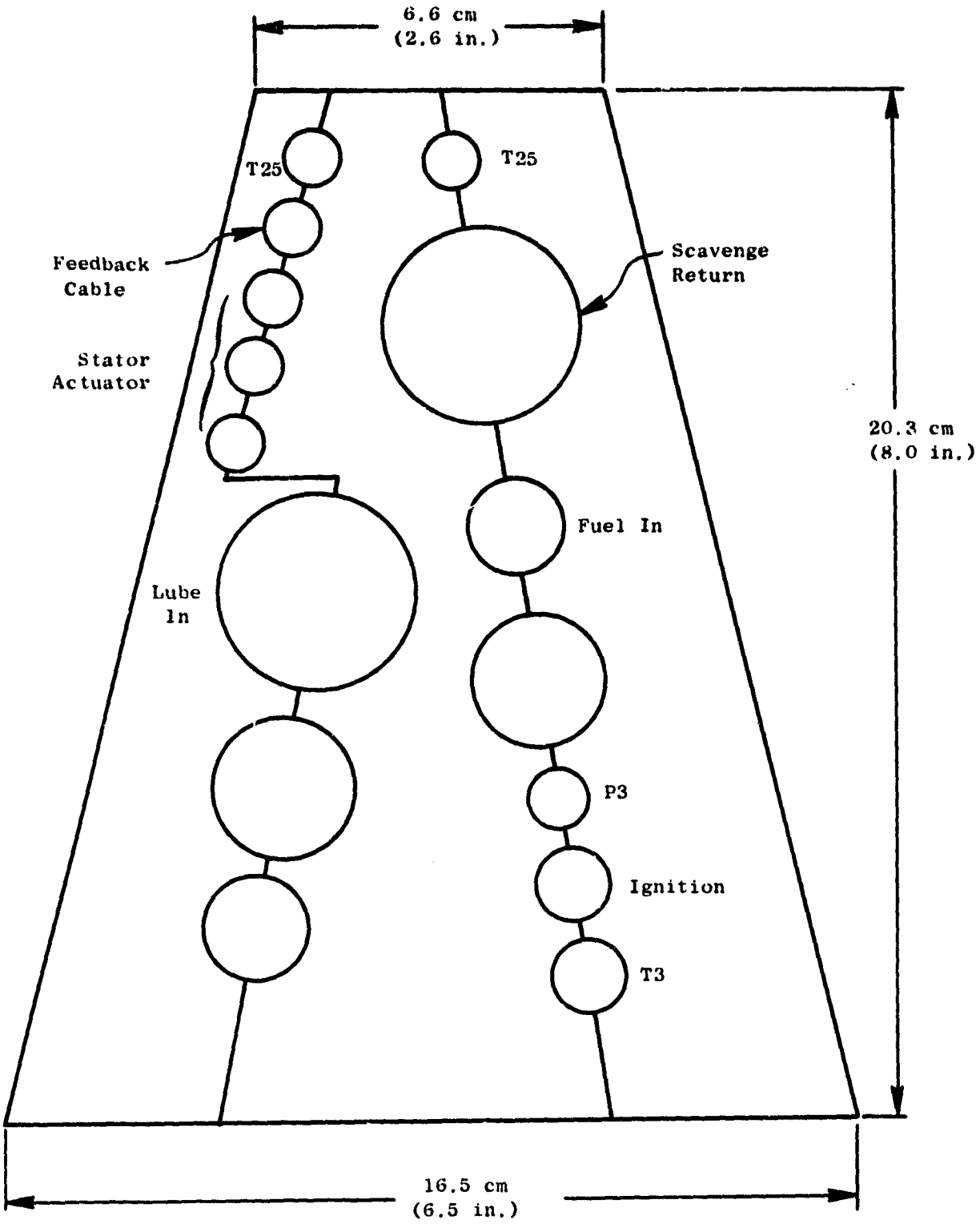

Figure 14.16. Pylon Service Area.

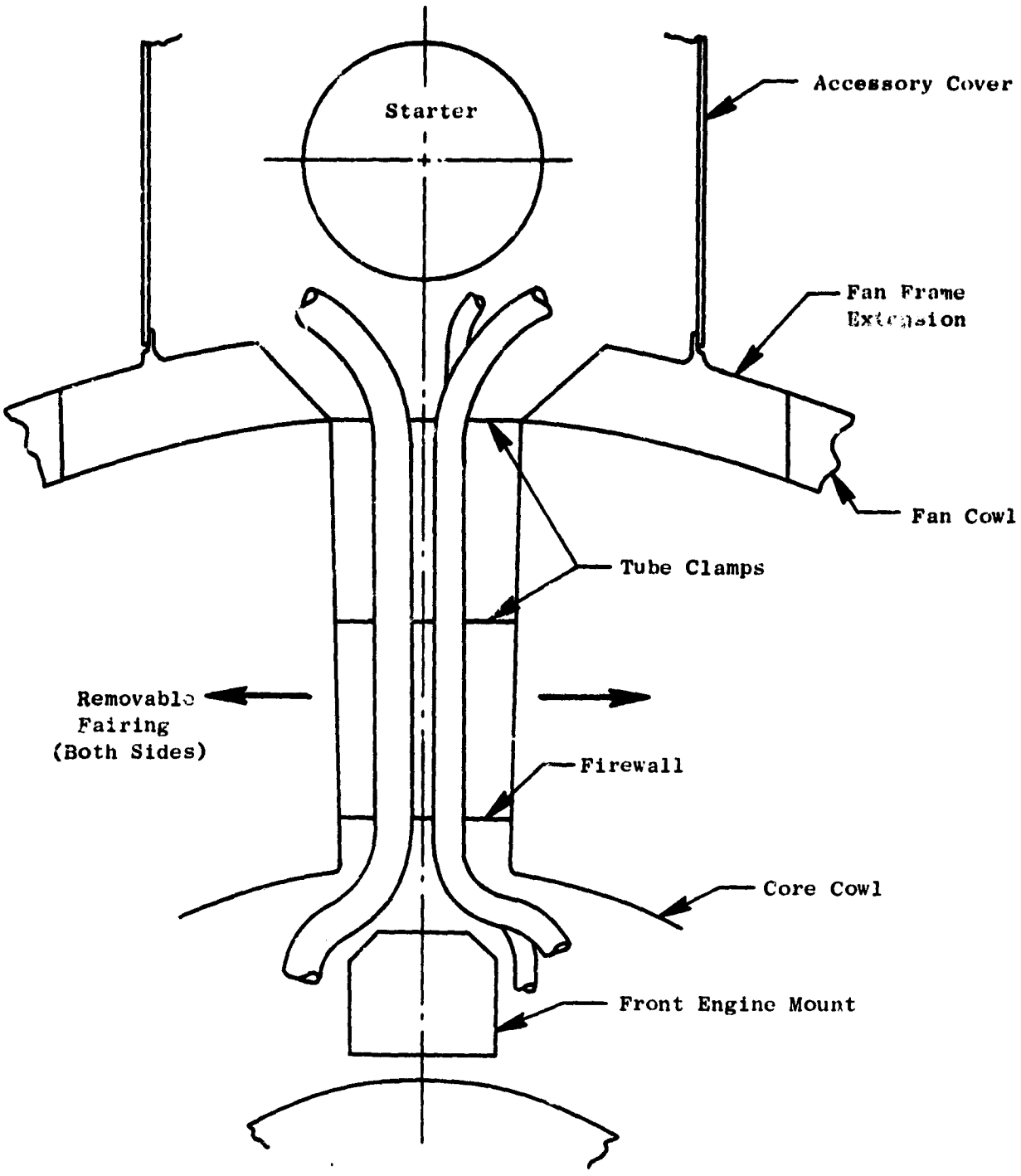

Figure 14.17. Pylon Service Area, Cross Section.

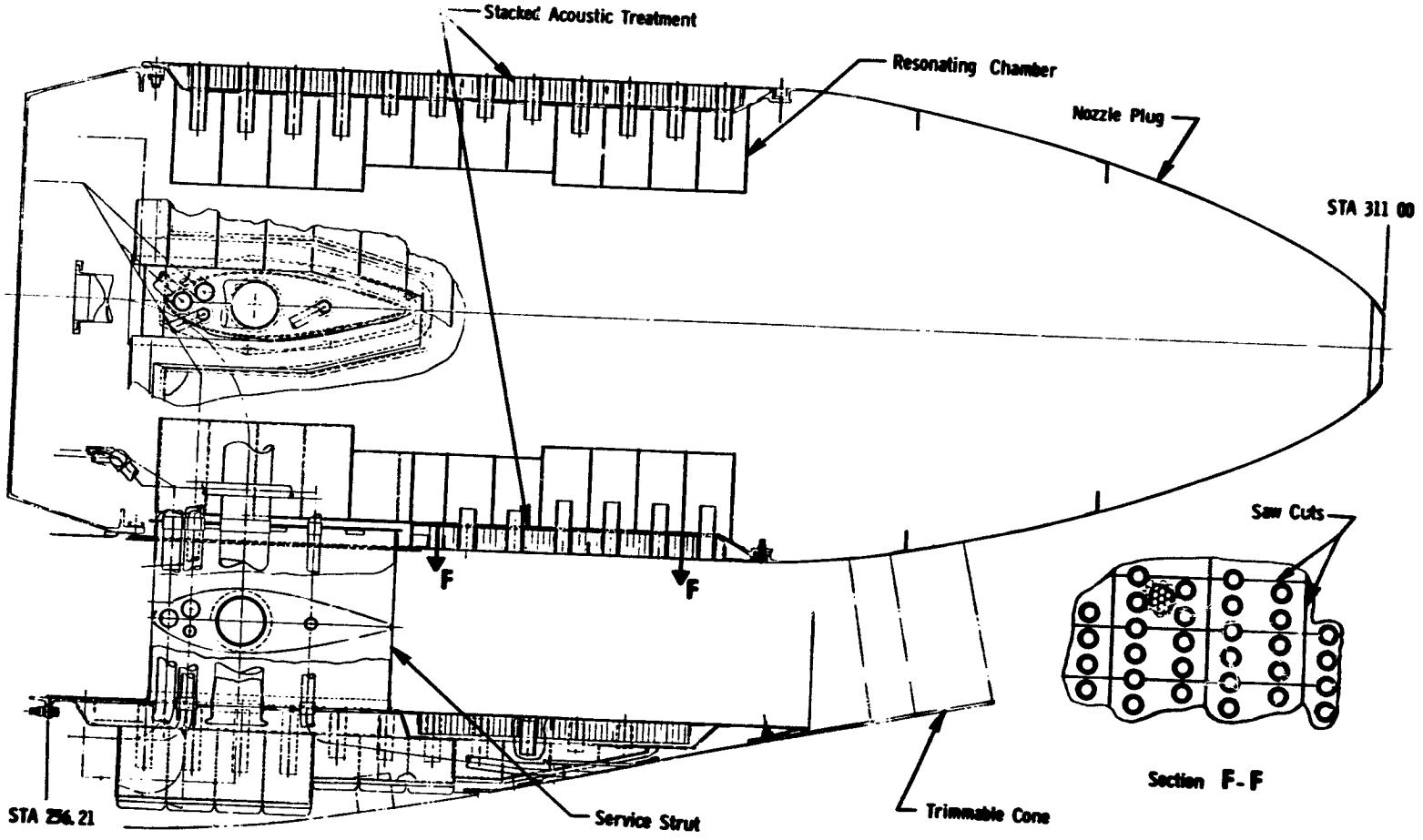

Figure 14.18. Boiler Plate Core Exhaust System.

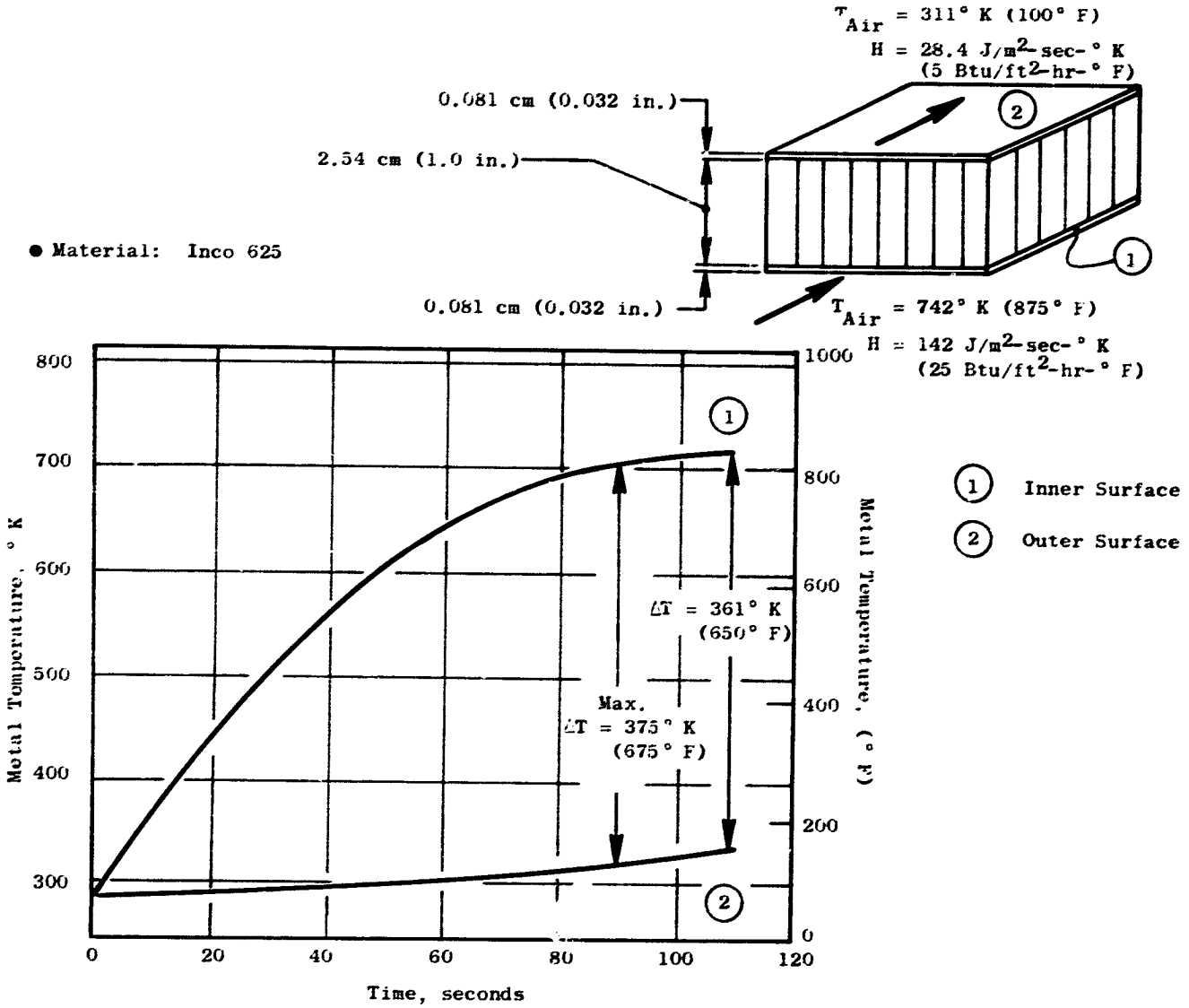

Figure 14.19. Core Exhaust Temperature Gradient.

duct treatment are saw cut as shown in Figure 14.18 (Section F-F). To accommodate the differential thermal expansion as gas temperatures approach 1089° K (1500° F) at the center of the stream and 922 - 978° K (1200 - 1300° F) at the walls, the honeycomb (acoustic treatment) section is designed to freely expand radially as shown in Figure 14.20 and axially as shown in Figure 14.21. Retaining rings at both ends of the inner and outer cylinders center the acoustic treatment. The 12 rows of tube holes in the inner treatment and the 11 rows in the outer treatment are oversized to provide a thermal expansion gap except for the closefitting center holes.

The radial service line struct located on the bottom centerline of the core exhaust nozzle provides an aerodynamic fairing over the oil-in line, the seal drain, the oil scavenge line, the auxiliary air line, and the compressor discharge air to the balance piston. In the experimental engine these lines are routed through the core nozzle to the sump.

- Forward and aft cavity seal drains are joined into a common line in the plug area. The single line comes out through the fairing and is discharged into the fan stream. Wetness or dripping of oil on the floor after testing would indicate seal leakage and the need for maintenance.

- Auxiliary (shop) air is required in the area surrounding the sump (not in balance piston cavity) for low speed (3-4% idle thrust) running where the third stage compressor air pressure goes below low-pressure-turbine discharge static pressure. If not pressurized with "shop" air, hot exhaust gas could circulate back over the turbine disks and forward into the compressor rotor. For the flight configuration a higher stage bleed will be required.

The aerodynamically shaped strut around the rear sump piping has a 4 to 1 fineness ratio to minimize pressure loss in the core exhaust duct. Disassembly of the strut and service lines is not required to change the acoustic treatment. The strut is designed with a fishmouth seal that engages the inner and outer acoustic treatment as they are assembled to the turbine frame flange. The strut is bolted to the outer acoustic treatment but has a slip joint between the strut and the centerbody to accommodate radial differential thermal expansion between the inner and outer acoustic treatment sections during transient conditions.

The core nozzle is a fixed-area nozzle with ± 5% area trim capability provided with interchangeable conical sections that are bolted to the nozzle cone as required in the test program. Finer control can be achieved by machining the cones to achieve the area desired.

14.4.2 OTW Flight Core Exhaust Nozzle

A preliminary design of the OTW flight core exhaust nozzle is shown in Figure 14.22. The core exhaust nozzle is angled 10° from the engine centerline to shorten the installation and to direct hot gas away from the wing.

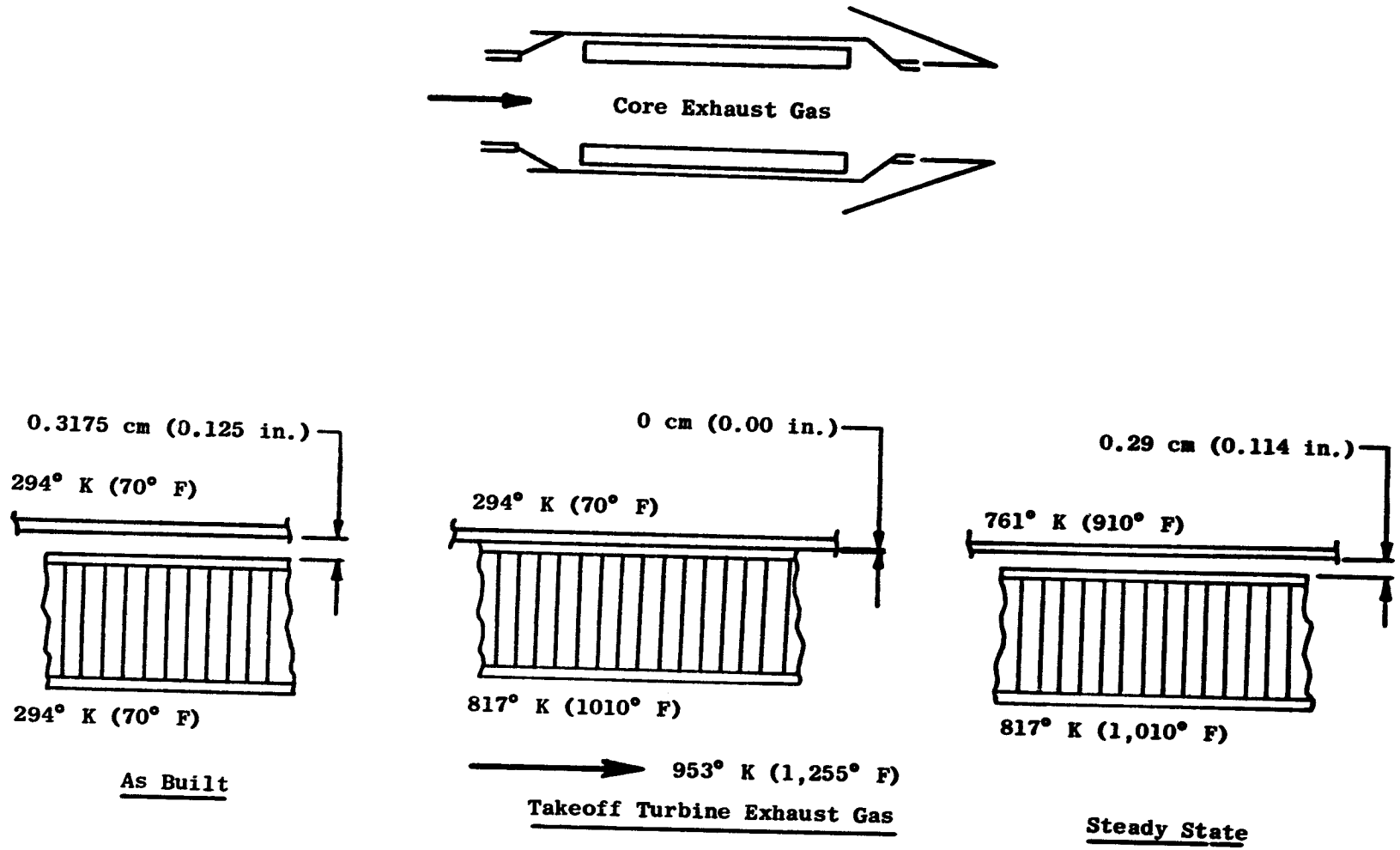

Figure 14.20. Outer Treatment, Radial Thermal Expansion.

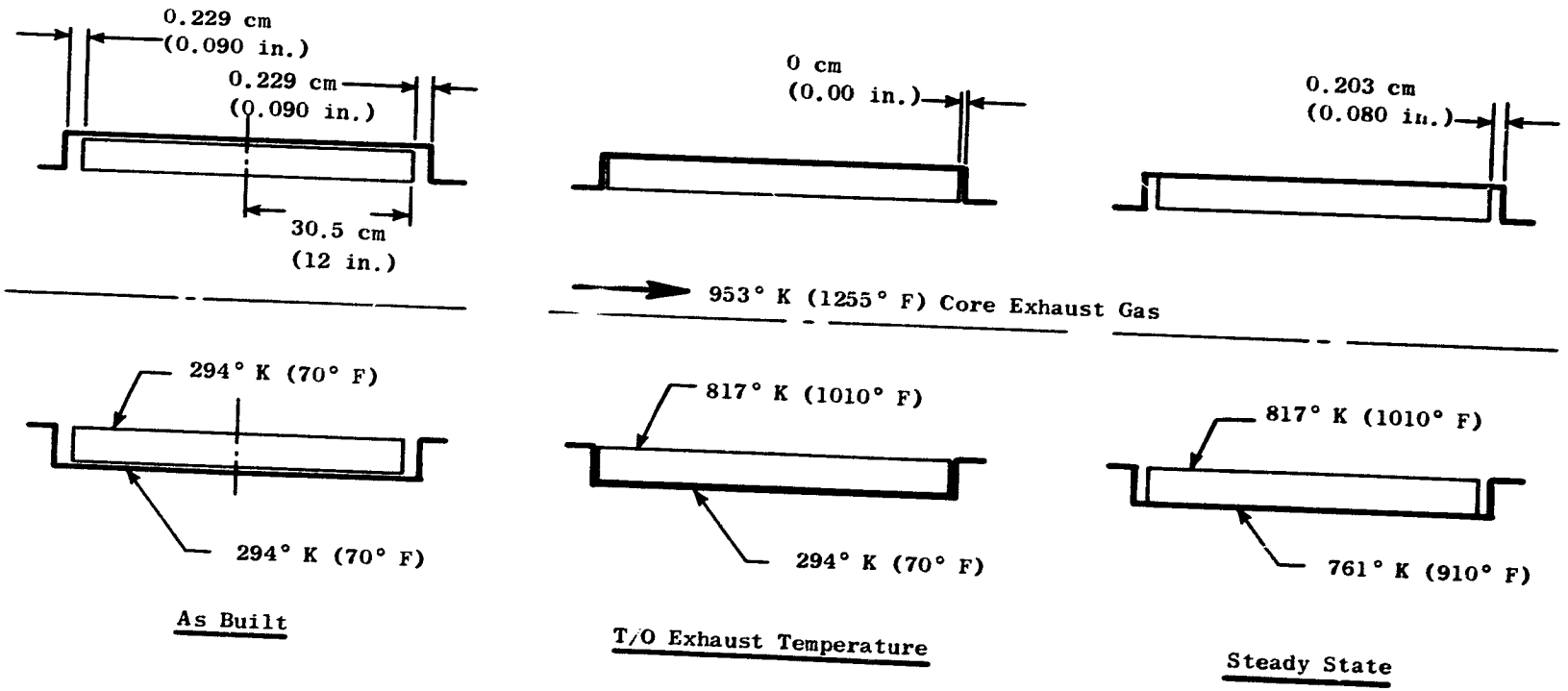

Figure 14.21. Outer Treatment, Axial Thermal Expansion.

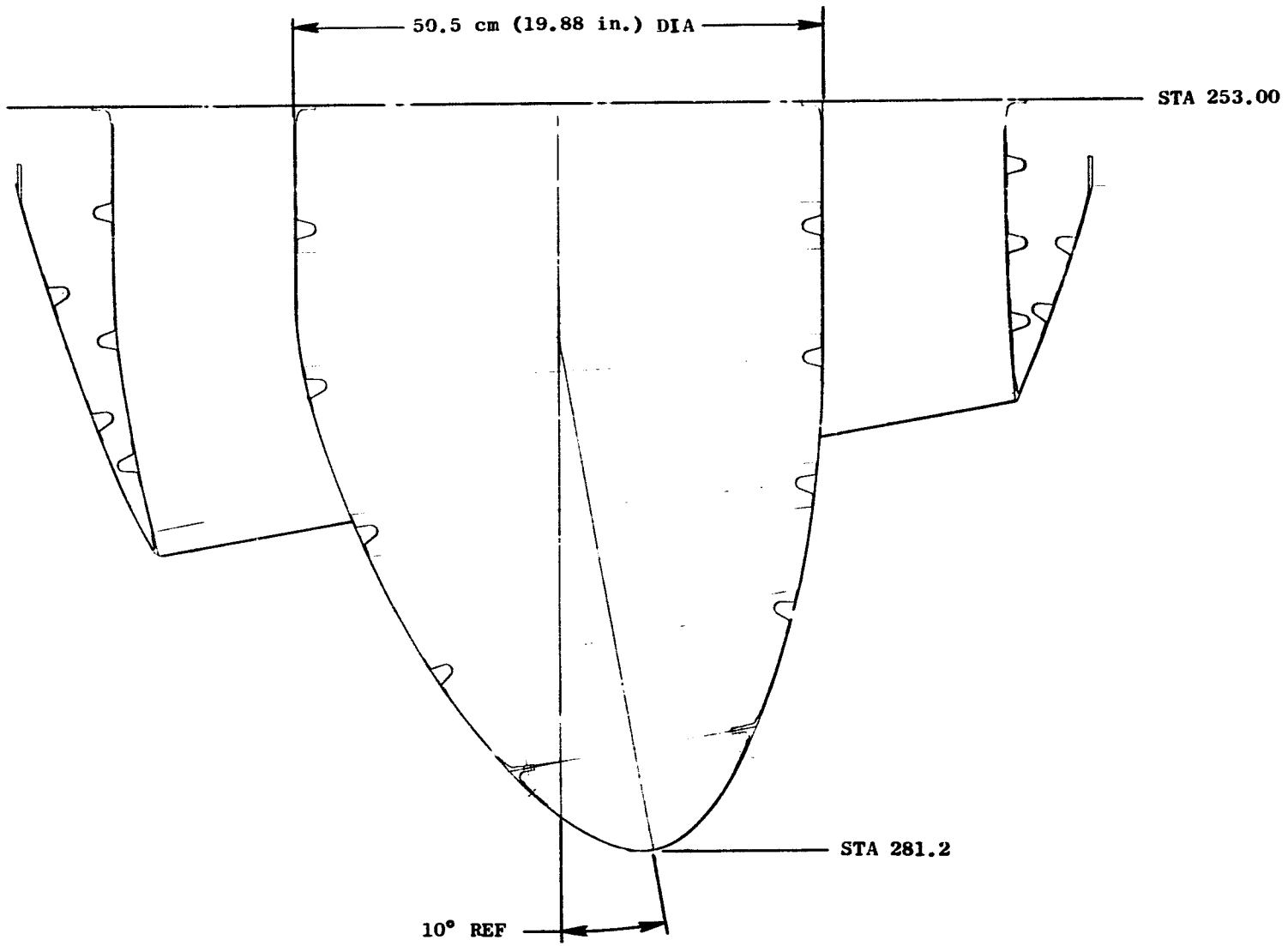

Figure 14.22. OTW Flight Core Exhaust System.

No acoustic treatment is required to meet the noise level requirements for operation on a 914.4 m (3000 foot) runway. The nozzle is a bolted assembly with reinforced sheet metal construction. The weight of the flight core exhaust nozzle is 38.1 kg (84 lbs).

14.5 ENGINE MOUNTING SYSTEM

14.5.1 Mounting System - Experimental Engine

The OTW experimental engine design utilizes the same mounting system as the UTW experimental engine. The front mount shown in Figure 14.23 has the vertical and side load uniball centerline at engine Station 199.0 on the rear structural ring of the composite fan frame. Thrust is taken through the short links and whiffletree. The two-point attachment moves the thrust reaction points closer to the engine centerline minimizing core bending, and, therefore, improving rotor-to-stator running clearance control.

The rear mount, shown in Figure 14.24, takes vertical, side, and torque loads through the outer ring at the turbine frame at engine Station 247.47. This engine mount system is composed of three links similar to that used on the DC-10/CF6 mount system. Uniballs at the ends of each of the links permit axial movement for differential thermal growth between the engine and the support structure.

When mounted as described, the engine and its mounting structure will withstand the flight maneuver forces described in Section 2.0. The precession rates used are consistent with the following normal commercial engine requirements:

> One radian/second in either pitch or yaw combined with the maximum resultant vertical, fore or aft, and angular acceleration loads at zero to maximum thrust combined with normal cycle pressure and thermal loads.

All engine-mounted equipment such as the inlet, fan exhaust cowls, and accessories have been included to determine mount loads. A forward thrust load of 81,400 N (21,000 lb) has been used in the design.

A summary of typical mount reactions for the mount system described above (Figures 14.23 and 14.24) for unit maneuver and "blade-out" loads is shown in Table 14-III for the OTW "Boilerplate" configuration with the fan cowl, "D" nozzle, and reverser supported from the facility thrust frame and no load attachments to the engine. This experimental engine mount system is identical to the system used on the UTW experimental and flight propulsion systems. All elements have been sized based on required operating maneuver load conditions.

Reacts Thrust, Vertical and Side Loads

- Blade Out Load: 204,608 N (46,000 lbs)
- Ultimate Allowable Load:

  Vertical and Side 591,584 N (133,000 lbs)

  Axial 155,680 N (35,000 lbs)

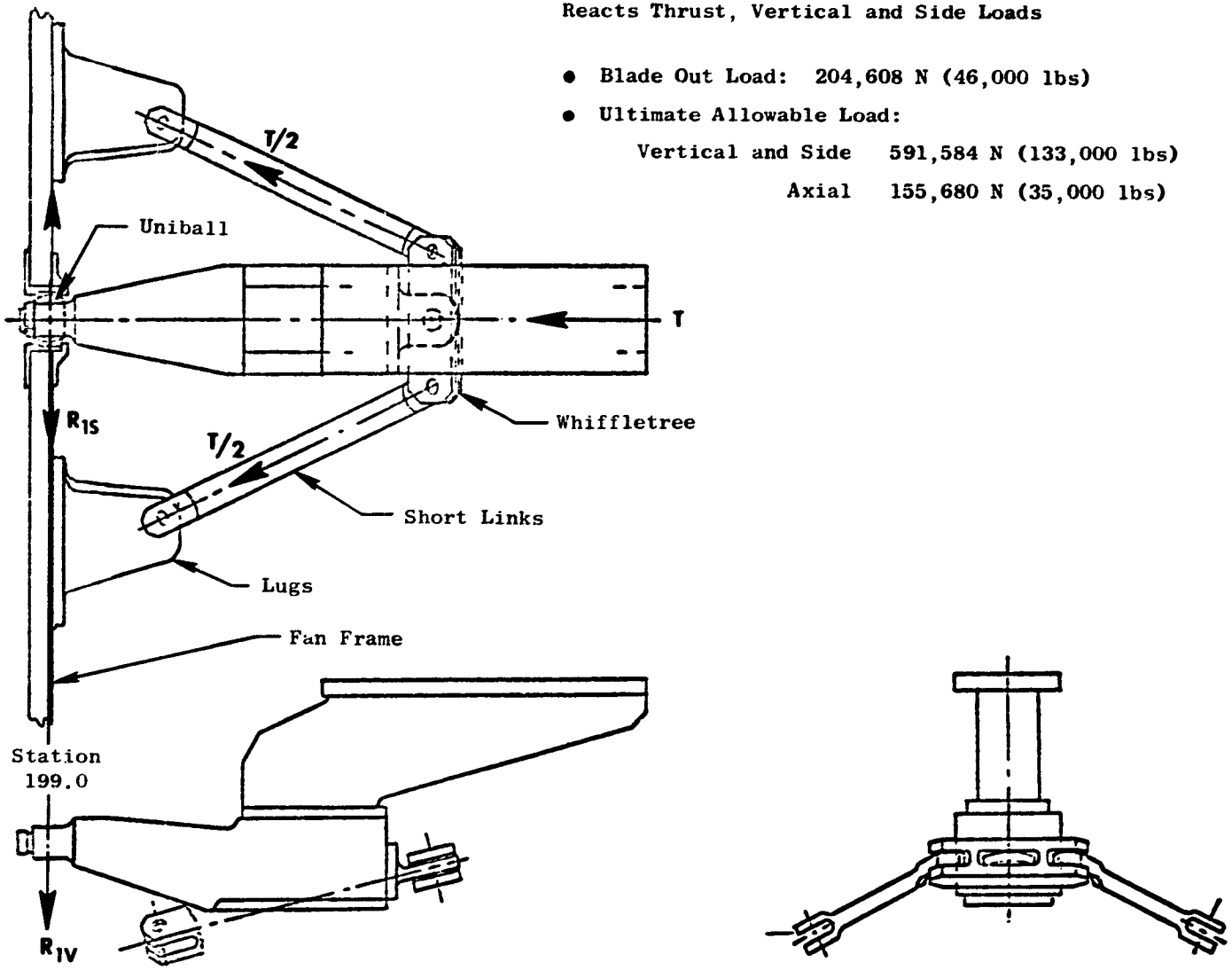

Figure 14.23. Front Mount, Experimental Engine.

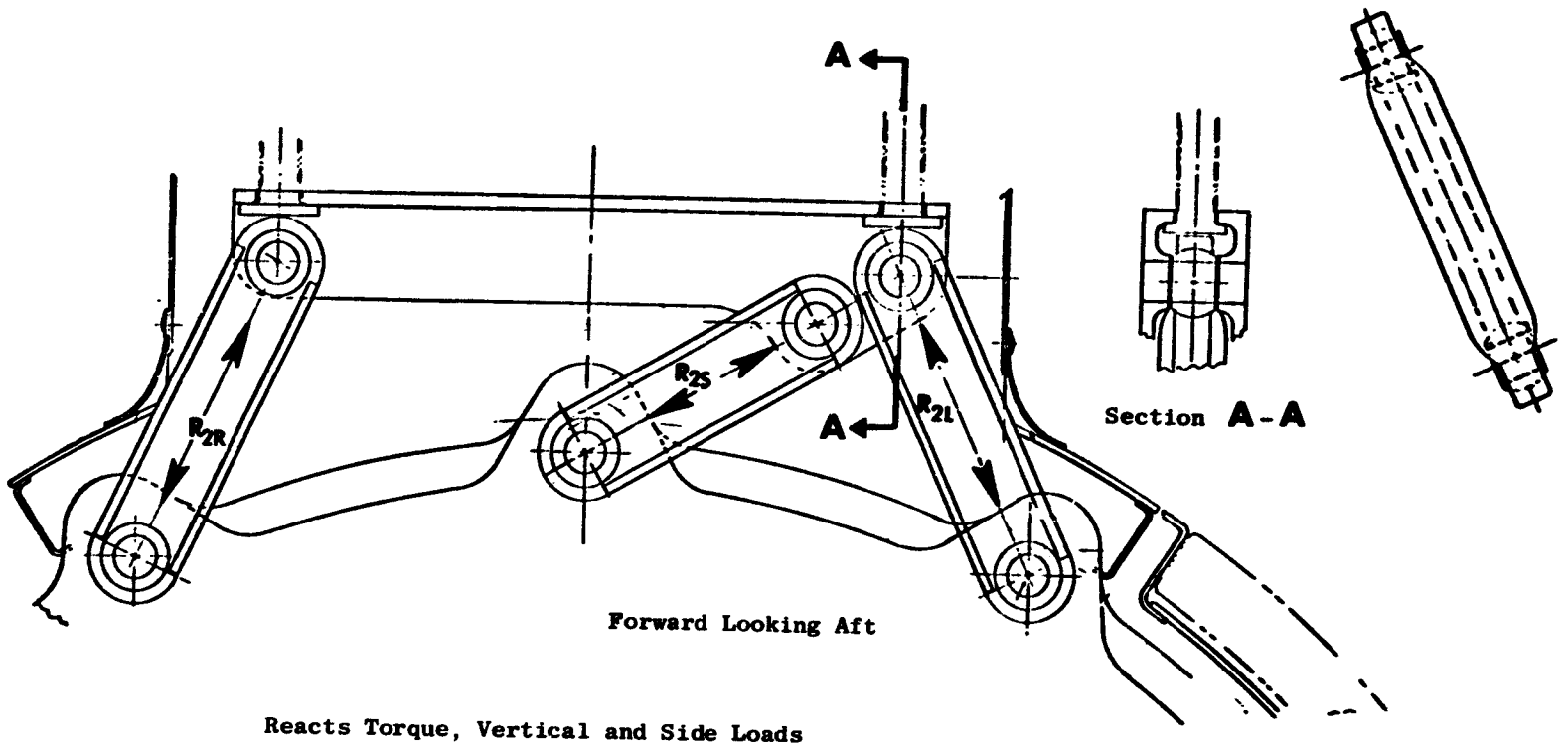

Reacts Torque, Vertical and Side Loads

- Links - Uniballs 2.223 cm (7/8 in.) Pin
- Blade Out - Max. Link Load 226,403 N (50,900 lbs)
  - Ultimate Allowable 420,336 N (94,500 lbs)

Figure 14.24. Rear Mount, Experimental Engine.

Table 14-III. OTW Experimental Propulsion System Mount Loads, Boilerplate Nacelle.

Maneuver		T	R 1V	R 1S	R 2R	R 2L	R 2S
1 G Down	N	---	+ 12,010	---	+ 6,295	+ 6,295	---
	(lb)	---	(+ 2,700)	---	(+ 1,415)	(+ 1,415)	---
1 G Side	N	---	---	± 12,010	∓ 14,635	∓ 30,400	± 28,560
	(lb)	---	---	(± 2,700)	(∓ 3,290)	(∓ 6,835)	(± 6,420)
1 $\dot{\theta}$ Pitch Velocity	N	---	---	± 17,325	± 4,400	∓ 7,450	∓ 21,485
	(lb)	---	---	(± 3,895)	(± 990)	(∓ 1,675)	(∓ 21,485)
1 $\dot{\psi}$ Yaw Velocity	N	---	± 17,325	---	± 9,560	± 9,560	---
	(lb)	---	(± 3,895)	---	(∓ 2,150)	(∓ 2,150)	---
1 $\ddot{\theta}$ Pitch Acceleration	N	---	± 1,270	---	± 690	∓ 690	---
	(lb)	---	(± 285)	---	(∓ 155)	(∓ 155)	---
1 $\ddot{\psi}$ Yaw Acceleration	N	---	---	± 1,270	± 535	± 335	∓ 1,580
	(lb)	---	---	(± 285)	(± 120)	(∓ 75)	(± 355)
1000 lbs Thrust	N	2225	+ 980	---	- 535	- 535	---
	(lb)	500	(+ 220)	---	(- 120)	(- 120)	---
1 Metal Blade Out †	N	---	±206,785	±206,785	∓185,115	∓185,115	±226,220
	(lb)	---	(± 46,490)	(± 46,490)	(∓ 41,620)	(∓ 46,620)	(± 50,860)

† Vertical and side loads do not act simultaneously.
‡ See Figures 14.23 and 14.24 for definition of load symbols.

14.6 ACCESSORIES

The accessory arrangement for the OTW experimental propulsion system is shown in Figure 14.25. To reduce cost, many of the experimental engine components are "off-the-shelf" items. The following list indicates the source of some of the items that are located in the accessory area of the experimental engine:

- Main fuel pump and control - modified F101
- Fuel shutoff valve - no flight design
- Water/oil cooler from LM2500*
- Lube tank from the CF6 modified
- Lube filters from the CF6 (supply)
- Industrial scavenge filter*
- Air/oil separator
- Lube and hydraulic pumps
- Magnetic chip detectors from the F101
- Alternator from the F101
- Digital control - non-flightweight design
- Ignition box from F101
- Control cables - nonflight design
- Power takeoff (PTO - used for starter mounting pad on experimental engine)

Optimized designs of the above items to meet flight system requirements would be mounted on the outer casing of the fan frame in the bottom accessory areas. Either location of these components will permit removal of the inlet without removing or uncoupling any of the engine fluid systems. On the experimental installation, the piping must be uncoupled from the facility-mounted components indicated above. The experimental engine casing is cast aluminum (heavier than flight design) using gears and gearbox gearings from the F101 gearbox.

Opening fan and core cowl doors will provide access to the core engine mounted equipment on the experimental system:

- Fuel manifold, valves, and tubes from the F101
- Stator actuators from the F101
- Scavenge pump

*Mounted to facility for experimental engine testing.

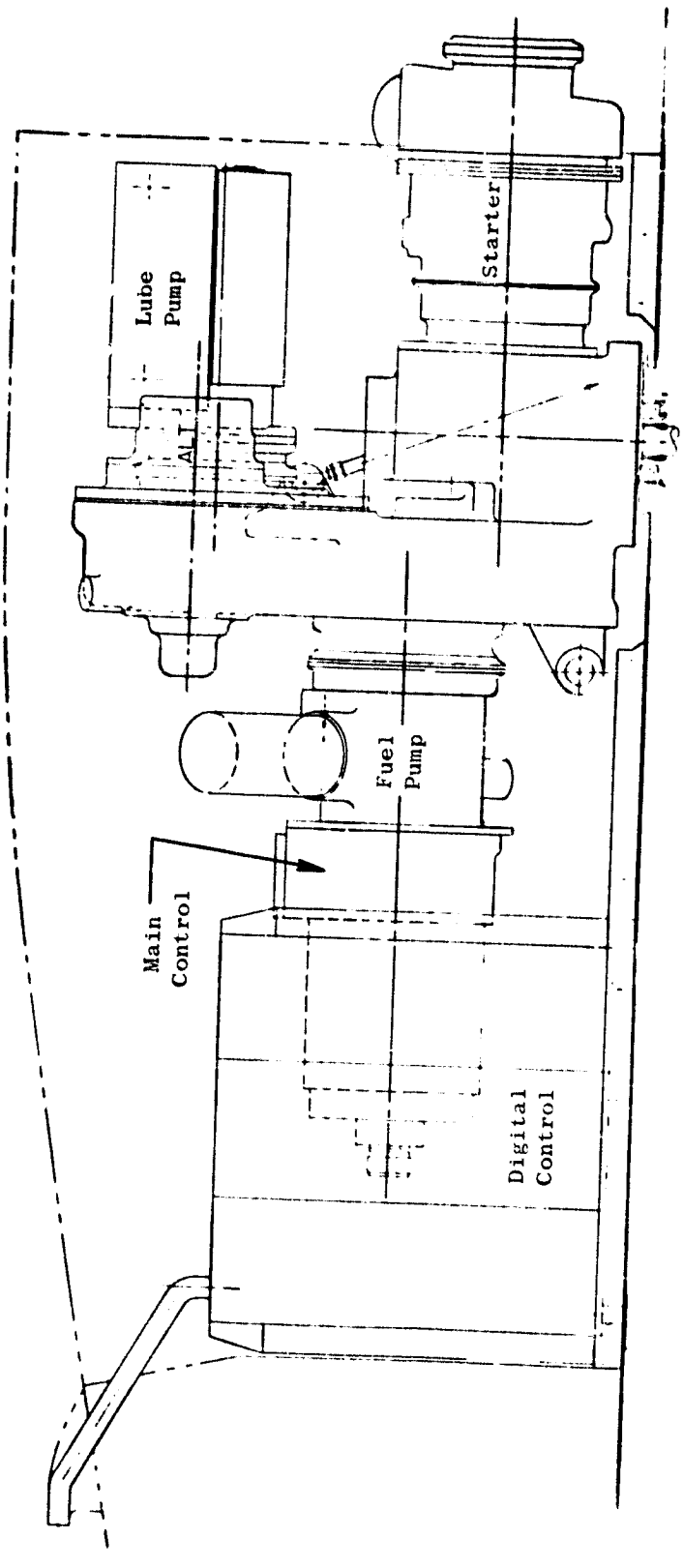

Figure 14.25. OTW Experimental Engine Accessories.

- Ignitors
- Instrumentation
- Speed sensors
- Vibration sensors
- Fire detection and extinguishing (aircraft hardware mounted on the pylon)

The scavenge pump with its own inlet gearbox and radial drive is on the bottom of the engine to provide a gravity-drain lube system. On the flight system, the scavenge pump would be mounted on the accessory gearbox.

The OTW flight system will include the following items not planned for the experimental engine:

- Flight-weight gearbox with provisions to drive: fuel pump and control, lube and scavenge pumps, alternator, and power-takeoff (PTO) for aircraft gearbox drive shaft
- Double-wall fuel piping and manifold
- Improved replaceability of fuel injection tubes
- Flight radial drive for scavenge pump
- "Hardwall" titanium piping in place of soft hardware coupling F101 engine pumping with accessories.

SECTION 15.0

ENGINE DYNAMICS

15.1 SUMMARY

A system vibration analysis of the QCSEE OTW experimental engine in the facility-mounted boilerplate nacelle configuration was performed to determine the critical speeds and corresponding amplitudes of vibration.

Results show that no serious vibration problems are anticipated assuming the engine rotating assemblies are balanced to within specified design tolerances using currently employed balancing technology.

15.2 DESIGN REQUIREMENTS

The propulsion system must be designed to be capable of operating within established safe operating vibration limits for excitation frequencies within all rotor speed ranges and for rotor unbalance not exceeding established allowable manufacturing tolerances. In addition, the system must be capable of withstanding, without further major structural failure, a transient loading caused by significant unbalance induced by blade loss resulting from foreign object damage (FOD). The transient consists of the time required for the pilot to recognize high vibration levels and take the necessary steps to shut down the engine.

Design vibration operating limits and the corresponding rotor balancing tolerances are established based upon the criteria that the rotor/bearing components and static structures shall not be subjected to vibratory loads in excess of those values which would reduce the life of those components below the established design life.

For the OTW propulsion system, there are actually three rotors which can serve as input sources for significant energy to excite a system mode. The three rotors are shown in Figure 15.1 along with their operating speeds. The range of frequencies for one per rev excitation is from approximately 9.55 Hz (573 rpm) for fan ground idle speed to 242.25 Hz (14,535 rpm) for maximum compressor speed. There are other sources of excitation such as the star gears, gear meshing frequencies, and blade passing frequencies; however, these sources do not have sufficient energy to drive the engine system modes being considered. Such component vibration is considered in the design criteria for the various engine parts by separate detail analyses of those components. It will be noted that the complexity of the propulsion system virtually precludes the avoidance of critical speeds in the operating speed range. Because of the structural damping inherent in the various components, the resonant amplitudes of the dynamic loads and displacements do not exceed acceptable limits if proper balancing of rotating components has been achieved.

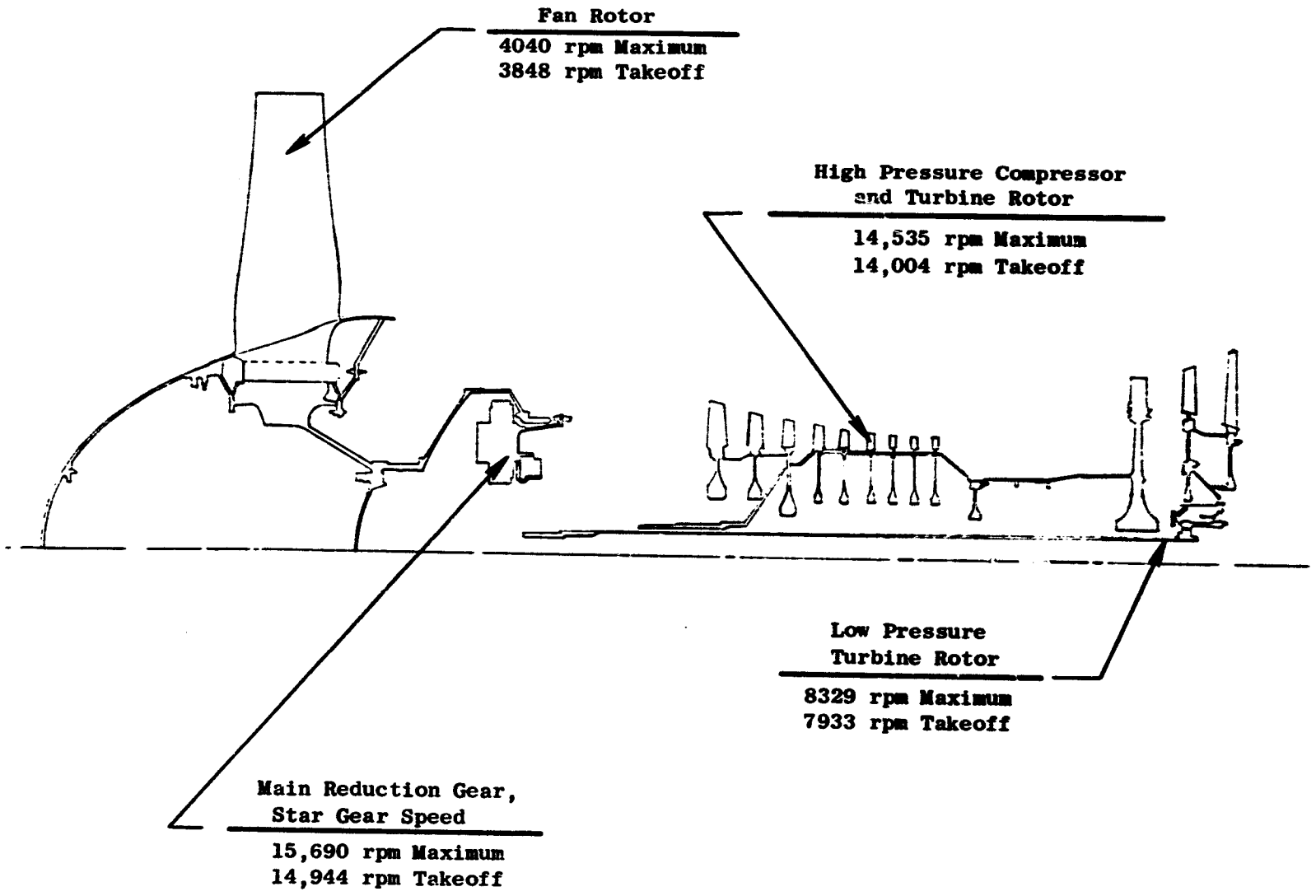

Figure 15.1. OTW Engine Rotating Subsystems.

However, there is one type of critical speed which must be avoided in order to avert possible serious problems, that being a rotor-dominated mode of the circular whirl-type where the rotor vibrates laterally or whirls at the same frequency at which it is rotating (forward synchronous precession). Therefore, the system must be carefully designed to ensure that rotor-dominated modes of the circular whirl-type do not exist in the operating speed range of the engine.

15.3 VIBRATION ANALYSES

15.3.1 Method of Analysis

The system was analyzed by use of the General Electric computer program VAST (Vibration Analysis System) which is used to calculate system critical speeds and vibratory estimated response at critical speeds for known unbalances. The VAST program has been in use at General Electric for a number of years and has consistently demonstrated the capability of accurately predicting engine critical speeds and responses for many types of engines and test vehicles developed by General Electric. A mathematical model of the engine system is constructed which includes all rotor components plus all stator components supported from the engine mounting system. The modeling procedure consists of establishing the geometric and physical properties and representing the various components by a series of lumped (or point) masses connected by flexible beam, cone, and spring elements. For more complex structures such as a fan frame or a bearing, special finite element models are constructed and/or tests of actual hardware are performed to determine their load/deflection characteristics. In summary form, the basic assumptions made in VAST are as follows:

1. The structure is axisymmetric and all deflections and vibrational modes will be based on beam-type behavior. No "shell modes" are considered.

2. Linear elastic behavior of materials for all elements modeled as beams or cones.

3. Elements modeled as beams follow classical beam small deflection theory in bending; shear deformation in beams is also considered.

4. All spring-type elements exhibit linear load-deflection characteristics.

5. Rotors exhibit gyroscopic stiffening due to whirling.

6. Damping coefficiencts are assumed to be constant. The structural damping factor is not considered to be a function of velocity.

7. Mass properties are considered as lumped at discrete points and are interconnected by massless generalized elastic (spring) elements.

8. A VAST analysis is an extension of the Prohl-Myklestad method of calculating the critical speeds of flexible rotors represented by beams.

9. The effects of flexible supports, multiple branches, and energy distribution schemes also are considered.

Critical speeds are calculated assuming an undamped system; however, estimated actual vibratory deflections and loads can be calculated by including damping coefficients for the various components along with possible unbalance locations on the rotors. Damping coefficients are based primarily on past performance of similar components as well as some analytical procedures in the case of friction dampers or journal bearings which are used in some vehicles.

15.3.2 Vibration Model

The VAST system vibration model is shown in Figure 15.2 in schematic form. The various frames and bearings are represented by springs whose flexibility coefficients have been determined by a separate analysis along with past experience with similar structures. For purposes of a VAST vibration analysis, the fan and LP turbine shafts, which turn at different speeds in opposite directions, are considered decoupled since no significant radial loads or shaft bending moments can be transmitted through the reduction gearing. For a torsional analysis, however, this decoupling assumption would not be true.

From a system vibration standpoint there are essentially three rotors involved due to the reduction gearing in the LP system, each rotor rotating at a different speed. Since the gyroscopic stiffening effects in the rotors depend upon the ratio of rotor speed, Ω, to the system vibratory frequency, ω, and since the source of system excitation is assumed to be an unbalance in one of the rotors causing harmonic excitation at the same frequency as the rotor speed (one per rev), it is required that three VAST vibration runs be made to determine all system criticals. Thus, the following cases are defined:

$$R = \Omega/\omega$$

Fan Excited Critical Speeds

$$R_{Fan} = 1.00$$

$$R_{LP} = -2.1$$

$$R_{HP} = -3.64$$

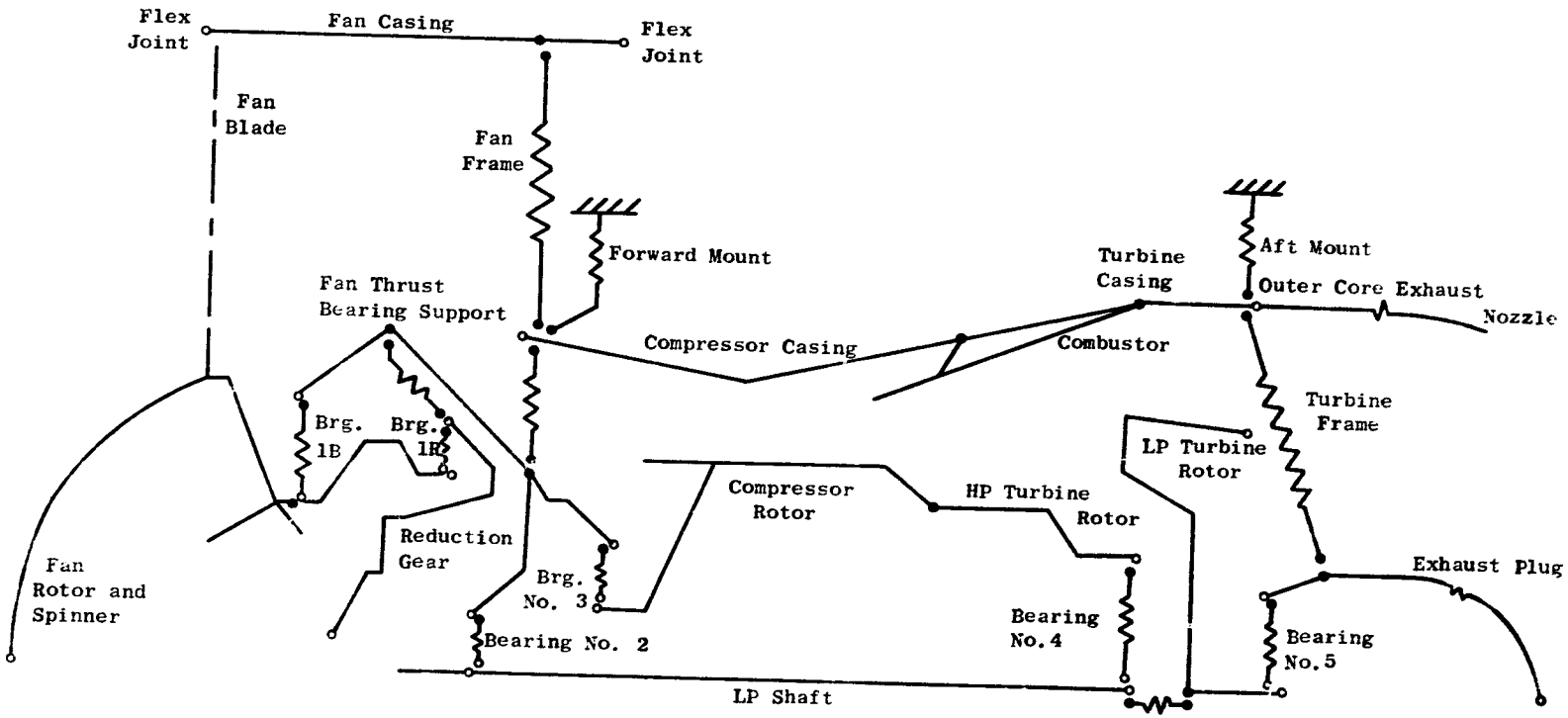

Figure 15.2. QCSEE OTW Experimental Engine Vibration Model.

LP Excited Reference Critical Speeds

$R_{Fan} = -0.49$

$R_{LP} = 1.00$

$R_{HP} = 1.77$

HP Excited Reference Critical Speeds

$R_{Fan} = -.27$

$R_{LP} = 0.57$

$R_{HP} = 1.00$

The negative sign on R represents a backward precession in whirling with respect to that component for which R = 1.

A series of VAST runs as outlined above was run for the experimental engine in the facility-mounted boilerplate nacelle configuration. In this configuration, the boilerplate nacelle components (inlet and fan aft duct) are supported by the facility and thus decoupled from the engine from a vibration standpoint.

15.3.3 Results

The results of the vibration analysis are shown in tabular form giving the critical speed in rpm along with the estimated maximum system response for both normal operation and the one-fan-blade-out condition. In the former case, the maximum system response is given for an unbalance of 25.4 gm-cm (10 gm-in.) at selected rotor planes.

Normal vibration data for the fan reference, LP turbine reference, and HP rotor reference are shown in Tables 15-I through 15-III. Blade-out fan reference data are presented in Tables 15-IV and 15-V.

As part of the output from VAST, a computer-generated plot of the system schematic with superimposed modal deflection pattern is produced. Also shown on these diagrams is a percentage distribution of kinetic and potential energies. This graphic output assists in identifying deflection patterns, and the energy distribution shows which parts are bending (high potential energy) and which are subject to highest g-loads (high kinetic energy). Figures 15.3 through 15.5 show typical mode shapes for various types of system modes for Configuration 1 (facility-mounted boilerplate nacelle configuration).

For both the vertical and horizontal directions, the forward and aft mount stiffnesses have been assumed to be 1.97 M-N/m (1×10^5 lb/in.). At

Table 15-I. Critical Speeds - Fan-Excited OTW - Boilerplate Nacelle.

Fan	Critical	Mode Description	Maximum Response* SA	
			mm	mils
573				
G1				
	803	FWD Mount, AFT Mount	.0074	.293
	1464	AFT Mount, FWD Mount	.0014	.055
	2180	LP Shaft, LP Turbine	.0025	.097
	2968	Core Casing, Fan Frame	.0012	.048
	3601	Turbine Frame, No. 1B Bearing, Fan Frame, Fan Rotor, Exhaust Plug	.0024	.093
3650 Maximum cruise				
3848 Hot day takeoff				
4040 Maximum				
	4144	Turbine Frame, Exhaust Plug, Fan Frame	.0017	.066

*Response at point of maximum deflection for 25.4 gm-cm (10 gm-in.) unbalance at fan (normal operating unbalance expected to be less than 50 gm-in.).

Table 15-II. Critical Speeds - LP Turbine and Shaft-Excited OTW - Boilerplate Nacelle.

LP Turbine rpm	Critical rpm	Mode Description	Maximum Response*			
			Unbalance At Center of LP Shaft		Unbalance At LP Turbine	
			mm-SA	Mils-SA	mm-SA	Mils-SA
1181						
G1	1464	AFT Mount, FWD Mount	.0008	.032	.0008	.033
	1859	Fan Rotor, IR, 1B Brg's, Fan Frame	.0002	.009	.0021	.085
	2991	Fan Frame, Core Casing, Exhaust Plug	.000025	.001	.0018	.072
	3922	Turbine Frame, Exhaust Plug, HP Turbine, LP Shaft, LP Turbine	.0670	2.64	.0406	1.6
	6084	Fan Frame, Fan Rotor, IR Brg. Core Casing	.0134	.528	.0035	.141
	7085	Turbine Frame, Exhaust	.1178	4.62	.0125	.495
7525 Maximum Cruise 7933 Hot Day Takeoff 8329		System, LP Shaft, HP Turbine, No. 5 Brg.				
	8493	Core Casing, Fan Frame, Exhaust Nozzle	.0052	.208	.0007	.029

*Response at point of maximum deflection for 25.4 gm-cm (10 gm-in.) unbalance. [Normal operating unbalance expected to be less the 50.8 gm-cm (20 gm-in.) for LP shaft and less than 101.6 gm-cm (40 gm-in.) for the LP turbine].

Table 15-III. Critical Speeds - Core-System-Excited OTW - Boilerplate Nacelle.

Core System rpm	Critical rpm	Mode Description	Maximum Response*			
			Unbalance At Compr. Stg. 1		Unbalance At HPT	
			mm-SA	Mils-SA	mm-SA	Mils-SA
	6591	LP Shaft, Fan Frame Turbine Frame, Fan Rotor	.001	.039	.001	.038
8093 G1						
	8484	Core Casing, Fan Frame, Exhaust Nozzle	.00025	.010	.00015	.006
	10616	LP Shaft, Core Rotors, No. 3 Brg.	.1275	5.02	.0439	1.73
	12288	LP Shaft, Fan Frame, Compressor Rotor	.0937	3.69	.0342	1.35
13237 Maximum Cruise 14004 Hot Day Takeoff 14535 Maximum						

* Response at point of maximum deflection for 25.4 gm-cm (10 gm-in.) unbalance. [Normal operating unbalance expected to be less than 50.8 gm-cm (20 gm-in.) for the compressor and less than 50.8 gm-cm (20 gm-in.) for the HPT].

Table 15-IV. One-Fan-Blade-Out Response, OTW - Boilerplate Nacelle.

Fan rpm	Critical rpm	Mode Description	Peak Response*	
			mm-SA	Mils-SA
573				
G1				
	803	FWD, Mount, AFT Mount	35.458	1396
	1464	AFT Mount, FWD Mount	6.6040	260
	2181	LP Shaft, LP Turbine	17.60	693
	2972	Core Casing, Fan Frame	.8890	35
3650 Maximum Cruise	3847	Turbine Frame, Fan Frame, Exhaust Plug, Fan Rotor	77.6224	3056
3848 Hot Day Takeoff				
4040 Maximum	4556	Fan Frame, Fan Rotor, Core Casing, Turbine Frame	65.8622	2593

*241,700 gm-cm (95,160) gm-in. unbalance for one titanium blade out.

Table 15-V. Fan-Blade-Out Response, OTW - Boilerplate Nacelle.

Critical (rpm)	Fan Relative Displacement		Mount Loads, SA				1-Titanium-Blade-Out Bearing Loads, SA											
			Fwd		Aft		No. 1B		No. 1R		No. 2		No. 3		No. 4		No. 5	
	mm-SA	mils-SA	N	lbs	N	lbs	N	lbs	N	lbs	N	lbs	N	lbs	N	lbs	N	lbs
803	1.651	65	206,797	46,490	85,072	19,125	103,372	23,239	36,920	8,300	3,229	726	5,662	1,273	2,477	557	4,617	1,038
1464	.838	33	24,189	5,438	59,282	13,327	12,081	2,716	6,485	1,458	2,090	470	3,278	737	9,394	2,112	14,634	3,290
2181	.299	11.8	14,567	3,275	27,000	6,070	25,870	5,816	10,361	2,330	29,522	6 637	4,430	996	24,613	5,585	18,882	4,200
2972	.236	9.3	1,757	395	1,258	283	1,467	330	1,187	267	177	40	1,205	271	484	109	756	170
3847	14.09	555	6,151	1,383	37,996	8,542	518,382	116,537	96,926	21,790	5,026	1,130	13,062	3,062	251,004	56,428	402,297	90,440
4556	55.13	2210	224,412	50,450	11,115	3,180	2.68×10^6	604,128	271,651	61,711	23,575	5,300	457,161	102,774	477,024	107,240	745,521	167,600

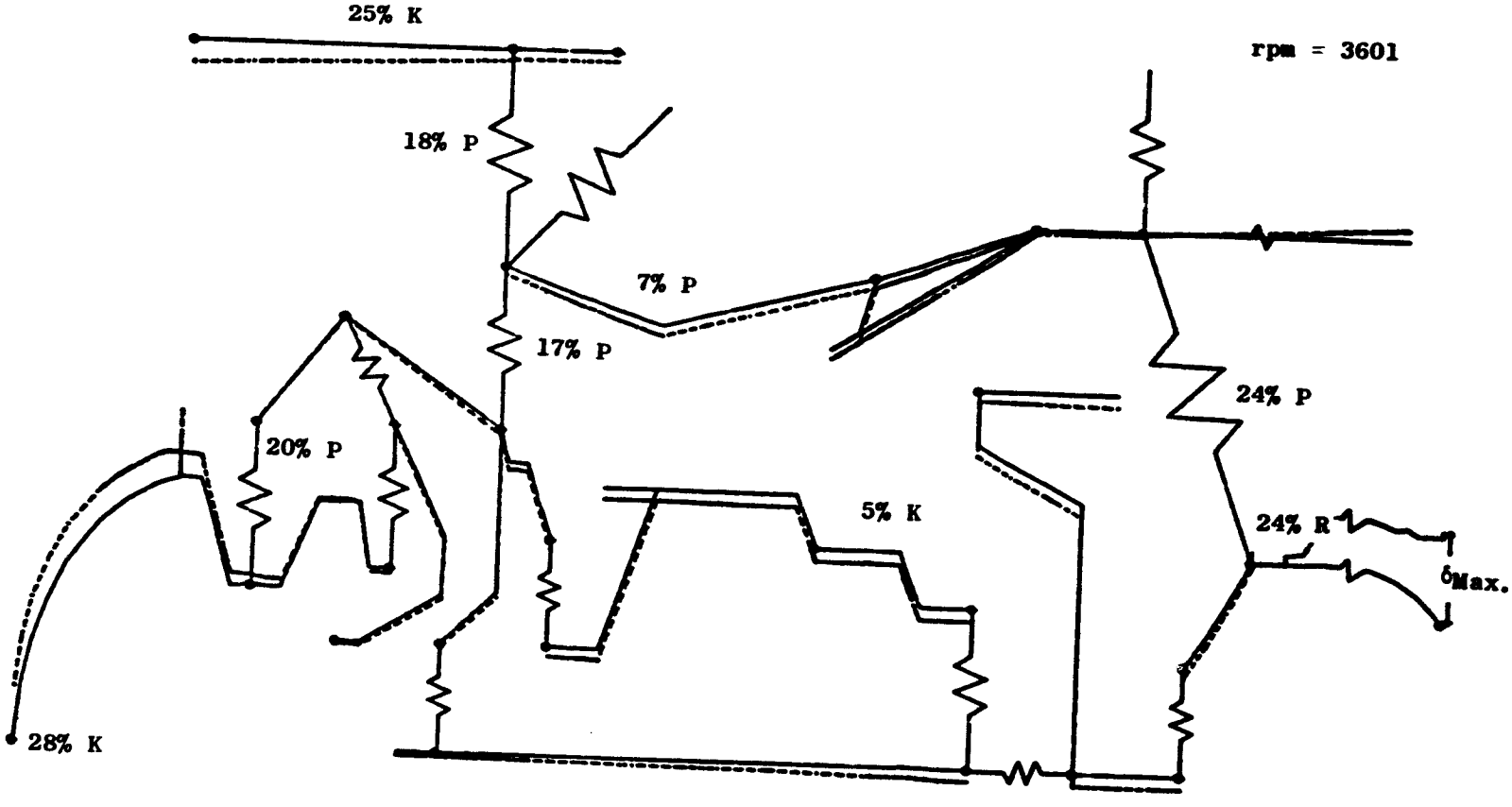

Figure 15.3. QCSEE OTW Configuration 1, Fan Reference.

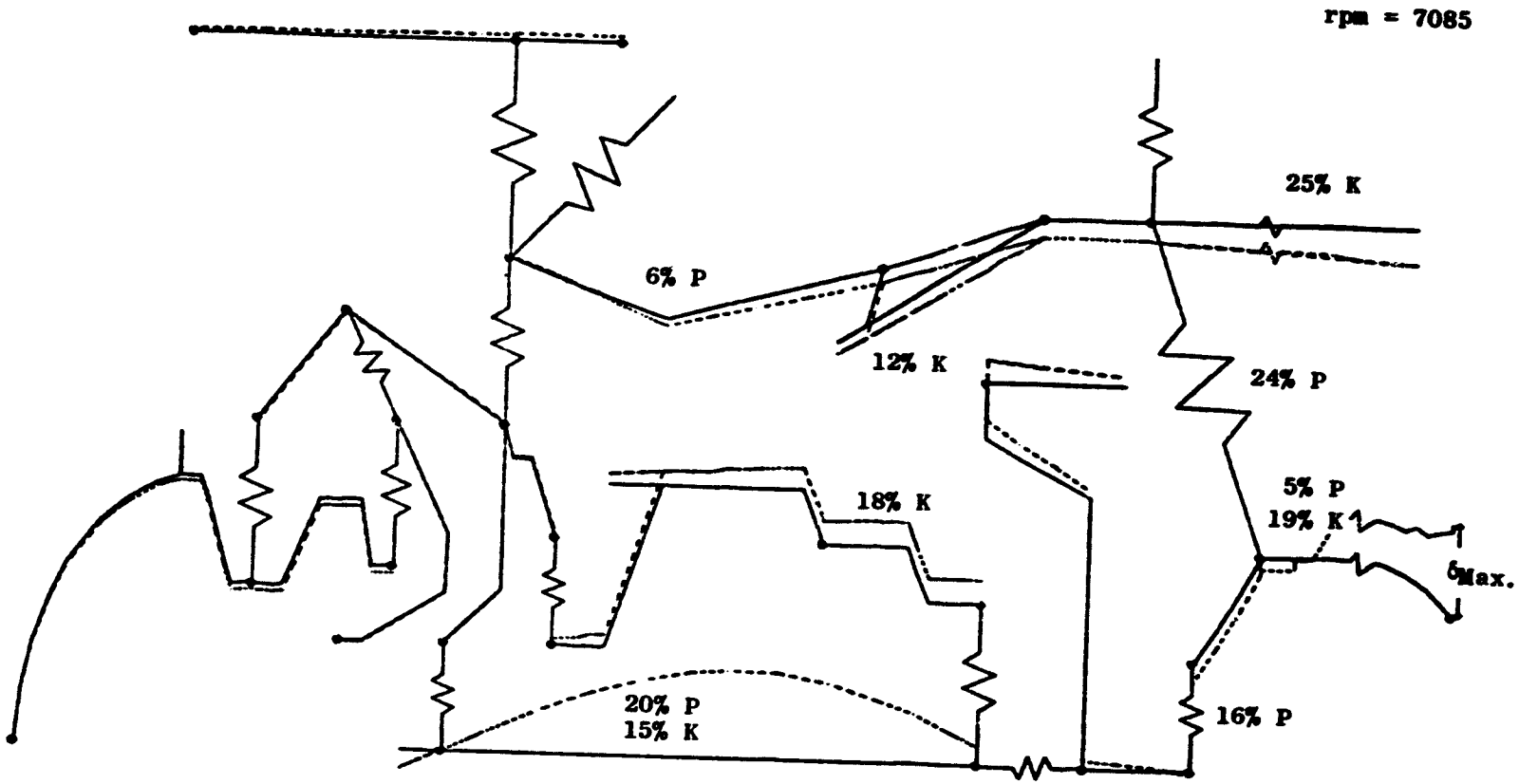

Figure 15.4. QCSEE OTW Configuration 1, LP Reference.

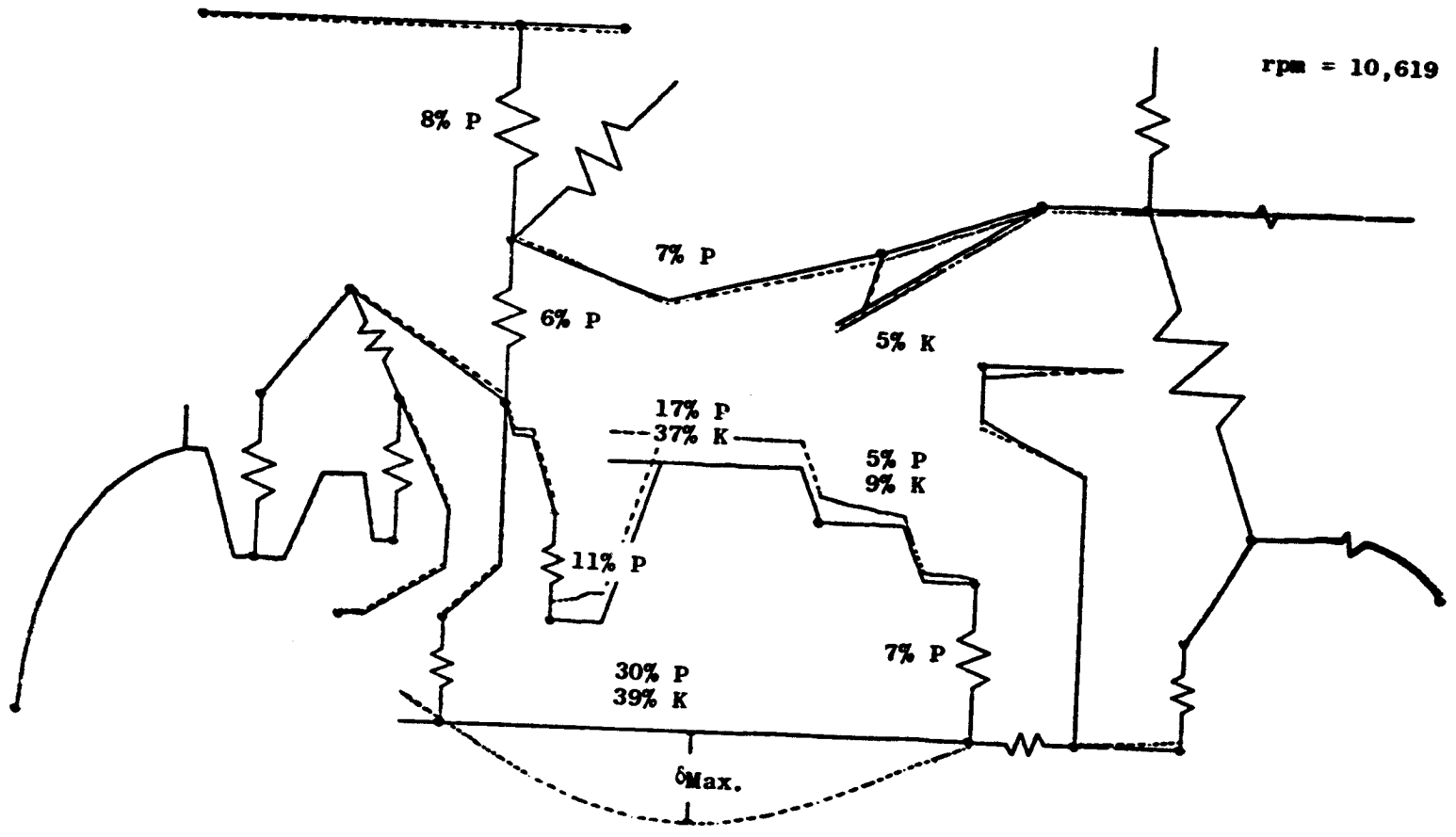

Figure 15.5. QCSEE OTW Configuration 1, HP Reference.

higher engine speeds the engine behaves like a seismic mass, and its response is little affected by the relatively soft mount spring rates. Therefore, the computed vibration spectrum for both normal operation and fan-blade-out condition is believed valid for the higher bending modes, and needs reexamination only at the low-frequency, rigid-body mount modes. The facility mount design will be completed by 9/75 and, if the structural analysis results in a spring constant significantly different from the original estimate, the effect will be reevaluated as required.

15.3.4 Conclusions

(Refer to Table 1-V and Figure 3.5).

The results of the VAST analysis indicate the following:

1. There are no rotor one-per-rev flexural criticals in the engine operating range.

2. For normal operation, unbalance in the compressor rotor and the LP shaft will result in the maximum response levels. The vibration amplitudes predicted are 0.1275 mm (5.02 mils) single amplitude at 10,616 rpm for compressor rotor unbalance and 0.1173 mm (4.62 mils) single amplitude at 7085 rpm for LP shaft unbalance.

3. For one-fan-blade-out, the following is indicated:

   - Low pressure shaft excursions will result in possible failure of the compressor air duct.

   - No. 5 bearing support cone may have localized yielding.

   - Secondary fan case damage will result from rubs.

   - The ultimate load capability of the mounts is not exceeded.

4. If proper rotor balancing procedures are followed, the system should not experience any serious vibration problems, since all modes involve significant bending of static structures or non-synchronous rotors which contribute to dissipation of energy. Utilizing current balancing technology, the rotors can be balanced to tolerances within those required to meet design criteria.

SECTION 16.0

WEIGHT

The OTW Propulsion System weight status at the completion of the Detail Design Phase is shown in Tables 16-I and 16-II. Table 16-I shows the breakdown of engine component weights. Differences between the experimental engine and projected flight engine weights are a result of material substitutions and design changes generally made to reduce cost and lead time of the experimental hardware. These differences are covered in detail in Table 16-III.

Table 16-II itemizes the installation components which, when added to the engine weight, result in the total propulsion system weight. In the case of the installation items no particular effort has been expended to control the weight of the boilerplate hardware.

As shown, the equivalent flight OTW propulsion system is expected to meet the contract goal of 4.7 installed thrust-to-weight ratio.

Table 16-1. OTW Engine Weight Summary.

	Experimental		Flight	
	kg	lb	kg	lb
F101 Core	433.2	955	424.6	936
F101 LPT	117.5	259	117.5	259
Mod. F101 Turbine Frame	83.9	185	47.6	105
Mod. F101 LPT Shaft	28.1	62	28.1	62
Total F101 Comp.	662.7	1461	617.8	1362
Fan Blades	166.5	367	59.0	130
Disk	142.0	313	69.9	154
Shaft	31.8	70	22.7	50
Spinner and Flowpath	31.3	69	22.2	49
Total Fan	371.5	819	173.3	382
Reduction Gear	89.8	198	77.1	170
Fan Frame Comp. Struct.	120.2	265	108.4	239
Casings and Flanges	48.1	106	45.8	101
Sump and Shields	0.9	2	0.9	2
Containment	20.9	46	20.9	46
Core OGV's	19.1	42	14.5	32
Total Fan Frame	209.1	461	190.5	420
Oil Tank	15.9	35	11.3	25
Bearing Supports	68.0	150	36.3	80
Bearings Sumps and Seals	98.4	217	86.2	190
Accessory Drives	64.9	143	44.9	99
Lube and Scavenge System	44.0	97	21.8	48
Total Brgs. Drives and Lube	291.2	642	200.5	442
Fuel System	33.6	74	20.0	44
Elect. System	26.3	58	25.4	56
Piping and Wiring	36.3	80	19.5	43
Total Controls System	96.6	213	64.9	143
Total Engine	1720.5	3794	1324.1	2919

Thrust/Weight Uninstalled - 21000/2919 = 7.19 (Goal 7.4)

Table 16-II. OTW Propulsion System Weight Summary.

	Experimental		Flight	
	kg	lb	kg	lb
Inlet	567	1250*	156.5	345
Fan Duct Doors	272.2	600*	95.3	210
Splitter	113.4	250*	-	-
Core Cowl	226.8	500	43.1	95
Core Exhaust	112.0	247	38.1	84
Aft Nacelle (see note)	212.7	469*	113.4	250
Nozzle/Reverser Doors and Linkage	241.3	532*	120.7	266
Nozzle/Reverser Actuation	-	-	25.9	57
Oil Cooler	99.8	220*	18.1	40
Fire Detection and Extinguishing	30.8	68*	-	-
Instrumentation	22.7	50	5.9	13
Drains and Vents	10.9	24	2.3	5
Total Installation	1909.7	4210	619.2	1365
Engine	1720.5	3794	1324.1	2919
Total Propulsion System	3630.1	8004	1943.3	4284

Thrust/Weight Installed - 20300/4284 = 4.74 (Goal 4.7)

---

*Facility-Mounted Component

Note: Aft Nacelle Definition:

Experimental Propulsion System - All static structure aft of the boilerplate fan cowl doors (Engine Station 245.5). Moveable components are listed separately.

Flight Propulsion System - Flowpath skin aft of Engine Station 200. Moveable components are listed separately. The engine supporting structure, corresponding to a pylon in a conventional installation, is included in the aircraft weight.

Table 16-III. Experimental and Flight Engine Weight Differences.

Component	Δ Weight kg	Δ Weight lb	Justification
F101 Core	-8.6	-19	Flight engine would use QT core. Many changes not under QCSEE Projects' control, are currently being formulated. These include a single-wall combustion casing. Also, titanium can be used further back in the compressor because of the subsonic operating envelope and lower fan pressure ratio. A QCSEE engine could also be designed lighter since max. P3 is 172.3 N/cm^2 (250 psia) instead of 344.8 N/cm^2 (500 psia).
Turbine Frame	-36.3	-80	The experimental frame retains the F101 structure consisting of 14 struts, uniball outer strut attachments and bolted inner strut attachments. The flight frame would be completely redesigned with 8 structural struts and 8 nonstructural vanes welded into the inner and outer casing. A lighter rear mounting would be used than in the UTW frame.
Fan Blades	-107.5	-237	The flight blades will be designed to use composite material in place of titanium. When flutter phenomena of composite blades are better understood, some relaxation in torsional stiffness may be permissible reducing the boron fiber content.
Fan Disk	-72.1	-159	This saving reflects the reduction in blade weight postulated above.
Fan Shaft	-9.1	-20	Saving is due to use of titanium in place of steel.
Spinner and Adaptors	-9.1	-20	Flight engine is assumed to use composite materials for these parts.
Reduction Gear	-12.7	-28	Saving is due to use of titanium in place of steel for support member.
Fan Frame	-18.6	-41	A 10% reduction in structural weight has been assumed on the basis that the 3X safety factor and 5-blade-out requirement will be relaxed after more composite test experience is gained. Also core OGV's would be titanium rather than steel.
Oil Tank	-4.5	-10	Saving is based on a new oil tank in place of TF-39 Component.
Bearing Supports	-31.8	-70	Saving is due to use of titanium in place of steel and using scalloped flanges.
Bearings	-12.2	-27	Experimental engine uses a modified CF6 No. 1 bearing. It is assumed that a smaller fan bearing could be developed for a flight engine. Also, lighter thermal shields and integral oil passages would be used on all of the low pressure rotor bearings.
Accessory Drives	-19.9	-44	The experimental gearboxes use available F101 gear trains and bearings. Lighter components could be used for the reduced QCSEE accessory loads. In the flight system only one accessory gearbox and drive is required on the bottom of the engine.
Lube and Scavenge System	-22.2	-49	Experimental engine uses an available CF6 lube pump and scavenge filter. Flight engine would allow redesign of these components. Also a combination lube and scavenge pump is used.
Fuel System	-13.6	-30	Most of this reduction is due to the use of an all digital control on the flight engine, substituting a fuel metering valve for the hydromechanical control.
Electrical System	-0.9	-2	A significant saving is projected by improved packaging of the digital control, but this is largely offset by returning to a dual ignition system.
Piping and Wiring	-16.8	-37	Both the experimental and flightweight estimates are still very approximate. The flight engine, however, will employ titanium tubing in place of steel, and the hydraulic lines are part of aircraft weight.
Inlet	-410.5	-905	Composite inlet in place of boilerplate.
Fan Duct Doors	-50.8	-390	The flight duct is composite material and is shorter.
Splitter	-113.4	-250	No splitter is required in flight duct.
Core Cowl	-83.3	-405	Saving due to shorter length and composite material.
Core Exhaust	-73.9	-163	Shorter, no acoustic treatment, and 0.038 cm (0.015 in.) stock in place of 0.079 cm (0.031 in.).
Aft Nacelle	-99.3	-219	In flight engine, this item is the nonstructural skin only.
Nozzle/Reverser Doors and Actuation	-94.8	-209	Composite construction in flight engine, includes actuators.
Oil Cooler	-81.6	-180	Experimental engine uses slave IM2500 water oil cooler. Flight engine uses new fuel/oil cooler.
Fire Detection and Exting.	-30.8	-68	This subsystem included as part of aircraft weight.
Instrumentation	-16.8	-37	Estimate based on reduced requirements and short lines in flight engine.
Drains and Vents	-8.6	-19	Reduction due to improved packaging of collector and shorter lines.

SECTION 17.0

SUMMARY OF RESULTS

The detail design phase of the QCSEE OTW engine has been completed as scheduled. Design analyses have shown no problems of a nature to prevent successful operation of the experimental propulsion system. The detail design has been approved by the NASA Project Office, authorizing the fabrication and procurement of all engine hardware needed to meet the scheduled start-of-test date of October 1, 1976.

Because of the high degree of integration of an OTW propulsion system with the aircraft, all installation features cannot be finalized until a specific airframe design is well underway. As a result of wind tunnel testing at NASA-Langley, a representative "D" nozzle/thrust reverser configuration has been selected for the QCSEE OTW experimental engine. This design has been approved, permitting fabrication of the boilerplate nacelle components to proceed except for final selection of the thrust reverser lip and side-wall configuration. These items will be defined on the basis of further wind tunnel testing, and a final design review is currently scheduled for January 7, 1976.